



Pilkington Library

Author/Filing Title GOETZ

Vol. No. Class Mark T

**Please note that fines are charged on ALL
overdue items.**

FOR REFERENCE ONLY

0402805658



POLYNUCLEAR COMPLEXES
OF MACROCYCLIC AND RELATED LIGANDS

by

Sandrine Goetz

A Doctoral Thesis

Submitted in partial fulfilment of the requirements for the award of
Doctor of Philosophy of Loughborough University

Department of Chemistry

Loughborough University

Loughborough

Leicestershire

LE11 3TU

© S. Goetz 2002

 Loughborough University Physical Library
Date <i>Aug 03</i>
Class <i>T</i>
Acc No. <i>040 280565</i>

ABSTRACT

A route to sodium salts of tetranuclear Schiff-base macrocyclic ligands (H_2Na_2L1 and H_2Na_2L2) derived from the condensation of 2,6-diformyl-4-(methyl or *tert*-butyl)phenol and 1,5-diaminopentan-3-ol has been developed, in order to compare two synthetic pathways namely the template synthesis and the “direct” synthesis of already known tetranuclear macrocyclic complexes. Subsequently, the complexation of H_2Na_2L1 and H_2Na_2L2 with nickel(II), copper(II), cobalt(II) and manganese(II) has been performed. The X-ray structures of tetranuclear nickel(II), copper(II) and manganese(II/III) complexes synthesised *via* the non-template route were determined and discussed. Furthermore, it is shown that the synthesis of tetranuclear complexes of metals inert towards template reactions like palladium is possible by complexing the pre-formed macrocycles H_2Na_2L1 and H_2Na_2L2 .

During this research, five dinuclear and two novel heptanuclear complexes of 2,6-diformyl-4-*tert*-butylphenol were isolated and fully characterised. The synthesis and structures along with some preliminary magnetic studies will be discussed.

To study the influence of extended versions of the tetranuclear macrocycles H_2Na_2L1 and H_2Na_2L2 , the synthesis of a new diphenolic precursor 2,2'-dihydroxy-5,5'-di-*tert*-butyl-3,3'-methanediyldibenzaldehyde (DHTMB) has been developed. Pseudocalixarene-like macrocyclic ligands were synthesised by condensation of DHTMB and a range of diamines in the presence of metal (Fe(II), Mn(II), Co(II), Ni(II), Cu(II) and Zn(II)) salts. The DHTMB group introduced multiple geometrical variations, largely due to the presence of the saturated carbon linking the two phenol rings. A range of di-, tri- and tetranuclear macrocyclic complexes accessible using DHTMB, have been synthesised and structurally characterised. Depending on the counter anions present, and the extent of deprotonation of the phenol groups, the nuclearity of the macrocycles can be manipulated. Similarly, bridging groups of various lengths can be accommodated between the bound metal ions.

DEDICATION

*I would like to dedicate this thesis to my late much beloved dad
who has always been there for me, supported every choice I made, seen me through
good and bad times and taught me to never give up.
You have had and will always have a very special place in my heart!*

ACKNOWLEDGEMENTS

I am especially grateful to my supervisor, Prof. Vickie McKee, for everything she has done for me during my Ph.D. Many thanks for your invaluable input and guidance throughout this project! I am also grateful to The Queen's University of Belfast and Loughborough University for financial support.

Furthermore, I wish to mention my late dad Gilbert, my mum Pierrette and Dominique for their love, support and encouragement throughout my years at University. I would like to give my very special thanks to Sean whose love, support and understanding has seen me through the last two years of my PhD. Your humour makes life funnier and more interesting! I would also like to thank David and Nellie for their support during my Ph.D. Special thanks go to all my friends who made my Ph.D such an enjoyable experience! From Belfast (very good craic!), Aine, Barbara, Cathy (& Peter), Antoinette, Clare, Connor, Fred, Nicolas, David F., David S., Maeve, Mannis, Béatrice, Stéphanie, Mark H., Woody and Jen; from Leicester, Neil, Steve, Peter, Jo, Luca, Lisa and Julia Z. I would also like to thank my work colleagues in Loughborough: Pauline, Sandra, Sean, Richard B., Julia B., Katie, Sarah, Richard W., Julia S., Liam, Jenny, Duncan, Pious, Emma and Sophie. I also wish to thank Prof. Jane Nelson for her general help and advice. I must also thank Drs Jon Parr, Sandra Dann, Mark Elsegood and Paul Kelly from the chemistry department at Loughborough University.

I am indebted to Pauline King at Loughborough University as well as ASEP at Queen's University of Belfast for the elemental analysis, Dr C.J. Harding for carrying out the variable-temperature magnetic measurements, Dr F. Marken for helping out with the voltammetry studies, the EPSRC National Mass Spectrometry Service Centre in Swansea for FAB (LSIMS) spectra and the Synchrotron Radiation Source at Daresbury for use of station 9.8. In addition, I wish to acknowledge the use of the EPSRC's Chemical Database Service at Daresbury. I would also like to thank Dr M. Tumer and Julia Barreira Fontecha for their assistance during this project.

CONTENTS

Title	i
Abstract	ii
Dedication	iii
Acknowledgements	iv
Contents	v
Ligand referred to in the thesis	xv
Colour pattern(s) of the atoms	xxv
Abbreviations and symbols	xxvii

TABLE OF CONTENTS

Chapter one	Introduction: Macrocyclic chemistry: from binuclear systems to polynuclear systems	1
Chapter two	Tetranuclear complexes of phenol head-unit Schiff-base macrocycles	51
Chapter three	Polynuclear complexes of new tetraphenolic Schiff-base macrocycles	100
Chapter four	Binuclear and mononuclear complexes of 2,6-diformyl-4- <i>tert</i> -butylphenol	177
Chapter five	Polynuclear clusters: a potential for high-spin molecules	216
Chapter six	Experimental	260

References	310
Single X-ray crystallography	324
Annex 1: Tables for crystal data and refinement for the compounds described in chapter 2	325
Annex 2: Tables for crystal data and refinement for the compounds described in chapter 3	329
Annex 3: Tables for crystal data and refinement for the compounds described in chapter 4	344
Annex 4: Tables for crystal data and refinement for the compounds described in chapter 5	351
Appendix - Single Crystal X-ray Crystallographic Data in CIF format	CD-ROM

Chapter one Introduction: Macrocyclic chemistry: from binuclear systems to polynuclear systems

1.1.	Introduction	2
1.2.	Binucleating Schiff-base macrocyclic systems	9
1.2.1.	Phenolic head-units	9
1.2.2.	Heterocyclic head-units	19
1.3.	From binuclear to tetranuclear complexes	26
1.4.	Tetranuclear and octanuclear macrocyclic complexes of H ₄ L1 and H ₄ L2	27
1.4.1.	Tetranuclear manganese complexes	30
1.4.2.	Tetranuclear cobalt complexes	31
1.4.3.	Tetranuclear nickel complexes	32
1.4.4.	Tetranuclear copper complexes	32
1.4.5.	Octanuclear copper complexes	35
1.5.	Tetranuclear complexes of H ₄ L34	37
1.6.	Tetranuclear complexes of H ₄ L36	41
1.7.	Tetranuclear complexes of H ₄ L37	44
1.8.	Tetranuclear complexes of H ₂ L38	45
1.9.	Hexanuclear complexes of H ₆ L39 and H ₆ L40	47
1.10.	Conclusion	50

Chapter two Tetranuclear complexes of phenol head-unit Schiff-base macrocycles

2.1.	Tetranuclear nickel complexes	52
2.1.1.	Introduction	52
2.1.2.	Tetranickel complexes with ClO ₄ ⁻ , NO ₃ ⁻ and Cl ⁻	54
2.1.2.1.	Synthesis and characterisation	54

2.2.	Sodium template approach for the synthesis of tetraimine macrocycles by condensing NaDFMP/NADFTP and NaDFMOP with DAHP or 1,3-diaminopropan-2-ol	61
2.2.1.	Synthesis and characterisation of the sodium salts of DFMP, DFTP and DFMOP	63
2.2.2.	Synthesis and characterisation of the sodium salts of the ligands L1, L2, L3, L4 and L5	63
2.3.	Complex syntheses using the “free macrocycles” H_2Na_2L1 and H_2Na_2L2	72
2.3.1.	Complexes with nickel perchlorate and nickel nitrate	72
2.3.2.	Structures with nickel acetate	78
2.3.3.	Structures with manganese acetate	82
2.3.4.	Structures with cobalt acetate	87
2.3.5.	Structures with copper nitrate	89
2.3.6.	Dinuclear and tetranuclear palladium complexes	95
2.4.	Conclusion	97

Chapter three Polynuclear complexes of new tetraphenolic Schiff-base macrocycles

3.1.	Introduction	101
3.2.	Synthesis of 2,2'-dihydroxy-5,5'-di- <i>tert</i> -butyl-3,3'-methanediyl dibenzaldehyde (DHTMB)	104
3.2.1.	Characterisation of 2,2'-diallyloxy-5,5'-di- <i>tert</i> -butyl-3,3'-methanediyl dibenzyl alcohol (AOTMBA)	106
3.2.2.	Characterisation of 2,2'-diallyloxy-5,5'-di- <i>tert</i> -butyl-3,3'-methanediyl dibenzaldehyde (AOTMB)	110
3.2.3.	Characterisation of 2,2'-dihydroxy-5,5'-di- <i>tert</i> -butyl-3,3'-methanediyl dibenzaldehyde (DHTMB)	113

3.3.	Pseudo-cryptate structures: pendent arm macrocycle	117
3.3.1.	Synthesis of $[\text{Mn}_2(\text{L8})](\text{ClO}_4)_2$ and $[\text{Co}_2(\text{L8})](\text{ClO}_4)_2$	117
3.3.2.	IR and FAB characterisation of $[\text{Mn}_2(\text{L8})](\text{ClO}_4)_2$	118
3.3.3.	Structure of $[\text{Mn}_2(\text{L8})](\text{ClO}_4)_2$	119
3.3.4.	IR and FAB characterisation of $[\text{Co}_2(\text{L8})](\text{ClO}_4)_2$ and $[\text{Co}_2(\text{L8a})](\text{ClO}_4)(\text{OH})(\text{MeOH})$	122
3.4.	Dinuclear bridged complexes of L9	123
3.4.1.	Synthesis of $[\text{Ni}_2(\text{H}_4\text{L9})(\mu_2\text{-H}_2\text{O})(\text{EtOH})_2](\text{ClO}_4)_2$ and $[\text{Co}_2(\text{H}_4\text{L9})(\mu_2\text{-H}_2\text{O})(\text{H}_2\text{O})_2](\text{ClO}_4)_2$	124
3.4.2.	IR and FAB characterisation of $[\text{Ni}_2(\text{H}_4\text{L9})(\mu_2\text{-H}_2\text{O})(\text{EtOH})_2](\text{ClO}_4)_2$ and $[\text{Co}_2(\text{H}_4\text{L9})(\mu_2\text{-H}_2\text{O})(\text{H}_2\text{O})_2](\text{ClO}_4)_2$	125
3.4.3.	Structures of $[\text{Ni}_2(\text{H}_4\text{L9})(\mu_2\text{-H}_2\text{O})(\text{EtOH})_2](\text{ClO}_4)_2$ and $[\text{Co}_2(\text{H}_4\text{L9})(\mu_2\text{-H}_2\text{O})(\text{H}_2\text{O})_2](\text{ClO}_4)_2$	127
3.4.4.	Synthesis of $[\text{Ni}_2(\text{H}_4\text{L9})(\text{H}_2\text{O})_3](\text{NO}_3)_2$ and $[\text{Ni}_2(\text{H}_4\text{L9})(\text{NO}_3)(\text{DMF})_2](\text{NO}_3)$	132
3.4.5.	Structure of $[\text{Ni}_2(\text{H}_4\text{L9})(\text{NO}_3)(\text{DMF})_2](\text{NO}_3)$	133
3.5.	Dinuclear complexes of L10	137
3.5.1.	Synthesis and characterisation of $[\text{Ni}_2(\text{L10})]$	137
3.5.2.	Synthesis and characterisation of $[\text{Mn}_2(\text{L10})(\text{EtOH})_2(\text{OAc})_2]$	138
3.6.	Dinuclear trimeric complexes of L9	139
3.6.1.	Synthesis of $[(\text{Mn}_2(\text{H}_2\text{L9})(\text{OAc})(\text{H}_2\text{O}))_3\text{CO}_3]$	139
3.6.2.	Structure of $[(\text{Mn}_2(\text{H}_2\text{L9}))_3(\text{OAc})_3(\text{H}_2\text{O})(\text{EtOH})_2\text{CO}_3]$	141
3.6.3.	Synthesis of $[(\text{Co}_2(\text{H}_2\text{L9})(\text{OAc})(\text{H}_2\text{O}))_3\text{CO}_3]$ and $[(\text{Fe}_2(\text{H}_2\text{L9})(\text{OAc})(\text{H}_2\text{O}))_3\text{CO}_3]$	144
3.7.	A trinuclear complex of L9	146
3.7.1.	Synthesis and structure of $[\text{Cu}_3(\text{L9})(\text{MeOH})_2]_n$	146
3.8.	Tetranuclear complexes of L9	152
3.8.1.	Synthesis of $[\text{Ni}_4(\text{H}_2\text{L9})(\mu_2\text{-OH})_2(\mu_2\text{-H}_2\text{O})_2(\text{EtOH})_4](\text{ClO}_4)_2$	152
3.8.2.	Structure of $[\text{Ni}_4(\text{H}_2\text{L9})(\mu_2\text{-OH})_2(\mu_2\text{-H}_2\text{O})_2(\text{EtOH})_4](\text{ClO}_4)_2$	152

3.8.3.	Synthesis and characterisation of $[\text{Cu}_4(\text{H}_2\text{L9})(\text{OH})_2(\text{H}_2\text{O})_2(\text{H}_2\text{O})(\text{MeOH})_3](\text{NO}_3)_2$	155
3.8.4.	Synthesis and characterisation of $[\text{Cu}_4(\text{L9})(\text{OAc})_2(\text{AcOH})_3(\text{DMF})]$	158
3.8.5.	Synthesis and characterisation of $[\text{Co}_4(\text{H}_2\text{L9})(\text{OH})_4(\text{MeOH})_4](\text{ClO}_4)_2$	159
3.9.	Tetranuclear complexes of L11	160
3.9.1.	Synthesis of $[\text{Mn}_4(\text{L11})(\text{MeOH})_4(\text{MeO})_2(\text{OAc})_2]\text{Cl}_2$ and $[\text{Mn}_4(\text{L11})(\text{MeOH})_6(\text{MeO})_2\text{Cl}_2](\text{ClO}_4)_2$	160
3.9.2.	Structures of $[\text{Mn}_4(\text{L11})(\text{MeOH})_6(\text{MeO})_2\text{Cl}_2](\text{ClO}_4)_2$ and $[\text{Mn}_4(\text{L11})(\text{MeOH})_4(\text{MeO})_2(\text{OAc})_2]\text{Cl}_2$	162
3.9.3.	Magnetic behaviour	168
3.9.4.	Preliminary electrochemistry studies	168
3.9.5.	Synthesis and characterisation of $[\text{Co}_4(\text{L11})(\text{MeOH})(\text{HOAc})_3(\text{MeO})_2(\text{OAc})_2]\text{Cl}_2$	173
3.9.6.	Synthesis and characterisation of $[\text{Ni}_4(\text{L11})(\text{MeOH})_5(\text{HOAc})_3(\text{OAc})_2]$	174
3.10.	Conclusion	175

Chapter four Binuclear and mononuclear complexes of 2,6-diformyl-4-*tert*-butylphenol

4.1.	Introduction	178
4.1.1.	Review on a few dioximato systems	178
4.1.2.	Binuclear and mononuclear complexes of 2,6-diformyl-4- <i>tert</i> -butylphenol	183
4.2.	Dinuclear complexes of 2,6-diformyl-4- <i>tert</i> -butylphenol	184
4.2.1.	Synthesis	184
4.2.2.	IR characterisation	186
4.2.3.	Structure of $[\text{Ni}_2(\text{C}_{12}\text{H}_{13}\text{O}_3)_2(\text{MeOH})_4](\text{ClO}_4)_2 \cdot 2\text{MeOH}$	187

4.2.4. Structure of $[\text{Co}_2(\text{C}_{12}\text{H}_{13}\text{O}_3)_2(\text{MeOH})_4](\text{ClO}_4)_2 \cdot 2\text{MeOH}$	192
4.2.5. Structure of $[\text{Mn}_2(\text{C}_{12}\text{H}_{13}\text{O}_3)_2(\text{MeOH})_4](\text{ClO}_4)_2 \cdot 2\text{MeOH}$	196
4.2.6. Structure of $[\text{Cu}_2(\text{C}_{12}\text{H}_{13}\text{O}_3)_2(\text{MeOH})_2(\text{ClO}_4)_2]$	198
4.2.7. Structure of $[\text{Ni}_2(\text{C}_{12}\text{H}_{13}\text{O}_3)_2(\text{MeOH})_2(\text{NO}_3)_2]$	202
4.2.8. Magnetic behaviour	204
4.3. Mononuclear complex of 2,6-diformyl-4- <i>tert</i> -butylphenol	212
4.3.1. Synthesis and IR characterisation of $\text{Cu}(\text{C}_{12}\text{H}_{13}\text{O}_3)_2$	212
4.3.2. Structure of $\text{Cu}(\text{C}_{12}\text{H}_{13}\text{O}_3)_2$	212
4.4. Conclusion	214

Chapter five Polynuclear clusters: a potential for high-spin molecules

5.1. Introduction	217
5.2. Homoheptanuclear complexes with Ni(II) and Co(II)	238
5.2.1. Synthesis of $[\text{Ni}_7(\text{C}_{12}\text{H}_{13}\text{O}_3)_6(\text{OH})_4(\text{MeO})_2](\text{ClO}_4)_2$ and $[\text{Co}_7(\text{C}_{12}\text{H}_{13}\text{O}_3)_6(\text{OH})_4(\text{MeO})_2](\text{ClO}_4)_2$	238
5.2.2. Structures of $[\text{Ni}_7(\text{C}_{12}\text{H}_{13}\text{O}_3)_6(\text{OH})_4(\text{MeO})_2](\text{ClO}_4)_2$ and $[\text{Co}_7(\text{C}_{12}\text{H}_{13}\text{O}_3)_6(\text{MeO})_6](\text{ClO}_4)_2$	240
5.2.3. FAB characterisation of $[\text{Ni}_7(\text{C}_{12}\text{H}_{13}\text{O}_3)_6(\text{OH})_4(\text{MeO})_2](\text{ClO}_4)_2$ and $[\text{Co}_7(\text{C}_{12}\text{H}_{13}\text{O}_3)_6(\text{OH})_4(\text{MeO})_2](\text{ClO}_4)_2$	245
5.2.4. Magnetic studies	250
5.2.4.1. $[\text{Ni}_7(\text{C}_{12}\text{H}_{13}\text{O}_3)_6(\text{OH})_4(\text{MeO})_2](\text{ClO}_4)_2$	250
5.2.4.2. $[\text{Co}_7(\text{C}_{12}\text{H}_{13}\text{O}_3)_6(\text{OH})_4(\text{MeO})_2](\text{ClO}_4)_2$	251
5.3. A trinuclear Mn(II) complex	252
5.3.1. Synthesis and characterisations (IR and FAB) of $[\text{Mn}_3(\text{C}_{23}\text{H}_{26}\text{O}_4)_2(\text{CH}_3\text{OH})_4(\text{H}_2\text{O})](\text{ClO}_4)_2$	252
5.3.2. Structure of $[\text{Mn}_3(\text{C}_{23}\text{H}_{26}\text{O}_4)_2(\text{CH}_3\text{OH})_4(\text{H}_2\text{O})](\text{ClO}_4)_2$	253
5.4. Conclusion	258

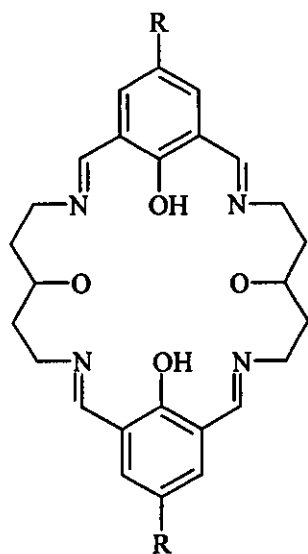
Chapter 6 Experimental

E.1.	General experimental conditions	261
E.1.1.	Solvents and reagents	261
E.1.2.	Physical measurements	262
E.2.	Chapter 2	263
E.2.1.	Organic preparations	263
E.2.1.1.	1,5-diaminopentan-3-ol dihydrochloride (DAHP.2HCl) (2.1)	263
E.2.1.2.	2,6-diformyl-4-methylphenol (DFMP) (2.2)	268
E.2.1.3.	2,6-diformyl-4- <i>tert</i> -butylphenol (DFTP) (2.3)	270
E.2.1.4.	2,6-diformyl-4-methoxyphenol (DFMOP) (2.4)	271
E.2.2.	Complex syntheses	272
E.2.2.1.	$[\text{Ni}_4(\text{L1})(\text{OH})](\text{ClO}_4)_3$ (2.5)	272
E.2.2.2.	$[\text{Ni}_4(\text{L1})(\text{OH})](\text{NO}_3)_3$ (2.6), $[\text{Ni}_4(\text{L1})(\text{OH})](\text{Cl})_3$ (2.7) and $[\text{Ni}_4(\text{L2})(\text{OH})](\text{ClO}_4)_3$ (2.8)	273
E.2.3.	Preparation of the sodium salts of DFMP, DFTP and DFMOP	277
E.2.3.1.	NaDFMP (2.9)	277
E.2.3.2.	NaDFTP (2.10) and NaDFMOP (2.11)	277
E.2.4.	Preparation of the sodium salts of the ligands L1, L2, L3, L4, L5, L6 and L7	278
E.2.4.1.	$\text{H}_2\text{Na}_2\text{L2}$ (2.12)	278
E.2.4.2.	$\text{H}_2\text{Na}_2\text{L1}$ (2.13) and $\text{H}_2\text{Na}_2\text{L3}$ (2.14)	278
E.2.4.3.	$\text{H}_2\text{Na}_2\text{L4}$ (2.15)	279
E.2.4.4.	$\text{H}_2\text{Na}_2\text{L5}$ (2.16)	279
E.2.5.	Complex syntheses	280
E.2.5.1.	$[\text{Ni}_4(\text{L2})(\text{OH})(\text{MeOH})_4(\text{H}_2\text{O})_4](\text{ClO}_4)_3$ (2.19)	280
E.2.5.2.	$[\text{Ni}_4(\text{L2})(\text{OH})(\text{NO}_3)_2(\text{MeOH})_4](\text{NO}_3)$ (2.20)	280
E.2.5.3.	$[\text{Ni}_4(\text{L2})(\text{OH})(\text{OAc})_2(\text{MeOH})_4](\text{OAc})$ (2.21)	281

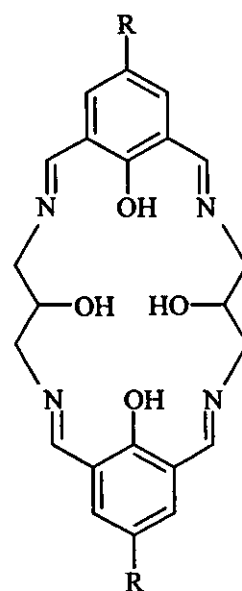
E.2.5.4.	$[\text{Mn}_4(\text{L}2)(\text{O})(\text{OAc})_4]$ (2.22)	281
E.2.5.5.	$[\text{Co}_4(\text{L}2)(\text{O})(\text{OAc})_4](\text{OAc})$ (2.23)	282
E.2.5.6.	$[\text{Cu}_4(\text{L}2)(\text{OH})(\text{NO}_3)_2](\text{NO}_3)$ (2.24)	282
E.3.	Chapter 3	283
E.3.1.	Organic preparations	283
E.3.1.1.	Synthesis of 2,2'-dihydroxy-5,5'-di- <i>tert</i> -butyl-3,3'-methanediyl dibenzyl alcohol (DHTMBA) (3.1)	283
E.3.1.2.	Synthesis of 2,2'-diallyloxy-5,5'-di- <i>tert</i> -butyl-3,3'-methanediyl dibenzyl alcohol (AOTMBA) (3.2)	284
E.3.1.3.	Synthesis of 2,2'-diallyloxy-5,5'-di- <i>tert</i> -butyl-3,3'-methanediyl dibenzaldehyde (AOTMB) (3.3)	285
E.3.1.4.	Synthesis of 2,2'-dihydroxy-5,5'-di- <i>tert</i> -butyl-3,3'-methanediyl dibenzaldehyde (DHTMB) (3.4)	286
E.3.2.	Complex syntheses	287
E.3.2.1.	$[\text{Mn}_2(\text{L}8)](\text{ClO}_4)_2$ (3.5)	287
E.3.2.2.	$[\text{Co}_2(\text{L}8)](\text{ClO}_4)_2$ (3.6)	288
E.3.2.3.	$[\text{Ni}_2(\text{H}_4\text{L}9)(\mu_2\text{-H}_2\text{O})(\text{EtOH})_2](\text{ClO}_4)_2$ (3.8)	289
E.3.2.4.	$[\text{Co}_2(\text{H}_4\text{L}9)(\mu_2\text{-H}_2\text{O})(\text{EtOH})_2](\text{ClO}_4)_2$ (3.10)	290
E.3.2.5.	$[\text{Ni}_2(\text{H}_4\text{L}9)(\mu_2\text{-H}_2\text{O})(\text{H}_2\text{O})_2](\text{NO}_3)_2$ (3.12) / $[\text{Ni}_2(\text{H}_4\text{L}9)(\text{NO}_3)(\text{DMF})_2](\text{NO}_3)_2$ (3.13)	291
E.3.2.6.	$[\text{Ni}_2(\text{L}10)]$ (3.14)	292
E.3.2.7.	$[\text{Mn}_2(\text{L}10)(\text{EtOH})_2(\text{OAc})_2]$ (3.15)	293
E.3.2.8.	$[\text{Mn}_6(\text{H}_2\text{L}9)_3(\text{H}_2\text{O})_6(\text{CO}_3)](\text{ClO}_4)_2$ (3.17)	293
E.3.2.9.	$[\text{Mn}_6(\text{H}_2\text{L}9)_3(\text{OAc})_3(\text{H}_2\text{O})_3(\text{CO}_3)](\text{ClO}_4)_2$ (3.18)	294
E.3.2.10.	$[\text{Co}_6(\text{H}_2\text{L}9)_3(\text{H}_2\text{O})_3(\text{OAc})_3(\text{CO}_3)]$ (3.19)	295

E.3.2.11.	$[\text{Fe}_6(\text{H}_2\text{L9})_3(\text{H}_2\text{O})_3(\text{OAc})_3(\text{CO}_3)]$ (3.20)	296
E.3.2.12.	$[\text{Cu}_4(\text{H}_2\text{L9})(\mu_2\text{-OH})_2(\mu_2\text{-H}_2\text{O})_2](\text{NO}_3)_2$ (3.21) / $[\text{Cu}_3(\text{L9})(\text{MeOH})_2]_n$ (3.22)	296
E.3.2.13.	$[\text{Ni}_4(\text{H}_2\text{L9})(\mu_2\text{-OH})_2(\mu_2\text{-H}_2\text{O})_2(\text{EtOH})_4]\text{-}$ $(\text{ClO}_4)_2$ (3.23)	297
E.3.2.14.	$[\text{Cu}_4(\text{H}_2\text{L9})(\mu_2\text{-OH})_2(\mu_2\text{-H}_2\text{O})_2](\text{NO}_3)_2$ (3.21)	298
E.3.2.15.	$[\text{Cu}_4(\text{L9})(\text{OAc})_2(\text{HOAc})_3(\text{DMF})]$ (3.24)	299
E.3.2.16.	$[\text{Co}_4(\text{H}_2\text{L9})(\mu_2\text{-OH})_4(\text{MeOH})_4](\text{ClO}_4)_2$ (3.25)	299
E.3.2.17.	$[\text{Mn}_4(\text{L11})(\text{MeOH})_4(\text{MeO})_2(\text{OAc})_2]\text{Cl}_2$ (3.26)	300
E.3.2.18.	$[\text{Mn}_4(\text{L11})(\text{MeOH})_6(\text{MeO})_2\text{Cl}_2](\text{ClO}_4)_2$ (3.27)	301
E.3.2.19.	$[\text{Co}_4(\text{L11})(\text{MeOH})(\text{MeO})_2(\text{HOAc})_3\text{-}$ $(\text{OAc})_2]\text{Cl}_2$ (3.28)	301
E.3.2.20.	$[\text{Ni}_4(\text{L11})(\text{MeOH})_5(\text{HOAc})_3(\text{OAc})_2]$ (3.29)	302
E.3.2.21.	$[\text{Cu}_4(\text{L11})(\text{OAc})_2(\text{HOAc})_3(\text{MeOH})]$ (3.30) / $[\text{Cu}_3(\text{L11})]_n$ (3.31)	303
E.4./E.5. Chapter 4 and chapter 5		303
E.4.1.	$[\text{Ni}_2(\text{C}_{12}\text{H}_{13}\text{O}_3)_2(\text{MeOH})_4](\text{ClO}_4)_2$ (4.1) / $[\text{Ni}_7(\text{C}_{12}\text{H}_{13}\text{O}_3)_6(\text{OH})_4(\text{MeO})_2](\text{ClO}_4)_2$ (5.1)	304
E.4.2.	$[\text{Co}_2(\text{C}_{12}\text{H}_{13}\text{O}_3)_2(\text{MeOH})_4](\text{ClO}_4)_2$ (4.2) / $[\text{Co}_7(\text{C}_{12}\text{H}_{13}\text{O}_3)_6(\text{OH})_4(\text{MeO})_2](\text{ClO}_4)_2$ (5.2)	305
E.4.3.	$[\text{Mn}_2(\text{C}_{12}\text{H}_{13}\text{O}_3)_2(\text{MeOH})_4](\text{ClO}_4)_2$ (4.3)	306
E.4.4.	$[\text{Cu}_2(\text{C}_{12}\text{H}_{13}\text{O}_3)_2(\text{MeOH})_2(\text{ClO}_4)_2]$ (4.4)	307
E.4.5.	$[\text{Ni}_2(\text{C}_{12}\text{H}_{13}\text{O}_3)_2(\text{MeOH})_2(\text{NO}_3)_2]$ (4.5)	307
E.4.6.	$[\text{Cu}_2(\text{C}_{12}\text{H}_{13}\text{O}_3)_2]$ (4.6)	308
E.5. Chapter 5		309
E.5.1.	$[\text{Mn}_3(\text{C}_{23}\text{H}_{26}\text{O}_4)(\text{MeOH})_4(\text{H}_2\text{O})](\text{ClO}_4)_2$ (5.3)	309

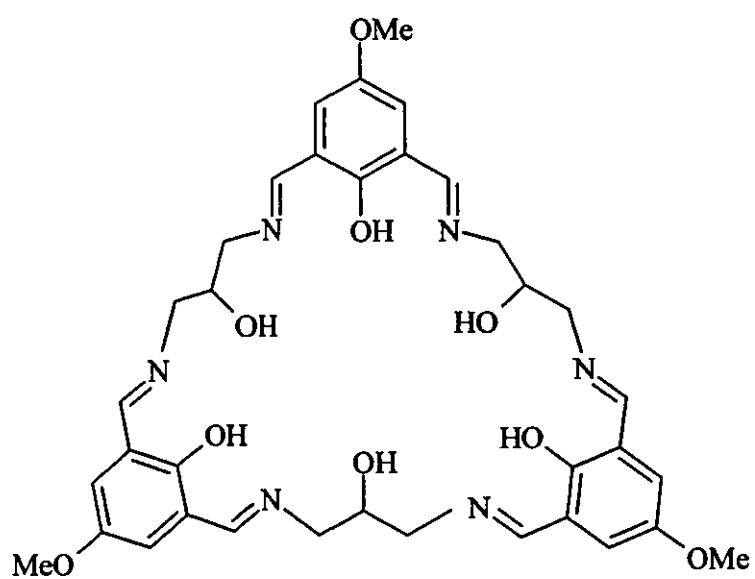
LIGANDS REFERRED TO IN THE THESIS



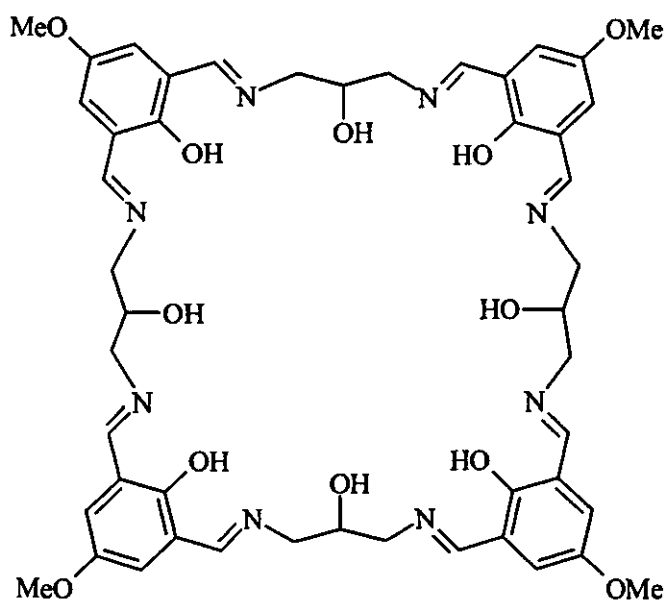
$R = C(CH_3)_3$ **H₄L1**
 $R = CH_3$ **H₄L2**
 $R = OCH_3$ **H₄L3**



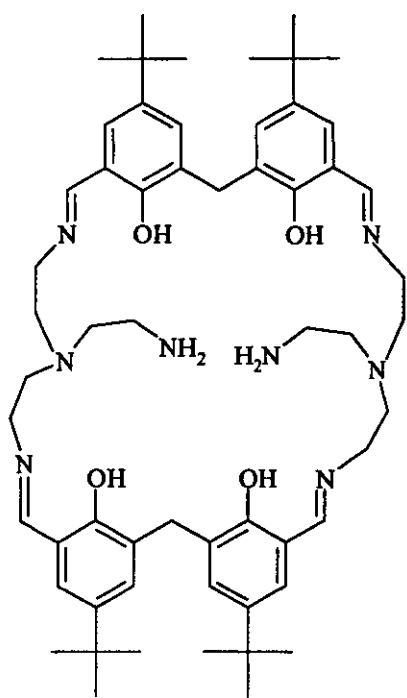
$R = CH_3$ **H₄L4**
 $R = OCH_3$ **H₄L5**



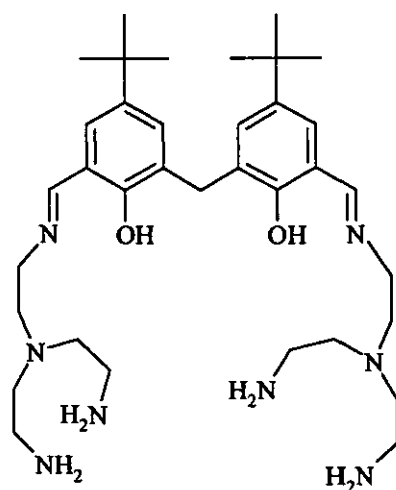
H₆L6



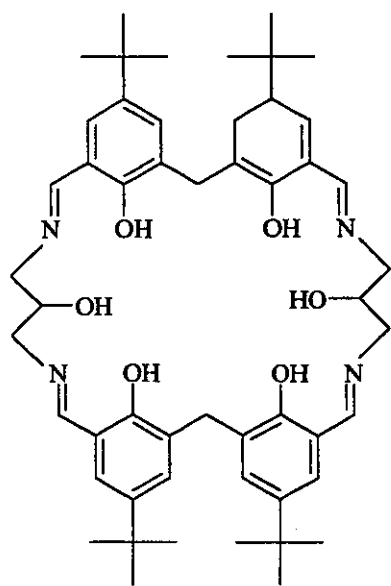
H₃L7



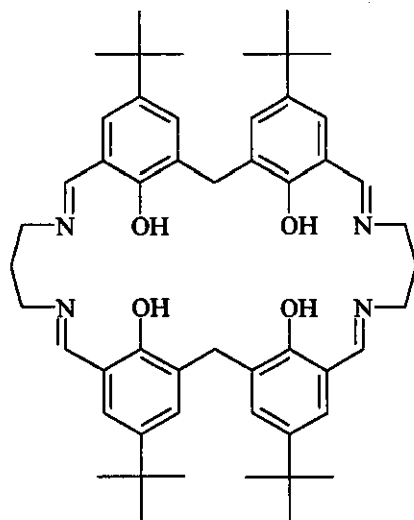
H₄L8



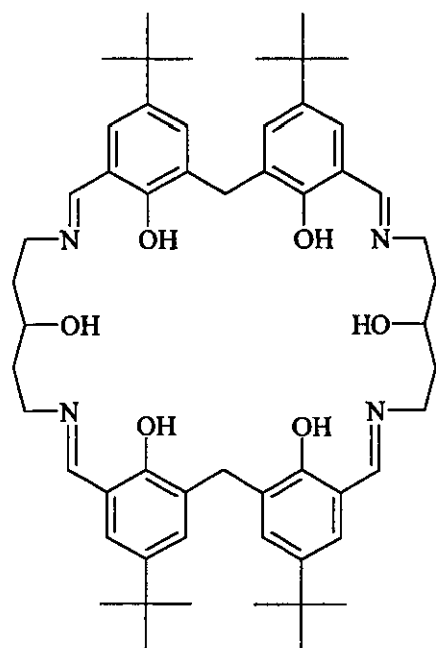
H₂L8a



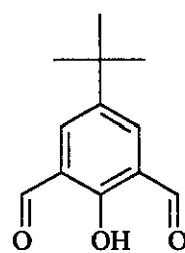
H₆L9



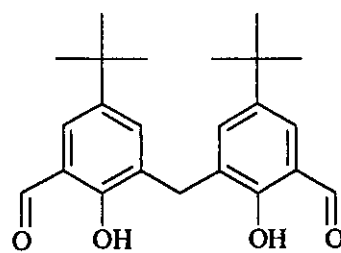
H₄L10



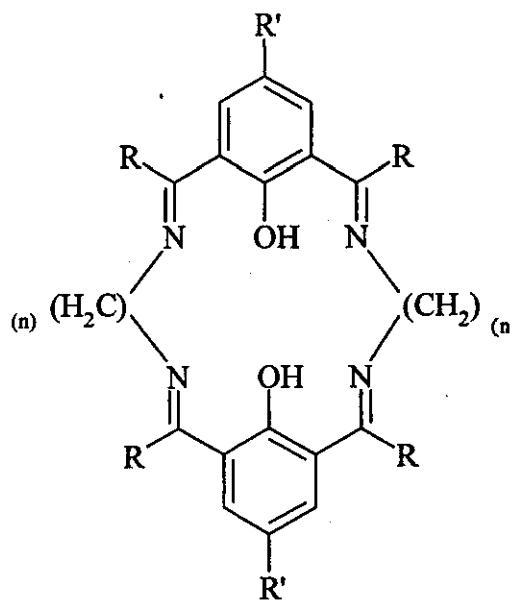
H₆L11



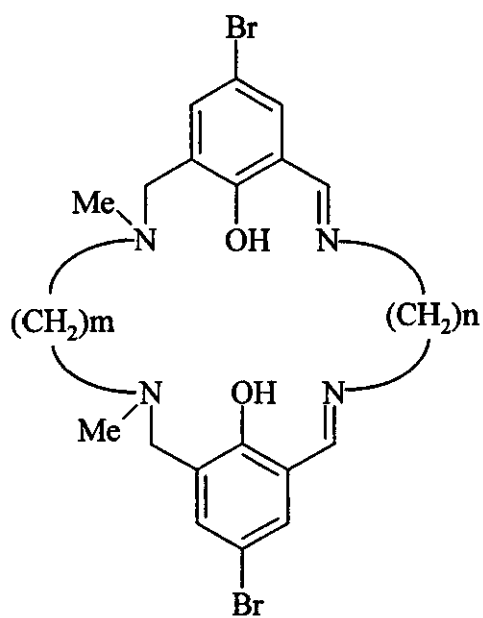
C₁₂H₁₄O₃



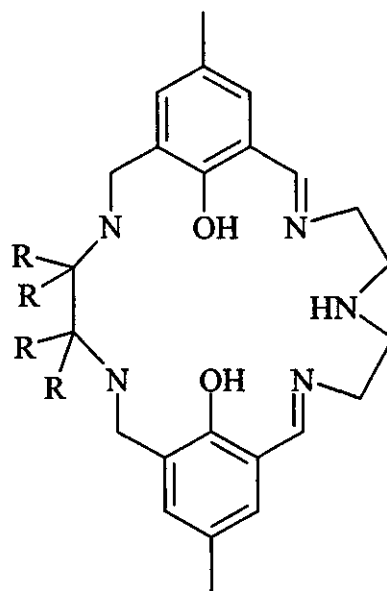
C₂₃H₂₆O₄



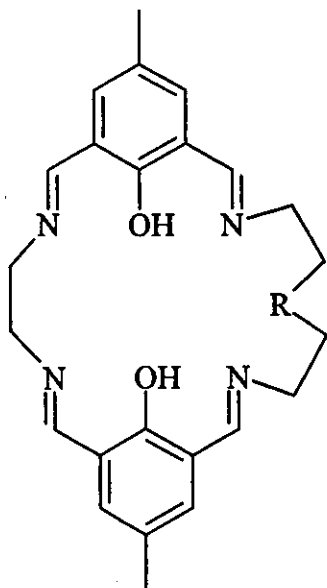
$n = 2$ R = H R' = Me **H₂L12**
 $n = 2$ R = Me R' = Me **H₂L13**
 $n = 3$ R = H R' = Me **H₂L14**
 $n = 3$ R = H R' = ^tBu **H₂L15**



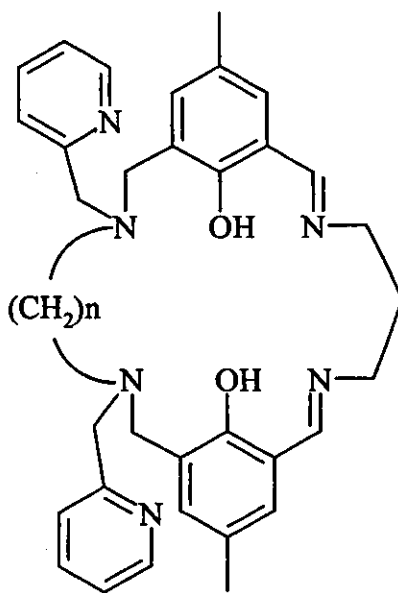
H₂L16



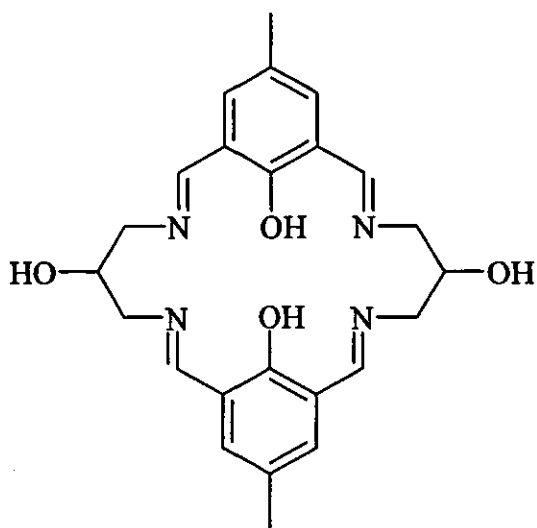
R = H **H₃L17**
R = Me **H₃L18**



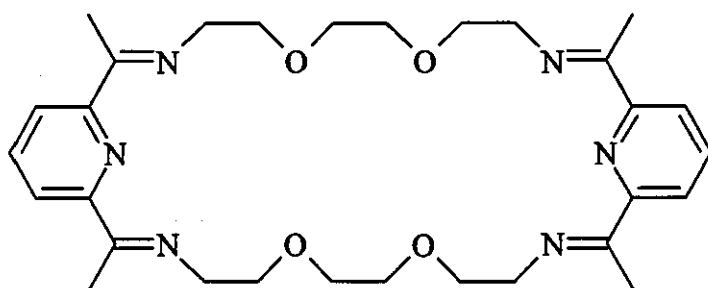
R = NH **H₃L19**
 R = S **H₂L20**



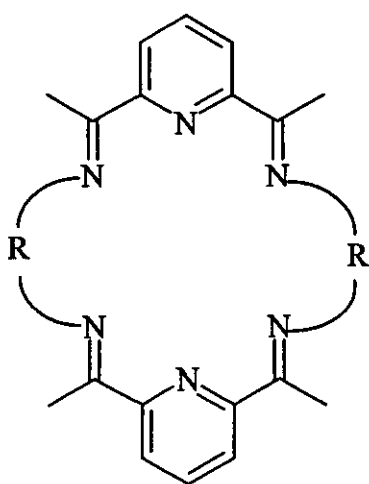
n = 2 **H₂L21**
 n = 3 **H₂L22**



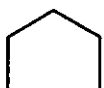
H₄L23



L24



L25



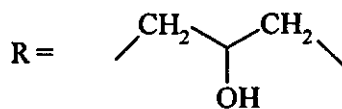
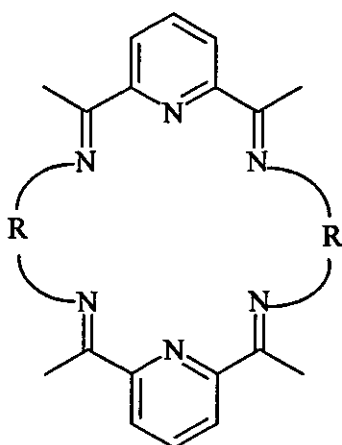
L26



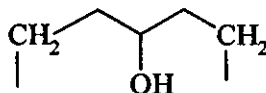
L27



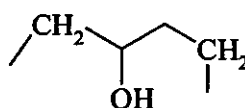
H₂L28



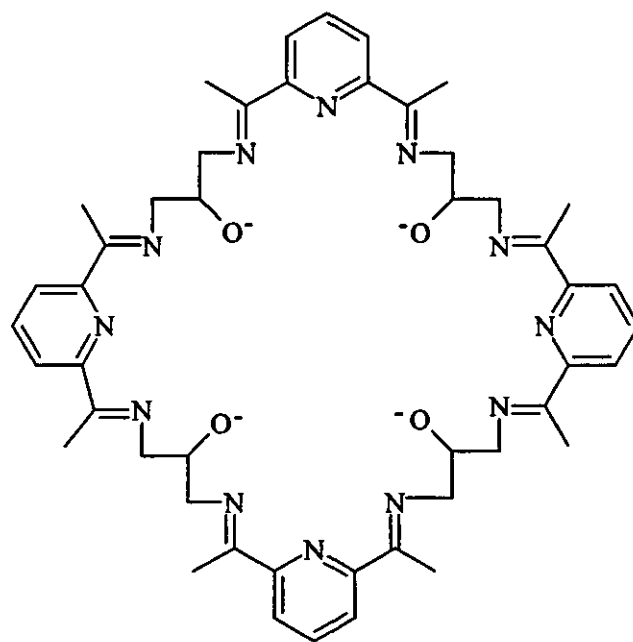
H₂L29



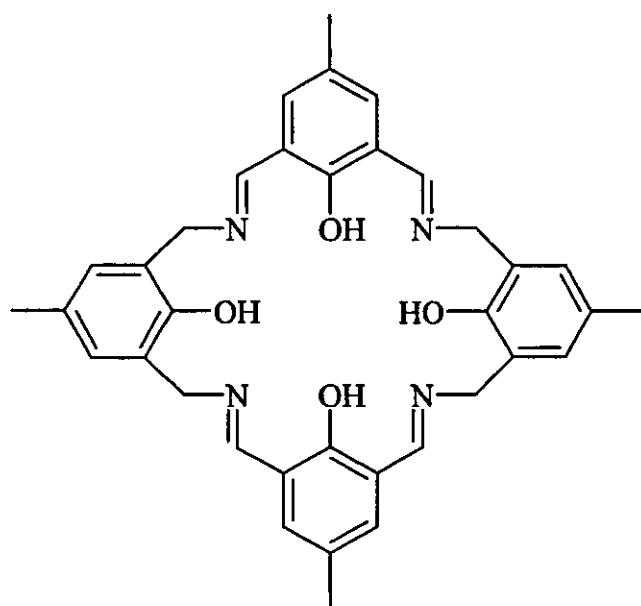
H₂L30



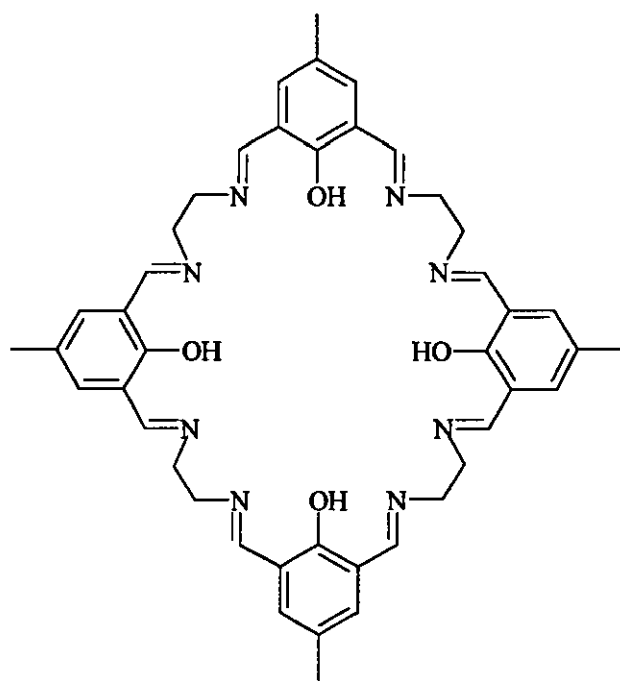
H₂L31 and H₂L32



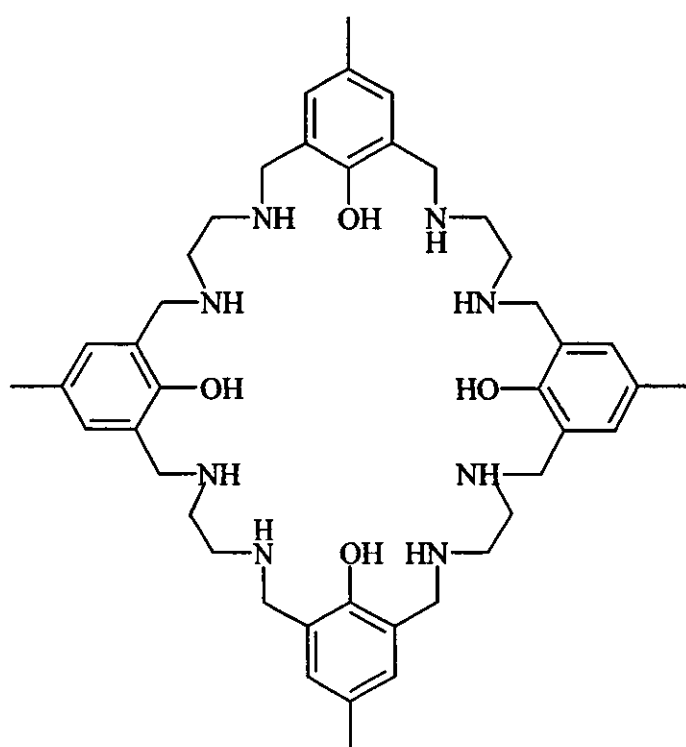
L33



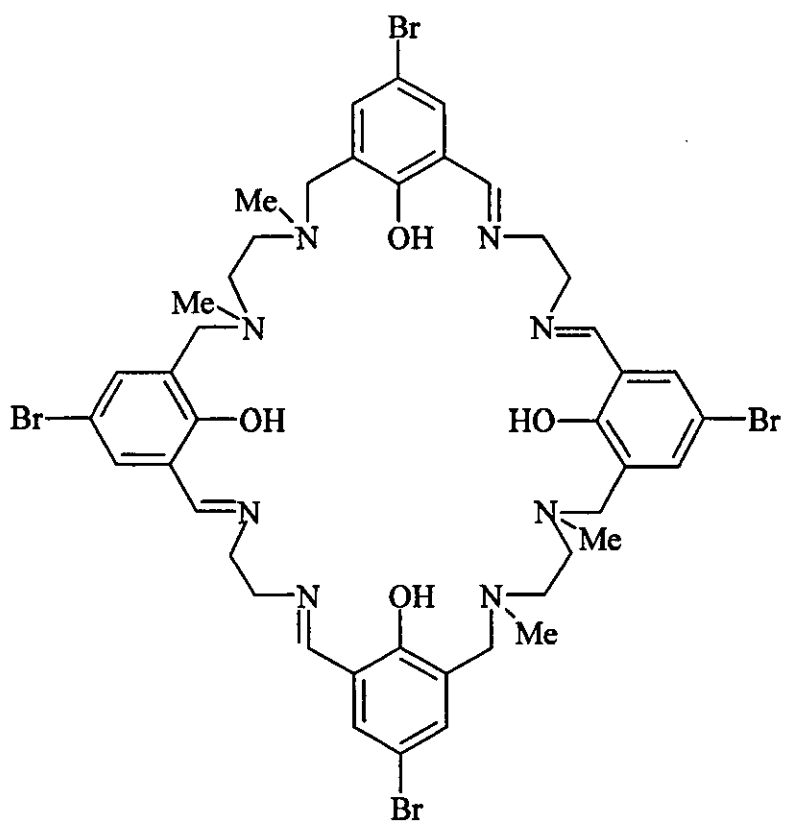
H₄L34



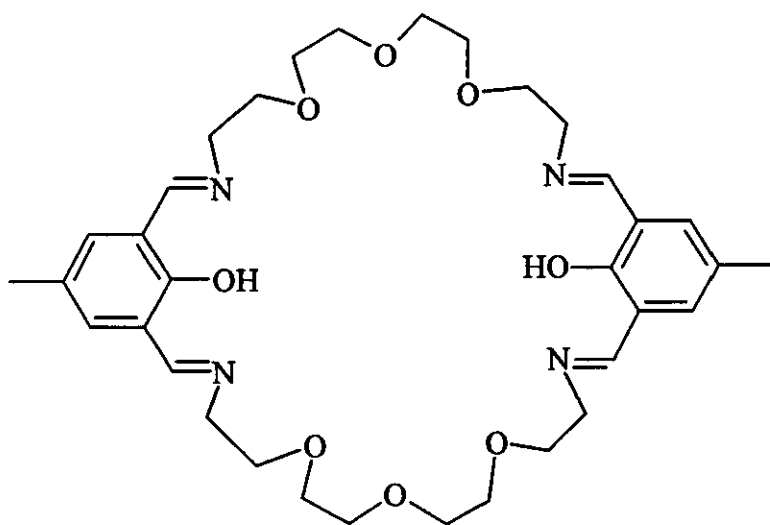
H₄L35



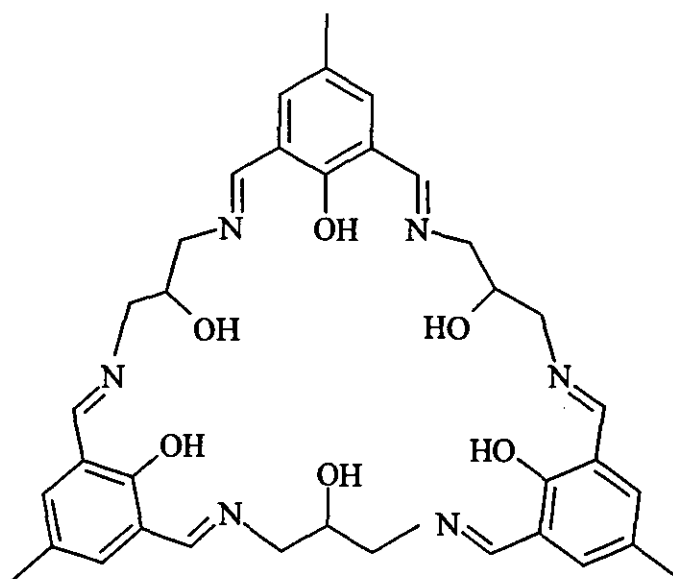
H₄L36



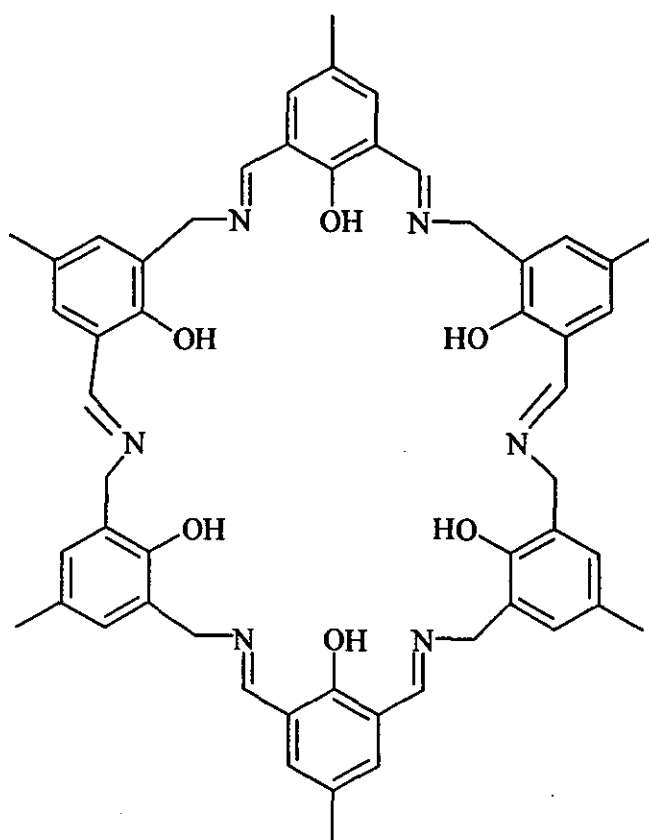
H₄L37



H₂L38



H₆L39



H₆L40

COLOUR PATTERN(S) OF THE ATOMS

Carbon: 

Hydrogen: 

Oxygen:    or 

Nitrogen:   or 

Sulfur: 

Chlorine:  or 

Bromine: 

Sodium: 

Manganese:  or 

Iron:   or 

Cobalt:  or 

Nickel:  or 

Copper:   or 

Zinc: 

Vanadium: 

Lead: 

ABBREVIATIONS AND SYMBOLS

DAHP	1,5-Diaminopentan-3-ol
DFTP	2,6-Diformyl-4- <i>tert</i> -butylphenol
DFMP	2,6-Diformyl-4-methylphenol
DFMOP	2,6-Diformyl-4-methoxyphenol
DHTMBA	2,2'-Dihydroxy-5,5'-di- <i>tert</i> -butyl-3,3'-methanedioldibenzyl- alcohol
OATMBA	2,2'-Diallyloxy-5,5'-di- <i>tert</i> -butyl-3,3'-methanedioldibenzyl- alcohol
OATMB	2,2'-Diallyloxy-5,5'-di- <i>tert</i> -butyl-3,3'-methanedioldibenzal- dehyde
DHTMB	2,2'-Dihydroxy-5,5'-di- <i>tert</i> -butyl-3,3'-methanedioldibenzal- dehyde
NaDFMP	Sodium 2,6-diformyl-4- <i>tert</i> -butylphenol
NaDFTP	Sodium 2,6-diformyl-4-methylphenol
NaDFMOP	Sodium 2,6-diformyl-4-methoxyphenol
HPyr	Pyrazole (pyrazolate)
Pyr	Pyrazolate
Py	Pyridine
DMF	N,N-dimethylformamide
d-DMF	Deuterated N,N-dimethylformamide
DMSO	Dimethylsulfoxide
Pet-ether	Petroleum ether
PTSA	Paratoluene sulfonic acid
Pd/C	Palladium on activated charcoal
OAc	Acetate
HOAc	Acetic acid
Ar.	Aryl ring
HPLC	High pressure liquid chromatography

TLC	Thin layer chromatography
Noba	3-Nitrobenzyl alcohol
IR	Infra-red
NMR	Nuclear magnetic resonance
EPR	Electron paramagnetic resonance
ESR	Electron spin resonance
MS	Mass spectrometry
FAB	Fast atom bombardment
EI	Electronic impact
E.A	Elemental analysis
LFSE	Ligand field stabilisation energy
TIP	Temperature independent magnetism
SCE	Standard calomel electrode
SMM	Single-molecule magnet
Anal.	Analysis (elemental)
Calc.	Calculated
Rel.	Relative
Lit.	Literature
fig.	figure(s)
min.	minute(s)
sec.	second(s)
conc.	Concentrated or concentration
ref.	reference
<i>ca.</i>	circa
h.	hour(s)
bp	boiling point
<i>p</i>	para
T	Temperature or tesla
T_b	Blocking temperature
T_c	Critical temperature

FT	Fourier transform
L	Litre(s)
mL	milliliter(s)
M	Molar
mM	millimolar
mm	millimeter(s)
V	Volt
Å	Angström unit 10^{-10} m
mMol	millimole
mol	mole
m/z	mass-to-charge ratio
Hz	Hertz, sec^{-1}
ppm	parts per million
$\Delta\nu$	wavelength separation
ν	mu, wavelength
δ	chemical shift in ppm
χ	molar magnetic susceptibility
μ_{eff}	effective magnetic moment
J	exchange coupling constant
K	Boltzmann constant
K	Kelvin
N	Avogadro number
B.M.	Bohr magneton
S	Spin quantum number
\hat{H}	Hamiltonian
°	degrees
°C	degrees centigrade
g	gram or g-factor or Landé factor
cm^{-1}	wave number
Rf	Retention factor
sh.	shoulder

<i>cf.</i>	confer
b.	broad
w.	weak
m.	medium
s.	strong
vs.	versus
equiv.	equivalent(s)

Chapter one

Introduction

Macrocyclic Chemistry: from binuclear systems to polynuclear systems

1.1. Introduction

Over the last 40 years, an ever-growing interest has developed in the investigation of polynuclear metal arrays based on macrocyclic ligands.¹⁻³ For a coordination chemist, a macrocyclic ligand is seen as a polydentate ligand containing donor atoms either incorporated in or, less commonly, attached to a cyclic skeleton, which is able to bind one or more metal ions within the central cavity. Such ligands consist of a minimum of three donor atoms in a ring of at least nine atoms. The coordination behaviour of macrocycles is no different in principle from that of open-chain polydentate ligands, although in practice the unusual and often unexpected properties of the systems justify them being given special treatment. One of the big advantages of this type of ligand is that a majority of them are kinetically and thermodynamically more stable than analogous compounds with non-cyclic ligands. This phenomenon is known as the *macrocyclic effect*.^{1,4} Moreover, the study of macrocyclic ligands and their complexes allows us to probe more subtle aspects of the reactivity of coordination compounds which would not be possible in less stable complexes with non-cyclic ligands.

Bioinorganic chemistry is just one area in many that received a considerable stimulus from the employment of macrocyclic ligands. As outlined by Guerriero,³ macrocyclic ligands have been synthesised to study the influence of different factors on the metal ion binding and selectivity (e.g. the nature of the donor atoms and their relative position, the number and size of the chelate ring formed, the flexibility and the shape of the coordinating moiety, their planar or tridimensional architecture). By varying these parameters, a control over different metal-metal interactions, redox and magnetic properties can be achieved for such systems. The transport and activation of small molecules has been another focus in this research.⁵

Bioinorganic aspects

The development of synthetic macrocyclic chemistry has resulted in an increased understanding of the functions and properties of naturally occurring biological macrocycles. Indeed, macrocyclic ligand complexes are involved in a number of fundamental biological processes such as photosynthesis (chlorophylls) (fig. 1.1), dioxygen transport in vertebrate and other respiratory systems (hemoglobin-myoglobin family) (fig. 1.2), ion transport across lipid barriers (nonactin) (fig. 1.3), electron transport (cytochromes) (fig. 1.2), rearrangements like vicinal 1,2 interchange (vitamin and coenzyme B₁₂) (fig. 1.4), just to mention a few.⁶⁻⁸

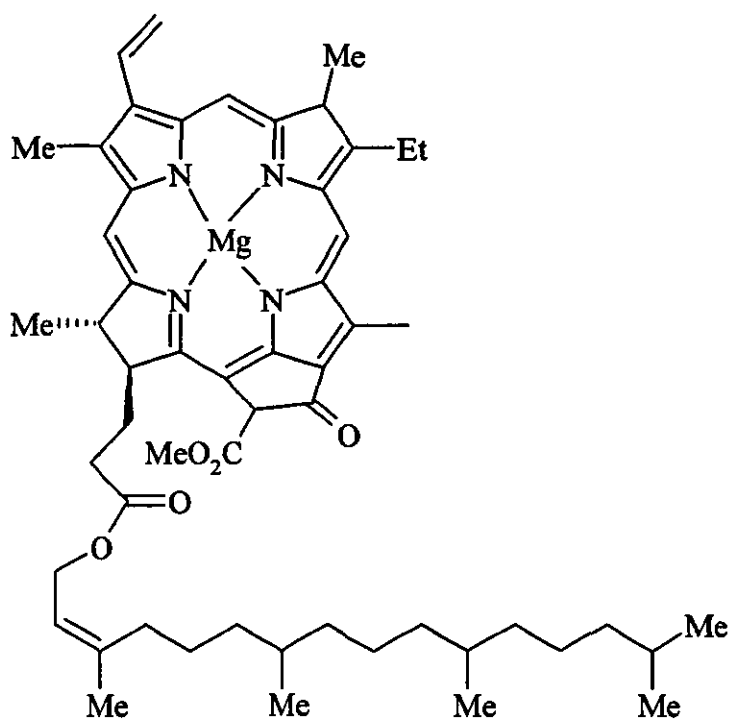
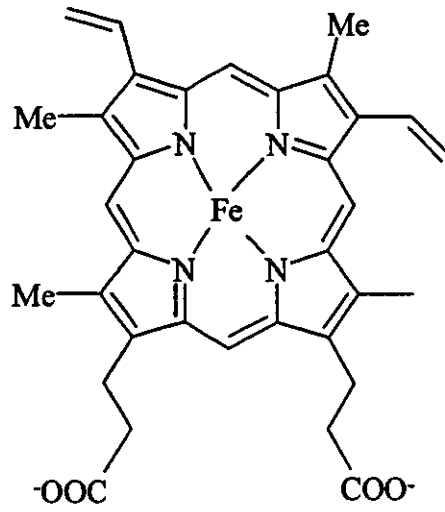


Fig. 1.1: Chlorophyll *a*



In the case of Hemoglobin

In the case of Cytochrome *c*

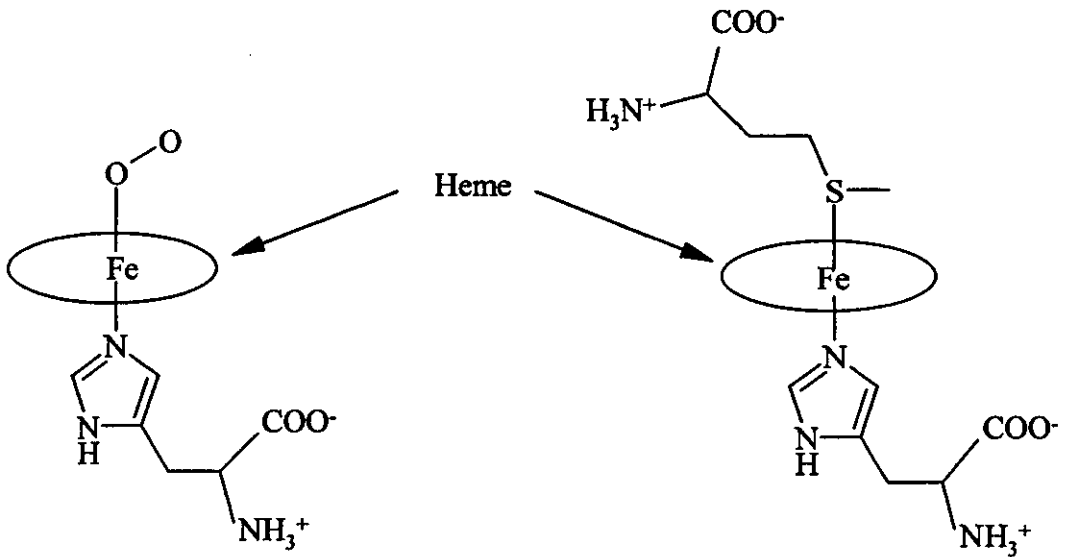


Fig. 1.2: Hemoglobin and Cytochrome *c*

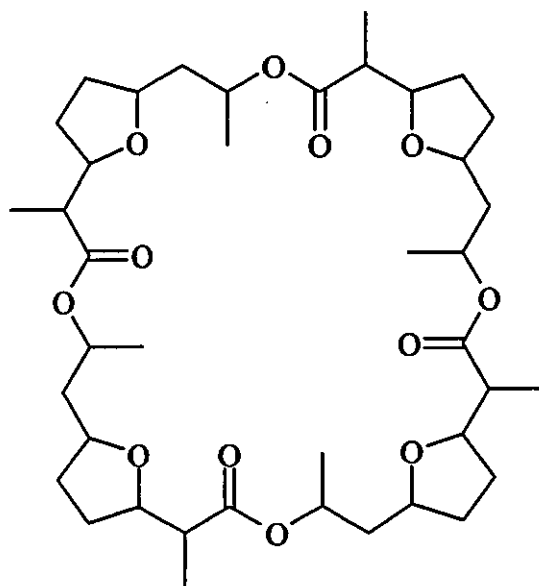


Fig. 1.3: Nonactin

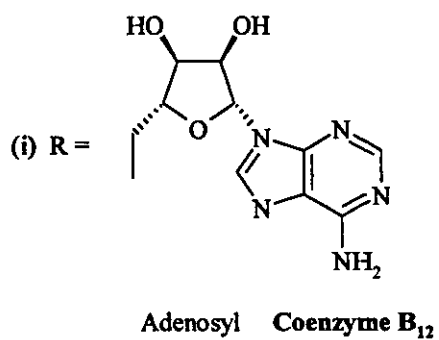
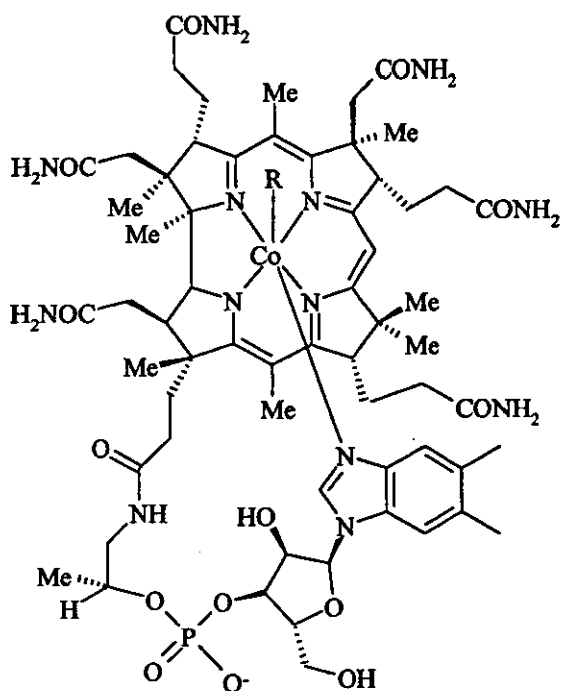


Fig. 1.4: Vitamin and Coenzyme B₁₂

Prior to 1960 the phthalocyanines (Fig. 1.5) were the only well-established category of synthetic cyclic ligands. Some of the complexes containing phthalocyanine behave as semiconductors,⁹ as catalysts for a variety of chemical transformations,^{10,11} as pigments and as model compounds in biochemical research.^{12,13}

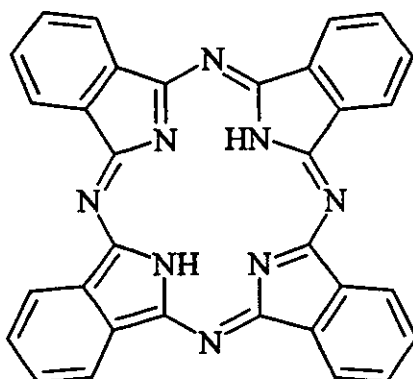


Fig. 1.5: Phthalocyanine

It is now well established that macrocyclic complexes can be used as models for metalloprotein and metalloenzyme active sites (macrocyclic and non-macrocyclic) or mimic their chemistry.^{2,14-17} Indeed, macrocyclic ligands can prove to be perfect candidates to mimic the unusual properties of certain enzymes by providing an unusual donor set for the metal and/or imposing a particular geometry or environment on the metal. Although the preparation of structural models that reproduce spectroscopic or other features of the enzymes has proved to be successful, devising functional models that replicate the biological and chemical reactivity has encountered more difficulties. However, negative results are often valuable in modifying the models and are, in any case, useful in expanding the underlying coordination chemistry. The huge development in this area of macrocyclic chemistry means that the main target is no longer to produce structural and/or functional models only but to introduce some selectivity.

A large variety of macrocyclic ligands and their complexes has been synthesised and characterised over the last few decades. Despite all the progress that has been made

in this field, there is always a challenge to synthesise new types of macrocycles showing different properties in their coordination chemistry influencing electronic, magnetic or redox features of those systems. So far, known systems include macrocycles providing mixed donor atoms, pendent functional groups macrocycles, interlocked macrocyclic ligands, binucleating/polynucleating macrocyclic complexes, cage macrocycles and bicyclic ligands. Discussing the different categories of synthetic macrocyclic ligands is beyond the scope of this introduction due to the extent of the subject. Therefore the following discussion will be focused on polynucleating Schiff-base macrocyclic complexes containing two to eight metal ions with the macrocycle contributing at least three nitrogen or oxygen donor atoms in the coordination sphere of each metal.

Synthesis

Concerning the synthesis of macrocyclic ligands, two main procedures can be outlined. The first is the traditional approach involving the “direct” synthesis in which the cyclisation occurs by a conventional organic route. However, the organic synthetic methods for medium (8-11) and large (≥ 12) rings, which are of interest for the coordination chemists, are not well-developed. As stressed by Constable,⁴ the dominant factor controlling the synthesis of large ring compounds is entropic. Indeed, the final cyclisation process can only occur if the two reactive functional groups are in the right conformation and close together but statistically it is more likely that those groups meet another reactive functionality of a second molecule. Consequently, the formation of polymeric species will be a substantial alternative pathway to the desired macrocyclisation reaction. A widely adopted method that overcomes those problems involves the use of “*high dilution*” reaction conditions. In this case, the more dilute the solution, the better the ratio of macrocycle to polymer because the probability of a molecule meeting a second molecule decreases with the concentration. This can be achieved by ensuring that the reactants are mixed at a very slow rate so that the concentrations of unreacted materials are always very small. Despite some scattered examples of Schiff-base derived macrocycles,¹⁸⁻²³ and

cryptands^{24,25} obtained by direct synthesis, template synthesis (described below) is generally favoured in order to get better yields or because the free ligand is not stable. Nevertheless, Schiff-base derived macrocycles have been recently synthesised directly with high yields of 80%²⁶ to > 90%.²⁷ Furthermore, fairly recently Nelson *et al.*²⁸ have obtained high yields (*ca.* 50 to 70%) of several symmetric hexa-Schiff-base cryptands.

Template synthesis involves an *in situ* approach wherein the presence of a metal ion in the cyclisation reaction markedly increases the yield of the cyclic product. The metal ion plays a significant role in directing the pathway of the reaction. This is known as the metal template effect and can be of two kinds. One is the *kinetic template effect* where the role of the metal is to control the stereochemistry in the intermediates such that the cyclisation is the favoured pathway. In the case of the second effect termed the *thermodynamic template effect*, the metal ion shifts the equilibria existing between the different species formed by coordinating to the desired cyclic product. Whilst these two types of template effect appear very clear in principle, the role of the metal is often more obscure and might involve aspects of both effects⁴ as well as combining less obvious roles such as masking or activating functional groups or influencing the reaction in other ways not related to the stereochemistry of the cyclisation itself.¹

The size of the cation used as a template has, in fact, proved to be of importance in directing the synthetic pathway in the Schiff-base systems. Indeed, the success of the synthesis and the geometry of the resulting product are dependent on the compatibility of the macrocyclic cavity with the metal cation radius combined with the strength of the interaction between the donor atoms and the metal ion.^{1,3} Because of the synthetic difficulty and instability of the macrocyclic Schiff-base ligands in the uncomplexed state (hydrolysis of the imine bond being the main reason²⁹), it seems, as observed by Nelson³⁰ *ca.* 20 years ago, that the synthesis of metal macrocyclic complexes is often restricted to those metal ions which are effective as templates.

However, Nelson *et al.*³⁰ found that these complexes are usually kinetically labile and that the complexed template ion can be exchanged in many cases with other metal ions present in solution. This observation led to another process to synthesise the desired Schiff-base macrocyclic complexes known as transmetallation. This method proved to be an effective route to complexes of metal ions, which were not effective if used in the direct template route. For the larger metal binding sites in polynuclear Schiff-base macrocycles, it has been generally found that the transition metals cations are ineffective as templates. In those cases the use of alkaline earth, lanthanide and main group metal ions has enabled the formation of the corresponding transition metal complexes through transmetallation.^{3,31-35} This is mainly due to the kinetic lability of these metal ions, which form weaker bonds with the ligand donor set and are therefore readily exchanged. Furthermore, the use of transmetallation sometimes yielded new types of macrocyclic ligands arising from ring expansions or contractions.^{3,30-34} This remarkable aspect is dependent on the demands and the size of the transmetalling ion.

1.2. Binucleating Schiff-base macrocyclic systems

1.2.1. Phenolic head-units

Binucleating macrocyclic compounds have been extensively studied over the last 30 years since these structural units are thought to be involved in a variety of biochemical¹⁴ and industrial processes. In 1970 Robson and Pilkington reported the first synthesis of a compartmental macrocyclic system based upon the metal template Schiff-base condensation of 2,6-diformyl-4-methylphenol with 1,3-diaminopropane in the presence of a range of first row transition metal ions (Mn^{2+} , Fe^{2+} , Co^{2+} , Ni^{2+} , Cu^{2+} and Zn^{2+}).^{36,37} These compounds were initially used in attempts to construct synthetic systems capable of binding and possibly activating molecular nitrogen. Binucleating ligands and their complexes have developed into a vast area of research with the activation of small molecules still being the central theme,⁵ although the

activation of dioxygen has taken the focal point. The systems first described by Robson *et al.* achieve the aim of bringing two metal centres into close proximity (less than 4 Å), which has important implications for metal-metal interactions and magnetic exchange (observed in a number of natural systems) and a potential for binuclear metal reactivity. Since then a large variety of binucleating ligands including macrocyclic compounds of different kinds has been synthesised. Many of them are Schiff-base derived from the condensation of dicarbonyl species with diamines.

Since its first use by Robson *et al.* many derivatives of 2,6-diformyl-4-methylphenol (fig. 1.6) were synthesised and extensively studied in the formation of binuclear complexes. Variations of X have included H,^{15,38} CH₃,³⁹ C(CH₃)₃,⁴⁰ Cl,^{41,42} CF₃,^{43,44} NO₂,⁴⁵ F,³ Br,^{3,46,47} and OH.⁴⁸

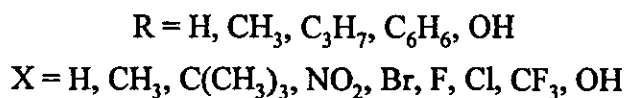
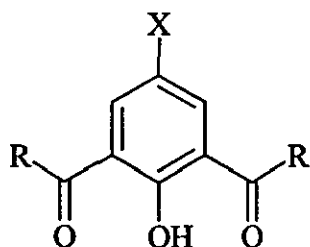


Fig. 1.6: Phenol head unit

The diamines units can be simple alkane chains but they can also contain alcohol, amine or other functional groups.

Since the first compartmental ligands described by Robson (examples given in fig. 1.7), these “Robson-type” macrocycles have been extensively studied, in some cases with variations on the nature of the condensed diamines and many complexes have been fully characterised.

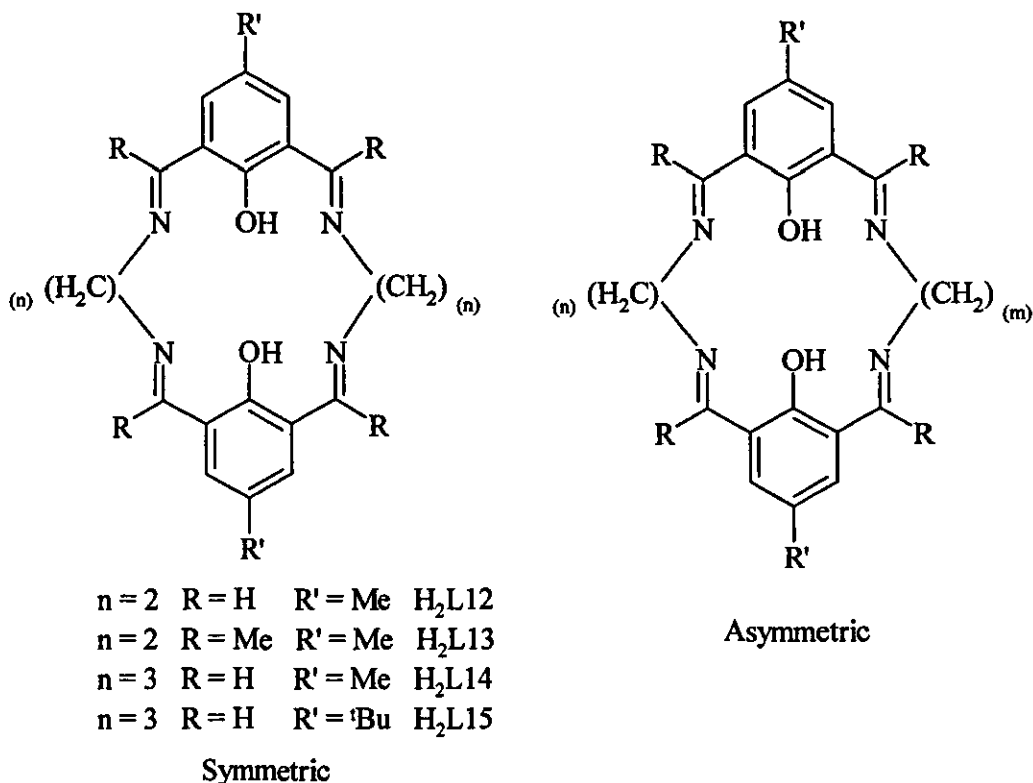


Fig. 1.7: Examples of “Robson-type” macrocycles

In 1970, the crystal structure of a dicopper(II) complex of the symmetric macrocyclic ligand L14 was determined by Robson³⁷ ($[L14Cu_2Cl_2] \cdot 6H_2O$) and showed a square-pyramidal environment for both metal ions with the macrocyclic ligand adopting a roughly planar geometry. Given the evidence provided by the electronic spectra (observed d-d transitions), the geometry around the metals (Cu(II), Co(II), Fe(II) and Ni(II)) in the other dinuclear complexes ($[L14Co_2Cl_2]$, $[L14Fe_2Cl_2]$, $[L14Ni_2Cl_2]$, $[L14Cu_2(ClO_4)_2]$ and $[L14Cu_2(SO_4)]$) was also determined to be square pyramidal. Later, in 1976, Hoskins *et al.*⁴⁹ reported the structure of $[L14Cu_2Cl_2]$.

According to Robson,³⁷ this geometry is probably due to the fact that the cavities are slightly too small to allow incorporation of the cation within the N₂O₂ plane at normal metal-nitrogen and metal-oxygen bond distances. In this case the macrocycle seems to impose the geometry around metal ions that are unsuited to five-coordination. Some other examples of very similar dinuclear copper(II) complexes of L14 were isolated by Thompson *et al.*^{44,50} (fig. 1.8) along with a dinuclear Cu(I)/Cu(II) complex of L14 synthesised by Gagné,⁵¹ just to mention a few.

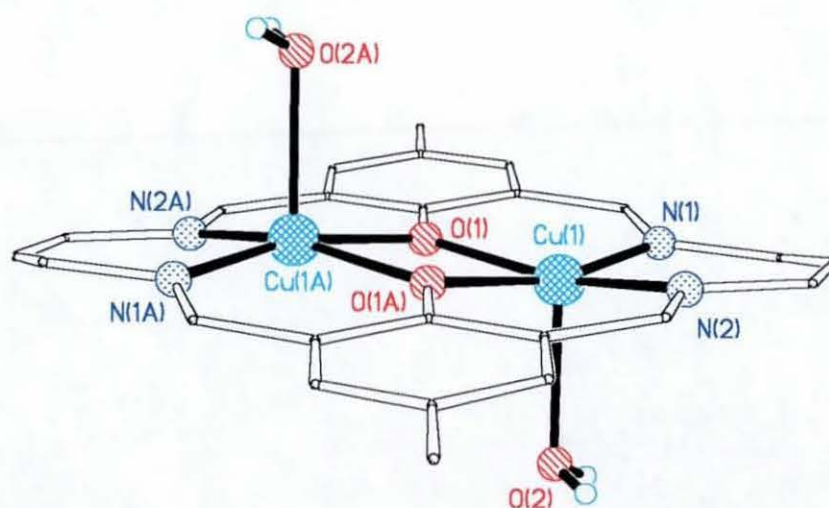


Fig. 1.8: Structure⁵² of the cation $[(L14)Cu_2(H_2O)_2]^{2+}$ (in contrast to Robson, chloride anions were replaced by water molecules)

Crystallographic confirmation of the square pyramidal geometry of the dinuclear cobalt(II) complex has been given by Hoskins and Williams⁵³ while that of the dinuclear manganese(II) complex was reported by Hendrickson *et al.*⁵⁴ (fig. 1.9).

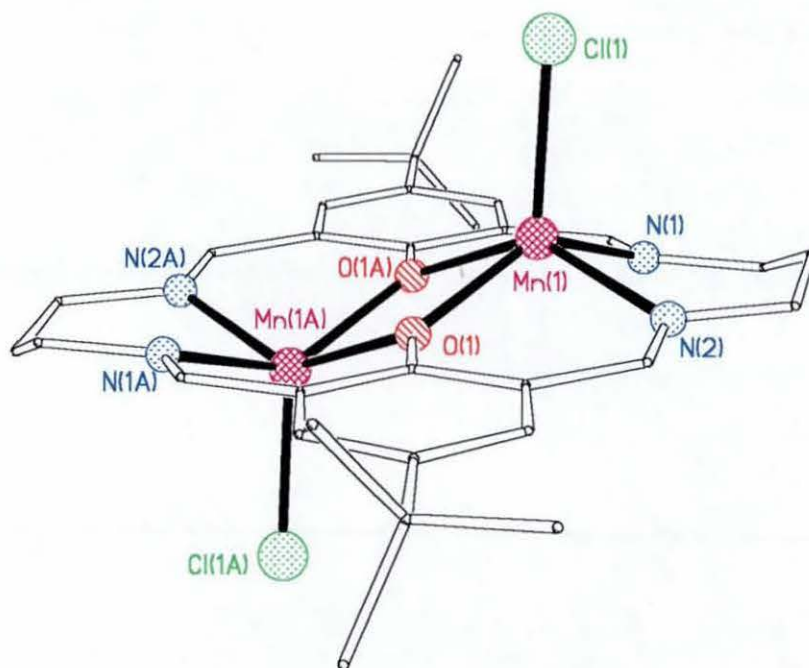


Fig. 1.9: Structure⁵² of $[L14Mn_2Cl_2]$

The geometry around the zinc atoms in a dinuclear complex of L14 ($[Zn_2(L14)(N_3)_2]$) was confirmed to be square pyramidal in the case of five-coordination by Fenton *et al.*⁵⁵ The study of complexes of L14 performed by Lambert and Hendrickson⁵⁶ has shown an antiferromagnetic exchange interaction between the two metal ions, with a magnitude that markedly decreases across the series from Cu(II) to Fe(II). Mn(II) is found to exhibit a ferromagnetic exchange interaction. According to Hendrickson *et al.*⁵⁶ the reduction of the net antiferromagnetic exchange interaction is partially a consequence of the increased displacement from the macrocyclic ligand plane of the metal ions across the series from Cu(II) to Mn(II) (the $d_{x^2-y^2}$ -(s,p)- $d_{x^2-y^2}$ overlap is reduced). Moreover, across the series there is an addition of one more unpaired d-electron per metal until Mn(II) is reached, which opens the pathway for ferromagnetic interactions. In the case of Mn(II) the appreciable metal ion displacement coupled with a large number of ferromagnetic exchange pathways leads to a net ferromagnetic interaction.

There are also reports on octahedral dinuclear complexes of L14 with Ni(II),^{39,57} Fe(II),⁵⁷ Co(II)/Co(III),⁵⁸ Co(II)⁵⁷ which shows that the metal ion can be constrained to lie in the N₂O₂ plane of the ligand. This is not the case for the Mn(II) ion in the mixed valence (Mn(II)/Mn(III)) complex L15Mn₂Cl₂Br,⁵⁴ where Mn(II), being significantly bigger than Mn(III), sits above the distorted N₂O₂ plane (fig. 1.10).

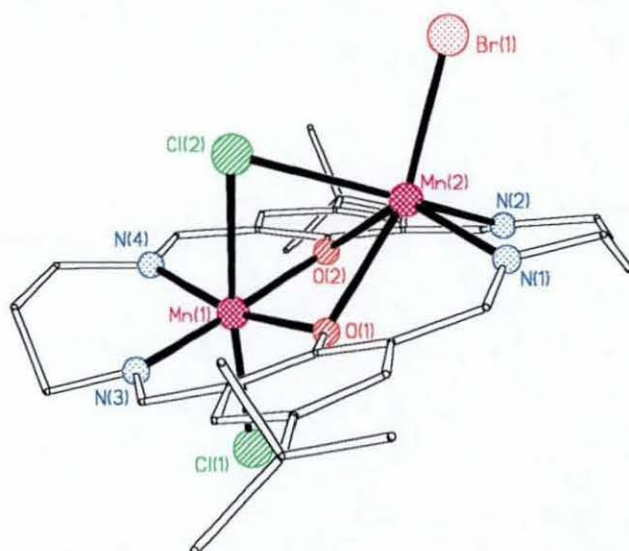
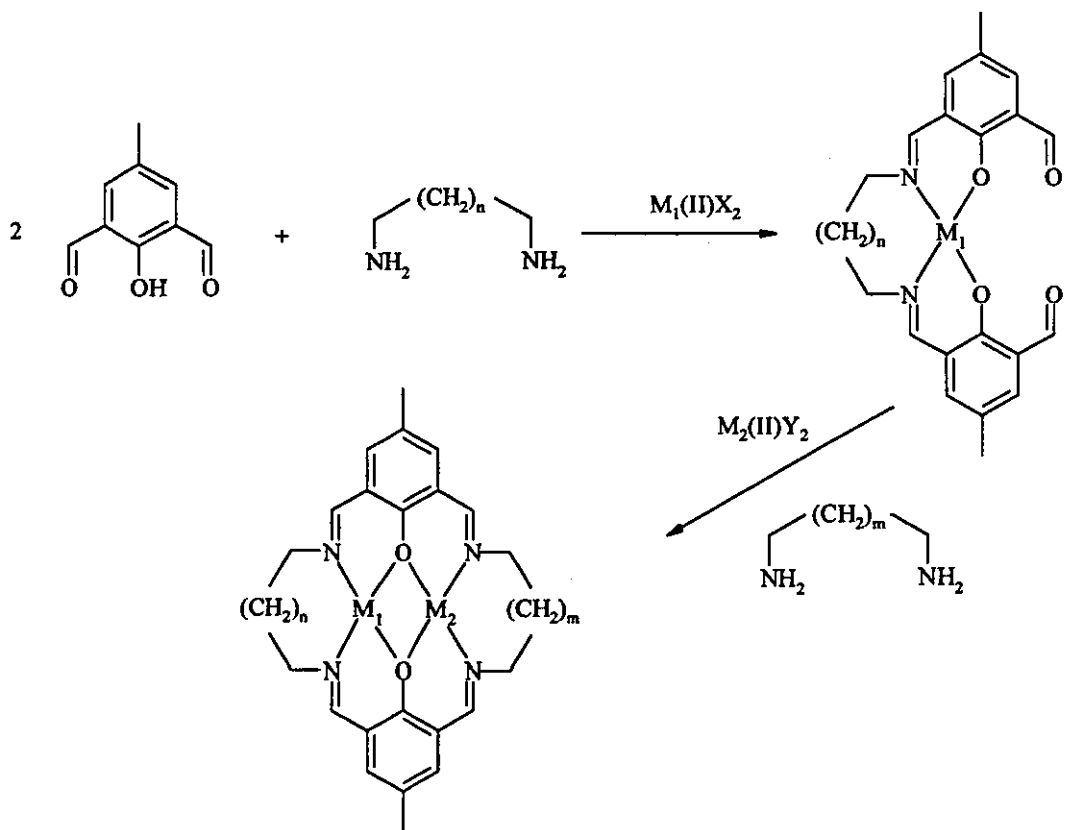


Fig. 1.10: Structure⁵² of [L15Mn₂Cl₂Br]

In the octahedral dinuclear Mn(II) complex of L14 reported by Okawa *et al.*⁵⁹ both Mn(II) ions deviate from the basal N₂O₂ plane by 0.75 Å due to the mismatch of the cavity size and the ionic radius of the Mn(II) ions. However, Fenton *et al.*⁶⁰ observed that it is possible for Mn(II) to lie in the N₂O₂ plane by enlarging the carbon side chain to four carbon atoms instead of three. Each atom is in a distorted octahedral environment with two acetate molecules bridging the metal centre above and below the dinuclear skeleton. In the case of the dinuclear Ni(II) complex with the ligand L13 reported by Schröder *et al.*,³⁹ reducing the ring size increased the ligand field affording a square-planar Ni(II) complex. Therefore the stereochemistry can potentially be controlled by the ring size. More recently, Gou *et al.*^{41,61} reported octahedral zinc(II) complexes of L14 acting as platforms in molecular ladders.

H₂L14 was synthesised by Schröder *et al.*,³⁹ as a free ligand to complex inert metal ions such as those of the platinum group which are ineffective in template reactions. The complexation with Pd(II) and Pt(II) proved successful and afforded dinuclear complexes in high yields. The structure of the dinuclear Pd(II) showed both metal centres in a square-planar environment

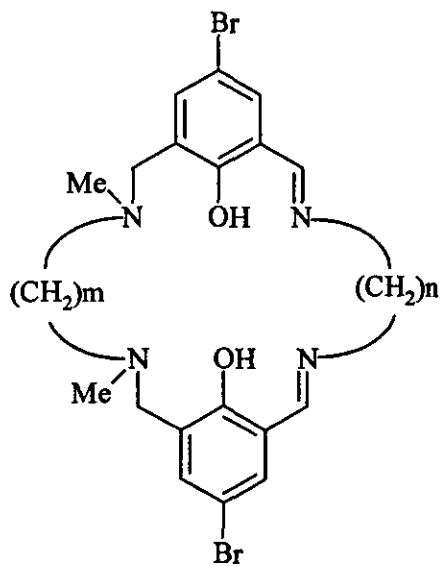
Although heteronuclear complexes of dinucleating “Robson-type” macrocycles have been known for many years,⁶²⁻⁶⁵ the study of this type of complexes has recently become important due to original physicochemical properties and functions arising from a pair of dissimilar metal ions in close proximity.⁶⁵⁻⁶⁷ In order to provide discrete heteronuclear core complexes, many efforts have been devoted to the design of unsymmetric compartmental ligands where the two metal-binding sites are not equivalent with respect to the cavity size, coordination mode or the nature of the donor atoms. Most commonly these complexes are synthesised, using ligands with dissimilar binding sites in either the final macrocyclic product or in a key non-cyclic intermediate in a step-wise synthesis (fig. 1.11).



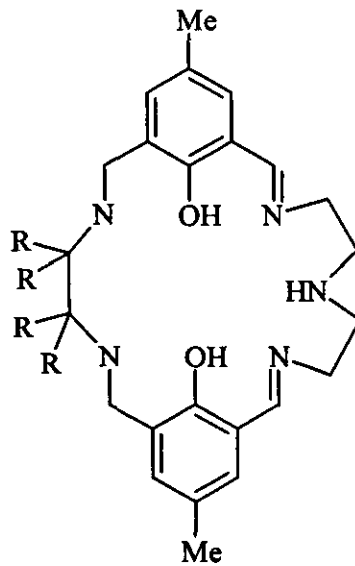
X and Y = counteranions (X and Y can be identical)
 M_1 = metal 1
 M_2 = metal 2

Fig. 1.11: An example of step-wise synthesis leading to heteronuclear macrocyclic complexes

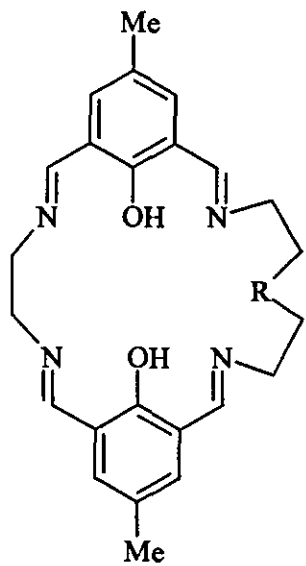
Some examples of asymmetric macrocycles^{3,17,47,68} are given in fig. 1.12.



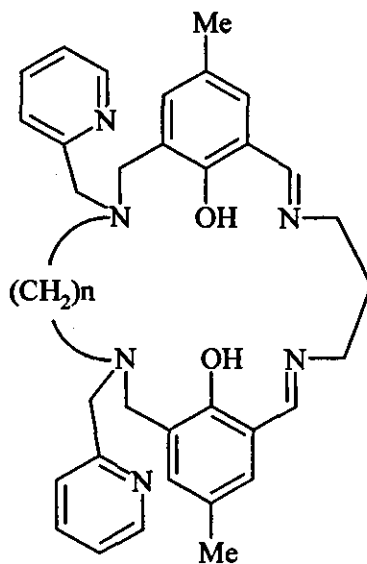
H₂L16 (ref. 47)



R = H H₃L17 (ref. 68)
R = Me H₃L18 (ref. 68)



R = NH H₃L19 (ref. 17)
R = S H₂L20 (ref. 17)



n = 2 H₂L21 (ref. 17)
n = 3 H₂L22 (ref. 17)

Fig. 1.12: Examples of asymmetric macrocycles

The condensation of the phenol head-unit with a 1,3-diaminopropan-2-ol side arm yielded binuclear [2+2] complexes of H₂L23 with Cu(II),⁶⁹⁻⁷¹ Ni(II)⁷² (fig. 1.13), Mn(II)⁷² (fig. 1.14) and Pb(II) (fig. 1.15).²¹

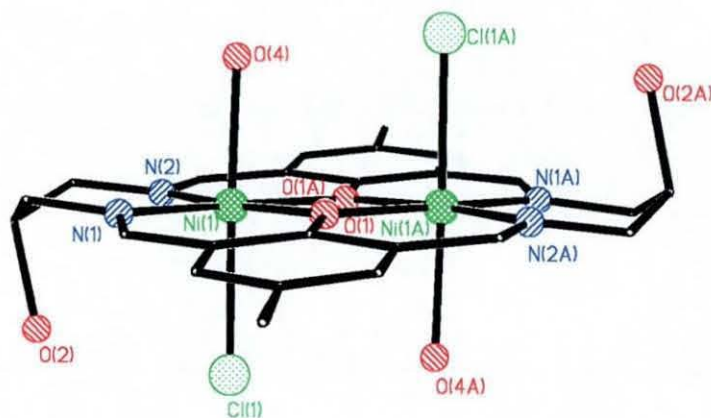


Fig. 1.13: Structure⁵² of [Ni₂(H₂L23)(H₂O)₂(Cl)₂]

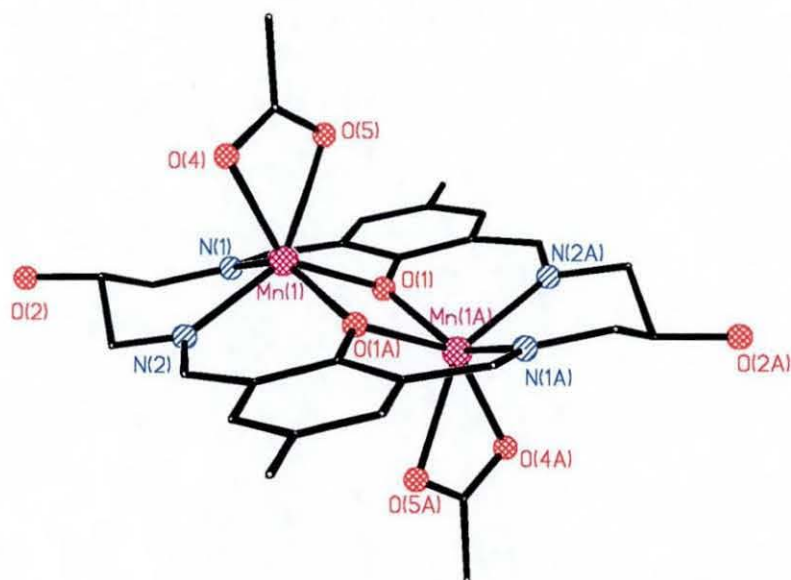


Fig. 1.14: Structure⁵² of [Mn₂(H₂L23)(OAc)₂]

Essentially, these complexes are structurally very similar to the complexes of the simple Robson-type ligands discussed previously. In the case of smaller ions like copper, nickel and manganese, the pendant alcohol groups on the side chains remain protonated and pointing outside the cavity of the macrocycle. Therefore they are not involved in the coordination. However, in the case of bigger cations such as Pb(II) (fig. 1.15) the alcohol groups are weakly interacting with the metal in the apical position.

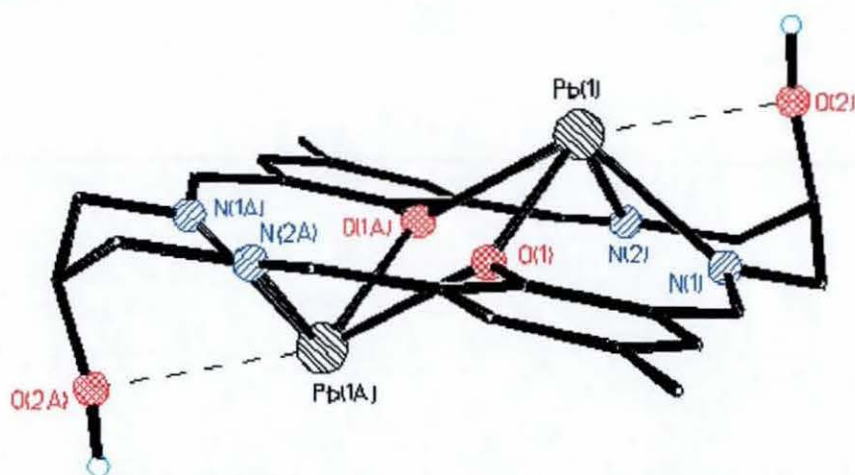
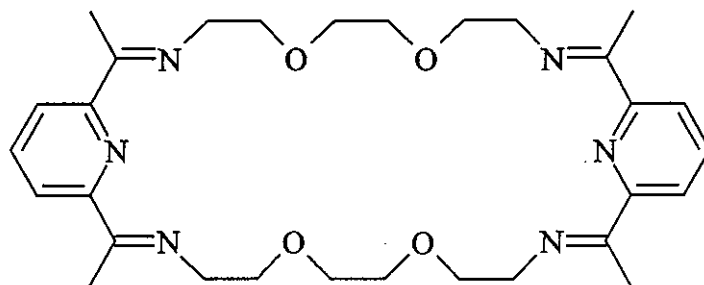


Fig. 1.15: Structure⁵² of the cation $[\text{Pb}_2(\text{H}_2\text{L23})]^{2+}$

1.2.2. Heterocyclic head-units

Since Nelson *et al.*⁷³ first communicated the use of 2,6-diacetylpyridine in the formation of [2+2] macrocyclic complexes using Pb^{2+} (fig. 1.16), 2,6-diacetylpyridine has been quite commonly used, in template [2+2] condensation affording a range of binucleating macrocycles using other template agents, such as Ag^+ , Sr^{2+} and Ba^{2+} .⁷⁴⁻⁷⁹ Some examples of those are gathered in fig. 1.17. Subsequent studies by Nelson⁸⁰ showed that the transmetallation route could be used to synthesise the otherwise inaccessible dicopper(II) species. Generally, the Cu(II) centres are coordinated to two imine donors and one pyridyl donor and two exogenous donors. It has been

shown that groups or molecules such as OH^- , N_3^- , imidazolate and pyrazolate can act as bridging units between the metal centres. These observations mean that these macrocycles can also be used as hosts for exogenous substrates of various sizes.



L24

Fig. 1.16: Nelson-type binucleating macrocycle

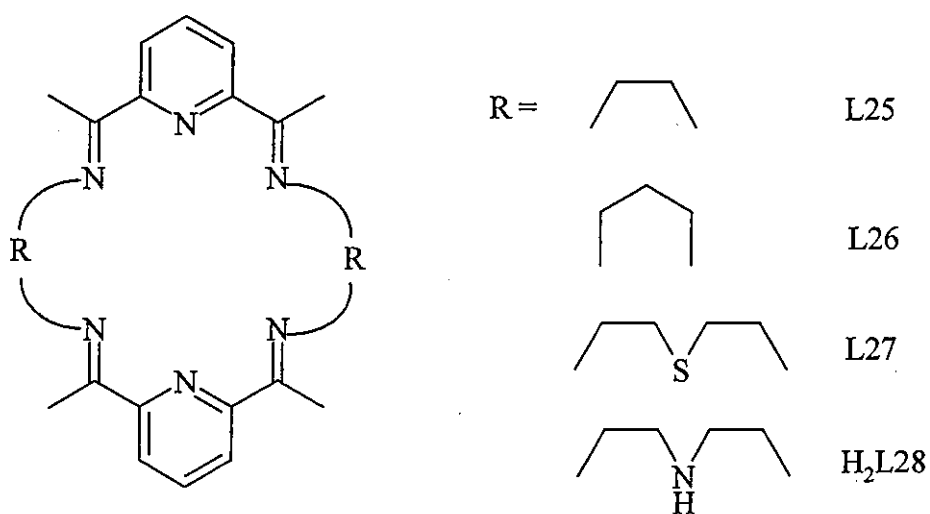


Fig. 1.17: Nelson-type binucleating macrocycles

McKee *et al.*^{32,33} and Fenton *et al.*³¹ reported related systems incorporating pendent alcohol groups in the side chain because they are capable of providing endogenous bridging between the metal ions (fig. 1.18).

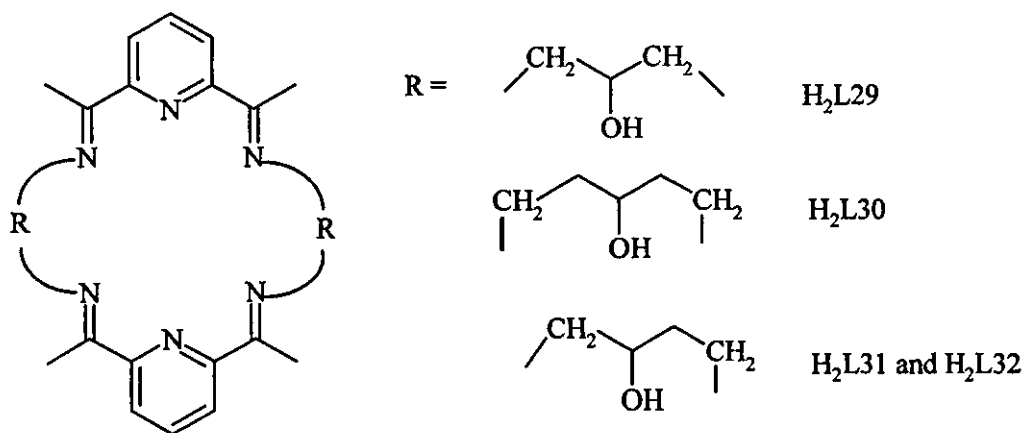


Fig. 1.18: Macrocycles containing pendent alcohol side arms

The synthesis of dinuclear Cu(II) complexes of the ligands H₂L29, H₂L30, H₂L31 and H₂L32 is performed via transmetallation of a mononuclear Ba²⁺ complex of the respective ligands. Mononuclear Pb²⁺ complexes can be obtained with H₂L30, H₂L31 and H₂L32 but with H₂L29 the macrocycle undergoes a ring contraction. In each dinuclear complex³² the Cu(II) atoms are coordinated to two imine donors, one pyridyl donor and one of the endogenous hydroxyl group acting as a bridge between the metal centres. Only one hydroxyl group in each macrocycle has been deprotonated. The geometry around the metal can be approximately square-pyramidal (fig. 1.19)⁸¹ or tetragonal depending on the diamine used. Binuclear Mn(II) (fig. 1.20),^{33,34,82} Fe(III),⁸³ and V(III) (fig. 1.21)⁸⁴ complexes of H₂L29 have been reported with the metal centres bridged by both alkoxy groups. However metals such as Ni(II), which are more sensitive about the coordination geometry of the donor set of the macrocycles do not form complexes with H₂L29 or the related macrocycles shown in fig. 1.18.

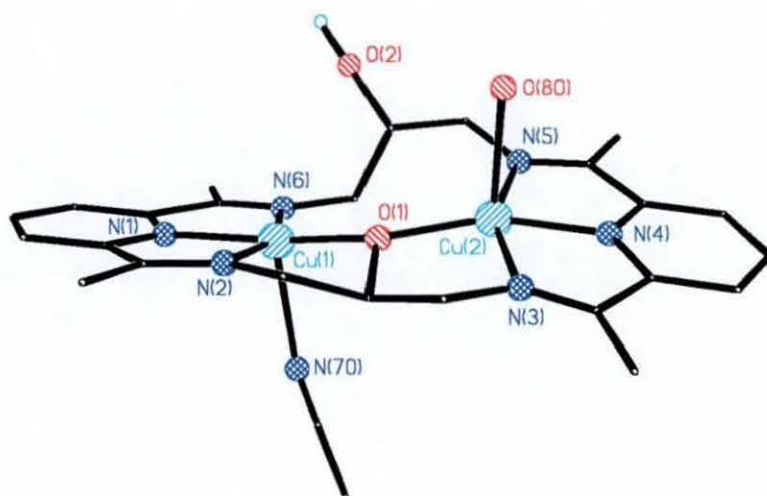


Fig. 1.19: Structure⁵² of the cation $[\text{Cu}_2(\text{HL29})(\text{CH}_3\text{CN})(\text{H}_2\text{O})]^{3+}$

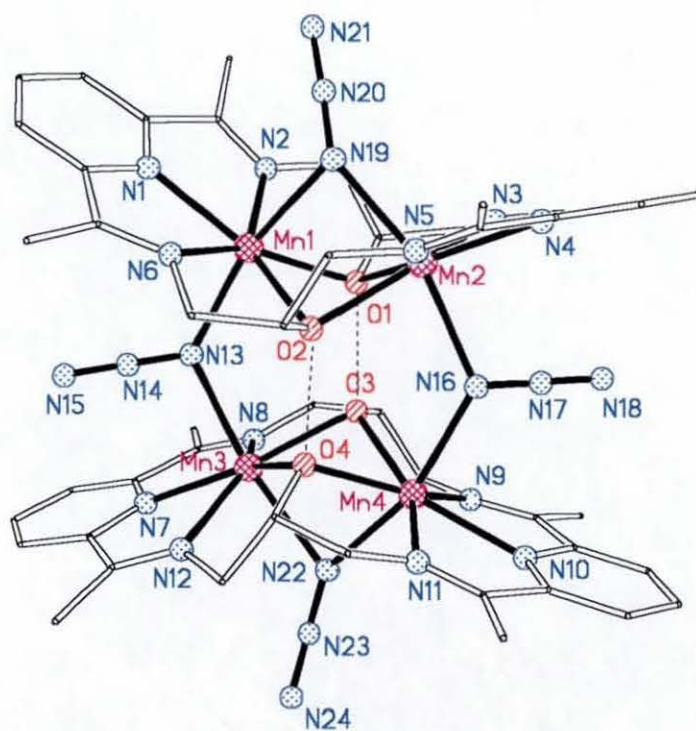


Fig. 1.20: Structure⁵² of the dimeric cation $[\text{Mn}_2(\text{HL29})(\text{N}_3)_2]^{2+}$

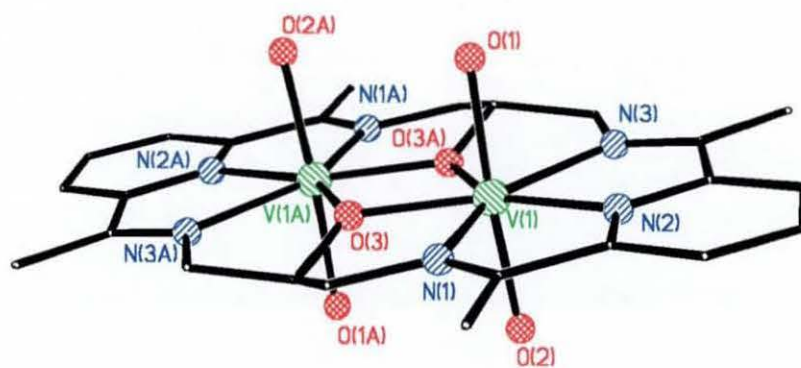


Fig. 1.21: Structure⁵² of the cation $[V_2(L29)(H_2O)_4]^{4+}$

Neither template synthesis using $Mn(ClO_4)_2 \cdot 6H_2O$ nor transmetallation of a Ba^{2+} complex of H_2L23 by $Mn(ClO_4)_2 \cdot 6H_2O$ produced the expected binuclear $Mn(II)$ complex. The compound obtained proved to be a tetramanganese(II) complex $([Mn_4(L33)](ClO_4)_4)$ (fig. 1.23) resulting from the [4+4] condensation of 2,6-diacetylpyridine and 1,3-diaminopropan-2-ol.^{34,82}

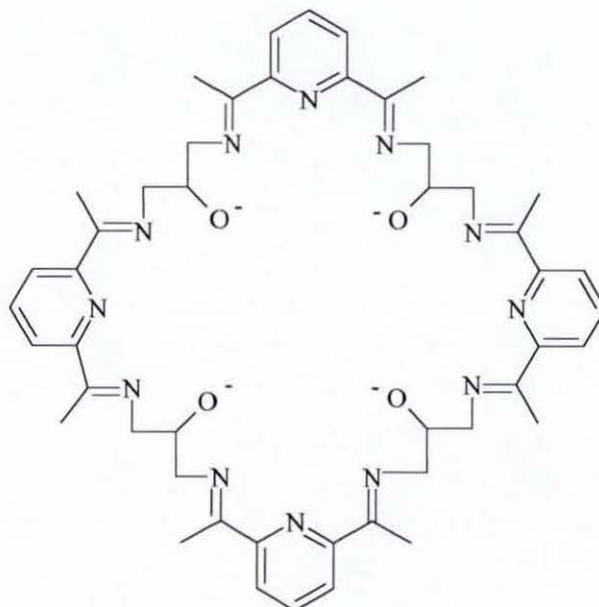


Fig. 1.22: Ligand L33

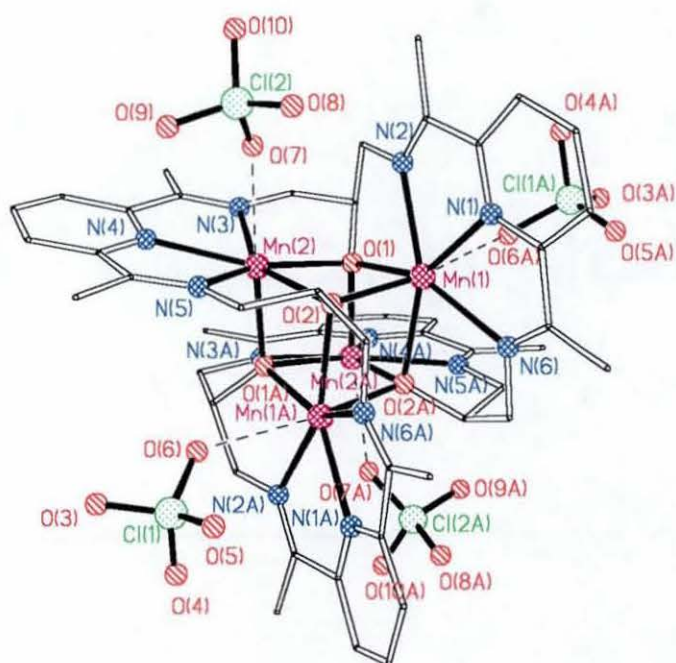


Fig. 1.23: Structure⁵² of $[\text{Mn}_4(\text{L33})](\text{ClO}_4)_2$

The macrocycle is folded in such a way that the manganese cluster has a cubane-type core structure (full bonds in fig. 1.23).

Other heterocyclic head-units^{20,35,85,86} have been used to form binuclear macrocycles like those shown in fig. 1.24.

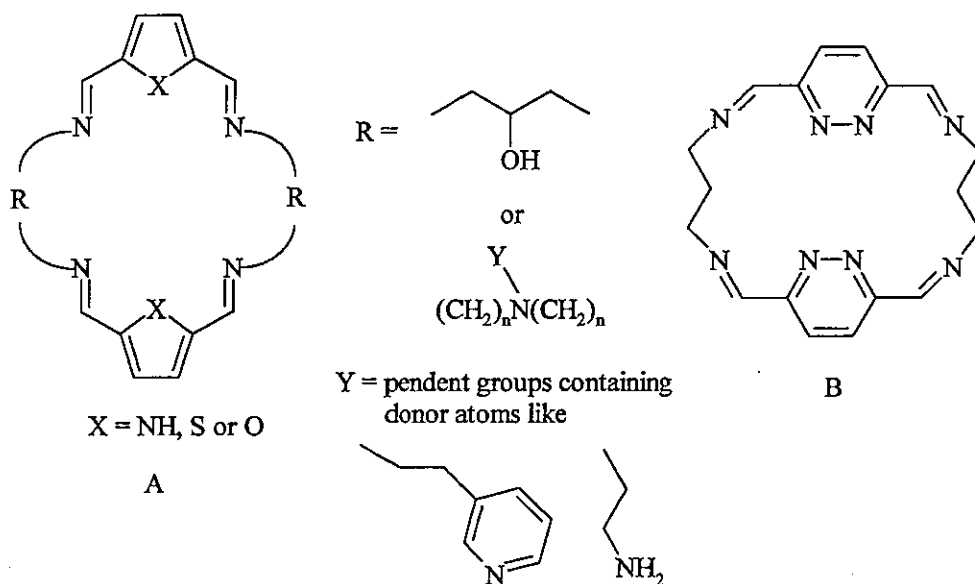


Fig. 1.24: Example of other binuclear macrocycles

In the case of the macrocycles of type A, metals have been found to coordinate in the same way as in the examples with the pyridine-based head-unit. The arrangement and nature of the donor atoms in the pyridazine head-unit of macrocycle B are different to the macrocycles discussed before. The rigid part contains two nitrogen donors next to each other, which leads to a side-by-side arrangement as in the case of ligand L23 (fig. 1.25). However, in this case, the metal ions are linked by a two-atom bridge.

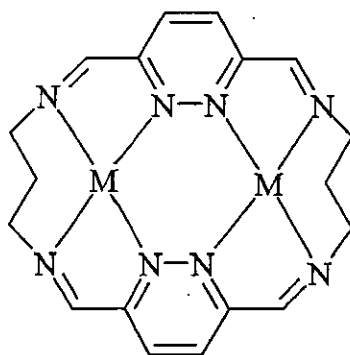


Fig. 1.25: Metal arrangement with binuclear macrocycle B

1.3. From binuclear complexes to tetranuclear complexes

Complexes containing several metal centres (3, 4, 6, 8, 12) in some predetermined arrangement can exhibit quite peculiar chemical and/or physical behaviour.^{2,87} The relatively accessible arrangement of the metal centres provided by the organising ligand may enable substrates to be brought under the influence of some or even all the metals simultaneously, which offers the possibility of subsequent activation, multi-electron reduction or oxidation for the substrates. Therefore, these complexes are the focus of a wide interest because they can act as models for polynuclear structures in a number of metalloproteins (e.g. tetranuclear manganese complexes as models for the Oxygen-Evolving Complex of photosystem II in green plants) and potential homogeneous catalysts and they can provide opportunities for the investigation of magnetic interactions. Thus, the design of tetranuclear macrocyclic complexes is a natural progression from the numerous binuclear systems that have been reported.

As shown in the previous section, the pyridine-based units have resulted in two metal atoms being able to coordinate along the axis between the two head-units, in an end-to-end manner (fig. 1.26). However, this arrangement has limited the number of metal ion being coordinated to two as each pyridine head-unit has a cavity into which only one metal ion can coordinate. Changing the head-unit from pyridine to phenol, permitted a side by side arrangement of the metal ion but disallowed the end-to-end arrangement (fig. 1.26). This is a consequence of the inability of the 1,3-diaminopropan-2-ol side chains to bring the pendant alcohol functions into the coordination sphere of the metal ions due to the small size of the macrocyclic cavity. A way to overcome this issue is to lengthen the carbon side arm of the macrocycle.

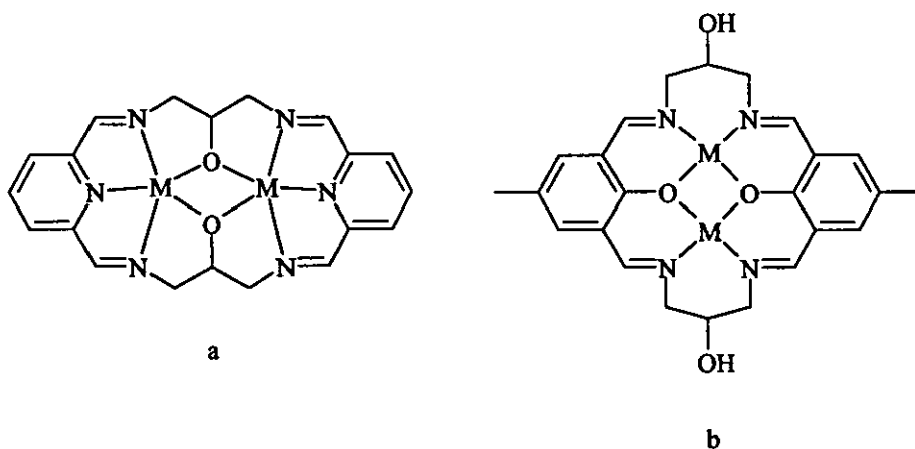


Fig. 1.26: Dipyridine-dialcohol binuclear arrangement (a) and diphenol-dialcohol (b) favoured arrangement

1.4. Tetranuclear and octanuclear macrocyclic complexes of H_4L1 and H_4L2

The tetranuclear macrocycles developed by the McKee group are the result of the [2+2] Schiff-base condensation of 2,6-diformyl-4-(methyl or *tert*-butyl)phenol with 1,5-diaminopentan-3-ol upon a metal template (fig. 1.27). As shown in fig. 1.27, the pendent alcohol groups belonging to the side chain are now involved in the coordination sphere of the metal ions allowing both end-to-end and side-by-side arrangement of metal ions.

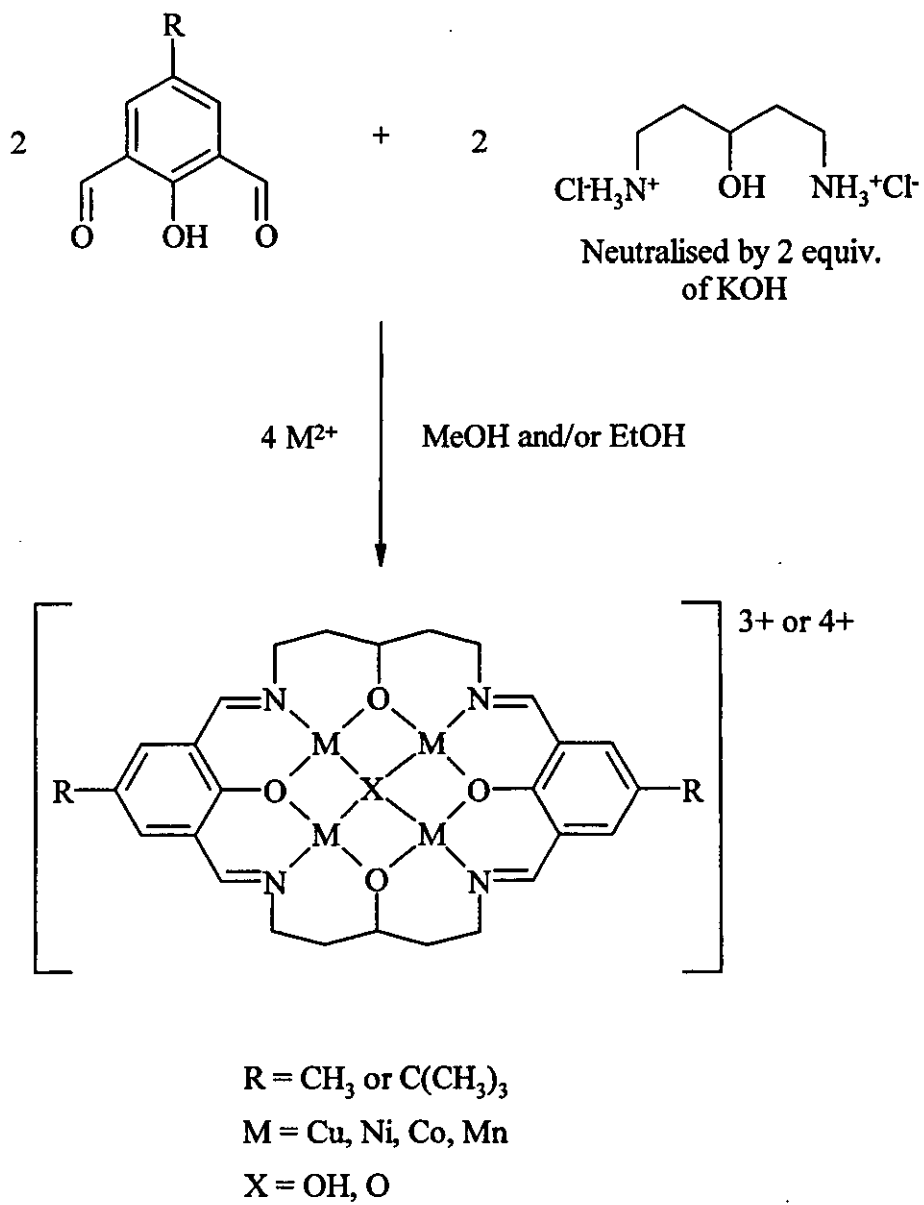


Fig. 1.27: [2+2] macrocycle synthesised *via* template condensation

The resulting macrocycles H₄L1 and H₄L2 (fig. 1.28) can be regarded as being formed of two distinct parts, the rigid phenoldiimine and the saturated side chains containing alcohol groups, which impart some flexibility to the system. This latter feature allows the macrocycle to partially adapt to the coordination preferences of the metal ions.

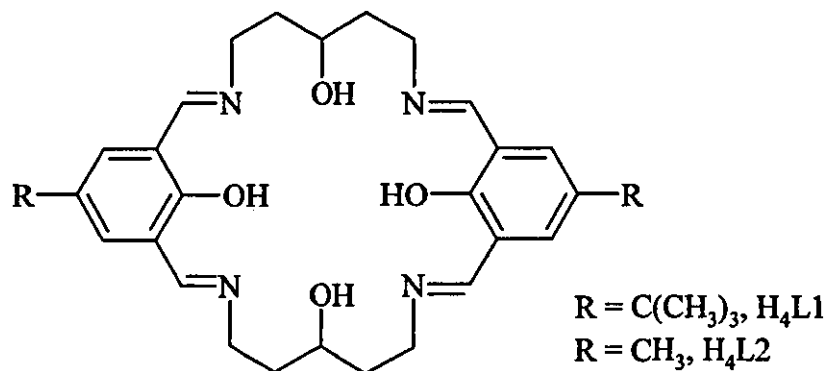


Fig. 1.28: Macrocycles H₄L1 and H₄L2

In this case, the coordination sphere of each metal ion consists of three donors provided by the macrocycle (one phenoxo, one alkoxo and one imine donor) and usually two or three exogenous ligands. In most of the examples the central donor is an oxo or hydroxo group shared by all four metals. The phenol and alcohol are generally deprotonated and act as bridges between the metal centres.

The ability of these macrocycles to form tetranuclear arrays has been demonstrated with a variety of metal complexes with both geometrically demanding metal ions such as nickel and geometrically undemanding like manganese(II), cobalt(II) and copper(II). Although several structures were confirmed by crystallography, many were inferred from combining the results from mass spectrometry, infra-red spectroscopy and elemental analysis.

1.4.1. Tetranuclear manganese complexes

$[\text{Mn}_4(\text{L}2)\text{O}(\text{OAc})_3\text{Cl}(\text{MeOH})]$ (fig. 1.29) was the first tetramanganese complex of $\text{H}_4\text{L}2$ communicated by McKee and Tandon⁸⁸ in 1988. Since then, another structurally similar tetramanganese complex of the same ligand ($[\text{Mn}_4(\text{L}2)\text{O}(\text{OAc})_4(\text{H}_2\text{O})]$) was reported by McKee *et al.*⁸⁹ They both proved to be of mixed valence with two Mn(II) and two Mn(III) ions. These structures are described in detail in the next chapter. Other tetramanganese complexes containing nitrate, perchlorate and chloride counteranions have been suggested by FAB but none of them have been structurally characterised, as yet.

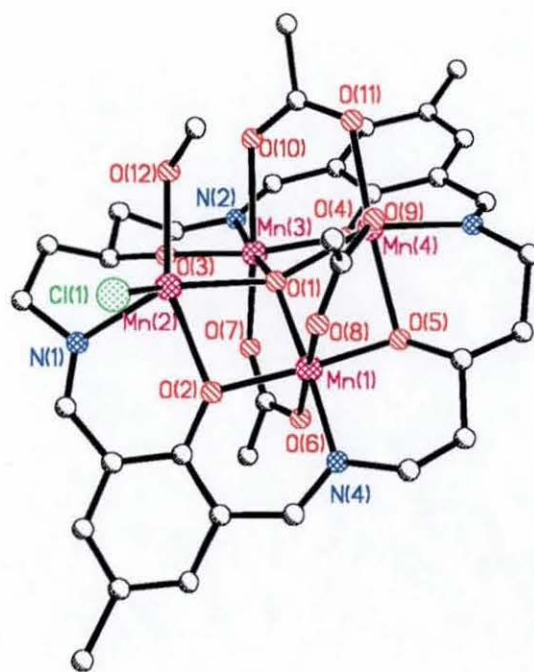


Fig. 1.29: Structure⁵² of $[\text{Mn}_4(\text{L}2)\text{O}(\text{OAc})_3\text{Cl}(\text{MeOH})]$

1.4.2. Tetranuclear cobalt complexes

Tetranuclear cobalt complexes have been identified with acetate, perchlorate, thiocyanate and nitrate counteranions, though crystal structures have been limited to compounds with acetate anions. Two of those structures are of mixed valence, while a third one contains only Co(II). The mixed valence structures $[\text{Co(II)Co(III)}_3(\text{L2})\text{O}(\text{OAc})_3\text{Cl}](\text{ClO}_4)$ and $[\text{Co(II)Co(III)}_3(\text{L2})\text{O}(\text{OAc})_4]\text{Cl}$ are very similar to that of the mixed valence manganese compounds.⁸⁹ However, the Co(II) structure $[\text{Co(II)}_4(\text{L2})(\text{OAc})_2\text{Cl}_2]$ (fig. 1.30) is somewhat unusual in the current set in that it does not contain a central oxo donor and unlike the other structures the macrocycle is close to planar with the exception of the saturated section. Each cobalt is in a trigonal pyramidal environment with two acetate triply bridging (act as both one and three atom bridges) the cobalt centres. This arrangement removed the need for a central bridging group.

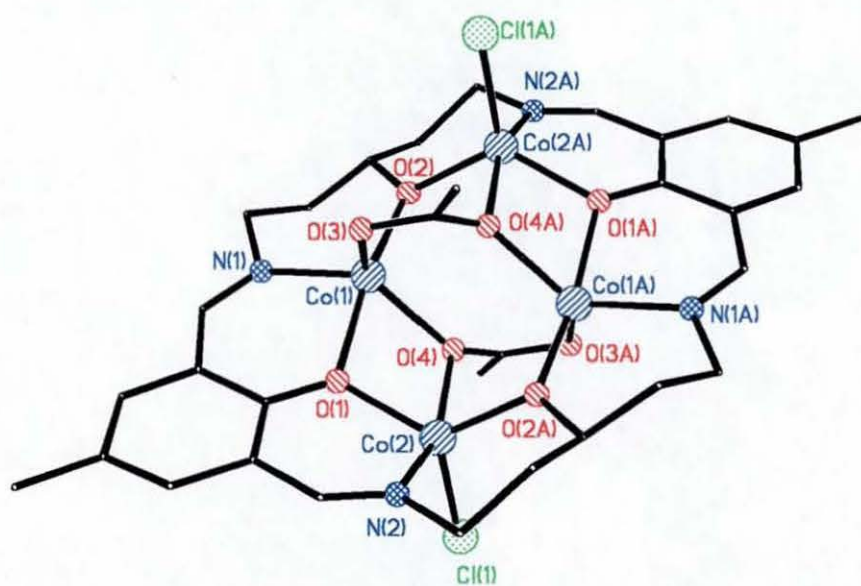


Fig. 1.30: Structure⁵² of $[\text{Co}_4(\text{L2})(\text{OAc})_2\text{Cl}_2]$

1.4.3. Tetranuclear nickel complexes

Two tetranuclear nickel complexes, $[\text{Ni}_4(\text{L1})(\text{OH})(\text{OAc})_3(\text{HOAc})_2]$ and $[\text{Ni}_4(\text{L1})(\text{OH})(\text{OAc})_3(\text{HOAc})(\text{H}_2\text{O})]$, were first isolated and fully characterised by Kruger⁹⁰ and Metcalfe⁹¹ respectively. The structures showed four nickel atoms separated by *ca.* 3 Å in a roughly planar array. This arrangement is notable for the similarities the tetranickel-pentaoxygen core bears with metal oxide surfaces.⁹² These structures will be described in more detail in the following chapter because of their relevance to the work described there. Tetranickel complexes with weakly coordinating axial ligands such as solvent molecules (methanol or ethanol), perchlorates or nitrates are detectable by FAB but have, so far, proved to be difficult to crystallise. However, one example of a tetranickel complexes containing coordinated nitrate anions has been characterised in the course of this work.

1.4.4. Tetranuclear copper complexes

McKee and Tandon⁹³⁻⁹⁵ reported a series of seven tetracopper complexes and three octacopper complexes, which were formed by face to face dimerisation of two tetranuclear copper arrays. Launay,⁹⁶ in the course of his work isolated two new tetracopper complexes along with another octacopper complex containing tetrafluoroborate, all similar to known copper structures. As for the tetranuclear nickel complexes, the structure isolated with copper showed four metal ions separated from each other by *ca.* 3 Å in a roughly planar array reminiscent of a metal-oxide layer. Consequently, the study of the interaction of exogenous ligands with the tetracopper macrocyclic core was undertaken. This work has been described in detail in Launay's thesis.⁹⁶ Only a few examples will be described here.

There are numerous examples of tetranuclear copper complexes illustrating the ability of the copper array to behave like a surface to which a variety of species can be bound. The species that were found to coordinate to the "surface" were both anionic

and neutral, and frequently both at the same time. Perchlorate,⁹⁷ nitrate,⁹⁵ formate,⁹⁸ thiocyanate, pyrazolate,^{96,99} benzotriazole,⁹⁶ acetonitrile⁹⁷ and water⁹⁸ were observed.

The structure of complex $[\text{Cu}_4(\mu_4\text{-OH})(\text{L1})(\text{H}_2\text{O})_2](\text{NO}_3)_3$ was first reported by McKee and Tandon and will be described in detail in the next chapter due to its relevance to the subsequent work in this thesis, the main feature being four copper ions coordinated within the macrocyclic cavity with a central $\mu_4\text{-OH}$ donor (fig. 1.31). At first, the tetranuclear copper complexes containing perchlorate anions were assumed to be similar to the previous nitrate complexes according to analytical data and spectroscopic studies. This assumption was later confirmed by Wikaira⁹⁷ who isolated the complex $[\text{Cu}_4(\mu_4\text{-OH})(\text{L2})(\text{CH}_3\text{CN})_3(\text{ClO}_4)_2](\text{ClO}_4)$. In this case, three acetonitrile molecules and one perchlorate ion are bound on one face while on the opposite face another perchlorate anion is bound in a tripod fashion to three copper ions.

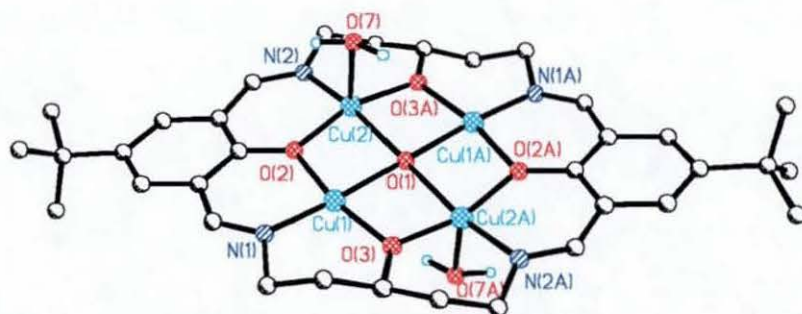


Fig. 1.31: Structure⁵² of the cation $[\text{Cu}_4(\text{L1})(\mu_4\text{-OH})(\text{H}_2\text{O})_2]^{3+}$

McKee and Tandon⁹³ showed that the central $\mu_4\text{-OH}$ can be replaced by two μ -azido ligands, yielding the complex presented in fig. 1.32. The two independent copper atoms have very different coordination environments. The geometry about one copper is square pyramidal with the phenoxy oxygen being the axial ligand and the imine, alkoxy, μ -azido and terminal azido donors forming the base of the pyramid. In

contrast, the other copper centre is four-coordinate with no terminal azido donor in its coordination sphere. The geometry around the metal is somewhat irregular. The two μ -azido ligands lie on either side of the macrocyclic plane.

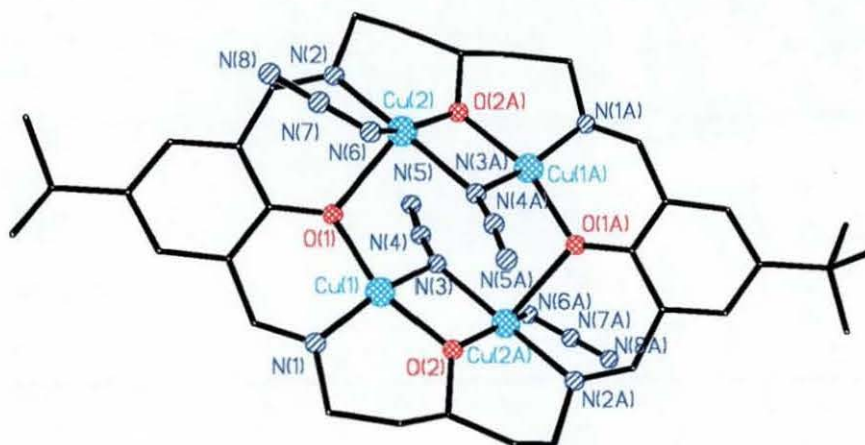


Fig. 1.32: Structure⁵² of the complex $[\text{Cu}_4(\mu\text{-N}_3)_2(\text{L1})(\text{N}_3)_2]$

During his study, Launay⁹⁶ proved that other species can displace the central μ -OH. Benzotriazole was thought to be an ideal candidate being a well-known agent for the protection of copper from corrosion.¹⁰⁰ However, the coordination of the bulky benzotriazole results in a significant bend of the macrocycle and the ejection of two copper ions. Subsequently, pyrazole being less bulky and having the same coordination mode as benzotriazole was used. In this instance, the central cavity is occupied by two pyrazolate molecules bridging two copper centres that lie side by side along the long axis of the macrocyclic ligand. The pyrazolate molecules are sitting on either side of the macrocyclic plane (fig. 1.33). This arrangement has been encountered before in the case of the azido ligands. Each copper ion is in a distorted planar environment. The tetracopper complex is evidently sterically strained on binding pyrazolate anions. Indeed, a dinuclear copper complex containing one bridging pyrazolate with a similar structure to the benzotriazole version was also isolated.

The possibility of varying the central species opens up the potentiality of activating it to further reaction by placing it in an unusual geometric and electronic environment.

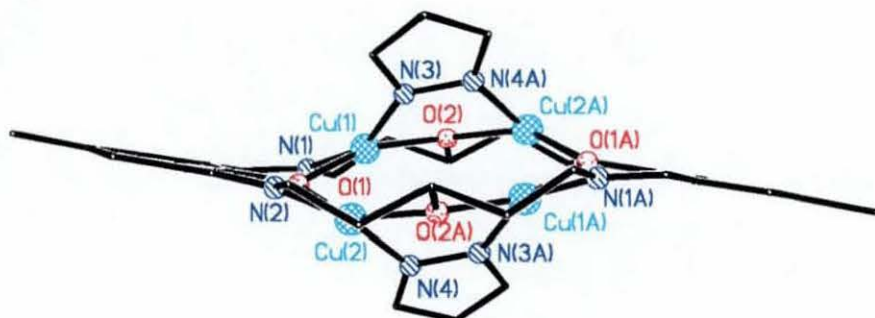


Fig. 1.33: Structure⁵² of the cation $[\text{Cu}_4(\text{L}2)(\mu\text{-pyr})_2]^{2+}$

1.4.5. Octanuclear copper complexes

As mentioned in the previous section, McKee *et al.*^{93,94,96} reported the synthesis and characterisation of four interesting octanuclear copper complexes formed by face to face dimerisation (e.g. $[\{\text{Cu}_4(\mu_5\text{-O})(\text{L}2)(\text{ClO}_4)\}_2](\text{ClO}_4)_2 \cdot 3\text{DMF}$, $[\{\text{Cu}_4(\mu_5\text{-O})(\text{L}1)(\text{ClO}_4)\}_2](\text{ClO}_4)_2$, $[\{\text{Cu}_4(\mu_5\text{-O})(\text{L}2)(\text{NO}_3)\}_2](\text{NO}_3)_2 \cdot 2\text{H}_2\text{O}$, $[\{\text{Cu}_4(\mu_5\text{-O})(\text{L}2)(\text{BF}_4)\}_2](\text{BF}_4)_2$). The structures with perchlorate and tetrafluoroborate are very similar. The compound $[\{\text{Cu}_4(\mu_5\text{-O})(\text{L}2)(\text{ClO}_4)\}_2](\text{ClO}_4)_2$ is shown in fig. 1.34.

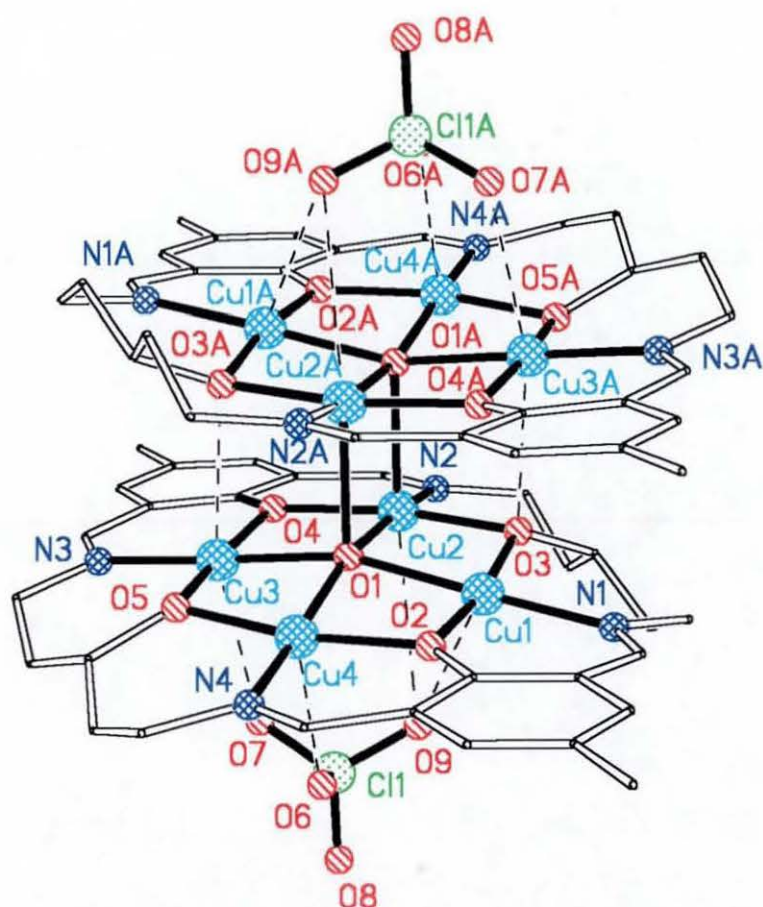


Fig. 1.34: Structure⁵² of $[\{Cu_4(\mu_5-O)(L_2)(ClO_4)\}_2](ClO_4)_2$

All three structures are centrosymmetric dimers and, within each macrocycle, the arrangement is analogous to that observed in the corresponding tetranuclear complexes. However, one major difference in the dimers is the central oxygen, which in those cases is a five coordinate oxo anion (O1), which is displaced from the mean plane of the four copper atoms by *ca.* 0.3 Å and axially linked to Cu2A, a copper atom from the second macrocyclic unit. This bond and the symmetry-related Cu2-O1A linkage hold the dimer together along with weaker interactions involving Cu1 and Cu3. The outer faces of the dimers are blocked by perchlorate or tetrafluoroborate anions bound in a tripod fashion to the tetracopper array. It is

interesting to notice that the *tert*-butyl groups do not appear to present any steric barrier to the dimerisation. The difference between the structures $[\{\text{Cu}_4(\mu_5\text{-O})(\text{L2})(\text{ClO}_4)\}_2](\text{ClO}_4)_2$ and $[\{\text{Cu}_4(\mu_5\text{-O})(\text{L1})(\text{ClO}_4)\}_2](\text{ClO}_4)_2$ occurs at the outer face where the perchlorate anions are coordinated. Indeed, the strengths of the Cu-O(ClO₃) bonds differ due to the distinct orientations of the perchlorate anions. Nonetheless, one significant feature in both complexes is that the shortest bond involves Cu₄, which has no axial interaction on the opposite side of the macrocycle, and the longest distance is that to Cu₂ which has a strong axial bond to O1A.

This dimerisation process has been shown⁹³ to be reversible under the addition of acids and bases and can be monitored by electronic spectroscopy. This observation proves that substrates can be coordinated and released without a major change in the geometry of the copper array, which is encouraging for the possibility of carrying out homogeneous metal-promoted reactions on the metal array.

1.5. Tetranuclear complexes of H₄L34

In 1987, Robson *et al.*¹⁰¹ first communicated the condensation of 2,6-diformyl-4-methylphenol with 2,6-bis(aminoethyl)-4-methylphenol in the presence of nickel acetate, which produced a tetranuclear complex of L34 (fig. 1.35 and fig. 1.36) with similar coordination geometries to those of the macrocycles L1 and L2.

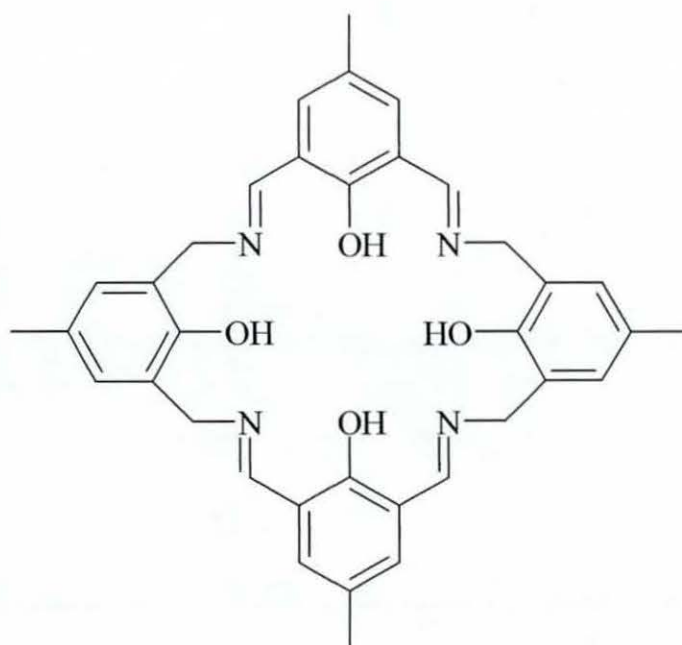


Fig. 1.35: Ligand H₄L34

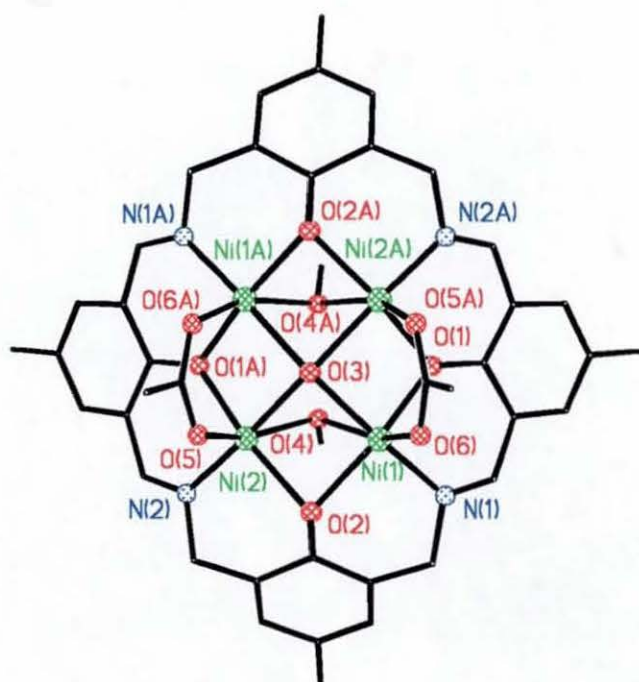


Fig. 1.36: Structure⁵² of [Ni₄(L34)(μ₄-OH)(OAc)₂(MeO·H·OMe)]

The ligand L34 having four phenol units interconnected by carbons ortho to the hydroxyl groups is reminiscent of calixarenes. The molecule is situated around a crystallographic two-fold axis of symmetry and the four nickel atoms are located at the corners of an approximate square. The four aromatic rings are inclined, all on the same side of the Ni₄ plane, at considerable angle to that plane, giving the overall molecular arrangement the shape of a bowl. The extent of the inclination is demonstrated in fig. 1.37.

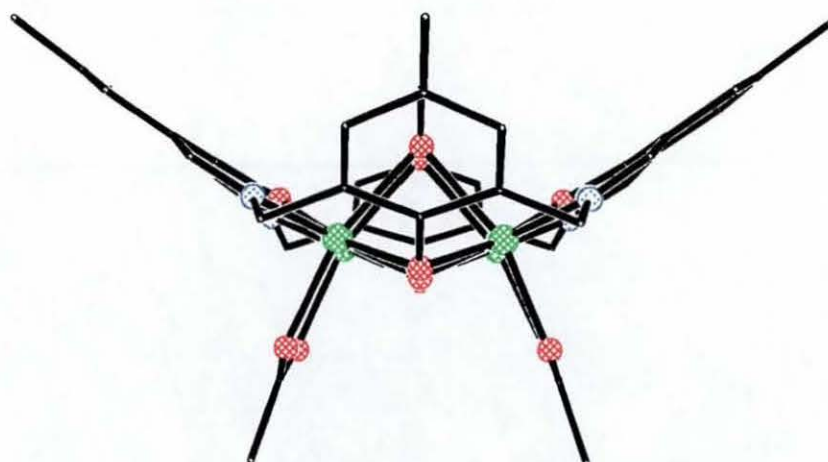


Fig. 1.37: Side-on view of $[\text{Ni}_4(\text{L34})(\mu_4\text{-OH})(\text{OAc})_2(\text{MeO}\cdot\text{H}\cdot\text{OMe})]$

As for the complexes described in the previous section, all four nickel atoms are bound to a central $\mu_4\text{-OH}$ group, which is located 0.6 Å below the Ni₄ plane. The pseudo-octahedral arrangement around each nickel is completed by a bridging acetate ion on the convex side of the macrocycle and one methoxy group on the concave side of the macrocycle. Two methoxy groups are interacting through a hydrogen bond yielding the following system (MeO·H·OMe). Two other tetranickel complexes have also been isolated by Robson *et al.*¹⁰² In complex $[\text{Ni}_4(\text{L34})(\mu_4\text{-OH})(\text{N}_3)_2(\text{H}_2\text{O})_2(\text{MeO}\cdot\text{H}\cdot\text{OMe})]$, the axial acetate ligands have been substituted by azide and water while in complex $[\text{Ni}_4(\text{L34})(\mu_4\text{-OH})(\text{MeO}\cdot\text{H}\cdot\text{OMe})_3]$ the axial acetate ligands have been replaced by two pairs of hydrogen-bonded methoxy groups.

A tetranuclear zinc(II) complex (fig. 1.38) was also characterised by Robson *et al.*¹⁰³ The general bowl-like arrangement encountered in the Ni₄ complexes is present in the Zn₄ complex in less symmetrical form. The phenol rings are all inclined on the same side of the Zn₄ cluster but at four different angles to the mean plane that passes through the metals. The four zinc centres are not coplanar and the arrangement of the Zn₄ cluster is markedly distorted from a square, the two “diagonals” differing significantly in length (Zn(2)-Zn(4) 3.632(7) Å and Zn(1)-Zn(3) 4.742(7) Å). The geometry around the metal ions varies between distorted square pyramidal and tetragonal. As in the tetranickel complexes the central cavity of the macrocycle is occupied by a μ₄-OH group. However, with the loss of symmetry, probably due to a mismatch in size between the metal ions and the macrocyclic ligand, the strength of the four bonds linking the central group to the zinc centres differs. Indeed, two bonds are rather weak with one being much weaker (O(11)-Zn(3) 2.60(3) Å) than the others (O(11)-Zn(2) 2.06(3) Å, O(11)-Zn(4) 1.97(3) Å, O(11)-Zn(1) 2.17(2) Å).

It is clearly apparent that this macrocycle (L34) has provided less flexibility than the macrocycles L1 and L2. However, the rigidity of L34 is not such that the ligand completely dictates the geometry of the final product, since the Ni₄ and Zn₄ structures are different.

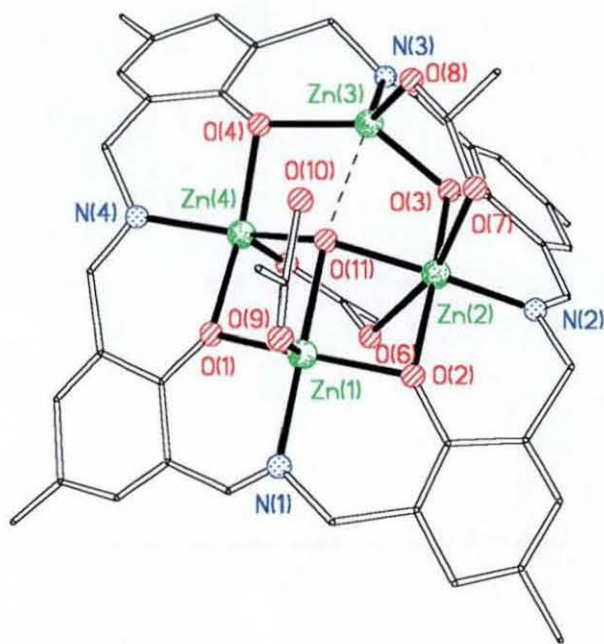


Fig. 1.38: Structure⁵² of $[Zn_4(L34)(\mu_4-OH)(OAc)_3]$

The amine version of macrocycle L34 yielded another strikingly similar tetranuclear zinc(II) complex and a trinuclear Co(III) complex.¹⁰⁴ Additionally, a dinuclear Mn(II) complex of L34 has also been isolated by Robson *et al.*¹⁰⁵

1.6. Tetranuclear complexes of H₄L36

A more flexible tetranuclear macrocycle H₄L36 (fig. 1.40) has been reported by Nag *et al.*¹⁰⁶ The macrocycle is the result of the reduction of the macrocycle H₄L35 (fig. 1.39), which was formed by template condensation of 2,6-diformyl-4-methylphenol and 1,2-diaminoethane in the presence of magnesium acetate.

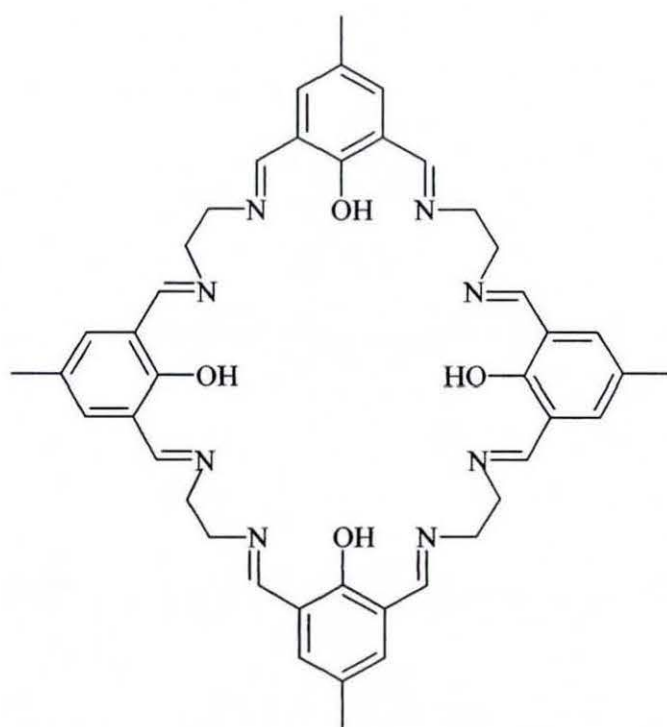


Fig. 1.39: Ligand H₄L35

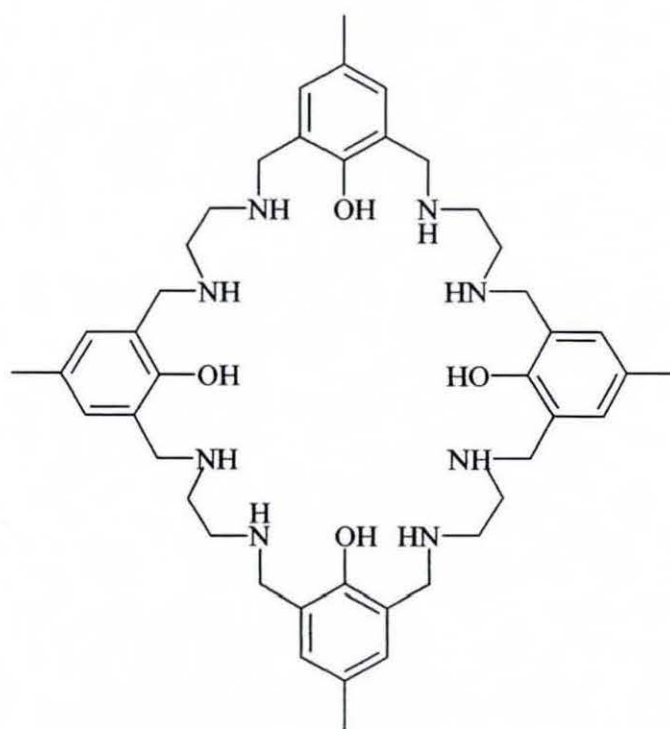


Fig. 1.40: Ligand H₄L36

The synthesis of tetranickel(II) and tetracopper(II) complexes is achieved on reaction of H₄L36 with the appropriate metal salt in the presence of Et₃N. The structure of one tetranickel complex ([Ni₄(L36)(μ₂-NCS)₂(μ₂-H₂O)₂](ClO₄)₂) was described (fig. 1.41). Here again, the structure is centrosymmetric with the four nickel ions forming a square. Two pairs of two nickel atoms are triply-bridged by one phenoxo oxygen, one aqua oxygen, and the thiocyanate nitrogen. An additional bridge between the two pairs is provided by the two remaining phenoxo oxygen donors. The coordination sphere of each nickel is completed by two secondary amines from the macrocyclic ligand.

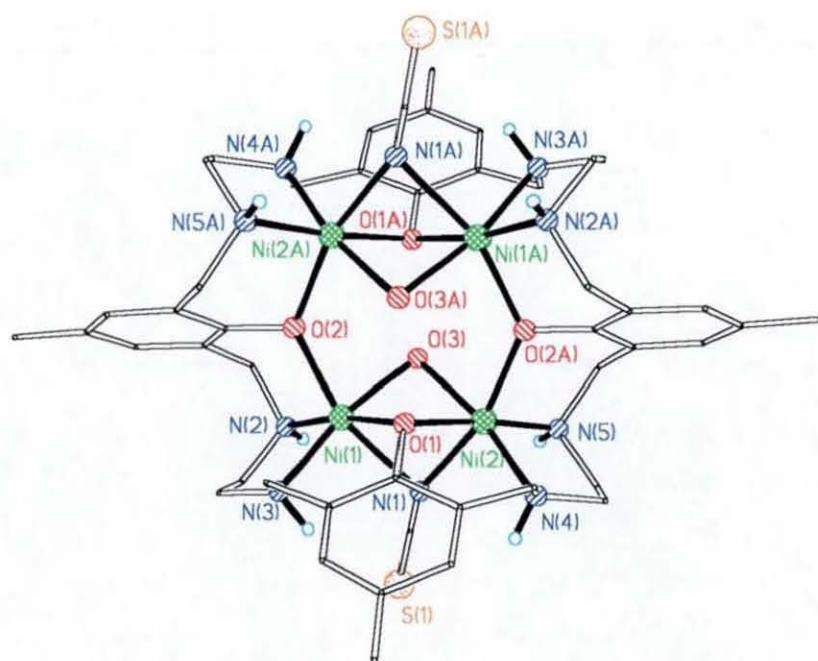


Fig. 1.41: Structure⁵² of the cation [Ni₄(L36)(μ₂-NCS)₂(μ₂-H₂O)₂]²⁺

A non-centrosymmetric tetranuclear Ni(II) structure with a central hydroxy group bonded to three nickel atoms was also reported earlier by Nag *et al.*¹⁰⁷ The coordination sphere of the fourth nickel atom is completed by one perchlorate anion.

1.7. Tetranuclear complexes of H₄L37

Okawa *et al.*^{108,109} reported a heterotetranuclear Ni₂Cu₂ complex with a derivative of the macrocyclic ligand H₄L37 shown in fig. 1.42. The environment of both Ni(II) atoms is nearly octahedral while the geometry around the Cu(II) atoms is trigonal pyramidal forming a defective double-cubane structure (fig. 1.43). Here, we have to stress the fact that there are two types of coordination sites provided by the macrocycle: N_(amine)2O₂ and N_(imine)2O₂. In this case, copper is opting for the softer imine donors while nickel prefers the harder amine donors. This preference mainly originates from the favoured geometry adopted by the metals. Copper is not geometrically demanding whereas nickel is. The two amine side-chains give the macrocycle a certain degree of flexibility not possible with only imine donors. Consequently, the macrocycle can provide nickel with its favoured octahedral environment.

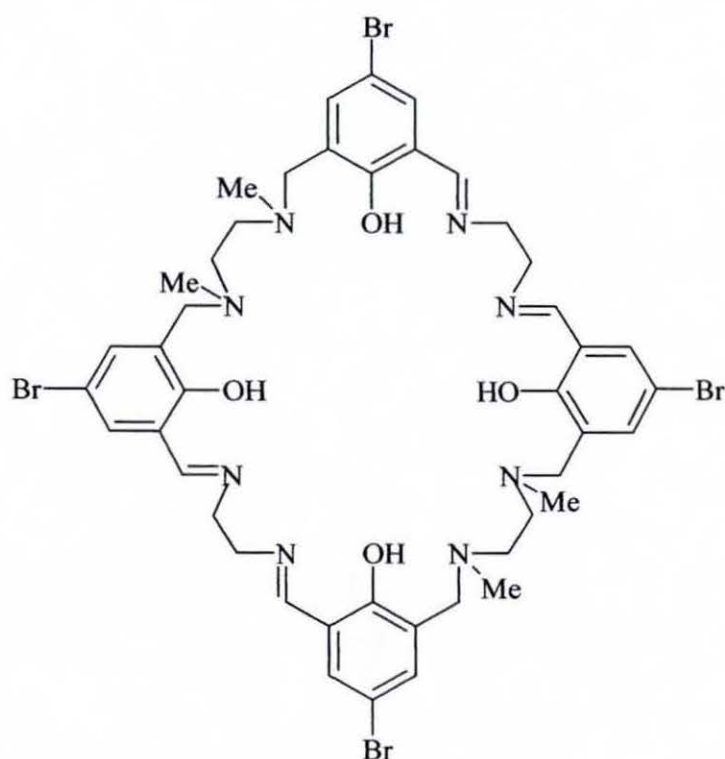


Fig. 1.42: Ligand H₄L37

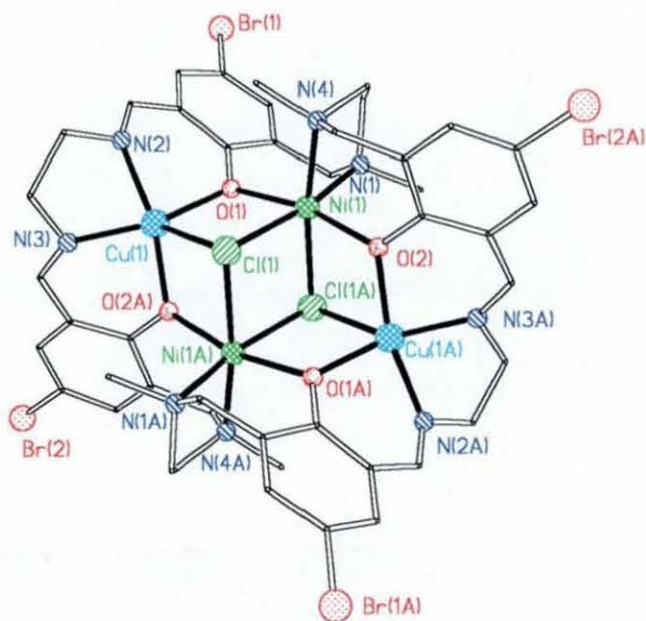


Fig. 1.43: Structure⁵² of the cation $[\text{Ni}_2\text{Cu}_2(\text{L37})\text{Cl}_2]^{2+}$

1.8. Tetranuclear complexes of H₂L38

Asato *et al.*¹¹⁰ reported another tetranuclear macrocycle H₂L38 (fig. 1.44), which was obtained by template condensation of 2,6-diformyl-4-methylphenol and 1,11-diamino-3,6,9-trioxaundecane using zinc acetate as the template core.

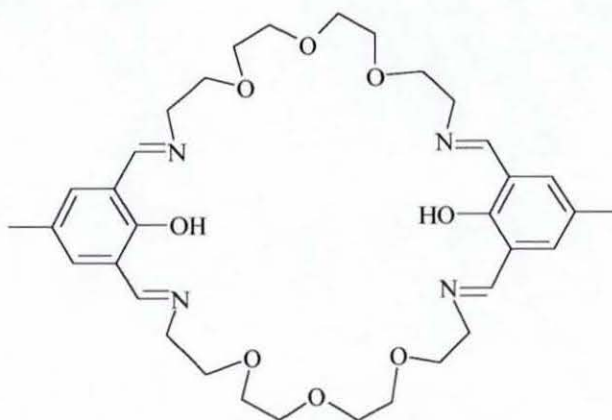


Fig. 1.44: Ligand H₂L38

Two tetrazinc(II) complexes were isolated, $[\text{Zn}_4(\text{L38})(\text{OAc})_4](\text{ClO}_4)_2$ and $[\text{Zn}_4(\text{L38})(\text{OH})_2(\text{OAc})_2](\text{ClO}_4)_2$. In complex $[\text{Zn}_4(\text{L38})(\text{OAc})_4](\text{ClO}_4)_2$ (fig. 1.45) the macrocycle has a planar form with the polyether chains adopting a linear conformation. This ligand arrangement produces a large cavity in the centre of the ring, into which four zinc ions are encapsulated as a pair of μ -phenoxo-bis(μ -carboxylato)dizinc species. Each metal has essentially the same coordination geometry which is distorted trigonal pyramidal.

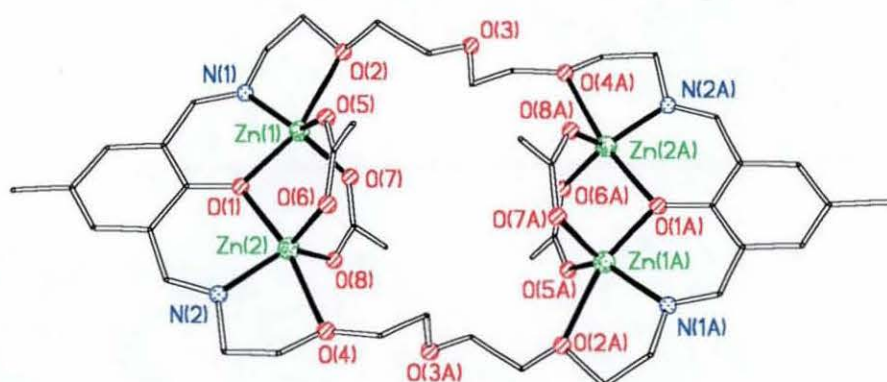


Fig. 1.45: Structure⁵² of the cation $[\text{Zn}_4(\text{L38})(\text{OAc})_4]^{2+}$

The structure of $[\text{Zn}_4(\text{L38})(\text{OH})_2(\text{OAc})_2](\text{ClO}_4)_2$ (fig. 1.46) differs significantly from that of $[\text{Zn}_4(\text{L38})(\text{OAc})_4](\text{ClO}_4)_2$, at each dinuclear zinc core there is only one bridging acetate. The other acetate groups at each dinuclear zinc core have been replaced by two hydroxo ions which further coordinate to the other zinc pair thereby linking the two dimer units, yielding a Zn_4O_4 cluster-like ring core. Unlike in complex $[\text{Zn}_4(\text{L38})(\text{OAc})_4](\text{ClO}_4)_2$, the two polyether chains of the ligand L38 are folded and the two dimeric units formed by the phenoxo bridges are paired parallel to each other by π - π stacking of two phenolate rings. This feature may contribute to the close proximity of the two dimeric units, finally yielding the bis- μ -hydroxo dimer pair.

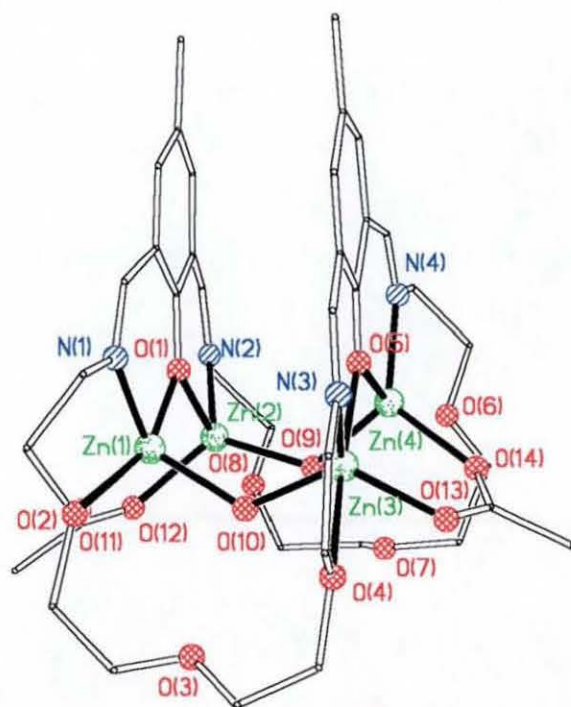


Fig. 1.46: Structure⁵² of the cation $[\text{Zn}_4(\text{L38})(\text{OH})_2(\text{OAc})_2]^{2+}$

1.9. Tetranuclear complexes of H₆L39 and H₆L40

Tandon *et al.*^{69,111} reported the [3+3] condensation of 2,6-diformyl-4-methyl phenol with 1,3-diaminopropan-2-ol in the presence of copper nitrate and perchlorate or nickel nitrate and perchlorate as the template agents, yielding the ligand H₆L39, which can accommodate six metal centres (fig. 1.47). The hexacopper(II) complex described by Tandon, is in fact a dodecanuclear dimer and can be described as hexagonal cyclic arrays of metal centres linked axially through hydroxo bridges. No structure of related nickel complexes have been determined as yet, but they are assumed to be similar to the copper complexes.

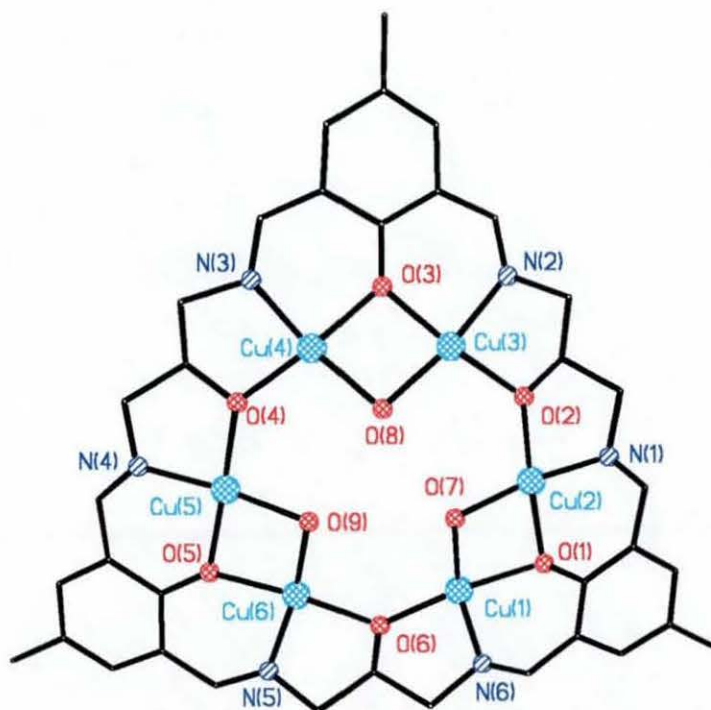


Fig. 1.47: Structural representation⁵² of one hexanuclear ring for $[\text{Cu}_6(\text{L39})(\mu_2\text{-OH})_3]_2(\text{NO}_3)_6$

The copper-copper distances can be subdivided in two sets: one set where the copper centres are bridged by a phenoxy and a hydroxy oxygen atom with a Cu---Cu distance of *ca.* 2.942(4) Å and the other set where the copper centres are bridged by an alkoxy oxygen atom with a longer Cu---Cu distance of *ca.* 3.560(5) Å.

As shown on the structural representation there is a potential for the coordination of a seventh metal in the empty central cavity. However, the choice is restricted to metals with no particular preference in their coordination geometry.

A comparable Cu_6 complex of a more flexible macrocyclic ligand ($\text{H}_6\text{L40}$) derived from the [3+3] template condensation of 2,6-diformyl-4-methylphenol and 2,6-bis(aminomethyl)-4-methylphenol in the presence of copper acetate reported by Robson *et al.*,¹¹² leads to a “cyclohexane boat” arrangement of six copper(II) centres. Five of the copper centres are essentially square pyramidal while the sixth copper ion is in an elongated tetragonal environment (fig. 1.48).

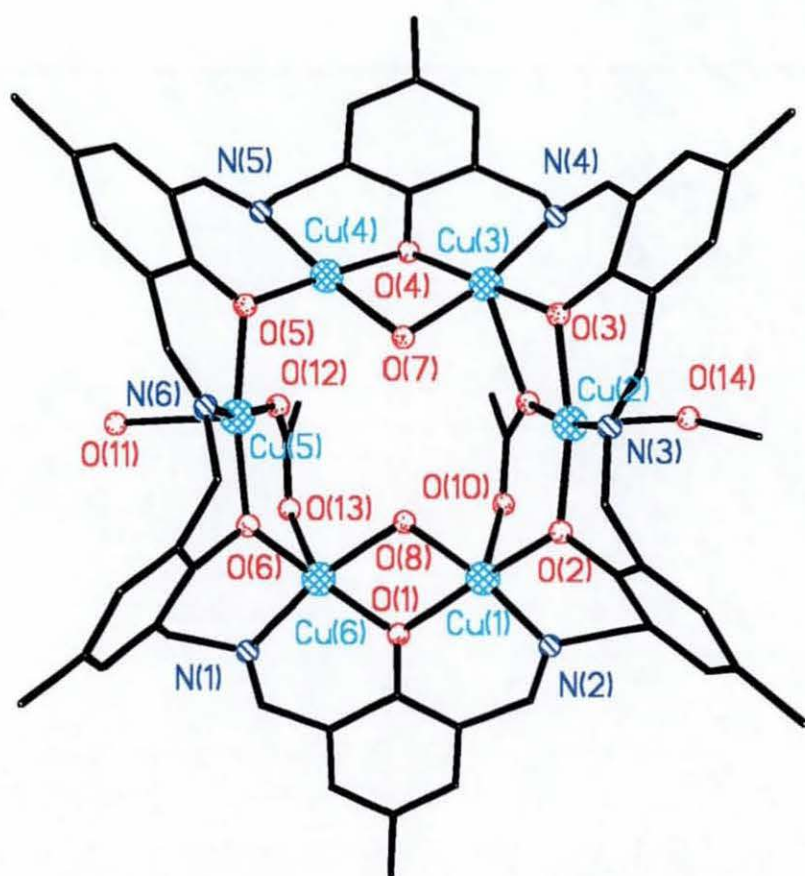


Fig. 1.48: Structure⁵² of the cation $[\text{Cu}_6(\text{L40})(\text{OAc})_2(\mu_2\text{-OH})_2(\text{MeOH})_2(\text{H}_2\text{O})]^{2+}$

1.10. Conclusion

Most of the polynuclear (≥ 4 metal ions) systems described previously have achieved the aim of bringing the metal centres into close proximity (between 2.5 and 5 Å) with various degrees of constraint to the metal and distortion of the macrocycles. It has been shown that the macrocycles containing imine donors have provided less flexibility than those containing amine donors. However, within the group of imine-donors-macrocycles the flexibility can be enhanced by the introduction of side chains of different lengths. In cases where the macrocycles are more flexible, the metals tend to impose their favoured geometry on the macrocycle whereas for more rigid macrocycles the situation is reversed. Generally, a compromise has to be found somewhere in between the two extreme positions.

Some macrocycles can afford complexes with the metal centres situated either far apart or in close proximity. The tetranuclear zinc complexes isolated by Asato *et al.*¹¹⁰ are a perfect example for this particular feature. Here, the length and flexibility of the side-chain plays an important role allowing the macrocycle to adopt two different conformations.

In a large majority of examples, the polynuclear macrocyclic systems possess a central cavity, which can be occupied by different bridging groups, which opens up the potentiality of activating them to further reaction depending on the environment. Another possible aspect is the study of host-guest chemistry with the aim of selective coordination of certain species by varying the environment of the central cavity.

The introduction of different coordination sites within polynuclear (≥ 3 metal centres) macrocycles to render mixed-metal complexes is an interesting perspective due to already known dinuclear complexes exhibiting original physicochemical properties and functions arising from dissimilar metal ions in close proximity.

Chapter two

Tetranuclear Complexes

of

Phenol Head-unit Schiff-base Macrocycles

2.1. Tetranuclear nickel complexes

2.1.1. Introduction

The [2+2] macrocycles H_4L1 and H_4L2 (fig. 2.1), formed by template condensation of 2,6-diformyl-4-R-phenol ($R = CH_3$ or $C(CH_3)_3$) and 1,5-diaminopentan-3-ol upon nickel acetate has yielded interesting tetranuclear complexes reported by Kruger,⁹⁰ $[Ni_4(L1)(\mu_4-OH)(OAc)_3(HOAc)_2]$, and Metcalfe,⁹¹ $[Ni_4(L1)(\mu_4-OH)(OAc)_3(HOAc)-(H_2O)]$. This work was initially an extension of the investigation into copper complexes of these macrocycles.⁹³⁻⁹⁶

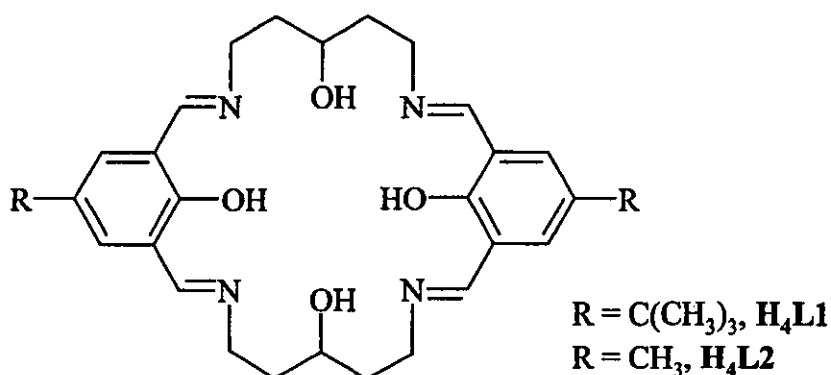


Fig. 2.1: Ligand H_4L1 and H_4L2

In those complexes, the four metal ions are separated from each other by *ca.* 3 Å in a roughly planar array with a central hydroxy group bridging all four metal atoms (fig. 2.2).

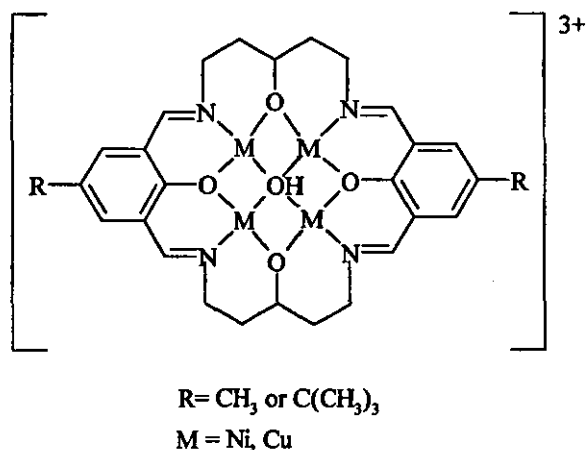


Fig. 2.2: Metal complexes with nickel and copper

The complexes $[\text{Ni}_4(\text{L1})(\mu_4\text{-OH})(\text{OAc})_3(\text{HOAc})_2]$ and $[\text{Ni}_4(\text{L1})(\mu_4\text{-OH})(\text{OAc})_3(\text{HOAc})(\text{H}_2\text{O})]$ possess a superstructure of three bridging acetate groups and two neutral ligands (L) as shown in fig. 2.3.

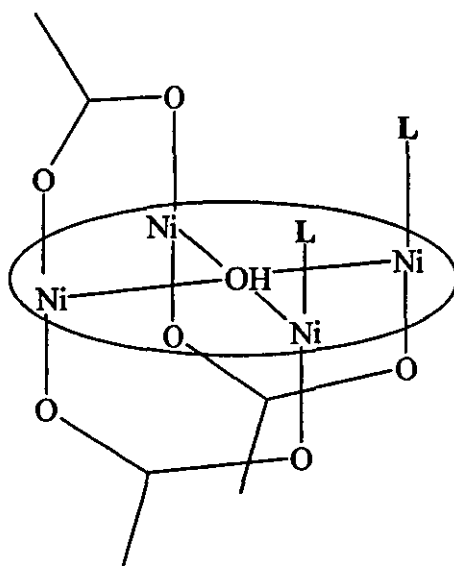


Fig. 2.3: Acetate superstructure of $[\text{Ni}_4(\text{L1})(\mu_4\text{-OH})(\text{OAc})_3(\text{L})_2]$

The structural results suggest that neutral ligand exchange can take place on the metal "surface". One of the neutral acetic acid molecules can be replaced by a water

molecule. The neutral $[\text{Ni}_4(\text{L1})(\mu_4\text{-OH})(\text{OAc})_3]$ core remains largely unaffected by the changes due to the exchange of the L ligands. This ability suggests that the investigation of interactions of exogenous species with macrocyclic “pseudo surfaces” may be a first step towards the project of carrying out and understanding homogeneous metal promoted reactions by binding the substrate to the array. In order to exploit the ability displayed by these complexes^{90,91} it is of interest to prepare tetranickel complexes in which more of the axial sites are not occupied by strongly coordinated acetate anions. Such complexes can be detected by IR and FAB spectrometry but to date have proved difficult to crystallise. However, one example with NO_3^- anions was isolated in the course of this work (section 2.3 of this chapter).

As the previously reported structures^{90,91} are relevant to the work discussed in this chapter, they will be described in more detail in section 2.3.1.

2.1.2. Tetranickel complexes with ClO_4^- , NO_3^- and Cl^-

2.1.2.1. Synthesis and characterisation

The $[\text{Ni}_4(\text{L1})(\text{OH})(\text{OAc})_3]$ core is neutral and relatively easy to isolate. Tetranuclear complexes with less strongly bound anions formulated as $[\text{Ni}_4(\text{L1})(\mu_4\text{-OH})(\text{MeOH})_4(\text{H}_2\text{O})_4](\text{ClO}_4)_3$, $[\text{Ni}_4(\text{L2})(\mu_4\text{-OH})(\text{MeOH})_6(\text{H}_2\text{O})_2](\text{ClO}_4)_3$, $[\text{Ni}_4(\text{L1})(\mu_4\text{-OH})(\text{MeOH})_7(\text{H}_2\text{O})](\text{NO}_3)_3$ and $[\text{Ni}_4(\text{L1})(\mu_4\text{-OH})(\text{MeOH})_8]\text{Cl}_3$ present more synthetic difficulties. These complexes were synthesised *via* a template route by the condensation of DFTP or DFMP and DAHP using the appropriate nickel salts and characterised by FAB spectrometry, infra-red spectroscopy and elemental analysis. The FAB mass spectra indicated the formation of tetranuclear entities in each complex. For $[\text{Ni}_4(\text{L1})(\mu_4\text{-OH})(\text{MeOH})_4(\text{H}_2\text{O})_4](\text{ClO}_4)_3$, the spectrum shows two main peaks at m/z 953 and 971 attributable to $[\text{Ni}_4(\text{L1})(\mu_4\text{-OH})(\text{MeOH})_3(\text{H}_2\text{O})_2]^{3+}$ and $[\text{Ni}_4(\text{L1})(\mu_4\text{-OH})(\text{MeOH})_3(\text{H}_2\text{O})_3]^{3+}$, which, combined with the elemental analysis data, supports the coordination of solvent molecules as described in the

experimental section. These two peaks are a common feature in the three tetranuclear complexes containing L1.

Another five peaks of lower intensity were assigned to $[\text{Ni}_4(\text{L1})(\mu_4\text{-OH})(\text{MeOH})(\text{H}_2\text{O})_4(\text{ClO}_4)_2]^{2+}$ (m/z 1027), $[\text{Ni}_4(\text{L1})(\mu_4\text{-OH})(\text{MeOH})(\text{ClO}_4)_3 + \text{H}]^+$ (m/z 1146), $[\text{Ni}_4(\text{L1})(\mu_4\text{-OH})(\text{H}_2\text{O})_2(\text{ClO}_4)_3 + \text{H}]^+$ (m/z 1159), $[\text{Ni}_4(\text{L1})(\text{OH})(\text{MeOH})_4(\text{ClO}_4)]^{2+} \cdot 2\text{MeOH}$ (m/z 1253) and $[\text{Ni}_4(\text{L1})(\text{OH})(\text{MeOH})(\text{ClO}_4)_3 + \text{Na}]^+$ (m/z 1316). For $[\text{Ni}_4(\text{L1})(\mu_4\text{-OH})(\text{MeOH})_7(\text{H}_2\text{O})](\text{NO}_3)_3$, another main peak attributed to $[\text{Ni}_4(\text{L1})(\mu_4\text{-OH})(\text{MeOH})_7(\text{NO}_3)_3 + \text{Na}]^+$ appears at 1252. The remaining peaks were attributed as displayed in table 2.2.

The complete peak assignments for each complex are given in tables 2.1, 2.2 and 2.3.

Note: peak attribution in mass spectrometry

In mass spectrometry a molecule is ionised (for the compounds described in this thesis, the method of ionisation is FAB) and fragmented into different ions. The spectrum shows different clusters of peaks at different m/z (m = mass of the observed ion and z = charge of the observed ion) values corresponding to different fragmented ions. Each cluster represents an isotopic distribution for one fragment (fig. 2.4) due to the different isotopes of the atoms present in the molecule. The value taken for m/z in the data table is that of the highest peak belonging to a set of peaks in the experimental spectrum. The value for the calculated mass is obtained by taking that of the peak of highest intensity in the isotopic distribution pattern calculated by the Isotopic Distribution Calculator program developed by J.J. Manura and D.J. Manura.¹¹³

In FAB spectrometry, it is known that metal ions can be reduced during the experiment. Therefore if one peak fits the formula with a charge of +2 or +3, the charge is effectively +1 with the molecule gaining one or two electrons through the metal.

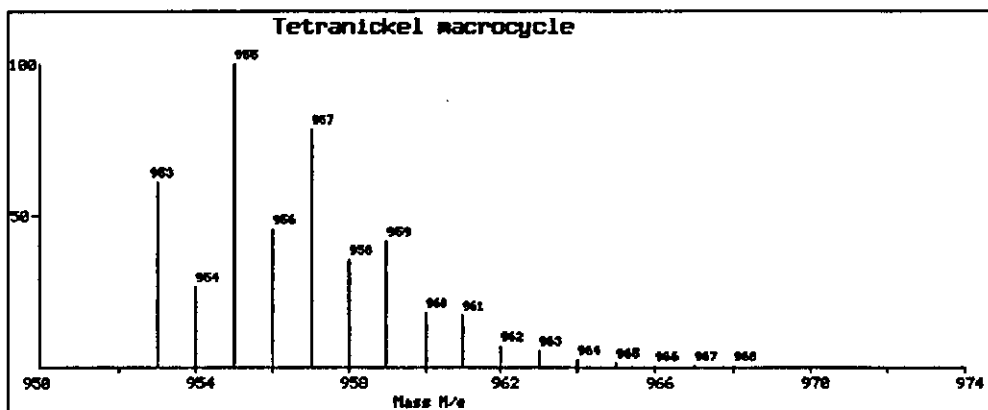


Fig. 2.4: Example of calculated isotopic distribution for the fragment $[\text{Ni}_4(\text{L1})(\text{OH})(\text{H}_2\text{O})_2(\text{MeOH})_3]^{3+}$

Table 2.1: Peak attributions for $[\text{Ni}_4(\text{L1})(\mu_4\text{-OH})(\text{MeOH})_7(\text{H}_2\text{O})](\text{ClO}_4)_3$

m/z	Rel. Intensities (%)	Fragments	Calc. Mass
219	100	fragmentation peak of noba or tetranickel complex	
953	70	$[\text{Ni}_4(\text{L1})(\text{OH})(\text{H}_2\text{O})_2(\text{MeOH})_3]^{3+}$	955
971	80	$[\text{Ni}_4(\text{L1})(\text{OH})(\text{H}_2\text{O})_3(\text{MeOH})_3]^{3+}$	973
1027	25	$[\text{Ni}_4(\text{L1})(\text{OH})(\text{H}_2\text{O})_4(\text{MeOH})(\text{ClO}_4)]^{2+}$	1027
1146	25	$[\text{Ni}_4(\text{L1})(\text{OH})(\text{MeOH})(\text{H}_2\text{O})_5(\text{ClO}_4)_2+\text{H}]^+$	1146
1159	20	$[\text{Ni}_4(\text{L1})(\text{OH})(\text{H}_2\text{O})_2(\text{ClO}_4)_3+\text{H}]^+$	1159
1253	15	$[\text{Ni}_4(\text{L1})(\text{OH})(\text{MeOH})_3(\text{H}_2\text{O})_2(\text{ClO}_4)_3+\text{H}]^{2+}$	1253
1316	15	$[\text{Ni}_4(\text{L1})(\text{OH})(\text{MeOH})_3(\text{H}_2\text{O})_2(\text{ClO}_4)_3+\text{H}]^{2+}$.2MeOH	1317

Table 2.2: Peak attributions for $[\text{Ni}_4(\text{L1})(\mu_4\text{-OH})(\text{MeOH})_7(\text{H}_2\text{O})](\text{NO}_3)_3$

M/Z	Rel. Intensities	Fragments	Calc. Mass
907	30	$[\text{Ni}_4(\text{L1})(\text{OH})(\text{H}_2\text{O})_3(\text{MeOH})]^{3+}$	909
953	100	$[\text{Ni}_4(\text{L1})(\text{OH})(\text{H}_2\text{O})_2(\text{MeOH})_3]^{3+}$	955
971	100	$[\text{Ni}_4(\text{L1})(\text{OH})(\text{H}_2\text{O})_3(\text{MeOH})_3]^{3+}$	973
1013	15	$[\text{Ni}_4(\text{L1})(\text{OH})(\text{H}_2\text{O})_2(\text{MeOH})(\text{NO}_3)_2]^+$	1015
1027	55	$[\text{Ni}_4(\text{L1})(\text{OH})(\text{H}_2\text{O})(\text{NO}_3)_3+\text{H}]^+$	1027
1083	50	$[\text{Ni}_4(\text{L1})(\text{OH})(\text{H}_2\text{O})_4(\text{MeOH})_2(\text{NO}_3)_2]^+$	1083
1107	20	$[\text{Ni}_4(\text{L1})(\text{OH})(\text{MeOH})_5(\text{NO}_3)_2]^+$	1107
1159	20	$[\text{Ni}_4(\text{L1})(\text{OH})(\text{H}_2\text{O})_3(\text{CH}_3\text{OH})_3(\text{NO}_3)_3+\text{H}]^+$	1160
1252	80	$[\text{Ni}_4(\text{L1})(\text{OH})(\text{CH}_3\text{OH})_7(\text{H}_2\text{O})(\text{NO}_3)_3+\text{H}]^+$	1252

In the case of $[\text{Ni}_4(\text{L1})(\mu_4\text{-OH})(\text{MeOH})_8]\text{Cl}_3$, the relative intensity of the peaks is quite weak with respect to the peak at m/z 219(100) corresponding to the noba matrix or a fragmentation peak of $[\text{Ni}_4(\text{L1})(\mu_4\text{-OH})(\text{MeOH})_8]\text{Cl}_3$. The peak attributions are shown in table 2.3.

Table 2.3: Peak attributions for $[\text{Ni}_4(\text{L1})(\mu_4\text{-OH})(\text{MeOH})_8]\text{Cl}_3$

m/z	Rel. Intensities (%)	Fragments	Calc. Mass
907	15	$[\text{Ni}_4(\text{L1})(\text{OH})(\text{H}_2\text{O})_3(\text{MeOH})]^{3+}$	909
953	13	$[\text{Ni}_4(\text{L1})(\text{OH})(\text{H}_2\text{O})_2(\text{MeOH})_3]^{3+}$	955
971	30	$[\text{Ni}_4(\text{L1})(\text{OH})(\text{H}_2\text{O})_3(\text{MeOH})_3]^{3+}$	973
1083	10	$[\text{Ni}_4(\text{L1})(\text{OH})(\text{MeOH})_6\text{Cl}_2]^+$	1082
1101	20	$[\text{Ni}_4(\text{L1})(\text{OH})(\text{MeOH})_6(\text{H}_2\text{O})\text{Cl}_2]^+$	1100
1256	15	$[\text{Ni}_4(\text{L1})(\text{OH})(\text{MeOH})_8\text{Cl}_3+\text{H}]^+ \cdot 4\text{H}_2\text{O}$	1255
1275	15	$[\text{Ni}_4(\text{L1})(\text{OH})(\text{MeOH})_8\text{Cl}_3+\text{H}]^+ \cdot 5\text{H}_2\text{O}$	1273

Some peaks at higher mass (m/z 1555, 1622, 1702 and 1903) suggest the formation of polymeric species. The relative intensity is very weak ($< 5\%$), which could suggest a lack of solubility in the FAB medium (noba matrix). Another possibility is the

formation of a species like the high nuclearity cluster $\text{Ni}_7(\text{OH})_4(\text{MeO})_2(\text{C}_{12}\text{H}_{13}\text{O}_3)(\text{ClO}_4)_2$ discussed in chapter 5 of this thesis.

In the case of complex $[\text{Ni}_4(\text{L2})(\mu_4\text{-OH})(\text{MeOH})_6(\text{H}_2\text{O})_2](\text{ClO}_4)_3$, the relative intensity of the peaks observed is also quite weak with respect to the highest peak at 219(100). The peak attributions are displayed in table 2.4.

Table 2.4: Peak attribution for $[\text{Ni}_4(\text{L2})(\mu_4\text{-OH})(\text{MeOH})_6(\text{H}_2\text{O})_2](\text{ClO}_4)_3$

m/z	Rel. Intensities (%)	Fragments	Calc. Mass
738	15	$[\text{Ni}_4(\text{L2})(\text{OH})]^{3+}$	739
775	20	$[\text{Ni}_4(\text{L2})(\text{OH})(\text{H}_2\text{O})]^{3+}$	775
795	20	$[\text{Ni}_4(\text{L2})(\text{OH})(\text{H}_2\text{O})_3]^{3+}$	793
837	10	$[\text{Ni}_4(\text{L2})(\text{OH})(\text{ClO}_4)]^{2+}$	838
859	10	$[\text{Ni}_4(\text{L2})(\text{OH})(\text{ClO}_4)(\text{H}_2\text{O})]^{2+}$	856

The macrocyclic nature of all the complexes was supported by the IR spectra with the absence of the amine and carbonyl vibrations associated with the reactants and the presence of an imine stretch at 1645-1649 cm^{-1} . A band at 1540-1545 cm^{-1} can be assigned to the skeletal vibration of the aromatic ring.¹¹⁴ For complex $[\text{Ni}_4(\text{L2})(\mu_4\text{-OH})(\text{MeOH})_6(\text{H}_2\text{O})_2](\text{ClO}_4)_3$ the $\nu_3(\text{ClO}_4^-)$ vibration is clearly split into three bands 1088, 1130 and 1146 cm^{-1} therefore it implies that the counter anion might be weakly coordinated or involved in hydrogen-bonding with the coordinated solvent molecules. The $\nu_4(\text{ClO}_4^-)$ deformation vibration is detected at 626 cm^{-1} . As for complex $[\text{Ni}_4(\text{L1})(\mu_4\text{-OH})(\text{MeOH})_4(\text{H}_2\text{O})_4](\text{ClO}_4)_3$, the $\nu_3(\text{ClO}_4^-)$ stretching vibration and $\nu_4(\text{ClO}_4^-)$ deformation vibration appear at 1104 and 626 cm^{-1} respectively. The broadness of the $\nu_3(\text{ClO}_4^-)$ vibration suggests a relatively unsymmetric environment. For complex $[\text{Ni}_4(\text{L1})(\mu_4\text{-OH})(\text{MeOH})_7(\text{H}_2\text{O})](\text{NO}_3)_3$ the broad $\nu_3(\text{NO}_3^-)$ stretching vibration appears at 1383 cm^{-1} .

The products that were isolated by precipitation using diethylether, after concentration of the reaction mixture, were waxy and turned into a hard solid under vacuum. The recurring problem encountered during the attempts to successively recrystallise the complexes using different combinations of solvents was that the compounds seemed to evolve into oils. This observation is consistent with the large amount of solvent in the formulae. The yields range from *ca.* 25 to 30% and even lower (13%) for $[\text{Ni}_4(\text{L1})(\mu_4\text{-OH})(\text{MeOH})_8]\text{Cl}_3$, which is significantly lower than the yield reported by Kruger for the acetate complex (80%). Also, $[\text{Ni}_4(\text{L1})(\mu_4\text{-OH})(\text{MeOH})_7(\text{H}_2\text{O})](\text{NO}_3)_3$ and $[\text{Ni}_4(\text{L1})(\mu_4\text{-OH})(\text{MeOH})_8]\text{Cl}_3$ are contaminated by $\text{Ni}(\text{NO}_3)_2$ and NiCl_2 , respectively, according to the elemental analysis. Purification of the complexes was tried by chromatography on sephadex LH-20^a (extends gel-filtrations to polar organic solvents) as reported by Schröder *et al.*¹¹⁶ for charged inorganic complexes. Molecules with a molecular weight superior to 3500-5000 cannot diffuse into the gel particles. Consequently, if polymeric species were present in the compounds they would have been separated from the tetranickel complexes. Unreacted starting material was separated first because their diffusion was faster (lower weight molecules). Unfortunately, the attempts to recover the tetranickel species proved unsuccessful, as the complexes tend to decompose on the gel or fail to diffuse through the gel.

The geometry of Ni(II) in a high-spin configuration is preferably octahedral or tetragonal because of its higher LFSE in those configurations. In the tetranuclear nickel(II) complexes described previously the macrocyclic ligand occupies the equatorial coordination sites of the Ni(II) ions, which leaves the axial positions vacant. Ni(II) having a high-spin configuration, tends to complete its coordination sphere. Consequently, forming ladder type complexes,^{41,61} superstructural complexes¹¹⁷ or even polymeric structures is conceivable. It has been seen that

^a Sephadex is a cross-linked polymer derived from dextran (polysaccharide). The chains of dextran are cross-linked by glyceryl bridges. The type of sephadex, LH-20 was prepared by alkylation of most of the hydroxyl groups of sephadex G-25. The proportion of cross-linking determines the size of the largest molecule able to diffuse into the sephadex matrix.¹¹⁵

the core $\text{Cu}_4(\mu_4\text{-OH})(\text{L}2)$ of tetracopper(II) complexes can form a dimer with another tetracopper core, leading to an octanuclear structure.^{94,95} Moreover, the McKee group has previously undertaken some work concerning the aggregation of nickel complexes as molecular building blocks via self-assembly.⁹¹ The aim was to form molecular ladders with macrocyclic molecules as platforms interconnected with bridging dicarboxylic acids. Unfortunately, the polymeric nature of those compounds hindered their isolation and characterisation. Another example of a polymer of a binuclear Ni(II) macrocyclic complex bridged by 1,3-diaminopropane has been reported by Manoharan *et al.*¹¹⁸ (fig. 2.5). The macrocycle was formed by the condensation of 2,6-diformyl-4-methylphenol and 1,3-diaminopropane in boiling water.

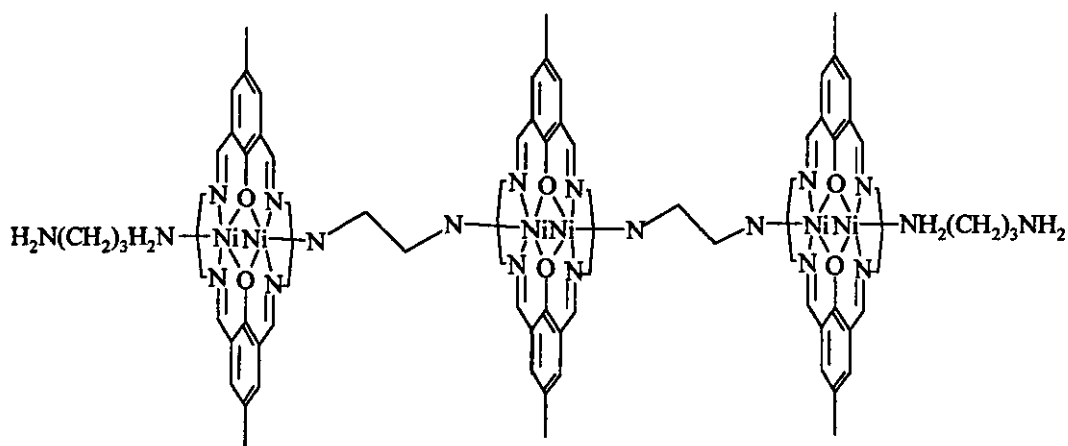


Fig. 2.5: Polymer based on a dinickel(II) Robson-type macrocyclic complex

The water molecules completing the coordination sphere of the nickel ions were omitted in fig. 2.5 for clarity. The isolation of such a complex leads us to think that the formation of a polymeric compound with the macrocyclic units bridged by 1,5-diaminopentan-3-ol could be possible. 1,5-diaminopentan-3-ol, if present in excess, can act as a bidentate axial ligand linking individual tetranuclear macrocyclic complexes of L1 or L2 in an end-to-end fashion as shown in fig. 2.5 for the dinuclear species. The other prospect is the coordination of solvent molecules as neutral

ligands at the vacant sites as in the isolated complexes. All these enumerated tendencies might have an influence on the synthesis and lower the yield of the complexes $[\text{Ni}_4(\text{L1})(\mu_4\text{-OH})(\text{MeOH})_4(\text{H}_2\text{O})_4](\text{ClO}_4)_3$, $[\text{Ni}_4(\text{L2})(\mu_4\text{-OH})(\text{MeOH})_6(\text{H}_2\text{O})_2](\text{ClO}_4)_3$, $[\text{Ni}_4(\text{L1})(\mu_4\text{-OH})(\text{MeOH})_7(\text{H}_2\text{O})](\text{NO}_3)_3$ and $[\text{Ni}_4(\text{L1})(\mu_4\text{-OH})(\text{MeOH})_8]\text{Cl}_3$.

The change of counter anions did not seem to have any influence on the crystallisation in the complexes containing perchlorate, nitrate or chloride. Only complexes with acetate were isolated more easily, presumably because they rendered a neutral compound.

However, the isolation of complexes with weakly coordinating counter anions is encouraging for the study of binding species to the pseudo surface because solvent molecules are easily displaced compared to strongly coordinated acetate molecules.

2.2. Sodium template approach for the synthesis of tetraimine macrocycles by condensing NaDFMP/NaDFTP/NaDFMOP with DAHP or 1,3-diaminopropan-2-ol

Since the size of the cation used as template has proved to be of importance in controlling the synthetic pathway in the Schiff-base system,³ transition metals are generally used for the smaller rings, and rare earth metals for the larger ones. Alkali metals are seldom involved in the formation of a Schiff-base derived macrocycle. They are more commonly used in the synthesis of crown ethers.⁴ However, Fenton *et al.*¹¹⁹ reported a way to employ the sodium ion as an effective template in the synthesis of a series of macrocycles using 2,6-diformyl-4-methylphenolate as a precursor. The yields vary from 26% to 90% depending on the diamine used in the condensation. They have shown, in the case of the Robson macrocycle displayed in fig. 2.6, that the disodium macrocyclic complex used as the “free ligand” readily undergoes transmetallation by transition metals to form dinuclear macrocyclic

complexes with a high yield.⁵⁵ These complexes can also be viewed as sodium salts. Sodium would not be expected to coordinate strongly to medium-soft donors such as nitrogen and might in fact not act as a strong template as in the synthesis of crown-ethers where all the coordinating atoms are oxygens.

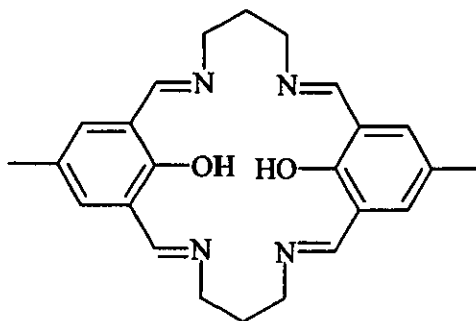


Fig. 2.6: Robson macrocycle

It was decided to employ a similar method to Fenton *et al.*¹¹⁹ to synthesise the disodium complexes of H₄L1, H₄L2, H₄L3, H₄L4 and H₄L5 for several reasons. First, it was expected that these complexes would behave as a “free macrocycle equivalent” and should yield cleaner nickel complexes with nitrate and perchlorate counter-anions, which might be easier to crystallise. Secondly, as the template method previously employed by the McKee group is not well-suited to the preparation of complexes with substitution inert metal ions such as Pd(II) complexes, this method seemed a promising route to new complexes. Complexes with nickel acetate, copper nitrate, manganese acetate and cobalt acetate synthesised *via* the template route using 2,6-diformyl-4-methylphenol (DFMP) or 2,6-diformyl-4-*tert*-butylphenol (DFTP) and 1,5-diaminopentane-2-ol have been previously reported by the McKee group.^{89-91,93,95} Four of those complexes were synthesised using the modified procedure used by Fenton *et al.*¹¹⁹ in order to compare the two methods.

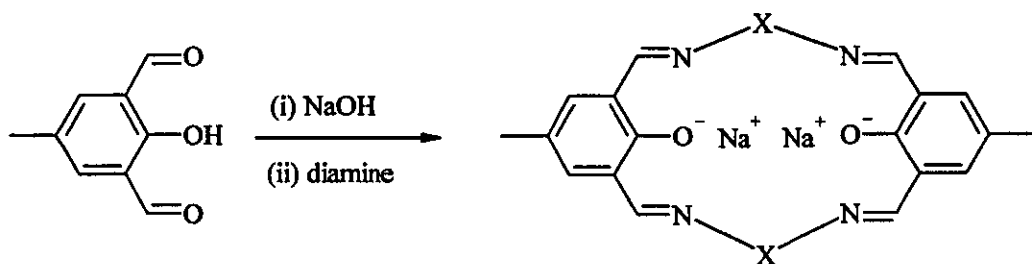
2.2.1. Synthesis and characterisation of the sodium salt of DFMP, DFTP and DFMOP

The synthesis of the sodium salts of DFMP, DFTP and DFMOP were carried out in the presence of NaOH following the procedure described by Fenton *et al.*¹¹⁹ with a similar yield varying from 75 to 85%. Their IR spectra are similar to the protonated ligand, showing the main C=O vibration at *ca.* 1685 cm⁻¹.

2.2.2. Synthesis and characterisation of the sodium salt of the ligand L1, L2, L3, L4, L5

A scheme of the synthetic route is given for L1, L2, L3, L4 and L5 in fig. 2.8.

L1, L2 and L3 were formed by the condensation of DAHP with the corresponding sodium 2,6-diformylphenolate whereas 1,3-diaminopropan-2-ol was used in the synthesis of L4 and L5. The yields for H₂Na₂L1, H₂Na₂L2 and H₂Na₂L4 are 50, 55 and 41% respectively, which is lower than the majority of macrocycles reported by Fenton *et al.*¹¹⁹ (68 to 90%). However, the efficiency of the template reaction depends on the size of the metal ion, the size of the cavity and the donor-atoms of the macrocycle. Therefore the use of other cations like K⁺ or Cs⁺, might improve the yield of the template reaction. The nature of the diamine is likely to have an effect as well; Fenton *et al.*¹¹⁹ did not use amines with pendent alcohol groups. The donor-atoms on the flexible side-chain were incorporated in the carbon backbone, which makes the macrocycles similar to crown ethers or oxo-azacryptands and might be more suited to the use of sodium as a template. A few examples are gathered in fig. 2.7.



Example of diamines used

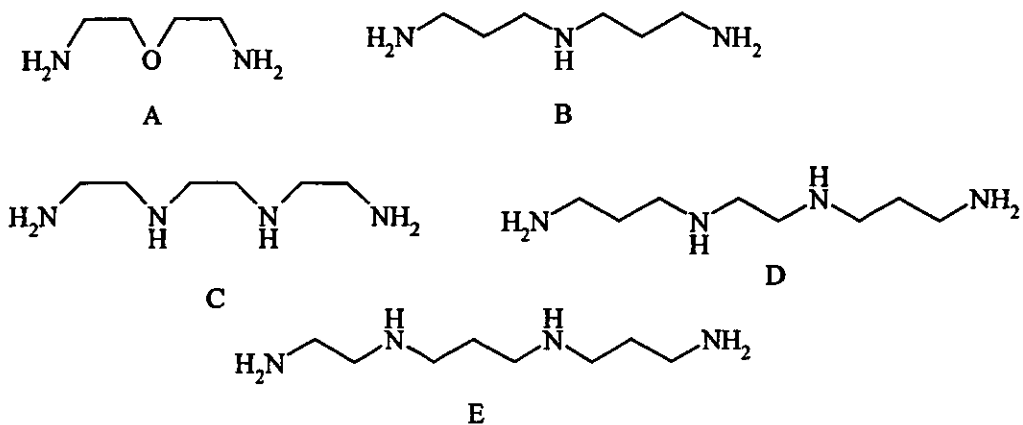


Fig. 2.7: Reaction scheme for Fenton's "free macrocycles"

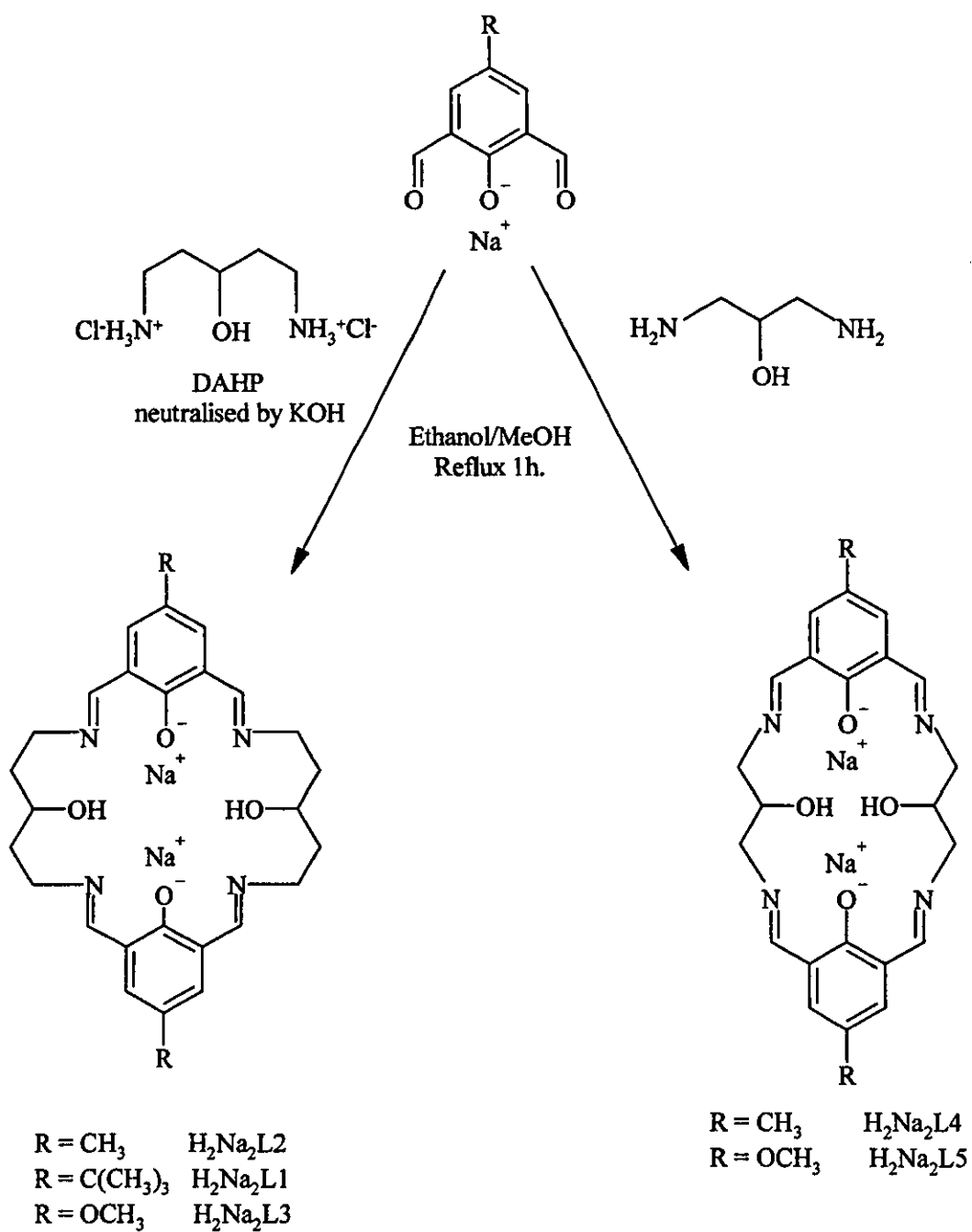


Fig. 2.8: Synthetic route to the “free macrocycles”

For H_2Na_2L3 the synthesis was unfruitful. The product had a gummy texture and was not isolated with reasonable purity. Moreover, it proved to be quite insoluble, which can be characteristic of a polymeric compound. Since the product is quasi insoluble, the FAB spectrum obtained is very weak. Nevertheless FAB results suggest the [2+2]-condensation product did form but as a minor product. Two peaks at m/z 615 and m/z 637 can be assigned to $[Na_4L3+H]^+$ and $[Na_4L3+Na]^+$ respectively. This observation could mean that the complex lost two protons and gained two sodium ions to balance the charge during the FAB experiment but the possibility that this occurred during the synthesis cannot be rejected.

In the case of H_2Na_2L1 , H_2Na_2L2 and H_2Na_2L4 the FAB spectra confirmed the formation of the [2+2]-condensation product. The peak assignments are displayed in tables 2.5, 2.6 and 2.7.

Table 2.5: Peak attributions for H_2Na_2L1

m/z	Rel. Intensities (%)	Fragments	Calc. Mass
577	100	$[H_4L1+H]^+$	577
593	7	$[H_4L1+H]^+ \cdot H_2O$	595
599	30	$[H_3NaL1+H]^+$ or $[H_4L1+Na]^+$	600

The minor peaks observed are due to fragmentation (m/z 560, 545, 516, 413, 390, 344 and below).

Table 2.6: Peak attributions for H_2Na_2L2

m/z	Rel. Intensities (%)	Fragments	Calc. Mass
493	30	$[H_4L2+H]^+$	493
515	10	$[H_3NaL2+H]^+$ or $[H_4L2+Na]^+$	515
535	7	$[H_2Na_2L2+H]^+$	537
561	5	$[H_2Na_2L2+Na]^+$	560

Three main peaks at m/z 165(80), 192(85), 286(65) and two other minor peaks at m/z 345(25) and 433(10) are a result of the fragmentation of the macrocycle.

Table 2.7: Peak attributions for H_2Na_2L4

m/z	Rel. Intensities (%)	Fragments	Calc. Mass
437	18	$[H_4L4+H]^+$	437
458	20	$[H_3NaL4+H]^+$ or $[H_4L4+Na]^+$	459
527	15	$[Na_4L2+H]^+$	525
549	40	$[Na_4L2+Na]^+$	547

The minor peaks observed are due to the fragmentation (m/z 413, 391, 375, 353 and below).

The parent molecular ion was observed for H_2Na_2L2 (m/z 537) but not for H_2Na_2L1 and H_2Na_2L4 .

The peak at m/z 599 for H_2Na_2L1 , m/z 515 for H_2Na_2L2 and m/z 458 for H_2Na_2L4 can be attributed to the fully protonated neutral ligand or the complex with the loss of one sodium ion and the gain of one proton. The peaks at m/z 577 and 593 for H_2Na_2L1 and m/z 493 for H_2Na_2L2 can be attributed to the fully protonated neutral ligand. For H_2Na_2L4 , the peak at m/z 437 can be attributed to the fully protonated neutral ligand and the peaks at m/z 527 and m/z 549 can be assigned to $[Na_4L4+H]^+$ and $[Na_4L4+Na]^+$ respectively. The presence of four sodium cations has been observed previously for H_2Na_2L3 .

In the complexes reported by Fenton *et al.*,¹¹⁹ (with one exception for the Robson-type macrocycle) the parent sodium complex (Na_2L) was not observed. For all the complexes with one exception (condensation with diamine C in fig. 2.7), peaks for the fully protonated neutral ligand were observed. Peaks attributed to the loss of a sodium cation with the gain of one proton were also detected. However, the detection

of peaks assigned to the fully protonated neutral ligand leads to the hypothesis of the synthesis of a “free macrocyclic ligand” and not the actual disodium complex but the elemental analysis is consistent with the latter in the case of H_2Na_2L1 , H_2Na_2L2 and H_2Na_2L4 . Very recently, Schröder *et al.*⁴⁰ reported the synthesis of the Robson macrocycle derived from 2,6-diformyl-4-*tert*-butylphenol as a genuine free ligand (H_2L). The reaction of equimolar amount of 2,6-diformyl-4-*tert*-butylphenol and 1,3-diaminopropane with an excess of HBr in MeOH followed by the addition of excess NH_4PF_6 afforded the diprotonated ligand $[H_4L](PF_6)_2$ which, when reacted with five equivalents of Et_3N , afforded the free Robson ligand H_2L . Previous communications by Schröder *et al.*,^{39,120} reported the synthesis of the diprotonated salt $[H_4L]^{2+}$ *via* cyclisation of components under acidic conditions. Consequently, it would be interesting to carry out the synthesis of H_4L1 , H_4L2 , H_4L3 , H_4L4 and H_4L5 under acidic conditions in order to obtain genuine free ligands. McKee¹²¹ proved to be successful in producing the diprotonated ligand $[H_6L4(H_2O)_2](ClO_4)_2$ by reacting DFMP and 1,3-diaminopropan-2-ol in the presence of $HClO_4$. However, Kruger found that the reaction in MeOH of DFMP with DAHP in the presence of HBr and an excess of Br_2 did not afford the desired salt of the macrocycle but the hydrobromo salt of the diamine. Furthermore, the reaction of DFMP with DAHP.2HCl in an acetic acid/acetate buffered solution, whilst indicating the presence of some macrocyclic species, was found not to be suitable for the isolation of pure product. Moreover, the use of $HClO_4$ instead of HBr in refluxed MeOH did not generate any macrocyclic species but a mixture of starting materials.

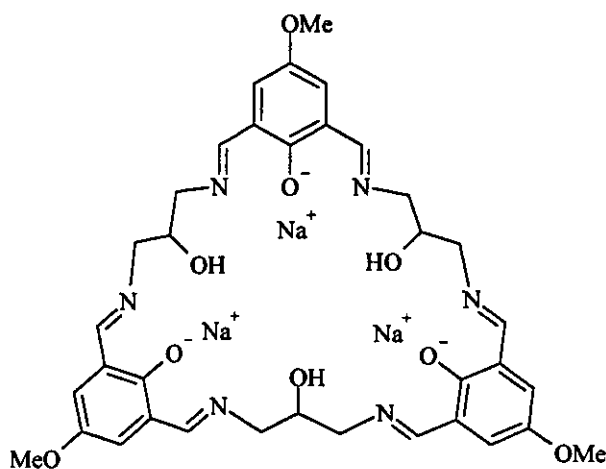
The synthesis of H_2Na_2L5 , unfortunately led to a mixture of compounds. The peak attributions are given in table 2.8.

Table 2.8: Peak attributions for the synthesis of H₂Na₂L5

m/z	Rel. Intensities (%)	Fragments	Calc. Mass
491	100	[H ₃ NaL5+H] ⁺ or [H ₄ L5+Na] ⁺	491
703	15	[H ₄ L5+H] ⁺	703
725	25	[H ₃ NaL6+H] ⁺ or [H ₆ L6+Na] ⁺	725
743	10	[H ₃ NaL6+H] ⁺ .H ₂ O or [H ₆ L6+Na] ⁺ .H ₂ O	743
959	15	[H ₇ NaL7+H] ⁺ or [H ₈ L7+Na] ⁺	959
981	5	[H ₇ NaL7+Na] ⁺	983

The main peak at m/z 491(100) is assigned to the [2+2]-condensation product and can be attributed to the protonated ligand or the complex with the loss of one sodium ion ([H₃NaL5+H]⁺ or [H₄L5+Na]⁺). Peaks detected at m/z 905, 671, 665, 437, 413 and below are due to the fragmentation processes for the different ligands present.

The peak at m/z 725(25) can be assigned to the [3+3]-condensation product shown in fig. 2.9. The formation of this ligand is not totally surprising. Indeed, the condensation of DFMP or DFTP with 1,3-diaminopropan-2-ol in the presence of copper or nickel has rendered similar ligands.^{69,111}

**Fig. 2.9:** H₃Na₃L6

A very important fact that is essential in the synthesis of the [3+3]-condensation product is that the reaction has to be performed in the presence of triethylamine to deprotonate the secondary alcohol group of 1,3-diaminopropan-2-ol, which is then involved in the metal coordination. Consequently, those [3+3] macrocycles can accommodate six metal ions but the reported structures consist of a dodecanuclear dimer and can be described as hexagonal cyclic arrays of metal centres linked axially through hydroxo bridges. It is very interesting to note that it is possible to synthesise this macrocycle using sodium as a template and obtain a “free ligand”. The FAB results mainly show the protonated ligand but it does not rule out that during the reaction three or more sodium cations were necessary for the synthesis of the [3+3]-condensation product. The reason why it formed in those conditions is not known but an alkaline impurity might be enough to trigger the reaction as triethylamine was necessary in Tandon’s synthesis.^{69,111} The sodium salt of DFMOP might have been slightly contaminated by NaOH.

The peak at m/z 959(25) can be assigned to the [4+4]-condensation product shown in fig. 2.10.

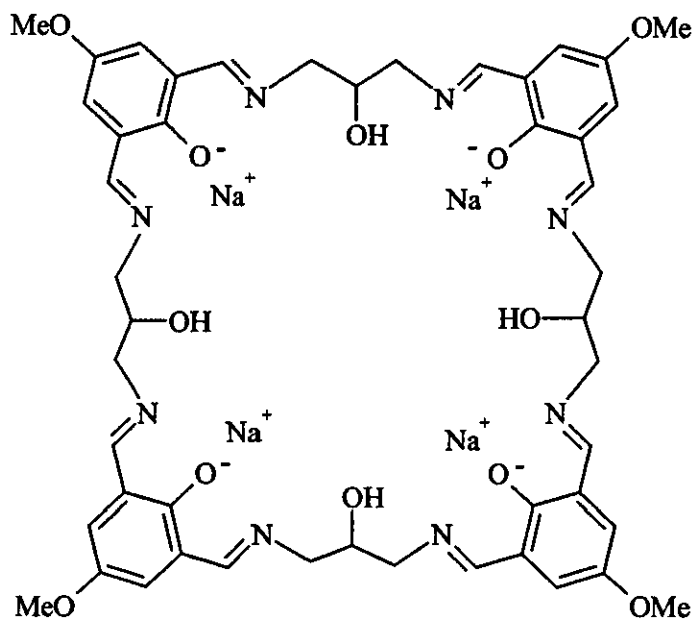


Fig. 2.10: $H_4Na_4L_7$

A similar ligand using 2,6-diacetylpyridine instead of DFMOP has been reported by McKee.⁸² Template (Ba^{2+}) condensation of 2,6-diacetylpyridine with 1,3-diaminopropan-2-ol, followed by transmetallation produces a tetranuclear [4+4] $\text{Mn}(\text{ClO}_4)_2$ complex, with deprotonation and coordination of the hydroxo group belonging to the diamine. In this case the macrocycle is forming during the transmetallation followed by the formation of Mn-alkoxide bonds between two binuclear macrocyclic units in a cofacial orientation. This configuration allows the two units to react *via* transamination to form the [4+4] macrocycle. Again, it is of interest to note that this type of macrocycle can be synthesised using sodium as a template to obtain a “free ligand”. Indeed, the ligand $\text{H}_8\text{L7}$ could accommodate a large number of metals and be interesting in the study of magnetic interactions. The FAB results mainly show the protonated ligand but it does not rule out that during the reaction four or more sodium cations were necessary for the synthesis of the [4+4]-condensation product. The reason why it formed in those conditions is not known but it might be related with the number of sodium cations available.

The IR spectra of complexes $\text{H}_2\text{Na}_2\text{L1}$, $\text{H}_2\text{Na}_2\text{L2}$ and $\text{H}_2\text{Na}_2\text{L4}$ showed no bands characteristic of the stretching frequency of the C=O groups in sodium 2,6-diformyl-R-phenolate, nor the symmetric and unsymmetric stretching frequencies for the primary amine groups. Sodium complexes, however, all possess a very strong band at *ca.* 1638 cm^{-1} assigned to the imino stretching mode, supporting the Schiff-base linkage. Strong peaks in the range $1522\text{-}1529\text{ cm}^{-1}$ are attributable to the phenolic C-O groups acquiring partial double bond character through conjugation with the imine system in the chelate ring.⁴² All compounds exhibit strong broad bands between 3375 and 3395 cm^{-1} indicative of $\nu(\text{OH})$ stretching vibrations of water, which is not surprising because Fenton *et al.*¹¹⁹ reported the hygroscopic character of similar compounds.

2.3. Complex syntheses using the “free macrocycles” H₂Na₂L1 and H₂Na₂L2

2.3.1. Complexes with nickel perchlorate and nickel nitrate

Nickel complexes containing non-coordination or weakly coordinating anions have been detected by IR and FAB spectrometry but, so far, they proved to be difficult to crystallise. The nickel complex formed by complexation of Na₂H₂L1 with nickel perchlorate seems to be a tetranuclear species according to the FAB (table 2.9). However, the fact that the relative intensity of the peaks is very weak leads to the hypothesis of a polymeric product with a small amount of tetranuclear species. So far, this method employed with perchlorate anions does not seem to have improved the outcome of the reaction. Purification of the compound by recrystallisation failed because the product turned into an oil.

Table 2.9: Peak attributions for [Ni₄(L1)(OH)(H₂O)₄(MeOH)₄](ClO₄)₃

m/z	Rel. Intensities (%)	Fragments	Calc. Mass
953	5	[Ni ₄ (L1)(OH)(H ₂ O) ₂ (MeOH) ₃] ³⁺	955
971	5	[Ni ₄ (L1)(OH)(H ₂ O) ₃ (MeOH) ₃] ³⁺	973
1027	5	[Ni ₄ (L1)(OH)(H ₂ O) ₄ (MeOH)(ClO ₄)] ²⁺	1027

However, in the course of this work a complex with coordinated nitrate anions and MeOH molecules was isolated. The complex [Ni₄(L2)(OH)(NO₃)₂(MeOH)₄](NO₃) was synthesised by complexation of the pseudo-free ligand Na₂H₂L2 with nickel nitrate. The synthesis was carried out twice. The first time, only the crystal structure was determined. Green crystals of [Ni₄(L2)(OH)(NO₃)₂(MeOH)₄](NO₃). 3.5MeOH suitable for X-ray studies were grown by slow evaporation of a methanol solution of the compound. The second time however, no crystals suitable for X-ray studies were isolated. Nevertheless, the elemental analysis results combined with those of IR spectroscopy seem to confirm the crystal structure determined previously. The IR shows nitrate vibrations indicative of both coordinated (1331 and 1439 cm⁻¹) and free

(1385 cm^{-1}) nitrate ions, which is consistent with the formula. The structure of the cation $[\text{Ni}_4(\text{L2})(\text{OH})(\text{NO}_3)_2(\text{MeOH})_4]^+$ is shown in fig. 2.11.

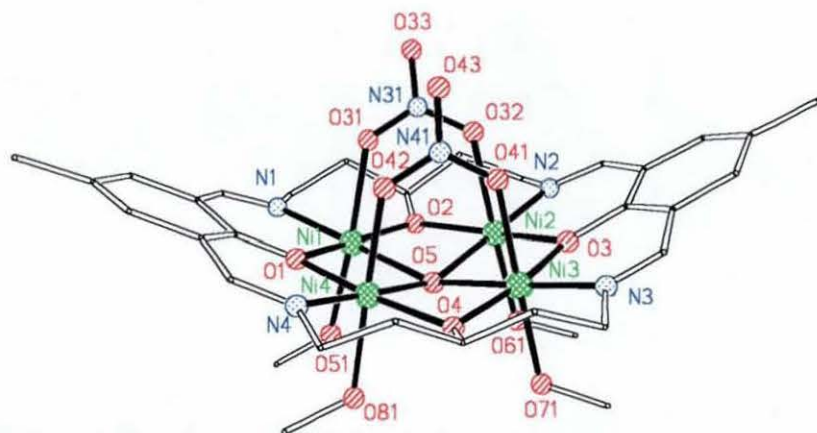


Fig. 2.11: Structure of the cation $[\text{Ni}_4(\text{L2})(\text{OH})(\text{NO}_3)_2(\text{MeOH})_4]^+$

The complex $[\text{Ni}_4(\text{L2})(\text{OH})(\text{NO}_3)_2(\text{MeOH})_4](\text{NO}_3) \cdot 3.5\text{MeOH}$ contains four nickel ions separated each by *ca.* 3 Å in a roughly planar array. The macrocycle provides three donors for each nickel, one phenoxy oxygen, one alkoxo oxygen and one imine nitrogen. The nickel ions are closely interacting through phenoxo and alkoxo bridges and share a central hydroxy donor. The four nickel ions form a tetranickel array in which the Ni-O distance is on average 2.038(6) Å. The central μ_4 -hydroxy donor sits slightly out of the plane (0.41(1) Å) giving the array a convex and a concave side, which is accentuated by the bending of the macrocyclic molecule. The bending of the nickel oxo array along the axis that passes through the pendent alkoxo groups and the central μ_4 -hydroxy is caused by two bridging nitrate molecules situated on the concave side of the macrocycle. The bending of the macrocycle appears necessary in order to have a geometry as near to octahedral as possible around the nickel atoms. Both nitrate anions form three-atom bridges between a pair of nickel ions, parallel to the long axis of the macrocycle. On the convex side of the array the coordination sphere of each nickel atoms is completed by one MeOH molecule. All the X-ray data collection parameters for $[\text{Ni}_4(\text{L2})(\text{OH})(\text{NO}_3)_2(\text{MeOH})_4](\text{NO}_3) \cdot 3.5\text{MeOH}$ are

summerised in table 1 in annex 1, along with the details concerning the refinement and disorders. The selected bond lengths and angles are displayed in table 2.10.

Table 2.10: Selected bond lengths [Å] and angles [°] for
 $[\text{Ni}_4(\text{L2})(\text{OH})(\text{NO}_3)_2(\text{MeOH})_4](\text{NO}_3)_3 \cdot 3.5\text{MeOH}$

Ni(1)-O(2)	1.946(5)	Ni(2)-Ni(3)	3.0571(15)
Ni(1)-N(1)	1.987(7)	Ni(3)-O(4)	1.959(5)
Ni(1)-O(1)	1.995(5)	Ni(3)-N(3)	1.962(7)
Ni(1)-O(51)	2.118(5)	Ni(3)-O(3)	1.992(5)
Ni(1)-O(5)	2.170(5)	Ni(3)-O(71)	2.109(5)
Ni(1)-O(31)	2.236(6)	Ni(3)-O(41)	2.153(5)
Ni(1)-Ni(2)	2.9928(13)	Ni(3)-O(5)	2.169(5)
Ni(1)-Ni(4)	3.0532(14)	Ni(3)-Ni(4)	2.9472(14)
Ni(2)-O(2)	1.971(6)	Ni(4)-O(4)	1.955(6)
Ni(2)-O(3)	1.972(5)	Ni(4)-O(1)	1.996(5)
Ni(2)-N(2)	1.983(7)	Ni(4)-N(4)	2.000(7)
Ni(2)-O(61)	2.121(5)	Ni(4)-O(81)	2.107(5)
Ni(2)-O(5)	2.181(5)	Ni(4)-O(42)	2.129(6)
Ni(2)-O(32)	2.261(6)	Ni(4)-O(5)	2.155(5)
O(2)-Ni(1)-N(1)	97.7(3)	O(51)-Ni(1)-O(31)	175.9(2)
O(2)-Ni(1)-O(1)	168.2(2)	O(5)-Ni(1)-O(31)	91.8(2)
N(1)-Ni(1)-O(1)	91.5(3)	O(2)-Ni(1)-Ni(2)	40.49(16)
O(2)-Ni(1)-O(51)	94.3(3)	N(1)-Ni(1)-Ni(2)	136.1(2)
N(1)-Ni(1)-O(51)	89.2(2)	O(1)-Ni(1)-Ni(2)	128.47(15)
O(1)-Ni(1)-O(51)	93.2(2)	O(51)-Ni(1)-Ni(2)	103.68(17)
O(2)-Ni(1)-O(5)	85.6(2)	O(5)-Ni(1)-Ni(2)	46.70(13)
N(1)-Ni(1)-O(5)	176.2(3)	O(31)-Ni(1)-Ni(2)	79.31(14)
O(1)-Ni(1)-O(5)	85.0(2)	O(2)-Ni(1)-Ni(4)	129.87(16)
O(51)-Ni(1)-O(5)	92.3(2)	N(1)-Ni(1)-Ni(4)	131.5(2)
O(2)-Ni(1)-O(31)	86.2(2)	O(1)-Ni(1)-Ni(4)	40.11(14)
N(1)-Ni(1)-O(31)	86.7(2)	O(51)-Ni(1)-Ni(4)	95.02(19)
O(1)-Ni(1)-O(31)	86.9(2)	O(5)-Ni(1)-Ni(4)	44.88(13)

O(31)-Ni(1)-Ni(4)	87.72(16)	O(4)-Ni(3)-O(3)	169.5(2)
Ni(2)-Ni(1)-Ni(4)	89.53(4)	N(3)-Ni(3)-O(3)	92.8(3)
O(2)-Ni(2)-O(3)	167.7(2)	O(4)-Ni(3)-O(71)	88.7(2)
O(2)-Ni(2)-N(2)	97.5(3)	N(3)-Ni(3)-O(71)	91.5(3)
O(3)-Ni(2)-N(2)	92.5(3)	O(3)-Ni(3)-O(71)	92.5(2)
O(2)-Ni(2)-O(61)	93.6(2)	O(4)-Ni(3)-O(41)	91.2(2)
O(3)-Ni(2)-O(61)	93.6(2)	N(3)-Ni(3)-O(41)	88.2(3)
N(2)-Ni(2)-O(61)	90.3(3)	O(3)-Ni(3)-O(41)	87.6(2)
O(2)-Ni(2)-O(5)	84.71(19)	O(71)-Ni(3)-O(41)	179.7(2)
O(3)-Ni(2)-O(5)	84.9(2)	O(4)-Ni(3)-O(5)	84.8(2)
N(2)-Ni(2)-O(5)	176.2(3)	N(3)-Ni(3)-O(5)	177.6(3)
O(61)-Ni(2)-O(5)	92.7(2)	O(3)-Ni(3)-O(5)	84.8(2)
O(2)-Ni(2)-O(32)	85.5(2)	O(71)-Ni(3)-O(5)	88.4(2)
O(3)-Ni(2)-O(32)	88.2(2)	O(41)-Ni(3)-O(5)	92.0(2)
N(2)-Ni(2)-O(32)	84.8(3)	O(4)-Ni(4)-O(1)	170.5(2)
O(61)-Ni(2)-O(32)	174.8(2)	O(4)-Ni(4)-N(4)	98.5(3)
O(5)-Ni(2)-O(32)	92.2(2)	O(1)-Ni(4)-N(4)	90.9(3)
O(2)-Ni(2)-Ni(1)	39.86(15)	O(4)-Ni(4)-O(81)	87.3(2)
O(3)-Ni(2)-Ni(1)	128.35(16)	O(1)-Ni(4)-O(81)	93.6(2)
N(2)-Ni(2)-Ni(1)	135.0(2)	N(4)-Ni(4)-O(81)	92.2(3)
O(61)-Ni(2)-Ni(1)	103.30(15)	O(4)-Ni(4)-O(42)	90.9(2)
O(5)-Ni(2)-Ni(1)	46.39(12)	O(1)-Ni(4)-O(42)	88.3(2)
O(32)-Ni(2)-Ni(1)	79.22(15)	N(4)-Ni(4)-O(42)	87.1(3)
O(2)-Ni(2)-Ni(3)	129.31(16)	O(81)-Ni(4)-O(42)	178.0(2)
O(3)-Ni(2)-Ni(3)	39.78(15)	O(4)-Ni(4)-O(5)	85.3(2)
N(2)-Ni(2)-Ni(3)	132.1(2)	O(1)-Ni(4)-O(5)	85.3(2)
O(61)-Ni(2)-Ni(3)	95.69(15)	N(4)-Ni(4)-O(5)	176.2(3)
O(5)-Ni(2)-Ni(3)	45.20(12)	O(81)-Ni(4)-O(5)	87.4(2)
O(32)-Ni(2)-Ni(3)	88.82(16)	O(42)-Ni(4)-O(5)	93.5(2)
O(4)-Ni(3)-N(3)	97.6(3)		

As shown in fig. 2.12, both nitrate anions lean away from the vertical to the plane of the four nickel atoms ($56.30(25)^\circ$ and $88.02(21)^\circ$). For the nitrate bridging Ni1 and Ni2 the angle is bigger; this is probably a consequence from the packing mainly

dictated by the hydrogen-bonding linking individual macrocyclic molecules. Each nitrate ion is hydrogen-bonded to two MeOH molecules belonging to an adjacent tetranuclear array. The stronger hydrogen-bonds involve the nitrate anion (N(31)O(31)O(32)O(33)) and the MeOH molecules C(51A)O(51A)H(51A) C(61A)O(61A)H(61A), 2.712(8) Å and 2.694(7) Å respectively, which explains the weaker coordination of this nitrate anion to the nickel atoms. The bond lengths and angles involved in hydrogen-bonding are displayed in table 2.11.

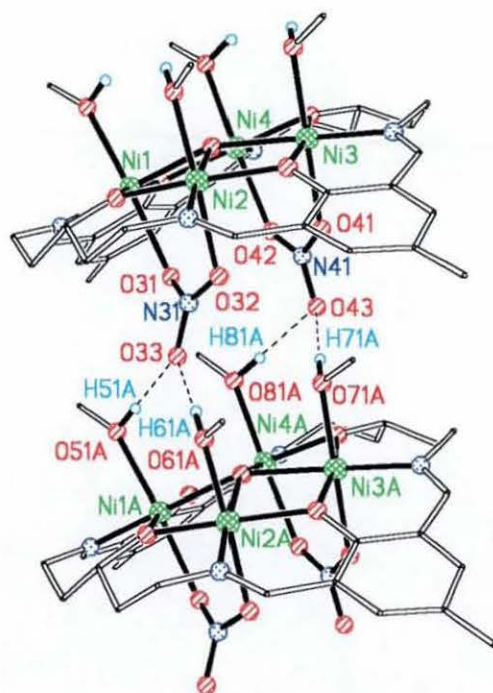


Fig. 2.12: Structure of the cation $[\text{Ni}_4(\text{L}2)(\text{OH})(\text{NO}_3)_2(\text{MeOH})_4]^+$ showing two individual macrocyclic molecules linked *via* hydrogen-bonding

Table 2.11: Hydrogen bonds [\AA and $^\circ$] for $[\text{Ni}_4(\text{L1})(\text{OH})(\text{MeOH})_4(\text{NO}_3)_2] \cdot (\text{NO}_3) \cdot 3.5\text{MeOH}$

D-H...A	d(D-H)	d(H...A)	d(D...A)	<(DHA)
O(51)-H(51)...O(33)*	0.86	1.86	2.721(8)	179.0
O(61)-H(61)...O(33)*	0.86	1.83	2.694(7)	179.0
O(71)-H(71)...O(43)*	0.85	1.91	2.755(8)	179.0
O(81)-H(81)...O(43)*	0.85	1.93	2.782(8)	179.9

Symmetry transformations used to generate equivalent atoms: (*) x-1, y, z

Table 2.12: Peak attributions for $[\text{Ni}_4(\text{L1})(\text{OH})(\text{MeOH})_4(\text{NO}_3)_2] \cdot (\text{NO}_3) \cdot 3.5\text{MeOH}$

m/z	Rel. Intensities (%)	Fragments	Calc. Mass
739	25	$[\text{Ni}_4(\text{C}_{28}\text{H}_{32}\text{N}_4\text{O}_4)(\text{OH})]^{3+}$	737
750	20	$[\text{Ni}_4(\text{C}_{28}\text{H}_{32}\text{N}_4\text{O}_4)(\text{OH})(\text{H}_2\text{O})]^{3+}$	755
772	15	$[\text{Ni}_4(\text{C}_{28}\text{H}_{32}\text{N}_4\text{O}_4)(\text{OH})(\text{H}_2\text{O})_2]^{3+}$	773
800	7	$[\text{Ni}_4(\text{C}_{28}\text{H}_{32}\text{N}_4\text{O}_4)(\text{OH})(\text{NO}_3)]^{2+}$	799
891	10	$[\text{Ni}_4(\text{C}_{28}\text{H}_{32}\text{N}_4\text{O}_4)(\text{OH})(\text{MeOH})(\text{NO}_3)_2]^+$	893
833	15	$[\text{Ni}_4(\text{C}_{28}\text{H}_{32}\text{N}_4\text{O}_4)(\text{OH})(\text{MeOH})(\text{NO}_3)]^{2+}$	831
905	10	$[\text{Ni}_4(\text{C}_{28}\text{H}_{32}\text{N}_4\text{O}_4)(\text{OH})(\text{MeOH})(\text{H}_2\text{O})(\text{NO}_3)_2]^+$	910

The FAB spectrum shows the formation of the tetranuclear nickel complex but does not give any information concerning the coordination or non-coordination of the nitrate anions. The relative intensity of the peaks is weak in respect to the highest peak at m/z 115(100) (fragmentation of the compound or noba matrix) and might be indicative of a poor solubility in the noba matrix. Indeed, once isolated, it is more difficult to resolubilise the compound. This feature is not totally surprising considering that each macrocyclic molecule is linked to adjacent molecules through a network of hydrogen-bonding (difficult to break) forming chains as depicted in fig. 2.13.

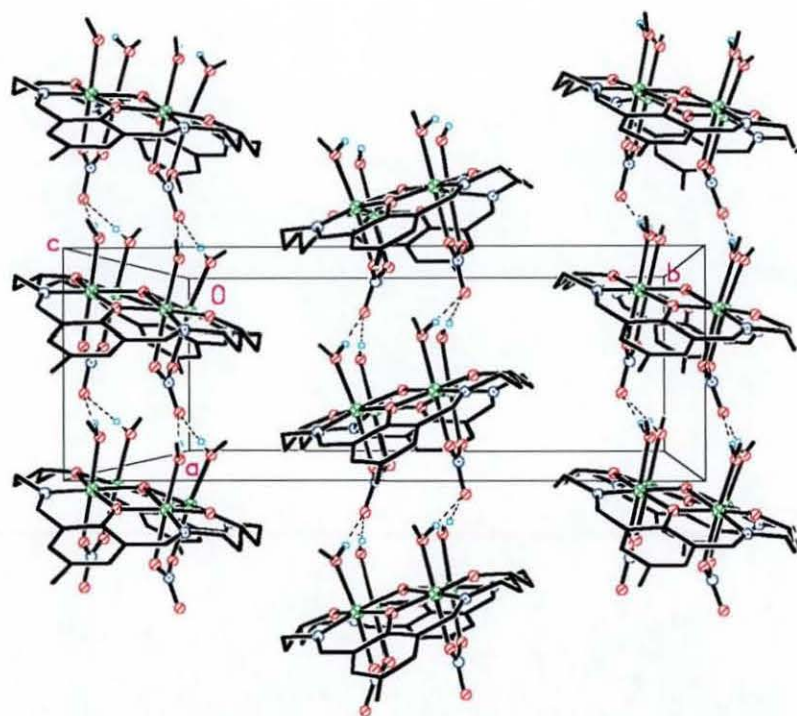


Fig. 2.13: Packing diagram of the cation $[\text{Ni}_4(\text{L1})(\text{OH})(\text{MeOH})_4(\text{NO}_3)_2]^+$

2.3.2. Structures with nickel acetate

In the course of this work a tetranickel complex was prepared by complexation of nickel acetate with the already pre-formed macrocycle $\text{H}_2\text{Na}_2\text{L2}$. No crystals suitable for X-ray analysis were isolated. According to the elemental analysis the formula could be $[\text{Ni}_4(\text{L2})(\text{OH})(\text{OAc})_2(\text{MeOH})_4](\text{OAc})$ or $[\text{Ni}_4(\text{L2})(\text{OH})(\text{OAc})_3(\text{MeOH})_2] \cdot 2\text{MeOH}$. In this case, the yield (34%) was not improved compared to the complex isolated by Kruger⁹⁰ (80%) but significantly improved the yield reported by Metcalfe⁹¹ (15%). The IR spectrum is consistent with acetate being present. Two strong bands at 1456 and 1406 cm^{-1} can be assigned to symmetrical $\nu(\text{COO})$ vibrations. The bands corresponding to the asymmetrical $\nu(\text{COO})$ vibrations are likely to be found in the strong band at 1592 cm^{-1} where $\nu(\text{C}=\text{C})$, $\nu(\text{C}-\text{O})$ and $\nu(\text{COO})$ vibrations can overlap. The presence of two symmetrical bands can be indicative of

two acetate anions in a different environment. In this case, it is difficult to predict if all acetate anions adopt a bridging coordination mode or if one is non-coordinating without crystallographic evidence. The FAB spectrum shows three peaks, consistent with the formula. The peak assignments are displayed in table 2.13.

Table 2.13: Peak attributions for $[\text{Ni}_4(\text{L2})(\text{OH})(\text{OAc})_2(\text{MeOH})_4](\text{OAc})$ or $[\text{Ni}_4(\text{L2})(\text{OH})(\text{OAc})_3(\text{MeOH})_2].2\text{MeOH}$.

m/z	Rel. Intensities (%)	Fragments	Calc. Mass
738	25	$[\text{Ni}_4(\text{L2})(\text{OH})]^{3+}$	739
797	20	$[\text{Ni}_4(\text{L2})(\text{OH})(\text{OAc})]^{2+}$	798
859	5	$[\text{Ni}_4(\text{L2})(\text{OH})(\text{OAc})(\text{MeOH})_2]^{2+}$	862

If the formula $[\text{Ni}_4(\text{L2})(\text{OH})(\text{OAc})_2(\text{MeOH})_4](\text{OAc})$ proves to be correct, a possible structure (A) could be similar to that of $[\text{Ni}_4(\text{L1})(\text{OH})(\text{MeOH})_4(\text{NO}_3)_2](\text{NO}_3)$ with the bridging nitrate anions replaced by bridging acetate molecules. If, on the other hand, the synthesised complex is $[\text{Ni}_4(\text{L2})(\text{OH})(\text{OAc})_3(\text{MeOH})_2]$, the structure (B) is very likely to be similar to the first tetranickel complex $[\text{Ni}_4(\text{L1})(\mu_4\text{-OH})(\text{OAc})_3(\text{HOAc})_2]$ of this system, isolated and fully characterised by Kruger⁹⁰ (fig. 2.14). In the complex $[\text{Ni}_4(\text{L2})(\text{OH})(\text{OAc})_3(\text{MeOH})_2]$, both acetic acid molecules are replaced by MeOH molecules. The complex $[\text{Ni}_4(\text{L1})(\mu_4\text{-OH})(\text{OAc})_3(\text{HOAc})_2]$ was formed *via* a template route using 2,6-diformyl-4-*tert*-butylphenol (DFTP) and 1,5-diaminopentan-3-ol (DAHP).

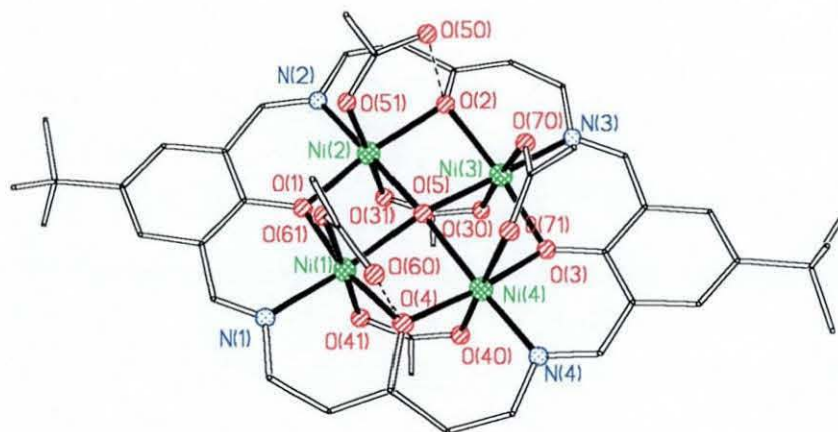


Fig. 2.14: Structure of $[\text{Ni}_4(\text{L1})(\mu_4\text{-OH})(\text{OAc})_3(\text{HOAc})_2]$

The tetranickel array is similar to that of complex $[\text{Ni}_4(\text{L1})(\text{OH})(\text{MeOH})_4(\text{NO}_3)_2](\text{NO}_3) \cdot 3.5\text{MeOH}$ described previously in section 2.3.1. Here again, the central μ_4 -hydroxy donor sits slightly out of the plane giving the array a concave and a convex side but not as pronounced as in complex $[\text{Ni}_4(\text{L1})(\text{OH})(\text{MeOH})_4(\text{NO}_3)_2](\text{NO}_3) \cdot 3.5\text{MeOH}$. Three bridging acetate molecules are causing a slight bending of the nickel oxo array along the axis that passes through the pendent alkoxy groups and the central μ_4 -hydroxy. Both acetate molecules situated on the concave side of the array form three-atom bridges between a pair of nickel ions, parallel to the long axis of the macrocycle, similar to the nitrate anions in complex $[\text{Ni}_4(\text{L1})(\text{OH})(\text{MeOH})_4(\text{NO}_3)_2](\text{NO}_3) \cdot 3.5\text{MeOH}$. In complex $[\text{Ni}_4(\text{L1})(\mu_4\text{-OH})(\text{OAc})_3(\text{HOAc})_2]$ the bending of the macrocycle is smaller probably due to the third bridging acetate molecule (bridges two nickel ions in the parallel direction to the short axis of the macrocycle) coordinated on the convex side of the array partially compensating the effect of the acetate molecules situated on the other side of the array. Another factor that could influence this latter feature (bending of the macrocycle) is the different bridge sizes of the nitrate and acetate bridges. The acetate groups are roughly orthogonal to the plane of the array and slightly twisted in the plane of coordination. The twist in the coordination plane appears necessary for the oxygen to coordinate as near as possible

to 90° to the plane of each nickel and allow a geometry as near to octahedral as possible around the metal. The two other nickel ions are coordinated each to an acetic acid molecule making each nickel 6-coordinate. Each alkoxo group is pulled up from the Ni-O array by the hydrogen-bonding to one of the acetic acid molecules.

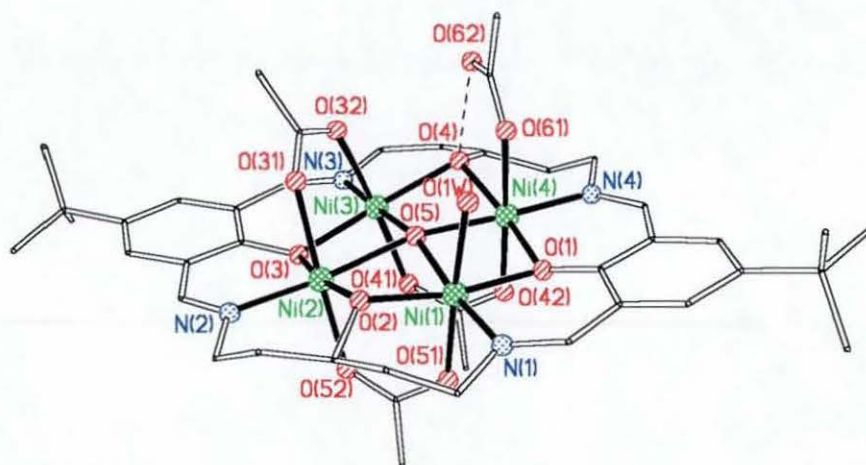


Fig. 2.15: Structure of $[\text{Ni}_4(\text{L1})(\mu_4\text{-OH})(\text{OAc})_3(\text{HOAc})(\text{H}_2\text{O})]$

Another similar structure, $[\text{Ni}_4(\text{L1})(\mu_4\text{-OH})(\text{OAc})_3(\text{HOAc})(\text{H}_2\text{O})]$, has been isolated by Metcalfe⁹¹ using the same procedure. The different structure might have been a result of the recrystallisation process. In this complex (fig. 2.15), one acetic acid molecule has been replaced by a water molecule. The three acetate groups remain largely unaffected by the changes to the macrocyclic geometry due to the replacement of a non-bridging acetic acid molecule. The macrocycle is slightly less constrained because one of the alkoxo groups on the side chain is not involved in hydrogen-bonding.

2.3.3. Structures with manganese acetate

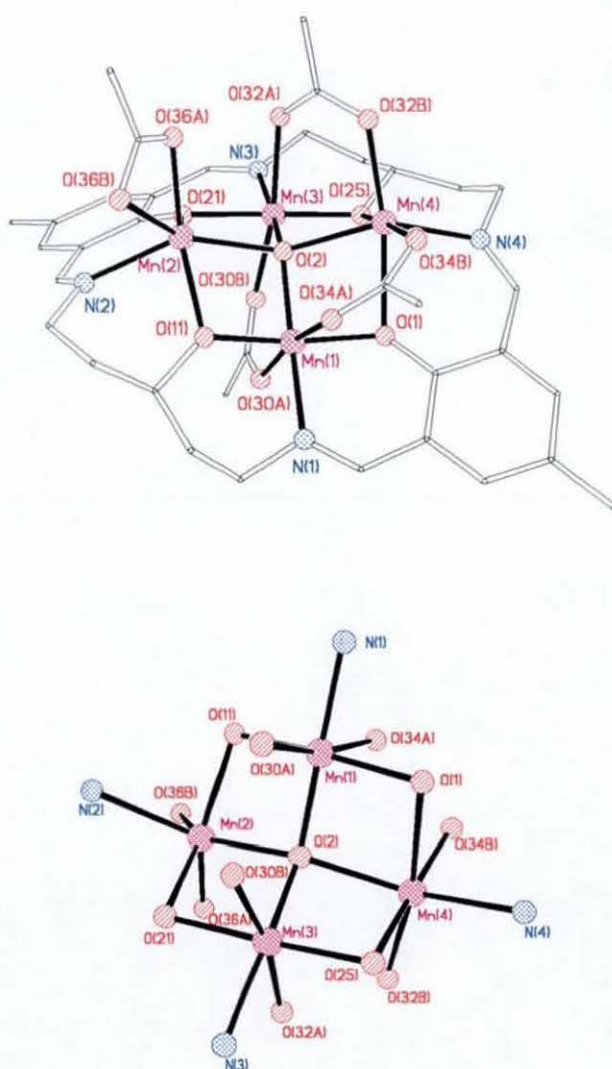


Fig. 2.16: Structure of $[\text{Mn}_4(\text{L}2)(\mu_4\text{-O})(\text{OAc})_4]$

The complex $[\text{Mn}_4(\text{L}2)(\mu_4\text{-O})(\text{OAc})_4]$ was prepared by complexation of manganese acetate with the already pre-formed macrocycle $\text{H}_2\text{Na}_2\text{L}2$. Using this method has improved the yield by almost 20% compared to the same compound obtained *via* template synthesis⁸⁹ (from 30 to 48%). The IR shows a strong broad band (shoulder to the left) at 1411 cm^{-1} , characteristic of the symmetric $\nu(\text{COO})$ vibration of acetate anions. The broadness of the band might be indicative of acetate ions in a different

environment. The strong band at 1570 cm^{-1} can be partially attributed to the asymmetric $\nu(\text{COO})$ vibrations (likely overlap with $\nu(\text{C}=\text{C})$ and $\nu(\text{C}-\text{O})$ vibrations). According to Deacon *et al.*¹²² the separation between the symmetrical and asymmetrical $\nu(\text{COO})$ vibrations can be used to predict the coordination mode of the acetate molecules. For $[\text{Mn}_4(\text{L2})(\mu_4\text{-O})(\text{OAc})_4]$, the separation is $\Delta\nu < 160\text{ cm}^{-1}$. Following Deacon's classification, the IR data suggest that the acetate ions are likely to adopt a chelating or bridging coordination mode; this is confirmed by crystallography.

Brown crystals of $[\text{Mn}_4(\text{L2})(\mu_4\text{-O})(\text{OAc})_4]$ suitable for X-ray studies were grown by slow diffusion of diethylether into an acetonitrile solution of the compound. The structure (fig. 2.16) contains two Mn(II) and two Mn(III) ions. The four metal ions are bound to the same set of macrocyclic donors and to a central μ_4 -oxo group. Two acetate ions link two adjacent metal ions on the same side of the macrocycle and one bridges one set of diagonal metal sites on the opposite face. The coordination sphere of the fourth metal ion is completed by a bidentate acetate ligand. The macrocyclic ligand is significantly twisted in this complex compared to the roughly planar Cu_4 and Ni_4 analogues. The twist enables the central oxo group to achieve a pseudotetrahedral geometry and is also necessary to accommodate the acetate bridge linking diagonally-related metal ions. The Mn(III) centres clearly show the expected Jahn-Teller distortions resulting in the extension of Mn-OAc bonds but the metal-phenoxo, metal-alkoxo, metal-oxo and metal-imine distances are markedly shorter in the +3 oxidation state than for the +2 ions in similar environment. The distortion from octahedral geometry is much greater for the Mn(II) ions. The selected bonds and angles are displayed in table 2.14. All the X-ray data collection parameters for $[\text{Mn}_4(\text{L2})(\mu_4\text{-O})(\text{OAc})_4]$ are summarised in table 2 in annex 1, along with the details concerning the refinement and disorders.

Table 2.14: Selected bond lengths [\AA] and angles [$^\circ$] for $[\text{Mn}_4(\text{L}2)(\mu_4\text{-O})(\text{OAc})_4]$

Mn(1)-O(11)	1.892(2)	Mn(2)-Mn(3)	3.1230(7)
Mn(1)-O(2)	1.904(2)	Mn(3)-O(25)	1.885(2)
Mn(1)-O(1)	1.946(2)	Mn(3)-O(2)	1.911(2)
Mn(1)-N(1)	1.997(3)	Mn(3)-O(21)	1.967(2)
Mn(1)-O(30A)	2.157(2)	Mn(3)-N(3)	2.034(3)
Mn(1)-O(34A)	2.279(2)	Mn(3)-O(30B)	2.181(2)
Mn(1)-Mn(4)	3.0518(7)	Mn(3)-O(32A)	2.213(2)
Mn(1)-Mn(2)	3.0734(7)	Mn(3)-Mn(4)	3.0212(7)
Mn(2)-O(36A)	2.080(3)	Mn(4)-O(32B)	2.114(2)
Mn(2)-O(11)	2.089(2)	Mn(4)-O(34B)	2.122(2)
Mn(2)-O(21)	2.183(2)	Mn(4)-O(2)	2.153(2)
Mn(2)-O(2)	2.190(2)	Mn(4)-N(4)	2.181(3)
Mn(2)-N(2)	2.208(3)	Mn(4)-O(25)	2.266(2)
Mn(2)-O(36B)	2.523(5)	Mn(4)-O(1)	2.311(2)
O(11)-Mn(1)-O(2)	86.85(9)	O(36A)-Mn(2)-O(2)	107.27(14)
O(11)-Mn(1)-O(1)	169.25(10)	O(11)-Mn(2)-O(2)	75.10(8)
O(2)-Mn(1)-O(1)	88.68(9)	O(21)-Mn(2)-O(2)	74.90(8)
O(11)-Mn(1)-N(1)	93.66(11)	O(36A)-Mn(2)-N(2)	113.57(16)
O(2)-Mn(1)-N(1)	178.89(10)	O(11)-Mn(2)-N(2)	82.01(11)
O(1)-Mn(1)-N(1)	90.65(10)	O(21)-Mn(2)-N(2)	82.61(11)
O(11)-Mn(1)-O(30A)	93.81(11)	O(2)-Mn(2)-N(2)	135.39(11)
O(2)-Mn(1)-O(30A)	96.79(9)	O(36A)-Mn(2)-O(36B)	54.11(15)
O(1)-Mn(1)-O(30A)	96.43(10)	O(11)-Mn(2)-O(36B)	97.97(13)
N(1)-Mn(1)-O(30A)	84.17(10)	O(21)-Mn(2)-O(36B)	140.67(13)
O(11)-Mn(1)-O(34A)	86.03(10)	O(2)-Mn(2)-O(36B)	134.83(14)
O(2)-Mn(1)-O(34A)	93.60(9)	N(2)-Mn(2)-O(36B)	85.47(15)
O(1)-Mn(1)-O(34A)	84.49(9)	O(25)-Mn(3)-O(2)	90.05(9)
N(1)-Mn(1)-O(34A)	85.46(10)	O(25)-Mn(3)-O(21)	176.55(10)
O(30A)-Mn(1)-O(34A)	169.59(9)	O(2)-Mn(3)-O(21)	86.57(9)
O(36A)-Mn(2)-O(11)	144.07(13)	O(25)-Mn(3)-N(3)	94.27(10)
O(36A)-Mn(2)-O(21)	97.49(12)	O(2)-Mn(3)-N(3)	172.68(11)
O(11)-Mn(2)-O(21)	117.12(10)	O(21)-Mn(3)-N(3)	89.03(11)

O(25)-Mn(3)-O(30B)	97.00(9)	O(34B)-Mn(4)-O(25)	174.07(9)
O(2)-Mn(3)-O(30B)	97.08(9)	O(2)-Mn(4)-O(25)	74.81(8)
O(21)-Mn(3)-O(30B)	84.13(9)	N(4)-Mn(4)-O(25)	79.76(9)
N(3)-Mn(3)-O(30B)	88.26(10)	O(32B)-Mn(4)-O(1)	170.84(9)
O(25)-Mn(3)-O(32A)	89.64(10)	O(34B)-Mn(4)-O(1)	85.54(8)
O(2)-Mn(3)-O(32A)	90.40(9)	O(2)-Mn(4)-O(1)	74.05(8)
O(21)-Mn(3)-O(32A)	89.69(10)	N(4)-Mn(4)-O(1)	78.79(9)
N(3)-Mn(3)-O(32A)	83.73(11)	O(25)-Mn(4)-O(1)	89.63(8)
O(30B)-Mn(3)-O(32A)	169.97(9)	Mn(3)-O(21)-Mn(2)	97.46(9)
O(32B)-Mn(4)-O(34B)	95.01(10)	Mn(1)-O(2)-Mn(3)	131.20(12)
O(32B)-Mn(4)-O(2)	97.11(9)	Mn(1)-O(2)-Mn(4)	97.40(9)
O(34B)-Mn(4)-O(2)	107.05(9)	Mn(3)-O(2)-Mn(4)	95.88(9)
O(32B)-Mn(4)-N(4)	110.20(11)	Mn(1)-O(2)-Mn(2)	97.06(9)
O(34B)-Mn(4)-N(4)	95.89(10)	Mn(3)-O(2)-Mn(2)	98.97(9)
O(2)-Mn(4)-N(4)	142.54(10)	Mn(4)-O(2)-Mn(2)	144.03(11)
O(32B)-Mn(4)-O(25)	90.30(9)		

The FAB spectrum shows three peaks, consistent with the formula. The peak assignments are displayed in table 2.15.

Table 2.15: Peak attributions for $[\text{Mn}_4(\text{L}2)(\text{O})(\text{OAc})_4]$

m/z	Rel. Intensities (%)	Fragments	Calc. Mass
783	70	$[\text{Mn}_4(\text{L}2)(\text{O})(\text{OAc})]^{3+}$	783
842	100	$[\text{Mn}_4(\text{L}2)(\text{O})(\text{OAc})_2]^{2+}$	842
901	25	$[\text{Mn}_4(\text{L}2)(\text{O})(\text{OAc})_3]^+$	901

Two similar mixed-valence tetranuclear manganese complexes have been isolated and characterised by McKee *et al.*⁸⁹ They were formed *via* a template route using 2,6-diformyl-4-methylphenol (DFMP) and 1,5-diaminopentan-3-ol (DAHP). The reported tetramanganese structures slightly differ from the structure of $[\text{Mn}_4(\text{L}2)(\text{O})(\text{OAc})_4]$, although the bond lengths and angles are similar in the three

complexes and three of the acetate groups adopt the same bridging mode as in complex $[\text{Mn}_4(\text{L}2)(\text{O})(\text{OAc})_4]$. The environment of the second Mn(II) is different; in the case of the complex shown in fig. 2.17 the coordination of the fourth metal ion is completed by a chloride ion and a solvent MeOH whereas for the complex shown in fig. 2.18, the coordination sphere is completed by a monodentate acetate group and a water molecule, which are linked by an intramolecular hydrogen bond (dotted line).

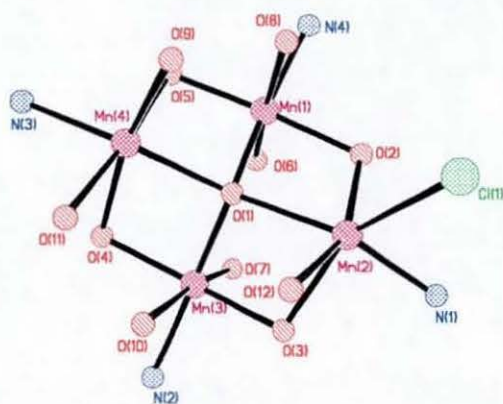
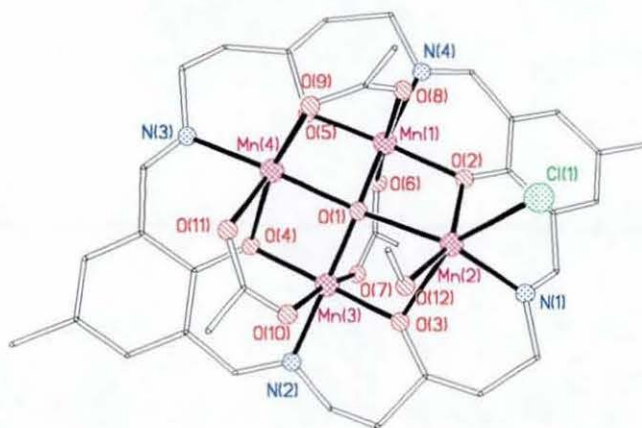


Fig. 2.17: Structure of $[\text{Mn}_4(\text{L}2)(\mu_4\text{-O})(\text{OAc})_3(\text{MeOH})\text{Cl}]$

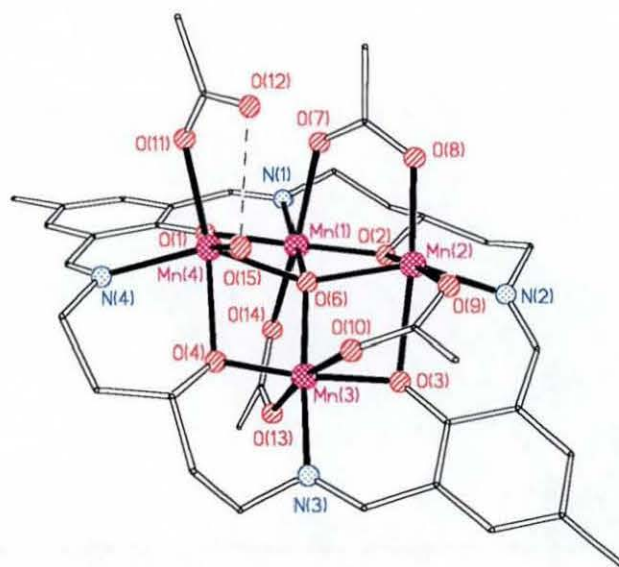


Fig. 2.18: Structure of $[\text{Mn}_4(\text{L}2)(\mu_4\text{-O})(\text{OAc})_4(\text{H}_2\text{O})]$

2.3.4. Structures with cobalt acetate

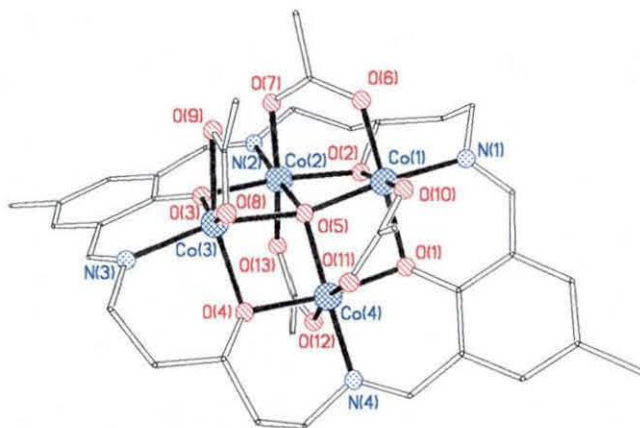
Complexation of cobalt acetate with the already pre-formed macrocycle $\text{H}_2\text{Na}_2\text{L}2$ yielded $[\text{Co}_4(\text{L}2)(\mu_4\text{-O})(\text{OAc})_4](\text{OAc})$. Using this method has improved the yield of the template synthesis⁸⁹ by *ca.* 20% (from 30 to 52%). The IR shows two strong broad bands at 1411 cm^{-1} (slightly split) and 1443 cm^{-1} characteristic of the symmetrical $\nu(\text{COO})$ vibration of acetate anions. The presence of two stretches might be an indication of acetate anions in a different environment. The strong band at 1581 cm^{-1} can be partially attributed the asymmetric $\nu(\text{COO})$ vibrations (likely overlap with $\nu(\text{C}=\text{C})$ and $\nu(\text{C}-\text{O})$ vibrations). Again here (separation $\Delta\nu < 160\text{ cm}^{-1}$), following Deacon's classification, the IR data suggest that the acetate anions are likely to adopt a chelating or bridging coordination mode.

The FAB spectrum shows five peaks, consistent with the formula. The peak assignments are displayed in table 2.16. The peaks represent the successive loss of one acetate group.

Table 2.16: Peak attributions for $[\text{Co}_4(\text{L2})(\text{O})(\text{OAc})_4](\text{OAc})$

m/z	Rel. Intensities (%)	Fragments	Calc. Mass
738	60	$[\text{Co}_4(\text{L2})(\text{O})]^{5+}$	740
799	85	$[\text{Co}_4(\text{L2})(\text{O})(\text{OAc})]^{4+}$	799
858	87	$[\text{Co}_4(\text{L2})(\text{O})(\text{OAc})_2]^{3+}$	858
917	95	$[\text{Co}_4(\text{L2})(\text{O})(\text{OAc})_3]^{2+}$	917
976	35	$[\text{Co}_4(\text{L2})(\text{O})(\text{OAc})_4]^+$	976

No crystals suitable for X-ray studies were obtained. However, combining the results obtained for the elemental analysis and the FAB spectrometry, it is reasonable to assume that the structure is similar to the reported structure,⁸⁹ $[\text{Co}_4(\text{L2})(\mu_4\text{-O})(\text{OAc})_4]\text{Cl}$, but with a free acetate instead of a chloride counteranion (fig. 2.19). This cobalt structure contains three Co(II) and one Co(III) and is similar to the manganese complex $[\text{Mn}_4(\text{L2})(\mu_4\text{-O})(\text{OAc})_4]$ prepared from $\text{H}_2\text{Na}_2\text{L2}$. The presence of the chloride ion in the reported structure can be explained by the incomplete neutralisation of $\text{DAHP}\cdot 2\text{HCl}$ or the small portion of KCl that stayed in solution.

**Fig. 2.19:** Structure of the cation $[\text{Co}_4(\text{L2})(\mu_4\text{-O})(\text{OAc})_4]^+$

McKee *et al.*⁸⁹ reported another mixed-valence tetranuclear cobalt complex with L2 containing three Co(II) and one Co(III): $[\text{Co}_4(\text{L}2)(\mu_4\text{-O})(\text{OAc})_3\text{Cl}](\text{ClO}_4)$ is shown in fig. 2.20 and is broadly similar to the manganese complex $[\text{Mn}_4(\text{L}2)(\mu_4\text{-O})(\text{OAc})_3\text{Cl}]$.

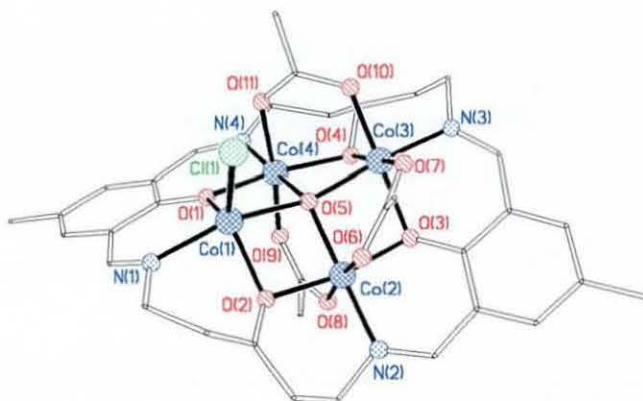


Fig. 2.20: Structure of the cation $[\text{Co}_4(\text{L}2)(\mu_4\text{-O})(\text{OAc})_3\text{Cl}]^+$

2.3.5. Structures with copper nitrate

The structure of $[\text{Cu}_4(\text{L}1)(\mu_4\text{-OH})(\text{NO}_3)_3 \cdot 3\text{H}_2\text{O}]$ has been communicated by McKee *et al.* in 1988.⁹⁵ Later in 1991,⁹³ a series of six tetranuclear copper complexes synthesised by template condensation of DFTP or DFMP with the corresponding copper salt (copper nitrate, copper perchlorate and copper acetate) was also reported. In 2001, Launay reported similar structures with copper tetrafluoroborate.⁹⁶ A perspective view of the cation $[\text{Cu}_4(\text{L}1)(\mu_4\text{-OH})(\text{H}_2\text{O})_2]^{3+}$ is shown in fig. 2.21.

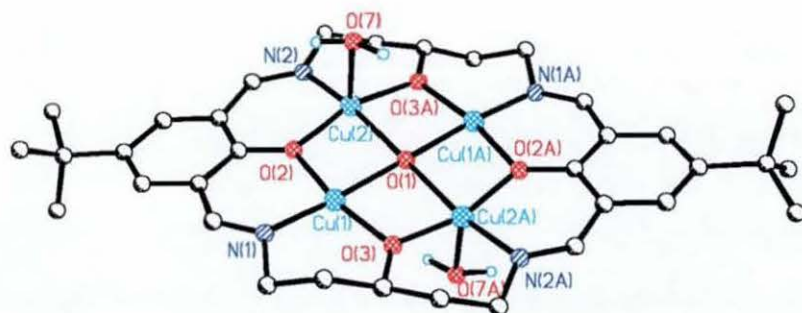


Fig. 2.21: Structure of the cation $[\text{Cu}_4(\text{L1})(\mu_4\text{-OH})(\text{H}_2\text{O})_2]^{3+}$

The cation is centrosymmetric. Four copper(II) ions are bound within the macrocycle, each coordinated to one imine nitrogen, one phenoxide oxygen, one alkoxide oxygen, the central μ_4 -hydroxy ion and to one axial donor (water or nitrate). The copper ions are bridged either through alkoxo or phenoxo oxygen atoms. The Cu---Cu distances are quite short but not bonding (3.000(1) and 2.953(1) Å). Similarly to the tetranickel systems described previously, the M- $\mu_4\text{OH}$ distances (2.082(1) and 2.127(1) Å) are significantly longer. Here again, the size of the central cavity does not seem to be a perfect fit for the hydroxy group. The axial donor is different for the copper centres (Cu(1) and Cu(2)). One is coordinated to a water molecule (Cu(2)-O(1w) 2.249(5) Å), while the other Cu(II) exhibits a longer interaction with either a 50/50 disordered water (Cu(1)-O(2w) 2.48(1) Å) or nitrate moiety (Cu(1)-O(22) 2.82(2) Å). Individual macrocyclic units are linked by hydrogen bonds involving the nitrate anions and the coordinated water molecule (O(1w)). The $\mu_4\text{-OH}$ is disordered between two positions slightly above and below the ring.

The complex $[\text{Cu}_4(\text{L2})(\mu_4\text{-OH})(\text{NO}_3)_3]$ isolated in the course of this work was synthesised using a different procedure. The complex was formed from the complexation of copper nitrate with $\text{H}_2\text{Na}_2\text{L2}$. The obtained yield is higher (57%) than the reported yield for the same complex (45%) prepared by template synthesis.⁹³ The IR shows nitrate vibrations indicative of both coordinated (1333 and 1439 cm^{-1})

and free (1384 cm^{-1}) nitrate anions. This differs slightly from the reported⁹³ similar tetracopper complexes with DFMP and DFTP in which the nitrate vibration was around 1375 cm^{-1} .

The FAB spectra indicate the presence of the tetranuclear entity. However the relative intensity of the peaks is weak, which is similar to the reported structures.^{93,96} The peak assignments are given in table 2.17.

Table 2.17: Peak attributions for $[\text{Cu}_4(\text{L}2)(\mu_4\text{-OH})(\text{NO}_3)_2](\text{NO}_3)$

m/z	Rel. Intensities (%)	Fragments	Calc. Mass
783	5	$[\text{Cu}_4(\text{L}2)(\mu_4\text{-OH})(\text{H}_2\text{O})_{1.5}]^{3+}$	785
1015	5	$[\text{Cu}_4(\text{L}2)(\mu_4\text{-OH})(\text{NO}_3)_3+\text{Na}]^+.\text{EtOH}$	1014
1127	5	$[\text{Cu}_4(\text{L}2)(\mu_4\text{-OH})(\text{NO}_3)_3+\text{H}]^+.\text{4EtOH}$	1130

The FAB and elemental analysis results on the powdered sample show that the structure of the isolated crystals is different to the powdered sample as well as the reported structure.⁹⁵ Green crystals of $[\text{Cu}_4(\text{L}2)(\mu_4\text{-OH})(\text{OH})_2(\text{NO}_3)]$ suitable for X-ray studies were grown by slow diffusion of diethylether into a DMF/MeOH solution of the compound. Indeed, two hydroxy groups replaced two nitrate anions. The structure was refined in the space group $C2/m$ with a disorder between the coordinated nitrate anion and the two adjacent OH groups on either side of the plane defined by the macrocycle (fig. 2.22).

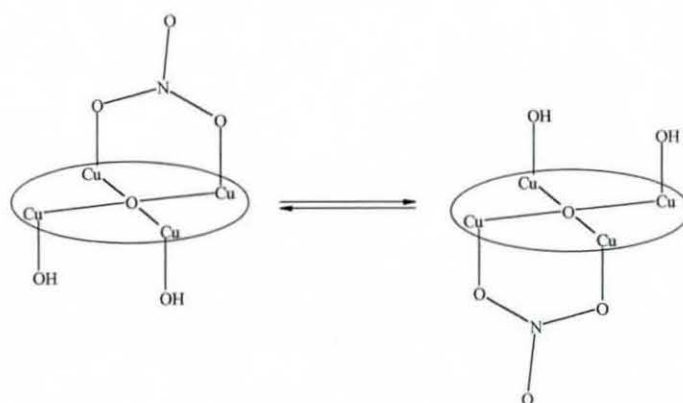


Fig. 2.22: Diagram showing the disorder between NO_3^- and two OH^-

This disorder could not be removed by reducing the symmetry except in the space group P1. Unfortunately, the refinement was unstable in this space group, so the structure was completed using a disorder model in C2/m.

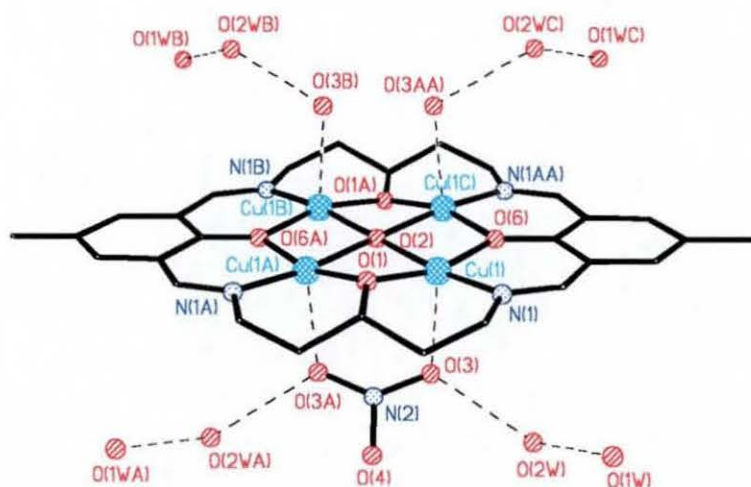


Fig. 2.23: Structure of $[\text{Cu}_4(\text{L}2)(\mu_4\text{-OH})(\text{OH})_2(\text{NO}_3)] \cdot 6\text{H}_2\text{O}$

The atoms N(2) and O(4) belonging to the nitrate moiety are half occupancy whereas O(3) belonging to both nitrate and hydroxy groups is full occupancy. As the picture shows, the hydroxy groups are stabilised by hydrogen-bonding to the H_2O network. The network shown in the packing diagram (fig. 2.24 and fig. 2.25) links the individual macrocycles as in the structure reported by McKee *et al.*⁹⁵ Selected bond

lengths and angles for $[\text{Cu}_4(\text{L}2)(\mu_4\text{-OH})(\text{OH})_2(\text{NO}_3)].6\text{H}_2\text{O}$ are displayed in table 2.18. All the X-ray data collection parameters for $[\text{Cu}_4(\text{L}2)(\mu_4\text{-OH})(\text{OH})_2(\text{NO}_3)].6\text{H}_2\text{O}$ are summarised in table 3 in annex 1, along with the details concerning the refinement and disorders.

Table 2.18: Selected bond lengths [Å] and angles [°] for $[\text{Cu}_4(\text{L}2)(\mu_4\text{-OH})(\text{OH})_2(\text{NO}_3)].6\text{H}_2\text{O}$

Cu(1)-O(1)	1.878(4)	Cu(1)-O(3)	2.496(6)
Cu(1)-O(6)	1.912(3)	Cu(1)-Cu(1)*	2.8708(16)
Cu(1)-N(1)	1.953(5)	Cu(1)-Cu(1)**	2.9344(15)
Cu(1)-O(2)	2.0526(8)		
O(1)-Cu(1)-O(6)	163.2(2)	O(2)-Cu(1)-O(3)	92.12(13)
O(1)-Cu(1)-N(1)	96.8(2)	Cu(1)-O(1)-Cu(1)*	99.7(3)
O(6)-Cu(1)-N(1)	93.2(2)	Cu(1)*-O(2)-Cu(1)**	180.0
O(1)-Cu(1)-O(2)	84.31(14)	Cu(1)*-O(2)-Cu(1)	88.74(4)
O(6)-Cu(1)-O(2)	84.25(13)	Cu(1)**-O(2)-Cu(1)	91.26(4)
N(1)-Cu(1)-O(2)	173.08(17)	Cu(1)*-O(2)-Cu(1) [#]	91.26(4)
O(1)-Cu(1)-O(3)	94.7(2)	Cu(1)**-O(2)-Cu(1) [#]	88.74(4)
O(6)-Cu(1)-O(3)	98.05(14)	Cu(1)-O(2)-Cu(1) [#]	180.00(3)
N(1)-Cu(1)-O(3)	94.6(2)		

Symmetry transformations used to generate equivalent atoms: (*) x, -y, z (**)-x, y, -z+2 ([#])-x, -y, -z+2

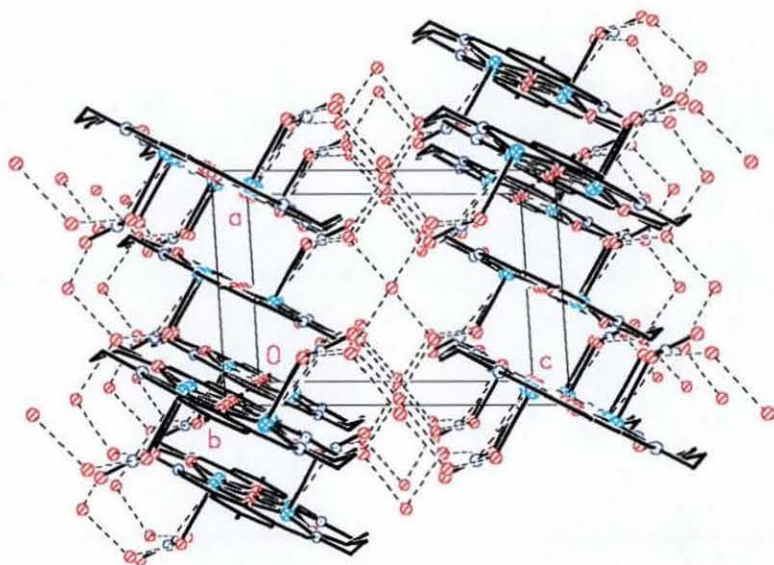


Fig. 2.24: Packing diagram for $[\text{Cu}_4(\text{L}2)(\mu_4\text{-OH})(\text{OH})_2(\text{NO}_3)].6\text{H}_2\text{O}$
(along the b axis)

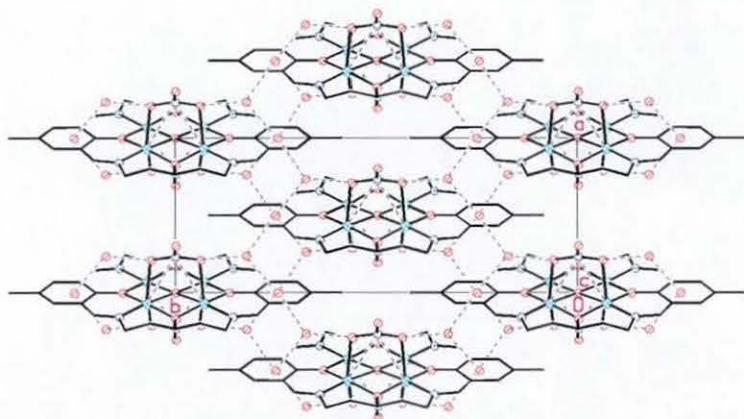


Fig. 2.25: Packing diagram for $[\text{Cu}_4(\text{L}2)(\mu_4\text{-OH})(\text{OH})_2(\text{NO}_3)].6\text{H}_2\text{O}$

The packing diagram reflects the nitrate/hydroxy disorder. It is not possible to show on which side of the macrocyclic plane the hydroxy groups or nitrate anions are in each molecule (might be different for each). Therefore, in fig. 2.24 and 2.25, two nitrate anions are depicted for each macrocyclic molecule.

2.3.6. Dinuclear and tetranuclear palladium complexes

As it has been stated before, palladium, and generally metals of the second and third row of transition metals, are relatively more inert than the metals of the first row towards template reaction. They have been usually found to form macrocyclic compounds when reacted with pre-formed ligand species^{120,123} but are poor template ions. Launay,⁹⁶ in the course of his studies aimed at controlling the synthesis of heterotetranuclear complexes, found some mass spectral evidence suggesting the formation of a tetrapalladium complex rather than the heteronuclear Cu_2Pd_2 . This complex arose from the reaction of a dicopper complex $[\text{Cu}_2(\text{H}_3\text{L1})(\mu\text{-Pyr})](\text{BF}_4)_2$ with an excess of palladium acetate in $\text{MeOH}/\text{CH}_3\text{CN}$ refluxed overnight, however, elemental analysis suggested the product was impure. Unfortunately, due to poor solubility the recrystallisation and further analyses were unsuccessful. The alternative template route was attempted to try and synthesise “diagonal” dinuclear palladium double-bridged by chloride anions like the dinuclear $\text{Co}(\text{II})$ complex reported by Wikaira⁹⁷ (fig. 2.26). Again, there was some mass spectral evidence of the formation of di-, tri- or even tetranuclear palladium species but no pure compound was isolated.

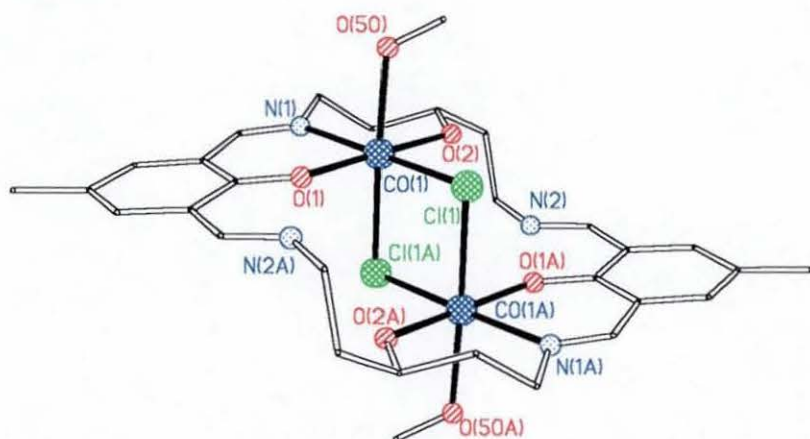


Fig. 2.26: Structure of the cation $[\text{Co}_2(\text{H}_4\text{L1})(\text{Cl})_2(\text{MeOH})_2]^{2+}$

Whilst these palladium complexes have not been fully characterised as yet, their detection confirms that polynuclear palladium complexes are accessible. In the course of this work, some additions have been made to the previous results reported by Launay. This study has been performed with the assistance of Dr M. Tumer. A dinuclear palladium complex containing chloride ions was synthesised by complexation of the pre-formed disodium salt of the ligand H_4L1 with two equivalents of $PdCl_2$ in MeOH refluxed overnight. So far, no crystals suitable for X-ray studies have been isolated but there is a clear mass spectral evidence of the formation of this complex. A main peak is found at m/z 739, which can be attributed to the complex with the loss of three chloride ions, $[Pd_2(H_4L1)Cl]^{3+}$. Minor peaks (weak) at m/z 704, 757 and 774 can be assigned to $[Pd_2(H_4L1)]^{4+}$, $[Pd_2(H_4L1)Cl]^{3+} \cdot H_2O$ and $[Pd_2(H_4L1)Cl_2]^{2+}$ respectively. The IR spectrum reveals some differences with that of the ligand Na_2H_2L2 , which suggest the coordination of palladium. The split in the imine band (1649 and 1621 cm^{-1}) implies an unsymmetric coordination of the palladium leaving both imine in a different environment. This observation gives a hint concerning the way by which the palladium ions are coordinated. Therefore, it seems reasonable to think that the structure is similar to the dicobalt structure mentioned before (fig. 2.27).

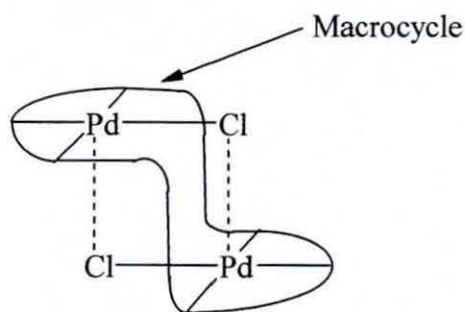


Fig. 2.27: Proposed geometry for the dipalladium complex

However, as palladium(II) complexes are usually square planar, the geometry adopted by the macrocycle might be different and all the available donors might not be involved in the coordination. To establish the existence of the double chloride bridge

between the metals beyond doubt, some structural information is needed. Another attempt, reacting $\text{Na}_2\text{H}_2\text{L1}$ and $\text{Pd}(\text{NH}_3)_4(\text{NO}_3)_2$ in refluxing $\text{MeOH}/\text{CH}_3\text{CN}$ over a period of two days, was performed. The product isolated was not pure but again there was some mass spectral evidence of the formation of tetranuclear palladium species (table 2.19). However, the spectral evidence of a dinuclear species (table 2.19) combined with the isolation of unreacted palladium salt suggest that either the reaction period needs to be longer or that the cavity of the macrocycle might be too small to accommodate four palladium ions. Moreover, $\text{Pd}(\text{II})$ is a soft metal centre and therefore has a preference for soft donors which means that the coordination to donors in the macrocycle might be more difficult. However, the size of the cavity should not be the main issue because structures with the Robson macrocycle (fig. 2.6) accommodating two $\text{Pd}(\text{II})$ have been reported.¹²⁰

Table 2.19: Peak attributions for $\text{Pd}_4(\text{L1})(\text{NH}_3)_4(\text{NO}_3)_3\text{Cl}$

m/z	Rel. Intensities (%)	Fragments	Calc. Mass
825	20	$[\text{Pd}_2(\text{H}_4\text{L1})\text{Cl}]^{3+}$	825
1229	5	$[\text{Pd}_4(\text{L1})(\text{NH}_3)_4(\text{NO}_3)_2]^{2+} \cdot \text{MeCN}$	1231
1240	5	$[\text{Pd}_4(\text{L1})(\text{NH}_3)_4(\text{NO}_3)_2]^{2+} \cdot \text{MeOH} \cdot \text{H}_2\text{O}$	1236
1327	5	$[\text{Pd}_4(\text{L1})(\text{NH}_3)_4(\text{NO}_3)_3\text{Cl} + \text{H}]^+ \cdot \text{MeCN}$	1329
1363	10	$[\text{Pd}_4(\text{L1})(\text{NH}_3)_4(\text{NO}_3)_3\text{Cl} + \text{H}]^+ \cdot \text{MeCN} \cdot 2\text{H}_2\text{O}$	1365
1378	10	$[\text{Pd}_4(\text{L1})(\text{NH}_3)_4(\text{NO}_3)_3\text{Cl} + \text{Na}]^+ \cdot \text{MeOH} \cdot 2\text{H}_2\text{O}$	1378

2.4. Conclusion

The results obtained in this chapter have shown that tetranuclear nickel complex with weakly coordinated anions like perchlorate can be synthesised and detected by FAB or IR. The use of template synthesis rendered unclean products (oily) contaminated by polymeric material due to the tendency of $\text{Ni}(\text{II})$ to complete its coordination sphere and form polymeric compounds. Complexation with the already pre-formed macrocycles L1 or L2 as sodium salts did not improve the purity of the complex.

However, this method employed with nickel nitrate afforded an interesting complex in which the nitrate anions are coordinated to the Ni(II) centres on one side of the macrocycle. Individual macrocycles are linked through hydrogen-bonding *via* the coordinated MeOH and nitrate anions. The isolation of this complex is encouraging in the pursuit of our goal of forming complexes with weakly coordinated anions or molecules that have a potential of performing homogeneous metal promoted reactions as the weakly coordinated ligands can be easily replaced by other substrates.

Another important finding in the course of this work is that the macrocycles L1 and L2 previously synthesised *via* template routes can be synthesised in reasonable yield as sodium salts. This is very interesting because transmetallation with any transition metals is accessible, Na^+ being easily exchanged. In a few observed cases with manganese acetate, cobalt acetate and copper nitrate the yields are improved. The use of pre-formed macrocycles avoids the formation of complexes with the starting materials, which can contaminate the template reaction. Moreover, metals inert towards template reactions like palladium can be complexed by the already formed macrocycles. No palladium complexes have been structurally characterised yet but their detection by FAB is encouraging.

An additional feature of this research is the difference between the complex synthesis *via* template route and that of the complexation of the pre-formed ligand. In the template synthesis the metal assists the Schiff-base reaction that leads to the formation of the macrocycle. Therefore in this case, the structure of the final product is dependent on the order in which the different parts come together, hence on the way the metal ions is directing the course of the reaction. This order is changed if the pre-formed ligand is used and the result might be slightly different. Some differences have been noticed in the copper complex. Two nitrate molecules are found weakly bridging two separate pairs of copper ions, which has not been observed in the template synthesis. In the case of the nickel acetate structure, two structures are possible [(A) and (B)]. If structure (A) proves to be the right one, it would mean that the number of acetate molecules involved in the bridging pattern is lower in the non-

template synthesis, which implies that acetate molecules might be playing a role in the formation of the stable macrocyclic structure in the Ni(II) template synthesis. For the tetramanganese complex there is no difference in the bridging pattern of the acetate molecules. This probably means that the acetate molecules can only bridge in a certain way to accommodate the four metal ions in the cavity of the macrocycle as well as the pseudo-tetrahedral geometry of the central oxo ion. The only difference in the structure is the additional bidentate acetate coordinating the fourth metal ion in contrast to methanol, water or chloride in the template synthesis.

Chapter three

Polynuclear Complexes

of

New Tetraphenolic Schiff-base Macrocycles

3.1. Introduction

As mentioned in the two previous chapters, the McKee group has been mainly interested in Schiff-base derived macrocycles with one phenol-head unit (H_4L1 and H_4L2). More recently, the results discussed in the previous chapters led to the investigation of extended versions of these macrocycles (fig. 3.1).

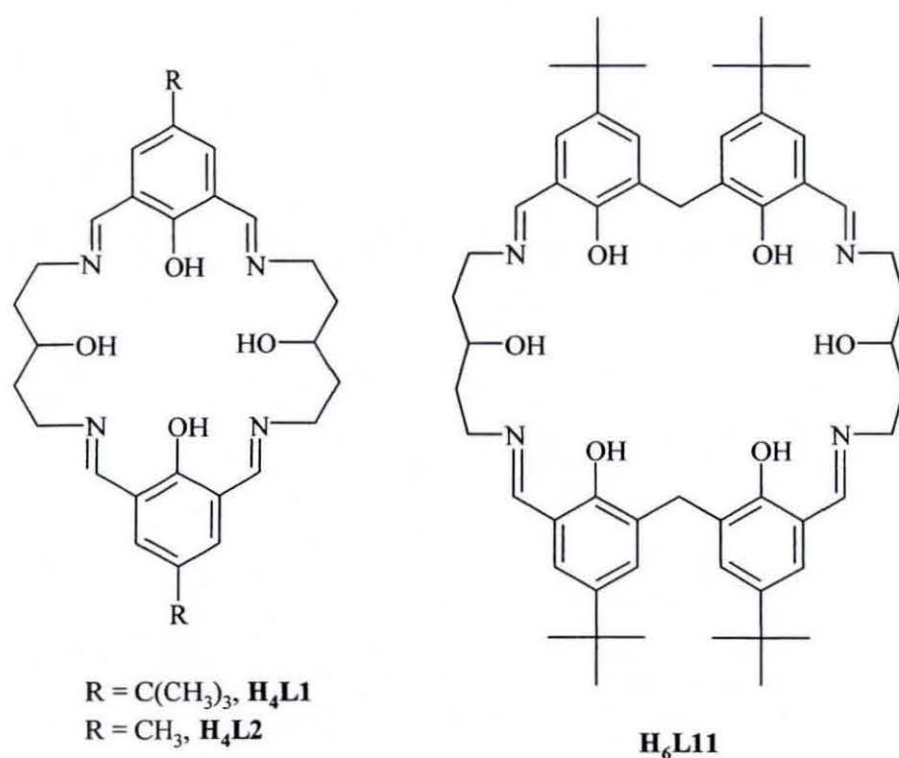


Fig. 3.1: Schiff-base derived macrocycles

The diphenolic head-unit DHTMB (2,2'-dihydroxy-5,5'-di-*tert*-butyl-3,3'-methane-diyldibenzaldehyde) (fig. 3.4) has been prepared with the intention of synthesising the macrocycles shown in fig. 3.2 and 3.3. The DHTMB group introduces a range of geometrical variations, largely due to the presence of the saturated carbon linking the two phenol rings. In calixarenes these possibilities are restricted by the geometry of the ring system but the introduction of longer, flexible links in the chain extends the range of conformational possibilities. Depending on the counterion present, the metal:ligand ratio, and the extent of deprotonation of the phenol groups, the

nuclearity of the macrocycles can be manipulated. Similarly, bridging groups of various lengths could be accommodated between the bound metal ions. The work described in this chapter comprises a preliminary investigation of the chemistry of these ligands and provides a foundation for future work.

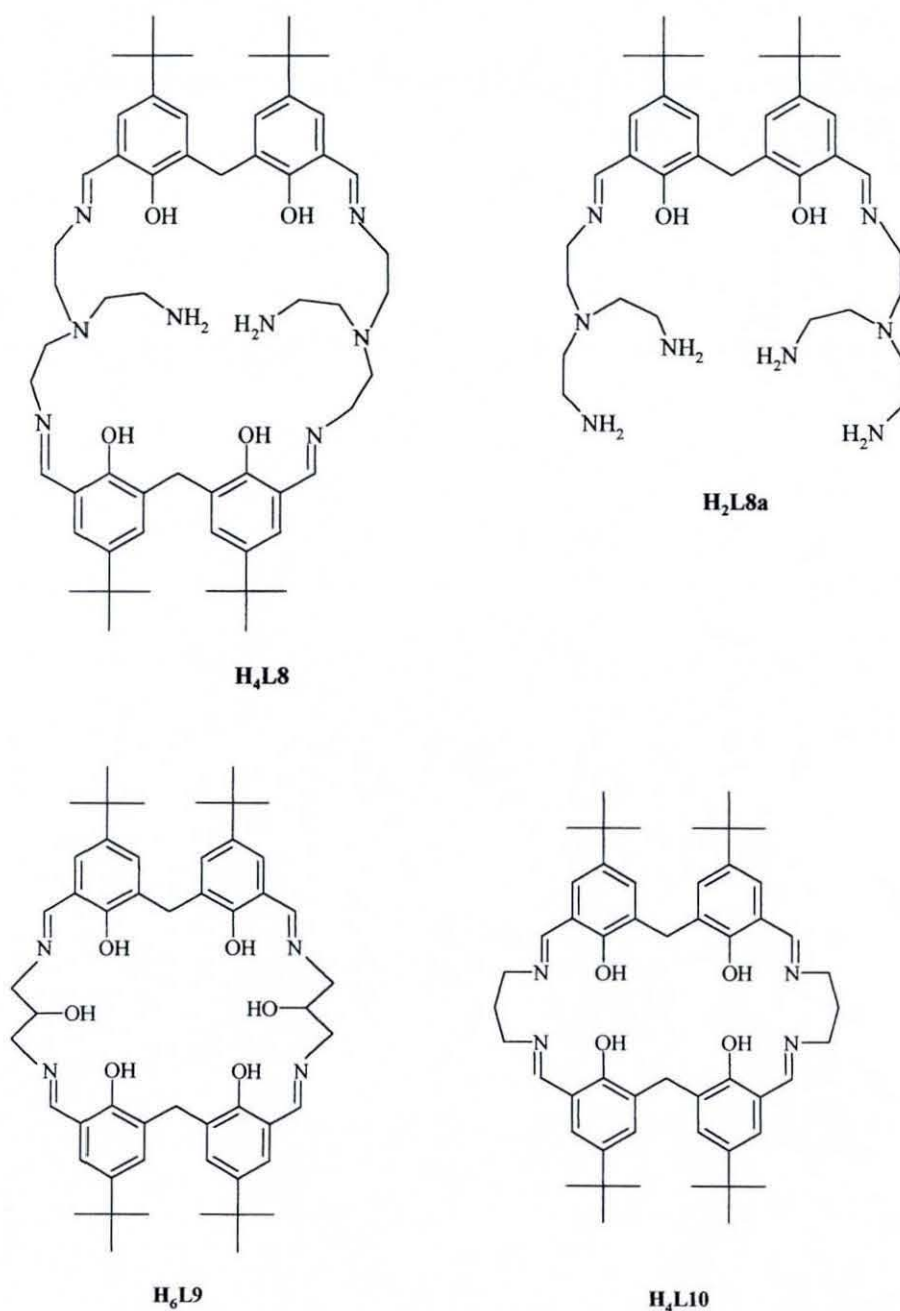
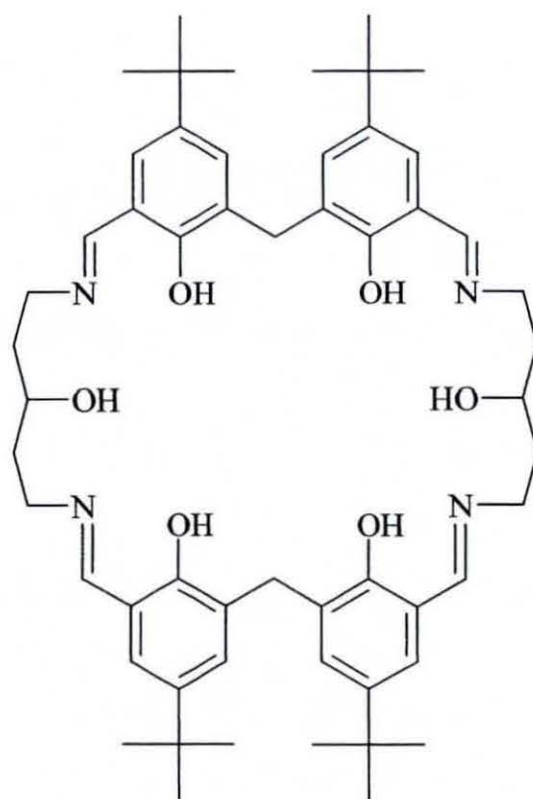
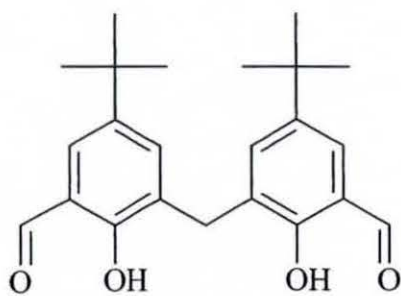


Fig. 3.2: Diphenolic and tetraphenolic ligands



H₆L11

Fig. 3.3: Tetraphenolic ligand



C₂₃H₂₈O₄ (DHTMB)

Fig. 3.4: 2,2'-dihydroxy-5,5'-di-*tert*-butyl-3,3'-methanediyl dibenzaldehyde (DHTMB)

3.2. Synthesis of 2,2'-dihydroxy-5,5'-di-*tert*-butyl-3,3'-methanediyl-dibenzaldehyde (DHTMB)

DHTMB was synthesised from 4-*tert*-butylphenol in three steps. The overall yield is 5%, which is very low.

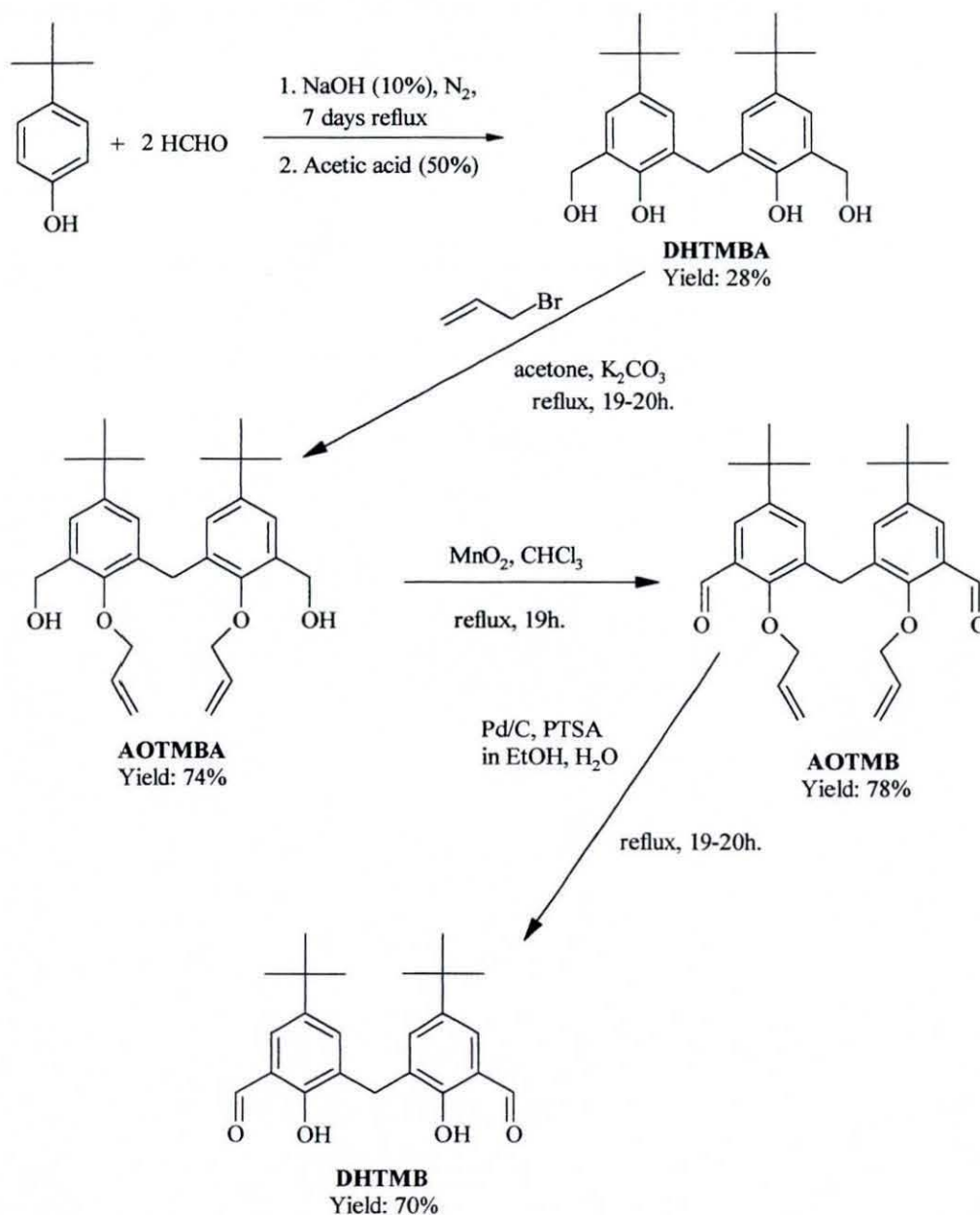


Fig. 3.5: Synthesis of DHTMB

The precursor (DHTMBA) to the synthesis of DHTMB was synthesised following the literature procedure reported by Gutsche *et al.*¹²⁴ in 1983 but the work up of the reaction was slightly changed. The oil that formed upon acidification was not separated but directly extracted from the aqueous layer with diethylether. The diethylether fractions were then washed several times with water to eliminate the residual acetic acid. The recrystallisation was performed as reported by Gutsche, with a comparable yield (*ca.* 28%). The low yield of this reaction, in addition to the following 3-step-reaction process, contributes to the very low overall yield.

To oxidise the two alcohol functions into aldehyde functions, it was found necessary to protect the phenol groups. The protection reaction was carried out in the presence of allyl bromide and potassium carbonate in acetone, a method frequently applied to phenols.¹²⁵ The protected compound was obtained with a reasonable yield of 74%. Indeed, the value reported for the protection of one phenol group is 85%, which applied to the protection of two groups would give a yield of 72%. The method used to synthesise AOTMB is similar to that reported by Taniguchi *et al.*¹²⁶ The reaction is carried out using activated MnO₂ in chloroform with a yield of 78%. The method used to deprotect the phenol groups is similar to the one described by Boss *et al.*¹²⁷ The reaction was carried out using Pd on activated charcoal and *p*-toluenesulfonic acid in ethanol with a yield of 70%, which seems quite low compared to the reported value. The value reported for the deprotection of one phenol group is 95%, which applied to the deprotection of two groups would give a yield of 90%.

The oxidation of the alcohol groups with MnO₂ without protecting the phenol groups was unfruitful. The brown colour of the isolated product might suggest an oxidation of the phenol groups into semi-quinones. In addition, purification of the product by column chromatography only yielded a very small amount of DHTMB. Another possibility, which might improve the yield, is the use of a weaker oxidant that would not attack the phenol groups, hence reduce the number of steps used to one.

3.2.1. Characterisation of 2,2'-diallyloxy-5,5'-di-*tert*-butyl-3,3'-methanediyl-dibenzyl alcohol (AOTMBA)

¹H NMR, IR and E.A characterisations

There are not many changes in the ¹H NMR spectrum compared to the precursor except for the appearance of four new peaks at 6.07 ppm, 5.34 ppm, 5.30 ppm and 4.34 ppm assigned to the allyl groups as stated in the experimental section. The peaks assigned to the protons on the aromatic rings and the saturated carbon linking the two phenol rings are slightly shifted downfield. In the case of the precursor, the protons on the phenol and alcohol groups are not seen. Therefore the fact that the protons belonging to the phenol groups are not detected in AOTMBA does not corroborate the protection. There is additional confirmation of the protection shown in the IR spectrum. Indeed, only one broad band corresponding to the OH stretching vibration of the alcohol groups is to be seen at 3272 cm⁻¹. Moreover, there is a weak band at 3085 cm⁻¹ that can be assigned to the allyl (=CH₂) stretching vibration. The peak corresponding to the phenolic-OH bending vibration is not seen, which is another indication of the protection. The results obtained combined with the elemental analysis are consistent with the formation of AOTMBA.

X-ray characterisation

Colourless crystals suitable for X-ray studies were obtained by slow evaporation of a solution of petroleum ether/diethylether (50:50). All the X-ray data collection parameters for AOTMBA are summarised in table 1 in annex 2 along with details of the refinement and disorders (fig. 3.6). The molecule shown in fig. 3.6 is non-planar due to the saturated carbon C(15) linking the two aromatic rings. Indeed, the two aryl rings are inclined at an angle of 78.93(1)° with respect to one another. The *tert*-butyl groups situated in the para position to the oxoallyl groups are on opposite sides of the core of the molecule formed by the linked aromatic rings. This conformation adopted by the molecule is a consequence of the ability of the two phenyl rings to rotate about

the C(15)-C(5) or C(15)-C(20) bond respectively and is likely to be the result of the packing partially dictated by the hydrogen-bonding network throughout the lattice (fig. 3.7).

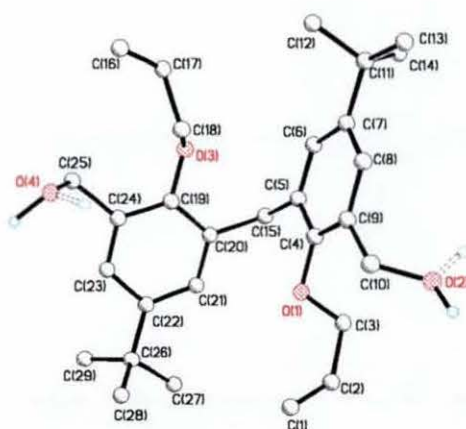


Fig. 3.6: Structure of 2,2'-diallyloxy-5,5'-di-*tert*-butyl-3,3'-methanedioldibenzyl alcohol (AOTMBA) showing the disordered hydrogen atoms

The values of the torsion angles relative to this particular part of the molecule are gathered in table 3.1.

Table 3.1: Torsion angles [°] for AOTMBA

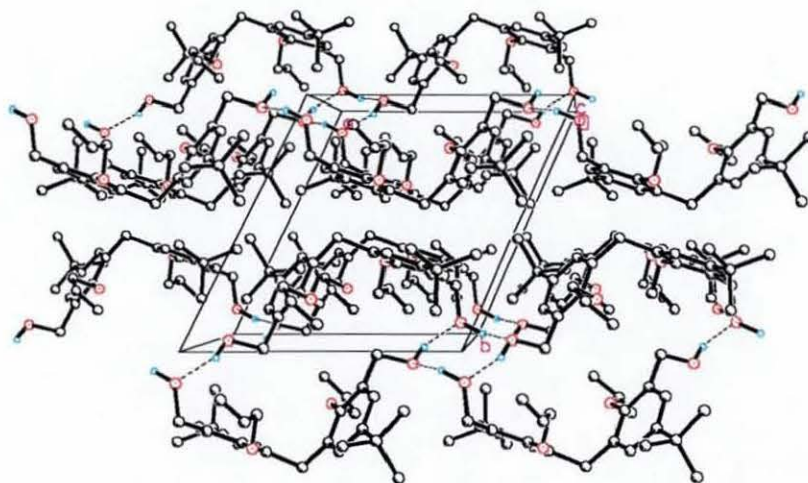
	Torsion angles in (°)
C(19)-C(20)-C(15)-C(5)	64.0(4)
C(21)-C(20)-C(15)-C(5)	-118.1(3)
C(4)-C(5)-C(15)-C(20)	65.8(4)
C(6)-C(5)-C(15)-C(20)	-114.4(3)

The -CH₂OH and oxoallyl groups are not situated in the plane formed by each aryl ring. The torsion angles are displayed in table 3.2.

Table 3.2: Torsion angles [$^{\circ}$] for AOTMBA

	Torsion angles in ($^{\circ}$)
C(19)-C(24)-C(25)-O(4)	-104.0(3)
C(23)-C(24)-C(25)-O(4)	74.5(4)
C(4)-C(9)-C(10)-O(2)	95.1(3)
C(8)-C(9)-C(10)-O(2)	-81.8(3)
C(24)-C(19)-O(3)-C(18)	71.3(3)
C(20)-C(19)-O(3)-C(18)	-112.2(3)
C(9)-C(4)-O(1)-C(3)	-83.0(3)
C(5)-C(4)-O(1)-C(3)	97.7(3)

All the bond lengths and angles are typical and merit no further discussion.

**Fig. 3.7:** Packing diagram for AOTMBA

As depicted in fig. 3.7, along the *a* axis, each molecule is hydrogen-bonded to the next one through the hydroxy groups, forming a chain of symmetry equivalent molecules related to each other by translation. Along the *b* axis, the molecules are facing each other in pairs. Within each pair the molecules are related by an inversion

centre and hydrogen-bonded through both of their hydroxy groups. The packing can be seen as a succession of parallel double chains. One of those chains is depicted in fig. 3.8.

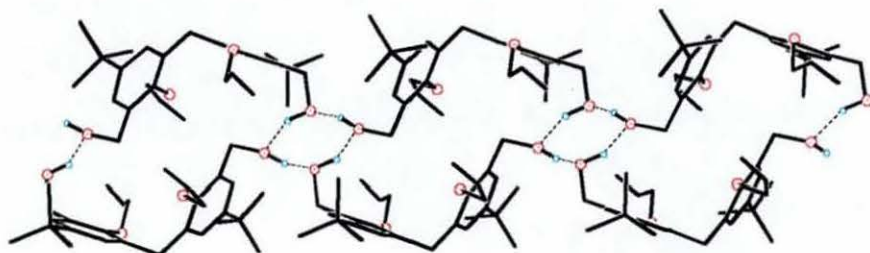


Fig. 3.8: Section of the packing showing one double chain

The bond lengths and angles relative to the hydrogen-bonding are displayed in table 3.3.

Table 3.3: Hydrogen bonds [\AA and $^\circ$] for AOTMBA

D-H...A	d(D-H)	d(H...A)	d(D...A)	$\angle(\text{DHA})$
O(4)-H(4B)...O(2)*	0.99	1.88	2.751(3)	145.8
O(2)-H(2A)...O(4)*	0.91	1.88	2.751(3)	158.6
O(4)-H(4A)...O(2)**	1.09	1.70	2.732(3)	157.1
O(2)-H(2B)...O(4) [#]	1.00	1.78	2.732(3)	158.4

Symmetry transformations used to generate equivalent atoms: (*) $-x+1, -y+2, -z$ (**) $x-1, y, z$
[#] $x+1, y, z$

3.2.2. Characterisation of 2,2'-diallyloxy-5,5'-di-*tert*-butyl-3,3'-methanediyl-dibenzaldehyde (AOTMB)

¹H NMR, IR and E.A characterisations

The notable difference in the ¹H NMR compared to AOTMBA is the peak at 10.4 ppm assigned to the aldehyde protons. The other peaks are slightly shifted as a consequence of the transformation of the alcohol groups into aldehyde groups. The same remark can be made of the IR spectrum where a characteristic peak at 1660 cm⁻¹ corresponding to the C=O stretching vibration is to be seen. The combined data, IR, ¹H NMR and elemental analysis confirm the formation of AOTMB.

X-ray characterisation

Colourless crystals suitable for X-ray studies were obtained by slow evaporation of a diethylether solution. All the X-ray data collection parameters for AOTMB are summarised in table 2 in annex 2 along with details of the refinement and disorders (fig. 3.9). There are a few differences in this structure compared to that of AOTMBA. The length of the bonds C(10)-O(2) and C(25)-O(4) are 1.213(3) and 1.207(3) Å respectively and confirm the double-bond character of the carbonyl groups. In this case the *tert*-butyl groups are on the same side of the core of the molecule formed by the two linked aryl rings, which are inclined at an angle of 74.11(6)° with respect to each other. This value is almost 4° smaller than that of AOTMBA.

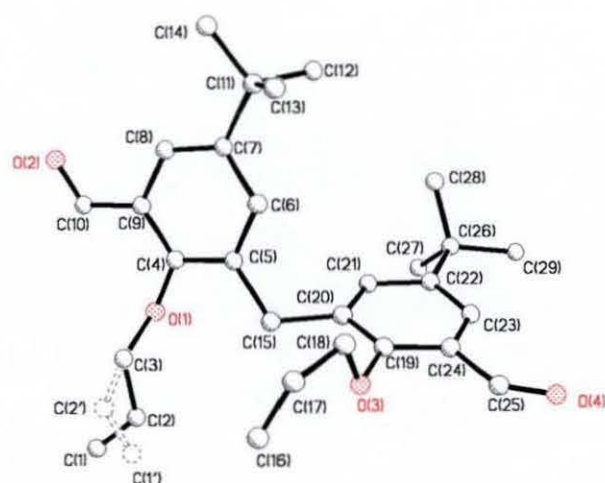


Fig. 3.9: Structure of AOTMB showing the disordered oxoallyl group

Table 3.4: Torsion angles [$^{\circ}$] for AOTMBA and AOTMB

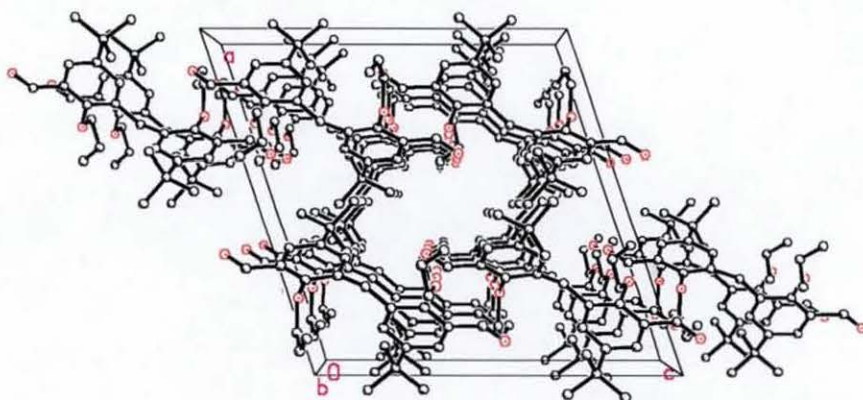
	Torsion angles in ($^{\circ}$) for AOTMBA	Torsion angles in ($^{\circ}$) for AOTMB
C(19)-C(20)-C(15)-C(5)	64.0(4)	128.2(2)
C(21)-C(20)-C(15)-C(5)	-118.1(3)	-57.3(3)
C(4)-C(5)-C(15)-C(20)	65.8(4)	151.1(3)
C(6)-C(5)-C(15)-C(20)	-114.4(3)	-29.1(3)

In the case of AOTMB, the torsion angles stated in table 3.4, are significantly different to AOTMBA.

As in the case of AOTMBA, the oxoallyl groups are not situated in the plane formed by each aryl ring. There is a 10 to 20 $^{\circ}$ difference in the torsion angles. Moreover, in contrast to the alcohol groups, both aldehyde groups are almost in the plane formed by each phenyl ring (table 3.5). All those features are probably the consequence of a different packing, which in this case is probably directed by the π -stacking between the aromatic ring and the carbonyl C=O of adjacent molecules (fig. 3.11).

Table 3.5: Torsion angles [°] for AOTMBA and AOTMB

	Torsion angles in (°) for AOTMBA	Torsion angles in (°) for AOTMB
C(19)-C(24)-C(25)-O(4)	-104.0(3)	170.8(2)
C(23)-C(24)-C(25)-O(4)	74.5(4)	-8.5(4)
C(4)-C(9)-C(10)-O(2)	95.1(3)	-176.3(2)
C(8)-C(9)-C(10)-O(2)	-81.8(3)	3.0(3)
C(24)-C(19)-O(3)-C(18)	71.3(3)	-84.3(3)
C(20)-C(19)-O(3)-C(18)	-112.2(3)	100.4(2)
C(9)-C(4)-O(1)-C(3)	-83.0(3)	-102.0(2)
C(5)-C(4)-O(1)-C(3)	97.7(3)	83.4(2)

**Fig. 3.10:** Packing diagram for AOTMB

The packing diagram (fig. 3.10) shows that along the b axis the molecules are parallel to each other forming rows. However, the packing seems to be dictated by pairs of molecules π -stacked together. The π -stacking occurs between the carbonyl group and the aromatic ring of adjacent molecules as depicted in fig. 3.11.

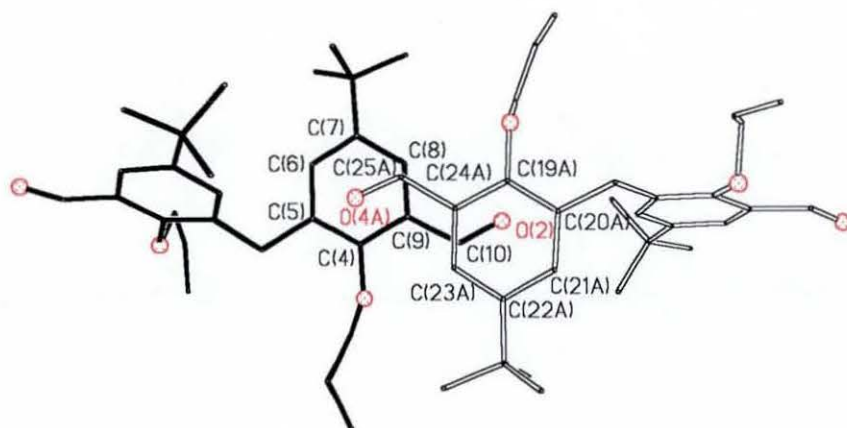


Fig. 3.11: Section of the packing showing the π -stacking

π -stacking distances:

phenyl ring C(4)C(5)C(6)C(7)C(8)C(9)/carbonyl C(25A)O(4A):

3.2834(8)-3.3652(9) Å

phenyl ring C(19A)C(20A)C(21A)C(22A)C(23A)C(24A)/carbonyl C(10)O(2):

3.2856(7)-3.4776(9) Å

3.2.3. Characterisation of 2,2'-dihydroxy-5,5'-di-*tert*-butyl-3,3'-methanediyl-dibenzaldehyde (DHTMB)

¹H NMR, IR and E.A characterisations

The ¹H NMR shows the disappearance of the peaks assigned to the allyl groups while the IR spectrum shows the characteristic C=O stretching vibration at 1658 cm⁻¹ and the appearance of one peak at 1270 cm⁻¹ corresponding to the phenolic-OH bending vibration of the two phenol groups. These features combined with the elemental analysis results confirm the formation of DHTMB.

X-ray characterisation

The very interesting feature about this compound is the fact that it can be obtained as two polymorphic crystal forms. If it is crystallised by slowly evaporating a diethylether solution of the product, it crystallises (pale yellow crystals) in the tetragonal space group $I4_1/a$. However, if the crystallisation conditions are changed it crystallises (pale yellow crystals) in a monoclinic space group $C2/c$. The latter structure has been obtained while recrystallising a nickel complex of the macrocyclic ligand H₆L11 from methanol. All the X-ray data collection parameters for DHTMB are summarised in table 3 ($I4_1/a$) and 4 ($C2/c$) in annex 2 along with details of the refinement.

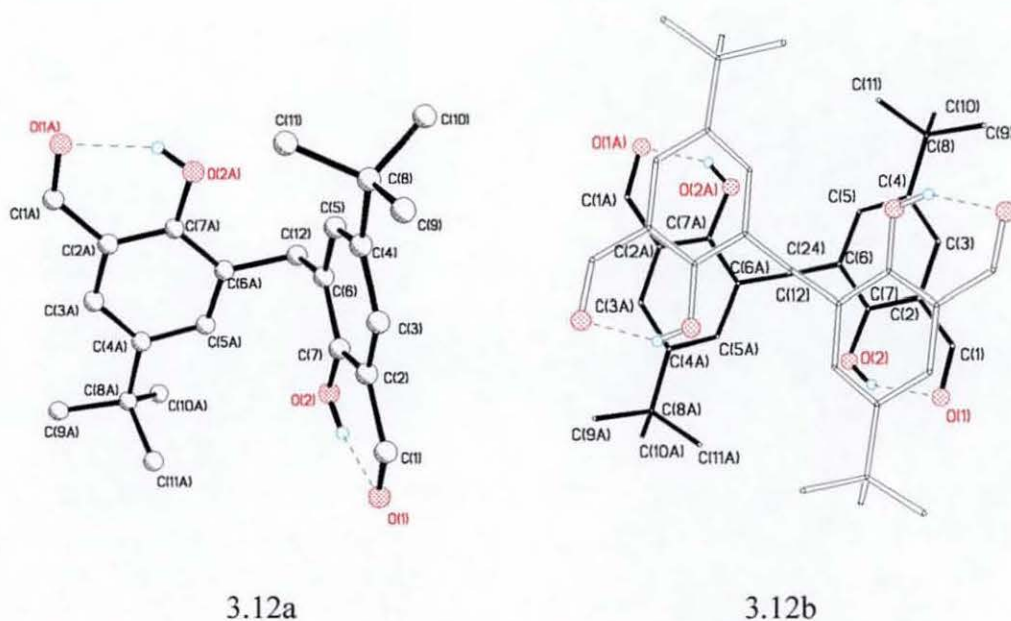


Fig. 3.12: Structure of DHTMB in the tetragonal space group (3.12a) and in the monoclinic space group (3.12b) (2 molecules in the asymmetric unit)

In the tetragonal space group, the asymmetric unit contains one molecule with a 2-fold axis passing through C(12) while in the monoclinic space group the asymmetric unit contains two molecules each having a 2-fold symmetry.

In each space group the bond lengths and angles are similar. The *tert*-butyl groups are on opposite side of the core of the molecule formed by the linked aryl rings. The phenolic hydrogen atoms are involved in an intramolecular hydrogen-bonding interaction with the oxygen atom belonging to the carbonyl groups forming a pseudo-six membered ring (dotted lines in fig. 3.12). As in the structures discussed previously, the phenyl rings are inclined at an angle with respect to each other. However, the values differ from one space group to the other. Indeed, in the tetragonal space group the value ($61.48(5)^\circ$) is much smaller than that obtained for AOTMBA ($74.11(6)^\circ$) and AOTMB ($78.93(1)^\circ$) whereas in the monoclinic space group the values are similar to AOTMBA. In the monoclinic space group, there is one difference between the two molecules in the asymmetric unit: for one set of molecules the phenyl-inclination angle is $73.58(5)^\circ$ while for the other set the value is $75.04(5)^\circ$. The values of the torsion angles C(5)-C(6)-C(12)-C(6)* ($-100.6(2)^\circ$) and C(7)-C(6)-C(12)-C(6)* ($78.27(18)^\circ$); C(17)-C(18)-C(24)-C(18)* ($101.5(2)^\circ$) and C(19)-C(18)-C(24)-C(18)* ($-76.82(18)^\circ$) in the monoclinic space groups and the values of the torsion angles C(7)-C(6)-C(12)-C(6)* ($-101.12(19)^\circ$) and C(5)-C(6)-C(12)-C(6)* ($81.89(18)^\circ$) in the tetragonal space group are closer to those obtained for AOTMBA (table 3.4). However, the twist around the saturated carbon in DHTMB is slightly bigger.

The differences for DHTMB in torsion angles and inclination angle of the two phenyl rings arise from the packing, which is different in each space groups. In the monoclinic system, the molecules are stacked along the *a* axis forming rows as depicted in fig. 3.13. As shown in fig. 3.12b, the way successive molecules are stacked (slightly tilted) there are no overlap between parts (C=O, allyl C=C and aryl ring) of the molecule that can be involved in π -stacking. Along the *a* axis, the molecules are stacked in an ABAB fashion. The *tert*-butyl groups of successive molecules are pointing in opposite directions to reduce the steric hindrance (fig. 3.12b).

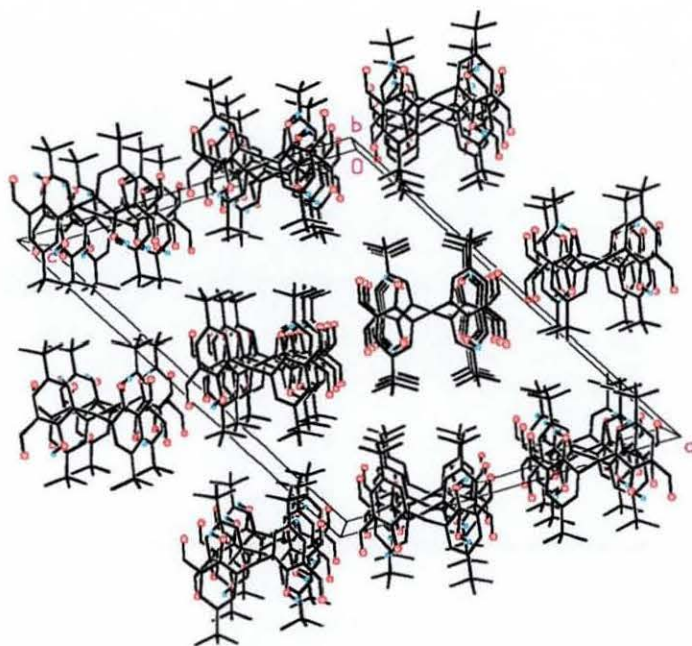


Fig. 3.13: Packing diagram (view down the a axis) of DHTMB (monoclinic)

In the tetragonal space group, the molecules are arranged as depicted in fig. 3.14 and 3.15. Some molecules form rows along b while others form rows along a.

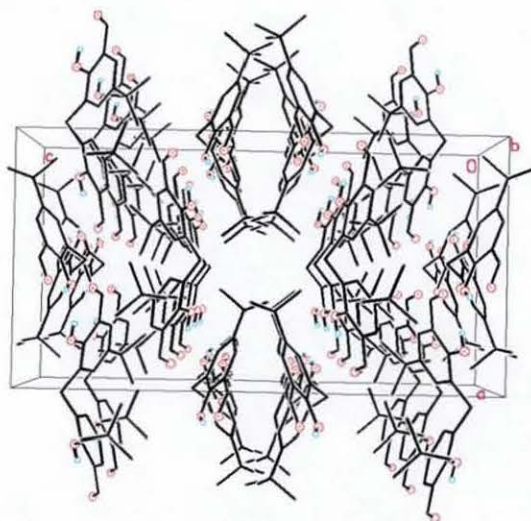


Fig. 3.14: Packing diagram (along the b-axis) of DHTMB (tetragonal)

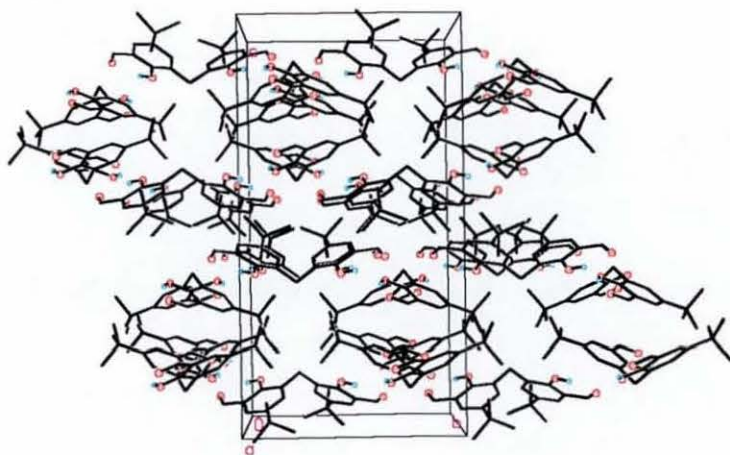


Fig. 3.15: Packing diagram (along the a-axis) of DHTMB (tetragonal)

3.3. Pseudo-cryptate structures: pendent arm macrocycle

3.3.1. Synthesis of $[\text{Mn}_2(\text{L8})](\text{ClO}_4)_2$ and $[\text{Co}_2(\text{L8})](\text{ClO}_4)_2$

DHTMB can be used to prepare a range of [2+2] Schiff-base macrocycles using standard metal ion template methods with a range of amines. Reaction with tris(2-aminoethyl)amine (tren) in the presence of Mn(II) or Co(II) produces dinuclear complexes of the pendent arm ligand $\text{H}_4\text{L8}$ (fig. 3.16) with a yield of 48% and 29% respectively. Even if the DHTMB:tren ratio is 3:3, the condensation of a third link to form the cryptate-like structure is prevented probably by the geometry adopted by the DHTMB fragment as described below. Moreover, a range of different geometries might be possible and favoured over the cryptate-like structure. In the case of cobalt, a small amount of a dinuclear complex of the ligand $\text{H}_2\text{L8a}$ containing only one DHTMB fragment, $([\text{Co}_2(\text{L8a})](\text{ClO}_4)(\text{OH})(\text{CH}_3\text{OH}))$, was isolated.

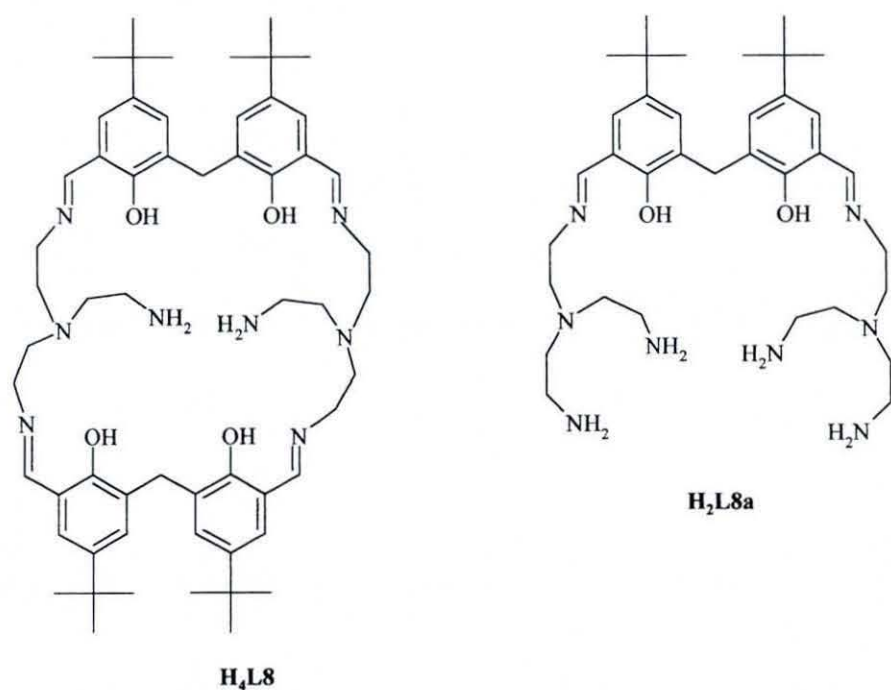


Fig. 3.16: Ligands H₄L8 and H₂L8a

3.3.2. IR and FAB characterisation of [Mn₂(L8)](ClO₄)₂

The macrocyclic nature of the complexes is suggested by the absence of the carbonyl vibration associated with DHTMB and the presence of the imine stretches at 1631 cm⁻¹, 1616 cm⁻¹ and 1599 cm⁻¹. The three bands observed are indicative of a non-symmetric environment for the imine groups, which is confirmed by the structure of the complex described later. The band at 1545 cm⁻¹ can be assigned to the C-O vibration of the phenol groups.¹²⁸ The vibrations at 1089 and 624 cm⁻¹ are assigned to the ν_3 and ν_4 vibrations of the perchlorate anion. The strong broad peak at 3400 cm⁻¹ might be indicative of the hygroscopic character of the compound. Two bands at 3135 and 3247 cm⁻¹ can be assigned to the symmetric and asymmetric -NH₂ stretching vibrations of the primary amine. This is an indication that one branch of tren is not condensed as shown in the crystal structure.

The FAB spectrum shows a major peak at m/z 1063(100) that can be assigned to the cation $[\text{Mn}_2(\text{L8})]^{2+}$ and a smaller peak at m/z 1163(5) that can be assigned to the cation $[\text{Mn}_2(\text{L8})(\text{ClO}_4)]^+$. This attribution supports the formation of the complex $[\text{Mn}_2(\text{L8})](\text{ClO}_4)_2$.

3.3.3. Structure of $[\text{Mn}_2(\text{L8})](\text{ClO}_4)_2$

Pale green crystals of $[\text{Mn}_2(\text{L8})](\text{ClO}_4)_2 \cdot 4\text{CH}_3\text{CN}$ suitable for X-ray studies were grown by slow diffusion of diethylether into an acetonitrile solution of the compound. The complex contains two well-separated metal ions, encapsulated by the ligand in a pseudo-cryptate structure. Two views of the cation are depicted in fig. 3.17 and 3.18. All the X-ray data collection parameters for $[\text{Mn}_2(\text{L8})](\text{ClO}_4)_2 \cdot 4\text{CH}_3\text{CN}$ are summarised in table 5 in annex 2 along with the details concerning the refinement and disorders.

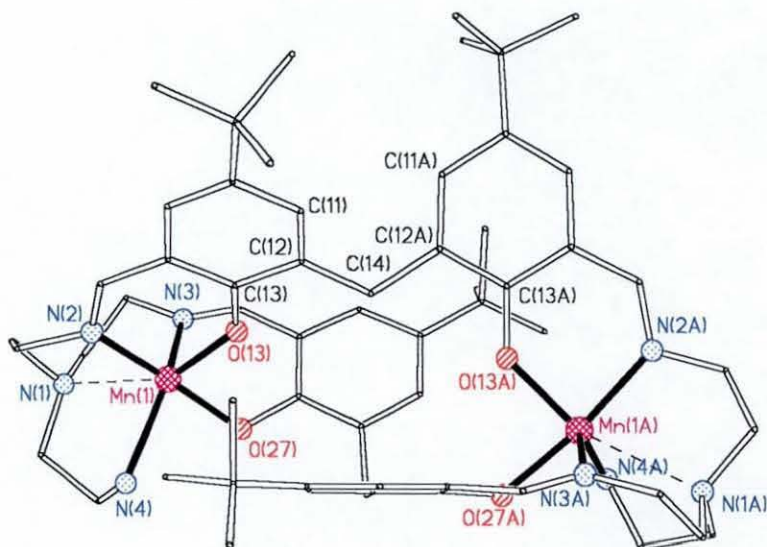


Fig. 3.17: Structure of the cation $[\text{Mn}_2(\text{L8})]^{2+}$

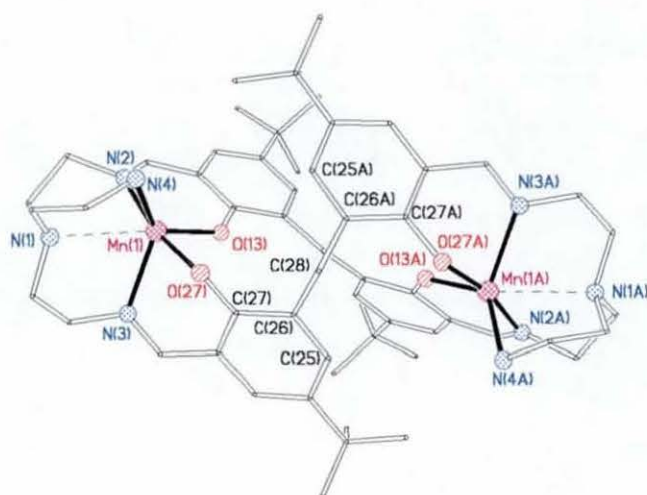


Fig. 3.18: Structure of the cation $[\text{Mn}_2(\text{L8})]^{2+}$

The DHTMB fragment is able to adopt a variety of geometrical conformations due to the saturated carbon linking the two phenyl rings. In this instance, the saturated carbons for the two fragments are C(14) and C(28) and the two fragments adopt different conformations. The view in fig. 3.17 shows that one DHTMB link has a *syn*-conformation (both phenolic oxygen atoms O(13) and O(13A) on the same side) with the two phenyl rings tilted with respect to each other. This tilted geometry is enabled due to the ability of the two aryl rings to rotate around the saturated carbon C(14) (torsion angles are given in table 3.6). The view in fig. 3.18 shows that the conformation of the second strand is *anti* (both phenolic oxygen atoms on opposite sides) with the molecule adopting a folded geometry due to the rotation around the saturated carbon (C(28)), which enables the rings to come closer together, facing each other. The value of the angle between the plane formed by the two phenyl rings is $63.35(12)^\circ$. Furthermore, the phenyl rings can rotate about the bond linking the ring to C(28) (see torsion angles in table 3.6), which permits some flexibility for the coordination of the oxygen atoms. In this case, they opt for the *syn*-conformation. In this complex, binding of a third link to form a genuine cryptate is sterically prevented by the figure-8 *anti* geometry of the DHTMB section of the macrocycle. This complex is a perfect example of how the flexibility of the DHTMB fragment can give

rise to an interesting twisted geometry. The distance separating the two manganese ions (7.98(6) Å) seems too big for them to interact.

Table 3.6: Torsion angles [°] for [Mn₂(L8)](ClO₄)₂

	Torsion angles in (°)
C(11)-C(12)-C(14)-C(12A)	-31.9(4)
C(13)-C(12)-C(14)-C(12A)	153.2(4)
C(25)-C(26)-C(28)-C(26A)	88.5(4)
C(27)-C(26)-C(28)-C(26A)	-92.3(4)

The geometry at the metal ions could be regarded as irregular 6-coordinate or as approximately trigonal bipyramidal. The interaction between the manganese ion and the bridged nitrogen atom N(1) is rather long at 2.515(4) Å. The selected bond lengths and angles are given in table 3.7.

Table 3.7: Selected bond lengths [Å] and angles [°] for [Mn₂(L8)](ClO₄)₂

Mn(1)-O(27)	1.890(3)	Mn(1)-N(4)	2.150(4)
Mn(1)-O(13)	1.908(3)	Mn(1)-N(3)	2.184(4)
Mn(1)-N(2)	2.021(4)	Mn(1)-N(1)	2.515(4)
O(27)-Mn(1)-O(13)	86.17(14)	N(2)-Mn(1)-N(3)	107.70(16)
O(27)-Mn(1)-N(2)	168.56(15)	N(4)-Mn(1)-N(3)	130.02(16)
O(13)-Mn(1)-N(2)	88.14(15)	O(27)-Mn(1)-N(1)	113.84(13)
O(27)-Mn(1)-N(4)	81.04(15)	O(13)-Mn(1)-N(1)	153.39(14)
O(13)-Mn(1)-N(4)	129.77(15)	N(2)-Mn(1)-N(1)	74.83(15)
N(2)-Mn(1)-N(4)	95.08(16)	N(4)-Mn(1)-N(1)	73.06(15)
O(27)-Mn(1)-N(3)	82.75(14)	N(3)-Mn(1)-N(1)	71.13(15)
O(13)-Mn(1)-N(3)	95.63(15)		

The oxidation state of the manganese ions is not unambiguous. The distorted geometry feature would be more typical for Mn(II), which is not as demanding for its geometric environment as Mn(III) but some bond lengths are very short for a Mn(II) ion (e.g. 1.890(3) and 1.908(3) Å) (table 3.7). In addition, the pale green colour of the complex would suggest that it contains Mn(III) ions and not Mn(II) ions. The oxidation states of the two manganese ions can be assigned as + (III), assuming the four phenolate groups are deprotonated. The distance between the two phenolic oxygen atoms O(13) and O(13A) belonging to the DHTMB fragment with the *syn*-conformation is 5.12(5) Å. This distance is too far for a proton to be shared between the two oxygen atoms, which leaves the case of a mixed-valence (II/III) complex unlikely. However, there is a possibility that the oxygen atoms O(13) and O(27) separated by 2.594(4) Å share one hydrogen. As O(13A) and O(27A) are the symmetry equivalents of O(13) and O(27) respectively, they would also share one hydrogen. Consequently, the oxidation state of both manganese ions is likely to be + (II). In this case, as the X-ray data are not good enough to be able to find protons, it is difficult to reach a decision without further evidence. The measurement of the magnetic susceptibility at room temperature should give an idea as to the oxidation states of the manganese ions. However, the value of the calculated effective magnetic moment per Mn ions is $3.97\mu_B$, which is very low for the expected spin-only value of two non-interacting Mn(II) ($S = 5/2$, $5.92\mu_B$) or two non-interacting Mn(III) ($S = 2$, $4.90\mu_B$). This might be due to impurities present in the sample or the container. Carrying out the experiment on more sample or possibly on a better quality sample might shed a light on the oxidation states of the manganese ions. Nevertheless, further magnetic studies are needed to be able to determine beyond doubt the oxidation states of the two manganese ions.

3.3.4. IR and FAB characterisation of $[\text{Co}_2(\text{L8})(\text{ClO}_4)_2]$ and $[\text{Co}_2(\text{L8a})(\text{ClO}_4)(\text{OH})(\text{CH}_3\text{OH})]$

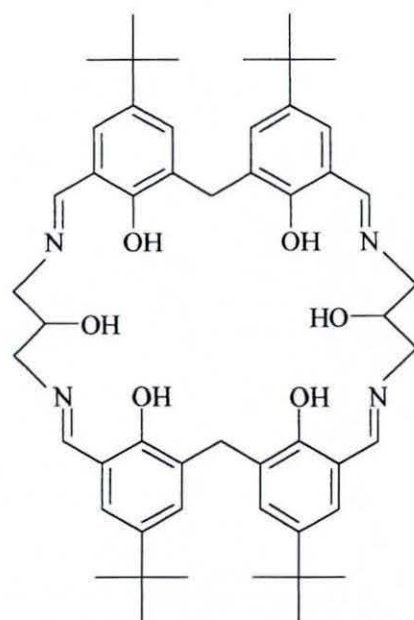
No crystals suitable for X-ray studies were isolated for $[\text{Co}_2(\text{L8})(\text{ClO}_4)_2]$ and $[\text{Co}_2(\text{L8a})(\text{ClO}_4)(\text{OH})(\text{CH}_3\text{OH})]$. The main product isolated is assumed to be

$[\text{Co}_2(\text{L8})](\text{ClO}_4)_2$ (yellow powder) mainly because of the results of the elemental analysis. Unfortunately, probably due to a poor solubility of the sample in the noba matrix, only a small amount of $[\text{Co}_2(\text{L8a})](\text{ClO}_4)(\text{OH})(\text{CH}_3\text{OH})$ was detected at m/z 840 ($[\text{Co}_2(\text{L8a})(\text{ClO}_4)]^+$). This does not give an indication whether the complex $[\text{Co}_2(\text{L8})](\text{ClO}_4)_2$ did or did not form.

Similarly to the dinuclear manganese complex, the condensation of DHTMB with tren is suggested by the absence of the carbonyl vibration associated with DHTMB and the presence of an imine stretch at, respectively for $[\text{Co}_2(\text{L8})](\text{ClO}_4)_2$ and $[\text{Co}_2(\text{L8a})](\text{ClO}_4)(\text{OH})(\text{CH}_3\text{OH})$, 1631 cm^{-1} and 1643 cm^{-1} . The detection of only one imine stretch for both cobalt complexes might be an indication of a different structure compared to the manganese complex as in the manganese structure the imine groups are not equivalent. The expected vibrations at *ca.* 1090 and 624 cm^{-1} for the perchlorate counteranions are observed. As for the dimanganese complex, the strong peak at 3423 cm^{-1} might be indicative of the hygroscopic character of the compound. The band at 3269 cm^{-1} and a weaker shoulder at *ca.* 3120 cm^{-1} can be assigned to the symmetric and asymmetric $-\text{NH}_2$ stretching vibrations of the primary amine. The second peak is stronger in the case of the manganese complex.

3.4. Dinuclear bridged complexes of L9

The reaction of DHTMB with 1,3-diaminopropan-2-ol yields di-, tri- and tetranuclear complexes of $\text{H}_6\text{L9}$ (fig. 3.19) with very interesting conformations, again, because of the partial flexibility of the DHTMB head-unit.



H₆L9

Fig. 3.19: Ligand H₆L9

3.4.1. Synthesis of [Ni₂(H₄L9)(μ₂-H₂O)(EtOH)₂](ClO₄)₂ and [Co₂(H₄L9)(μ₂-H₂O)(H₂O)₂](ClO₄)₂

The complex [Ni₂(H₄L9)(μ₂-H₂O)(EtOH)₂](ClO₄)₂ was isolated as green crystals with a yield of 61%. However, the green crystalline powder turned red under vacuum due to the loss of solvent molecules. The dried complex is [Ni₂(H₄L2)](ClO₄)₂·3H₂O, as confirmed by elemental analysis. The water molecules are thought to be non-coordinated as the geometry around the metal is usually found to be square planar or tetrahedral for Ni(II) complexes isolated as red powders. If the complex is square planar, the complex is expected to be diamagnetic. Preliminary variable-temperature magnetic studies showed that the sample is not diamagnetic but that the moment per nickel atom is 2.19 B.M at T = 80 K and 2.26 B.M at T = 280 K, which is too low for Ni(II) in a high spin configuration. However, it is possible that the solvent has not all been removed under vacuum and that the sample contains a mixture of complexes with the two nickel atoms in an octahedral environment, hence paramagnetic and

complexes with the two nickel atoms in a square planar environment, hence diamagnetic. Further studies are needed to shed a light on the behaviour of this compound.

The complex $[\text{Co}_2(\text{H}_4\text{L9})(\mu_2\text{-H}_2\text{O})(\text{H}_2\text{O})_2](\text{ClO}_4)_2$ was synthesised under nitrogen because it was found to slowly oxidise in solution. Once isolated as a pale yellow-orange powder (45%) the complex seems stable. In the structure of $[\text{Co}_2(\text{H}_4\text{L9})(\mu_2\text{-H}_2\text{O})(\text{EtOH})_2](\text{ClO}_4)_2$ described later, the geometry around the cobalt is octahedral, thus, it can be assumed that the bridging water molecule and the water molecule occupying the remaining axial coordination site of each cobalt are all coordinated as there is no change in colour when the yellow-orange powder is solubilised in ethanol. Moreover, the value of the room-temperature effective magnetic moment is $4.74\mu_{\text{B}}$, which falls within the range expected for high-spin Co(II) in an octahedral environment.^{129,130} Over a short period of time, an ethanol solution of the complex, which was yellow-orange at the beginning turned dark brown suggesting that other Co(III) products can be formed.

3.4.2. IR and FAB characterisation of $[\text{Ni}_2(\text{H}_4\text{L9})(\mu_2\text{-H}_2\text{O})(\text{EtOH})_2](\text{ClO}_4)_2$ and $[\text{Co}_2(\text{H}_4\text{L9})(\mu_2\text{-H}_2\text{O})(\text{H}_2\text{O})_2](\text{ClO}_4)_2$

The macrocyclic nature of the two complexes is suggested by the absence of the carbonyl vibration associated with DHTMB and the presence of the imine stretch at 1636 cm^{-1} for $[\text{Ni}_2(\text{H}_4\text{L9})(\mu_2\text{-H}_2\text{O})(\text{EtOH})_2](\text{ClO}_4)_2$ and 1630 cm^{-1} for $[\text{Co}_2(\text{H}_4\text{L9})(\mu_2\text{-H}_2\text{O})(\text{H}_2\text{O})_2](\text{ClO}_4)_2$. The weak band at 1560 cm^{-1} for both complexes can be assigned to the C-O vibration of the phenol groups.¹²⁸ In both cases the structure is symmetric as demonstrated later therefore only one imine stretch is expected. For the cobalt complex the expected ν_3 and ν_4 vibrations for the perchlorate anions are detected at ca. 1117 cm^{-1} and 626 cm^{-1} . The ν_3 vibration is split into three bands 1088 , 1117 and 1134 cm^{-1} , which indicates an unsymmetrical environment for ClO_4^- . For the nickel complex, the ν_3 and ν_4 vibrations for the perchlorate anions are

detected at 1120 cm^{-1} (broad) and 626 cm^{-1} . There is no real indication of the coordinated bridging water molecule in neither of the complexes, probably overlapped by the strong broad band at 3433 cm^{-1} that might be indicative of the hygroscopic character of the compound. It could also be an indication that the coordinated water molecule is involved in hydrogen-bonding.

In both complexes, the FAB data (table 3.8 and 3.9) support the formation of the dinuclear macrocyclic species. In each complex, the ligands completing the coordination sphere are different to the crystal structure (water and methanol instead of ethanol). For the nickel complex, there is no supporting evidence of the presence of water bridging the two metal ions as will be described in the structure further on in the discussion. For the cobalt complex, there might be an indication with the peak at m/z 1126 but the relative intensity of the peak (3) is very weak.

Table 3.8: Peak attributions for $[\text{Ni}_2(\text{H}_4\text{L9})(\mu_2\text{-H}_2\text{O})(\text{EtOH})_2](\text{ClO}_4)_2$

m/z	Rel. Intensity (%)	Fragments	Calc. Mass
901	10	$[\text{Ni}(\text{H}_4\text{L9})+\text{H}]^+$	901
941	25	$[\text{Ni}(\text{H}_4\text{L9})(\text{H}_2\text{O})+\text{Na}]^+$	941
957	100	$[\text{Ni}_2(\text{H}_4\text{L9})]^{2+}$	958
995	5	$[\text{Ni}_2(\text{H}_4\text{L9})(\text{H}_2\text{O})_2]^{2+}$	994
1094	5	$[\text{Ni}_2(\text{H}_4\text{L9})(\text{H}_2\text{O})_2(\text{ClO}_4)]^+$	1093
1108	5	$[\text{Ni}_2(\text{H}_4\text{L9})(\text{H}_2\text{O})(\text{MeOH})(\text{ClO}_4)]^+$	1107

Table 3.9: Peak attributions for $[\text{Co}_2(\text{H}_4\text{L9})(\mu_2\text{-H}_2\text{O})(\text{H}_2\text{O})_2](\text{ClO}_4)_2$

m/z	Rel. Intensity (%)	Fragments	Calc. Mass
903	< 5	$[\text{Co}(\text{H}_4\text{L9})+\text{H}]^+$	902
943	< 5	$[\text{Co}(\text{H}_4\text{L9})(\text{H}_2\text{O})+\text{Na}]^+$	942
959	25	$[\text{Co}_2(\text{H}_4\text{L9})]^{2+}$	960
995	100	$[\text{Co}_2(\text{H}_4\text{L9})(\text{H}_2\text{O})_2]^{2+}$	996
1011	3	$[\text{Co}_2(\text{H}_4\text{L9})(\text{H}_2\text{O})(\text{MeOH})]^{2+}$	1010
1126	3	$[\text{Co}_2(\text{H}_4\text{L9})(\text{H}_2\text{O})_2(\text{MeOH})(\text{ClO}_4)]^+$	1127

3.4.3. Structures of $[\text{Ni}_2(\text{H}_4\text{L9})(\mu_2\text{-H}_2\text{O})(\text{EtOH})_2](\text{ClO}_4)_2$ and $[\text{Co}_2(\text{H}_4\text{L9})(\mu_2\text{-H}_2\text{O})(\text{EtOH})_2](\text{ClO}_4)_2$

Green crystals of $[\text{Ni}_2(\text{H}_4\text{L9})(\mu_2\text{-H}_2\text{O})(\text{EtOH})_2](\text{ClO}_4)_2$ and yellow crystals of $[\text{Co}_2(\text{H}_4\text{L9})(\mu_2\text{-H}_2\text{O})(\text{EtOH})_2](\text{ClO}_4)_2$ suitable for X-ray studies were grown by slow evaporation of an ethanol solution of $[\text{Ni}_2(\text{H}_4\text{L9})(\mu_2\text{-H}_2\text{O})(\text{EtOH})_2](\text{ClO}_4)_2$ and $[\text{Co}_2(\text{H}_4\text{L9})(\mu_2\text{-H}_2\text{O})(\text{H}_2\text{O})_2](\text{ClO}_4)_2$ respectively. For the cobalt complex, an exchange of exogenous ligands took place. Moreover, beside the yellow crystals of $[\text{Co}_2(\text{H}_4\text{L9})(\mu_2\text{-H}_2\text{O})(\text{H}_2\text{O})_2](\text{ClO}_4)_2$ a brown product formed that has not been identified but is likely to contain Co(III).

The two structures are isomorphous, thus only one will be described. All the X-ray data collection parameters for $[\text{Ni}_2(\text{H}_4\text{L9})(\mu_2\text{-H}_2\text{O})(\text{EtOH})_2](\text{ClO}_4)_2$ and $[\text{Co}_2(\text{H}_4\text{L9})(\mu_2\text{-H}_2\text{O})(\text{EtOH})_2](\text{ClO}_4)_2$ are summarised in table 6 and 7 respectively in annex 2 along with the details concerning the refinement and disorders.

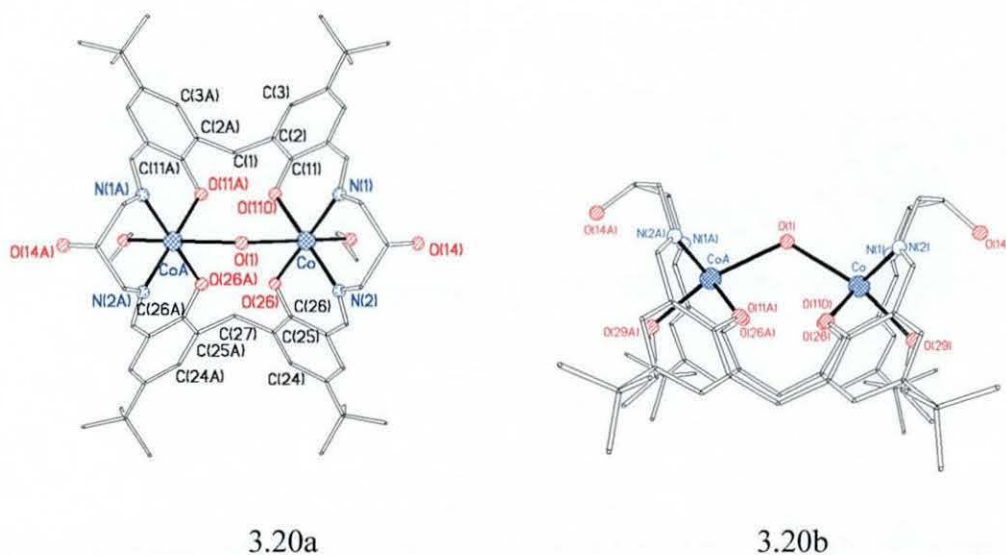


Fig. 3.20: Two views of the cation $[\text{Co}_2(\text{H}_4\text{L9})(\mu_2\text{-H}_2\text{O})(\text{EtOH})_2]^{2+}$

With 1,3-diaminopropan-2-ol another conformation is accessible for the macrocycle containing DHTMB as a head-unit. As demonstrated in fig. 3.20, the structure is symmetric with a mirror plane passing through C(1), O(1) and C(27). The alcohol groups are not involved in bonding, which partially allows the macrocycle to adopt the saddle conformation (fig. 3.21). Fig. 3.20b clearly shows that the hydroxy groups are pointing outside the cavity of the macrocycle. The diphenolic head-unit plays a big part in the flexibility of the macrocyclic complex compared to more planar macrocyclic complexes formed by the condensation of 1,3-diaminopropan-2-ol with single phenolic head-units like DFTP or DFMP.⁶⁹⁻⁷² As described previously, the two phenyl rings can rotate in different ways, which gives a certain degree of freedom to the macrocycle. Here, the rotation of the aryl rings around the saturated carbon C(1) or C(27) enables the two rings to face each other with the molecule adopting a folded geometry. The conformation of both DHTMB fragments is *syn*. The value of the angle between the planes formed by the two phenyl rings is $69.41(17)^\circ$ for $[\text{Co}_2(\text{H}_4\text{L9})(\mu_2\text{-H}_2\text{O})(\text{EtOH})_2](\text{ClO}_4)_2$ and $72.34(16)^\circ$ for $[\text{Ni}_2(\text{H}_4\text{L9})(\mu_2\text{-H}_2\text{O})(\text{EtOH})_2](\text{ClO}_4)_2$. Relevant torsion angles for both complexes are given in table 3.10. As the data were weak, it was not possible to find if the phenolic oxygen atoms were protonated or not. However, in a closely related structure, $[\text{Zn}_2(\text{H}_4\text{L9})(\mu_2\text{-Cl})]\text{Cl}$

synthesised by J. Barreira Fontecha, two hydrogen atoms, each shared between the adjacent phenolic oxygen atoms of the DHTMB fragment, were detected. Thus, it is not unreasonable to think that this is also the case for the dinuclear cobalt and nickel complexes. It is thought that the folded geometry adopted by the macrocycle is mainly due to these hydrogen bonded links and not to the bridging groups (H₂O or Cl), whose coordination to the metal is relatively weak (*ca.* 2.5 Å). Those features control the metal-metal distance, which is 4.213(15) Å for the dicobalt complex and 4.223(13) Å for the dinickel complex.

Table 3.10: Torsion angles [°] for [Co₂(H₄L9)(μ₂-H₂O)(EtOH)₂](ClO₄)₂ and [Ni₂(H₄L9)(μ₂-H₂O)(EtOH)₂](ClO₄)₂

	Torsion angles in (°) for [Co ₂ (H ₄ L9)(μ ₂ - H ₂ O)(EtOH) ₂](ClO ₄) ₂	Torsion angles in (°) for [Ni ₂ (H ₄ L9)(μ ₂ - H ₂ O)(EtOH) ₂](ClO ₄) ₂
C(24)-C(25)-C(27)-C(25A)	94.5(7)	96.7(6)
C(26)-C(25)-C(27)-C(25A)	-82.0(8)	-83.6(7)

The two metal ions are in a tetragonal environment, with the macrocycle providing two imine nitrogen atoms and two phenolic oxygen atoms. The axial sites are occupied by one bridging water molecule and one ethanol molecule. The selected bond lengths and angles for [Co₂(H₄L9)(μ₂-H₂O)(EtOH)₂](ClO₄)₂ are given in table 3.11. The bridging water molecule is coordinated relatively weakly to the metal ions at a distance of *ca.* 2.4 Å in both complexes. There are few reports on water bridging nickel complexes.^{106,107,131-134} Most of the distances recorded are *ca.* 2.1 Å. Only a couple of examples with longer distances of *ca.* 2.4 Å are accounted for.^{107,133} In these latter cases, the bridge is not symmetric: one distance is *ca.* 2.2 Å and the other is 2.4 Å. There are hydrogen-bonding distances between O(1) and two methanol solvate molecules with one of the methanol molecules hydrogen-bonded to one of the perchlorate ions (table 3.12). Considering this observation, there is at least one

hydrogen on the bridging oxygen O(1). However, the distance would be too long for a bridging hydroxy group, therefore it can reasonably be assumed that the bridging unit is a water molecule (fig. 3.21).

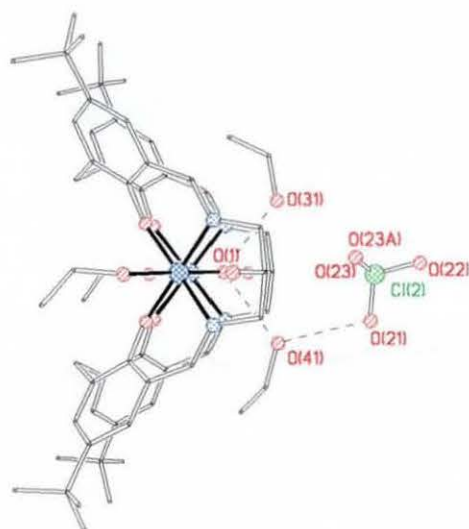


Fig. 3.21: Structure of the cation $[\text{Co}_2(\text{H}_4\text{L9})(\mu_2\text{-H}_2\text{O})(\text{EtOH})_2(\text{ClO}_4)]^+$ showing the hydrogen-bonding

Table 3.11: Selected bond lengths [\AA] and angles [$^\circ$] for $[\text{Co}_2(\text{H}_4\text{L9})(\mu_2\text{-H}_2\text{O})(\text{EtOH})_2](\text{ClO}_4)_2$

Co-O(26)	2.012(4)	Co-O(29)	2.156(4)
Co-O(110)	2.020(4)	Co-O(1)	2.400(3)
Co-N(1)	2.055(5)	O(1)-Co*	2.400(3)
Co-N(2)	2.056(5)		
O(26)-Co-O(110)	92.47(15)	O(26)-Co-O(29)	88.33(16)
O(26)-Co-N(1)	179.16(18)	O(110)-Co-O(29)	89.61(15)
O(110)-Co-N(1)	86.97(16)	N(1)-Co-O(29)	91.04(18)
O(26)-Co-N(2)	86.72(17)	N(2)-Co-O(29)	89.21(18)
O(110)-Co-N(2)	178.59(18)	O(26)-Co-O(1)	81.58(17)
N(1)-Co-N(2)	93.83(19)	O(110)-Co-O(1)	81.58(16)

N(1)-Co-O(1)	98.94(19)	O(29)-Co-O(1)	166.26(17)
N(2)-Co-O(1)	99.44(19)	Co*-O(1)-Co	122.7(2)

Symmetry transformations used to generate equivalent atoms: (*) x, -y+1/2, z

Table 3.12: Hydrogen bonds [\AA] for $[\text{Co}_2(\text{H}_4\text{L9})(\mu_2\text{-H}_2\text{O})(\text{EtOH})_2](\text{ClO}_4)_2$

D---A	d(D---A)
O(1)...O(31)	2.707(9)
O(1)...O(41)	2.711(9)
O(41)...O(21)	2.877(12)

Symmetry transformations used to generate equivalent atoms: (*) x, -y+1/2, z

Fig. 3.22 shows that the individual macrocyclic complexes are linked *via* perchlorate anions through hydrogen-bonding forming chains.

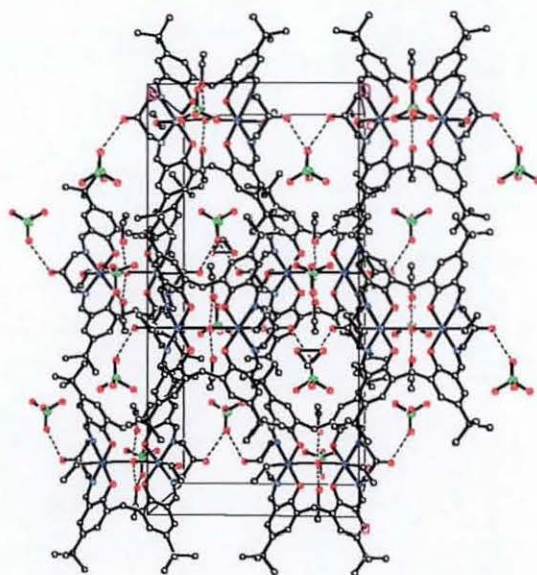


Fig. 3.22: Packing diagram of $[\text{Co}_2(\text{H}_4\text{L9})(\mu_2\text{-H}_2\text{O})(\text{EtOH})_2](\text{ClO}_4)_2$ showing the hydrogen-bonding

3.4.4. Synthesis of $[\text{Ni}_2(\text{H}_4\text{L9})(\mu_2\text{-H}_2\text{O})(\text{H}_2\text{O})_2](\text{NO}_3)_2$ and $[\text{Ni}_2(\text{H}_4\text{L9})(\text{NO}_3)(\text{DMF})_2](\text{NO}_3)$

When refluxed for 6-7 hours, the complex formed is similar to $[\text{Ni}_2(\text{H}_4\text{L9})(\mu_2\text{-H}_2\text{O})(\text{EtOH})_2](\text{ClO}_4)_2$ with nitrate as counteranions. As no crystals suitable for X-ray studies were isolated, the elemental analysis data combined with the IR and FAB results supported the formation of $[\text{Ni}_2(\text{H}_4\text{L9})(\mu_2\text{-H}_2\text{O})(\text{H}_2\text{O})_2](\text{NO}_3)_2$. In the IR spectrum there was no indication of a bridging nitrate anion as only a strong sharp band at 1383 cm^{-1} characteristic of free nitrate anions was detected. The FAB shows one major peak at m/z 958 attributed to $[\text{Ni}_2(\text{H}_4\text{L9})]^{2+}$ and a minor peak attributed to $[\text{Ni}_2(\text{H}_4\text{L9})(\text{H}_2\text{O})_2]^{2+}$. However, when the reaction time was scaled down to 4 hours and the crude product washed with dichloromethane, green crystals of $[\text{Ni}_2(\text{H}_4\text{L9})(\text{NO}_3)(\text{DMF})_2](\text{NO}_3)$ grew by slow evaporation of a DMF solution of the compound with a yield of 54%. As DMF was not present during the reaction, it is reasonable to assume that water or ethanol molecules were displaced by DMF molecules, which is consistent with the elemental analysis data. Considering that in the reaction mixture the amount of water was superior to that present during the recrystallisation in DMF, the initial complex formed might have been similar to $[\text{Ni}_2(\text{H}_4\text{L9})(\mu_2\text{-H}_2\text{O})(\text{H}_2\text{O})_2](\text{NO}_3)_2$ with a bridging water molecule, which would have been replaced by a nitrate molecule during the recrystallisation process to yield $[\text{Ni}_2(\text{H}_4\text{L9})(\text{NO}_3)(\text{DMF})_2](\text{NO}_3)$. The product of the 7 hour-reflux reaction was not recrystallised with DMF, thus the isolation of the product of the 4-hour reaction might not, in fact, be due to the reduced reaction time but to the DMF recrystallisation. No crystals were isolated with other exogenous ligands such as water or ethanol. The IR spectrum of $[\text{Ni}_2(\text{H}_4\text{L9})(\text{NO}_3)(\text{DMF})_2](\text{NO}_3)$ is very similar to the dinuclear water bridged complexes described previously except for the vibrations of the DMF molecules and the nitrate counteranions. The nitrate vibrations are indicative of both coordinated (1366 and 1436 cm^{-1}) and free (1385 cm^{-1}) nitrate ions, which is consistent with the formula. The FAB (table 3.13) supports the formation of the dinuclear macrocycle but also shows peaks with a very low intensity at higher mass (m/z 1916, 1954 and 2044). This could mean two things: the fragmentation might

have initiated the formation of polynuclear nickel species during the FAB experiment or there is a small contamination of the sample by polynuclear species formed from the bridging of individual macrocycles.

Table 3.13: Peak attributions for $[\text{Ni}_2(\text{H}_4\text{L9})(\text{NO}_3)(\text{DMF})_2](\text{NO}_3)$

m/z	Rel. Intensity (%)	Fragments	Calc. Mass
903	5	$[\text{Ni}(\text{H}_4\text{L9})+\text{H}]^+$	901
941	15	$[\text{Ni}(\text{H}_4\text{L9})(\text{H}_2\text{O})+\text{Na}]^+$	941
973	100	$[\text{Ni}_2(\text{H}_4\text{L9})(\text{H}_2\text{O})]^{2+}$	976
995	20	$[\text{Ni}_2(\text{H}_4\text{L9})(\text{H}_2\text{O})_2]^{2+}$	994
1085	13	$[\text{Ni}_2(\text{H}_4\text{L9})(\text{NO}_3)(\text{MeOH})_2]^+$	1084
1916	< 5		
1954	< 5		
2044	< 5		

3.4.5. Structure of $[\text{Ni}_2(\text{H}_4\text{L9})(\text{NO}_3)(\text{DMF})_2](\text{NO}_3)$

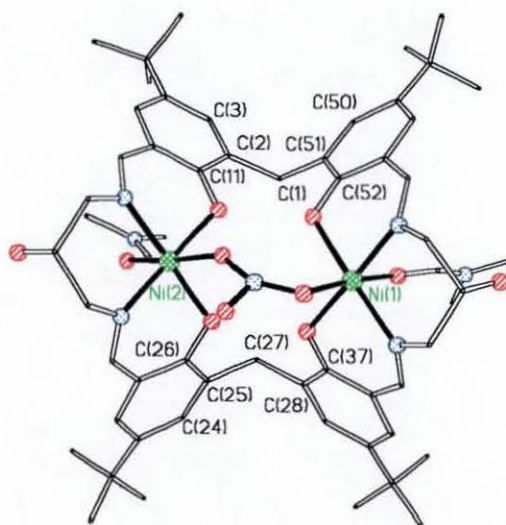


Fig. 3.23: Structure of the cation $[\text{Ni}_2(\text{H}_4\text{L9})(\text{NO}_3)(\text{DMF})_2]^+$

In complex $[\text{Ni}_2(\text{H}_4\text{L9})(\text{NO}_3)(\text{DMF})_2](\text{NO}_3)$ the Ni-Ni separation has expanded (4.6049(10) Å) to accommodate a longer *syn-anti* nitrate bridge. The two bonds linking the bridging unit to the nickel atoms are of different lengths. Consequently, this insertion resulted in a loss of symmetry as shown in fig. 3.24 where the two saturated carbon atoms (C(1) and C(27)) belonging to the two different DHTMB fragments are not aligned anymore. The relevant torsion angles are given in table 3.14. The values of the angle between the two phenyl rings of each DHTMB fragment are $64.42(15)^\circ$ and $58.95(18)^\circ$.

Table 3.14: Torsion angles [$^\circ$] for $[\text{Ni}_2(\text{H}_4\text{L9})(\text{NO}_3)(\text{DMF})_2](\text{NO}_3)$

	Torsion angles in ($^\circ$)
C(51)-C(1)-C(2)-C(3)	100.3(6)
C(51)-C(1)-C(2)-C(11)	-80.5(6)
C(26)-C(25)-C(27)-C(28)	89.6(6)
C(24)-C(25)-C(27)-C(28)	-93.0(6)

As in the previous dinickel complex, the nickel atoms are in a tetragonal environment with a DMF molecule and a bridging nitrate occupying the axial sites. The selected bond lengths and angles are given in table 3.15. For the same reasons mentioned for the dinickel and dicobalt complexes, the two phenoxy hydrogen atoms were not found. In this dinuclear nickel complex, the nitrate-bridging unit is coordinated more strongly (Ni(1)-O(71) 2.123(4) Å and Ni(2)-O(73) 2.092(5) Å) to the nickel atoms than the water molecule bridging (*ca.* 2.4 Å) the metal atoms in complex $[\text{Ni}_2(\text{H}_4\text{L9})(\mu_2\text{-H}_2\text{O})(\text{EtOH})_2](\text{ClO}_4)_2$.

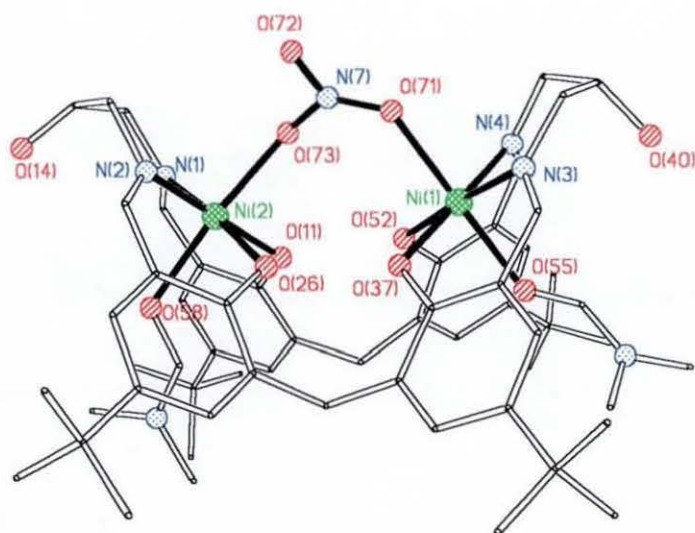


Fig. 3.24: Side-on view of the cation $[\text{Ni}_2(\text{H}_4\text{L9})(\text{NO}_3)(\text{DMF})_2]^+$

Fig. 3.24 shows that the four phenolic oxygen donors are positioned to provide a potential binding site for a third metal ion. This was also the case for the similar dinickel and dicobalt complexes. As the binding site is harder, we would expect a harder metal ion, like iron, to be preferred. Green crystals of $[\text{Ni}_2(\text{H}_4\text{L9})(\text{NO}_3)(\text{DMF})_2](\text{NO}_3)$ suitable for X-ray studies were grown by slow evaporation of a DMF solution of the compound over two weeks. A very similar zinc(II) complex with a bridging nitrate anion $[\text{Zn}_2(\text{H}_4\text{L9})(\text{NO}_3)(\text{EtOH})](\text{NO}_3)$ has also been isolated.

Table 3.15: Selected bond lengths [\AA] and angles [$^\circ$] for $[\text{Ni}_2(\text{H}_4\text{L9})(\text{NO}_3)(\text{DMF})_2](\text{NO}_3)$

Ni(1)-N(4)	2.033(5)	Ni(2)-N(2)	2.012(5)
Ni(1)-N(3)	2.038(5)	Ni(2)-O(11)	2.011(4)
Ni(1)-O(37)	2.043(4)	Ni(2)-N(1)	2.039(5)
Ni(1)-O(52)	2.061(4)	Ni(2)-O(26)	2.040(4)
Ni(1)-O(55)	2.079(4)	Ni(2)-O(73)	2.092(5)
Ni(1)-O(71)	2.123(4)	Ni(2)-O(58)	2.129(4)
Ni(1)-Ni(2)	4.6049(10)		

N(4)-Ni(1)-N(3)	94.64(19)	N(2)-Ni(2)-O(11)	178.18(18)
N(4)-Ni(1)-O(37)	178.02(18)	N(2)-Ni(2)-N(1)	94.53(19)
N(3)-Ni(1)-O(37)	87.33(17)	O(11)-Ni(2)-N(1)	87.02(17)
N(4)-Ni(1)-O(52)	84.99(18)	N(2)-Ni(2)-O(26)	87.18(17)
N(3)-Ni(1)-O(52)	176.01(17)	O(11)-Ni(2)-O(26)	91.34(15)
O(37)-Ni(1)-O(52)	93.06(15)	N(1)-Ni(2)-O(26)	175.73(18)
N(4)-Ni(1)-O(55)	93.31(18)	N(2)-Ni(2)-O(73)	95.4(2)
N(3)-Ni(1)-O(55)	90.25(17)	O(11)-Ni(2)-O(73)	83.5(2)
O(37)-Ni(1)-O(55)	86.86(16)	N(1)-Ni(2)-O(73)	92.8(2)
O(52)-Ni(1)-O(55)	85.81(15)	O(26)-Ni(2)-O(73)	90.95(19)
N(4)-Ni(1)-O(71)	89.94(19)	N(2)-Ni(2)-O(58)	92.16(17)
N(3)-Ni(1)-O(71)	85.70(18)	O(11)-Ni(2)-O(58)	88.85(15)
O(37)-Ni(1)-O(71)	90.02(17)	N(1)-Ni(2)-O(58)	87.58(17)
O(52)-Ni(1)-O(71)	98.26(17)	O(26)-Ni(2)-O(58)	88.45(15)
O(55)-Ni(1)-O(71)	175.00(17)	O(73)-Ni(2)-O(58)	172.3(2)

These dinuclear complexes show a real potential for host-guest chemistry as they can bind anions or neutral molecules acting as a bridge between the two metal centres and they could also bind further metal ions within the central cavity. The ability to accommodate different size of bridging molecules can be used in modelling studies of dinickel enzymes such as urease.¹³²⁻¹³⁷

3.5. Dinuclear complexes of L10

3.5.1. Synthesis and characterisation of $[\text{Ni}_2(\text{L10})]$

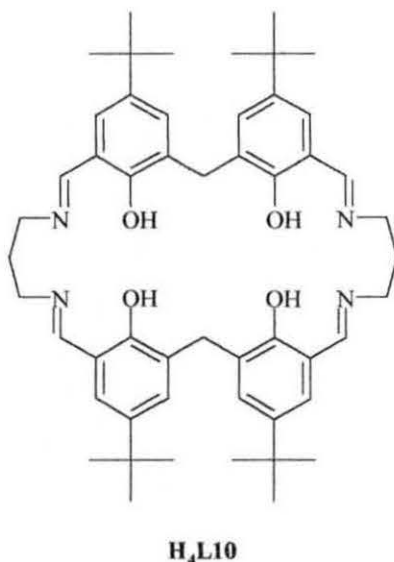


Fig. 3.25: Ligand H₄L10

$[\text{Ni}_2(\text{L10})]$ formed as a rusty-brown precipitate (58%) after the condensation of DHTMB with 1,3-diaminopropane. The product is not very soluble in any of the solvents tried from low to high polarity, which is the reason why no crystals could be grown so far. This observation points to the possibility that the compound might in fact be a polymer. The IR shows a band at 1617 cm^{-1} , which can be attributed to the vibration of the imine groups. However, it is lower than for every other macrocyclic complex that was formed from the condensation of DHTMB with 1,3-diaminopropan-2-ol or DAHP. There is no trace of ClO_4^- anion stretches. The elemental analysis is consistent with the formula but it does not prove whether the species is polymeric or not. The FAB results (table 3.16) are also consistent with the formula but in FAB spectrometry, only the species soluble in the solvent used are seen.

Table 3.16: Peak attributions for [Ni₂(L10)]

m/z	Rel. Intensity (%)	Fragments	Calc. Mass
925	100	[Ni ₂ (L10)+H] ⁺	925
947	50	[Ni ₂ (L10)+Na] ⁺	947
963	10	[Ni ₂ (L10)+H] ⁺ .2H ₂ O	961
1007	7	[Ni ₂ (L10)+H] ⁺ .2H ₂ O,EtOH	1007

The rusty-brown colour of the complex is an indication in itself because octahedral complexes of Ni(II) are usually green. In this case, the geometry might be square planar or tetrahedral. If the geometry is square planar the complex is expected to be diamagnetic. The value of the room-temperature molar susceptibility is almost 0 (-1.56×10⁻⁵) within the error range, which agrees with a diamagnetic compound.

3.5.2. Synthesis and characterisation of [Mn₂(L10)(EtOH)₂(OAc)₂]

In the case of manganese, two compounds have been isolated. They were identified as [Mn₂(L10)(EtOH)₂(OAc)₂] and [Mn₂(L10)(MeOH)(OAc)₂] by combining the IR, elemental analysis and FAB results. The formation of both complexes can be explained by the different conformations available to the macrocycle. The macrocycle can opt for a folded conformation like in the dinickel and dicobalt complexes with one acetate molecule bridging the two manganese centres yielding the complex [Mn₂(L10)(MeOH)(OAc)₂]. The macrocycle can also fold so that one manganese ion lies on either side of the macrocyclic plane (fig. 3.26) yielding the complex [Mn₂(L10)(EtOH)₂(OAc)₂]. This conformation is adopted in the manganese complex [(Mn₂(H₂L9)(OAc)(H₂O))₃CO₃] described in section 3.6.2. The IR spectra of complexes [Mn₂(L10)(EtOH)₂(OAc)₂] and [Mn₂(L10)(MeOH)(OAc)₂] are similar and show a band at 1621 cm⁻¹, attributed to the vibration of the imine groups. The FAB results (table 3.17 and table 3.18) support the formation of both complexes but for complex [Mn₂(L10)(MeOH)(OAc)₂] two peaks of low relative intensity at m/z

1837 and 1860 indicate the small contamination by a complex possibly containing two or more macrocyclic units. No structural data are available at the moment.

Table 3.17: Peak attributions for $[\text{Mn}_2(\text{L10})(\text{EtOH})_2(\text{OAc})_2]$

m/z	Rel. Intensity (%)	Fragments	Calc. Mass
919	80	$[\text{Mn}_2(\text{L10})]^{2+}$	918
979	100	$[\text{Mn}_2(\text{L10})(\text{OAc})]^+$	977
1087	5	$[\text{Mn}_2(\text{L10})(\text{EtOH})_2(\text{OAc})]^+ \cdot \text{H}_2\text{O}$	1087

Table 3.18: Peak attributions for $[\text{Mn}_2(\text{L10})(\text{MeOH})(\text{OAc})_2]$

m/z	Rel. Intensity (%)	Fragments	Calc. Mass
918	100	$[\text{Mn}_2(\text{L10})]^{2+}$	918
978	80	$[\text{Mn}_2(\text{L10})(\text{OAc})]^+$	977
1087	10	$[\text{Mn}_2(\text{L10})(\text{MeOH})(\text{OAc})]^+ \cdot \text{MeOH}, \text{EtOH}$	1087
1837	5	$[(\text{Mn}_2(\text{L10}))_2 + \text{H}]^+$	1836
1860	5	$[(\text{Mn}_2(\text{L10}))_2 + \text{Na}]^+$	1859

3.6. Dinuclear trimeric complexes of L9

3.6.1. Synthesis of $[(\text{Mn}_2(\text{H}_2\text{L9})(\text{OAc})(\text{H}_2\text{O}))_3\text{CO}_3]$

$[(\text{Mn}_2(\text{H}_2\text{L9})(\text{OAc})(\text{H}_2\text{O}))_3\text{CO}_3]$ was first isolated in our attempts to synthesise dinuclear manganese complexes of L9. When the reaction was stopped, the yellow colour immediately changed to dark green/brown, which is an indication of the oxidation of Mn(II) to Mn(III). The crystal structure revealed the presence of a carbonate anion in the complex, which was thought to originate from the carbon dioxide present in the air that dissolved in the reaction solution. Subsequently, to try and synthesise the complex systematically, it was decided to add dry-ice to the

solution. This procedure proved successful in synthesising complex $[(\text{Mn}_2(\text{H}_2\text{L9})(\text{OAc})(\text{H}_2\text{O}))_3\text{CO}_3]$. The elemental analysis and FAB results (table 3.19) were consistent with the formation of $[(\text{Mn}_2(\text{H}_2\text{L9})(\text{OAc})(\text{H}_2\text{O}))_3\text{CO}_3]$. The macrocyclic nature of the compound is supported by the band at 1619 cm^{-1} assigned to the vibration of the imine groups. A broad band at 1440 cm^{-1} can be assigned to carbonate and acetate vibrations. The band at 875 cm^{-1} could be assigned to the second vibration expected for carbonate anions. However, it is difficult to detect the vibration of a single CO_3^{2-} anion in such a large structure. The asymmetric vibration of the acetate anions is probably overlapped by C=C and C-O vibrations at 1551 cm^{-1} (strong band).

Adding dry-ice would make the solution more acidic but in this case it did not seem to have an effect on the outcome of the reaction. As a source of CO_3^{2-} , it would be interesting to use an alkaline source like Na_2CO_3 to study the effect of the pH on the reaction.

Table 3.19: Peak assignments for $[(\text{Mn}_2(\text{H}_2\text{L9})(\text{OAc})(\text{H}_2\text{O}))_3\text{CO}_3]$

m/z	Rel. Intensity (%)	Fragments	Calc. Mass
949	30	$[\text{Mn}_2(\text{H}_2\text{L9})]^{2+}$	950
971	25	$[\text{Mn}_2(\text{H}_2\text{L9})(\text{H}_2\text{O})]^{2+}$	968
1040	15	$[\text{Mn}_2(\text{H}_2\text{L9})(\text{OAc})]^+ \cdot \text{MeOH}$	1041
1882	30	$[\text{Mn}_3(\text{H}_2\text{L9})_2]^{+} \cdot 2\text{H}_2\text{O}$	1881
1891	40	$[(\text{Mn}(\text{H}_4\text{L9})(\text{H}_2\text{O})(\text{MeOH}))_2]^{2+}$	1894
1899	100	$[(\text{Mn}_2(\text{H}_2\text{L9}))_2]^{2+}$	1900
1915	30	$[(\text{Mn}(\text{H}_4\text{L9})(\text{H}_2\text{O})(\text{MeOH}))_2]^{2+} \cdot \text{H}_2\text{O}$	1913
1920	30	$[(\text{Mn}_2(\text{H}_2\text{L9}))_2]^{2+} \cdot \text{H}_2\text{O}$	1918
1935	30	$[(\text{Mn}_2(\text{H}_2\text{L9}))_2]^{2+} \cdot \text{MeOH}$	1933
2847	10	$[\text{Mn}_5(\text{H}_2\text{L9})_3]^{3+} \cdot 3\text{H}_2\text{O}$	2850
2885	8	$[\text{Mn}_5(\text{H}_2\text{L9})_3(\text{OAc})]^{2+} \cdot \text{MeOH}$	2887
2934	5	$[\text{Mn}_5(\text{H}_2\text{L9})_3(\text{OAc})_2]^+ \cdot \text{H}_2\text{O}$	2932
2976	< 3	$[\text{Mn}_5(\text{H}_2\text{L9})_3(\text{OAc})_3 + \text{H}]^+$	2974
3062	< 3	$[(\text{Mn}_2(\text{H}_2\text{L9})(\text{OAc}))_3(\text{H}_2\text{O})_2]^{2+}$	3064

3.6.2. Structure of $[(\text{Mn}_2(\text{H}_2\text{L9}))_3(\text{OAc})_3(\text{H}_2\text{O})(\text{EtOH})_2\text{CO}_3]$

Brown crystals of $[(\text{Mn}_2(\text{H}_2\text{L9}))_3(\text{OAc})_3(\text{H}_2\text{O})(\text{EtOH})_2\text{CO}_3]$ suitable for X-ray studies were grown by slow diffusion of diethylether into a methanol solution $[(\text{Mn}_2(\text{H}_2\text{L9})(\text{OAc})(\text{H}_2\text{O}))_3\text{CO}_3]$. All the X-ray data collection parameters for $[(\text{Mn}_2(\text{H}_2\text{L9}))_3(\text{OAc})_3(\text{H}_2\text{O})(\text{EtOH})_2\text{CO}_3]$ are summarised in table 9 in annex 2 along with the details concerning the refinement and disorders. The structure contains three dimanganese macrocyclic units, $[\text{Mn}_2(\text{H}_2\text{L9})(\text{OAc})(\text{H}_2\text{O})]$ (fig. 3.26), $[\text{Mn}_2(\text{H}_2\text{L9})(\text{EtOH})_2]$ and $[\text{Mn}_2(\text{H}_2\text{L9})(\text{OAc})_2]$ linked into a ring centred on a carbonate anion (fig. 3.27). The formula of the structure $[(\text{Mn}_2(\text{H}_2\text{L9}))_3(\text{OAc})_3(\text{H}_2\text{O})(\text{EtOH})_2\text{CO}_3]$ is slightly different to the formula of the complex fitting the elemental analysis $[(\text{Mn}_2(\text{H}_2\text{L9})(\text{OAc})(\text{H}_2\text{O}))_3\text{CO}_3]$, axial ligands are different). Therefore, it is reasonable to assume that the axial ligands (water or ethanol) of the manganese ions can be exchanged. The structure is maintained by three Mn-carbonate bonds, three intermacrocyclic Mn-alcohol links and four hydrogen bonds (dotted line in fig. 3.27). A similar complex $[(\text{Mn}_2(\text{H}_2\text{L9})(\text{H}_2\text{O})_2)_3\text{CO}_3](\text{ClO}_4)_2$ was isolated but the refinement was very poor due to disorders. Uniquely among the dinuclear complexes of L9 structurally characterised to date, the macrocycle folds so that one manganese ion lies on either side of the macrocyclic plane (fig. 3.26). The relevant torsion angles are given in table 3.20.

Table 3.20: Torsion angles [$^\circ$] for $[(\text{Mn}_2(\text{H}_2\text{L9}))_3(\text{OAc})_3(\text{H}_2\text{O})(\text{EtOH})_2\text{CO}_3]$

	Torsion angles in ($^\circ$)
C(1)-C(10)-C(11)-C(12)	-165.9(12)
C(9)-C(10)-C(11)-C(12)	12.9(19)
C(34)-C(35)-C(37)-C(38)	98.2(17)
C(36)-C(35)-C(37)-C(38)	-81.5(18)

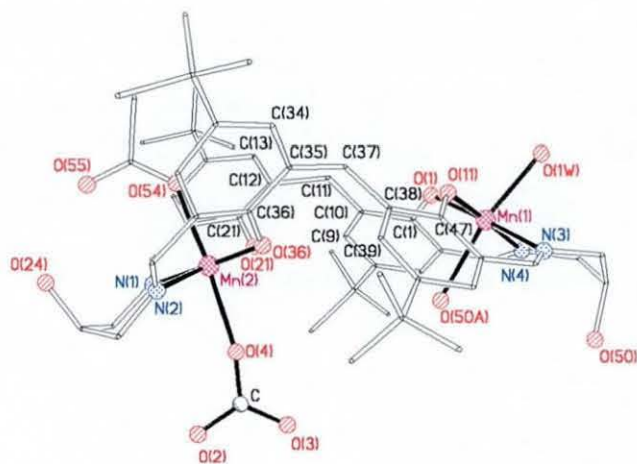


Fig. 3.26: Dimanganese macrocyclic unit

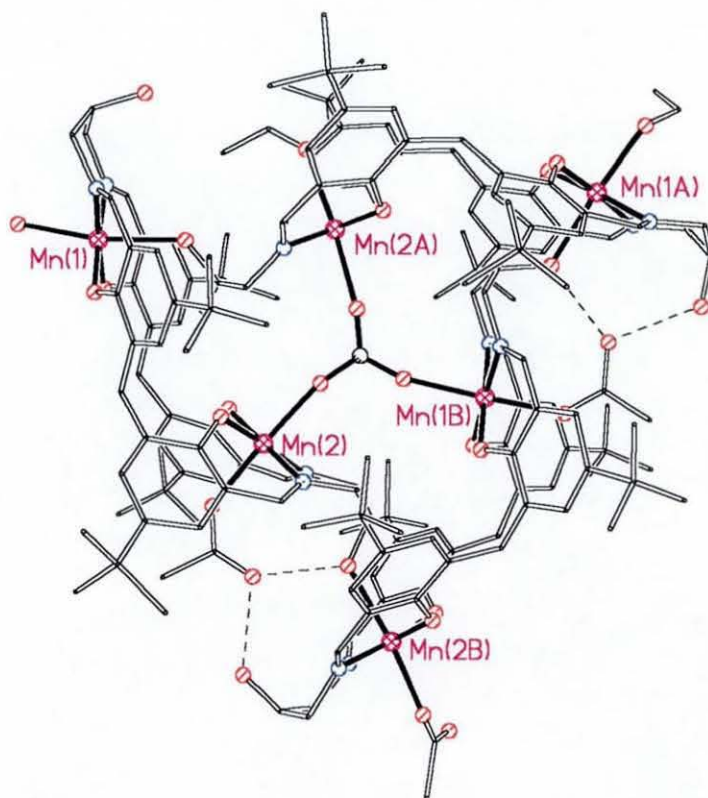


Fig. 3.27: Structure of $[(\text{Mn}_2(\text{H}_2\text{L}9))_3(\text{OAc})_3(\text{H}_2\text{O})(\text{EtOH})_2\text{CO}_3]$

The manganese ions are in a tetragonal octahedral environment. The axial coordination sites are occupied by acetate anions, water molecules, carbonate anion or pendent alcohol groups from the neighbouring macrocyclic unit. The elongated geometry is characteristic of a Mn(III) ion exhibiting a Jahn-Teller distortion. The selected bond lengths and angles are given in table 3.21.

Table 3.21: Selected bond lengths [Å] and angles [°] for
 $[(\text{Mn}_2(\text{H}_2\text{L9})(\text{OAc})(\text{H}_2\text{O}))_3\text{CO}_3]$

Mn(1)-O(1)	1.885(10)	Mn(2)-O(21)	1.877(10)
Mn(1)-O(11)	1.881(10)	Mn(2)-N(1)	2.032(12)
Mn(1)-N(4)	2.002(13)	Mn(2)-N(2)	2.022(11)
Mn(1)-N(3)	2.035(13)	Mn(2)-O(36)	1.881(9)
Mn(1)-O(1W)	2.177(10)	Mn(2)-O(54)	2.186(10)
Mn(1)-O(50A)	2.309(9)	Mn(2)-O(4)	2.223(14)
O(1)-Mn(1)-O(11)	88.7(4)	O(36)-Mn(2)-O(21)	91.2(4)
O(1)-Mn(1)-N(4)	91.4(5)	O(36)-Mn(2)-N(2)	89.3(4)
O(11)-Mn(1)-N(4)	176.9(4)	O(21)-Mn(2)-N(2)	178.8(4)
O(1)-Mn(1)-N(3)	175.0(5)	O(36)-Mn(2)-N(1)	178.0(5)
O(11)-Mn(1)-N(3)	87.7(5)	O(21)-Mn(2)-N(1)	89.4(5)
N(4)-Mn(1)-N(3)	91.9(5)	N(2)-Mn(2)-N(1)	90.1(5)
O(1)-Mn(1)-O(1W)	98.3(4)	O(36)-Mn(2)-O(54)	90.2(4)
O(11)-Mn(1)-O(1W)	98.2(4)	O(21)-Mn(2)-O(54)	89.4(4)
N(4)-Mn(1)-O(1W)	84.9(5)	N(2)-Mn(2)-O(54)	91.7(4)
N(3)-Mn(1)-O(1W)	85.7(5)	N(1)-Mn(2)-O(54)	87.9(4)
O(1)-Mn(1)-O(50A)	88.8(4)	O(36)-Mn(2)-O(4)	95.0(5)
O(11)-Mn(1)-O(50A)	89.7(3)	O(21)-Mn(2)-O(4)	91.3(5)
N(4)-Mn(1)-O(50A)	87.2(4)	N(2)-Mn(2)-O(4)	87.6(5)
N(3)-Mn(1)-O(50A)	87.6(4)	N(1)-Mn(2)-O(4)	86.9(6)
O(1W)-Mn(1)-O(50A)	169.4(4)	O(54)-Mn(2)-O(4)	174.8(5)

Considering that the structure contains six Mn(III) ions, electroneutrality requires an overall negative charge of -18 for the complex. The three macrocycles each provide four negative charges, the carbonate anion provides two negative charges and the three acetate anions provide three negative charges, which makes a total of -17. Consequently, one additional negative charge is required. It is difficult to determine whether all the alkoxy oxygen atoms are protonated or not (lower quality of the data and size of the structure), therefore the additional negative charge can be provided by one of the coordinated ethanol or water molecules or by the non-hydrogen-bonded pendent alkoxy oxygen atom.

Very recently a dinuclear manganese complex $[(\text{Mn}_2(\text{H}_2\text{L9})(\text{Cl})_2(\text{DMF})(\text{DMSO}))]$ was isolated by J. Barreira Fontecha. The shape adopted by the macrocycle in this latter complex is the same as that adopted by the macrocyclic unit in the structure of $[(\text{Mn}_2(\text{H}_2\text{L9}))_3(\text{OAc})_3(\text{H}_2\text{O})(\text{EtOH})_2\text{CO}_3]$. This observation stresses the fact that the shape of the macrocyclic unit is not the driving force for the formation of this remarkable circular hexamanganese structure. Similarly, it means that the formation of the circular hexamanganese structure does not influence the shape of the macrocycle. So far, the only dimanganese complex was isolated with chloride counter anions, which might suggest that the counter anion (coordinating or non-coordinating) has an influence on the outcome of the final product. There is no apparent reason why this complex differs from the other dinuclear complexes of L9.

3.6.3. Synthesis of $[(\text{Co}_2(\text{H}_2\text{L9})(\text{OAc})(\text{H}_2\text{O}))_3\text{CO}_3]$ and $[(\text{Fe}_2(\text{H}_2\text{L9})(\text{OAc})(\text{H}_2\text{O}))_3\text{CO}_3]$

A cobalt complex of L9, thought to have a similar structure to $[(\text{Mn}_2(\text{H}_2\text{L9}))_3(\text{OAc})_3(\text{H}_2\text{O})(\text{EtOH})_2\text{CO}_3]$ has also been isolated. This synthesis differs from the dinuclear cobalt complex in that the reaction time was scaled up to 24 hours. Similarly to the hexamanganese complex, a colour change from light orange-brown to dark brown occurred upon cooling. The elemental analysis combined with the FAB data (table 3.22) seems to support the formation of the complex $[(\text{Co}_2(\text{H}_2\text{L9})(\text{OAc})(\text{H}_2\text{O}))_3\text{CO}_3]$.

Table 3.22: Peak attributions for $[(\text{Co}_2(\text{H}_2\text{L9})(\text{OAc})(\text{H}_2\text{O}))_3\text{CO}_3]$

m/z	Rel. Intensity (%)	Fragments	Calc. Mass
952	80	$[\text{Co}_2(\text{H}_2\text{L9})]^{2+}$	958
981	100	$[\text{Co}_2(\text{H}_2\text{L9})+\text{Na}]^+$	981
1016	25	$[\text{Co}_2(\text{H}_2\text{L9})(\text{OAc})]^+$	1017
1076	10	$[\text{Co}_2(\text{H}_2\text{L9})(\text{OAc})_2+\text{H}]^+$	1077
1937	50	$[(\text{Co}_2(\text{H}_2\text{L9}))_2]^{2+} \cdot \text{H}_2\text{O}$	1935
1993	20	$[(\text{Co}_2(\text{H}_2\text{L9}))_2(\text{OAc})]^+ \cdot \text{H}_2\text{O}$	1994

Furthermore, an iron complex of L9 with a supposed similar structure to $[(\text{Mn}_2(\text{H}_2\text{L9})(\text{OAc})(\text{H}_2\text{O}))_3\text{CO}_3]$ was also synthesised. However, the FAB data (table 3.23) do not seem to agree with the formation of $[(\text{Fe}_2(\text{H}_2\text{L9})(\text{OAc})(\text{H}_2\text{O}))_3\text{CO}_3]$ but with a mixture of tetranuclear compounds and polynuclear complexes containing two macrocyclic ligands. The elemental analysis results support the possible formation of $[(\text{Fe}_2(\text{H}_2\text{L9})(\text{OAc})(\text{H}_2\text{O}))_3\text{CO}_3]$ but as for the previously described hexacobalt complex, without structural data, it is difficult to speculate on the nature of the isolated complex.

Table 3.23: Peak attributions for $[(\text{Fe}_2(\text{H}_2\text{L9})(\text{OAc})(\text{H}_2\text{O}))_3\text{CO}_3]$

m/z	Rel. Intensity (%)	Fragments	Calc. Mass
951	85	$[\text{Fe}_2(\text{H}_2\text{L9})]^{2+}$	952
975	100	$[\text{Fe}_2(\text{H}_2\text{L9})+\text{Na}]^+$	975
1007	60	$[\text{Fe}_2(\text{H}_2\text{L9})(\text{OAc})]^+$	1011
1078	15	$[\text{Fe}_2(\text{H}_2\text{L9})(\text{OAc})]^+ \cdot 2\text{MeOH}$	1075
1426	10	$[\text{Fe}_4(\text{H}_2\text{L9})(\text{OAc})_2(\text{H}_2\text{O})_2(\text{OH})_2(\text{EtOH})_3+\text{H}]^+ \cdot \text{MeOH}$	1426
1535	7	$[\text{Fe}_4(\text{H}_2\text{L9})(\text{OAc})_2(\text{H}_2\text{O})_2(\text{OH})_2(\text{EtOH})_4+\text{H}]^+ \cdot 4\text{H}_2\text{O}$	1536
1798	7	$[\text{Fe}_2(\text{H}_4\text{L9})_2]^{2+}$	1797

All the bridged (H_2O or Cl^-) dinuclear nickel, cobalt, copper and zinc complexes of $\text{H}_6\text{L9}$ structurally characterised so far are virtually identical in that the folded conformation of the macrocycle is the same in each case (superimposable). This is thought to be a consequence of the hydrogen links between the phenolate oxygen atoms of each DHTMB unit. The insertion of a nitrate bridge, which is a three-atom-bridge removes part of the symmetry present in the water or chloride bridged complexes. In those complexes the saddle shape of the macrocycle is maintained but there is no mirror plane passing through the saturated carbons of each DHTMB unit. However, the dinuclear manganese complex is an exception in this series due to the different conformation adopted by the DHTMB head-unit of the macrocycle.

3.7. A trinuclear complex of L9

3.7.1. Synthesis and structure of $[\text{Cu}_3(\text{L9})(\text{MeOH})_2]_n$

In the course of attempts to synthesise tetranuclear species of the macrocyclic ligand L9, a trinuclear complex was also isolated in addition to tetranickel, tetracobalt and tetracopper complexes of L9. At first, it was thought that the formation of tetranuclear products might require sodium hydroxide to deprotonate the alcohol groups of the side-chain allowing them to bind to the metal. When the ratio ligand: NaOH is 1:1 a mixture of trinuclear and tetranuclear complexes was isolated. The slow evaporation of an ethanol solution (green) of the reaction mixture yielded orange and green crystals. Only the orange crystals were suitable for X-ray studies and these proved to be a one-dimensional chain of a trinuclear macrocyclic copper complex of L9 ($[\text{Cu}_3(\text{L9})(\text{CH}_3\text{OH})_2]_n$). All the X-ray data collection parameters for $[\text{Cu}_3(\text{L9})(\text{CH}_3\text{OH})_2]_n$ are summarised in table 10 in annex 2 along with the details concerning the refinement and disorders. The amount of orange crystals isolated was too small to perform other analyses than X-ray crystallography. Nonetheless, the presence of the chain was detected by FAB (table 3.24) in a contaminated sample of a tetranuclear copper complex.

Table 3.24: Peak attributions for $[\text{Cu}_3(\text{L9})(\text{CH}_3\text{OH})_2]_n$

m/z	Rel. Intensity (%)	Fragments	Calc. Mass
2137	45	$[(\text{Cu}_3(\text{L9})(\text{MeOH})_2)_2+\text{H}]^+ \cdot \text{H}_2\text{O}$	2137
2202	15	$[(\text{Cu}_3(\text{L9})(\text{MeOH})_2)_2\text{Cu}]^{2+}$	2200

The tricopper complex is very similar to the previous binuclear structures except that the central binding site is occupied (fig. 3.28). The macrocycle adopts the same saddle-shape conformation and is almost superimposable (fig. 3.29). The torsion angles related to the DHTMB unit, remain largely unchanged (table 3.25) for the trinuclear species compared to the dinuclear nickel and cobalt species. However, in this case the saddle shape is maintained by the copper ion in the central site rather than by two hydrogen bonds.

Table 3.25: Torsion angles [$^\circ$] for $[\text{Cu}_3(\text{L9})(\text{CH}_3\text{OH})_2]_n$

	Torsion angles in ($^\circ$)
C(11)-C(10)-C(12)-C(13)	-90.1(8)
C(9)-C(10)-C(12)-C(13)	84.5(8)

As shown in fig. 3.28 and fig. 3.30, Cu(1) and Cu(2) are in square planar environments, while the remaining copper atom Cu(3) is in a square pyramidal environment. The copper atoms are separated from the central copper atom Cu(3) by 2.808(3) and 2.867(2) Å respectively. The distance separating Cu(1) and Cu(3) is 5.162(3) Å, which is longer than the metal-metal distances in the dinuclear complexes of ligand L9. The insertion of the third metal in the central cavity causes the macrocycle to open with the angle between the two phenyl rings of each DHTMB unit being 80.87(24) $^\circ$, which is almost 10 $^\circ$ bigger than in the dinuclear species.

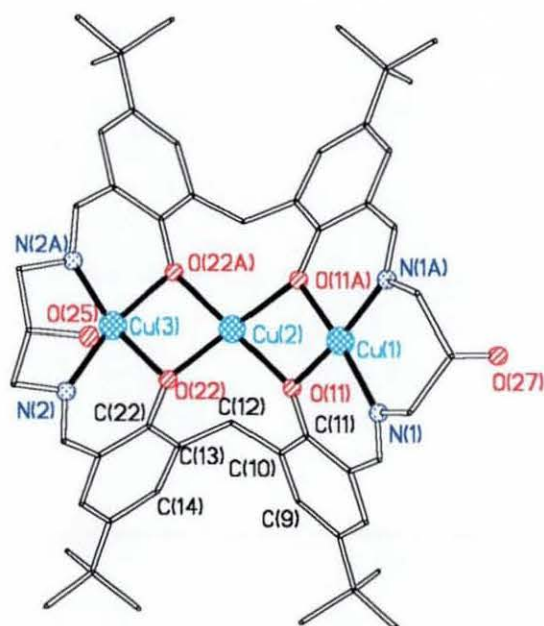


Fig. 3.28: Structure of $[\text{Cu}_3(\text{L9})]$

The selected bond lengths and angles are given in table 3.26. This trinuclear complex is another good example of how the macrocycle, due to its flexibility, can accommodate different nuclearities.

Table 3.26: Selected bonds [\AA] and angles [$^\circ$] for $[\text{Cu}_3(\text{L9})(\text{CH}_3\text{OH})_2]_n$

Cu(1)-N(1)	1.924(7)	Cu(2)-O(11)	1.912(5)
Cu(1)-N(1)*	1.924(7)	Cu(2)-O(11)*	1.912(5)
Cu(1)-O(11)	1.960(5)	Cu(2)-Cu(3)	2.867(2)
Cu(1)-O(11)*	1.960(5)	Cu(3)-N(2)*	1.917(7)
Cu(1)-Cu(2)	2.808(3)	Cu(3)-N(2)	1.917(7)
Cu(1)-Cu(3)	5.162(3)	Cu(3)-O(22)	1.969(5)
Cu(2)-O(22)	1.897(5)	Cu(3)-O(22)*	1.969(5)
Cu(2)-O(22)*	1.897(5)	Cu(3)-O(27)**	2.309(8)
N(1)-Cu(1)-N(1)*	99.3(4)	N(1)-Cu(1)-O(11)	91.2(2)

N(1)*-Cu(1)-O(11)	168.8(3)	N(2)*-Cu(3)-O(22)	167.6(3)
N(1)-Cu(1)-O(11)*	168.8(3)	N(2)-Cu(3)-O(22)	91.7(3)
N(1)*-Cu(1)-O(11)*	91.2(2)	N(2)*-Cu(3)-O(22)*	91.7(3)
O(11)-Cu(1)-O(11)*	78.1(3)	N(2)-Cu(3)-O(22)*	167.6(3)
O(22)-Cu(2)-O(22)*	81.2(3)	O(22)-Cu(3)-O(22)*	77.7(3)
O(22)-Cu(2)-O(11)	98.3(2)	N(2)#1-Cu(3)-O(27)**	95.3(3)
O(22)*-Cu(2)-O(11)	170.0(2)	N(2)-Cu(3)-O(27)**	95.3(3)
O(22)-Cu(2)-O(11)*	170.0(2)	O(22)-Cu(3)-O(27)**	91.4(2)
O(22)*-Cu(2)-O(11)*	98.3(2)	O(22)*-Cu(3)-O(27)**	91.4(2)
O(11)-Cu(2)-O(11)*	80.4(3)		
N(2)*-Cu(3)-N(2)	97.9(5)		

Symmetry transformations used to generate equivalent atoms: (*) $x, y, -z+1$ (**) $-x+1/2, y-1/2, -z+1$

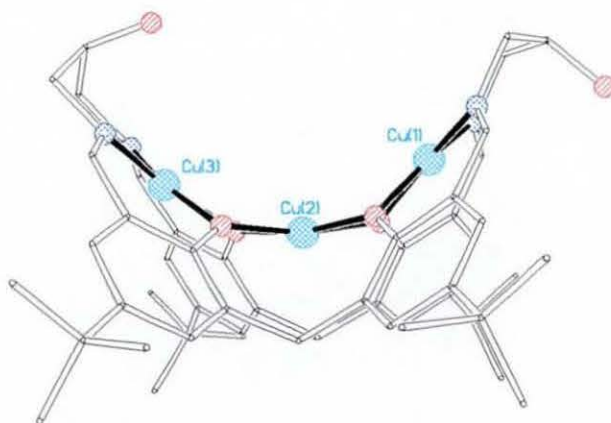


Fig. 3.29: Side-on view of $[\text{Cu}_3(\text{L}9)]$

As depicted in fig. 3.29, one of the pendent alkoxy groups points inside the cavity of the macrocycle while the other one points outside. The latter one acts as an axial ligand (2.309(8) Å) to one of the copper ions belonging to the neighbouring macrocyclic unit resulting in a one-dimensional chain (fig. 3.30). The remaining alkoxy group is involved in hydrogen-bonding with solvate molecules (MeOH).

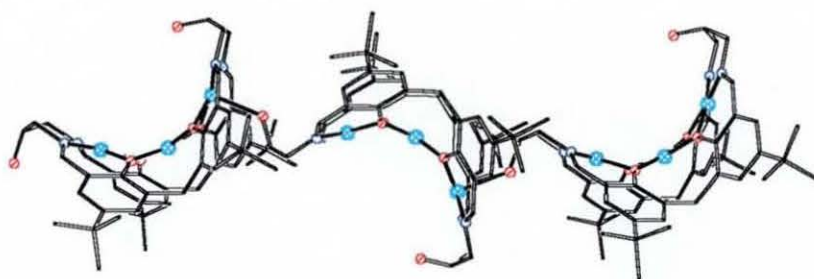


Fig. 3.30: One dimensional chain of $[\text{Cu}_3(\text{L}9)]$

When the ratio ligand:NaOH is 1:2, only the tetranuclear complex seems to form. Green crystals suitable for X-ray studies were grown from slow evaporation of an ethanol solution of the complex $[\text{Cu}_4(\text{H}_2\text{L}9)(\mu_2\text{-H}_2\text{O})_2(\mu_2\text{-OH})_2(\text{H}_2\text{O})(\text{MeOH})_3](\text{NO}_3)_2$, which will be described in section 3.8.

Further studies performed with the assistance of J. Barreira Fontecha have demonstrated that without the use of sodium hydroxide and with the reaction time scaled up to 24 hours, only the trinuclear copper complex formed. In this case, without the use of sodium hydroxide, the alkoxy oxygen atoms belonging to the side chain of the macrocycle are protonated and two nitrate anions provide the two additional negative charges required for electroneutrality. However, if the reaction time is 1-2 hours, only the tetranuclear copper complex forms. Consequently, the trinuclear copper complex seems to be the thermodynamic product of the reaction and the tetranuclear copper complex the kinetic product. It has also been found that the use of base favoured the formation of the tetranuclear species as it assists the deprotonation of the alcohol groups. In addition, when the counter ion used is chloride and the reaction time is short (*ca.* 1 hour), a dinuclear copper complex with a chloride ion bridging the two copper centres forms. The only dinuclear copper complex obtained is the chloride bridged complex $([\text{Cu}_2(\text{H}_4\text{L}9)(\mu_2\text{-Cl})]\text{Cl})$ and there is no evidence, as yet, of the isolation of a water or nitrate bridged dicopper complex in the other cases involving $\text{Cu}(\text{NO}_3)_2$ or $\text{Cu}(\text{ClO}_4)_2$. In those latter cases, copper seems to opt for the tetranuclear or trinuclear option. A great amount of

rearrangement would not be necessary to pass from the dinuclear species to the tetranuclear or the trinuclear species. However, if as we assume the tetranuclear species forms before the trinuclear species, the process would involve a lot of rearrangement (more bonds to be broken and major geometrical change), which does not seem straightforward as shown in fig. 3.31. The reasons or driving forces of the processes occurring in this reaction are still obscure and need further investigation.

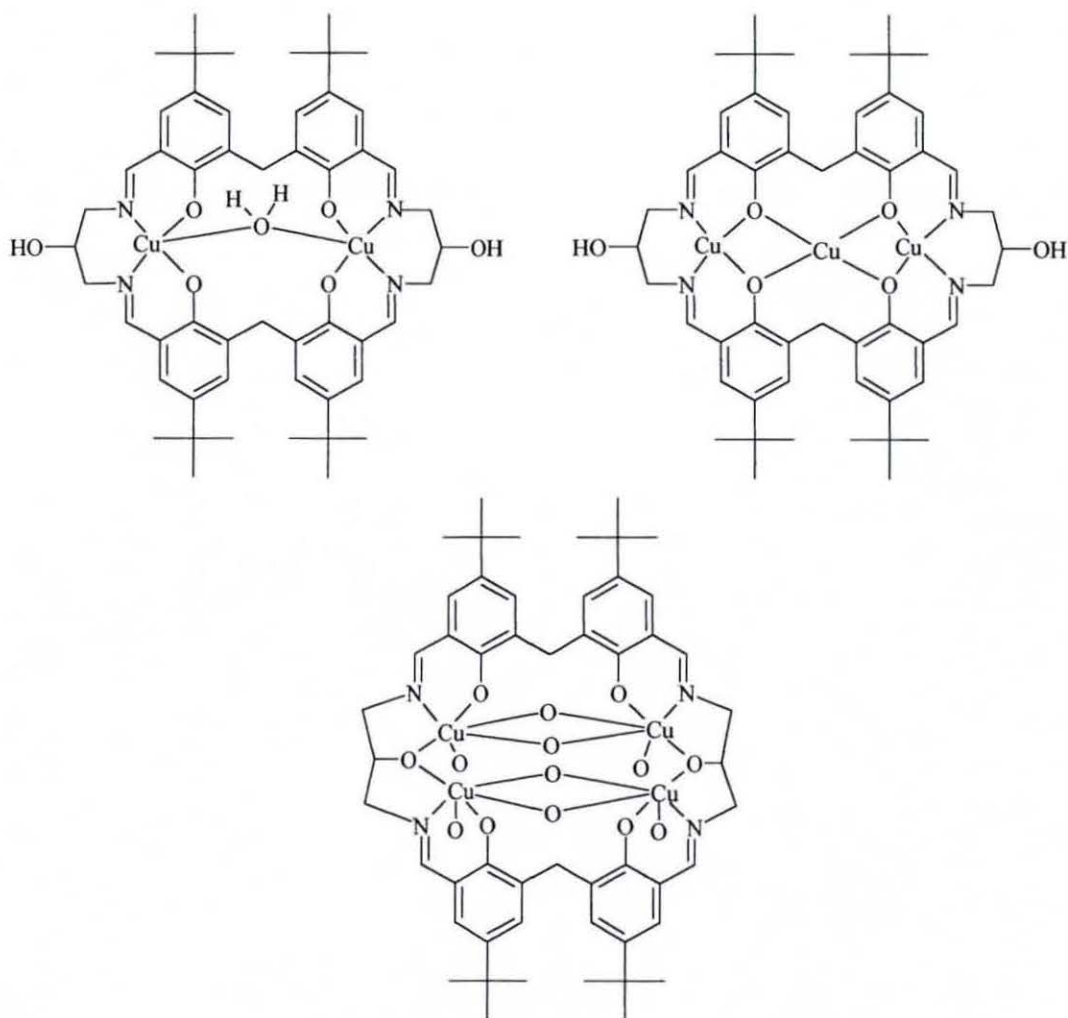


Fig. 3.31: Schematic representation of the di-, tri- and tetranuclear copper species

3.8. Tetranuclear complexes of L9

3.8.1. Synthesis of $[\text{Ni}_4(\text{H}_2\text{L9})(\mu_2\text{-OH})_2(\mu_2\text{-H}_2\text{O})_2(\text{EtOH})_4](\text{ClO}_4)_2$

As already mentioned in the previous section, the synthesis of tetranuclear complexes prepared from 1,3-diaminopropan-2-ol and DHTMB can be achieved and has shown that, contrary to our experience with single phenol head-units, tetranuclear species from 1,3-diaminopropan-2-ol are accessible. These results demonstrate that with the change of the head-unit to a bigger and more flexible one it is possible to play with the nuclearity of the final product.

In contrast to the tetranuclear copper complex that can be synthesised with or without base, the tetranickel complex $[\text{Ni}_4(\text{H}_2\text{L9})(\mu_2\text{-OH})_2(\mu_2\text{-H}_2\text{O})_2(\text{EtOH})_4](\text{ClO}_4)_2$ only forms when sodium hydroxide is added to the reaction mixture. There is no evidence, as yet, of the synthesis of a tetranuclear nickel complex without the use of base. The elemental analysis data are consistent with the formation of $[\text{Ni}_4(\text{H}_2\text{L9})(\mu_2\text{-OH})_2(\mu_2\text{-H}_2\text{O})_2(\text{EtOH})_4](\text{ClO}_4)_2$. The IR spectra is showing evidence that the condensation has taken place with the band at 1633 cm^{-1} that can be assigned to the vibration of the imine groups. The expected vibrations for the perchlorate anions are observed at 1089 and 624 cm^{-1} .

3.8.2. Structure of $[\text{Ni}_4(\text{H}_2\text{L9})(\mu_2\text{-OH})_2(\mu_2\text{-H}_2\text{O})_2(\text{EtOH})_4](\text{ClO}_4)_2$

Green crystals of $[\text{Ni}_4(\text{H}_2\text{L9})(\mu_2\text{-OH})_2(\mu_2\text{-H}_2\text{O})_2(\text{EtOH})_4](\text{ClO}_4)_2$ suitable for X-ray studies were grown by slow evaporation of an ethanol solution of the compound. All the X-ray data collection parameters for $[\text{Ni}_4(\text{H}_2\text{L9})(\text{OH})_2(\text{H}_2\text{O})_2(\text{EtOH})_4](\text{ClO}_4)_2$ are summarised in table 11 in annex 2 along with the details concerning the refinement and disorders.

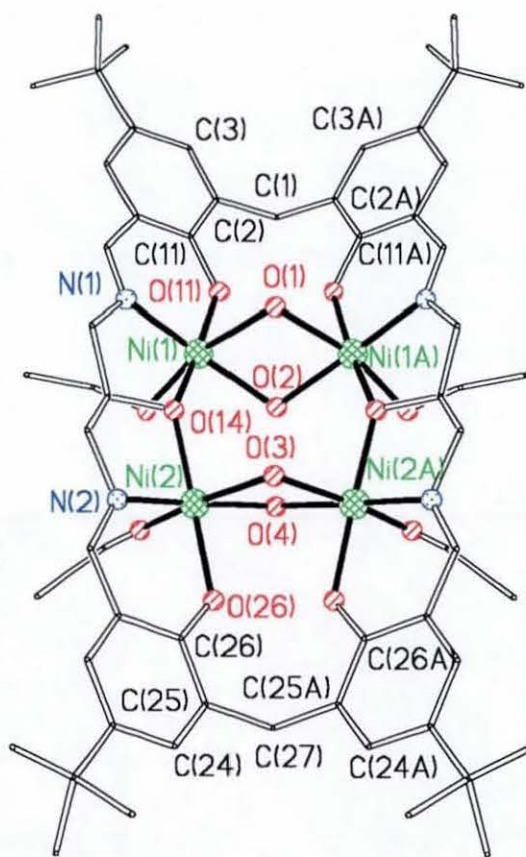


Fig. 3.32: Structure of the cation $[\text{Ni}_4(\text{H}_2\text{L9})(\mu_2\text{-OH})_2(\mu_2\text{-H}_2\text{O})_2(\text{EtOH})_4]^{2+}$

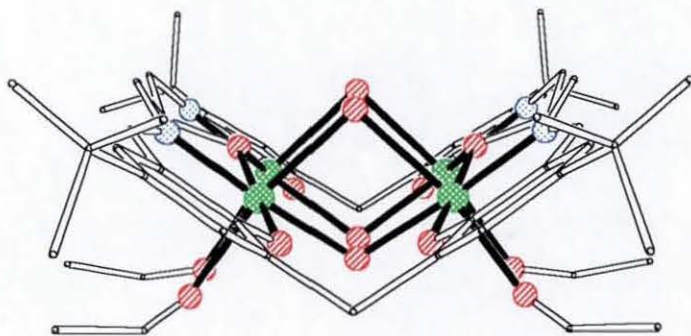


Fig. 3.33: Side-on view of the cation $[\text{Ni}_4(\text{H}_2\text{L9})(\mu_2\text{-OH})_2(\mu_2\text{-H}_2\text{O})_2(\text{EtOH})_4]^{2+}$ showing the sharp fold of the macrocycle

As pictured in fig. 3.33, the macrocycle is sharply folded at the saturated carbon of the DHTMB unit, allowing the two octahedrally coordinated nickel ions to share an edge. The value of the angle between the planes formed by the two phenyl rings of each DHTMB fragment is $65.30(42)^\circ$, which is *ca.* 10° smaller than in the related dinuclear species. The values of the torsion angles involving the saturated carbon are very similar to the dinuclear complexes $[\text{Ni}_2(\text{H}_4\text{L9})(\mu_2\text{-H}_2\text{O})(\text{EtOH})_2](\text{ClO}_4)_2$ and $[\text{Co}_2(\text{H}_4\text{L9})(\mu_2\text{-H}_2\text{O})(\text{EtOH})_2](\text{ClO}_4)_2$. The distance separating Ni(1) from Ni(1A) is $3.204(3)$ Å, which is one angström smaller than the Ni-Ni distance in the complex $[\text{Ni}_2(\text{H}_4\text{L9})(\mu_2\text{-H}_2\text{O})(\text{EtOH})_2](\text{ClO}_4)_2$. The two sets of opposite nickel ions are doubly bridged; one bridging unit is coordinated more strongly to the nickel ions at a distance of $2.048(7)$ Å, while the other unit is at a distance of $2.199(8)$ Å. This observation might indicate that one bridge is a hydroxo group and the other a water molecule. Similarly to the dinuclear water bridged species, a water bridge occupies one of the apical positions on the concave side of the macrocycle. There is also a second bridge that occupies one of the equatorial positions in the nickel octahedral environment and is situated in the fold of the macrocycle. The coordination of a hydroxo group might influence the metal-metal distance by pulling the nickel ions together, in contrast to the dinickel complex where no hydroxo groups are present. On each side of the macrocycle an alkoxo group bridges the set of nickel atoms. Four ethanol molecules complete the coordination sphere of the nickel ions. Similarly to the dinuclear species, the nickel ions are in a tetragonal environment. The selected bond lengths and angles are given in table 3.27. As a result of accommodating four metal centres the macrocycle is quite constrained, which shows the extent of flexibility of the macrocyclic ligand L9. Similarly to the dinuclear complexes, it can be assumed that the fold of the macrocycle is the consequence of a hydrogen link between the adjacent phenolic oxygen atoms of each DHTMB fragment.

As pictured in fig. 3.33, the macrocycle is sharply folded at the saturated carbon of the DHTMB unit, allowing the two octahedrally coordinated nickel ions to share an edge. The value of the angle between the planes formed by the two phenyl rings of each DHTMB fragment is $65.30(42)^\circ$, which is *ca.* 10° smaller than in the related dinuclear species. The values of the torsion angles involving the saturated carbon are very similar to the dinuclear complexes $[\text{Ni}_2(\text{H}_4\text{L9})(\mu_2\text{-H}_2\text{O})(\text{EtOH})_2](\text{ClO}_4)_2$ and $[\text{Co}_2(\text{H}_4\text{L9})(\mu_2\text{-H}_2\text{O})(\text{EtOH})_2](\text{ClO}_4)_2$. The distance separating Ni(1) from Ni(1A) is $3.204(3) \text{ \AA}$, which is one angström smaller than the Ni-Ni distance in the complex $[\text{Ni}_2(\text{H}_4\text{L9})(\mu_2\text{-H}_2\text{O})(\text{EtOH})_2](\text{ClO}_4)_2$. The two sets of opposite nickel ions are doubly bridged; one bridging unit is coordinated more strongly to the nickel ions at a distance of $2.048(7) \text{ \AA}$, while the other unit is at a distance of $2.199(8) \text{ \AA}$. This observation might indicate that one bridge is a hydroxo group and the other a water molecule. Similarly to the dinuclear water bridged species, a water bridge occupies one of the apical positions on the concave side of the macrocycle. There is also a second bridge that occupies one of the equatorial positions in the nickel octahedral environment and is situated in the fold of the macrocycle. The coordination of a hydroxo group might influence the metal-metal distance by pulling the nickel ions together, in contrast to the dinickel complex where no hydroxo groups are present. On each side of the macrocycle an alkoxo group bridges the set of nickel atoms. Four ethanol molecules complete the coordination sphere of the nickel ions. Similarly to the dinuclear species, the nickel ions are in a tetragonal environment. The selected bond lengths and angles are given in table 3.27. As a result of accommodating four metal centres the macrocycle is quite constrained, which shows the extent of flexibility of the macrocyclic ligand L9. Similarly to the dinuclear complexes, it can be assumed that the fold of the macrocycle is the consequence of a hydrogen link between the adjacent phenolic oxygen atoms of each DHTMB fragment.

hydroxide with the ratio ligand:NaOH being 1:2. Green crystals suitable for X-ray studies were grown by slow evaporation of an ethanol solution of the compound. All the X-ray data collection parameters for $[\text{Cu}_4(\text{H}_2\text{L9})(\mu_2\text{-OH})_2(\mu_2\text{-H}_2\text{O})_2](\text{NO}_3)_2$ are summarised in table 12 in annex 2 along with the details concerning the refinement and disorders. As the tetracopper structure is very similar to the tetranickel complex, only the selected bond lengths and angles will be given in table 3.28.

Table 3.28: Selected bond lengths [\AA] and angles [$^\circ$] for $[\text{Cu}_4(\text{H}_2\text{L9})(\mu_2\text{-OH})_2(\mu_2\text{-H}_2\text{O})_2](\text{NO}_3)_2$

Cu(1)-O(2)	1.905(12)	Cu(2)-O(1)	2.393(14)
Cu(1)-N(1)	1.925(16)	Cu(3)-O(4)	1.899(16)
Cu(1)-O(52)	1.939(12)	Cu(3)-N(4)	1.936(17)
Cu(1)-O(11)	1.999(12)	Cu(3)-O(52)	1.990(12)
Cu(1)-O(1)	2.390(13)	Cu(3)-O(48)	2.010(14)
Cu(1)-Cu(2)	3.137(4)	Cu(3)-O(3)	2.42(2)
Cu(1)-Cu(3)	3.692(4)	Cu(4)-O(4)	1.886(16)
Cu(2)-O(2)	1.903(12)	Cu(4)-N(3)	1.889(18)
Cu(2)-N(2)	1.933(17)	Cu(4)-O(25)	1.977(12)
Cu(2)-O(25)	1.950(12)	Cu(4)-O(37)	2.023(12)
Cu(2)-O(22)	2.004(12)	Cu(4)-O(3)	2.418(15)
O(2)-Cu(1)-N(1)	176.9(7)	N(2)-Cu(2)-O(25)	86.5(6)
O(2)-Cu(1)-O(52)	94.4(5)	O(2)-Cu(2)-O(22)	89.4(5)
N(1)-Cu(1)-O(52)	85.9(6)	N(2)-Cu(2)-O(22)	89.8(6)
O(2)-Cu(1)-O(11)	89.1(5)	O(25)-Cu(2)-O(22)	172.2(5)
N(1)-Cu(1)-O(11)	90.2(6)	O(2)-Cu(2)-O(1)	81.8(5)
O(52)-Cu(1)-O(11)	171.0(5)	N(2)-Cu(2)-O(1)	100.7(7)
O(2)-Cu(1)-O(1)	81.8(5)	O(25)-Cu(2)-O(1)	99.2(5)
N(1)-Cu(1)-O(1)	101.2(6)	O(22)-Cu(2)-O(1)	88.3(5)
O(52)-Cu(1)-O(1)	100.4(5)	O(4)-Cu(3)-N(4)	174.9(8)
O(11)-Cu(1)-O(1)	88.3(5)	O(4)-Cu(3)-O(52)	94.5(6)
O(2)-Cu(2)-N(2)	177.4(7)	N(4)-Cu(3)-O(52)	85.9(6)
O(2)-Cu(2)-O(25)	94.0(5)	O(4)-Cu(3)-O(48)	89.5(6)

N(4)-Cu(3)-O(48)	89.5(6)	N(3)-Cu(4)-O(25)	86.7(7)
O(52)-Cu(3)-O(48)	171.7(5)	O(4)-Cu(4)-O(37)	88.8(6)
O(4)-Cu(3)-O(3)	82.7(7)	N(3)-Cu(4)-O(37)	89.9(7)
N(4)-Cu(3)-O(3)	102.2(9)	O(25)-Cu(4)-O(37)	170.7(5)
O(52)-Cu(3)-O(3)	100.0(7)	O(4)-Cu(4)-O(3)	82.6(5)
O(48)-Cu(3)-O(3)	87.7(7)	N(3)-Cu(4)-O(3)	103.1(8)
O(4)-Cu(4)-N(3)	175.0(8)	O(25)-Cu(4)-O(3)	100.1(5)
O(4)-Cu(4)-O(25)	93.9(6)	O(37)-Cu(4)-O(3)	89.2(5)

The elemental analysis and FAB data (table 3.29) support the formation of $\text{Cu}_4(\text{H}_2\text{L9})(\mu_2\text{-OH})_2(\mu_2\text{-H}_2\text{O})_2(\text{NO}_3)_2$. The IR shows a band corresponding to the vibration of the imine groups and the expected band at 1384 cm^{-1} characteristic of free nitrate anions is also observed.

Table 3.29: Peak attributions for $[\text{Cu}_4(\text{H}_2\text{L9})(\mu_2\text{-OH})_2(\mu_2\text{-H}_2\text{O})_2](\text{NO}_3)_2$

m/z	Rel. Intensity (%)	Fragments	Calc. Mass
969	55	$[\text{Cu}_2(\text{H}_2\text{L9})+\text{H}]^+$	967
1031	65	$[\text{Cu}_3(\text{H}_2\text{L9})]^{2+}$	1029
1091	25	$[\text{Cu}_3(\text{H}_2\text{L9})(\text{NO}_3)]^+$	1091
1109	20	$[\text{Cu}_4(\text{H}_2\text{L9})(\text{OH})]^{3+}$	1109
1264	35	$[\text{Cu}_4(\text{H}_2\text{L9})(\mu_2\text{-OH})_2(\mu_2\text{-H}_2\text{O})_2]^{2+}$	1262
1514	7	$[\text{Cu}_4(\text{H}_2\text{L9})(\mu_2\text{-OH})_2(\mu_2\text{-H}_2\text{O})_2(\text{NO}_3)_2+\text{H}]^+ \cdot 5\text{EtOH}$	1516
1576	5	$[\text{Cu}_4(\text{H}_2\text{L9})(\mu_2\text{-OH})_2(\mu_2\text{-H}_2\text{O})_2(\text{NO}_3)_2+\text{Na}]^+ \cdot 5\text{EtOH}, 2\text{H}_2\text{O}$	1576

3.8.4. Synthesis and characterisation of $[\text{Cu}_4(\text{L9})(\text{OAc})_2(\text{AcOH})_3(\text{DMF})]$

Another tetranuclear complex was isolated but in this case no sodium hydroxide was used. The macrocyclic nature of the complex is supported by the presence of an imine vibration at 1628 cm^{-1} in the IR spectrum. The symmetric vibration of the acetate groups is observed at 1438 cm^{-1} . It can be assumed that the asymmetric vibration associated with the acetate can be found in the band at 1567 cm^{-1} where C=C and C-O vibrations also overlap. The formula, $[\text{Cu}_4(\text{L9})(\text{OAc})_2(\text{AcOH})_3(\text{DMF})]$, is consistent with the elemental analysis and the FAB data (table 3.30). However, some of the peaks observed in FAB are of low relative intensity, which suggests that the complex is not very soluble within the noba matrix.

Table 3.30: Peak attributions for $[\text{Cu}_4(\text{L9})(\text{OAc})_2(\text{AcOH})_3(\text{DMF})]$

m/z	Rel. Intensity (%)	Fragments	Calc. Mass
989	45	$[\text{Cu}_2(\text{H}_2\text{L9})+\text{Na}]^+$	989
1448	< 5	$[\text{Cu}_4(\text{L9})(\text{OAc})_2(\text{AcOH})_4+\text{H}]^+$	1449
1472	< 5	$[\text{Cu}_4(\text{L9})(\text{OAc})_2(\text{AcOH})_4+\text{Na}]^+$	1471
1579	< 5	$[\text{Cu}_4(\text{L9})(\text{OAc})_2(\text{AcOH})_4+\text{H}]^+.\text{DMF},\text{AcOH}$	1582

Without any structural information, it is difficult to speculate on the nature of this copper complex. If the structure is related to the tetracopper complex $[\text{Cu}_4(\text{H}_2\text{L9})(\text{OH})_2(\text{H}_2\text{O})_2(\text{H}_2\text{O})_4](\text{NO}_3)_2$, it can be assumed that the two acetate molecules are bridging the two opposite sets of copper ions. The separation between the symmetric and asymmetric vibrations is *ca.* 129 cm^{-1} , which according to Deacon *et al.*¹²² would suggest that the acetate anions adopt a bridging mode.

3.8.5. Synthesis and characterisation of $[\text{Co}_4(\text{H}_2\text{L9})(\text{OH})_4(\text{MeOH})_4](\text{ClO}_4)_2$

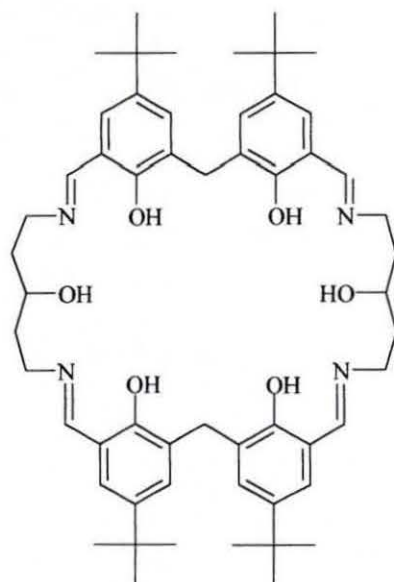
In this series of tetranuclear species of the ligand L9, a tetranuclear cobalt complex thought to be similar to the tetranuclear nickel complex has been synthesised. Similarly to the tetranickel complexes, the use of sodium hydroxide seemed necessary. The elemental analysis and the FAB results (table 3.31) are consistent with the formation of a mixed-valence complex ($[\text{Co}_2^{\text{II}}\text{Co}_2^{\text{III}}(\text{H}_2\text{L9})(\text{OH})_4(\text{MeOH})_4](\text{ClO}_4)_2$). After 24 hours reflux the solution had turned dark brown, which is indicative of a mixed-valence Co(II/III) or Co(III) complex. The IR spectrum shows a band at 1624 cm^{-1} assigned to the vibration of the imine groups, which supports the macrocyclic nature of the compound. The expected vibrations attributed to the perchlorate anions are observed at 1090 and 625 cm^{-1} .

Table 3.31: Peak attributions for $[\text{Co}_4(\text{H}_2\text{L9})(\text{OH})_4(\text{MeOH})_4](\text{ClO}_4)_2$

m/z	Rel. Intensity (%)	Fragments	Calc. Mass
959	100	$[\text{Co}_4(\text{H}_2\text{L9})]^+$	958
1016	40	$[\text{Co}_3(\text{H}_2\text{L9})]^{3+}$	1017
1059	95	$[\text{Co}_3(\text{H}_2\text{L9})]^{3+}.\text{EtOH}$	1063
1116	60	$[\text{Co}_4(\text{H}_2\text{L9})(\text{OH})_2]^{4+}$	1110
1183	5	$[\text{Co}_4(\text{H}_2\text{L9})(\text{OH})_4]^{2+}.2\text{H}_2\text{O}$	1180
1384	20	$[\text{Co}_4(\text{H}_2\text{L9})(\text{OH})_4(\text{MeOH})_3(\text{ClO}_4)]^+.\text{H}_2\text{O}$	1389
1439	7	$[\text{Co}_4(\text{H}_2\text{L9})(\text{OH})_4(\text{MeOH})_3(\text{ClO}_4)_2+\text{H}]^+$	1439
1496	7	$[\text{Co}_4(\text{H}_2\text{L9})(\text{OH})_4(\text{MeOH})_4(\text{ClO}_4)_2+\text{Na}]^+$	1493

3.9. Tetranuclear complexes of L11

3.9.1. Synthesis of $[\text{Mn}_4(\text{L11})(\text{MeOH})_4(\text{MeO})_2(\text{OAc})_2]\text{Cl}_2$ and $[\text{Mn}_4(\text{L11})(\text{MeOH})_6(\text{MeO})_2\text{Cl}_2](\text{ClO}_4)_2$



$\text{H}_6\text{L11}$

Fig. 3.34: Ligand $\text{H}_6\text{L11}$

Using the longer diamine 1,5-diaminopentane-3-ol, the synthesis of two tetranuclear manganese complexes, $[\text{Mn}_4(\text{L11})(\text{MeOH})_4(\text{MeO})_2(\text{OAc})_2]\text{Cl}_2$ and $[\text{Mn}_4(\text{L11})(\text{MeOH})_6(\text{MeO})_2\text{Cl}_2](\text{ClO}_4)_2$, has been achieved with yields of 57 and 50% respectively. One remarkable fact during the synthesis was the change of colour from brown-green to deep dark green (almost black) upon cooling of the reaction mixture. This might be an indication that the exposure to even more air completed the oxidation of the manganese ions to produce Mn(III)_4 complexes. Further investigation is needed to study the influence of oxygen on the reaction and see if the outcome of the reaction is dramatically changed or not. The macrocyclic nature of both complexes is supported by the presence of an imine vibration at *ca.* 1618 cm^{-1} . For $[\text{Mn}_4(\text{L11})(\text{MeOH})_6(\text{MeO})_2\text{Cl}_2](\text{ClO}_4)_2$, the expected perchlorate vibrations are observed at 1088 and 626 cm^{-1} , while for $[\text{Mn}_4(\text{L11})(\text{MeOH})_4(\text{MeO})_2(\text{OAc})_2]\text{Cl}_2$, the

symmetric vibration of the acetate anions can be detected at 1443 and 1439 cm^{-1} and the asymmetric vibration at *ca.* 1552 cm^{-1} . The separation between the symmetric and asymmetric vibrations is *ca.* 109 cm^{-1} , which according to Deacon *et al.*¹²² would suggest that the acetate anions adopt a bridging mode. The FAB results are consistent with the formation of both complexes (tables 3.32 and 3.33).

Table 3.32: Peak attributions for $[\text{Mn}_4(\text{L11})(\text{MeOH})_6(\text{MeO})_2\text{Cl}_2](\text{ClO}_4)_2$

m/z	Rel. Intensity (%)	Fragments	Calc. Mass
955	55	$[\text{Mn}(\text{H}_3\text{L11})+\text{H}]^+$	953
991	100	$[\text{Mn}(\text{H}_4\text{L11})\text{Cl}+\text{H}]^+$	989
1044	70	$[\text{Mn}_2(\text{H}_3\text{L11})\text{Cl}]^{2+}$	1043
1096	25	$[\text{Mn}_2(\text{H}_3\text{L11})\text{Cl}_2]^+\cdot\text{H}_2\text{O}$	1095
1108	20	$[\text{Mn}_2(\text{H}_3\text{L11})\text{Cl}_2]^+\cdot\text{CH}_3\text{OH}$	1109
1223	25	$[\text{Mn}_4(\text{L11})\text{Cl}_2]^{4+}\cdot 2\text{H}_2\text{O}$	1223
1287	10	$[\text{Mn}_4(\text{L11})(\text{MeO})_2\text{Cl}_2]^{2+}\cdot 2\text{H}_2\text{O}$	1285
1337	10	$[\text{Mn}_4(\text{L11})(\text{MeO})_2(\text{H}_2\text{O})_3\text{Cl}_2]^{2+}\cdot 2\text{H}_2\text{O}$	1336
1490	10	$[\text{Mn}_4(\text{L11})(\text{MeO})_2(\text{MeOH})_6\text{Cl}_2]^{2+}\cdot\text{H}_2\text{O},\text{MeOH}$	1488
1518	10	$[\text{Mn}_4(\text{L11})(\text{MeO})_2(\text{H}_2\text{O})_6(\text{MeOH})_2\text{Cl}_2(\text{ClO}_4)]^+$	1517

Table 3.33: Peak attributions for $[\text{Mn}_4(\text{L11})(\text{MeOH})_4(\text{MeO})_2(\text{OAc})_2]\text{Cl}_2$

m/z	Rel. Intensity (%)	Fragments	Calc. Mass
901	40	$[(\text{H}_6\text{L11})+\text{H}]^+$	901
954	80	$[\text{Mn}(\text{H}_4\text{L11})]^+$	953
990	75	$[\text{Mn}(\text{H}_4\text{L11})\text{Cl}+\text{H}]^+$	989
1043	100	$[\text{Mn}_2(\text{H}_3\text{L11})\text{Cl}]^{2+}$	1043
1096	45	$[\text{Mn}_2(\text{H}_3\text{L11})\text{Cl}_2]^+\cdot\text{H}_2\text{O}$	1095
1150	45	$[\text{Mn}_3(\text{L11})\text{Cl}]^{2+}\cdot 3\text{H}_2\text{O}$	1148
1185	30	$[\text{Mn}_4(\text{L11})\text{Cl}_2]^{4+}$	1184
1489	25	$[\text{Mn}_4(\text{L11})(\text{MeO})_2(\text{MeOH})_4(\text{OAc})_2\text{Cl}]^+$ MeOH	1489
1512	10	$[\text{Mn}_4(\text{L11})(\text{MeO})_2(\text{MeOH})_4(\text{OAc})_2\text{Cl}_2+\text{Na}]^+$	1515
1584	5	$[\text{Mn}_4(\text{L11})(\text{MeO})_2(\text{MeOH})_4(\text{OAc})_2\text{Cl}_2+\text{Na}]^+$ MeOH, 2H ₂ O	1583

3.9.2. Structures of $[\text{Mn}_4(\text{L11})(\text{MeOH})_6(\text{MeO})_2\text{Cl}_2](\text{ClO}_4)_2$ and $[\text{Mn}_4(\text{L11})-(\text{MeOH})_4(\text{MeO})_2(\text{OAc})_2]\text{Cl}_2$

Dark green crystals of $[\text{Mn}_4(\text{L11})(\text{MeOH})_6(\text{MeO})_2\text{Cl}_2](\text{ClO}_4)_2$ and $[\text{Mn}_4(\text{L11})-(\text{MeOH})_4(\text{MeO})_2(\text{OAc})_2]\text{Cl}_2$ suitable for X-ray studies were grown by slow diffusion of diethylether into a methanol solution of the compounds. All the X-ray data collection parameters for $[\text{Mn}_4(\text{L11})(\text{MeOH})_6(\text{MeO})_2\text{Cl}_2](\text{ClO}_4)_2$ and $[\text{Mn}_4(\text{L11})-(\text{MeOH})_4(\text{MeO})_2(\text{OAc})_2]\text{Cl}_2$ are summarised in table 13 and table 14 respectively in annex 2 along with the details concerning the refinement and disorders.

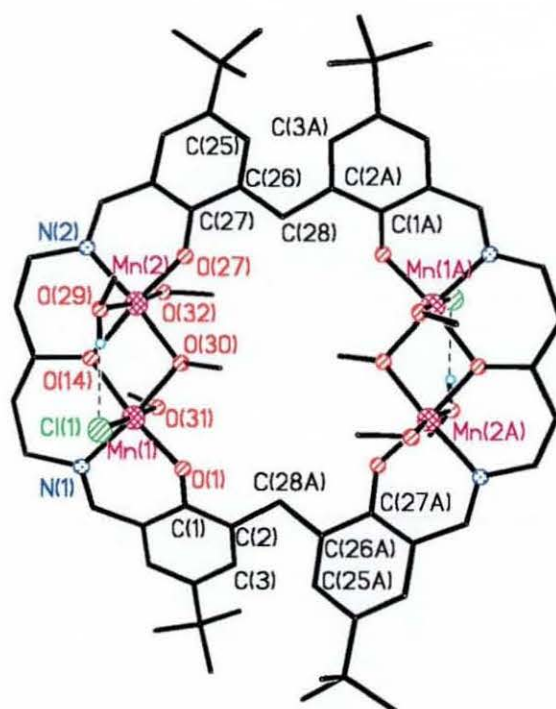


Fig. 3.35: Structure of the cation $[\text{Mn}_4(\text{L11})(\text{MeOH})_6(\text{MeO})_2\text{Cl}_2]^{2+}$

The two centrosymmetric structures are very similar except for the axial ligands. The manganese ions are co-planar in the centre of the macrocycle with a dimer-of-dimer geometry and an elongated octahedral environment (fig. 3.36 and 3.37), which is consistent with Mn(III) centres exhibiting a Jahn-Teller distortion. The lengths of the equatorial Mn-O and Mn-N bonds are typical of Mn(III) ions.⁸⁹ The selected bond lengths and angles for both complexes are given in table 3.34.

Table 3.34: Selected bond lengths [Å] and angles [°] for
 $[\text{Mn}_4(\text{L11})(\text{MeOH})_6(\text{MeO})_2\text{Cl}_2](\text{ClO}_4)_2$ and
 $[\text{Mn}_4(\text{L11})(\text{MeOH})_4(\text{MeO})_2(\text{OAc})_2]\text{Cl}_2$

$[\text{Mn}_4(\text{L11})(\text{MeOH})_6(\text{MeO})_2\text{Cl}_2](\text{ClO}_4)_2$

Mn(1)-O(1)	1.8515(16)	O(14)-Mn(2)	1.9304(16)
Mn(1)-O(30)	1.9464(16)	N(2)-Mn(2)	1.992(2)
Mn(1)-O(14)	1.9469(16)	O(27)-Mn(2)	1.8558(16)
Mn(1)-N(1)	1.991(2)	O(29)-Mn(2)	2.2412(19)
Mn(1)-O(31)	2.2619(19)	Mn(2)-O(30)	1.9187(16)
Mn(1)-Cl(1)	2.5499(7)	Mn(2)-O(32)	2.2618(19)
Mn(1)-Mn(2)	2.9635(5)		
O(1)-Mn(1)-O(30)	94.27(7)	O(14)-Mn(1)-O(31)	86.24(7)
O(1)-Mn(1)-O(14)	170.47(7)	N(1)-Mn(1)-O(31)	88.17(8)
O(30)-Mn(1)-O(14)	79.45(7)	O(1)-Mn(1)-Cl(1)	95.55(6)
O(1)-Mn(1)-N(1)	91.48(8)	O(30)-Mn(1)-Cl(1)	92.50(5)
O(30)-Mn(1)-N(1)	173.47(8)	O(14)-Mn(1)-Cl(1)	91.91(5)
O(14)-Mn(1)-N(1)	94.46(7)	N(1)-Mn(1)-Cl(1)	90.01(6)
O(1)-Mn(1)-O(31)	86.50(7)	O(31)-Mn(1)-Cl(1)	177.30(5)
O(30)-Mn(1)-O(31)	89.10(7)		

$[\text{Mn}_4(\text{L11})(\text{MeOH})_4(\text{MeO})_2(\text{OAc})_2]\text{Cl}_2$

Mn(1)-O(1)	1.8621(14)	O(14)-Mn(2)	1.9333(14)
Mn(1)-O(31)	1.9281(13)	N(2)-Mn(2)	2.0000(17)
Mn(1)-O(14)	1.9533(14)	O(27)-Mn(2)	1.8480(14)
Mn(1)-N(1)	1.9779(18)	O(30A)-Mn(2)	2.1588(16)
Mn(1)-O(30B)	2.1487(16)	Mn(2)-O(31)	1.9425(13)
Mn(1)-O(32)	2.3308(16)	Mn(2)-O(33)	2.2521(15)
Mn(1)-Mn(2)	2.9155(4)		

O(1)-Mn(1)-O(31)	93.75(6)	O(14)-Mn(1)-O(30B)	88.14(6)
O(1)-Mn(1)-O(14)	171.37(7)	N(1)-Mn(1)-O(30B)	93.02(7)
O(31)-Mn(1)-O(14)	81.08(6)	O(1)-Mn(1)-O(32)	89.12(6)
O(1)-Mn(1)-N(1)	91.61(7)	O(31)-Mn(1)-O(32)	90.51(6)
O(31)-Mn(1)-N(1)	173.45(7)	O(14)-Mn(1)-O(32)	84.04(6)
O(14)-Mn(1)-N(1)	93.14(7)	N(1)-Mn(1)-O(32)	85.81(7)
O(1)-Mn(1)-O(30B)	98.82(7)	O(30B)-Mn(1)-O(32)	172.01(6)
O(31)-Mn(1)-O(30B)	89.88(6)		

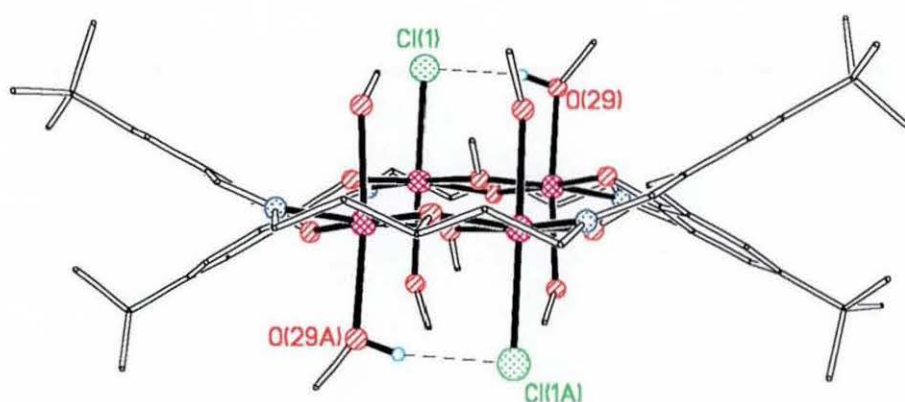


Fig. 3.36: Side-on view of the cation $[\text{Mn}_4(\text{L11})(\text{MeOH})_6(\text{MeO})_2\text{Cl}_2]^{2+}$

As shown in fig. 3.35 and 3.36, the coordination sphere of the manganese ions in $[\text{Mn}_4(\text{L11})(\text{MeOH})_6(\text{MeO})_2\text{Cl}_2](\text{ClO}_4)_2$ is completed with methanol molecules and chloride anions, while in $[\text{Mn}_4(\text{L11})(\text{MeOH})_4(\text{MeO})_2(\text{OAc})_2]\text{Cl}_2$ the coordination sphere is completed by methanol molecules and acetate anions bridging two adjacent manganese ions on each side of the macrocycle (fig. 3.37).

In complex $[\text{Mn}_4(\text{L11})(\text{MeOH})_6(\text{MeO})_2\text{Cl}_2](\text{ClO}_4)_2$ (fig. 3.36), each coordinated chloride anion is involved in hydrogen-bonding with the methanol molecule coordinated to the neighbouring manganese ion. One of the coordinated methanol molecules is also involved in hydrogen-bonding with a solvate molecule (MeOH)

while the other methanol molecule is hydrogen-bonded to a perchlorate anion. The bond lengths and angles associated with hydrogen-bonding are given in table 3.35.

Table 3.35: Hydrogen bonds [\AA and $^\circ$] for $[\text{Mn}_4(\text{L11})(\text{MeOH})_6(\text{MeO})_2\text{Cl}_2](\text{ClO}_4)_2$

D-H...A	d(D-H)	d(H...A)	d(D...A)	<(DHA)
O(29)-H(29)...Cl(1)	0.85	2.17	2.9926(19)	163.8
O(31)-H(31)...O(33)	0.94	1.72	2.651(3)	169.3
O(32)-H(32)...O(23)**	0.85	2.00	2.834(3)	167.9
O(33)-H(33)...O(24) [#]	0.85	1.91	2.739(4)	162.1

Symmetry transformations used to generate equivalent atoms: (***) $-x+1/2, y+1/2, -z+1/2$

([#]) $x, -y+2, z+1/2$

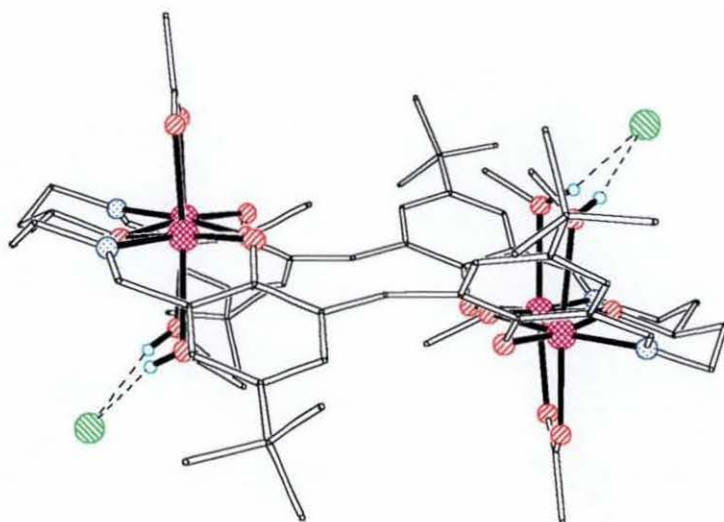


Fig. 3.37: Side-on view of $[\text{Mn}_4(\text{L11})(\text{MeOH})_4(\text{MeO})_2(\text{OAc})_2]\text{Cl}_2$ showing the hydrogen-bonding

In complex $[\text{Mn}_4(\text{L11})(\text{MeOH})_4(\text{MeO})_2(\text{OAc})_2]\text{Cl}_2$ (fig. 3.37), on each side of the macrocyclic plane the two adjacent coordinated methanol molecules are hydrogen-bonded to one free chloride anion. The bond lengths and angles involved in hydrogen-bonding are given in table 3.36.

Table 3.36: Hydrogen bonds [\AA and $^\circ$] for $[\text{Mn}_4(\text{L11})(\text{MeOH})_4(\text{MeO})_2(\text{OAc})_2]\text{Cl}_2$

D-H...A	d(D-H)	d(H...A)	d(D...A)	<(DHA)
O(32)-H(32)...Cl(1)	0.85	2.25	3.0855(18)	166.2
O(33)-H(33)...Cl(1)	0.85	2.18	2.9999(17)	164.2

As shown in fig. 3.35, 3.36 and 3.37, the twist around the saturated carbon of the DHTMB head-unit is similar to the dinuclear manganese complex, $[(\text{Mn}_2(\text{H}_2\text{L9}))_3(\text{OAc})_3(\text{H}_2\text{O})(\text{EtOH})_2\text{CO}_3]$, described previously. The macrocycle does not adopt a folded conformation with the two phenyl rings facing each other. In this case, the phenyl rings are tilted with one oxygen atom pointing up while the other oxygen atom is pointing down (fig. 3.37). The torsion angles (table 3.37) are slightly different in both complexes, probably due to the bridging acetate anions.

Table 3.37: Torsion angles [$^\circ$] for $[\text{Mn}_4(\text{L11})(\text{MeOH})_6(\text{MeO})_2\text{Cl}_2](\text{ClO}_4)_2$ and $[\text{Mn}_4(\text{L11})(\text{MeOH})_4(\text{MeO})_2(\text{OAc})_2]\text{Cl}_2$

	Torsion angles in ($^\circ$) for $[\text{Mn}_4(\text{L11})(\text{MeOH})_6(\text{MeO})_2\text{Cl}_2](\text{ClO}_4)_2$	Torsion angles in ($^\circ$) for $[\text{Mn}_4(\text{L11})(\text{MeOH})_4(\text{MeO})_2(\text{OAc})_2]\text{Cl}_2$
C(25)-C(26)-C(28)-C(2A)	17.8(4)	-31.3(3)
C(27)-C(26)-C(28)-C(2A)	-163.0(2)	153.9(2)

The remarkable feature of this complex is that the change to a longer alkoxy side-chain only changed the nuclearity of the macrocycle with the macrocycle H₆L11 keeping a similar shape to the smaller macrocycle H₆L9. This shows that the DHTMB unit mainly dictates the shape of the macrocycle rather than the diamine. No tetranuclear manganese complexes of the macrocycle H₆L9 have been isolated so far.

In contrast to the other complexes described previously, except [Mn₂(L8)](ClO₄)₂, there is a big gap (8.289(1) Å) between the manganese ions on opposite sides of the macrocycle. This feature is very interesting because it opens the way to host-guest chemistry. Consequently, the macrocyclic complex could potentially accommodate different bridging units with various sizes depending on the extent of its flexibility. Finally, it is striking that the structural differences between the M₄ complexes of H₆L9 and H₆L11 are primarily due to the DHTMB group rather than to the diamines used.

3.9.3. Magnetic behaviour

Magnetic data confirm that both manganese complexes behave as isolated dimeric Mn(III) units. This is not surprising considering the large distance separating the two sets of manganese ions with no bridge able to mediate any magnetic exchange. ESR data showed traces of Mn(II) but the compound is essentially ESR-silent, which is expected for Mn(III) compounds.

3.9.4. Preliminary electrochemistry studies

In this study the redox properties of the complex [Mn₄(L11)(MeOH)₄(MeO)₂(OAc)₂]-Cl₂ are studied and compared dissolved in methanol solution and as a solid in aqueous buffer solution environments by cyclic voltammetry. Rather than dissolving the sensitive metal complexes in the solution phase, they can be mechanically adhered to a suitable electrode surface (basal plane pyrolytic graphite) in form of

microcrystalline solid and investigated by solid state voltammetry.¹³⁸⁻¹⁴⁰ As a result, the redox properties of $[\text{Mn}_4(\text{L11})(\text{MeOH})_4(\text{MeO})_2(\text{OAc})_2]\text{Cl}_2$ can be studied at the solid/solution phase boundary in purely aqueous media.

Tetramanganese(III) metal complexes may be expected to undergo both reduction and oxidation processes within a relatively narrow potential range (usually Mn(III) has a narrow range of stability). This unusual feature is detected here in solid state voltammograms but not in experiments conducted in organic solution.

Fig. 38A shows cyclic voltammograms for the reduction of 2 mM of $[\text{Mn}_4(\text{L11})(\text{MeOH})_4(\text{MeO})_2(\text{OAc})_2]\text{Cl}_2$ in methanol/0.1 M Nbu_4PF_6 . A chemically reversible reduction response is detected at $E_{1/2} = 0.0$ V vs. SCE. Experiments at a range of different scan rates indicate the formation of a relatively stable reduction product. In order to determine the number of electrons transferred at the electrode surface per tetramanganese molecule, microelectrode experiments were conducted. Fig. 38B shows a typical steady state voltammogram obtained at a 10 mm diameter platinum microelectrode. The limiting current at a microelectrode is given by equation 1.

$$I_{\text{lim}} = 4 n F D c r \quad (1)$$

With the diffusion coefficient, D , known, the number of electrons transferred, n , can be calculated from the limiting current, I_{lim} , the Faraday constant, F , the concentration, C , and the electrode radius, $r = 5$ mm. An estimate for the diffusion coefficient, $D = 4.0 \times 10^{-6} \text{ cm}^2 \text{ s}^{-1}$, was obtained from the Wilke-Chang expression.¹⁴¹ With this estimate, the approximate number of electrons transferred, $n = 2$, is obtained. Therefore only two of the four manganese(III) centres are reduced.

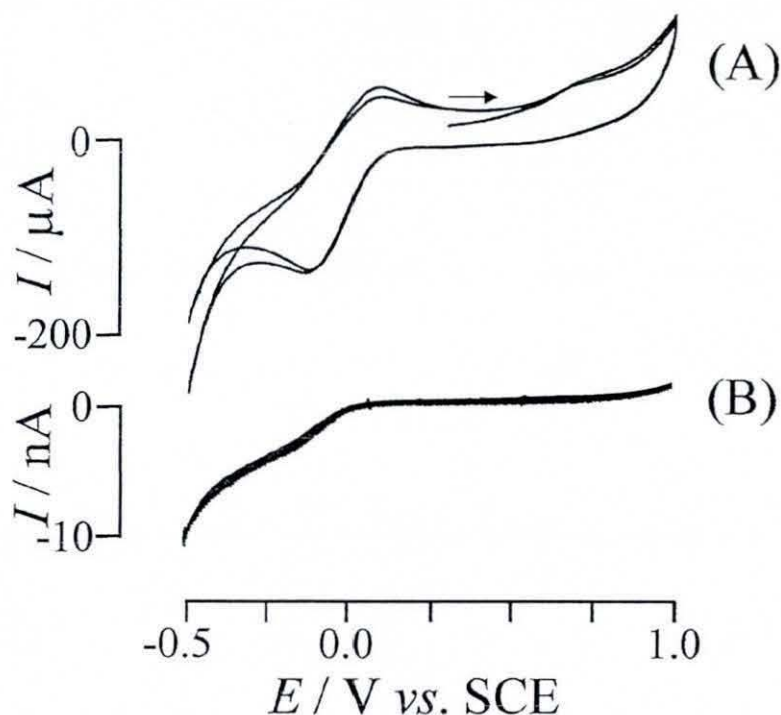


Fig. 3.38: (A) Multicycle cyclic voltammogram (scan rate 0.02 V s^{-1}) for the reduction of $[\text{Mn}_4(\text{L11})(\text{MeOH})_4(\text{MeO})_2(\text{OAc})_2]\text{Cl}_2$ (conc. 2 mM) dissolved in methanol/0.1 M NBu_4PF_6 at a 3 mm diameter glassy carbon electrode.

(B) Cyclic steady state voltammogram (scan rate 0.01 V s^{-1}) for the reduction of $[\text{Mn}_4(\text{L11})(\text{MeOH})_4(\text{MeO})_2(\text{OAc})_2]\text{Cl}_2$ (conc. 2 mM) dissolved in methanol/0.1 M NBu_4PF_6 at a $10 \mu\text{m}$ diameter platinum microelectrode.

Very different electrochemical characteristics were observed for solid $[\text{Mn}_4(\text{L11})(\text{MeOH})_4(\text{MeO})_2(\text{OAc})_2]\text{Cl}_2$. Fig. 39A and 39B show cyclic voltammograms for the reduction and oxidation of solid microcrystalline powder adhered to the surface of a basal plane pyrolytic graphite electrode and immersed in aqueous acetate

buffer solution. Fig. 39B shows that in the first potential cycle a chemically reversible oxidation is detected. In the corresponding solution voltammogram (see Fig. 38A) only a minor signal probably due to water traces in methanol was observed. The chemically reversible oxidation process suggests formation of Mn(IV). However, the number of electrons involved is currently not known.

The solid state voltammogram depicted in Fig. 39A shows that the reduction of Mn(III) to Mn(II) is detected in the first cycle of the solid state voltammogram. However, in the presence of water the process is irreversible and the product of the reduction process gives rise to new oxidation signals at more positive potentials. Varying the pH causes both oxidation and reduction signals to shift in potential. Qualitatively, this behaviour is indicating that the exchange of protons is part of the overall mechanism for both processes.

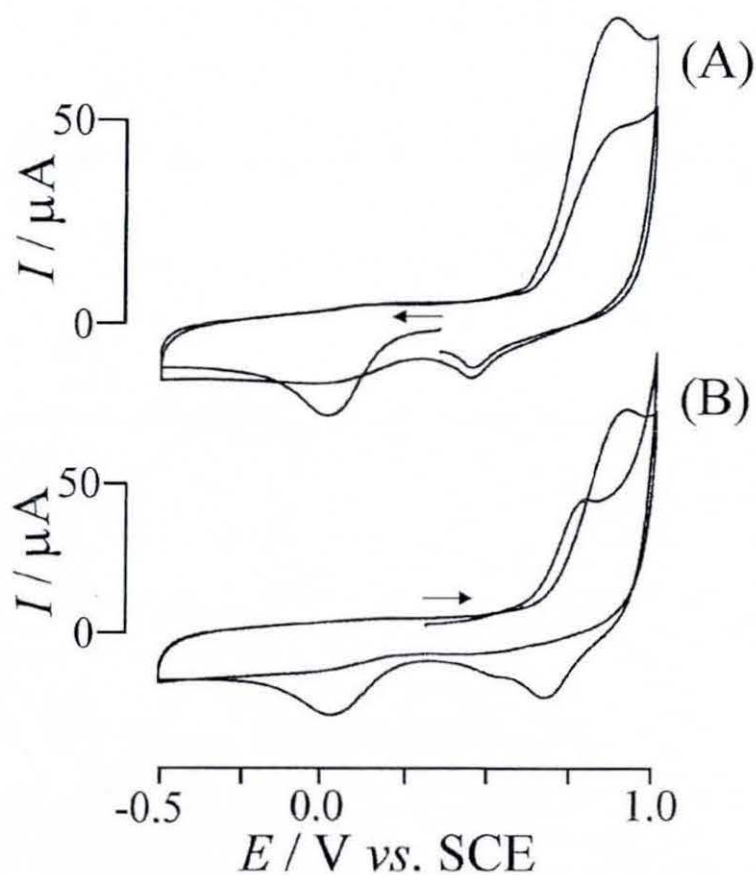


Fig. 3.39: Multicycle cyclic voltammograms (scan rate 0.1 V s^{-1}) for the reduction and oxidation of $[\text{Mn}_4(\text{L11})(\text{MeOH})_4(\text{MeO})_2(\text{OAc})_2]\text{Cl}_2$ adhered in solid microcrystalline form to a 4.9 mm diameter basal plane pyrolytic graphite electrode and immersed in aqueous 0.1 M acetate buffer at pH 6. In (A) reduction is followed by oxidation and in (B) oxidation is followed by reduction.

3.9.5. Synthesis and characterisation of $[\text{Co}_4(\text{L11})(\text{MeOH})(\text{HOAc})_3(\text{MeO})_2(\text{OAc})_2]\text{Cl}_2$

The cobalt complex, $[\text{Co}_4(\text{L11})(\text{MeOH})(\text{HOAc})_3(\text{MeO})_2(\text{OAc})_2]\text{Cl}_2$, synthesised with a yield of 57%, is thought to be similar to the tetramanganese complexes according to the IR, elemental analysis and FAB data (table 3.38). The IR spectrum shows a band at 1623 cm^{-1} assigned to the vibration of the imine groups, which supports the formation of the macrocycle. The symmetric vibration of the acetate anions is observed at 1450 cm^{-1} while the asymmetric vibration can be observed at *ca.* 1553 cm^{-1} . Similarly to the manganese complexes, the separation between the symmetric and asymmetric vibrations is *ca.* 103 cm^{-1} , which, according to Deacon *et al.*¹²² would suggest that the acetate anions adopt a bridging mode. Considering the elemental analysis, the axial ligands of the cobalt complex are slightly different to the manganese complex containing acetate anions; three of the methanol molecules have been replaced by acetic acid molecules. A similar coordination of acetic acid molecules has been observed⁹⁰ in tetranuclear nickel complexes of $\text{H}_4\text{L1}$.

Table 3.38: Peak attributions for $[\text{Co}_4(\text{L11})(\text{MeOH})(\text{HOAc})_3(\text{MeO})_2(\text{OAc})_2]\text{Cl}_2$

m/z	Rel. Intensity (%)	Fragments	Calc. Mass
950	40	$[\text{Co}(\text{H}_4\text{L11})]^+$	955
990	100	$[\text{Co}(\text{H}_4\text{L11})\text{Cl}+\text{H}]^+$	993
1038	100	$[\text{Co}_2(\text{L11})+\text{Na}]^+$	1035
1065	45	$[\text{Co}_2(\text{H}_3\text{L11})\text{Cl}]^{2+} \cdot \text{H}_2\text{O}$	1068
1438	38	$[\text{Co}_4(\text{L11})(\text{MeO})_2(\text{OAc})_2(\text{HOAc})(\text{MeOH})]^{2+} \cdot 2\text{H}_2\text{O}$	1438
1496	65	$[\text{Co}_4(\text{L11})(\text{MeO})_2(\text{OAc})_2(\text{HOAc})_2(\text{MeOH})_2]^{2+}$	1494

3.9.6. Synthesis and characterisation of $[\text{Ni}_4(\text{L11})(\text{MeOH})_5(\text{HOAc})_3(\text{OAc})_2]$

The synthesis of a tetranickel complex has also been achieved. However, no structural data are available, as yet. According to the IR, elemental analysis and FAB data (table 3.39), the structure differs from the other tetranuclear complexes. The IR shows a band at 1639 cm^{-1} assigned to the vibration of the imine groups, which is consistent with the formation of the macrocycle. Furthermore, the symmetric vibration of the acetate anions is observed at 1420 cm^{-1} while the asymmetric vibration can be detected at *ca.* 1581 cm^{-1} . Here, the separation between the symmetric and asymmetric vibrations is *ca.* 160 cm^{-1} , which according to Deacon *et al.*¹²² would still be in the range of vibrations observed for acetate anions adopting a bridging mode.

Table 3.39: Peak attributions for $[\text{Ni}_4(\text{L11})(\text{MeOH})_5(\text{HOAc})_3(\text{OAc})_2]$

m/z	Rel. Intensity (%)	Fragments	Calc. Mass
990	30	$[\text{Ni}(\text{H}_4\text{L11})+\text{H}]^+ \cdot \text{MeOH}$	990
1062	65	$[\text{Ni}_2(\text{H}_2\text{L11})+\text{H}]^+ \cdot \text{MeOH}, \text{H}_2\text{O}$	1063
1188	100	$[\text{Ni}_4(\text{L11})(\text{HOAc})+\text{H}]^{2+}$	1186
1338	80	$[\text{Ni}_4(\text{L11})(\text{HOAc})(\text{OAc})_2+\text{H}]^+ \cdot \text{MeOH}$	1337
1397	20	$[\text{Ni}_4(\text{L11})(\text{HOAc})_2(\text{OAc})_2+\text{H}]^+ \cdot \text{MeOH}$	1397
1440	25	$[\text{Ni}_4(\text{L11})(\text{HOAc})_3(\text{OAc})_2+\text{H}]^+ \cdot \text{H}_2\text{O}$	1443
1496	30	$[\text{Ni}_4(\text{L11})(\text{MeOH})(\text{HOAc})_3(\text{OAc})_2+\text{H}]^+ \cdot 2\text{H}_2\text{O}$	1494
1574	20	$[\text{Ni}_4(\text{L11})(\text{MeOH})_4(\text{HOAc})_3(\text{OAc})_2+\text{Na}]^+$	1575

In our attempts to synthesise tetranuclear copper complexes of L11, some preliminary tests led to the conclusion that after 16 hours of reflux in the presence of base, the final product is a mixture of tetranuclear and trinuclear species of L11 according to the elemental analysis and FAB data (table 3.40). Knowing that, depending on the reaction conditions, it is possible to vary the nuclearity of the macrocyclic complexes

of L9, it is reasonable to assume that it is also possible with the bigger macrocycle L11. Thus, further investigations are needed to adjust the reaction conditions and be able to synthesise trinuclear or tetranuclear copper complexes of L11 systematically.

Table 3.40: Peak attributions for the tetracopper-tricopper mixture

m/z	Rel. Intensity (%)	Fragments	Calc. Mass
1515	15	$[\text{Cu}_4(\text{L11})(\text{H}_2\text{O})(\text{HOAc})_3(\text{OAc})_2+\text{H}]^+.3\text{H}_2\text{O}$	1517
2091	7	$[\text{Cu}_4(\text{H}_2\text{L11})_2+\text{H}]^{2+}.\text{MeOH},\text{H}_2\text{O}$	2092
2269	10	$[(\text{Cu}_3(\text{L11}))_2+\text{H}]^+.2\text{MeOH},2\text{H}_2\text{O}$	2268

3.10. Conclusion

The precursor DHTMB can be synthesised in a reasonable yield. However the number of steps (4) combined with the low yield of the first step reduces the overall yield considerably. Presumably, an effective way to improve the yield would be to find an appropriate oxidising agent so that the protection of the phenol group would not be necessary. Thus, reducing the number of steps to two.

The synthesis of a variety of Schiff-base derived macrocycles has been achieved by condensing DHTMB with tren, 1,3-diaminopropan-2-ol, 1,3-diaminopropane and DAHP in the presence of various metal (Ni(II), Co(II), Mn(II), Fe(II), Cu(II) and Zn(II)) salts. Nickel and manganese complexes of H₄L10 have been characterised by IR and FAB spectrometry but no structural data are available so far. However, it has been demonstrated that the DHTMB group introduces multiple geometrical variations, largely due to the presence of the saturated carbon linking the two phenol rings. Indeed, the formation of di-, tri- and tetranuclear complexes of H₆L9 indicates a range of coordination motifs, which can be accessed with this ligand system. Furthermore, tetranuclear manganese complexes of H₆L11 have been fully characterised and are potential candidates for carrying out host-guest chemistry due to

the large central cavity. It would also be interesting to investigate the possibility of varying the oxidation states of the manganese ions or inserting bridges across the cavity that could act as magnetic mediators. Magnetic data confirm that both manganese complexes behave as isolated dimeric Mn(III) units. The preliminary electrochemical studies of $[\text{Mn}_4(\text{L11})(\text{MeOH})_4(\text{MeO})_2(\text{OAc})_2]\text{Cl}_2$ have shown that in the absence of water chemically reversible reduction of manganese(III) is observed. However, in contrast in aqueous media a new chemically reversible oxidation of manganese(III) occurs and the reduction process becomes irreversible.

Moreover, the flexibility of the central cavity in $\text{H}_6\text{L9}$ and $\text{H}_6\text{L11}$ complexes suggests that a range of different bridging species could be accommodated, and perhaps activated to further reaction. Analogous tetranuclear complexes containing nickel, copper and cobalt have been detected by FAB and characterised by IR and elemental analysis. Their crystallisation has proven more difficult, therefore no structural data are available as yet.

Chapter four

Binuclear and Mononuclear Complexes

of

2,6-diformyl-4-*tert*-butylphenol

4.1. Introduction

4.1.1. Review on a few dioximato systems

As described in chapter one, dinuclear complexes with macrocycles derived from the condensation of 2,6-diformyl-4-*tert*-butylphenol, 2,6-diformyl-4-methylphenol and 2,6-diacetyl-4-methylphenol with N,N' -diaminoalkanes have been extensively studied.^{3,5,39} Those systems are remarkable because they bring two metal centres into close proximity through a phenoxo bridge, with important implications for metal-metal interaction and magnetic exchange, potential redox properties and the activation of small molecules. Therefore analogous binucleating dioximes such as 2,6-bis(oximato)-4-methylphenol have similar potential due to the fact that their dinuclear complexes have a pseudo-macrocyclic structure resulting from hydrogen-bonding between two dioxime ligands (fig. 4.1). In 1998, the synthesis, structures and magnetochemistry of dinuclear Co(II), Ni(II) and Cu(II) species of 2,6-bis(oximato)-4-methylphenol were reported by Schröder *et al.*¹⁴²

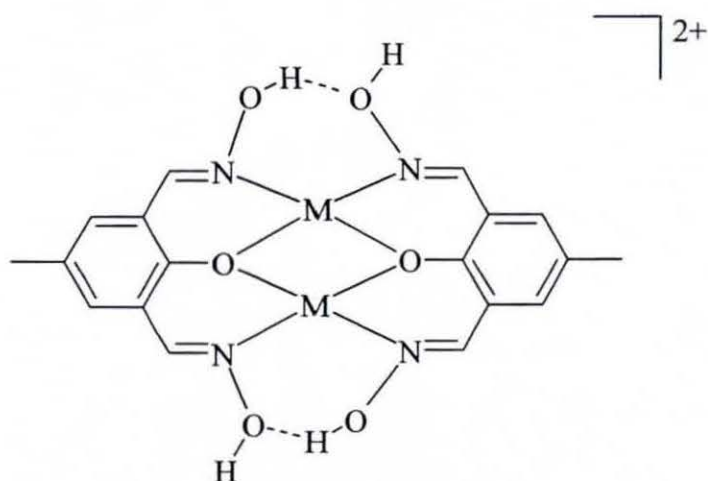


Fig. 4.1: Dinuclear complexes (Co(II), Ni(II) and Cu(II)) of 2,6-bis(oximato)-4-methylphenol

There have been relatively few reports dealing with the coordination chemistry of 2,6-bis(oximato)-4-methylphenol¹⁴³ and its derivatives.¹⁴⁴ In 1973, Okawa *et al.*¹⁴³ reported the synthesis of dicopper(II) and dinickel(II) complexes of 2,6-bis(oximato)-4-methylphenol (La) with the general formulation $[\text{Cu}_2(\text{HLa})_2]$ and $[\text{Ni}_2(\text{HLa})_2]$, while in 1998 Thompson *et al.*⁶⁵ reported magnetochemical and structural data on the related dinickel(II) and dicopper(II) complexes of 2,6-bis(acetoximato)-4-methylphenol and 2,6-bis(acetoximato)-4-*tert*-butylphenol.

Busch and co-workers¹⁴⁵ have been working with dicopper(II) complexes of the asymmetric dicompartmental Schiff-base-oxime ligand shown in fig. 4.2. Their studies were aiming to extend the Robson-type macrocycle into a multicompartmental chain-like ligand using two bimetallic units connected to each other by a fifth metal ion (fig. 4.3). Oxime groups are appropriate for this purpose because they provide “external” donors in the form of their oxygen atoms, while the oxime nitrogen coordinates to the metal ion within the dicompartmental ligand. In the absence of a fifth metal ion, the oxime oxygen coordinates axially to the Cu(II) centre from an other binuclear unit forming coordination tetramers or polymers.

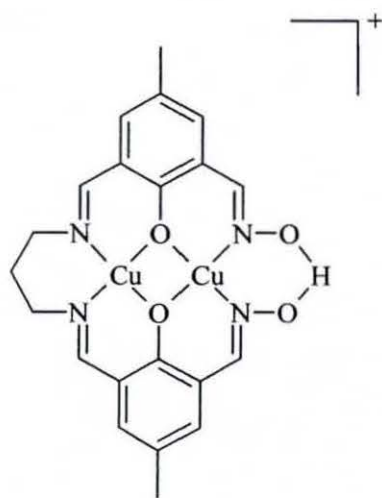


Fig. 4.2: DiCu(II) complex of a asymmetric dicompartmental Schiff-base oxime ligand prepared by Busch *et al.*¹⁴⁵

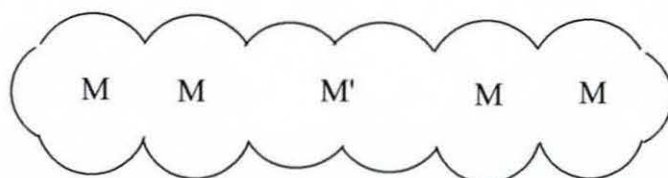


Fig. 4.3: One of the metal atom alignments discussed by Busch *et al.*¹⁴⁵

Dioximate bridges are known to act as good magnetic mediators between pairs of metal ions.¹⁴⁶⁻¹⁴⁸ Ligands possessing oximate groups are the ideal candidates for the synthesis of metal-condensed compounds,^{a,149} which are subject to many studies due to their physicochemical properties, particularly the existence of magnetic exchange interactions between metal ions in close proximity. Recent focus is placed on dinuclear and trinuclear complexes with *cis* dioximate groups as building blocks for providing those metal condensed systems. Wieghardt *et al.*¹⁵⁰ communicated the extension of a dinickel(II) complex (reported by Schröder *et al.*¹⁴²) to a tetranuclear Fe(III)Ni(II)Ni(II)Fe(III) system shown in fig. 4.4.

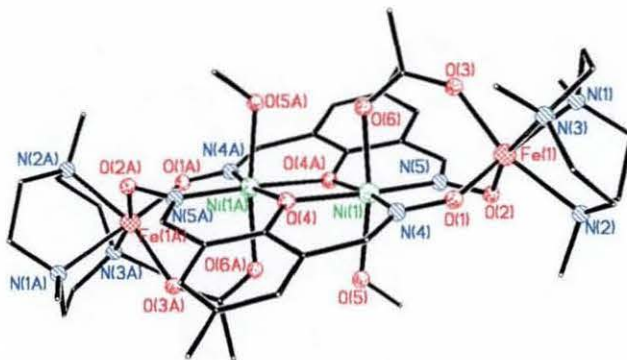


Fig. 4.4: Structure^{52,150} of the cation $[(C_9H_{21}N_3)_2Fe_2(\mu_2-OAc)_2-(C_9H_{10}N_2O_2)_2(MeOH)_2Ni_2]^{2+}$

^a Metal-condensed systems are compounds formed from complexes (building blocks) containing ligands possessing functional groups (oximate) able to coordinate to additional metals, thus forming polynuclear complexes.

Chaudhuri and co-workers have developed a route to extended heteronuclear complexes taking the dicompartmental Schiff-base oxime ligand reported by Busch *et al.*¹⁴⁵ In 1998, they communicated¹⁵¹ a trinuclear complex shown in fig. 4.5.

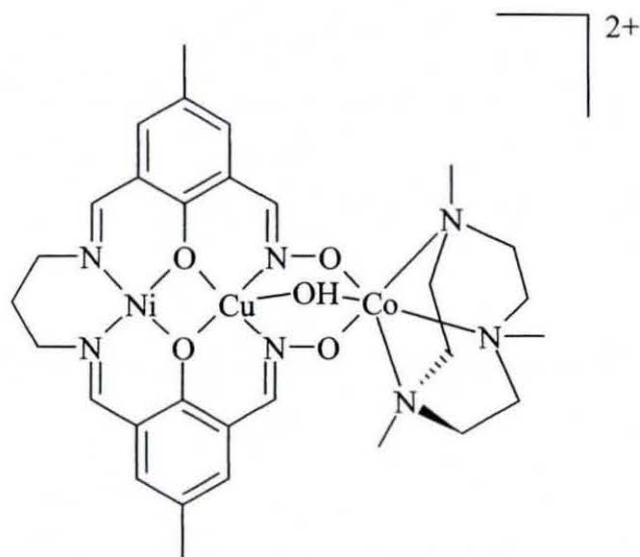


Fig. 4.5: Trinuclear species prepared by Chaudhuri and co-workers

More recently,¹⁵² they exchanged the paramagnetic Fe(III) ion with the diamagnetic Co(III) ion. The capping Fe(III) fragment (FeL) (fig. 4.6) is identical to the one reported by Wieghardt (fig. 4.4).

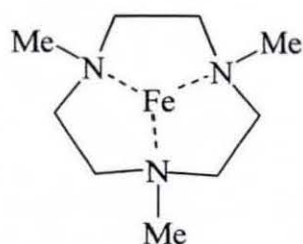


Fig. 4.6: Iron(III) fragment of 1,4,7-trimethyl-1,4,7-triazacyclononane

In this line of work Okawa *et al.*¹⁵³ extended a trinuclear Cu(II)Mn(II)Cu(II) complex to a polymeric $\{(\text{Cu(II)Mn(II)Cu(II)})\text{Mn(II)}\}_n$ system through *cis*-dioximate bridges using the ligand pictured in fig. 4.7. This oxamide/dioxime ligand is promising for providing complex-based magnetic materials. Indeed, the resulting polymeric compound (fig. 4.8) is a weak ferromagnet ($T_c = 5.5$ K) exhibiting a weak antiferromagnetic interaction between the ferrimagnetic chains.

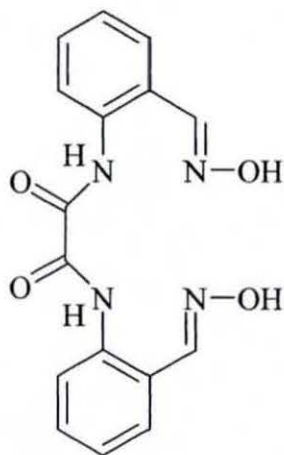


Fig. 4.7: N,N'-Bis[2-(hydroxyiminomethyl)phenyl]oxamide

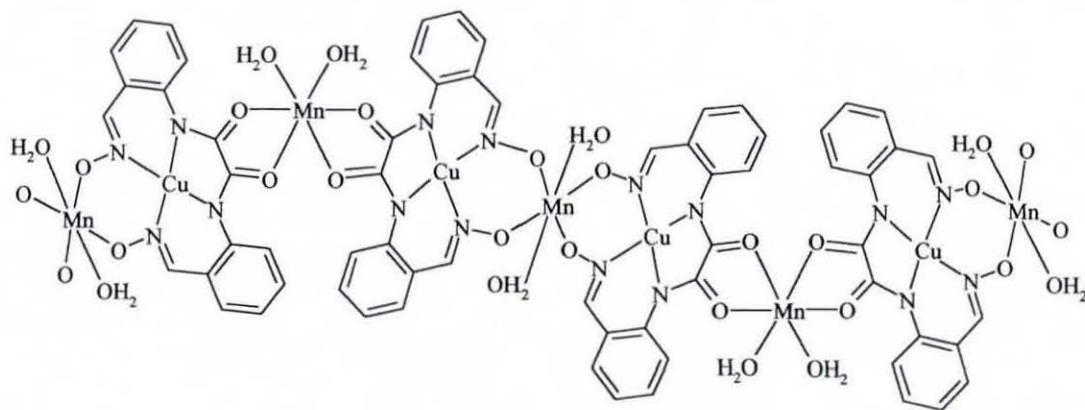


Fig. 4.8: Polymeric $\{(\text{Cu(II)Mn(II)Cu(II)})\text{Mn(II)}\}_n$ system

Another example of a dinuclear building block that shows a potential for forming metal condensed compounds has been reported by Okawa *et al.*¹⁴⁹ using 3-formylsalicylic acid oxime (fig. 4.9).

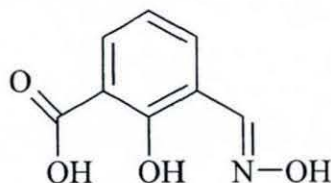


Fig. 4.9: 3-Formylsalicylic acid oxime

4.1.2. Binuclear and mononuclear complexes of 2,6-diformyl-4-*tert*-butylphenol

In the course of this work, five dinuclear species formed from 2,6-diformyl-4-*tert*-butylphenol and various salts ($\text{Ni}(\text{ClO}_4)_2$, $\text{Ni}(\text{NO}_3)_2$, $\text{Co}(\text{ClO}_4)_2$, $\text{Mn}(\text{ClO}_4)_2$ and $\text{Cu}(\text{ClO}_4)_2$) and one mononuclear species containing the same ligand and copper perchlorate have been isolated. These complexes are tabulated below in table 4.1.

Table 4.1: Complexes reported in this chapter

$[\text{Ni}_2(\text{C}_{12}\text{H}_{13}\text{O}_3)_2(\text{MeOH})_4](\text{ClO}_4)_2$ (4.1)
$[\text{Co}_2(\text{C}_{12}\text{H}_{13}\text{O}_3)_2(\text{MeOH})_4](\text{ClO}_4)_2$ (4.2)
$[\text{Mn}_2(\text{C}_{12}\text{H}_{13}\text{O}_3)_2(\text{MeOH})_4](\text{ClO}_4)_2$ (4.3)
$[\text{Cu}_2(\text{C}_{12}\text{H}_{13}\text{O}_3)_2(\text{MeOH})_2(\text{ClO}_4)_2]$ (4.4)
$[\text{Ni}_2(\text{C}_{12}\text{H}_{13}\text{O}_3)_2(\text{MeOH})_2(\text{NO}_3)_2]$ (4.5)
$[\text{Cu}(\text{C}_{12}\text{H}_{13}\text{O}_3)_2]$ (4.6)

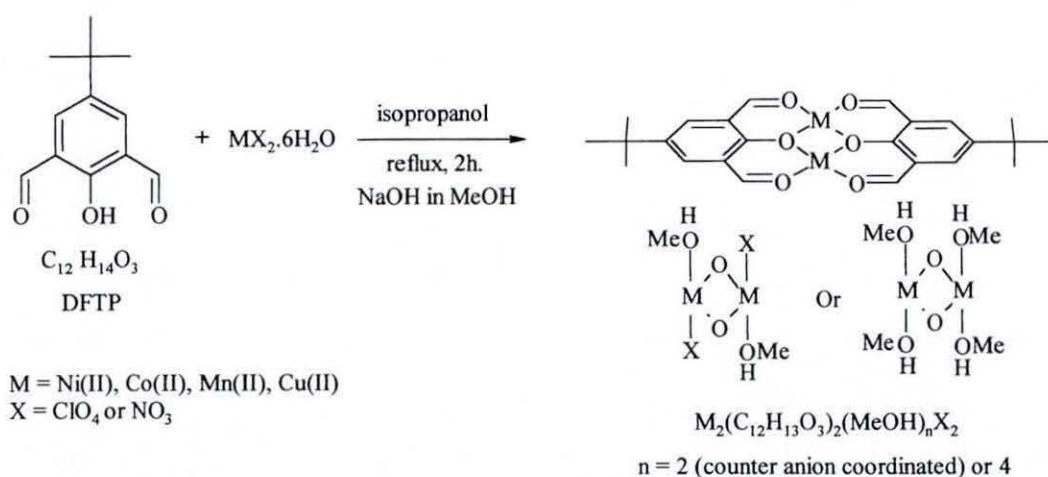
As, to the best of our knowledge, no dinuclear species containing 2,6-diformyl-4-*tert*-butylphenol have been reported, it was decided to fully characterise them and compare them to already known structures. Therefore, a report of the synthesis, structures and magnetochemistry of these complexes with Ni(II), Co(II), Mn(II) and

Cu(II) is given here. As for the mononuclear Cu(II) complex, only the synthesis and structure are described.

4.2. Dinuclear complexes of 2,6-diformyl-4-*tert*-butylphenol

4.2.1. Synthesis

Reaction scheme:



The dinuclear complexes $[\text{Ni}_2(\text{C}_{12}\text{H}_{13}\text{O}_3)_2(\text{MeOH})_4](\text{ClO}_4)_2$, $[\text{Co}_2(\text{C}_{12}\text{H}_{13}\text{O}_3)_2(\text{MeOH})_4](\text{ClO}_4)_2$, $[\text{Mn}_2(\text{C}_{12}\text{H}_{13}\text{O}_3)_2(\text{MeOH})_4](\text{ClO}_4)_2$ and $[\text{Cu}_2(\text{C}_{12}\text{H}_{13}\text{O}_3)_2(\text{MeOH})_2(\text{ClO}_4)_2]$ characterised in the course of this work were initially isolated in our attempts to synthesise polynuclear clusters using DFTP. They were all synthesised using the same procedure as described in the experimental chapter. The use of sodium hydroxide was thought to have an influence in the synthesis of high nuclearity clusters, therefore it was added to the reaction mixture. This aspect will be discussed in chapter 5. The use of sodium hydroxide has not proven to be essential in the direct synthesis of similar dinuclear complexes using 2,6-diformyl-4-methylphenol dioximes, which were reported by Schröder *et al.*¹⁴² (fig. 4.10). These workers varied the ligand:metal ratio as well as the synthetic methods depending on the metal used, in contrast to our conditions.

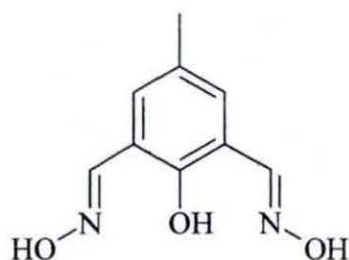


Fig. 4.10: 2,6-bis(oximato)-4-methylphenol

The complex $[\text{Ni}_2(\text{C}_{12}\text{H}_{13}\text{O}_3)_2(\text{MeOH})_2(\text{NO}_3)_2]$ was isolated as a by-product in the synthesis of the tetranuclear macrocyclic compound (**2.6**), as described in the experimental chapter.

For the dinuclear complexes $[\text{Ni}_2(\text{C}_{12}\text{H}_{13}\text{O}_3)_2(\text{MeOH})_4](\text{ClO}_4)_2$ and $[\text{Co}_2(\text{C}_{12}\text{H}_{13}\text{O}_3)_2(\text{MeOH})_4](\text{ClO}_4)_2$, the reaction afforded the same results at room temperature as the reaction under reflux, which proved that short heating time does not affect the synthesis. Both complexes were isolated with reasonable yields, 55% and 45% respectively, considering they are by-products of the reaction leading to high nuclearity clusters. However, the clusters were the minor products. This observation will be discussed in chapter 5.

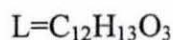
In the case of $[\text{Cu}_2(\text{C}_{12}\text{H}_{13}\text{O}_3)_2(\text{MeOH})_2(\text{ClO}_4)_2]$, as no other complex was identified, the low yield (44%) might be surprising. However the reported¹⁴² yield for the dinuclear copper complex of 2,6-diformyl-4-methylphenol dioximes is only 40%.

The lower yield observed for $[\text{Mn}_2(\text{C}_{12}\text{H}_{13}\text{O}_3)_2(\text{MeOH})_4](\text{ClO}_4)_2$ (34%) may be due to different reasons. The use of NaOH, which probably induced the partial oxidation of Mn(II) to Mn(III) and prevented the formation of the dinuclear Mn(II) species. Indeed, part of the ligand might have reacted with the Mn(III) or Mn(II) ion or both Mn(II) and Mn(III) to form a multinuclear complex containing hydroxy or methoxy bridges as is the case in reported¹⁵⁴ syntheses of polynuclear manganese clusters, in

which they use NaOMe. A small amount of brown powder was isolated and characterised by FAB. The peaks present at higher mass (m/z 1715, 1966, 2096, 2184, 2207) are very weak, which may be due to poor solubility of the cluster species. But it can also mean that there is only a small amount of cluster in the sample. The peaks shown in table 4.2 are assigned to polynuclear Mn(III) and Mn(II) species but this information is not enough to be sure about the nature of the compound(s). This result will be discussed further in chapter 5. As the amount of brown powder isolated is very small, it cannot alone account for the low yield obtained for $[\text{Mn}_2(\text{C}_{12}\text{H}_{13}\text{O}_3)_2(\text{MeOH})_4](\text{ClO}_4)_2$.

Table 4.2: Peak attributions for the Mn by-product

m/z	Rel. Intensities (%)	Fragments	Calc. Mass
1715	<5	$[\text{Mn}_7(\text{OH})_6(\text{L})_6]^{2+}$	1717
1966	<5	$[\text{Mn}_6(\text{MeO})_{12}(\text{L})_6\text{H}]^+ \cdot \text{MeOH}$	1965
2096	<5	$[\text{Mn}_7(\text{MeO})_{10}(\text{OH})_2(\text{L})_6(\text{ClO}_4)]^{2+} \cdot 2\text{H}_2\text{O}$	2094
2184	<5	$[\text{Mn}_7(\text{MeO})_{12}(\text{L})_6(\text{ClO}_4)_2]^+$	2185
2207	<5	$[\text{Mn}_7(\text{MeO})_{12}(\text{L})_6(\text{ClO}_4)_2]^+ \cdot \text{H}_2\text{O}$	2203



4.2.2. IR characterisation

The IR spectra of the binuclear complexes are quite similar due to the fact that the coordination mode of the DFTP unit is the same in each complex. The coordination of the ligand is confirmed by the shift of the bands attributed to the C=O and C=C stretches to lower wavelength. Indeed, the bonds are weakened due to the coordination of a metal ion.

The complexes $[\text{Ni}_2(\text{C}_{12}\text{H}_{13}\text{O}_3)_2(\text{MeOH})_4](\text{ClO}_4)_2$, $[\text{Co}_2(\text{C}_{12}\text{H}_{13}\text{O}_3)_2(\text{MeOH})_4](\text{ClO}_4)_2$ and $[\text{Mn}_2(\text{C}_{12}\text{H}_{13}\text{O}_3)_2(\text{MeOH})_4](\text{ClO}_4)_2$ have the same molecular formula and the

environment around the metal is identical. The bands at 1650-1654 cm^{-1} and 1623-1626 cm^{-1} (shoulders) are assigned to the C=O stretches, and the bands at 1534-1537 cm^{-1} are assigned to C=C stretches. The counter anion being ClO_4^- in each case, the two bands expected at 1088-1096 cm^{-1} and 624-626 cm^{-1} are observed. In the case of $[\text{Ni}_2(\text{C}_{12}\text{H}_{13}\text{O}_3)_2(\text{MeOH})_4](\text{ClO}_4)_2$ and $[\text{Co}_2(\text{C}_{12}\text{H}_{13}\text{O}_3)_2(\text{MeOH})_4](\text{ClO}_4)_2$ the $\nu_3(\text{ClO}_4^-)$ band is broad which is indicative of an unsymmetrical environment for the ClO_4^- anion. However for $[\text{Mn}_2(\text{C}_{12}\text{H}_{13}\text{O}_3)_2(\text{MeOH})_2](\text{ClO}_4)_2$ the band assigned to the $\nu_3(\text{ClO}_4^-)$ stretching is unusually thin, sharp and not that intense.

The complexes $[\text{Cu}_2(\text{C}_{12}\text{H}_{13}\text{O}_3)_2(\text{MeOH})_2(\text{ClO}_4)_2]$ and $[\text{Ni}_2(\text{C}_{12}\text{H}_{13}\text{O}_3)_2(\text{MeOH})_2](\text{NO}_3)_2$ are described separately from the three other complexes because their structure is slightly different in that the two counteranions are coordinated to the metal. The only difference between them is the counter anion, ClO_4^- detected at 1103 cm^{-1} and NO_3^- detected at 1384 cm^{-1} . There are some indications of the coordination of the anions. Indeed, in both complexes the C=O vibration is split, 1648 and 1628 cm^{-1} in the case of the nickel complex and 1635 and 1618 cm^{-1} in the case of the copper complex, which is indicative of a slightly different environment for the carbonyl groups. For the copper complex there is not a clear indication of the coordination of the perchlorate anions although the broadness of the band is characteristic of an unsymmetrical environment for the ClO_4^- anion. For the nickel complex, peaks at 1450 and 1322 cm^{-1} can be assigned to coordinated NO_3^- anions. Another peak at 1384 cm^{-1} that can be assigned to free nitrate anions but it is unusually small which might just indicate a slight contamination with nickel nitrate salts. However, this contamination does not appear in the elemental analysis results.

4.2.3. Structure of $[\text{Ni}_2(\text{C}_{12}\text{H}_{13}\text{O}_3)_2(\text{MeOH})_4](\text{ClO}_4)_2 \cdot 2\text{MeOH}$

Green crystals of $[\text{Ni}_2(\text{C}_{12}\text{H}_{13}\text{O}_3)_2(\text{MeOH})_4](\text{ClO}_4)_2 \cdot 2\text{MeOH}$ suitable for X-ray studies were grown by slow diffusion of diethylether into a methanol solution of the compound. The structure of $[\text{Ni}_2(\text{C}_{12}\text{H}_{13}\text{O}_3)_2(\text{MeOH})_4](\text{ClO}_4)_2 \cdot 2\text{MeOH}$ is (fig. 4.11, table 4.5) centrosymmetric with both Ni(II) centres in a tetragonal environment. The

two Ni(II) ions are linked through two phenoxo bridges. The bridge angle between the two metal ions is slightly bigger (by 2°) than that observed by Schröder *et al.*¹⁴² with 2,6-diformyl-4-methylphenol dioximes. The bridge angles for all the complexes are displayed in table 4.3. The Ni(1)---Ni(1A) distance is 3.0813(10) Å which is slightly bigger than the one for the reported structure (3.0495(8) Å).¹⁴² These two features are probably due to the hydrogen-bonds between the two oxime groups forcing the metal ions to get closer, which reduces the bridge angle. The observation concerning the bigger metal-metal distance and bridge angles in the nickel complex is valid for the structures of $[\text{Co}_2(\text{C}_{12}\text{H}_{13}\text{O}_3)_2(\text{MeOH})_4](\text{ClO}_4)_2 \cdot 2\text{MeOH}$, $[\text{Cu}_2(\text{C}_{12}\text{H}_{13}\text{O}_3)_2(\text{MeOH})_2(\text{ClO}_4)_2]$ and $[\text{Ni}_2(\text{C}_{12}\text{H}_{13}\text{O}_3)_2(\text{MeOH})_2(\text{NO}_3)_2]$ as displayed in table 4.3. Each Ni(II) is bound to two phenolic oxygen atoms and two carbonyl oxygen atoms in the equatorial plane. The coordination sphere is completed by two axially coordinated MeOH molecules. The solvent binding is stronger than that reported by Wieghardt¹⁵⁰ (2.116(3) Å) (fig. 4.12) in a similar structure, the Ni-O distance being shorter (2.055(4) to 2.082(4) Å).

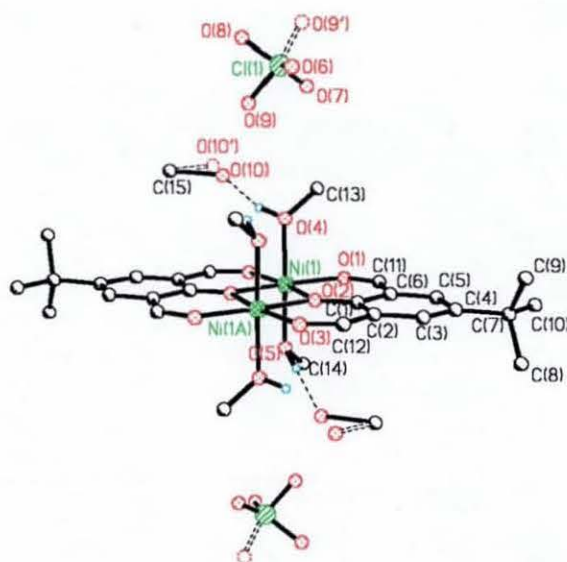


Fig. 4.11: Structure of complex (4.1).2MeOH showing the hydrogen-bonding and the disorders

Table 4.3: Phenoxo-bridge angles and metal-metal distances

Complexes	>(M-O-M) bridge angles(°)	M-M distances (Å)
[Ni ₂ (C ₁₂ H ₁₃ O ₃) ₂ (MeOH) ₄](ClO ₄) ₂ (4.1)	100.30(11)	3.0813(10)
[Ni ₂ (C ₉ H ₉ N ₂ O ₃) ₂ (H ₂ O) ₄](ClO ₄) ₂ ref. 142	98.12(6)	3.0495(8)
[Co ₂ (C ₁₂ H ₁₃ O ₃) ₂ (MeOH) ₄](ClO ₄) ₂ (4.2)	98.77(9) 98.40(11)	3.1216(6)
[Co ₂ (C ₉ H ₉ N ₂ O ₃) ₂ (H ₂ O) ₂ (MeOH) ₂]Cl ₂ ref. 142	96.9(2)	3.092(2)
[Mn ₂ (C ₁₂ H ₁₃ O ₃) ₂ (MeOH) ₄](ClO ₄) ₂ (4.3)	98.06(12) 97.63(11)	3.2482(10)
[Cu ₂ (C ₁₂ H ₁₃ O ₃) ₂ (MeOH) ₂ (ClO ₄) ₂] (4.4)	102.49(15)	3.0205(15)
[Cu ₂ (C ₉ H ₉ N ₂ O ₃) ₂ (ClO ₄) ₂] ref. 142	100.9(7) 99.2(8)	2.994(4)
[Ni ₂ (C ₁₂ H ₁₃ O ₃) ₂ (MeOH) ₂ (NO ₃) ₂] (4.5)	99.61(10)	3.0566(9)

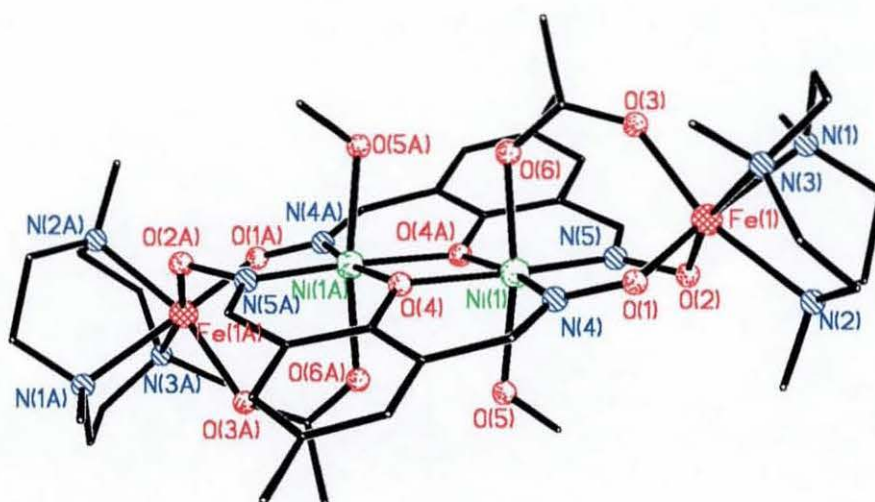


Fig. 4.12: Structure^{52,150} of the cation [(C₉H₂₁N₃)₂Fe₂(μ₂-OAc)₂-(C₉H₁₀N₂O₂)₂(MeOH)₂Ni₂]²⁺

All the X-ray data collection parameters for $[\text{Ni}_2(\text{C}_{12}\text{H}_{13}\text{O}_3)_2(\text{MeOH})_4](\text{ClO}_4)_2 \cdot 2\text{MeOH}$ are summarised in table 1 in annex 3 along with the details concerning the refinement and disorders (fig. 4.11). As shown in fig. 4.11 (dotted lines), the oxygen atom O(10) belonging to a MeOH solvate molecule is hydrogen-bonded to O(4), which belongs to the MeOH molecule coordinated to Ni(1). The symmetry equivalent of the disordered MeOH solvate molecule is involved in the same kind of hydrogen-bonding to O(5). The bond lengths and angles involved in hydrogen-bonding are shown in table 4.4.

Table 4.4: Hydrogen bonds [\AA and $^\circ$] for complex (4.1).2MeOH

D-H...A	d(D-H)	d(H...A)	d(D...A)	$\angle(\text{DHA})$
O(4)-H(4)...O(10)	0.84	1.81	2.574(12)	149.8
O(4)-H(4)...O(10')	0.84	1.95	2.733(17)	154.0
O(5)-H(5A)...O(10)*	0.86	1.93	2.795(12)	179.9

Symmetry transformations used to generate equivalent atoms: (*) -x+1, -y, -z+1

The hydrogen bonds are moderate (mostly electrostatic) according to the classification of Jeffrey,^{155,156} the distance being between 2.5 and 3.2 \AA .

The bond lengths in the equatorial plane of the metal ions are quite similar because all the donor atoms are almost identical, this is different from the structures with dioximes reported by Schröder *et al.*¹⁴² where the equatorial donor set is N_2O_2 . As observed by Schröder *et al.*,¹⁴² the two Ni(II) ions lie almost in the plane defined by the donor atoms of the two diformylphenol ligands.

Table 4.5: Selected bond lengths [Å] and angles [°] for complex **(4.1).2MeOH**

Ni(1)-O(1)	2.003(3)	Ni(1)-O(3)*	2.015(3)
Ni(1)-O(2)	2.006(3)	Ni(1)-O(5)	2.055(4)
Ni(1)-O(2)*	2.007(3)	Ni(1)-O(4)	2.082(4)
O(1)-Ni(1)-O(2)	90.45(11)	O(2)-Ni(1)-O(5)	90.42(14)
O(1)-Ni(1)-O(2)*	170.11(11)	O(3)*-Ni(1)-O(5)	88.71(17)
O(2)-Ni(1)-O(2)*	79.70(11)	O(1)-Ni(1)-O(4)	90.04(14)
O(1)-Ni(1)-O(3)*	99.58(12)	O(2)-Ni(1)-O(4)	92.16(15)
O(2)-Ni(1)-O(3)*	169.93(11)	O(2)*-Ni(1)-O(4)	89.41(14)
O(2)*-Ni(1)-O(3)*	90.28(11)	O(3)*-Ni(1)-O(4)	88.70(17)
O(1)-Ni(1)-O(5)	90.23(14)	O(5)-Ni(1)-O(4)	177.40(17)

Symmetry transformations used to generate equivalent atoms: (*) -x+1, -y, -z+1

The Ni-O(phenoxy) distances for $[\text{Ni}_2(\text{C}_{12}\text{H}_{13}\text{O}_3)_2(\text{MeOH})_2(\text{NO}_3)_2]$ and $\text{Ni}_2(\text{C}_{12}\text{H}_{13}\text{O}_3)_2(\text{MeOH})_4(\text{ClO}_4)_2$ are equal and shorter (*ca.* 2.006(3) Å) than in the Ni(II) complex described by Schröder *et al.* (2.0017(1)-2.0021(1) Å) whereas in the cases of $[\text{Co}_2(\text{C}_{12}\text{H}_{13}\text{O}_3)_2(\text{MeOH})_4(\text{ClO}_4)_2 \cdot 2\text{MeOH}]$ and $[\text{Cu}_2(\text{C}_{12}\text{H}_{13}\text{O}_3)_2(\text{MeOH})_2(\text{ClO}_4)_2]$, the equatorial bond lengths Co-O(phenoxy) (2.063(2)-2.056(19) Å) and Cu-O(phenoxy) (1.927(4)-1.946(4) Å) are similar to those observed by Schröder *et al.*¹⁴² (2.075(4)-2.055(4) Å and 1.941(10)-1.965(12) Å respectively). These features are gathered in table 4.6.

Table 4.6: M-O(phenoxo) distances in Å

Complexes	M-O(phenoxo) distances in Å
$[\text{Ni}_2(\text{C}_{12}\text{H}_{13}\text{O}_3)_2(\text{MeOH})_4](\text{ClO}_4)_2$ (4.1)	2.003(3) 2.006(3)
$[\text{Ni}_2(\text{C}_9\text{H}_9\text{N}_2\text{O}_3)_2(\text{H}_2\text{O})_4](\text{ClO}_4)_2$ ref. 142	2.017(1) 2.021(1)
$[\text{Co}_2(\text{C}_{12}\text{H}_{13}\text{O}_3)_2(\text{MeOH})_4](\text{ClO}_4)_2$ (4.2)	2.063(2) 2.056(19)
$[\text{Co}_2(\text{C}_9\text{H}_9\text{N}_2\text{O}_3)_2(\text{H}_2\text{O})_2(\text{MeOH})_2]\text{Cl}_2$ ref. 142	2.075(4) 2.055(4)
$[\text{Mn}_2(\text{C}_{12}\text{H}_{13}\text{O}_3)_2(\text{MeOH})_4](\text{ClO}_4)_2$ (4.3)	2.134(3) 2.182(3)
$[\text{Cu}_2(\text{C}_{12}\text{H}_{13}\text{O}_3)_2(\text{MeOH})_2(\text{ClO}_4)_2]$ (4.4)	1.947(4) 1.946(4)
$[\text{Cu}_2(\text{C}_9\text{H}_9\text{N}_2\text{O}_3)_2(\text{ClO}_4)_2]$ ref. 142	1.941(10) 1.965(12)
$[\text{Ni}_2(\text{C}_{12}\text{H}_{13}\text{O}_3)_2(\text{MeOH})_2(\text{NO}_3)_2]$ (4.5)	2.002(4) 2.004(4)

4.2.4. Structure of $[\text{Co}_2(\text{C}_{12}\text{H}_{13}\text{O}_3)_2(\text{MeOH})_4](\text{ClO}_4)_2 \cdot 2\text{MeOH}$

Orange crystals of $[\text{Co}_2(\text{C}_{12}\text{H}_{13}\text{O}_3)_2(\text{MeOH})_4](\text{ClO}_4)_2 \cdot 2\text{MeOH}$ suitable for X-ray studies were grown by slow diffusion of diethylether into a methanol solution of the compound. The structure of $[\text{Co}_2(\text{C}_{12}\text{H}_{13}\text{O}_3)_2(\text{MeOH})_4](\text{ClO}_4)_2 \cdot 2\text{MeOH}$ (fig. 4.13, table 4.7) is similar to that of Ni(II) discussed previously, though the cation is not centrosymmetric; the centrosymmetry is lost due to the relative orientation of the coordinated methanol. As it is shown in fig 4.13, above the plane of the molecule, the $\text{CH}_3\text{-O}$ bonds of each methanol molecule are positioned on each side of a plane passing through O(9), O(10), Co(1), Co(2), O(7) and O(8) whereas below the plane of the molecule the $\text{CH}_3\text{-O}$ bonds are positioned on the same side of the plane passing

through O(9), O(10), Co(1), Co(2), O(7) and O(8). Each Co(II) is in an approximately octahedral environment with axial distances, Co-O (MeOH) varying from 2.054(2) to 2.085(3) Å, which is shorter than those reported by Schröder *et al.*¹⁴¹ (2.102(4) and 2.133(4) Å). Both Co(II) ions are bridged the same way as the two Ni(II) ions were, through the phenolic oxygen atoms with a Co---Co distance of 3.1216(6) Å and bridge angles of 98.77(9)° and 98.40(11)° (table 4.3). The second main difference with the Ni(II) structure is the type of disorder of one of the perchlorate anions. This feature is described in annex 3. In contrast to the Ni(II) structure the solvate molecules are not disordered.

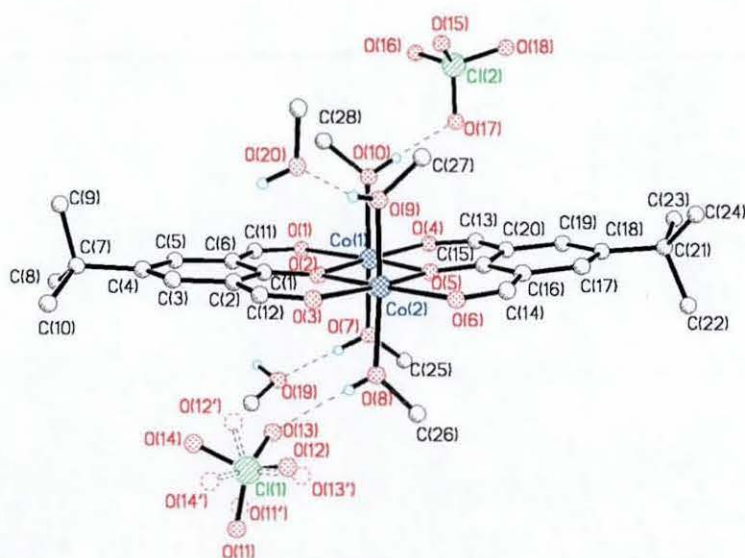


Fig. 4.13: Structure of complex (4.2).2MeOH showing the hydrogen-bonding and the disorder

Table 4.7: Selected bond lengths [Å] and angles [°] for complex (4.2).2MeOH

Co(1)-O(7)	2.054(2)	Co(1)-O(1)	2.076(2)
Co(1)-O(2)	2.063(2)	Co(2)-O(2)	2.050(2)
Co(1)-O(5)	2.0669(19)	Co(2)-O(5)	2.0565(19)
Co(1)-O(4)	2.070(2)	Co(2)-O(3)	2.059(2)
Co(1)-O(10)	2.074(2)	Co(2)-O(6)	2.065(2)

Co(2)-O(9)	2.082(3)	Co(2)-O(8)	2.085(3)
O(7)-Co(1)-O(2)	94.61(9)	O(2)-Co(2)-O(5)	81.67(8)
O(7)-Co(1)-O(5)	94.92(9)	O(2)-Co(2)-O(3)	88.66(9)
O(2)-Co(1)-O(5)	81.11(8)	O(5)-Co(2)-O(3)	170.29(8)
O(7)-Co(1)-O(4)	88.52(9)	O(2)-Co(2)-O(6)	169.63(8)
O(2)-Co(1)-O(4)	167.96(8)	O(5)-Co(2)-O(6)	88.08(8)
O(5)-Co(1)-O(4)	87.04(8)	O(3)-Co(2)-O(6)	101.61(9)
O(7)-Co(1)-O(10)	168.93(10)	O(2)-Co(2)-O(9)	93.19(10)
O(2)-Co(1)-O(10)	93.77(9)	O(5)-Co(2)-O(9)	94.43(9)
O(5)-Co(1)-O(10)	93.50(9)	O(3)-Co(2)-O(9)	85.21(11)
O(4)-Co(1)-O(10)	84.76(8)	O(6)-Co(2)-O(9)	89.11(10)
O(7)-Co(1)-O(1)	86.40(10)	O(2)-Co(2)-O(8)	92.60(10)
O(2)-Co(1)-O(1)	87.24(8)	O(5)-Co(2)-O(8)	97.06(10)
O(5)-Co(1)-O(1)	168.35(8)	O(3)-Co(2)-O(8)	84.18(11)
O(4)-Co(1)-O(1)	104.57(8)	O(6)-Co(2)-O(8)	87.12(10)
O(10)-Co(1)-O(1)	86.80(9)	O(9)-Co(2)-O(8)	167.78(11)

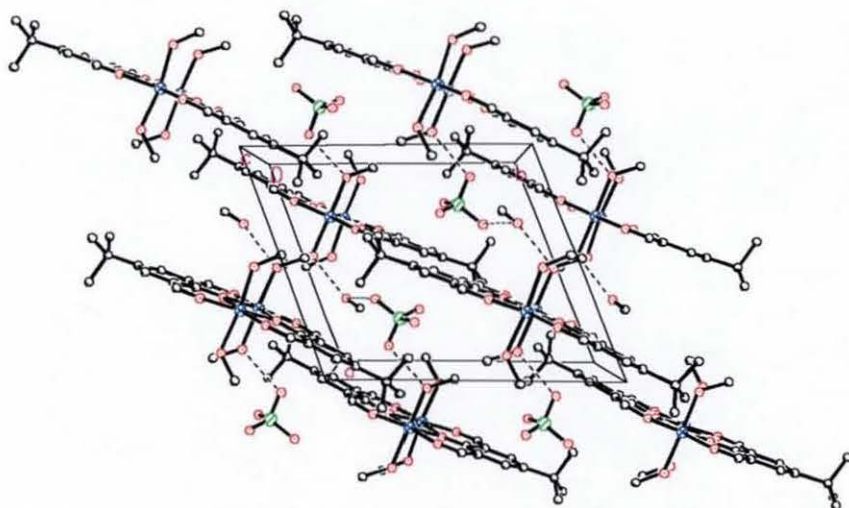
All the X-ray data collection parameters for this structure are summarised in table 2 in annex 3 along with the details concerning the refinement and disorders (fig. 4.13). As apparent (dotted lines) in fig. 4.13, both ClO_4^- counter-anions interact with two coordinated MeOH molecules through hydrogen-bonding (O(8)-H(8)----O(13) and O(10)-H(10)----O(17)). Two solvate molecules (MeOH) interact with the two remaining coordinated MeOH molecules through hydrogen-bonding (O(7)-H(7)----O(19) and O(9)-H(9)----O(20)). The bond lengths and angles involved in hydrogen-bonding are displayed in table 4.8.

Table 4.8: Hydrogen bonds [\AA and $^\circ$] for complex **(4.2).2MeOH**

D-H...A	d(D-H)	d(H...A)	d(D...A)	$\angle(\text{DHA})$
O(7)-H(7)...O(19)	0.85	1.81	2.655(4)	168.7
O(8)-H(8)...O(13)	0.72	2.05	2.760(8)	179.3
O(10)-H(10)...O(17)	0.90	1.84	2.737(4)	170.0
O(9)-H(9)...O(20)	0.85	1.87	2.701(4)	165.0
O(19)-H(19a)...O(18)*	0.88	2.03	2.911(6)	179.5
O(20)-H(H20a)...O(14)**	0.88	1.96	2.824(14)	165.5
O(20)-H(20a)...O(14')**	0.88	2.27	3.118(11)	162.9

Symmetry transformations used to generate equivalent atoms: (*) $1+x, y, z$ (**) $1-x, 1-y, z$

The hydrogen bonds are moderate (mostly electrostatic) according to the classification of Jeffrey,^{155,156} the distance being between 2.5 and 3.2 \AA .

**Fig. 4.14:** Packing diagram of **(4.2).2MeOH**

The packing diagram (fig. 4.14) shows the molecules arranged in parallel layers and linked by hydrogen-bonding *via* a MeOH solvate molecule and a ClO_4^- counter anion. The bond lengths and angles involved in hydrogen-bonding are displayed in table 4.8.

All the X-ray data collection parameters are summarised in table 3 in annex 3 along with the details concerning the refinement and disorders. Fig. 4.15 shows that the hydrogen-bonding network is the same as for $[\text{Co}_2(\text{C}_{12}\text{H}_{13}\text{O}_3)_2(\text{MeOH})_4](\text{ClO}_4)_2$ with the axial MeOH adopting the same relative orientations except for the disordered perchlorate anion, which is doubly hydrogen-bonded to the coordinated MeOH ($\text{O}(14)\cdots\text{H}(8)\text{O}(8)$ and $\text{O}(12')\cdots\text{H}(8)\text{O}(8)$). The bond lengths and angles involved in hydrogen-bonding are displayed in table 4.9. The disorder of one of the ClO_4^- counter-anions situated in the same position as in the Co(II) structure was modelled the same way (annex 3). However, there are some other slight differences between the Mn(II) and the Co(II) structures. One of the solvate MeOH molecule is disordered and was modelled as described in annex 3 and the second solvate MeOH molecule is not involved in hydrogen-bonding to any of the coordinated MeOH molecules. Consequently, in the packing diagram the individual molecules are not linked *via* a solvate molecule and a perchlorate anion but still adopt the same layer arrangement seen for the Co(II) complex.

Table 4.9: Hydrogen bonds [\AA and $^\circ$] for complex (4.3).2MeOH

D-H...A	d(D-H)	d(H...A)	d(D...A)	$\angle(\text{DHA})$
O(10)-H(10)...O(16)	0.71	2.03	2.740(5)	177.8
O(7)-H(7)...O	0.51	2.20	2.695(6)	165.0
O(8)-H(8)...O(14)	0.87	1.94	2.803(14)	179.8
O(8)-H(8)...O(12')	0.87	2.24	2.90(2)	132.5

Table 4.10: Selected bond lengths [\AA] and angles [$^\circ$] for complex (4.3).2MeOH

Mn(1)-O(4)	2.132(3)	Mn(1)-O(10)	2.172(3)
Mn(1)-O(1)	2.137(3)	Mn(1)-O(5)	2.182(3)
Mn(1)-O(7)	2.147(4)	Mn(2)-O(3)	2.120(4)
Mn(1)-O(2)	2.147(3)	Mn(2)-O(6)	2.130(3)

4.2.5. Structure of $[\text{Mn}_2(\text{C}_{12}\text{H}_{13}\text{O}_3)_2(\text{MeOH})_4](\text{ClO}_4)_2 \cdot 2\text{MeOH}$

Yellow crystals of $[\text{Mn}_2(\text{C}_{12}\text{H}_{13}\text{O}_3)_2(\text{MeOH})_4](\text{ClO}_4)_2 \cdot 2\text{MeOH}$ suitable for X-ray studies were grown by slow diffusion of diethylether into a methanol solution of the compound. The structure of $[\text{Mn}_2(\text{C}_{12}\text{H}_{13}\text{O}_3)_2(\text{MeOH})_4](\text{ClO}_4)_2$ (fig. 4.15, table 4.10) is isomorphous to the dinuclear Co(II) complex. Each Mn(II) is in an approximately octahedral environment. The equatorial bond lengths Mn-O(phenoxy) vary between 2.134(3) Å to 2.182(3) Å and are shorter than the equatorial Mn-O(carbonyl), which vary between 2.120(4) Å and 2.137(3) Å. These values are within the range of reported Mn(II)-O values.^{72,157-159} The selected bond lengths and angles are shown in table 4.10. The bridge angles between the two metal ions, 98.06(12)° and 97.63(11)° are similar to the dinuclear Co(II) complex 98.77(9)° and 98.40(11)° (table 4.3). The Mn-Mn separation is 3.248(1) Å.

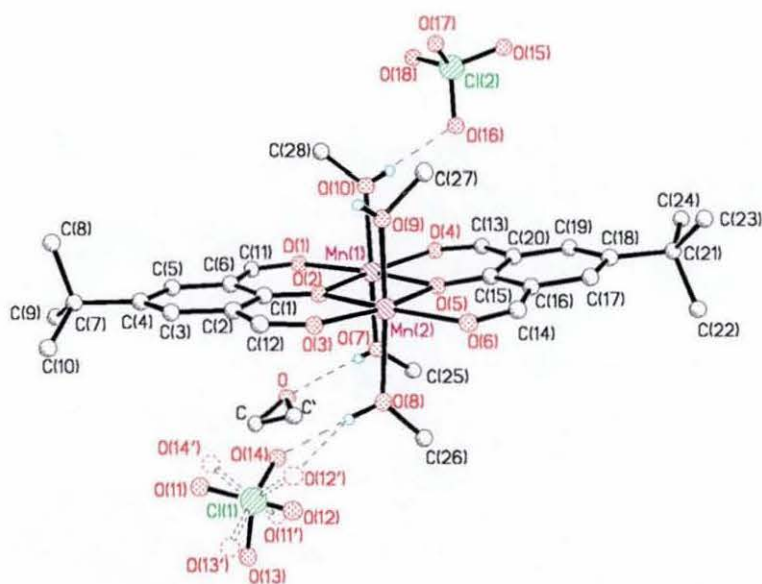


Fig. 4.15: Structure of complex (4.2).2MeOH showing the hydrogen-bonding and the disorders

Mn(2)-O(5)	2.134(3)	Mn(2)-O(9)	2.160(4)
Mn(2)-O(2)	2.155(3)	Mn(2)-O(8)	2.180(4)
O(4)-Mn(1)-O(1)	110.62(12)	O(3)-Mn(2)-O(5)	167.49(13)
O(4)-Mn(1)-O(7)	87.31(13)	O(6)-Mn(2)-O(5)	84.87(12)
O(1)-Mn(1)-O(7)	87.14(14)	O(3)-Mn(2)-O(2)	85.21(13)
O(4)-Mn(1)-O(2)	164.81(12)	O(6)-Mn(2)-O(2)	167.21(12)
O(1)-Mn(1)-O(2)	84.12(12)	O(5)-Mn(2)-O(2)	82.62(11)
O(7)-Mn(1)-O(2)	97.42(14)	O(3)-Mn(2)-O(9)	84.0(2)
O(4)-Mn(1)-O(10)	84.27(12)	O(6)-Mn(2)-O(9)	90.02(16)
O(1)-Mn(1)-O(10)	86.65(14)	O(5)-Mn(2)-O(9)	93.75(15)
O(7)-Mn(1)-O(10)	167.06(16)	O(2)-Mn(2)-O(9)	93.43(15)
O(2)-Mn(1)-O(10)	93.22(13)	O(3)-Mn(2)-O(8)	83.62(18)
O(4)-Mn(1)-O(5)	83.52(11)	O(6)-Mn(2)-O(8)	86.18(15)
O(1)-Mn(1)-O(5)	165.79(11)	O(5)-Mn(2)-O(8)	99.96(15)
O(7)-Mn(1)-O(5)	95.10(14)	O(2)-Mn(2)-O(8)	93.37(15)
O(2)-Mn(1)-O(5)	81.69(11)	O(9)-Mn(2)-O(8)	165.37(17)
O(10)-Mn(1)-O(5)	93.70(13)	Mn(1)-O(2)-Mn(2)	98.06(12)
O(3)-Mn(2)-O(6)	107.41(13)		

4.2.6. Structure of $[\text{Cu}_2(\text{C}_{12}\text{H}_{13}\text{O}_3)_2(\text{MeOH})_2(\text{ClO}_4)_2]$

Green crystals of $[\text{Cu}_2(\text{C}_{12}\text{H}_{13}\text{O}_3)_2(\text{MeOH})_2(\text{ClO}_4)_2]$ suitable for X-ray studies were grown by slow diffusion of diethylether into a methanol solution of the compound. The structure of $[\text{Cu}_2(\text{C}_{12}\text{H}_{13}\text{O}_3)_2(\text{MeOH})_2(\text{ClO}_4)_2]$ shows (fig. 4.17, table 4.13) a centrosymmetric binuclear structure with the Cu(II) centres in a tetragonal geometry. The two metal centres are bridged the same way as in the previous structures with a Cu(1)---Cu(1A) distance of 3.020(1) Å which is slightly bigger than the reported value.¹⁴² The bridge angles and the Cu-O(phenoxy) are displayed in table 4.3 and discussed in section 4.2. There is an almost identical centrosymmetrical structure reported in the literature with 2-hydroxybenzene-1,3-dicarbaldehyde¹⁶⁰ (fig. 4.16). The difference in the reported structure $[\text{Cu}_2(\text{C}_8\text{H}_5\text{O}_3)_2(\text{ClO}_4)_2]$ is that the Cu(II)

centres are in a tetragonal pyramidal environment with only one ligand (perchlorate anions) as an axial donor on opposite sides of the Cu_2O_6 plane (fig. 4.16) while in $[\text{Cu}_2(\text{C}_{12}\text{H}_{13}\text{O}_3)_2(\text{MeOH})_2(\text{ClO}_4)_2]$ the copper atoms are coordinated to an additional solvent molecule (MeOH). The bond distances around the metal are very similar (table 4.11). The phenoxo-bridge angle (101.7°)⁵² is very similar to the dicopper complex ($102.49(15)^\circ$) isolated in the course of this work. The slightly bigger value of the bridge angle in the latter case might be the result of the hydrogen-bonding interaction between the coordinated methanol molecule and the coordinated perchlorate anion.

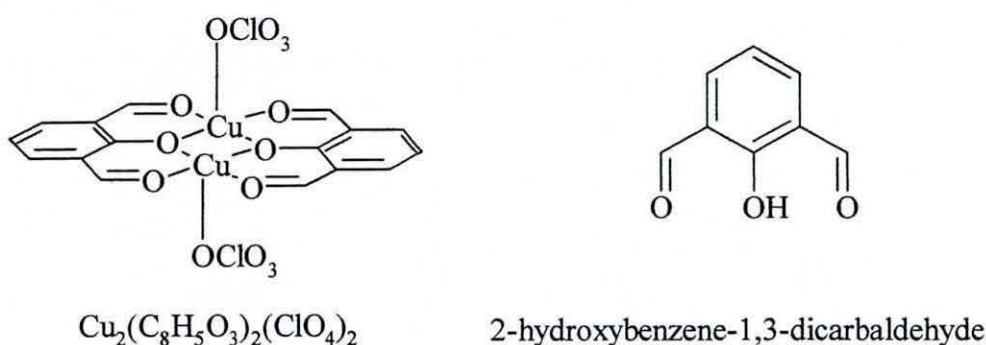


Fig. 4.16: Structural representation of $[\text{Cu}_2(\text{C}_8\text{H}_5\text{O}_3)_2(\text{ClO}_4)_2]$

Table 4.11: The bond distances around the metal for $[\text{Cu}_2(\text{C}_6\text{H}_5(\text{CHO})_2\text{O})_2(\text{ClO}_4)_2]$ and $[\text{Cu}_2(\text{C}_{12}\text{H}_{13}\text{O}_3)_2(\text{MeOH})_2(\text{ClO}_4)_2]$

Complexes	M-O (phenoxo) in Å	M-O (carbonyl) in Å	M-O (perchlorate) in Å
$[\text{Cu}_2(\text{C}_6\text{H}_5(\text{CHO})_2\text{O})_2(\text{ClO}_4)_2]$	1.951(4) 1.958(3)	1.923(4) 1.928(4)	2.050(1)
$[\text{Cu}_2(\text{C}_{12}\text{H}_{13}\text{O}_3)_2(\text{MeOH})_2(\text{ClO}_4)_2]$	1.947(4) 1.946(4)	1.926(4) 1.927(4)	2.469(4)

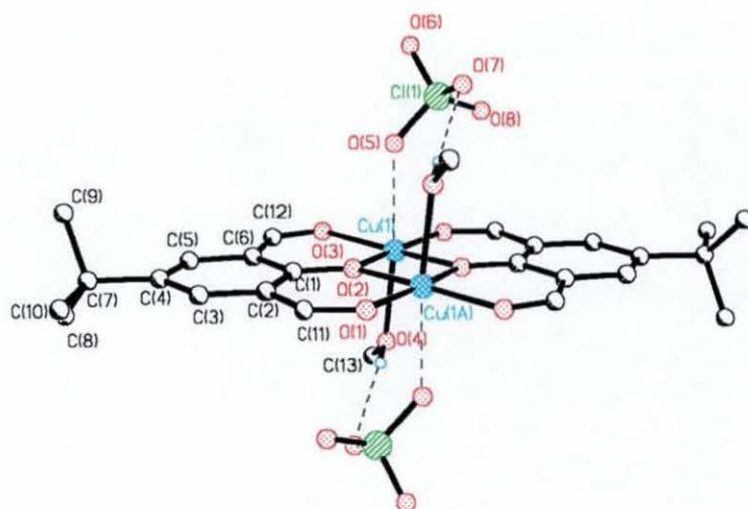


Fig. 4.17: Structure of complex **(4.4).2MeOH** showing the hydrogen-bonding

All the X-ray data collection parameters are summarised in table 4 in annex 3. The main difference with the previous structures is the coordination of the counter-anions to the metal. Indeed, as it is shown on fig. 4.17, two symmetry-related ClO_4^- anions are weakly coordinated ($2.469(4) \text{ \AA}$) to the Cu(II) atoms and hydrogen-bonded to the adjacent coordinated MeOH molecule.

Table 4.12: Hydrogen bond [\AA and $^\circ$] for complex **(4.4).2MeOH**

D-H...A	d(D-H)	d(H...A)	d(D...A)	$\angle(\text{DHA})$
O(4)-H(4)...O(7)*	0.69(6)	2.21(6)	2.890(10)	169(8)

Symmetry transformations used to generate equivalent atoms: (*) $-x+1, -y, -z$

The hydrogen bond is moderate (mostly electrostatic) according to the classification of Jeffrey,^{155,156} the distance being between 2.5 and 3.2 \AA .

In the case of the dinuclear Cu(II) complex synthesised by Schröder *et al.*,¹⁴² the Cu--O (ClO₄⁻) distance is longer (2.51(2)Å and 2.76(2)Å). However, the coordination mode of the ClO₄⁻ is different, the two copper atoms are bridged. Moreover, in our case the ClO₄⁻ anions are involved in hydrogen-bonding, which might have an influence on the strength of the interaction. The elongated axial interactions demonstrate the Jahn-Teller distortion expected for octahedrally coordinated Cu(II). The selected bond lengths and angles are displayed below in table 4.13.

There are a lot of examples in the literature of ClO₄⁻ interactions with transition metals, especially with Cu(II). The coordination can be monodentate in an axial position^{22,70,160-162} or bridging (μ_3).⁹³ Some examples are available with nickel mostly monodentate in an axial position.¹⁶³⁻¹⁶⁷ It is also possible to find a perchlorate anion bridging two nickel centres.¹³³ However, only a few structures are accounted for with cobalt,¹⁶⁸ iron^{169,170} and manganese.^{34,171,172}

Table 4.13: Selected bond lengths [Å] and angles [°] for complex (4.4).2MeOH

Cu(1)-O(1)*	1.926(4)	Cu(1)-O(4)	2.243(6)
Cu(1)-O(2)	1.947(4)	Cu(1)-O(5)	2.469(4)
Cu(1)-O(2)*	1.946(4)	Cu(1)-Cu(1)*	3.0205(15)
Cu(1)-O(3)	1.927(4)		
O(1)*-Cu(1)-O(2)	170.09(15)	O(2)*-Cu(1)-O(4)	95.7(2)
O(1)*-Cu(1)-O(2)*	93.19(16)	O(3)-Cu(1)-O(4)	89.5(2)
O(2)-Cu(1)-O(2)*	77.51(15)	O(1)*-Cu(1)-O(5)	88.37(16)
O(1)*-Cu(1)-O(3)	95.89(16)	O(2)-Cu(1)-O(5)	88.46(15)
O(2)-Cu(1)-O(3)	93.08(15)	O(2)*-Cu(1)-O(5)	91.40(15)
O(2)*-Cu(1)-O(3)	169.43(16)	O(3)-Cu(1)-O(5)	83.47(16)
O(1)*-Cu(1)-O(4)	91.2(2)	O(4)-Cu(1)-O(5)	172.90(19)
O(2)-Cu(1)-O(4)	93.1(2)		

Symmetry transformations used to generate equivalent atoms: (*) -x+1, -y, -z

4.2.7. Structure of $[\text{Ni}_2(\text{C}_{12}\text{H}_{13}\text{O}_3)_2(\text{MeOH})_2(\text{NO}_3)_2]$

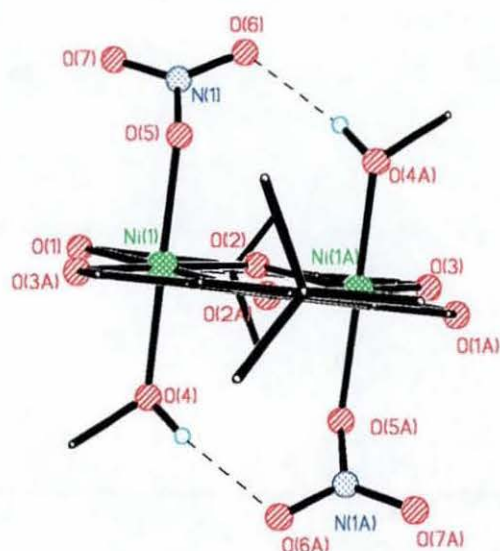
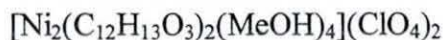


Fig. 4.18: Structure of complex (4.5) showing the hydrogen-bonding

The structure of $[\text{Ni}_2(\text{C}_{12}\text{H}_{13}\text{O}_3)_2(\text{MeOH})_2(\text{NO}_3)_2]$ (fig. 4.18, table 4.17) is isomorphous with the dicopper structure. The coordination sphere of the nickel centres is quite similar to the related dinuclear Ni(II) species discussed in section 4.2.1. except for the axial coordination of nitrate ions. The structural features concerning the two nickel complexes are gathered in table 4.14. and table 4.15.

Table 4.14: Bond distances around the metal for $[\text{Ni}_2(\text{C}_{12}\text{H}_{13}\text{O}_3)_2(\text{MeOH})_2(\text{NO}_3)_2]$ and $[\text{Ni}_2(\text{C}_{12}\text{H}_{13}\text{O}_3)_2(\text{MeOH})_4](\text{ClO}_4)_2$

Complexes	M-O(phenoxo)	M-O(carbonyl)	M-O(MeOH)
	in Å	in Å	in Å
$[\text{Ni}_2(\text{C}_{12}\text{H}_{13}\text{O}_3)_2(\text{MeOH})_4](\text{ClO}_4)_2$	2.006(3)	2.003(3)	2.055(4)
	2.007(3)	2.015(3)	2.082(4)
$[\text{Ni}_2(\text{C}_{12}\text{H}_{13}\text{O}_3)_2(\text{MeOH})_2(\text{NO}_3)_2]$	2.001(2)	2.004(3)	2.052(3)
	2.002(2)	2.018(2)	

Table 4.15: Metal-metal distance and M-O-M and angles for

Complexes	>(M-O-M) bridge angles in °	M-M distance in Å
$[\text{Ni}_2(\text{C}_{12}\text{H}_{13}\text{O}_3)_2(\text{MeOH})_4](\text{ClO}_4)_2$	100.30(11)	3.0813(10)
$[\text{Ni}_2(\text{C}_{12}\text{H}_{13}\text{O}_3)_2(\text{MeOH})_2(\text{NO}_3)_2]$	99.61(10)	3.0566(9)

The phenoxo bridge angle and the distance between the two metal ions is slightly smaller in complex $[\text{Ni}_2(\text{C}_{12}\text{H}_{13}\text{O}_3)_2(\text{MeOH})_2(\text{NO}_3)_2]$. This effect is most likely a consequence of the intra-molecular hydrogen-bonding (table 4.16) between the nitrate anions and the coordinated MeOH molecules.

Table 4.16: Hydrogen bond [Å and °] for complex (4.5)

D-H...A	d(D-H)	d(H...A)	d(D...A)	<(DHA)
O(4)-H(4)...O(6)*	0.84	2.01	2.851(6)	172.6

Symmetry transformations used to generate equivalent atoms: (*) -x, -y, -z+2

NO_3^- anions are known to be better coordinating ligands than ClO_4^- . The Ni-O(NO_3^-) distance, 2.072(3) Å is similar to that described for coordinated MeOH molecules in complex 4.1. The selected bond lengths and angles are shown below in table 4.17. All the X-ray data collection parameters are summarised in table 5 in annex 3.

Table 4.17: Selected bond lengths [Å] and angles [°] for complex (4.5)

Ni(1)-O(2)	2.001(2)	Ni(1)-O(1)	2.004(3)
Ni(1)-O(2)*	2.002(2)	Ni(1)-O(3)*	2.018(2)

Ni(1)-O(4)	2.052(3)	Ni(1)-O(5)	2.079(3)
O(2)-Ni(1)-O(2)*	80.39(10)	O(1)-Ni(1)-O(4)	87.43(12)
O(2)-Ni(1)-O(1)	90.44(10)	O(3)*-Ni(1)-O(4)	91.98(12)
O(2)*-Ni(1)-O(1)	170.34(10)	O(2)-Ni(1)-O(5)	91.64(11)
O(2)-Ni(1)-O(3)*	170.46(10)	O(2)*-Ni(1)-O(5)	88.95(11)
O(2)*-Ni(1)-O(3)*	90.17(10)	O(1)-Ni(1)-O(5)	94.37(12)
O(1)-Ni(1)-O(3)*	99.06(10)	O(3)*-Ni(1)-O(5)	86.80(11)
O(2)-Ni(1)-O(4)	89.30(11)	O(4)-Ni(1)-O(5)	177.96(12)
O(2)*-Ni(1)-O(4)	89.42(11)		

Symmetry transformations used to generate equivalent atoms: (*) -x, -y, -z+2

4.2.8. Magnetic behaviour

Variable-temperature magnetic measurements were carried out by Dr C.J. Harding at the Open University, Milton Keynes as described in the experimental section.

All the complexes were modelled using the general isotropic exchange Hamiltonian $\hat{H} = -2JS_1 \bullet S_2$ with $S_1 = S_2$ and $g_1 = g_2$. The solution to the Van Vleck equation using this Hamiltonian yields the magnetic susceptibility equations¹⁷³ in table 4.18 for the corresponding metal ions. In the case of complexes $[\text{Ni}_2(\text{C}_{12}\text{H}_{13}\text{O}_3)_2(\text{MeOH})_4](\text{ClO}_4)_2$, $[\text{Ni}_2(\text{C}_{12}\text{H}_{13}\text{O}_3)_2(\text{MeOH})_2(\text{ClO}_4)_2]$ and $[\text{Cu}_2(\text{C}_{12}\text{H}_{13}\text{O}_3)_2(\text{MeOH})_2(\text{ClO}_4)_2]$ the model was corrected for Temperature Independent Paramagnetism (TIP), which arises from the second order Zeeman effect. All the complexes exhibit antiferromagnetic coupling ($J < 0$), which can be fitted with a single J value. For all the complexes except the dinuclear Cu(II) complex, the susceptibility cusp lies below the minimum experimental temperature.

Table 4.18: Magnetic susceptibilities for the homodinuclear species

Metal ions	Equation for χ
DiNi(II) (S1=S2=1)	$\chi = C(2e^{2x} + 10e^{6x} / 1 + 3e^{2x} + 5e^{6x})$
DiCo(II) (S1=S2=3/2)	$\chi = C(2e^{2x} + 10e^{6x} + 28e^{12x} / 1 + 3e^{2x} + 5e^{6x} + 7e^{12x})$
DiMn(II) (S1=S2=5/2)	$\chi = C(2e^{2x} + 10e^{6x} + 28e^{12x} + 60e^{20x} + 110e^{30x} / 1 + 3e^{2x} + 5e^{6x} + 7e^{12x} + 9e^{20x} + 11e^{30x})$
DiCu(II) (S1=S2=1/2)	$\chi = C(2e^{2x} / 1 + 3e^{2x})$

$$C = Ng^2\mu_B^2/kT \text{ and } x = J/kT$$

Table 4.19: Magnetic data for the dinuclear complexes

Complexes	g	J in cm^{-1}	TIP correction
$[\text{Ni}_2(\text{C}_{12}\text{H}_{13}\text{O}_3)_2(\text{MeOH})_4](\text{ClO}_4)_2$	2.24	-10.29(0.05)	228.42(8.97)
$[\text{Ni}_2(\text{C}_{12}\text{H}_{13}\text{O}_3)_2(\text{MeOH})_2(\text{NO}_3)_2]$	2.21	-12.58(0.05)	226.83(10.13)
$[\text{Co}_2(\text{C}_{12}\text{H}_{13}\text{O}_3)_2(\text{MeOH})_4](\text{ClO}_4)_2$	2.68	-5.33(0.03)	0
$[\text{Mn}_2(\text{C}_{12}\text{H}_{13}\text{O}_3)_2(\text{MeOH})_4](\text{ClO}_4)_2$	2.02	-2.25(0.00)	0
$[\text{Cu}_2(\text{C}_{12}\text{H}_{13}\text{O}_3)_2(\text{MeOH})_2(\text{ClO}_4)_2]$	2.03	-315.34(4.51)	60

- $[\text{Ni}_2(\text{C}_{12}\text{H}_{13}\text{O}_3)_2(\text{MeOH})_4](\text{ClO}_4)_2$ (**4.1**)

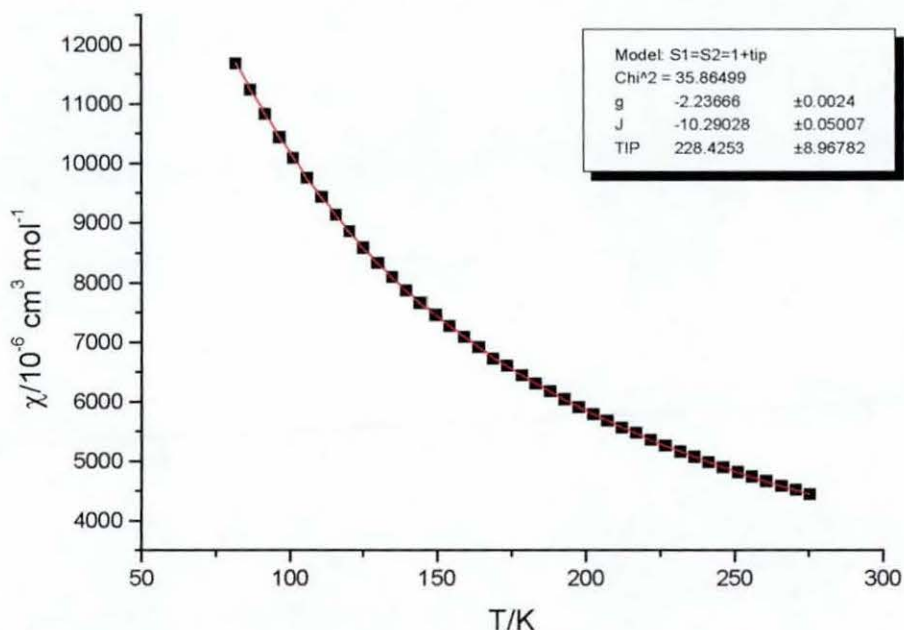


Fig. 4.19: Experimental (■) and calculated (—) magnetic susceptibility for (**4.1**)

The molecular magnetic susceptibility of $[\text{Ni}_2(\text{C}_{12}\text{H}_{13}\text{O}_3)_2(\text{MeOH})_4](\text{ClO}_4)_2$ displayed in fig. 4.19, was measured over the temperature range 81.7-275.4 K. The effective magnetic moment μ_{eff} , increases from 2.76 to 3.13 B.M with the increasing temperature. These values are in accordance with Ni(II) being in a high-spin state. The magnetic susceptibility is steadily increasing while the temperature is decreasing. The value of g fitting the measured magnetic susceptibility is consistent with the fact that in the case of Ni(II) the spin-orbit coupling is important enough to cause the g value to deviate measurably from the free ion value. The antiferromagnetic coupling is smaller than in the dinuclear Ni(II) complex described by Schröder *et al.*¹⁴² ($J = -17 \text{ cm}^{-1}$).

- $[\text{Co}_2(\text{C}_{12}\text{H}_{13}\text{O}_3)_2(\text{MeOH})_4](\text{ClO}_4)_2$ (**4.2**)

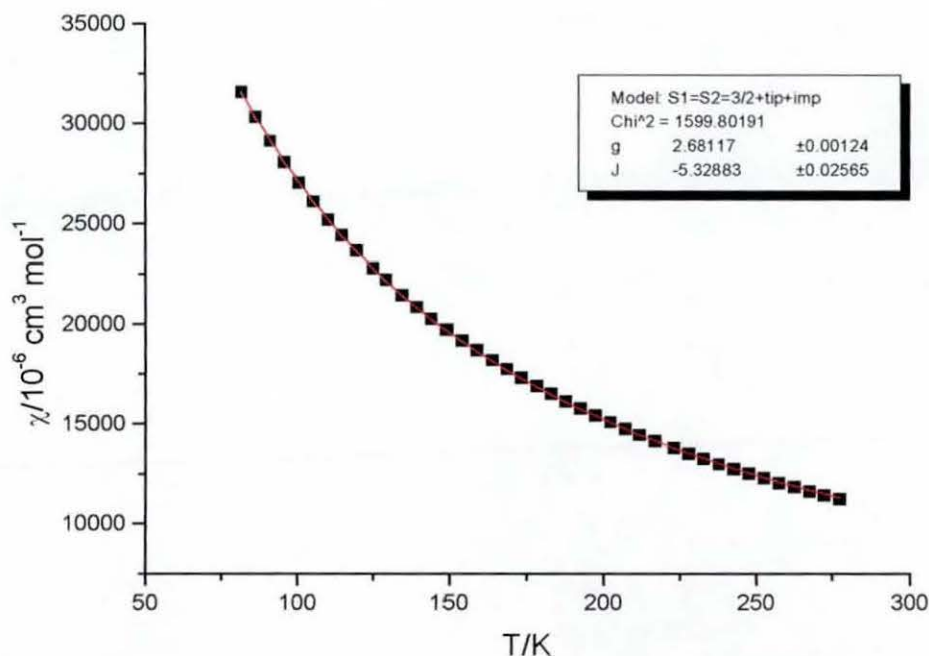


Fig. 4.20: Experimental (■) and calculated (—) magnetic susceptibility for (**4.2**)

The molecular magnetic susceptibility of $[\text{Co}_2(\text{C}_{12}\text{H}_{13}\text{O}_3)_2(\text{MeOH})_4](\text{ClO}_4)_2$ displayed in fig. 4.20, was measured over the temperature range 81.5-277.2 K. The effective magnetic moment μ_{eff} , increases from 4.53 to 4.98 B.M with the increasing temperature. These values are expected for high-spin Co(II) in an octahedral environment. Indeed, in a high-spin configuration one of the unpaired electron is in t_{2g} , which renders a 4T ground state. Therefore, Co(II) exhibits an important orbital contribution on the moment, raising it from the spin-only value to a value that lies typically in the range 4.5-5.1 μ_B .^{129,130} The antiferromagnetic coupling is smaller than in the dinuclear Co(II) complex described by Schröder *et al.*¹⁴² ($J = -6.9 \text{ cm}^{-1}$).

• $[\text{Mn}_2(\text{C}_{12}\text{H}_{13}\text{O}_3)_2(\text{MeOH})_4](\text{ClO}_4)_2$ (4.3)

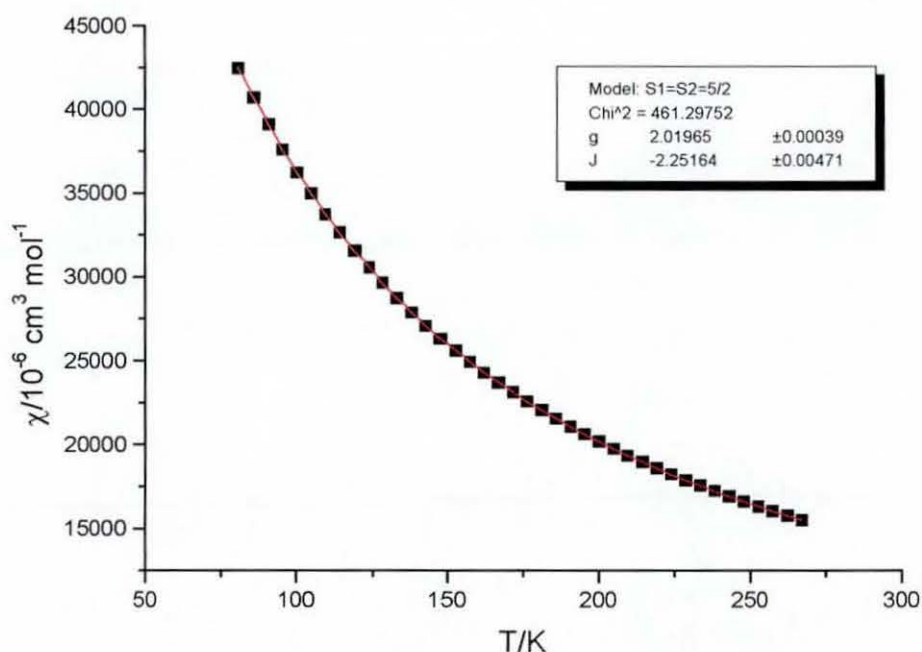


Fig. 4.21: Experimental (■) and calculated (—) magnetic susceptibility for (4.3)

The molecular magnetic susceptibility of $[\text{Mn}_2(\text{C}_{12}\text{H}_{13}\text{O}_3)_2(\text{MeOH})_4](\text{ClO}_4)_2$ displayed in fig. 4.21, was measured over the temperature range 80.8-272.2 K. The effective magnetic moment μ_{eff} , increases from 5.23 to 5.76 B.M with the increasing temperature. The model was calculated for $g = 2.01$, $J = -2.25 \text{ cm}^{-1}$ with each manganese atom having a spin value of $S = 5/2$. The g values for Mn(II) are generally isotropic around 2.0.¹³⁰ Mn(II) is known to exhibit only weak antiferromagnetic coupling.

• $[\text{Cu}_2(\text{C}_{12}\text{H}_{13}\text{O}_3)_2(\text{MeOH})_2(\text{ClO}_4)_2]$ (4.4)

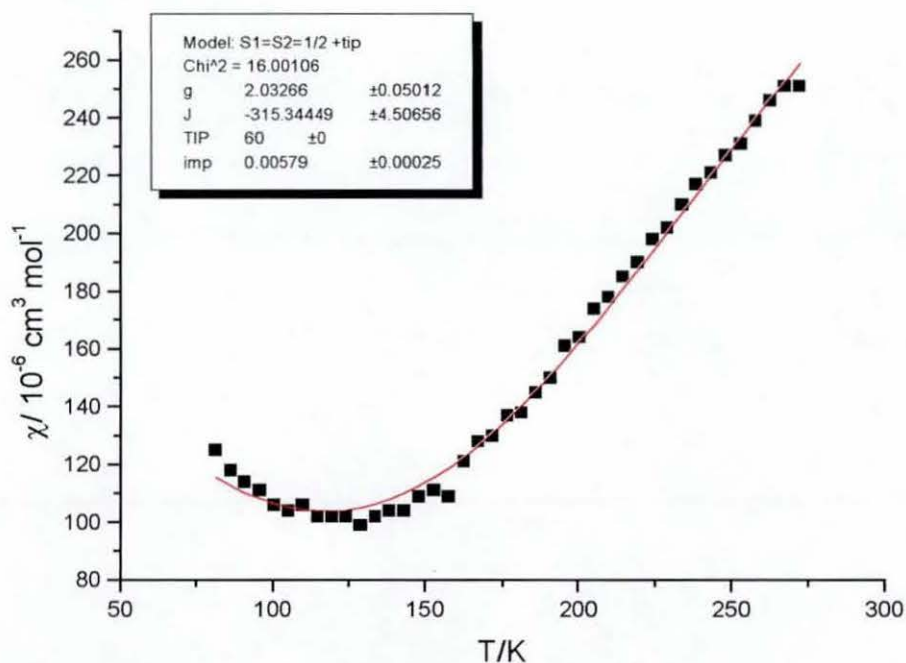


Fig. 4.22: Experimental (■) and calculated (—) magnetic susceptibility for (4.4)

The molecular magnetic susceptibility of $[\text{Cu}_2(\text{C}_{12}\text{H}_{13}\text{O}_3)_2(\text{MeOH})_2(\text{ClO}_4)_2]$ displayed in fig. 4.22, was measured over the temperature range 81.1-272.2 K. In this case the fit is not perfect due to the fact that the measurements were performed on a small sample (the spots on the graph obtained from the data do not form a smooth line as for the other complexes) which is more prone to fluctuations. The effective magnetic moment μ_{eff} , increases from 0.30 to 0.77 B.M with the decreasing temperature. Cu(II) has one unpaired electron whatever the geometry. We can also notice that there is a small contribution to the susceptibility at lower temperature, reflecting the presence of a small amount of paramagnetic impurity. The magnitude of the effective moment is quite small and the susceptibility is rising with the temperature, which implies that the exchange coupling (antiferromagnetic) in the binuclear complex is relatively strong. The susceptibility cusp lies well beyond the maximum experimental temperature. However, it is not as strong as that observed in the dinuclear Cu(II) described by Schröder *et al.*¹⁴² (between -415 and -452 cm^{-1}). The

perturbation caused by spin-orbit coupling with excited ligand-field states and a second order Zeeman contribution modify the spin-only value of g to lie typically in the range of 1.9-2.0.^{129,130} In this model, the TIP was fixed because the value obtained for g was too low if this parameter was left to vary freely.

- $[\text{Ni}_2(\text{C}_{12}\text{H}_{13}\text{O}_3)_2(\text{MeOH})_2](\text{NO}_3)_2$ (4.5)

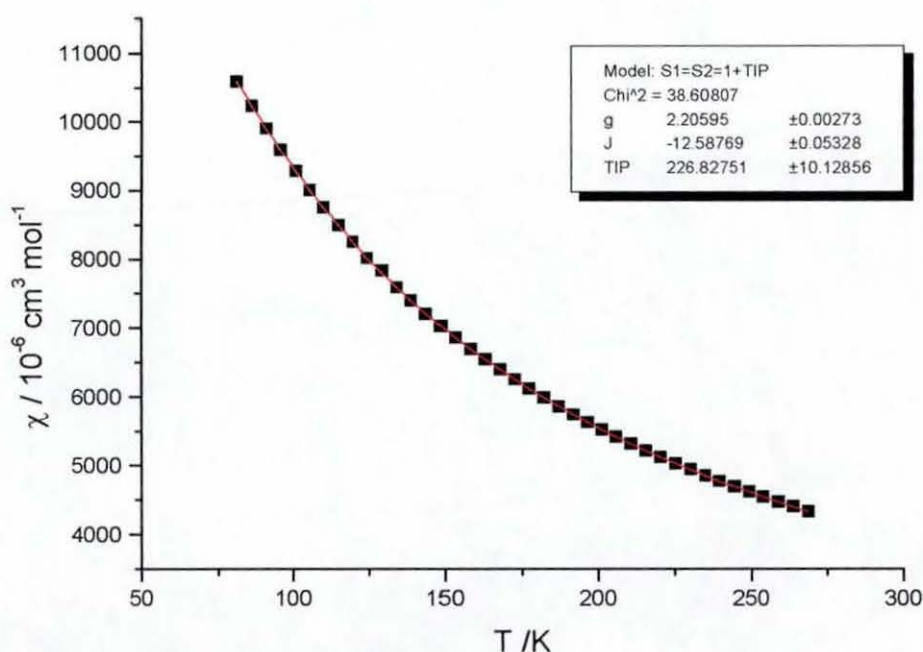


Fig. 4.23: Experimental (■) and calculated (—) magnetic susceptibility for (4.5)

This complex is similar to the dinuclear Ni(II) complex described before. The molecular magnetic susceptibility of $[\text{Ni}_2(\text{C}_{12}\text{H}_{13}\text{O}_3)_2(\text{MeOH})_2(\text{NO}_3)_2]$ displayed in fig. 4.23, was measured over the temperature range 81.3-268.9 K. The effective magnetic moment μ_{eff} increases from 2.73 to 3.18 B.M with the increasing temperature. The dinuclear complex shows antiferromagnetic coupling ($J < 0$) similar to the dinickel complex $[\text{Ni}_2(\text{C}_{12}\text{H}_{13}\text{O}_3)_2(\text{MeOH})_4](\text{ClO}_4)_2$.

- **Relation between the dinuclear complexes**

According to Kahn,¹⁷⁴ in a series of d^n dimers with a similar bridging structure, the value of n^2J should be constant (n is the number of unpaired electrons and J the exchange coupling constant). In our case, it is not exactly true because the environment of the metal ion is not identical in all synthesised complexes. The value of n^2J for complexes, $[\text{Ni}_2(\text{C}_{12}\text{H}_{13}\text{O}_3)_2(\text{MeOH})_4](\text{ClO}_4)_2$ (**4.1**), $[\text{Co}_2(\text{C}_{12}\text{H}_{13}\text{O}_3)_2(\text{MeOH})_4](\text{ClO}_4)_2$ (**4.2**), $[\text{Mn}_2(\text{C}_{12}\text{H}_{13}\text{O}_3)_2(\text{MeOH})_4](\text{ClO}_4)_2$ (**4.3**) and $[\text{Ni}_2(\text{C}_{12}\text{H}_{13}\text{O}_3)_2(\text{MeOH})_2(\text{NO}_3)_2]$ (**4.5**) is approximately the same and seems to follow that trend within the error range whereas for the dinuclear copper(II) complex this is far from being the case. There is no apparent reason why the dicopper complex, which is isomorphous to the dinuclear nickel complex (**4.5**), should be different. However, for the copper complex, the antiferromagnetic coupling between the two metal centres is much stronger than that observed for any other dinuclear complexes discussed in this chapter, yielding a n^2J value that is more than four times bigger than that of the other complexes. The values are displayed below in table 4.20.

Table 4.20: n^2J for the dinuclear complexes

Complexes	n (number of unpaired electrons)	n^2J
$[\text{Ni}_2(\text{C}_{12}\text{H}_{13}\text{O}_3)_2(\text{MeOH})_4](\text{ClO}_4)_2$	2	-41.16
$[\text{Co}_2(\text{C}_{12}\text{H}_{13}\text{O}_3)_2(\text{MeOH})_4](\text{ClO}_4)_2$	3	-47.96
$[\text{Mn}_2(\text{C}_{12}\text{H}_{13}\text{O}_3)_2(\text{MeOH})_4](\text{ClO}_4)_2$	5	-56.29
$[\text{Ni}_2(\text{C}_{12}\text{H}_{13}\text{O}_3)_2(\text{MeOH})_2(\text{NO}_3)_2]$	2	-50.34
$[\text{Cu}_2(\text{C}_{12}\text{H}_{13}\text{O}_3)_2(\text{MeOH})_2(\text{ClO}_4)_2]$	1	-315.34

4.3. Mononuclear complex of 2,6-diformyl-4-*tert*-butylphenol

4.3.1. Synthesis and IR characterisation of $\text{Cu}(\text{C}_{12}\text{H}_{13}\text{O}_3)_2$

This complex was synthesised in reasonable yield (54%) using a different procedure to the one used for the dinuclear complexes described in section 4.2. The reaction was carried out at room temperature in a different solvent (CH_3CN) and NaOH was added as an aqueous solution. However, the metal:ligand ratio was identical to the previous experiments. This demonstrates that it is possible to synthesise dinuclear as well as mononuclear species by changing the reaction conditions.

In this complex the coordination of the DFTP ligand is different from the dinuclear complexes described previously. This is reflected by slight changes in the IR spectrum. The bands at 1671 cm^{-1} and 1625 cm^{-1} are assigned to the C=O stretches, and the bands at 1527 cm^{-1} are assigned to C=C stretches but in this case, the carbonyl stretch at 1625 cm^{-1} is well separated from the stretch at 1671 cm^{-1} , which is indicative of a different coordination mode (see crystal structure in section 4.3.2). There is no trace of ClO_4^- anion stretches.

4.3.2. Structure of $\text{Cu}(\text{C}_{12}\text{H}_{13}\text{O}_3)_2$

Pale green crystals suitable for X-ray studies were obtained by slow diffusion of diethylether into a dichloromethane/acetonitrile solution of the complex. The structure of $\text{Cu}(\text{C}_{12}\text{H}_{13}\text{O}_3)_2$ shows (fig. 4.24, table 4.21) a centrosymmetric dinuclear structure with the Cu(II) centre in a square planar environment. The Cu-O distances ($1.900(1)$ - $1.960(2)$ Å) are similar to the dinuclear Cu(II) complex discussed in section 4.2. The torsion angles C(5)-C(6)-C(11)-O(1) and C(1)-C(2)-C(12)-O(3) are similar ($172.02(19)^\circ$ - $172.77(19)^\circ$) but opposite signs. Indeed, the non-coordinated carbonyl oxygen atom is pointing in the opposite direction. The selected bond lengths and angles are displayed in table 4.21. All the X-ray data collection parameters are summarised in table 6 in annex 3.

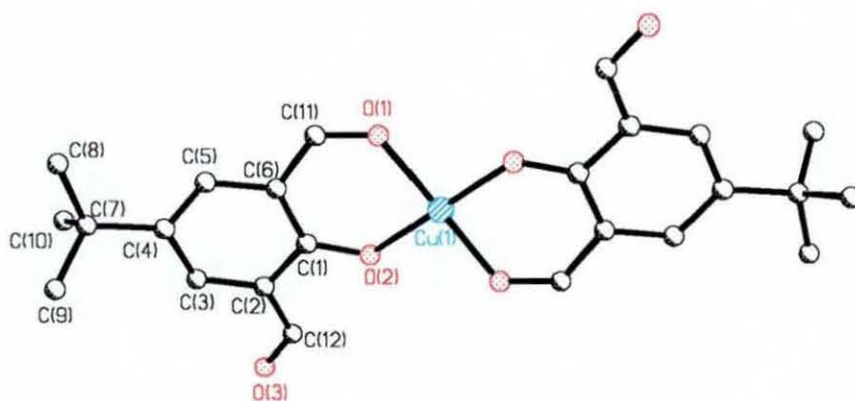


Fig. 4.24: Structure of complex (4.6)

Table 4.21: Selected bond lengths and angles for complex (4.6)

Cu(1)-O(2)	1.9007(14)	Cu(1)-O(3)*	2.5627(14)
Cu(1)-O(1)	1.9601(15)	Cu(1)-O(3)**	2.5627(14)
O(2)-Cu(1)-O(2)***	180.00(11)	O(2)-Cu(1)-O(3)*	87.81(5)
O(2)-Cu(1)-O(1)***	87.01(6)	O(1)***-Cu(1)-O(3)***	88.29(5)
O(2)-Cu(1)-O(1)	92.99(6)	O(1)-Cu(1)-O(3)*	91.71(5)
O(2)***-Cu(1)-O(1)	87.01(6)	O(2)-Cu(1)-O(3)**	92.19(5)
O(1)***-Cu(1)-O(1)	180.00(8)	O(3)*-Cu(1)-O(3)**	180.00(9)

Symmetry transformations used to generate equivalent atoms: (*) $x, -y+1/2, z+1/2$ (**) $-x+1, y-1/2, -z-1/2$ (***) $-x+1, -y, -z$

The Cu(II) centre is axially weakly interacting with two different symmetry related molecules through the uncoordinated carbonyl oxygen atom. Each mononuclear complex is coordinated to four different molecules as shown in the packing diagram in fig. 4.25.

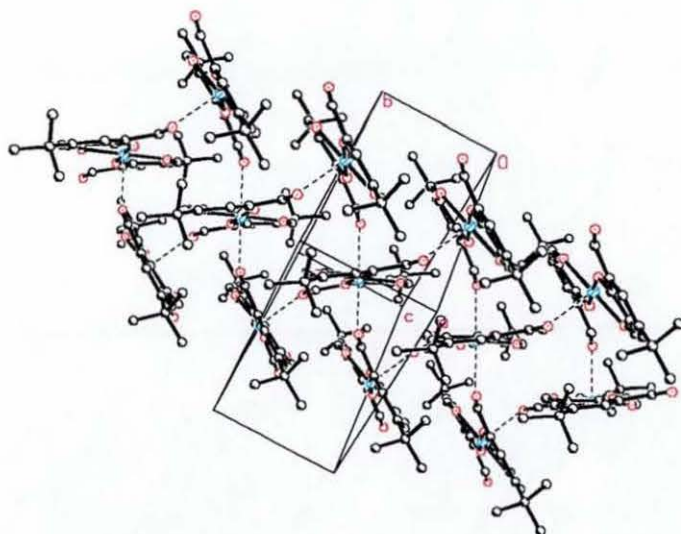


Fig. 4.25: Packing diagram of complex (4.6)

4.4. Conclusion

During this study, it has been shown that homodinuclear ($[\text{Ni}_2(\text{C}_{12}\text{H}_{13}\text{O}_3)_2(\text{MeOH})_4](\text{ClO}_4)_2$, $[\text{Co}_2(\text{C}_{12}\text{H}_{13}\text{O}_3)_2(\text{MeOH})_4](\text{ClO}_4)_2$, $[\text{Mn}_2(\text{C}_{12}\text{H}_{13}\text{O}_3)_2(\text{MeOH})_4](\text{ClO}_4)_2$, $[\text{Cu}_2(\text{C}_{12}\text{H}_{13}\text{O}_3)_2(\text{MeOH})_2](\text{ClO}_4)_2$ and $[\text{Ni}_2(\text{C}_{12}\text{H}_{13}\text{O}_3)_2(\text{MeOH})_2(\text{NO}_3)_2]$) as well as mononuclear ($[\text{Cu}(\text{C}_{12}\text{H}_{13}\text{O}_3)_2]$) complexes containing the deprotonated ligand DFTP can be synthesised. In all the dinuclear complexes, the metal centres (Ni(II), Co(II), Mn(II) and Cu(II)) are hexacoordinate and bridged through two phenoxo bridges. For two of those complexes, ($[\text{Cu}_2(\text{C}_{12}\text{H}_{13}\text{O}_3)_2(\text{MeOH})_2](\text{ClO}_4)_2$ and $[\text{Ni}_2(\text{C}_{12}\text{H}_{13}\text{O}_3)_2(\text{MeOH})_2(\text{NO}_3)_2]$), the counteranions are coordinated to the metal centres and are involved in intramolecular hydrogen-bonding with an adjacent coordinated MeOH molecule.

DFTP can adopt two coordination modes, bidentate observed with the dinuclear species and monodentate for the mononuclear Cu(II) complex. The latter complex does have an original structure with the Cu(II) centre joining two DFTP moieties in a square planar environment and two axial DFTP molecules weakly coordinated through one of the carbonyl group.

The five dinuclear complexes exhibit, as expected, an antiferromagnetic interaction between the two metal centres generally obeying the Kahn prediction.¹⁷⁴

Chapter five

Polynuclear Clusters: a potential for high-spin molecules

5.1. Introduction

Single-Molecule Magnets

The design of novel high-spin molecules represents a major goal of current research in the field of nanoscale materials. Since it was discovered in 1993 by Hendrickson *et al.*¹⁷⁵ that single molecules of $[\text{Mn}_{12}\text{O}_{12}(\text{O}_2\text{CMe})_{16}(\text{H}_2\text{O})_4]$ (Mn_{12}Ac) are superparamagnets and can thus function as magnets at temperatures lower than their blocking temperature (T_B), there has been great interest in trying to understand this new magnetic phenomenon of Single-Molecule Magnetism and in finding other compounds that exhibit similar properties. Such molecules were subsequently named single-molecule magnets (SMMs). The typical metal-core structure of Mn_{12}Ac clusters is depicted in fig. 5.1.

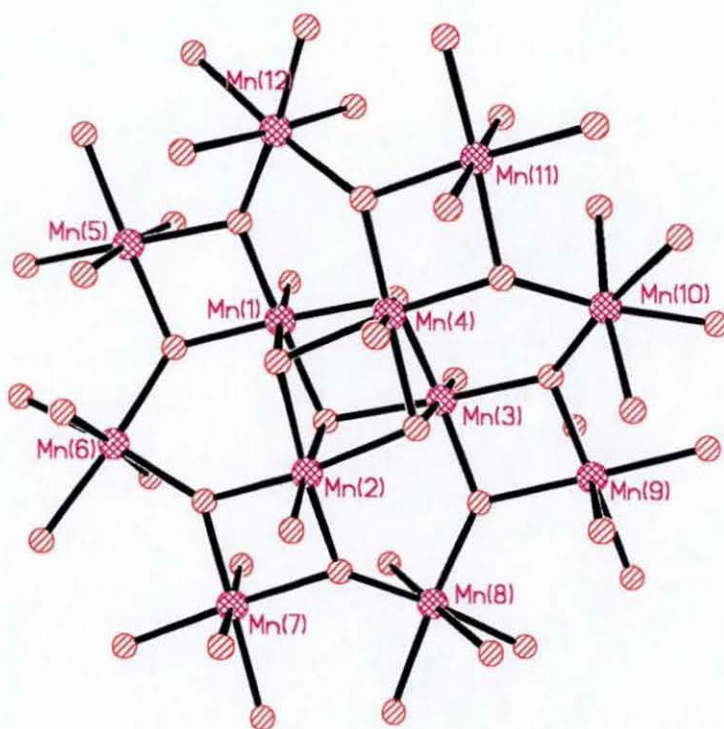


Fig. 5.1: Metal-core⁵² of a typical $[\text{Mn}_{12}\text{O}_{12}(\text{O}_2\text{CR})_{16}(\text{H}_2\text{O})_4]$ cluster

The complex can be conveniently described as a central $[\text{Mn}^{\text{IV}}_4\text{O}_4]^{8+}$ cubane held within a non-planar ring of eight additional Mn(III) atoms by $\mu_3\text{-O}$ atoms. All manganese atoms have a distorted octahedral environment with the Mn(III) centres showing the expected Jahn-Teller distortion.

Since then a few more manganese,¹⁷⁶⁻¹⁸⁴ vanadium¹⁸⁵ and iron¹⁸⁶⁻¹⁹² clusters have been found to possess the necessary properties to function as single-molecule magnets. All these molecules possess the combination of sufficiently large ground-state spin (S) and negative magnetoanisotropy required, to lead to the slow relaxation of magnetisation, which is the characteristic behaviour of a SMM.¹⁹³ This is due to the presence of an energy barrier for the reversal of the direction of their magnetisation and results in the appearance of an out-of-phase AC magnetic susceptibility signal⁸⁷ and magnetisation hysteresis loops. However, of the SMMs known to date, the $[\text{Mn}_{12}\text{O}_{12}(\text{O}_2\text{CR})_{16}(\text{H}_2\text{O})_4]$ ($R = \text{various}$) family possesses the best structural and electronic properties for this phenomenon, inasmuch as it displays the SMM behaviour at the highest temperature ($T_B \text{ ca. } 3 \text{ K}$). Also, relaxation times of the order of two months are observed at 2 K. Moreover, it was proven that molecules like $[\text{Mn}_{12}\text{O}_{12}(\text{O}_2\text{CR})_{16}(\text{H}_2\text{O})_4]$ exhibit quantum effects such as resonant quantum mechanical tunneling of the magnetisation,^{178,179,194-197} which was never clearly observed until Friedman *et al.*¹⁹⁸ first reported this phenomenon in 1996. The occurrence of this effect is reflected by the steps seen in the hysteresis loops. Quantum tunneling of the magnetisation takes place when there is an alignment of energy levels in the two parts of the double-well potential, the latter representing the change in potential energy as the molecules convert from the spin up to the spin down state. A very important aspect to the potential future use of SMMs in, for example, high density information storage (molecular memory devices) or quantum computers,^{191,199} is the ability to modify such molecules in a controllable fashion, both to assess the influence on the magnetic properties (e.g. mechanism of the tunneling) and to allow their assembly into ordered arrays. An additional interest in the study of molecular magnets stems from the possibility of observing macroscopic

quantum tunneling (MQT). Furthermore, manganese clusters are also investigated due to their relevance to the field of colossal magnetoresistance (magnetoresistance associated with a ferromagnetic-to-paramagnetic phase transition).^{200,201}

Rings and wheels

The understanding and exploitation of phenomena such as magnetic relaxation and hysteresis effects requires more examples and therefore the greatest need in this area remains the design of viable synthetic routes to produce nanoscale clusters with the potential for high-spin ground states. Those investigations have led to a particular aesthetic class of ring-shaped high-nuclearity clusters. The most common and homogeneous class of magnetic rings so far synthesised is a series of even-membered Fe(III) rings comprising six to eighteen metal centres denoted as molecular ferric wheels of which the decanuclear wheel $[\text{Fe}_{10}\{(\text{OMe})_2(\text{O}_2\text{CCH}_2\text{Cl})\}_{10}]$ reported by Lippard *et al.* may be regarded as the prototype of this class.^{202,203} The structure shown in fig. 5.2 consists of ten ferric ions essentially coplanar in a circular array. Each iron atom has a distorted octahedral geometry and is joined to its neighbours by edge-sharing methoxides and *cis*-carboxylate bridges, forming a molecular wheel of *ca.* 12 Å in diameter. The bridging methoxide ligands can be subdivided into two distinct sets by their orientation with respect to the ring of iron atoms. One set points into the centre of the circle while the second grouping is directed outward from the rim of the wheel.

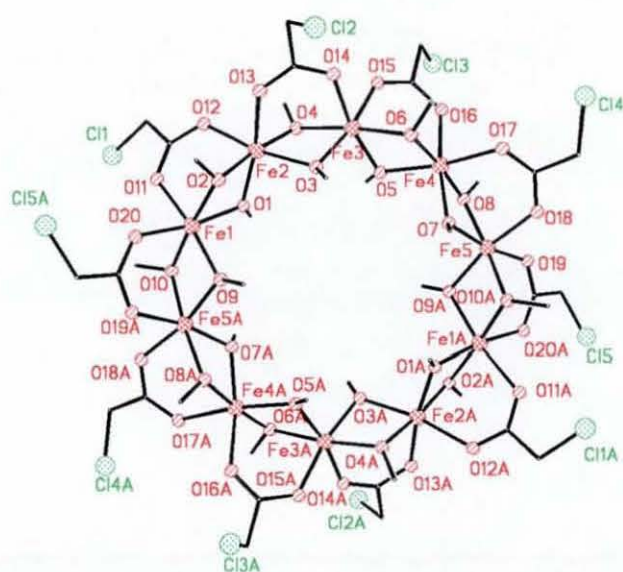


Fig. 5.2: Structure⁵² of a molecular ferric wheel: $[\text{Fe}_{10}\{(\text{OMe})_2(\text{O}_2\text{CCH}_2\text{Cl})\}_{10}]$

Both sets of bridging methoxide ligands are positioned alternatively above and below the plane of the circle in a staggered manner. The bridging monochloroacetate ligands exhibit a similar alternating orientation around the rim of the wheel. The repeated motifs afforded by the disposition of the ligands generate a structure composed of layers of iron, oxygen and carbon atoms when viewed parallel to the plane of the metal atoms (fig. 5.3).

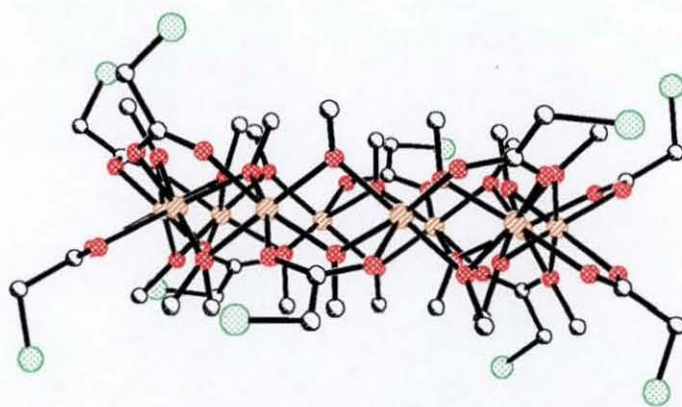


Fig. 5.3: Side-on view of $[\text{Fe}_{10}\{(\text{OMe})_2(\text{O}_2\text{CCH}_2\text{Cl})\}_{10}]$

The magnetic behaviour is typical of a linear chain of antiferromagnetically coupled $S_i = 5/2$ ions down to 50 K with a nearest-neighbour coupling constant J of *ca.* -10 cm^{-1} . Winpenny *et al.*²⁰⁴ reported a similar structure $[\text{Fe}_{10}\{(\text{OMe})_2(\text{O}_2\text{CMe})\}_{10}]$ with methylacetate ligands replacing the monochloroacetate ligands. Furthermore, Winpenny *et al.*²⁰⁵ illustrated the use of molecular ferric wheels in the modelling of relevant surface-active interactions in order to understand the modes of action of known corrosion inhibitors. This can be achieved by replacing the bridging acetate molecule with known organic active compounds like 3-(4-methylbenzoyl)-propionic acid used in water-borne coatings for mild steel. The ligand binds through the carboxylate function.

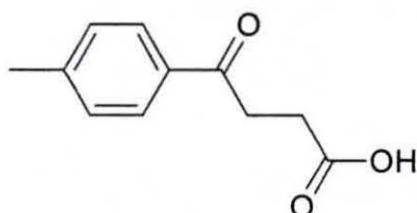


Fig. 5.4: 3-(4-methylbenzoyl)-propionic acid

These large Fe(III) rings are attractive models for one-dimensional quantum antiferromagnets (experimental comparison of rings and coordination polymeric chains) and for investigating the properties in increasingly larger assemblies of interacting metal ions at the simplest level. Further, large ferric wheels can be ideal candidates for the observation of macroscopic quantum size effects where the magnetisation of the wheels exhibits step-like field dependencies at low temperature due to the occurrence of field induced ground state level-crossing (tunneling of the magnetisation).²⁰⁶

So far, the largest cyclic ferric cluster reported is that described by Lippard *et al.*²⁰⁷ containing eighteen Fe(III) atoms in a ring, designated as the “molecular 18-wheeler”. The repeating unit comprises a (μ -hydroxo)bis-(carboxylato)-diiron(III) moiety linked by an acetate and two methoxide ions to a third iron atom (fig. 5.6). An

acetate and two additional methoxide ligands on the latter iron centre form bridges to the next trinuclear repeating unit. The *bis*-carboxylato bridging unit is the dianion of *m*-xylenediamine bis(Kemp's triacid imide) (XDK) depicted in fig. 5.5.

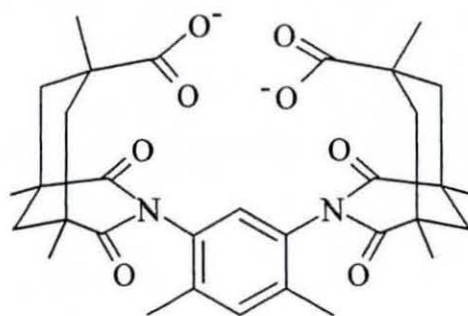


Fig. 5.5: *Bis*-carboxylato bridging unit XDK

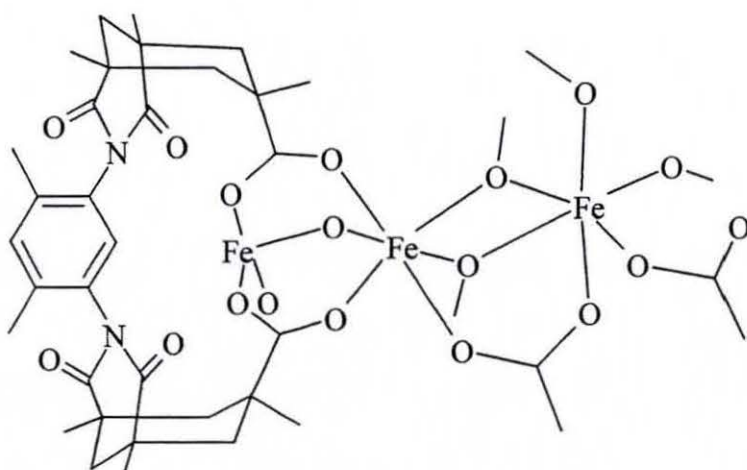


Fig. 5.6: Scheme representing the triiron(III) repeating motif

Each iron atom has distorted octahedral geometry. The magnetic behaviour of $[\text{Fe}(\text{OH})(\text{XDK})\text{Fe}_2(\text{OMe})_4(\text{O}_2\text{CMe})_2]_6$ is indicative of antiferromagnetic interactions between the high spin Fe(III) ions. Two magnetic interactions of different amplitude with exchange coupling constants of $J_A = -19.9 \text{ cm}^{-1}$ and $J_B = -6.8 \text{ cm}^{-1}$ were detected. This result probably reflects the presence of two different type of bridging units.

Gatteschi *et al.*²⁰⁸ reported another polymetallic ring consisting of twelve Fe(III) ions bridged by molecules of acetate and dibenzoylmethane (Hdbm). In this case, the ring is not planar and closely resembles a non-planar twisted “ribbon” (fig. 5.7).

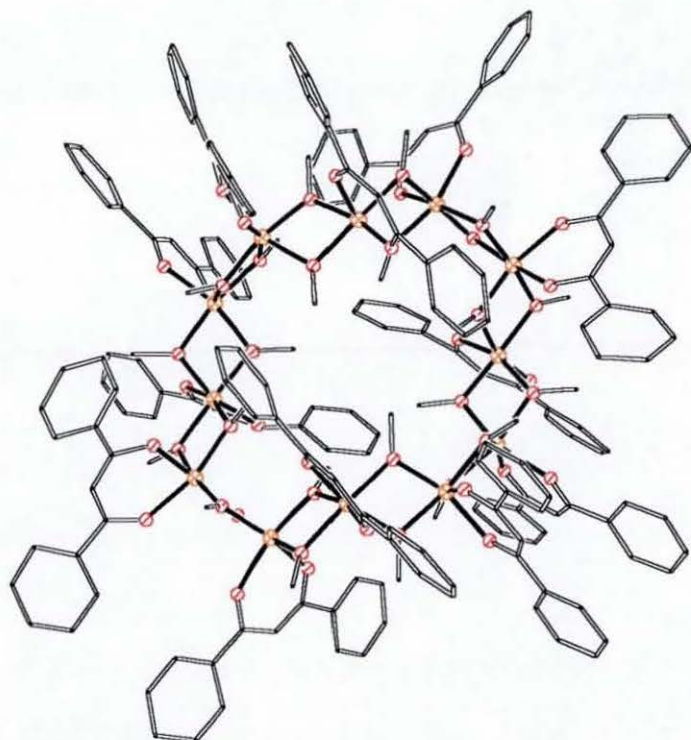


Fig. 5.7: Structure⁵² of $[\text{Fe}(\text{OMe})_2(\text{dbm})]_{12}$, Fe(III) atoms are depicted in yellow

Here again, the magnetic behaviour is that of antiferromagnetically coupled high spin Fe(III) ions with a exchange coupling constant of $J = -22.2 \text{ cm}^{-1}$.

In all those ferric systems, antiferromagnetic coupling results in complete cancellation of local spins to give a $S = 0$ ground state. However, the magnetic behaviour varies considerably depending on the chemical nature of the bridging ligands (carboxylates, alkoxide, hydroxides, etc.) and on the number of interacting spins. In principle, it would be possible to modulate the magnetic properties of the rings by playing with the coordination chemistry. In practice, the synthesis of ring-like molecules is quite challenging and most molecular rings have been obtained in a

serendipitous fashion. For instance, an odd-membered magnetic ring has apparently never been synthesised, although it would be highly frustrated and therefore extremely appealing for magnetic studies. However, attempts to use template ions like Na^+ , Li^+ , Cs^+ etc...in order to “drive” the combination of molecular fragments into a cyclic structure are giving promising results. The latter method is yielding a different class of polynuclear complexes known as “metallacrowns”. This class of compound will be dealt with in the next section entitled metallacrowns.

Other molecular rings (planar) have been reported with copper(II) ions by Ardizzoia *et al.*,^{209,210} $[\text{Cu}_8(\text{dmpz})_8(\text{OH})_8]$. Each copper atom is connected to two hydroxo and two 3,5-dimethylpyrazolate (dmpz) groups with almost square-planar coordination geometry (fig. 5.8).

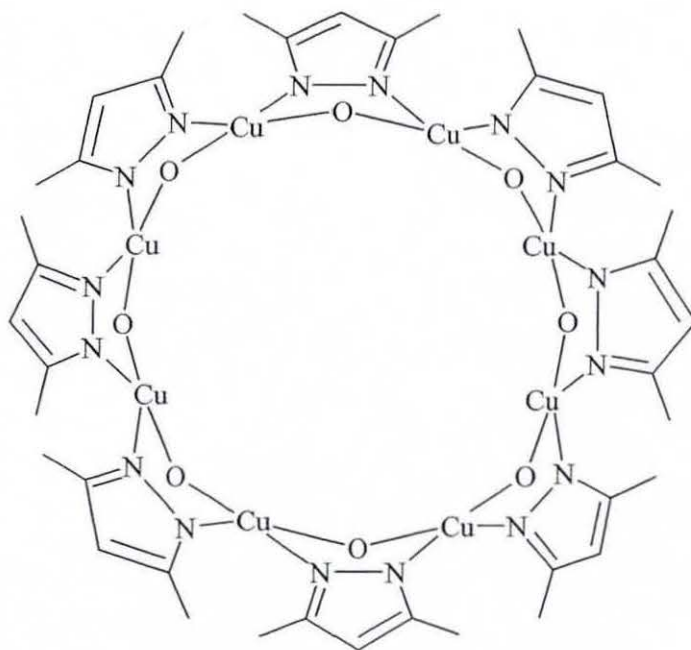


Fig. 5.8: Schematic representation of $[\text{Cu}_8(\text{dmpz})_8(\text{OH})_8]$

The magnetic studies indicate a strong antiferromagnetic superexchange interaction between the copper(II) centres with an exchange coupling constant $J = -950$ K leading to a $S = 0$ ground state.

Furthermore, in 1994, Winpenny *et al.*²¹¹ communicated the synthesis of a dodecanuclear nickel ring, $[\text{Ni}_{12}(\text{O}_2\text{CMe})_{12}(\text{chp})_{12}(\text{H}_2\text{O})_6(\text{THF})_6]$ where acetate, 6-chloropyridonate (chp) and water molecules are involved in bridging the nickel centres. The acetate groups can be subdivided in two sets: one set is situated in the outside of the ring while the other set is coordinated within the central cavity. The magnetic behaviour is indicative of ferromagnetic interactions between the nickel centres leading to a high-spin ground state $S = 12$ with a coupling constant $J = 4.7 \text{ cm}^{-1}$. More recently, Winpenny *et al.*²¹² reported what appears to be the largest homometallic wheel containing paramagnetic Ni(II) centres. The complicated set of interactions involving bridging 3-methyl-3-pyrazolin-5-onate (mpo), 3-methyl-3-pyrazolin-5-one (Hmpo), hydroxy and acetate ligands generates the Ni_{24} structure ($[\text{Ni}_{24}(\text{OH})_8(\text{mpo})_{16}(\text{O}_2\text{CMe})_{24}(\text{Hmpo})_{16}]$) (fig. 5.9), which is much less circular than other cyclic structures and can be described as an octamer of chemically equivalent trinuclear building blocks.

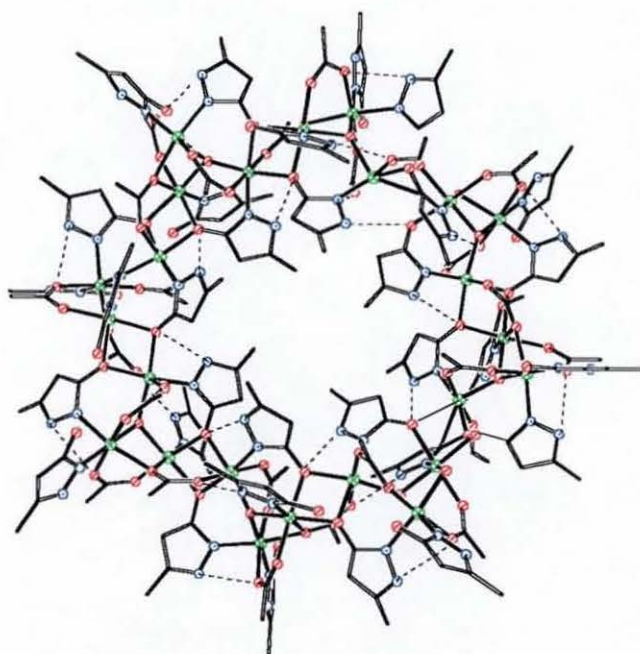


Fig. 5.9: Structure⁵² of $[\text{Ni}_{24}(\text{OH})_8(\text{mpo})_{16}(\text{O}_2\text{CMe})_{24}(\text{Hmpo})_{16}]$

The trinuclear fragments are so disposed that they point approximately at the centre of the neighbouring unit, rather than the end. In addition to metal-ligand bonding, the structure is stabilised by a large quantity of hydrogen-bonding (dotted lines in fig. 5.9). All the metal centres are six-coordinate, with approximately octahedral symmetry. The magnetic behaviour indicates an antiferromagnetic coupling between the nickel ions but it is rather weak and many magnetic states remain populated at even very low temperature (at 1.8 K, $\chi_m T$ is greater than $24 \text{ cm}^3 \text{Kmol}^{-1}$).

It is noticeable that, as with the Fe_{18} structure, it is not possible to generate a large 3d-metal wheel with only one type of bridging interaction. Therefore, while decanuclear ferric wheels can be accurately described as $([\{\text{Fe}(\text{OMe})_2(\text{O}_2\text{CR})\}_{10}])$, such a description as an oligomer of a mononuclear fragment is not accurate for Fe_{18} and Ni_{24} wheels. Therefore, if still larger wheels are to be constructed, a design principle might be to look for either larger oligomers of trinuclear fragments or oligomers of higher nuclearity building blocks.

Metallacrowns

As previously mentioned, large molecular clusters are, unfortunately, almost invariably obtained in a serendipitous manner from self-assembly reactions and general strategies for the synthesis of large clusters with preordained structures and properties have not yet been developed. However, the method using template ions like Na^+ , Li^+ , Cs^+ etc...in order to “drive” the combination of molecular fragments into a cyclic structure yielding a different class of polynuclear complexes known as “metallacrowns”²¹³⁻²¹⁶ has been successful to some extent.

Recently, Saalfrank *et al.*^{217,218} reported cyclic Fe(III) complexes with a [12]metallacrown-6 structure in which sodium or lithium is encapsulated in the centre. According to Lehn *et al.*²¹⁹ in the case of the template-mediated self-assembly of a supramolecular system, amidst a set of possibilities the one combination of building blocks that leads to the best receptor for the substrate is realised. Although

lithium has a smaller radius (0.68 Å) than sodium (0.97 Å), the reactions described by Saalfrank afforded the same type of structures, the isostructural complexes $[\text{Na}\text{CFe}_6\{\text{N}(\text{CH}_2\text{CH}_2\text{O})_3\}_6]^+$ and $[\text{Li}\text{CFe}_6\{\text{N}(\text{CH}_2\text{CH}_2\text{O})_3\}_6]^+$. The smaller radius of lithium led to a decrease in size of the metal ring and to a more regular topology of the oxygen atoms with respect to an idealised closest-packing CdI_2 -type arrangement. The six iron atoms of the centrosymmetric cation are located in the corners of a regular hexagon. Each Fe(III) ion is doubly bridged to its neighbour by two oxygen atoms belonging to two different bridging ligands (triethanolamine). In fact, triethanolamine acts as a tripodal tetradentate ligand and links three Fe(III) ions. Fig. 5.10 shows that two Fe(III) ions, the Na^+ ion and four oxygen atoms are situated at the corners of an open cube (one corner missing). The structure is constituted of three open cubes sharing two edges (red lines in fig 5.10). This type of metal-oxygen arrangement (CdI_2 -type) is found in similar structures with Mn and homoheptanuclear Mn and Zn complexes described later in this section.

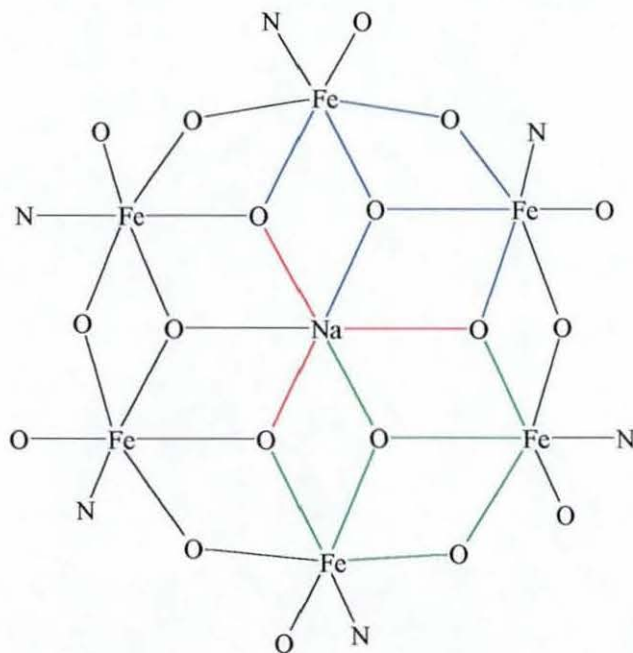


Fig. 5.10: Schematic representation of the backbone of $[\text{Na}\text{CFe}_6\{\text{N}(\text{CH}_2\text{CH}_2\text{O})_3\}_6]^+$

The magnetic behaviour of $[\text{Na}\text{CFe}_6\{\text{N}(\text{CH}_2\text{CH}_2\text{O})_3\}_6]^+$ indicates an antiferromagnetic interaction between the Fe(III) ions with an exchange coupling

constant of $J = -23.0$ K. For the isostructural complex $[\text{LiFe}_6\{\text{N}(\text{CH}_2\text{CH}_2\text{O})_3\}_6]^+$ the antiferromagnetic coupling constant is $J = -18.1$ K.

Similar Fe_6 structures containing either $\text{Na}^{220-222}$ (Fig. 5.11) or $\text{Li}^{221,222}$ in their central cavities have been isolated with different ligands such as Hdbm (1,3-diphenyl-1,3-propanedione) or Hpmdbm (1,3-di(4-methoxyphenyl)-1,3-propanedione) (table 5.1).

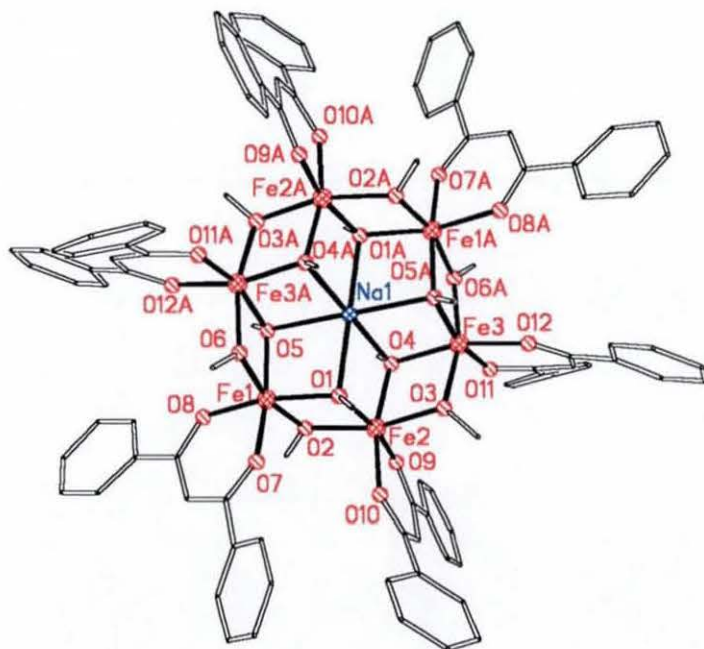


Fig. 5.11: Structure⁵² of the cation $[\text{NaFe}_6(\text{OMe})_{12}(\text{dbm})_6]^+$

Bis(methoxy) bridges connect adjacent iron atoms while the two remaining sites of the distorted octahedral coordination sphere of each iron(III) centre are occupied by a chelating dbm or pmdbm ligand. In those examples, the ligands, other than methoxy groups, are not involved in bridging the iron(III) ions.

Table 5.1: Exchange coupling constants for different Fe(III) clusters

Clusters	J in K
$[\text{Li}\text{-Fe}_6\{\text{N}(\text{CH}_2\text{CH}_2\text{O})_3\}_6]^+$	-18.1
$[\text{Na}\text{-Fe}_6\{\text{N}(\text{CH}_2\text{CH}_2\text{O})_3\}_6]^+$	-23.0
$[\text{Li}\text{-Fe}_6(\text{OMe})_{12}(\text{dbm})_6]^+$	-20.0
$[\text{Na}\text{-Fe}_6(\text{OMe})_{12}(\text{dbm})_6]^+$	-29.4
$[\text{Na}\text{-Fe}_6(\text{OMe})_{12}(\text{pmdbm})_6]^+$	-28.6

Studies by Gatteschi *et al.*^{221,222} concluded that the encapsulated alkali metal ion has a tuning effect on the magnetism of the core: the J value is related to the ionic radius of the guest ion, which determines the exact geometry at the methoxide ligands. Those observations showed that the possibility of controlling important magnetic parameters in the rings, such as exchange coupling (table 5.1) and zero-field splittings, by simply playing with the radius of the alkali metal template extends the potential uses of host-guest chemistry for fine tuning the magnetic properties of single-molecule magnets and for designing new magnetic clusters with preordained magnetic behaviour.

In this line of work, Gatteschi *et al.*¹⁵⁴ demonstrated that the magnetic properties of high-nuclearity clusters may be varied to a very large extent by acting on the electronic structure of the constituent metal ions. By substituting Fe(III) with Mn(III) in the core of the cyclic cluster $[\text{Na}\text{-Fe}_6(\text{OMe})_{12}(\text{dbm})_6]^+$, it was possible to switch from $S = 0$ to $S = 12$ ground state. Changing the number of d electrons on the metal centres may therefore represent a powerful tool for modulating the properties of single-molecule magnets. In the complex $[\text{Na}\text{-Mn}_6(\text{OMe})_{12}(\text{dbm})_6]^+$, the alkali metal ion has a trigonally distorted octahedral environment. Although the average nearest-neighbour Mn---Mn distance (3.21(2) Å) is comparable to that observed in the Fe(III) complex (3.194(9) Å), the coordination environment of the metal ions shows important differences (angles and bond lengths). There is an evident tetragonal elongation of the coordination polyhedra, which is typical of a Jahn-Teller distorted high-spin Mn(III). The magnetic behaviour is indicative of a ferromagnetic

interaction between the Mn(III) ions with two different coupling constants $J_A = 23.8 \text{ cm}^{-1}$ and $J_B = 2.6 \text{ cm}^{-1}$ due to the distorted geometry. Given the elongated nature of the distortion from octahedral geometry the metal x^2-y^2 orbitals are empty. Due to the arrangement of local elongation axes in the structure, the z^2 magnetic orbitals have non-zero overlap with the empty metal x^2-y^2 orbitals through the μ_3 -OMe ligands. As stated by Gatteschi and Ginsberg,²²³ the x^2-y^2/z^2 pathway is expected to provide a ferromagnetic coupling.

Using cesium, which is even bigger than lithium and sodium, Saalfrank *et al.*^{217,218} synthesised a larger [16]metallacrown-8 structure containing two additional ferric ions in which cesium is incorporated in the centre, $[\text{Cs} \subset \text{Fe}_8 \{ \text{N}(\text{CH}_2\text{CH}_2\text{O})_3 \}_8]^+$. In the case of the octanuclear complex, the eight iron atoms are located in the corners of a nearly regular octagon with a diameter of 8.224 \AA (fig. 5.12). Each Fe(III) ion is in a distorted octahedral environment. The Cs^+ ion lies directly above the centre of the cavity. The bridging pattern of the ligand triethanolamine is identical to the hexanuclear iron (III) complex $[\text{Na} \subset \text{Fe}_6 \{ \text{N}(\text{CH}_2\text{CH}_2\text{O})_3 \}_6]^+$.

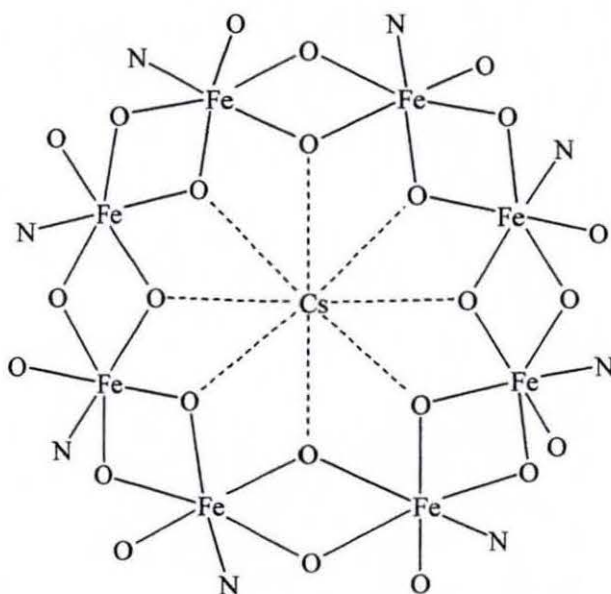


Fig. 5.12: Schematic representation of the backbone of $[\text{Cs} \subset \text{Fe}_8 \{ \text{N}(\text{CH}_2\text{CH}_2\text{O})_3 \}_8]^+$

The magnetic behaviour of $[\text{Cs}\text{Fe}_8\{\text{N}(\text{CH}_2\text{CH}_2\text{O})_3\}_8]^+$ indicates an antiferromagnetic exchange between the high-spin Fe(III) ions with a coupling constant $J = -22.5$ K.

Related metallacrown complexes of copper(II) ($[\text{Na}\text{C}\text{u}_6(\text{mhp})_{12}]$) and cobalt(II) ($[\text{Na}\text{C}\text{Co}_6(\text{mhp})_{12}]$) with an encapsulated sodium ion have been reported by Winpenny *et al.*²²⁴ and Thornton *et al.*²²⁵ with 2-hydroxy-6-methylpyridine (Hmhp). In those examples (e.g. fig. 5.13), no methoxo or hydroxo groups contribute to the bridging like in the Fe(III) and Mn(III) structures.

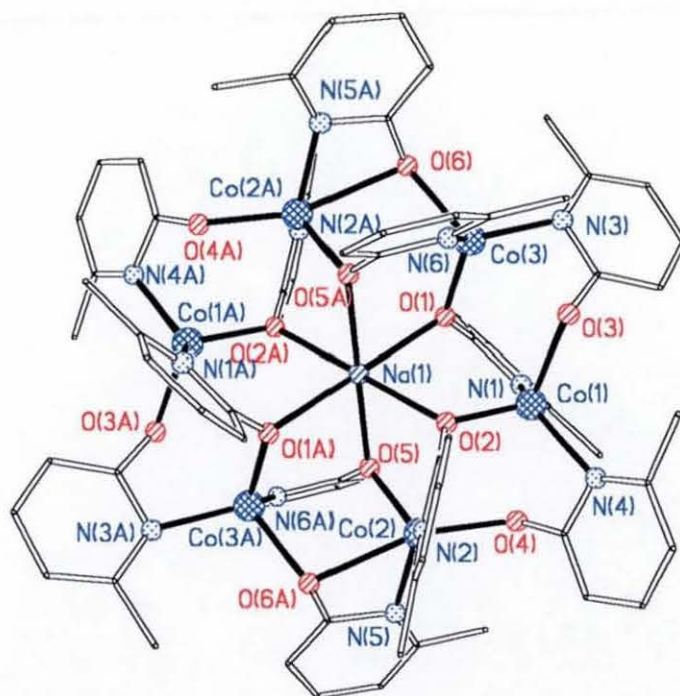


Fig. 5.13: Structure⁵² of $[\text{Na}\text{C}\text{Co}_6(\text{mhp})_{12}]$

Each cobalt(II) ion is coordinated tetrahedrally by two nitrogen and two oxygen atoms from four hydroxymethylpyridine ligands. Six of the twelve hydroxymethylpyridine oxygen atoms are located at the corners of an octahedron and coordinate the sodium ion at the centre of the cavity formed by the six cobalt atoms. Here, the

structure is quite distorted from an ideal CdI_2 -type structure mentioned previously. This is mainly due to the fact that the cobalt atoms are four-coordinate and the oxygen atoms are not involved in μ_3 -O bridges but μ_2 -O instead.

In the similar copper(II) complex ($[\text{NaCu}_6(\text{mhp})_{12}]$), the presence of the sodium ion is serendipitous. Each copper atom is in a distorted square-planar environment, with three symmetry equivalent coppers having a *trans*-arrangement of two nitrogen and two oxygen donors while the other three adopt a *cis*-arrangement. The central sodium ion has a trigonally distorted compressed octahedral array of oxygen atoms. The mhp ligands adopt the same bridging mode as in the cobalt complex. It is noteworthy that $[\text{NaCu}_6(\text{mhp})_{12}]$ shows occupation of the central cation cavity by Na^+ rather than K^+ , despite the latter's greater abundance in the preparative reaction, implying strong discrimination in favour of the less abundant smaller ion rather than forming a larger cavity to accommodate K^+ . Later, in 1994, Winpenny *et al.*²²⁶ showed that the sodium ion can be replaced by copper(II) without gross alteration of the structure (fig. 5.14).

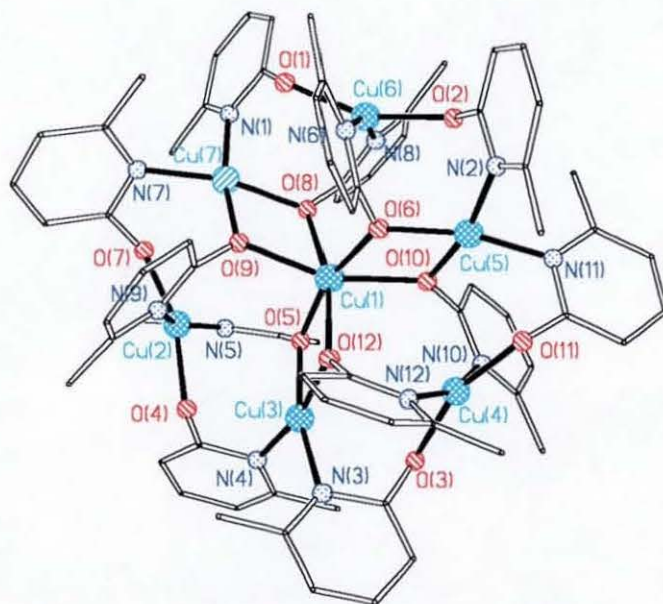


Fig. 5.14: Structure⁵² of $[\text{Cu}_7(\text{mhp})_{12}]$

Hepta-homonuclear complexes with a CdI_2 -type core structure (iron structure previously described) have also been encountered with manganese. Hendrickson *et al.*²²⁷ reported the synthesis of $[\text{Mn}_7(\text{OH})_3\text{Cl}_3(\text{hmp})_9]\text{Cl}[\text{MnCl}_4]$ (Hhmp = 2-hydroxymethylpyridine) consisting of a nearly planar Mn_7 unit comprising a central manganese ion held within a Mn_6 hexagon by three μ_3 -OH and three μ_3 -OR groups, the latter from three hmp^- chelates. The remaining hmp^- oxygen atoms doubly bridge Mn_2 pairs of the hexagon. Three terminal Cl^- ions complete peripheral ligation. Charge considerations require a four $\text{Mn}(\text{II})$ and three $\text{Mn}(\text{III})$ mixed-valence description and, on the basis of Mn^{III} Jahn-Teller distortions and bond valence sum calculations, they established Mn_2 , Mn_4 and Mn_6 to be $\text{Mn}(\text{III})$ (fig. 5.15).

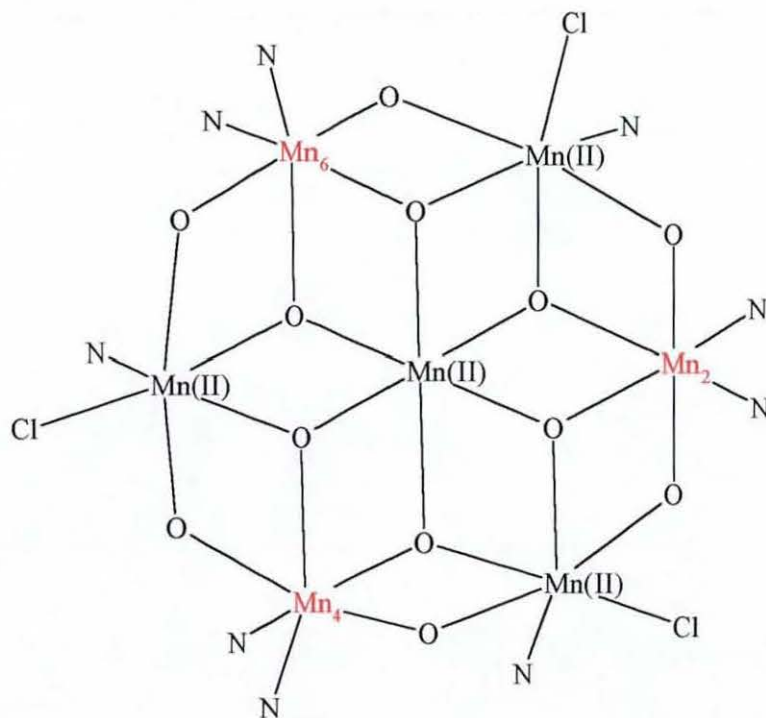


Fig. 5.15: Schematic representation of the Mn_7 core in $[\text{Mn}_7(\text{OH})_3\text{Cl}_3(\text{hmp})_9]\text{Cl}[\text{MnCl}_4]$

A topological M_7 equivalent of $[\text{Mn}_7(\text{OH})_3\text{Cl}_3(\text{hmp})_9]\text{Cl}[\text{MnCl}_4]$ was reported with zinc(II) by Tesmer *et al.*²²⁸ In $[\text{Zn}_7(\text{hmp})_{12}]\text{Cl}_2$, the ligand arrangement is slightly different; The μ_3 -O bridging the zinc centres all belong to hmp^- anions. Six hmp^-

anions bridge three zinc ions forming the coordination sphere of the central zinc ion while the remaining six hmp⁻ anions bridge two adjacent zinc centres forming the alternating Zn-O motif on the outer rim of the cluster (fig. 5.16).

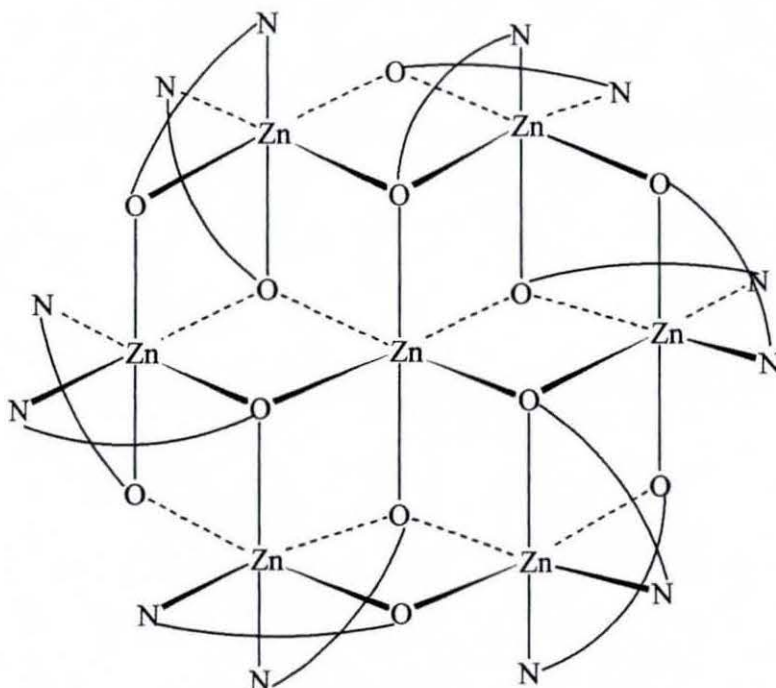


Fig. 5.16: Schematic representation of the cation $[Zn_7(hmp)_{12}]^{2+}$

The magnetic behaviour of $[Mn_7(OH)_3Cl_3(hmp)_9]Cl[MnCl_4]$ is consistent with a ground-state value of $S \geq 10$ and can be rationalised due to competing exchange interactions of comparable magnitude.²²⁹ The pair-wise exchange interactions are of two types: J_{io} and J_{oo} (I = inner, o = outer), the former comprising both J_{22} (Mn^{II} - Mn^{II}) and J_{23} (Mn^{II} - Mn^{III}) interactions and the latter only J_{23} . The ground-state of $[Mn_7(OH)_3Cl_3(hmp)_9]Cl[MnCl_4]$ will be dependent on the relative magnitudes of the competing J_{io} and J_{oo} interactions, which are usually weakly antiferromagnetic with comparable magnitude. Thus, it is impossible for the spins to align antiparallel to each of their neighbouring spins and the ground state consequently adopts an intermediate spin value.

A very similar high-spin mixed-valence heptanuclear manganese $[\text{Mn}_7(\text{OMe})_{12}(\text{dbm})_6]$ (Hdmb = dibenzoylmethane) cluster with a layered structure mimicking a fragment of the manganese oxide mineral lithiophorite was reported by Gatteschi *et al.*²³⁰ However, in Gatteschi's complex dbm⁻ anions are the organic ligands used, which chelate each metal and are not involved in bridging. The manganese ions are doubly bridged by μ_2 -OMe and μ_3 -OMe groups (fig. 5.17).

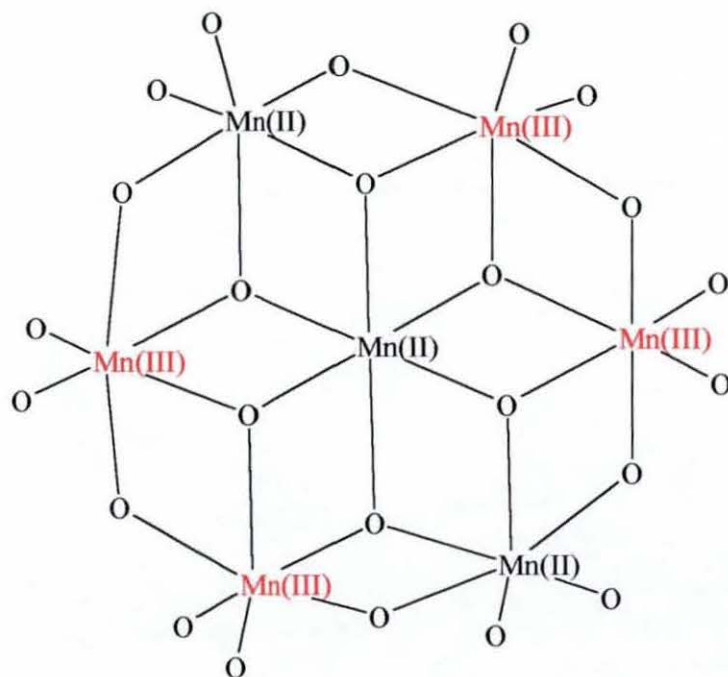


Fig. 5.17: Schematic representation of the Mn_7 core in $[\text{Mn}_7(\text{OMe})_{12}(\text{dbm})_6]$

Conductivity measurements confirmed the non-ionic character of $[\text{Mn}_7(\text{OMe})_{12}(\text{dbm})_6]$ and suggested a mixed valence $\text{Mn}^{\text{II}}_3\text{Mn}^{\text{III}}_4$ formulation. The magnetic behaviour is consistent with a ground-state spin value of 17/2. Here again, the result can be explained by the presence of competing exchange interactions of comparable magnitude²²⁹ ($\text{Mn}^{\text{II}}-\text{Mn}^{\text{II}}$; $\text{Mn}^{\text{II}}-\text{Mn}^{\text{III}}$; $\text{Mn}^{\text{III}}-\text{Mn}^{\text{III}}$). As for $[\text{Mn}_7(\text{OH})_3\text{Cl}_3(\text{hmp})_9]\text{Cl}$ [MnCl_4], spin frustration effects may play an important role and the spin multiplicity of the ground-state can easily escape prediction. Furthermore, high-spin Mn^{III} ions are susceptible of Jahn-Teller distortion. Superexchange interactions are strongly

influenced by the orientation of the Jahn-Teller axes, and a large number of different pair-wise interactions is therefore expected.

The same M_7 core, reminiscent of the CdI_2 -type lattice arrangement, is found at the centre of huge Fe_{19} structures reported by Heath *et al.*^{190,231,232} The organic ligands used are tetradentate derivatives of *N*-(1-hydroxyethyl)iminodiacetic (H_3 heidi) (fig. 5.18).

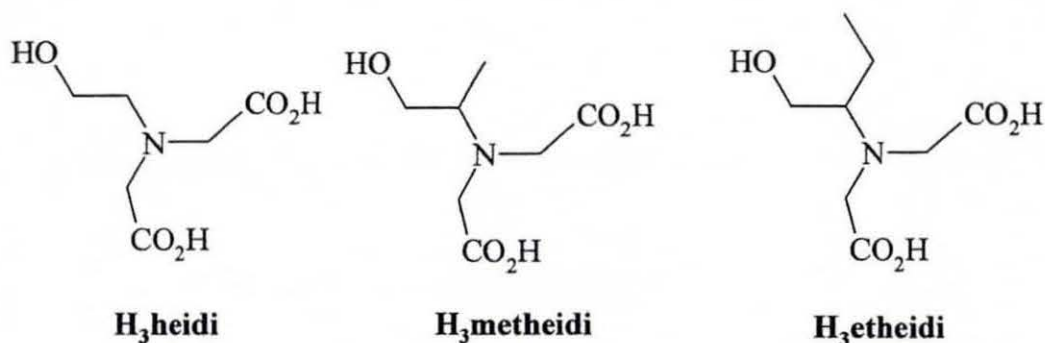


Fig. 5.18: Derivatives of H_3 heidi

An example of those structures is shown in fig. 5.19 with methheidi. The iron centres of the M_7 core are depicted in red while the additional iron ions of the periphery are depicted in yellow. This example demonstrates that the M_7 core employed as a building block can lead to higher nuclearity clusters. This synthetic strategy has a great potential in the field of high-spin polynuclear compounds for the design of ever-bigger clusters with bigger ground state spin value with the possibility of forming paramagnets. The magnetic data for $[Fe_{19}(\text{methheidi})_{10}(\text{OH})_{14}(\text{O})_6(\text{H}_2\text{O})_{12}](\text{NO}_3)$ suggest the presence of a range of antiferromagnetic pair-wise interactions that give rise to an uncompensated magnetic moment and are consistent with a ground state spin value of $33/2$. As for the Mn_{12} systems, the Fe_{19} systems show magnetic hysteresis at low temperatures ($< 1\text{K}$). However, the height of the magnetisation barrier for Fe_{19} clusters remains smaller than that of Mn_{12} single molecule magnets due to the very weak magnetoanisotropy.

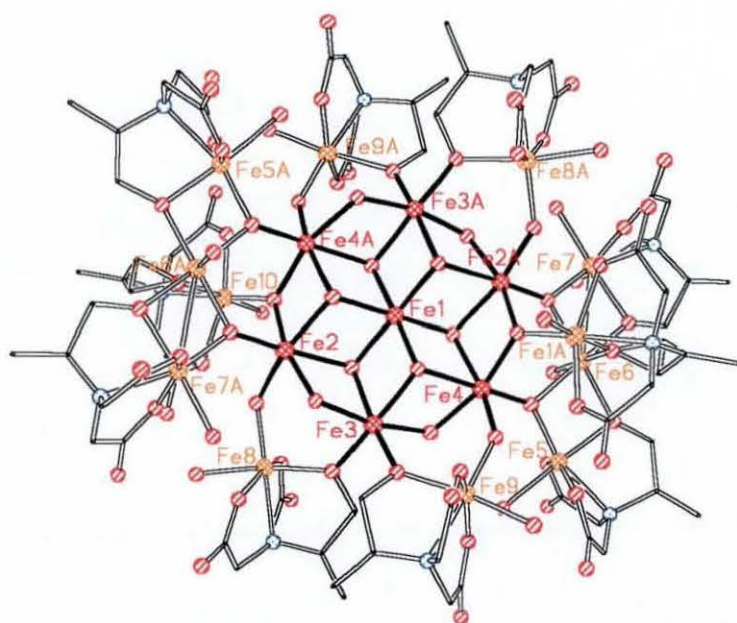


Fig. 5.19: Structure⁵² of the cation $[\text{Fe}_{19}(\text{metheidi})_{10}(\text{OH})_{14}(\text{O})_6(\text{H}_2\text{O})_{12}]^+$

In the course of the work described in this thesis, two homoheptanuclear clusters $[\text{Ni}_7(\text{C}_{12}\text{H}_{13}\text{O}_3)_6(\text{OH})_4(\text{MeO})_2](\text{ClO}_4)_2$ and $[\text{Co}_7(\text{C}_{12}\text{H}_{13}\text{O}_3)_6(\text{OH})_4(\text{MeO})_2](\text{ClO}_4)_2$ have been isolated. Their metal-core structure is similar to that of $[\text{Mn}_7(\text{OMe})_{12}(\text{dbm})_6]$, which is reminiscent to the CdI_2 -type lattice arrangement. Their synthesis and structure along with some preliminary magnetic studies are described here. During attempts to synthesis polynuclear clusters a trinuclear $\text{Mn}(\text{II})$ complex with the ligand DHTMB has been isolated as well.

5.2. Homoheptanuclear complexes with Ni(II) and Co(II)

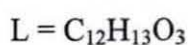
5.2.1. Synthesis of $[\text{Ni}_7(\text{C}_{12}\text{H}_{13}\text{O}_3)_6(\text{OH})_4(\text{MeO})_2](\text{ClO}_4)_2$ and $[\text{Co}_7(\text{C}_{12}\text{H}_{13}\text{O}_3)_6(\text{OH})_4(\text{MeO})_2](\text{ClO}_4)_2$

$[\text{Ni}_7(\text{C}_{12}\text{H}_{13}\text{O}_3)_6(\text{OH})_4(\text{MeO})_2](\text{ClO}_4)_2$ was initially isolated from a reaction which aimed to form tetranuclear macrocyclic Ni(II) complexes *via* the condensation of 2,6-diformyl-4-*tert*-butylphenol (DFTP) and 1,5-diaminopentan-3-ol in the presence of $\text{Ni}(\text{ClO}_4)_2$ in MeOH/EtOH. It was later noticed that in this particular reaction there was an excess of potassium hydroxide coming from the neutralisation of 1,5-diaminopentan-3-ol dihydrochloride. Consequently, attempts to directly synthesis this heptanuclear nickel complex were carried out reacting a solution of DFTP and $\text{Ni}(\text{ClO}_4)_2$ in methanol with a solution of sodium hydroxide in methanol. The use of sodium hydroxide in the synthesis of polynuclear clusters has been discussed previously in the introduction for the synthesis of heteronuclear complexes containing sodium (metallacrowns). However, sodium is not always incorporated in the compound as it is the case for a similar heteronuclear Mn(II/III) cluster reported by Gatteschi *et al.*²³⁰ In the example of $[\text{Ni}_7(\text{C}_{12}\text{H}_{13}\text{O}_3)_6(\text{OH})_4(\text{MeO})_2](\text{ClO}_4)_2$, sodium hydroxide was employed because it was thought to help the deprotonation of the ligand (weaker bases like pyridine have also been used in the synthesis of other polynuclear clusters¹⁹⁰). Nevertheless, it is possible that a sodium ion is incorporated to facilitate the formation of the cyclic structure and subsequently exchanged with a Ni(II) ion, yielding the final heptanickel cluster. The synthesis of a Co(II) analogue $[\text{Co}_7(\text{C}_{12}\text{H}_{13}\text{O}_3)_6(\text{OH})_4(\text{MeO})_2](\text{ClO}_4)_2$ was carried out following the same procedure used to synthesise the Ni_7 compound. The yields, however, are quite low *ca.* 12% but this is not surprising for this type of complexes as the reported yields of polynuclear clusters vary from as low as 5% to 60%. Furthermore, serendipity plays an important part in the synthesis of those assemblies and experimental design is often quite challenging. Different attempts were made to try and synthesise polynuclear clusters of copper, iron and manganese but led to the isolation of dinuclear species, which is the side-product of a wide range of those bigger assemblies. In the case of

manganese, some traces of polynuclear species have been detected by FAB (table 5.2) but it is difficult to attribute them beyond doubt as no structures have yet been determined to support the idea.

Table 5.2: Peak assignments for polynuclear by-products of
 $[\text{Mn}_2(\text{C}_{12}\text{H}_{13}\text{O}_3)_2(\text{MeOH})_4](\text{ClO}_4)_2$

m/z	Rel. Intensities (%)	Fragments	Calc. Mass
1715	<5	$[\text{Mn}_7(\text{OH})_6(\text{L})_6]^{2+}$	1717
1966	<5	$[\text{Mn}_6(\text{MeO})_{12}(\text{L})_6+\text{H}]^+ \cdot \text{MeOH}$	1965
2096	<5	$[\text{Mn}_7(\text{MeO})_{10}(\text{OH})_2(\text{L})_6(\text{ClO}_4)]^{2+} \cdot 2\text{H}_2\text{O}$	2094
2184	<5	$[\text{Mn}_7(\text{MeO})_{12}(\text{L})_6(\text{ClO}_4)_2]^+$	2185
2207	<5	$[\text{Mn}_7(\text{MeO})_{12}(\text{L})_6(\text{ClO}_4)_2]^+ \cdot \text{H}_2\text{O}$	2203



The reasons why one cluster forms in preference to the other or why not only polynuclear clusters are formed remain obscure and rely on many factors such as stability in solution, solubility, pH, ratio of the different components, the order in which building blocks come together etc. As stressed by Powell *et al.*²³² the use of a strong base such as sodium hydroxide in the case of polyiron aggregates, tends to shift the equilibrium existing between mononuclear and polynuclear species (fig. 5.20) completely to the right-hand side, producing "large" or "infinite" (polymeric) species like Fe(III) oxyhydroxide minerals (e.g. "Fe(OH)₃" which is a collection of mineral phases).

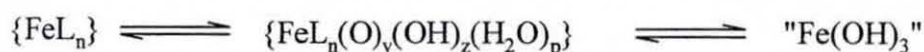


Fig. 5.20: Equilibrium existing in solution in the synthesis of polyiron species

Using a weaker base encourages the formation of smaller aggregated species. However, the use of pyridine in attempt to synthesise polyiron species with DFTP proved unsuccessful in the synthesis of a finite polynuclear species.

Both polynuclear Ni(II) and Co(II) species were characterised by elemental analysis, infra-red spectroscopy, FAB spectrometry and single crystal X-ray crystallography. The IR spectra of $[\text{Ni}_7(\text{C}_{12}\text{H}_{13}\text{O}_3)_6(\text{OH})_4(\text{MeO})_2](\text{ClO}_4)_2$ and $[\text{Co}_7(\text{C}_{12}\text{H}_{13}\text{O}_3)_6(\text{OH})_4(\text{MeO})_2](\text{ClO}_4)_2$ showed two strong sharp bands characteristic of $\nu(\text{C}=\text{O})$ vibrations at 1663 and 1625 cm^{-1} and 1664 and 1631 cm^{-1} respectively. The $\nu(\text{C}=\text{O})$ vibrations for the dimeric Ni(II) and Co(II) species appear at different wavelengths 1650 and 1630 cm^{-1} and 1654 and 1626 cm^{-1} respectively.

5.2.2. Structures of $[\text{Ni}_7(\text{C}_{12}\text{H}_{13}\text{O}_3)_6(\text{OH})_4(\text{MeO})_2](\text{ClO}_4)_2$ and $[\text{Co}_7(\text{C}_{12}\text{H}_{13}\text{O}_3)_6(\text{MeO})_6](\text{ClO}_4)_2$

Green crystals of $[\text{Ni}_7(\text{C}_{12}\text{H}_{13}\text{O}_3)_6(\text{OH})_4(\text{MeO})_2](\text{ClO}_4)_2$ and orange crystals of $[\text{Co}_7(\text{C}_{12}\text{H}_{13}\text{O}_3)_6(\text{MeO})_6](\text{ClO}_4)_2$ suitable for X-ray studies were isolated by slow diffusion of diethylether into methanol solutions of the compounds within a week.

To the best of our knowledge, no Ni_7 or Co_7 systems with the same metal core structure as $[\text{Ni}_7(\text{C}_{12}\text{H}_{13}\text{O}_3)_6(\text{OH})_4(\text{MeO})_2](\text{ClO}_4)_2$ and $[\text{Co}_7(\text{C}_{12}\text{H}_{13}\text{O}_3)_6(\text{MeO})_6](\text{ClO}_4)_2$ have been reported so far.

The structure of both complexes is centrosymmetric and consists of a nearly planar M_7 ($\text{M} = \text{Ni}^{2+}$ or Co^{2+}) unit comprising a central M held within the M_6 hexagon by four $\mu_3\text{-OH}^-$ and two MeO^- groups. The six DFTP⁻ ligands bridge two consecutive metal ions (M_6 hexagon), each through the phenoxo bridge forming two 6-membered chelate rings with each metal (fig. 5.21: cobalt cluster).

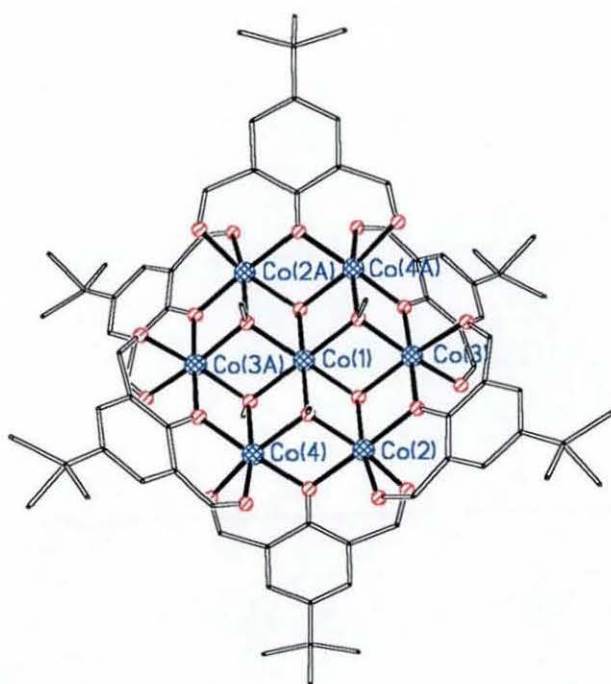


Fig. 5.21: Structure of the cation $[\text{Co}_7(\text{C}_{12}\text{H}_{13}\text{O}_3)_6(\text{MeO})_6]^{2+}$

As shown in fig. 5.22, the six metal ions are coplanar with the DFTP ligands alternatively pointing up and down around the circle formed by the six outer metal ions.

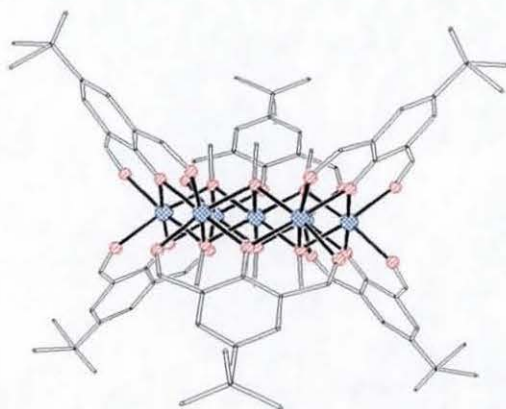


Fig. 5.22: Structure of the cation $[\text{Co}_7(\text{C}_{12}\text{H}_{13}\text{O}_3)_6(\text{MeO})_6]^{2+}$ showing the coordination of the DFTP in an up-and-down manner

The side view of the complex shows a M/O layered structure, with layers of oxygen atoms above and below the M₇ layer, reminiscent of the hexagonal close-packed layered structure of CdI₂.²³³

For the complexes [Ni₇(C₁₂H₁₃O₃)₆(OH)₄(MeO)₂](ClO₄)₂ and [Co₇(C₁₂H₁₃O₃)₆(MeO)₆](ClO₄)₂, each metal ion is in a compressed octahedral environment with two bond lengths significantly shorter than the four others. The Co-O distances are within the range of bond lengths observed for Co(II).⁸⁹ The selected bond lengths and angles for the nickel complex and the cobalt complex are given in table 5.3 and table 5.4 respectively. All the X-ray collection parameters for [Co₇(C₁₂H₁₃O₃)₆(MeO)₆](ClO₄)₂ and [Ni₇(C₁₂H₁₃O₃)₆(OH)₄(MeO)₂](ClO₄)₂ are summarised in table 1 and table 2 respectively, in annex 4.

Table 5.3: Selected bond lengths and angles for [Ni₇(C₁₂H₁₃O₃)₆(OH)₄(MeO)₂](ClO₄)₂

Ni(1)-O(3)*	2.058(6)	Ni(3)-O(2C)*	2.020(8)
Ni(1)-O(3)	2.058(6)	Ni(3)-O(3)*	2.064(6)
Ni(1)-O(1)	2.095(6)	Ni(3)-O(1)	2.074(6)
Ni(1)-O(1)*	2.095(6)	Ni(4)-O(3A)	2.035(8)
Ni(1)-O(2)*	2.165(7)	Ni(4)-O(3B)	2.036(7)
Ni(1)-O(2)	2.165(7)	Ni(4)-O(1B)	2.031(6)
Ni(2)-O(1C)	2.025(7)	Ni(4)-O(1A)	2.041(6)
Ni(2)-O(2B)	2.027(6)	Ni(4)-O(3)*	2.058(6)
Ni(2)-O(1B)	2.032(6)	Ni(4)-O(2)	2.105(6)
Ni(2)-O(3C)	2.033(7)	O(3)-Ni(4)*	2.058(6)
Ni(2)-O(1)*	2.074(6)	O(3)-Ni(3)*	2.064(6)
Ni(2)-O(2)	2.121(6)	O(1)-Ni(2)*	2.074(6)
Ni(3)-O(2A)	2.014(7)	O(1C)-Ni(3)*	2.019(6)
Ni(3)-O(1C)*	2.019(6)	O(2C)-Ni(3)*	2.020(8)
Ni(3)-O(1A)	2.027(7)		
O(3)*-Ni(1)-O(3)	180.0(5)	O(3)*-Ni(1)-O(1)	84.6(2)

O(3)-Ni(1)-O(1)	95.4(2)	O(2A)-Ni(3)-O(1A)	89.9(3)
O(3)*-Ni(1)-O(1)*	95.4(2)	O(1C)*-Ni(3)-O(1A)	178.2(3)
O(3)-Ni(1)-O(1)*	84.6(2)	O(2A)-Ni(3)-O(2C)*	88.8(3)
O(1)-Ni(1)-O(1)*	180.0(3)	O(1C)*-Ni(3)-O(2C)*	90.2(3)
O(3)*-Ni(1)-O(2)*	96.2(2)	O(1A)-Ni(3)-O(2C)*	91.2(3)
O(3)-Ni(1)-O(2)*	83.8(2)	O(2A)-Ni(3)-O(3)*	172.0(3)
O(1)-Ni(1)-O(2)*	84.9(2)	O(1C)*-Ni(3)-O(3)*	96.1(3)
O(1)*-Ni(1)-O(2)*	95.1(2)	O(1A)-Ni(3)-O(3)*	82.6(3)
O(3)*-Ni(1)-O(2)	83.8(2)	O(2C)*-Ni(3)-O(3)*	94.1(3)
O(3)-Ni(1)-O(2)	96.2(2)	O(2A)-Ni(3)-O(1)	93.0(3)
O(1)-Ni(1)-O(2)	95.1(2)	O(1C)*-Ni(3)-O(1)	82.4(3)
O(1)*-Ni(1)-O(2)	84.9(2)	O(1A)-Ni(3)-O(1)	96.3(3)
O(2)*-Ni(1)-O(2)	180.0(5)	O(2C)*-Ni(3)-O(1)	172.3(3)
O(1C)-Ni(2)-O(2B)	92.9(3)	O(3)*-Ni(3)-O(1)	85.1(2)
O(1C)-Ni(2)-O(1B)	176.1(2)	O(3A)-Ni(4)-O(3B)	87.9(3)
O(2B)-Ni(2)-O(1B)	90.2(3)	O(3A)-Ni(4)-O(1B)	94.4(3)
O(1C)-Ni(2)-O(3C)	88.7(3)	O(3B)-Ni(4)-O(1B)	89.3(3)
O(2B)-Ni(2)-O(3C)	88.2(3)	O(3A)-Ni(4)-O(1A)	87.9(3)
O(1B)-Ni(2)-O(3C)	93.8(3)	O(3B)-Ni(4)-O(1A)	93.1(3)
O(1C)-Ni(2)-O(1)*	82.2(2)	O(1B)-Ni(4)-O(1A)	176.8(3)
O(2B)-Ni(2)-O(1)*	91.6(3)	O(3A)-Ni(4)-O(3)*	170.3(3)
O(1B)-Ni(2)-O(1)*	95.3(3)	O(3B)-Ni(4)-O(3)*	92.6(3)
O(3C)-Ni(2)-O(1)*	171.0(3)	O(1B)-Ni(4)-O(3)*	95.3(3)
O(1C)-Ni(2)-O(2)	93.8(2)	O(1A)-Ni(4)-O(3)*	82.4(3)
O(2B)-Ni(2)-O(2)	172.7(3)	O(3A)-Ni(4)-O(2)	95.4(3)
O(1B)-Ni(2)-O(2)	82.9(2)	O(3B)-Ni(4)-O(2)	172.1(3)
O(3C)-Ni(2)-O(2)	94.7(3)	O(1B)-Ni(4)-O(2)	83.3(2)
O(1)*-Ni(2)-O(2)	86.5(3)	O(1A)-Ni(4)-O(2)	94.2(3)
O(2A)-Ni(3)-O(1C)*	91.4(3)	O(3)*-Ni(4)-O(2)	85.3(3)

Symmetry transformations used to generate equivalent atoms: (*) -x, -y, -z

Table 5.4: Selected bond lengths and angles for $[\text{Co}_7(\text{C}_{12}\text{H}_{13}\text{O}_3)_6(\text{MeO})_6](\text{ClO}_4)_2$

Co(1)-O(30)*	2.080(6)	Co(4)-O(1B)	2.060(8)
Co(1)-O(30)	2.080(6)	Co(4)-O(40)*	2.061(7)
Co(1)-O(40)	2.091(7)	Co(4)-O(3A)	2.077(9)
Co(1)-O(40)*	2.091(7)	Co(4)-O(30)	2.077(6)
Co(1)-O(50)*	2.093(7)	Co(4)-O(1A)	2.079(7)
Co(1)-O(50)	2.093(7)	Co(3)-O(1A)*	2.048(7)
Co(2)-O(3B)	2.050(10)	Co(3)-O(1C)	2.065(7)
Co(2)-O(2C)	2.067(9)	Co(3)-O(2A)*	2.075(8)
Co(2)-O(50)	2.063(7)	Co(3)-O(3C)	2.070(8)
Co(2)-O(1B)	2.064(8)	Co(3)-O(40)	2.084(7)
Co(2)-O(30)	2.073(7)	Co(3)-O(50)	2.083(7)
Co(2)-O(1C)	2.075(7)	O(40)-Co(4)*	2.061(7)
Co(4)-O(2B)	2.056(10)	O(1A)-Co(3)*	2.048(7)
O(30)*-Co(1)-O(30)	180.00(8)	O(2C)-Co(2)-O(1B)	94.4(3)
O(30)*-Co(1)-O(40)	81.7(3)	O(50)-Co(2)-O(1B)	96.3(3)
O(30)-Co(1)-O(40)	98.3(3)	O(3B)-Co(2)-O(30)	169.2(3)
O(30)*-Co(1)-O(40)*	98.3(3)	O(2C)-Co(2)-O(30)	98.6(3)
O(30)-Co(1)-O(40)*	81.7(3)	O(50)-Co(2)-O(30)	82.5(3)
O(40)-Co(1)-O(40)*	180.0(4)	O(1B)-Co(2)-O(30)	81.6(3)
O(30)*-Co(1)-O(50)*	81.7(3)	O(3B)-Co(2)-O(1C)	94.3(3)
O(30)-Co(1)-O(50)*	98.3(3)	O(2C)-Co(2)-O(1C)	87.3(3)
O(40)-Co(1)-O(50)*	97.1(3)	O(50)-Co(2)-O(1C)	82.0(3)
O(40)*-Co(1)-O(50)*	82.9(3)	O(1B)-Co(2)-O(1C)	177.5(3)
O(30)*-Co(1)-O(50)	98.3(3)	O(30)-Co(2)-O(1C)	96.3(3)
O(30)-Co(1)-O(50)	81.7(3)	O(2B)-Co(4)-O(1B)	87.6(4)
O(40)-Co(1)-O(50)	82.9(3)	O(2B)-Co(4)-O(40)*	96.6(3)
O(40)*-Co(1)-O(50)	97.1(3)	O(1B)-Co(4)-O(40)*	96.4(3)
O(50)*-Co(1)-O(50)	180.0(5)	O(2B)-Co(4)-O(3A)	84.1(4)
O(3B)-Co(2)-O(2C)	84.0(4)	O(1B)-Co(4)-O(3A)	94.3(3)
O(3B)-Co(2)-O(50)	96.9(3)	O(40)*-Co(4)-O(3A)	169.3(3)
O(2C)-Co(2)-O(50)	169.3(3)	O(2B)-Co(4)-O(30)	169.0(3)
O(3B)-Co(2)-O(1B)	87.8(3)	O(1B)-Co(4)-O(30)	81.6(3)

O(40)*-Co(4)-O(30)	82.6(3)	O(1C)-Co(3)-O(3C)	87.5(3)
O(3A)-Co(4)-O(30)	98.8(3)	O(2A)*-Co(3)-O(3C)	87.4(3)
O(2B)-Co(4)-O(1A)	94.6(3)	O(1A)*-Co(3)-O(40)	81.7(3)
O(1B)-Co(4)-O(1A)	177.2(3)	O(1C)-Co(3)-O(40)	96.9(3)
O(40)*-Co(4)-O(1A)	81.5(3)	O(2A)*-Co(3)-O(40)	168.9(3)
O(3A)-Co(4)-O(1A)	87.7(3)	O(3C)-Co(3)-O(40)	95.7(3)
O(30)-Co(4)-O(1A)	96.1(3)	O(1A)*-Co(3)-O(50)	96.7(3)
O(1A)*-Co(3)-O(1C)	178.0(3)	O(1C)-Co(3)-O(50)	81.8(3)
O(1A)*-Co(3)-O(2A)*	87.5(3)	O(2A)*-Co(3)-O(50)	95.6(3)
O(1C)-Co(3)-O(2A)*	93.9(3)	O(3C)-Co(3)-O(50)	169.1(3)
O(1A)*-Co(3)-O(3C)	94.0(3)	O(40)-Co(3)-O(50)	83.3(3)

Symmetry transformations used to generate equivalent atoms: (*) -x, -y, -z

5.2.3. FAB characterisation of $[\text{Ni}_7(\text{C}_{12}\text{H}_{13}\text{O}_3)_6(\text{OH})_4(\text{MeO})_2](\text{ClO}_4)_2$ and $[\text{Co}_7(\text{C}_{12}\text{H}_{13}\text{O}_3)_6(\text{OH})_4(\text{MeO})_2](\text{ClO}_4)_2$

The FAB results showed that $[\text{Ni}_7(\text{C}_{12}\text{H}_{13}\text{O}_3)_6(\text{OH})_4(\text{MeO})_2](\text{ClO}_4)_2$ and $[\text{Co}_7(\text{C}_{12}\text{H}_{13}\text{O}_3)_6(\text{OH})_4(\text{MeO})_2](\text{ClO}_4)_2$ are withstanding the FAB experiment (table 5.5 and table 5.6 respectively), which is a priori a little surprising for such big structures held together by large number of hydroxo and methoxo bridges. However, similar polynuclear assemblies have been seen to be stable in solution while running NMR,²³⁰ EPR and Mössbauer²³² experiments on these compounds. Fig. 5.23 shows the characteristic FAB spectra of $[\text{Ni}_7(\text{C}_{12}\text{H}_{13}\text{O}_3)_6(\text{OH})_4(\text{MeO})_2](\text{ClO}_4)_2$.

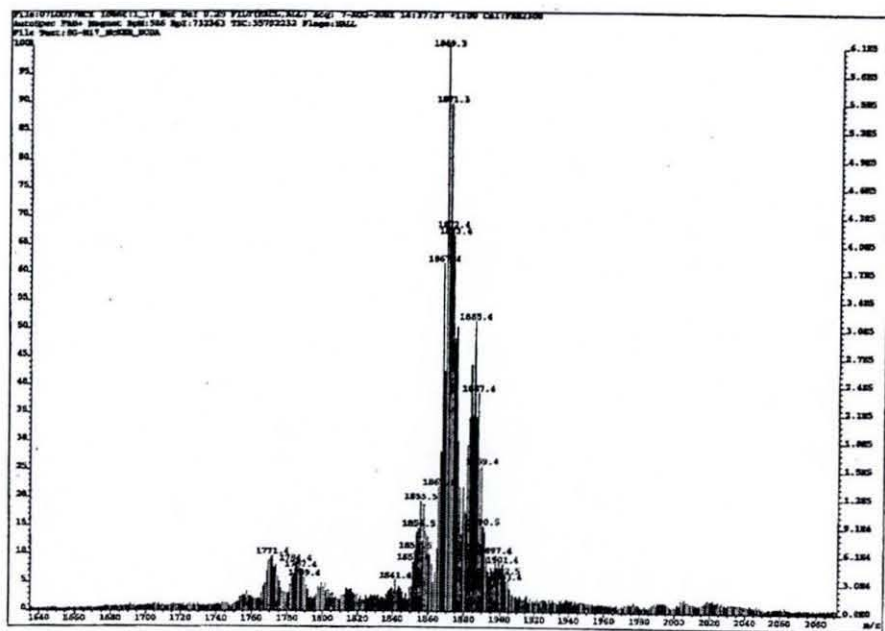
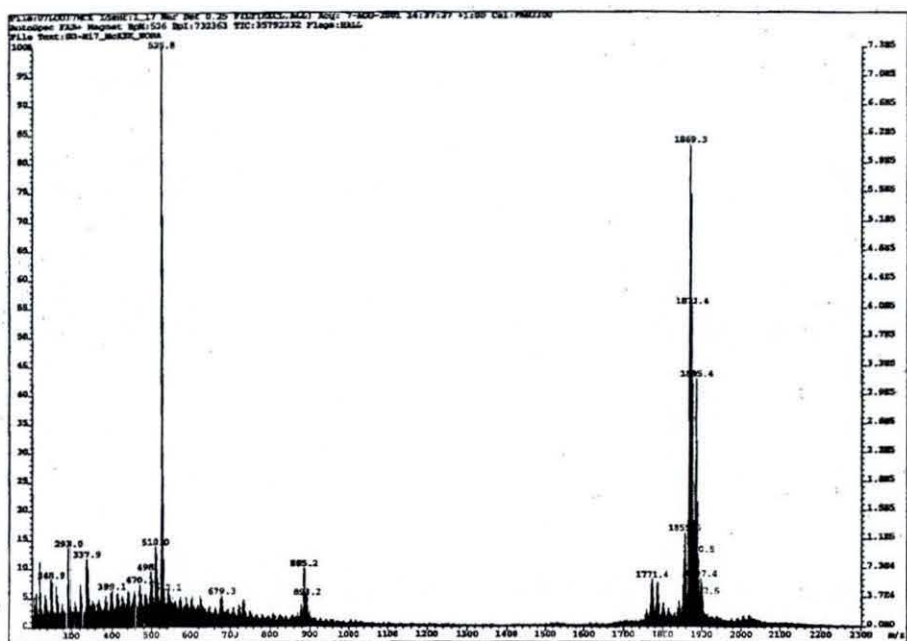


Fig. 5.23: Mass spectra of $[\text{Ni}_7(\text{C}_{12}\text{H}_{13}\text{O}_3)_6(\text{OH})_4(\text{MeO})_2](\text{ClO}_4)_2$

Table 5.5: Peak attributions for $[\text{Ni}_7(\text{C}_{12}\text{H}_{13}\text{O}_3)_6(\text{OH})_4(\text{MeO})_2](\text{ClO}_4)_2$

m/z	Rel. Intensity (%)	Fragments	Calc. Mass
526	100	$[\text{Ni}_2(\text{C}_{12}\text{H}_{13}\text{O}_3)_2]^{2+}$	526
878	< 5	$[\text{Ni}_3(\text{C}_{12}\text{H}_{13}\text{O}_3)_3(\text{OH})_3+\text{H}]^+ \cdot 2\text{H}_2\text{O}$	877
885	12	$[\text{Ni}_3(\text{C}_{12}\text{H}_{13}\text{O}_3)_3(\text{OMe})_2(\text{OH})+\text{H}]^+ \cdot \text{H}_2\text{O}$	887
892	5	$[\text{Ni}_3(\text{C}_{12}\text{H}_{13}\text{O}_3)_3(\text{OMe})(\text{OH})_2+\text{H}]^+ \cdot 2\text{H}_2\text{O}$	891
900	< 5	$[\text{Ni}_3(\text{C}_{12}\text{H}_{13}\text{O}_3)_3(\text{OMe})_3+\text{H}]^+ \cdot \text{H}_2\text{O}$	901
1771	10	$[\text{Ni}_7(\text{C}_{12}\text{H}_{13}\text{O}_3)_6(\text{OMe})_2(\text{OH})_4]^{2+}$	1766
1788	10	$[\text{Ni}_7(\text{C}_{12}\text{H}_{13}\text{O}_3)_6(\text{OMe})_2(\text{OH})_4]^{2+} \cdot \text{H}_2\text{O}$	1784
1800	5	$[\text{Ni}_7(\text{C}_{12}\text{H}_{13}\text{O}_3)_6(\text{OMe})_2(\text{OH})_4]^{2+} \cdot \text{MeOH}$	1798
1815	< 5	$[\text{Ni}_7(\text{C}_{12}\text{H}_{13}\text{O}_3)_6(\text{OMe})_2(\text{OH})_4]^{2+} \cdot \text{MeOH}, \text{H}_2\text{O}$	1816
1854	15	$[\text{Ni}_7(\text{C}_{12}\text{H}_{13}\text{O}_3)_6(\text{OMe})_6]^{2+} \cdot \text{MeOH}$	1854
1869	85	$[\text{Ni}_7(\text{C}_{12}\text{H}_{13}\text{O}_3)_6(\text{OMe})_2(\text{OH})_4(\text{ClO}_4)]^+$	1865
1885	15	$[\text{Ni}_7(\text{C}_{12}\text{H}_{13}\text{O}_3)_6(\text{OMe})_2(\text{OH})_4(\text{ClO}_4)]^+ \cdot \text{H}_2\text{O}$	1883
1897	5	$[\text{Ni}_7(\text{C}_{12}\text{H}_{13}\text{O}_3)_6(\text{OMe})_2(\text{OH})_4(\text{ClO}_4)]^+ \cdot \text{MeOH}$	1897
1925	< 5	$[\text{Ni}_7(\text{C}_{12}\text{H}_{13}\text{O}_3)_6(\text{OMe})_5(\text{OH})(\text{ClO}_4)]^+ \cdot \text{H}_2\text{O}$	1925
1936	< 5	$[\text{Ni}_7(\text{C}_{12}\text{H}_{13}\text{O}_3)_6(\text{OMe})_6(\text{ClO}_4)]^+ \cdot \text{H}_2\text{O}$	1939

Table 5.6: Peak attributions for $[\text{Co}_7(\text{C}_{12}\text{H}_{13}\text{O}_3)_6(\text{OH})_4(\text{MeO})_2](\text{ClO}_4)_2$

m/z	Rel. Intensity (%)	Fragments	Calc. Mass
528	100	$[\text{Co}_2(\text{C}_{12}\text{H}_{13}\text{O}_3)_2]^{2+}$	528
888	15	$[\text{Co}_3(\text{C}_{12}\text{H}_{13}\text{O}_3)_3(\text{OMe})_2(\text{OH})_2+\text{H}]^+$	889
1771	10	$[\text{Co}_7(\text{C}_{12}\text{H}_{13}\text{O}_3)_6(\text{OMe})_2(\text{OH})_4]^{2+}$	1773
1789	10	$[\text{Co}_7(\text{C}_{12}\text{H}_{13}\text{O}_3)_6(\text{OMe})_2(\text{OH})_4]^{2+} \cdot \text{H}_2\text{O}$	1791
1800	5	$[\text{Co}_7(\text{C}_{12}\text{H}_{13}\text{O}_3)_6(\text{OMe})_2(\text{OH})_4]^{2+} \cdot \text{MeOH}$	1805
1859	15	$[\text{Co}_7(\text{C}_{12}\text{H}_{13}\text{O}_3)_6(\text{OMe})_6]^{2+} \cdot \text{MeOH}$	1861
1870	80	$[\text{Co}_7(\text{C}_{12}\text{H}_{13}\text{O}_3)_6(\text{OMe})_2(\text{OH})_4(\text{ClO}_4)]^+$	1872
1888	15	$[\text{Co}_7(\text{C}_{12}\text{H}_{13}\text{O}_3)_6(\text{OMe})_2(\text{OH})_4(\text{ClO}_4)]^+ \cdot \text{H}_2\text{O}$	1890
1932	< 5	$[\text{Co}_7(\text{C}_{12}\text{H}_{13}\text{O}_3)_6(\text{OMe})_5(\text{OH})(\text{ClO}_4)]^+ \cdot \text{H}_2\text{O}$	1932
1947	< 5	$[\text{Co}_7(\text{C}_{12}\text{H}_{13}\text{O}_3)_6(\text{OMe})_6]^{2+} \cdot \text{MeOH}$	1946

The FAB spectra of $[\text{Ni}_7(\text{C}_{12}\text{H}_{13}\text{O}_3)_6(\text{OH})_4(\text{MeO})_2](\text{ClO}_4)_2$ and $[\text{Co}_7(\text{C}_{12}\text{H}_{13}\text{O}_3)_6(\text{OH})_4(\text{MeO})_2](\text{ClO}_4)_2$ are essentially quite similar. It is noteworthy that in both cases, there are not many peaks corresponding to the fragmentation of the cluster. Only two sets of peaks at *ca.* m/z 528 and 888-894 corresponding to the dinuclear and trinuclear fragment respectively. All the remaining peaks above *ca.* m/z 888 correspond to the complete M_7 cluster with the loss of one or both perchlorate anions. For both complexes, three peaks can be attributed to $[\text{M}_7(\text{C}_{12}\text{H}_{13}\text{O}_3)_6(\text{OMe})_6]^{2+} \cdot \text{MeOH}$ (m/z 1854 and 1859), $[\text{M}_7(\text{C}_{12}\text{H}_{13}\text{O}_3)_6(\text{OMe})_2(\text{OH})_4\text{ClO}_4]^+ \cdot \text{H}_2\text{O}$ (m/z 1885 and 1888) and $[\text{M}_7(\text{C}_{12}\text{H}_{13}\text{O}_3)_6(\text{OMe})_5(\text{OH})(\text{ClO}_4)]^+ \cdot \text{H}_2\text{O}$ (m/z 1925 and 1932), which implies that some rearrangements occur in solution with the possible existence of equilibria between molecules containing different numbers of hydroxy and methoxy bridges. The fact that, for the cobalt complex, the elemental analysis of the powder does not match the formula of the crystals might be an indication that some kind of rearrangement occurred during the crystallisation. According to the elemental analysis results, there is no mixture in the compounds isolated as $[\text{Ni}_7(\text{C}_{12}\text{H}_{13}\text{O}_3)_6(\text{OH})_4(\text{MeO})_2](\text{ClO}_4)_2$ and $[\text{Co}_7(\text{C}_{12}\text{H}_{13}\text{O}_3)_6(\text{OH})_4(\text{MeO})_2](\text{ClO}_4)_2$ so it can be assumed that these exchanges occur in solution.

To further study their stability in solution, it was decided to run a FAB experiment on $[\text{Ni}_7(\text{C}_{12}\text{H}_{13}\text{O}_3)_6(\text{OH})_4(\text{MeO})_2](\text{ClO}_4)_2$ over a period of three weeks. Slight variations have been observed in the spectrum but the peaks attributed to the Ni_7 cluster are still present after three weeks in solution (methanol) (table 5.7). The peaks corresponding to the M_7 cluster seem to diminish slightly in intensity, while the peaks corresponding to the trinuclear fragments seem to rise in intensity, which indicates that more fragments are present but not all originated from the FAB experiment only.

Table 5.7: Variations in the FAB spectra for $[\text{Ni}_7(\text{C}_{12}\text{H}_{13}\text{O}_3)_6(\text{OH})_4(\text{MeO})_2](\text{ClO}_4)_2$

m/z	Rel. Intensity (%)	Rel. Intensity (%) After 1 week	Rel. Intensity (%) After 2 week	Rel. Intensity (%) After 3 week
526	100	100	100	100
878	< 5	< 5	10	15
885	12	10	45	55
892	5	9	30	35
900	< 5	5	13	10
1771	10	12	17	30
1788	10	12	15	28
1800	5	5	10	20
1815	< 5	< 5	10	10
1854	15	15	< 5	10
1869	85	60	13	50
1885	15	60	10	25
1897	5	15	< 5	<5
1925	< 5	< 5	< 5	7
1936	< 5	< 5	< 5	5

5.2.4. Magnetic studies

Variable-temperature magnetic measurements were carried out by Dr C.J. Harding at the Open University, Milton Keynes as described in the experimental section.

5.2.4.1. $[\text{Ni}_7(\text{C}_{12}\text{H}_{13}\text{O}_3)_6(\text{OH})_4(\text{MeO})_2](\text{ClO}_4)_2$

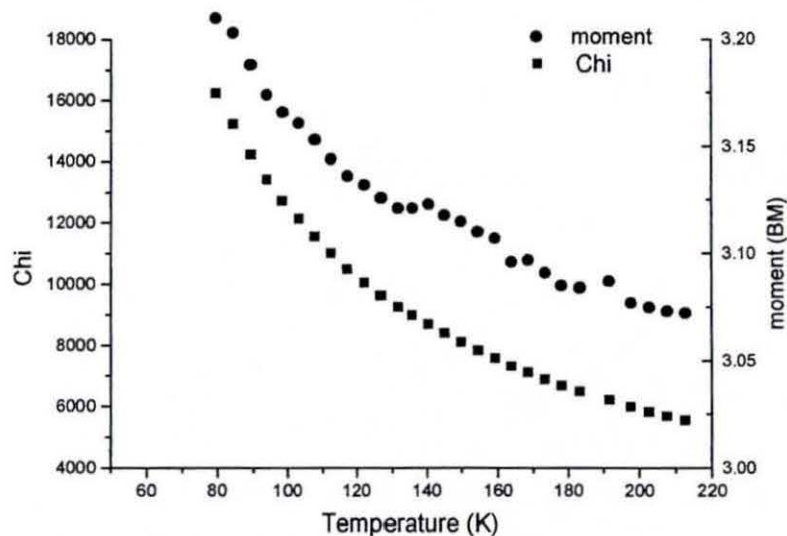


Fig. 5.24: Experimental (■) magnetic susceptibility and (●) magnetic moment for $[\text{Ni}_7(\text{C}_{12}\text{H}_{13}\text{O}_3)_6(\text{OH})_4(\text{MeO})_2](\text{ClO}_4)_2$

The molecular magnetic susceptibility of $[\text{Ni}_7(\text{C}_{12}\text{H}_{13}\text{O}_3)_6(\text{OH})_4(\text{MeO})_2](\text{ClO}_4)_2$ displayed in fig. 5.24, was measured over the temperature range 79.4-276.5 K. The effective magnetic moment μ_{eff} , increases from 3.067 to 3.210 B.M with the decreasing temperature. These values are in accordance with Ni(II) being in a high-spin state. The magnetic susceptibility is steadily increasing while the temperature is decreasing.

These preliminary magnetic studies show a net ferromagnetic interaction between the Ni(II) centres. In the light of the high-spin polynuclear cluster chemistry, this

observation is of interest and merits further investigations to study the magnetic behaviour at lower temperature and determine the spin value of the ground state.

5.2.4.2. $[\text{Co}_7(\text{C}_{12}\text{H}_{13}\text{O}_3)_6(\text{OH})_4(\text{MeO})_2](\text{ClO}_4)_2$

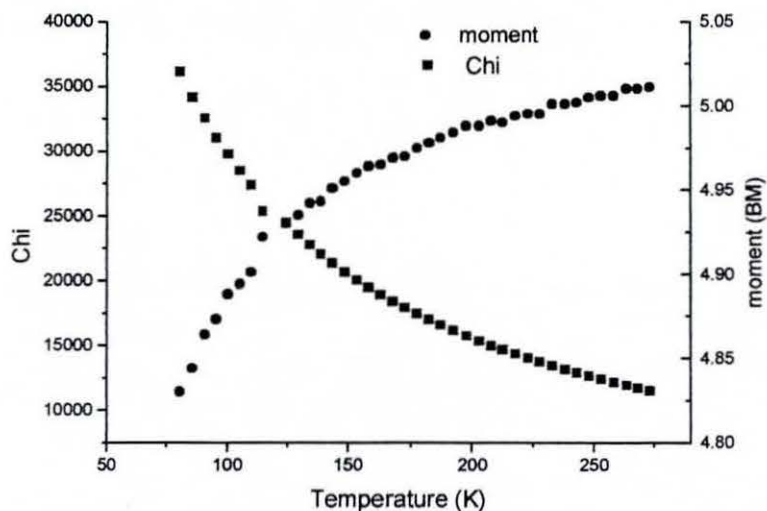


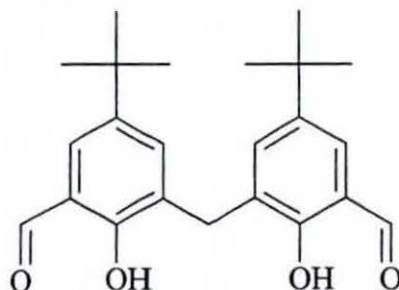
Fig. 5.25: Experimental (■) magnetic susceptibility and (●) magnetic moment for $[\text{Co}_7(\text{C}_{12}\text{H}_{13}\text{O}_3)_6(\text{OH})_4(\text{MeO})_2](\text{ClO}_4)_2$

The molecular magnetic susceptibility of $[\text{Co}_7(\text{C}_{12}\text{H}_{13}\text{O}_3)_6(\text{OH})_4(\text{MeO})_2](\text{ClO}_4)_2$ is displayed in fig. 5.25, was measured over the temperature range 80.8-278.2 K. The effective magnetic moment μ_{eff} , increases from 4.83 to 5.01 B.M with the increasing temperature. These values are expected for high-spin Co(II) in an octahedral environment. The magnetic susceptibility is steadily increasing while the temperature is decreasing.

These preliminary magnetic studies show a net antiferromagnetic interaction between the Co(II) centres.

5.3. A trinuclear Mn(II) complex

5.3.1. Synthesis and characterisations (IR and FAB) of $[\text{Mn}_3(\text{C}_{23}\text{H}_{26}\text{O}_4)_2(\text{CH}_3\text{OH})_4(\text{H}_2\text{O})](\text{ClO}_4)_2$



$\text{C}_{23}\text{H}_{28}\text{O}_4$ (DHTMB)

Fig. 5.26: Ligand DHTMB

$[\text{Mn}_3(\text{C}_{23}\text{H}_{26}\text{O}_4)_2(\text{CH}_3\text{OH})_4(\text{H}_2\text{O})](\text{ClO}_4)_2$ was isolated with a reasonable yield (57%) in our attempts to synthesise polynuclear clusters using DHTMB. This time, triethylamine was employed instead of sodium hydroxide, which is in some cases too strong to produce high-nuclearity cluster. However, the attempt failed to produce the desired aggregates with a number of metal ions superior to four.

A difference is seen in the IR spectra of the complex $[\text{Mn}_3(\text{C}_{23}\text{H}_{26}\text{O}_4)_2(\text{CH}_3\text{OH})_4(\text{H}_2\text{O})](\text{ClO}_4)_2$ in contrast to that of the non-coordinated ligand DHTMB. Instead of only one band attributed to the C=O stretch at 1658 cm^{-1} , the IR spectra shows two bands at 1591 and 1647 cm^{-1} . This observation supports the coordination of the ligand and gives an indication of an unsymmetrical coordination of the latter as demonstrated by the X-ray study. The counter anion being perchlorate the expected two bands at 1121 and 626 cm^{-1} are observed.

The FAB results support the formation of the trinuclear complex $[\text{Mn}_3(\text{C}_{23}\text{H}_{26}\text{O}_4)_2(\text{CH}_3\text{OH})_4(\text{H}_2\text{O})](\text{ClO}_4)_2$. The peak assignments are given in table 5.8. However, the peak at m/z 1288 can be attributed to $\text{Mn}_3(\text{C}_{23}\text{H}_{26}\text{O}_4)_2(\text{EtOH})_3^-$

$(\text{H}_2\text{O})(\text{ClO}_4)_2+\text{H}]^+ \cdot 2\text{H}_2\text{O}$, which implies a solvent exchange has taken place, methanol molecules being replaced by ethanol molecules. As the elemental analysis is consistent with the formula $[\text{Mn}_3(\text{C}_{23}\text{H}_{26}\text{O}_4)_2(\text{CH}_3\text{OH})_4(\text{H}_2\text{O})](\text{ClO}_4)_2$, the solvent exchange is likely to have happened during the FAB experiment within the noba matrix as the solvent used was ethanol.

Table 5.8: Peak attributions for $[\text{Mn}_3(\text{C}_{23}\text{H}_{26}\text{O}_4)_2(\text{CH}_3\text{OH})_4(\text{H}_2\text{O})](\text{ClO}_4)_2$

m/z	Rel. Intensity (%)	Fragments	Calc. Mass
1074	15	$\text{Mn}_3(\text{C}_{23}\text{H}_{26}\text{O}_4)_2(\text{MeOH})_4(\text{H}_2\text{O})]^+ \cdot \text{MeOH}$	1075
1265	50	$\text{Mn}_3(\text{C}_{23}\text{H}_{26}\text{O}_4)_2(\text{MeOH})_4(\text{H}_2\text{O})(\text{ClO}_4)_2 + \text{Na}]^+$	1264
1288	15	$\text{Mn}_3(\text{C}_{23}\text{H}_{26}\text{O}_4)_2(\text{EtOH})_3(\text{H}_2\text{O})(\text{ClO}_4)_2 + \text{H}]^+ \cdot 2\text{H}_2\text{O}$	1288

5.3.2. X-ray characterisation of $[\text{Mn}_3(\text{C}_{23}\text{H}_{26}\text{O}_4)_2(\text{CH}_3\text{OH})_4(\text{H}_2\text{O})](\text{ClO}_4)_2$

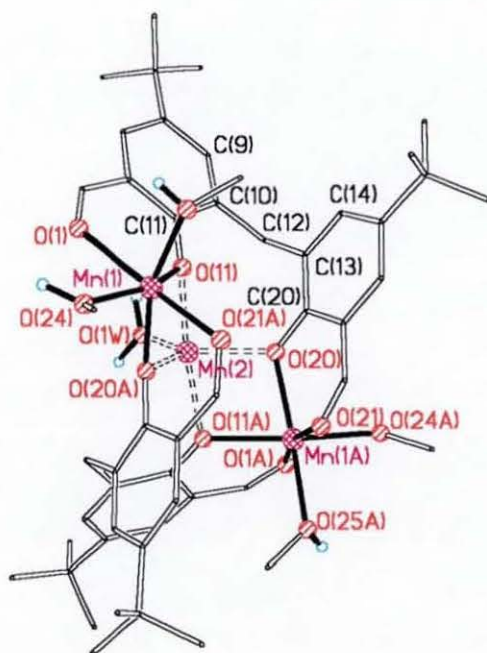


Fig. 5.27: Structure of the cation $[\text{Mn}_3(\text{C}_{23}\text{H}_{26}\text{O}_4)_2(\text{CH}_3\text{OH})_4(\text{H}_2\text{O})]^{2+}$

Here again, as demonstrated in chapter 3 for macrocyclic ligands containing a DHTMB head-unit, the DHTMB ligand alone can lead to the isolation of complexes with original and variable conformations; one example is the complex $[\text{Mn}_3(\text{C}_{23}\text{H}_{26}\text{O}_4)_2(\text{CH}_3\text{OH})_4(\text{H}_2\text{O})](\text{ClO}_4)_2$. Crystals of $[\text{Mn}_3(\text{C}_{23}\text{H}_{26}\text{O}_4)_2(\text{CH}_3\text{OH})_4(\text{H}_2\text{O})](\text{ClO}_4)_2$ suitable for X-ray studies were grown by slow diffusion of diethylether into a MeOH/CH₃CN solution of the compound. The structure (fig. 5.28) consists of three Mn(II), two of which are in a distorted octahedral environment (Mn(1) and Mn(1A)) while the remaining manganese ion in the centre (Mn(2)) adopts a distorted trigonal bipyramidal geometry (fig. 5.28). The three manganese ions are situated at the corners of a triangle.

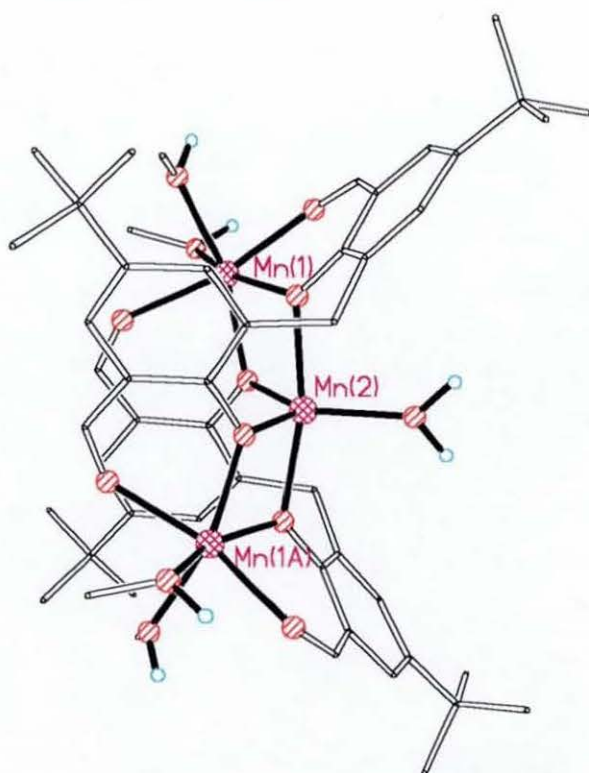


Fig. 5.28: Structure of the cation $[\text{Mn}_3(\text{C}_{23}\text{H}_{26}\text{O}_4)_2(\text{CH}_3\text{OH})_4(\text{H}_2\text{O})]^{2+}$

Mn(1A) is the symmetry equivalent of Mn(1), while Mn(2) is situated on the inversion centre. The two separate DHTMB fragments are bridging all three

manganese ions. Mn(1) is doubly chelated by the adjacent carboxy and phenoxy oxygen atoms (O(1) and O(11); O(21A) and O(20A)) of two symmetry equivalent DHTMB molecules forming a 6-membered ring. Its symmetry equivalent Mn(1A) is chelated by the adjacent carboxy and phenoxy oxygen atoms remaining on each DHTMB fragment. Their coordination sphere is completed by two methanol molecules. Mn(2) is doubly bridged to Mn(1) and Mn(1A) through two sets of phenoxy oxygen atoms (O(11) and O(20); O(11A) and O(20A)). A water molecule occupies the third coordination site of the trigonal plane formed by O(20), O(20A) and O(1W). The Mn-O distances are within the range of values observed for Mn(II) ions.⁸⁹ The selected bond lengths and angles are given in table 5.9. All the X-ray data collection parameters for $[\text{Mn}_3(\text{C}_{23}\text{H}_{26}\text{O}_4)_2(\text{CH}_3\text{OH})_4(\text{H}_2\text{O})](\text{ClO}_4)_2$ are summarised in table 3 in annex 4.

Table 5.9: Selected bond lengths [\AA] and angles [$^\circ$] for $[\text{Mn}_3(\text{C}_{23}\text{H}_{26}\text{O}_4)_2(\text{CH}_3\text{OH})_4(\text{H}_2\text{O})](\text{ClO}_4)_2$

Mn(2)-O(20)*	2.080(3)	Mn(1)-O(11)	2.146(3)
Mn(2)-O(20)	2.080(3)	Mn(1)-O(25)	2.177(4)
Mn(2)-O(1W)	2.086(5)	Mn(1)-O(24)	2.179(4)
Mn(2)-O(11)*	2.144(3)	Mn(1)-O(1)	2.188(3)
Mn(2)-O(11)	2.144(3)	Mn(1)-O(21)*	2.206(4)
Mn(1)-O(20)*	2.121(3)		
O(20)*-Mn(2)-O(20)	118.65(19)	O(20)*-Mn(1)-O(11)	78.71(13)
O(20)*-Mn(2)-O(1W)	120.68(10)	O(20)*-Mn(1)-O(25)	160.87(14)
O(20)-Mn(2)-O(1W)	120.68(10)	O(24)-Mn(1)-O(21)*	89.51(14)
O(20)*-Mn(2)-O(11)*	93.68(13)	O(11)-Mn(1)-O(25)	99.78(14)
O(20)-Mn(2)-O(11)*	79.64(13)	O(20)*-Mn(1)-O(24)	98.82(14)
O(1W)-Mn(2)-O(11)*	96.51(9)	O(11)-Mn(1)-O(24)	159.06(14)
O(20)*-Mn(2)-O(11)	79.64(13)	O(25)-Mn(1)-O(24)	89.20(15)
O(20)-Mn(2)-O(11)	93.68(13)	O(20)*-Mn(1)-O(1)	111.69(13)
O(1W)-Mn(2)-O(11)	96.51(9)	O(11)-Mn(1)-O(1)	81.41(13)
O(11)*-Mn(2)-O(11)	166.98(18)	O(25)-Mn(1)-O(1)	86.69(14)

O(24)-Mn(1)-O(1)	80.26(13)	O(11)-Mn(1)-O(21)*	110.14(13)
O(20)*-Mn(1)-O(21)*	79.01(13)	O(25)-Mn(1)-O(21)*	83.75(14)
O(1)-Mn(1)-O(21)*	166.09(13)		

Symmetry transformations used to generate equivalent atoms: (*) $-x+3/2, y, -z$

As described in chapter 3, the DHTMB fragment is able to adopt a variety of geometrical conformations due to the saturated carbon C(12) linking the two phenyl rings. The two aryl rings are able to rotate around the saturated carbon C(12), which enables the rings to come closer together, hence enables the molecule to adopt a folded conformation. The value of the angle between the planes of the two phenyl rings is $44.11(11)^\circ$. Furthermore, the phenyl rings can rotate along the bond linking the ring to C(12) (see torsion angles in table 5.10), which permits some flexibility for the coordination of the oxygen atoms. The oxygen atoms can be situated on the same side (*syn*-configuration), on the opposite side (*anti*-configuration) or in some position along the 360° of rotation available to the phenyl ring. For $[\text{Mn}_3(\text{C}_{23}\text{H}_{26}\text{O}_4)_2(\text{CH}_3\text{OH})_4(\text{H}_2\text{O})](\text{ClO}_4)_2$, the configuration adopted is *syn*.

Table 5.10: Selected torsion angles [$^\circ$] for $[\text{Mn}_3(\text{C}_{23}\text{H}_{26}\text{O}_4)_2(\text{CH}_3\text{OH})_4(\text{H}_2\text{O})](\text{ClO}_4)_2$

	Torsion angles in $^\circ$
C(9)-C(10)-C(12)-C(13)	126.0(5)
C(11)-C(10)-C(12)-C(13)	-58.7(6)
C(10)-C(12)-C(13)-C(14)	-69.9(6)
C(10)-C(12)-C(13)-C(20)	109.7(5)

Another notable feature is that both perchlorate anions are interacting with a coordinated methanol molecule through hydrogen bonding as shown in fig. 5.29.

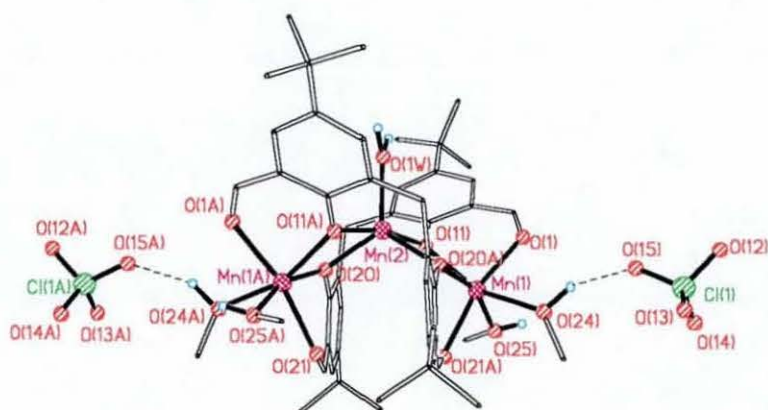


Fig. 5.29: Structure of $[\text{Mn}_3(\text{C}_{23}\text{H}_{26}\text{O}_4)_2(\text{CH}_3\text{OH})_4(\text{H}_2\text{O})](\text{ClO}_4)_2$ showing the hydrogen-bonding

The bond lengths and angles involved in hydrogen-bonding are given below in table 5.11.

Table 5.11: Hydrogen bonds [\AA and $^\circ$] for complex $[\text{Mn}_3(\text{C}_{23}\text{H}_{26}\text{O}_4)_2(\text{CH}_3\text{OH})_4(\text{H}_2\text{O})](\text{ClO}_4)_2$

D-H...A	d(D-H)	d(H...A)	d(D...A)	$\angle(\text{DHA})$
O(24)-H(24)...O(15)	1.02	1.91	2.854(5)	153.0
O(25)-H(25)...O(14)**	0.87	1.95	2.787(5)	162.0
O(1W)-H(1W)...O(15) [#]	1.06	1.71	2.764(5)	172.9

Symmetry transformations used to generate equivalent atoms: (*) $-x+3/2, y, -z$ (**) $-x+1/2, y, -z$

([#]) $x+1/2, -y+1, z$

As shown in the packing diagram (fig. 5.30), the perchlorate anions are hydrogen-bonded to the coordinated methanol molecule of an individual complex and to the water molecule of the adjacent complex forming chains (only one of those chains appears in the packing diagram for clarity).

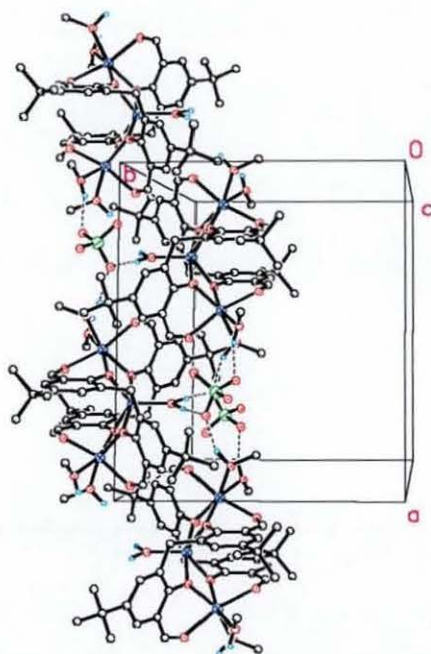


Fig. 5.30: Packing of $[\text{Mn}_3(\text{C}_{23}\text{H}_{26}\text{O}_4)_2(\text{CH}_3\text{OH})_4(\text{H}_2\text{O})](\text{ClO}_4)_2$ showing one hydrogen-bonded chain

5.4. Conclusion

Although the complex $[\text{Ni}_7(\text{C}_{12}\text{H}_{13}\text{O}_3)_6(\text{OH})_4(\text{MeO})_2](\text{ClO}_4)_2$ was first isolated by accident, the systematic synthesis of $[\text{Ni}_7(\text{C}_{12}\text{H}_{13}\text{O}_3)_6(\text{OH})_4(\text{MeO})_2](\text{ClO}_4)_2$ was achieved. Using the same procedure as for the Ni_7 complex, a very similar Co_7 complex $[\text{Co}_7(\text{C}_{12}\text{H}_{13}\text{O}_3)_6(\text{OH})_4(\text{MeO})_2](\text{ClO}_4)_2$ was synthesised. Further investigation will be needed to try and obtain better yields. The preliminary magnetic studies on $[\text{Co}_7(\text{C}_{12}\text{H}_{13}\text{O}_3)_6(\text{OH})_4(\text{MeO})_2](\text{ClO}_4)_2$ revealed a net antiferromagnetic interaction between the cobalt centres whereas for $[\text{Ni}_7(\text{C}_{12}\text{H}_{13}\text{O}_3)_6(\text{OH})_4(\text{MeO})_2](\text{ClO}_4)_2$ it revealed a net ferromagnetic interaction. For the Ni_7 complex, the magnetic behaviour merits a more in-depth study especially at lower temperature, as polynuclear paramagnetic compounds are of interest to both chemistry and physics

due to their potential to have a ground state with a large spin and possibly behave as paramagnets.

Preliminary studies on the stability in solution of those polynuclear complexes have been monitored by FAB spectrometry. They demonstrated that the complexes are relatively stable during the FAB experiment because the peak corresponding to the entire cluster can be observed. Even after a month in solution, the spectra still showed the presence of a reasonable amount of complex.

In the course of this study an interesting trinuclear Mn(II) complex $[\text{Mn}_3(\text{C}_{23}\text{H}_{26}\text{O}_4)_2(\text{CH}_3\text{OH})_4(\text{H}_2\text{O})](\text{ClO}_4)_2$ has been isolated, that shows that a variety of complexes could be accessible using the fragment DHTMB, which possesses some degree of flexibility.

Chapter six

Experimental

E.1. General experimental conditions

E.1.1. Solvents and reagents

Solvents for preparative chemistry were chemically pure grade or HPLC grade and were used without further purification unless stated otherwise. Reagents that were not prepared in this work were Analar or reagent grade and were used without further purification. For the electrochemistry experiments: KH_2PO_4 , K_2HPO_4 , KOH , H_3PO_4 , CH_3COOH (Aldrich) were obtained commercially and used without further purification. Distilled and filtered water with a resistivity of not less than $18 \text{ M}\Omega \text{ cm}$ was obtained from an Elgastat water purification system (Elga, Bucks, UK). Solutions were degassed with argon (Pureshield, BOC) for at least 15 minutes prior to undertaking experiments.

Methanol and ethanol were dried by conversion respectively to the methanoate and ethanoate²³⁴ as described below.

Magnesium turnings (5 g) and iodine (0.50 g) were refluxed in 100 mL of methanol for 30 min. to 1 h. (until all the iodine had disappeared and a white precipitate of methoxide or ethoxide had formed). Methanol or ethanol (1 L) dried on molecular sieves was then added and the solution refluxed for 3-4 h. The dry methanol or ethanol was finally distilled off into oven-dried bottles containing activated molecular sieves.

Dimethylformamide was dried over activated molecular sieves overnight.

E.1.2. Physical measurements

^1H NMR spectra (500 MHz) were recorded on a Bruker AC500FT spectrometer (Belfast) with δ referenced to CDCl_3 and on a Bruker AC250FT spectrometer with δ referenced to external SiMe_4 (Loughborough).

Infrared spectra were recorded as KBr pellets in the range $4000\text{--}450\text{ cm}^{-1}$ on a Bio-Rad FTS-185 Fourier Transform Infrared spectrometer (Belfast) and on a Perkin-Elmer System 2000 Fourier Transform spectrometer (Loughborough).

Variable-temperature magnetic measurements were carried out by Dr C.J. Harding at The Open University, Milton Keynes, on polycrystalline samples using a Faraday type magnetometer (Oxford Instruments), equipped with a helium continuous-flow cryostat working in the temperature range $80\text{--}280\text{ K}$, and an electromagnet operating at a magnetic field of 0.8 T . Diamagnetic corrections were estimated from standard Pascal values. Room temperature magnetic susceptibilities were measured using a Sherwood Scientific magnetic susceptibility balance within the chemistry department at Loughborough University.

Elemental analyses were performed by A.S.E.P. at the Queen's University of Belfast and by the Loughborough University Service within the chemistry department.

Low resolution Fast Atom Bombardment (FAB) and low resolution EI mass spectra were performed by the EPSRC National Mass Spectrometry Service Centre, Swansea.

Voltammetric experiments were carried out with a PGSTAT 30 Autolab potentiostat system (Eco Chemie, Netherlands) in a three-electrode conical glass cell. In aqueous solution the counter electrode was a Pt gauze, the reference electrode was a saturated Calomel electrode (SCE, Radiometer), and the working electrodes were prepared as follows. A 4.9 mm diameter basal plane pyrolytic graphite electrode, polished with a SiC paper (1200 grit), was pushed into a $1\text{--}3\text{ mg}$ quantity of the metal compound on a

clean filter paper (Whatman 1). By moving the electrode under gently applied pressure a reproducible and even coverage of mechanically adhered microcrystalline particles was achieved. After immersion of the modified electrode in aqueous buffer (phosphate (pH 7) or acetate (pH 6)) solution, conventional (staircase) voltammetry techniques were employed. Microelectrode experiments were conducted with a 10 mm diameter platinum electrode.

For the experiments conducted in an organic solution, a 2 mM MeOH solution of $[\text{Mn}_4(\text{L11})(\text{MeOH})_4(\text{MeO})_2(\text{OAc})_2]\text{Cl}_2$ containing NBu_4PF_6 (0.1 M) as an electrolyte was used.

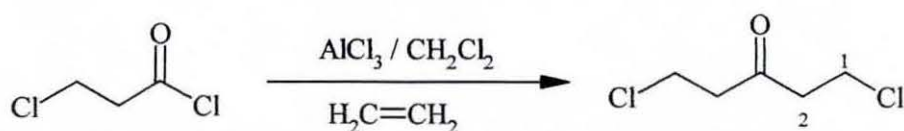
E.2. Chapter 2

E.2.1. Organic preparations

E.2.1.1. 1,5-Diaminopentan-3-ol dihydrochloride (DAHP.2HCl) (2.1)

1,5-Diaminopentan-3-ol was prepared in 68% overall yield from 3-chloropropionyl chloride in four steps using the method reported by Wikaira,⁹⁷ which is an adaptation of the overall method of Owen *et al.*²³⁵ and Murase *et al.*²³⁶

Step 1: 3-chloropropionyl chloride \rightarrow 1,5-dichloropentan-3-one



The Friedel-Crafts alkylation as reported by Owen²³⁵ was carried out.

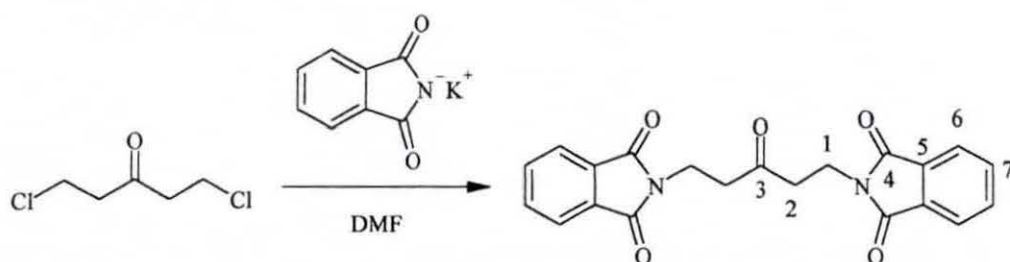
3-Chloropropionyl chloride (100 g, 0.76 mol) was added slowly to a mechanically stirred and cooled (ice bath) suspension of dry AlCl_3 (147 g, 1.10 mol) in

dichloromethane (200 mL - dried over molecular sieves). The reaction was carried out in a three-necked flask. HCl gas was evolved during the addition. The solution was allowed to warm up to ambient temperature and ethylene gas was flushed through the mixture for a minimum of 5 h. It was found that really vigorous stirring at this step of the reaction significantly increased the yield and that it was not necessary to have the gas bubbling through the mixture but simply replacing the ethylene atmosphere as it was used, was sufficient. The golden solution was then tested for starting material by taking about 0.1 mL, adding the same amount of water, separating the dichloromethane layer, and after evaporating the CH_2Cl_2 , examining the infrared spectrum of the remaining oil. The absorption at 1715 cm^{-1} was indicative of the product and the disappearance of the initial carbonyl band at 1790 cm^{-1} verified the completion of the reaction. The yield was further increased by continuing to stir the stoppered reaction for some time, e.g. overnight, after the gas flow had been discontinued. The resulting solution was then added cautiously, maintaining the temperature below 20°C , to a slush of ice (400 mL i.e. the aqueous layer), dichloromethane (100 mL) and conc. HCl (40 mL) in a high-sided beaker. A little extra HCl was added to ensure that all the AlCl_3 had been removed. The blue-black organic phase was separated, washed with $4 \times 400\text{ mL}$ of water, the water layers were saved and re-extracted with CH_2Cl_2 and the combined organic layers dried over MgSO_4 for 2 h. Evaporation of the dichloromethane under vacuum left 1,5-dichloropentan-3-one as a blue-black oil (114 g, 0.72 mol, 94%). The greatly improved yield (94% *cf.* lit. 55%) is partly attributed to the vigorous and prolonged mixing with ethylene at this step of the reaction.

IR (KBr, cm^{-1}): 2972(s,m); 1720(s, $\nu_{\text{C=O}}$)

NMR (CDCl_3 , ppm, ^1H): 2.94(t, 2H, $-\text{C}^1\text{H}_2-$); 3.76(t, 2H, $-\text{C}^2\text{H}_2-$)

Step 2: 1,5-dichloropentan-3-one → 1,5-diphthalimidopentan-3-one



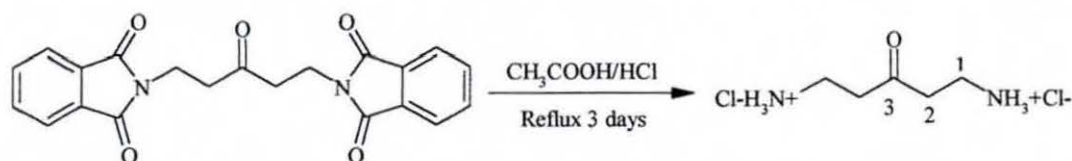
Phthalimide groups were substituted for chlorines by the method of Murase *et al.*²³⁶ As reported by Wikaira,⁹⁷ it was decided that the phthalimide should be at least a 2:1 ratio to the ketone at this step (for some reason none of the previously reported syntheses have a greater ratio than 1.3:1 ratio).

Potassium phthalimide (330 g, 1.78 mol) was vigorously stirred in dimethylformamide (630 mL, dried over molecular sieves), while crude 1,5-dichloropentan-3-one (138 g, 0.89 mol) was added drop-wise over 1 h. during which time the suspension increased in temperature and changed colour from white to brown. The resulting mixture was heated at 80-85°C for 6 h. and allowed to stand at room temperature overnight. The resulting 1,5-diphthalimidopentan-3-one was collected in a frit under vacuum and washed successively with chloroform (as this wash removes the excess organic product, it was repeated), water and acetone to produce a white powder. Yield: 226 g, 0.60 mol, 67.5%.

IR (KBr, cm^{-1}): 1774(s, $\nu_{\text{C}=\text{O}}$); 1708(s,b, phthalimido $\nu_{\text{C}=\text{O}}$)

NMR (d-DMF, ppm, ^{13}C): 33.37(C1); 40.87(C2); 206.92(C3); 168.50(C4);
132.73(C5); 123.55(C6); 134.9(C7)

Step 3: 1,5-diphtalimidopentan-3-one → 1,5-diaminopentan-3-one dihydrochloride



The harsh reaction conditions outlined by Murase *et al.*²³⁶ were used to cleave the five-membered phthalamide ring releasing phthalic acid and 1,5-diaminopentan-3-one dihydrochloride.

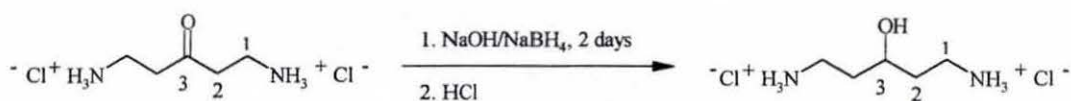
1,5-Diphtalimidopentan-3-one (226 g, 0.60 mol) was boiled in a mixture of acetic acid (560 mL) and conc. HCl (360 mL) with additional *ca.* 20 mL aliquots of conc. HCl being added at 8 hourly intervals over a period of 3 days until 200 mL had been added. On cooling, the fawn precipitate of phthalic acid was filtered off and washed with water. The combined filtrates and washings were evaporated nearly to dryness under reduced pressure, *ca.* 470 mL of water added and the non-dissolved phthalic acid filtered off. The filtrate was concentrated to *ca.* 50 mL under vacuum, *ca.* 800 mL of ethanol added and the resulting white precipitate, 1,5-diaminopentan-3-one dihydrochloride collected in a frit under vacuum. Yield: 110 g, 0.58 mol, 97%.

IR (KBr, cm^{-1}): 2997(s,b, NH_3^+ stretching); 1716(s, $\nu_{\text{C=O}}$); 1581(s, C- NH_3^+Cl^- vibration); 1520(s, C- NH_3^+Cl^- vibration)

NMR (D_2O , ppm, ^1H): 3.14(t, 2H, $-\text{C}^1\text{H}_2-$); 2.91(t, 2H, $-\text{C}^2\text{H}_2-$)

NMR (D_2O , ppm, ^{13}C): 39.33(C1); 34.75(C2); 209.10(C3)

Step 4: 1,5-diaminopentan-3-one dihydrochloride → 1,5-diaminopentan-3-ol dihydrochloride (DAHP.2HCl) (2.1)



Reduction of the carbonyl function to an alcohol was carried out using the method of Murase *et al.*²³⁶

Several aliquots of 1,5-diaminopentan-3-one dihydrochloride (37 g, 0.20 mol) were added to a solution, maintained below 20°C, of NaOH (15.6 g, 0.39 mol) and sodium borohydride (11 g, 0.29 mol) in 300 mL of water. The reaction solution was stirred at room temperature for 48 h. after which time 2M HCl was added slowly and carefully to the cold solution until the pH ~1. The solution appeared black during this step but reverted to colourless on standing. The solution was evaporated under vacuum to a dry white solid. Excess boric acid was removed, as its methyl ester, by adding methanol to this product and then evaporating off the ester under vacuum. The addition of methanol and the evaporation to dryness were repeated three times. 100 mL of methanol were added to the final residue, the mixture reflux 30 min., cooled and filtered to remove the resulting NaCl. The filtered solution was concentrated to *ca.* 90 mL and then added slowly to 900 mL of stirring diethylether. A white powdery product formed immediately on contact of the oil with ether and more product formed if the mixture was allowed to sit in the refrigerator at *ca.* 4°C overnight. The product was pure enough, not to require any further recrystallisation. This adaptation by Wikaira⁹⁷ is considered to be the second factor in the greatly improved overall yield of this preparation. Yield: 39-48 g, 0.21 mol, 99%. **Overall yield: 68%**

IR (KBr, cm^{-1}): 3380(s, b, OH stretch); 3030(s, b, NH_3^+ stretch); 1605(s, C- NH_3^+Cl^- vibration); 1570(s, C- NH_3^+Cl^- vibration)

NMR (CD_3OD , ppm, ^1H): 3.09(m, 2H, $-\text{C}^1\text{H}_2-$), 1.84(m, 2H, $-\text{C}^2\text{H}_2-$),
3.86(m, 2H, $-\text{C}^3\text{H}-$)

NMR (CD_3OD , ppm, ^{13}C): 68.58(C1); 38.60(C2); 335.66(C3)

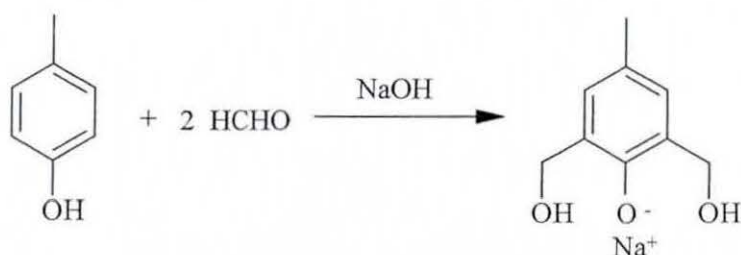
Note: neutralisation of DAHP.2HCl

DAHP is stored as a dihydrochloride salt and neutralised before each reaction.

In a typical neutralisation, DAHP.2HCl (0.24 g, 1.26 mmol) was dissolved in a minimum of dry MeOH (20 mL). Then, KOH (0.14 g, 2.50 mmol) was added to the solution. On solubilising KOH, KCl started to precipitate. To complete the precipitation of KCl, the solution was left in the freezer for *ca.* 30 min, then filtered into the reaction mixture.

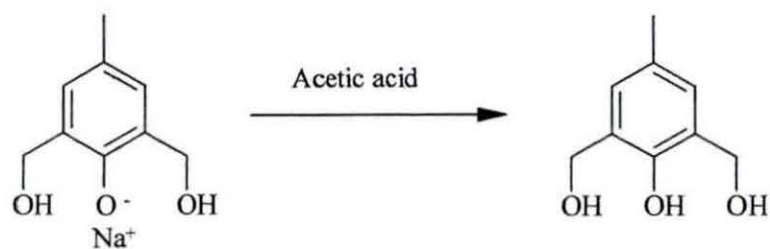
E.2.1.2. 2,6-Diformyl-4-methylphenol (DFMP) (2.2)

Step1:



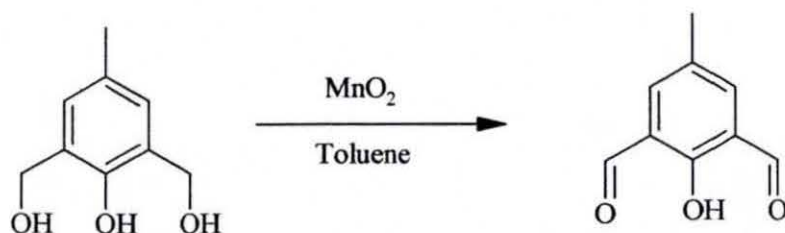
2,6-Dihydroxymethyl-4-methylphenol was prepared using the method of Gagné *et al.*⁶²

To a solution of NaOH (40 g, 1 mol) in water (160 mL) was added 4-methylphenol (*p*-cresol) (108 g, 1 mol). The mixture was stirred for up to 20 min. until a golden brown solution was formed. Next, 170 mL of formaldehyde (35% wt, 2 mol) was added while stirring. The mixture was left to stand for up to 2 days until an off-white solid precipitated. The solid was collected by filtration and the filtrate was left to stand to obtain a second crop of off-white solid. The solid was washed once with 100 mL of a saturated NaCl solution. (Caution!: excess washing dissolves the white solid).



The off-white solid was fully dissolved in water (~1 L), then acidified to pH ~5 with acetic acid while stirring, causing a fine powder (2,6-dihydroxymethyl-4-methylphenol) to precipitate. After stirring for 10 min. the white powder was collected by filtration and dried in a vacuum dessicator overnight. Yield: 100 g, 61%.

Step 2:



The preparation of 2,6-diformyl-4-methylphenol used the method of Taniguchi.¹²⁶

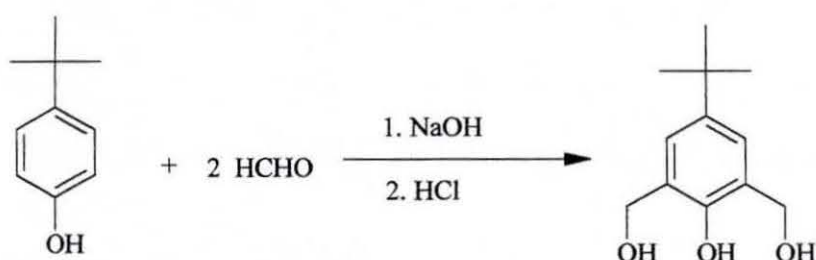
MnO₂ (130 g) was activated by heating in a furnace at 150°C overnight, then cooled to room temperature and added to a slurry of 50 g of 2,6-dihydroxymethyl-4-methylphenol in ca. 700 mL of toluene. The mixture was heated under reflux overnight with a constant overhead stirring. The solution developed a yellow colour and was then filtered and dried over MgSO₄. MgSO₄ was removed by filtration. Toluene was removed under vacuum to leave a yellow solid (2,6-diformyl-4-methylphenol). The product was dried under vacuum. Yield: 38 g, 78%.

IR (KBr, cm⁻¹): 3435(m,b, OH stretch); 2923(s,m); 1682(s, ν_{C=O}); 1613(s, ν_{C=O});
1303(s, OH bonding vibration); 926(s, 1,2,4,6-tetrasubstitution of Ar)

NMR (CDCl₃, ppm, ¹H): 2.38(s, 3H, CH₃), 7.39(s, 2H, ArH), 10.20(s, 2H, CHO),
11.44(s, 1H, -OH)

E.2.1.3. 2,6-Diformyl-4-*tert*-butylphenol (DFTP) (2.3)

Step1:

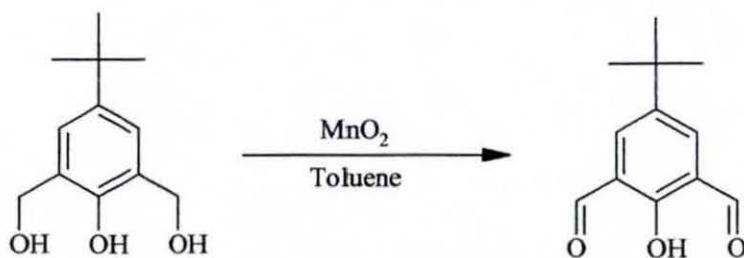


2,6-Dihydroxymethyl-4-*tert*-butylphenol was prepared using the method of Drago *et al.*²³⁷

NaOH (33.5 g, 0.84 mol) was dissolved in 800 mL of water. 4-*Tert*-butylphenol (100 g, 0.67 mol) was added to the NaOH solution and the mixture was stirred mechanically and heated gently until the solid was dissolved. The pale orange solution was cooled to room temperature before a 37%wt. solution of formaldehyde (115 mL, 1.42 mol) was added to the stirred solution. The solution was then stirred for 6 days at room temperature resulting in a yellow suspension. The mixture was then slowly neutralised with conc. HCl (74 mL). The solution turned from a reddish-brown suspension to a yellow suspension, then to an orange oil with a white aqueous suspension.

The aqueous layer was decanted and the organic phase washed with 3 lots of water (50 mL). Distilled water (300 mL) and chloroform (470 mL) were then added and the mixture was shaken. The mixture was allowed to separate. The chloroform layer was isolated and dried over MgSO₄ overnight. Chloroform was removed under vacuum to leave a golden-brown oil. The oil was dissolved in 200 mL of chloroform and cooled in the freezer. The product precipitated and was collected by filtration then dried under vacuum. Yield: 60 g, 50%.

Step2:



2,6-Diformyl-4-*tert*-butylphenol was synthesised using the method of Taniguchi.¹²⁶

MnO₂ (130 g) was activated by heating in a furnace at 150°C overnight, then cooled to room temperature and added to a slurry of 2,6-dihydroxymethyl-4-*tert*-butylphenol (50 g) in *ca.* 700 mL of toluene. The mixture was heated under reflux overnight with a constant overhead stirring. The solution developed a golden-brown colour. MnO₂ was removed by slow filtration through filter paper to remove the bulk and through a layer of silica to remove the traces. The liquor was dried over MgSO₄ overnight. MgSO₄ was removed by filtration and the remaining toluene removed under vacuum. The solution turned into a yellow-black oil which was dissolved in methanol and chilled in the freezer. The product precipitated slowly in low yield (20%).

IR (KBr, cm⁻¹): 2966(m); 2867(w); 1687(s, ν_{C=O}); 1659(s, ν_{C=O}); 1598(s);

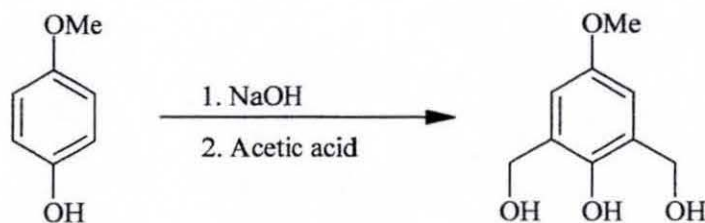
1224(m, OH bonding vibration); 980(s, 1,2,4,6-tetrasubstitution of an Ar); 554(m)

NMR (CDCl₃, ppm, ¹H): 1.4(s, 9H, C(CH₃)₃), 8(s, 2H, ArH), 10.8(s, 2H, CHO)

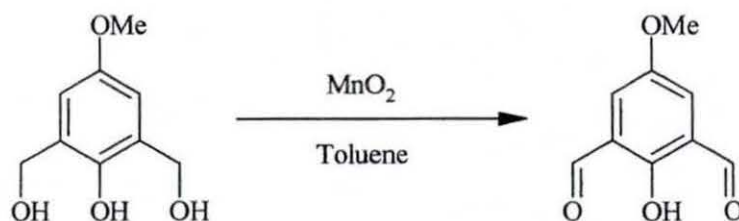
11.5(s, 1H, OH)

E.2.1.4. 2,6-Diformyl-4-methoxyphenol (DFMOP) (2.4)

Step1:



Step2:



DFMOP was synthesised by Sarah Cromie. The details of the synthesis will be reported in her thesis.

E.2.2. Complex syntheses

E.2.2.1. [Ni₄(L1)(OH)](ClO₄)₃ (2.5)

2,6-Diformyl-4-*tert*-butylphenol (DFTP) (0.26 g, 1.26 mmol) and Ni(ClO₄)₂·6H₂O (0.92 g, 2.52 mmol) were dissolved in hot dry ethanol (250 mL). 1,5-Diaminopentan-3-ol (DAHP) (0.24 g, 1.26 mmol) was directly filtered into the refluxing solution, which turned slightly darker olive green. The solution was left to reflux for 2 h. after which time it was allowed to cool then filtered and concentrated down to 20 mL. The solution was filtered again and the product was precipitated using diethylether. The product once filtered was waxy and turned into a hard solid under vacuum. This solid was ground and recrystallised from methanol. Slow evaporation to dryness left a hard waxy solid on the glass. A shiny green powder was obtained when the solid was scraped from the glass. Yield: 0.20 g. According to the FAB results and the elemental analysis we might have synthesised the following compound [Ni₄(L1)(OH)(MeOH)₄(H₂O)₄](ClO₄)₃. Indeed solvent molecules like MeOH and H₂O can complete the coordination sphere of Ni(II) (see tabulated data and section 2.1.2.1. in chap 2).

E.2.2.2. [Ni₄(L1)(OH)](NO₃)₃ (2.6), [Ni₄(L1)(OH)]Cl₃ (2.7) and [Ni₄(L2)(OH)](ClO₄)₃ (2.8)

These complexes were synthesised by the same procedure as complex 2.5. In the case of 2.6, 2.7 and 2.8, the amount of green powder obtained was 0.30 g, 0.10 g and 0.19 g respectively. According to the FAB results and elemental analysis for compound 2.6, we might have synthesised the following compound [Ni₄(L1)(OH)(MeOH)₄(MeOH)₇(H₂O)](NO₃)₃. (*cf.* tabulated data and section 2.1.2.2. in chapter 2). As for 2.7, the compound isolated might be [Ni₄(L1)(OH)-(MeOH)₈](Cl)₃ according to the FAB results. However some peaks of higher mass and the elemental analysis indicates contamination, which could be a polymeric compound. In the case of compound 2.8, the compound synthesised might be Ni₄(L2)(OH)(H₂O)₆(MeOH)₂](ClO₄)₃ for the same reasons mentioned for 2.5.

Complexes	IR (KBr, cm⁻¹)	Elemental analysis (calc.)
<p>[Ni₄(L1)(OH)](ClO₄)₃ or [Ni₄(L1)(OH)(MeOH)₄(H₂O)₄](ClO₄)₃ Yield: 24%</p>	<p>3424(s,b); 2960(w); 1646(s, ν_{C=N}); 1542(m, ν_{C=C}); 1104(b,s, ν₃(ClO₄⁻)); 626(m, ν₄(ClO₄⁻))</p>	<p>C: 34.88% (36.35) H: 4.91% (4.04) N: 3.89% (4.98) or C: 34.88% (34.48) H: 4.91% (5.25) N: 3.89% (4.23)</p>

Complexes	IR (KBr, cm ⁻¹)	Elemental analysis (calc.)
<p>[Ni₄(L1)(OH)](NO₃)₃ or [Ni₄(L1)(OH)(H₂O) (MeOH)₇](NO₃)₃ contaminated by 1.5 Ni(NO₃)₂</p> <p>Yield: 31%</p>	<p>3397(s,b); 2960(w); 1646(s, ν_{C=N}); 1542(m, ν_{C=C}); 1383(s, ν₃(NO₃⁻))</p>	<p>C: 32.02% (40.46) H: 5.02% (4.49) N: 9.24% (9.71) or C: 32.02% (32.28) H: 5.02% (4.95) N: 9.24% (9.18)</p>
<p>[Ni₄(L1)(OH)]Cl₃ or [Ni₄(L1)(OH)(MeOH)₈] (Cl)₃·4H₂O contaminated by 5 NiCl₂</p> <p>yield: 13%</p>	<p>3398(s,b); 2960(w); 1649(s, ν_{C=N}); 1540(m, ν_{C=C})</p>	<p>C: 26.25% (43.92) H: 5.04% (4.88) N: 3.81% (6.02) or C: 26.25% (26.43) H: 5.04% (4.07) N: 3.81% (2.95)</p>
<p>[Ni₄(L2)(OH)](ClO₄)₃ or [Ni₄(L2)(OH)(H₂O)₆ (MeOH)₂](ClO₄)₃</p> <p>yield: 25%</p>	<p>3390(s,b); 2960(w); 1645(s, ν_{C=N}); 1545(m, ν_{C=C}); 1088(s, ν₃(ClO₄⁻)); 626(m, ν₄(ClO₄⁻))</p>	<p>C: 29.43% (32.37) H: 4.69% (3.20) N: 3.76% (5.39) or C: 29.43% (29.75) H: 4.69% (4.41) N: 3.76% (4.62)</p>

Complex [Ni₄(L1)(OH)](ClO₄)₃ (2.5)

m/z	Rel. Intensities (%)	Fragments	Calc. Mass
953	70	[Ni ₄ (L1)(OH)(H ₂ O) ₂ (MeOH) ₃] ³⁺	953
971	80	[Ni ₄ (L1)(OH)(H ₂ O) ₃ (MeOH) ₃] ³⁺	971
1027	25	[Ni ₄ (L1)(OH)(H ₂ O) ₄ (MeOH)(ClO ₄)] ²⁺	1024
1146	25	[Ni ₄ (L1)(OH)(MeOH)(ClO ₄) ₃ +H] ⁺	1150
1159	20	[Ni ₄ (L1)(OH)(H ₂ O) ₂ (ClO ₄) ₃ +H] ⁺	1155
1253	15	[Ni ₄ (L1)(OH)(MeOH) ₄ (ClO ₄)] ²⁺ .2MeOH	1254
1316	15	[Ni ₄ (L1)(OH)(MeOH)(ClO ₄) ₃ +Na] ⁺	1315

Complex [Ni₄(L1)(OH)](NO₃)₃ (2.6)

m/z	Rel. Intensities (%)	Fragments	Calc. Mass
907	30	[Ni ₄ (L1)(OH)(H ₂ O) ₃ (MeOH)] ³⁺	907
953	100	[Ni ₄ (L1)(OH)(H ₂ O) ₂ (MeOH) ₃] ³⁺	953
971	100	[Ni ₄ (L1)(OH)(H ₂ O) ₃ (MeOH) ₃] ³⁺	971
1013	15	[Ni ₄ (L1)(OH)(H ₂ O) ₂ (MeOH)(NO ₃) ₂] ⁺	1013
1027	55	[Ni ₄ (L1)(OH)(H ₂ O)(NO ₃) ₃ +H] ⁺	1025
1083	50	[Ni ₄ (L1)(OH)(H ₂ O) ₄ (MeOH) ₂ (NO ₃) ₂] ⁺	1081
1107	20	[Ni ₄ (L1)(OH)(MeOH) ₅ (NO ₃) ₂] ⁺	1105
1159	20	[Ni ₄ (L1)(OH)(H ₂ O) ₅ (CH ₃ OH) ₂ (NO ₃) ₃ +H] ⁺	1162
1252	80	[Ni ₄ (L1)(OH)(CH ₃ OH) ₇ (NO ₃) ₃ +Na] ⁺	1254

Complex [Ni₄(L1)(OH)]Cl₃ (2.7)

m/z	Rel. Intensities (%)	Fragments	Calc. Mass
907	15	[Ni ₄ (L1)(OH)(H ₂ O) ₃ (MeOH)] ³⁺	907
953	13	[Ni ₄ (L1)(OH)(H ₂ O) ₂ (MeOH) ₃] ³⁺	953
971	30	[Ni ₄ (L1)(OH)(H ₂ O) ₃ (MeOH) ₃] ³⁺	971
1083	10	[Ni ₄ (L1)(OH)(MeOH) ₆ Cl ₂] ⁺	1083
1101	20	[Ni ₄ (L1)(OH)(MeOH) ₆ (H ₂ O)Cl ₂] ⁺	1101
1256	15	[Ni ₄ (L1)(OH)(MeOH) ₈ Cl ₃ +H] ⁺ .4H ₂ O	1256
1275	15	[Ni ₄ (L1)(OH)(MeOH) ₈ Cl ₃ +H] ⁺ .5H ₂ O	1274
1555	13		
1622	5		
1702	5		
1903	5		

Complex [Ni₄(L2)(OH)](ClO₄)₃ (2.8)

m/z	Rel. Intensities (%)	Fragments	Calc. Mass
738	15	[Ni ₄ (L2)(OH)] ³⁺	736
775	20	[Ni ₄ (L2)(OH)(H ₂ O)] ³⁺	773
795	20	[Ni ₄ (L2)(OH)(H ₂ O) ₃] ³⁺	791
837	10	[Ni ₄ (L2)(OH)(ClO ₄)] ²⁺	836
859	10	[Ni ₄ (L2)(OH)(ClO ₄)(H ₂ O)] ²⁺	854

E.2.3. Preparation of the sodium salts of DFMP, DFTP and DFMOP

E.2.3.1. NaDFMP (2.9)

DFMP (2 g, 12 mmol) was dissolved in a minimum of hot ethanol (50 mL). After cooling, a solution of NaOH (0.49 g, 12 mmol) in ethanol was added to the stirred solution of DFMP. The resulting solution turned brighter yellow and a yellow precipitate of NaDFMP started to form. The solution was left to stir for another 15 min. after which time the solution was filtered and the product dried in air first, then in vacuo. Yield: 1.90 g, 85%.

E.2.3.2. NaDFTP (2.10) and NaDFMOP (2.11)

The same procedure is carried out to obtain NaDFTP (2.10) with a yield of 80% and NaDFMOP (2.11) with a yield of 75%.

Complexes	IR (KBr, cm^{-1})	Elemental analysis (calc.)
NaDFMP	3384(m); 2971(w); 2861(w); 1684(s, $\nu_{\text{C=O}}$); 1515(s, $\nu_{\text{C=C}}$); 1225(m,s); 970(m,s, 1,2,4,6-tetrasubstitution of Ar)	C: 57.99% (58.07) H: 3.74% (3.79) N: % (0.00)
NaDFTP	3421(w); 2959(m); 2866(w); 1685(s, $\nu_{\text{C=N}}$); 1649(s, $\nu_{\text{C=O}}$); 1508(s, $\nu_{\text{C=C}}$); 1233(m); 987(s, 1,2,4,6-tetrasubstitution of Ar)	C: 62.98 % (63.15) H: 5.83% (5.74) N: 0.00% (0.00)
NaDFMOP	3433(w); 2938(w); 2835(w); 1686(s, $\nu_{\text{C=O}}$); 1655(s, $\nu_{\text{C=O}}$); 1610(m, $\nu_{\text{C=C}}$); 1526(s, $\nu_{\text{C=C}}$); 1275(m); 1219(m); 989(s, 1,2,4,6-tetrasubstitution of Ar)	C: 52.77% (53.47) H: 3.45% (3.49) N: 0.00% (0.00)

E.2.4. Preparation of sodium salts of the ligands L1, L2, L3, L4, L5, L6 and L7

E.2.4.1. $\text{H}_2\text{Na}_2\text{L2}$ (2.12)

The method used to synthesise **2.12** is similar to the ones reported by Gou *et al.*¹¹⁹

A solution of 1,5-diaminopentan-3-ol (0.53 g, 2.77 mmol) (neutralised by KOH) in dry methanol (48 mL) was filtered directly into a stirred suspension of NaDFMP (0.50 g, 2.69 mmol) in dry ethanol (55 mL). The solution became clear and was allowed to reflux for 1 h., then filtered hot to remove any insoluble product (polymers). The orange, slightly reddish, solution was concentrated until a yellow-orange precipitate appeared. Diethylether was added to complete the precipitation of the product. The product was then filtered, dried in air and in vacuo. Yield: 0.40 g, 55%.

Anal. Calc.: C 62.84%, H 6.92%, N 9.61%, for $\text{H}_2\text{Na}_2\text{L2} \cdot \text{EtOH}$

Found: C 62.79%, H 7.05%, N 8.95%

FAB-MS (% of relative abundance): 493(30); 515(10); 535(7); 561(5)

IR (KBr, cm^{-1}): 3396(s,b); 2917(s); 2846(s); 1638(s, $\nu_{\text{C=N}}$); 1599(s); 1529(m, $\nu_{\text{C=C}}$); 1459(s); 1382(m)

E.2.4.2. $\text{H}_2\text{Na}_2\text{L1}$ (2.13) and $\text{H}_2\text{Na}_2\text{L3}$ (2.14)

The procedure used to synthesise **2.13** (50%) and **2.14** is the same as that described for **2.12**, using DFTP and DFMOP respectively.

- $\text{H}_2\text{Na}_2\text{L1}$ (2.13):

Anal. Calc.: C 59.99%, H 7.81%, N 7.77%, for $\text{H}_2\text{Na}_2\text{L1} \cdot \text{EtOH} \cdot 3\text{H}_2\text{O}$

Found: C 60.16%, H 8.11%, N 7.25%

FAB-MS (% of relative abundance): 577(15); 593(7); 599(20)

IR (KBr, cm^{-1}): 3385(s,b); 2952(s); 1637(s, $\nu_{\text{C=N}}$); 1522(s, $\nu_{\text{C=C}}$); 1458(b,s);
1384(s)

• $\text{H}_2\text{Na}_2\text{L3}$ (**2.14**):

The product obtained had a gummy texture, it could not be isolated with reasonable purity and was quite insoluble. The isolated product is likely to be mainly a polymer.

FAB-MS (% of relative abundance): 615(5); 637(<5) very weak spectra

E.2.4.3. $\text{H}_2\text{Na}_2\text{L4}$ (2.15**)**

A solution of 1,3-diaminopropan-2-ol (0.26 g, 2.77 mmol) in dry methanol (20 mL) was added to a stirred suspension of NaDFMP (0.50 g, 2.69 mmol) in dry ethanol (55 mL). The solution became clear and was allowed to reflux for 1 h., then filtered hot to remove any insoluble product (polymers). The yellow-orange solution was concentrated until a yellow-orange precipitate appeared. Diethylether was added to complete the precipitation of the product. The yellow-orange powder is then filtered, dried in air and in vacuo. Yield: 0.24 g, 41%.

Anal. Calc.: C 62.64%, H 6.87%, N 11.23%, for $\text{H}_2\text{Na}_2\text{L4} \cdot \text{EtOH} \cdot \text{H}_2\text{O}$

Found: C 62.90%, H 6.79%, N 11.81%

FAB-MS (% of relative abundance): 437(18); 458(20); 527(15); 549(40)

IR (KBr, cm^{-1}): 3375(s,b); 2917(s); 1638(s, $\nu_{\text{C=N}}$); 1599(s); 1529(m, $\nu_{\text{C=C}}$);
1458(b,s); 1382(s)

E.2.4.4. $\text{H}_2\text{Na}_2\text{L5}$ (2.16**)**

The procedure carried out for the synthesis of **2.16** is identical to the one for **2.15**. Unfortunately, the reaction led to a mixture of different condensation products ([2+2], [3+3] ($\text{H}_3\text{Na}_3\text{L6}$, **2.17**) and [4+4] ($\text{H}_4\text{Na}_4\text{L7}$, **2.18**)) according to the FAB results. The conventional recrystallisation methods were not successful in separating the two compounds. No chromatographic separations were tried.

FAB-MS (% of relative abundance): 491(100); 725(25); 959(15)

E.2.5. Complex syntheses

E.2.5.1. $[\text{Ni}_4(\text{L2})(\text{OH})(\text{MeOH})_4(\text{H}_2\text{O})_4](\text{ClO}_4)_3$ (2.19)

A solution of $\text{Ni}(\text{ClO}_4)_2 \cdot 6\text{H}_2\text{O}$ (0.24 g, 0.64 mmol) in ethanol (10 mL) was added to a refluxing ethanol solution (50 mL) of $\text{H}_2\text{Na}_2\text{L2}$ (0.10 g, 0.16 mmol), while stirring. The reaction turned olive green and was left refluxing for 2 h. after which time it was allowed to cool, filtered and concentrated. The yellow-green solution was left to evaporate slowly. The green residue was washed with water to remove the excess of nickel salt as well as NaClO_4 . 0.095 g of olive green powder was collected and according to the FAB results and elemental analysis the compound isolated might be $[\text{Ni}_4(\text{L1})(\text{OH})(\text{H}_2\text{O})_4(\text{MeOH})_4](\text{ClO}_4)_3$.

Anal. Calc.: C 33.10%, H 5.50%, N 4.10%, for $[\text{Ni}_4(\text{L1})(\text{OH})(\text{H}_2\text{O})_4(\text{MeOH})_4](\text{ClO}_4)_3 \cdot 3\text{H}_2\text{O}$ (powder)

Found: C 33.10%, H 4.39%, N 3.49%

FAB-MS (% of relative abundance): 953(5); 971(5); 1028(5) very weak spectra

IR (KBr, cm^{-1}): 3405(s,b); 2959(m); 1646(s, $\nu_{\text{C}=\text{N}}$); 1543(s, $\nu_{\text{C}=\text{C}}$); 1145(s, $\nu_3(\text{ClO}_4^-)$); 1112(s, $\nu_3(\text{ClO}_4^-)$); 1090(s, $\nu_3(\text{ClO}_4^-)$); 626(m, $\nu_4(\text{ClO}_4^-)$)

E.2.5.2. $[\text{Ni}_4(\text{L2})(\text{OH})(\text{NO}_3)_2(\text{MeOH})_4](\text{NO}_3)$ (2.20)

A solution of $\text{Ni}(\text{NO}_3)_2 \cdot 6\text{H}_2\text{O}$ (0.22 g, 0.64 mmol) in ethanol (10 mL) was added to a refluxing ethanol solution (60 mL) of $\text{H}_2\text{Na}_2\text{L2}$ (0.10 g, 0.16 mmol), while stirring. The reaction turned green and was left refluxing for 2 h. after which time it was allowed to cool and left standing overnight. It was, then, filtered and the solvent removed. The green residue was washed with water to remove the excess of nickel salt. 0.085 g (46%) of green powder was collected. Green crystals suitable for X-ray were obtained by slow evaporation of a methanol solution of **2.20**.

Anal. Calc.: C 36.45%, H 4.68%, N 9.30%, (powder)

Found: C 36.33%, H 4.75%, N 9.51%

FAB-MS (% of relative abundance): 739(25); 750(20); 772(15); 800(7); 833(15);
891(10); 905(10)

IR (KBr, cm^{-1}): 3405(s,b); 2959(m); 1639(s, $\nu_{\text{C=N}}$); 1552(s, $\nu_{\text{C=C}}$); 1455(s);
1439($\nu_3(\text{NO}_3^-)$); 1404(s); 1384($\nu_3(\text{NO}_3^-)$); 1355(s); 1331(s,
 $\nu_3(\text{NO}_3^-)$)

E.2.5.3. [Ni₄(L2)(OH)(OAc)₂(MeOH)₄](OAc) (2.21)

A solution of Ni(OAc)₂·4H₂O (0.14 g, 0.56 mmol) in ethanol (10 mL) was added to a refluxing ethanol solution (40 mL) of H₂Na₂L2 (0.075 g, 0.14 mmol), while stirring. The reaction turned olive green and was left refluxing overnight. Then, the reaction was allowed to cool. After the solution was filtered and the solvent was removed, the green residue was dissolved in dichloromethane. A small amount of starting material was filtered off and the filtrate left to evaporate. Yield: 0.05 g, 34%.

Anal. Calc.: C 43.65%, H 5.59%, N 5.36%, (powder)

Found: C 44.05%, H 5.30%, N 4.94%

FAB-MS (% of relative abundance): 738(25); 797(20); 859(5)

IR (KBr, cm^{-1}): 3444(m,b); 2909(m); 1635(s, $\nu_{\text{C=N}}$); 1592(s); 1533(s);
1456(s, acetate ν_{COO}); 1406(s, acetate ν_{COO})

E.2.5.4. [Mn₄(L2)(O)(OAc)₄] (2.22)

A solution of Mn(OAc)₂·4H₂O (0.18 g, 0.74 mmol) in ethanol (10 mL) was added to a refluxing ethanol solution (50 mL) of H₂Na₂L2 (0.10 g, 0.18 mmol), while stirring. The reaction turned yellow-orange and was left refluxing for 1 h. On cooling the reaction turned dark brown-red. After the solution was filtered and the solvent was removed, the dark brown residue was dissolved in a minimum of acetonitrile (HPLC grade). A small amount of starting material was filtered off and the solvent removed. Yield: 0.09 g, 48%. Brown crystals suitable for X-ray studies were obtained by slow diffusion of diethylether into an acetonitrile solution of 2.22.

Anal. Calc.: C 42.57%, H 4.96%, N 5.51%, for $[\text{Mn}_4(\text{L2})(\text{O})(\text{OAc})_4] \cdot 3\text{H}_2\text{O}$
(powder)

Found: C 42.37%, H 4.83%, N 5.20%

FAB-MS (% of relative abundance): 783(70); 842(100); 901(25)

IR (KBr, cm^{-1}): 3423(m,b); 2920(w); 2852(w); 1645(m, $\nu_{\text{C}=\text{N}}$); 1570(s, $\nu_{\text{C}-\text{O}}$);
1444(sh, ν_{COO}); 1411(b,s, acetate ν_{COO})

E.2.5.5. $[\text{Co}_4(\text{L2})(\text{O})(\text{OAc})_4](\text{OAc})$ (2.23)

A solution of $\text{Co}(\text{OAc})_2 \cdot 4\text{H}_2\text{O}$ (0.19 g, 0.74 mmol) in ethanol (10 mL) was added to a refluxing ethanol solution (50 mL) of $\text{H}_2\text{Na}_2\text{L2}$ (0.10 g, 0.18 mmol), while stirring. The reaction turned orange and was left refluxing overnight after which time the solution had turned dark brown. The solution was left to cool, filtered and the solvent removed. The dark brown residue was dissolved in a minimum of dichloromethane. A small amount of starting material was filtered off and the solvent removed. Yield: 0.10 g, 52%.

Anal. Calc.: C 39.84%, H 4.26%, N 4.64%, for $[\text{Co}_4(\text{L2})(\text{O})(\text{OAc})_4](\text{OAc}) \cdot 2\text{CH}_2\text{Cl}_2$ (powder)

Found: C 39.55%, H 4.71%, N 4.06%

FAB-MS (% of relative abundance): 738(60); 799(85); 858(87); 917(95); 976(35)

IR (KBr, cm^{-1}): 3409(s,b); 2923(m); 1641(s, $\nu_{\text{C}=\text{N}}$); 1581(s, $\nu_{\text{C}-\text{O}}$); 1562(s); 1443(b,s, acetate ν_{COO}); 1413(b,s, acetate ν_{COO})

E.2.5.6. $[\text{Cu}_4(\text{L2})(\text{OH})(\text{NO}_3)_2](\text{NO}_3)$ (2.24)

A solution of $\text{Cu}(\text{NO}_3)_2 \cdot 6\text{H}_2\text{O}$ (0.18 g, 0.74 mmol) in ethanol (10 mL) was added to a refluxing ethanol solution of $\text{H}_2\text{Na}_2\text{L1}$ (0.10 g, 0.18 mmol). The solution turned green and a precipitate appeared. The solution was left refluxing for 3 h. The solution was filtered hot and the dark green powder was washed with methanol. Yield: 0.10 g, 57%. Green crystals suitable for X-ray studies were obtained by slow diffusion of

diethylether into a DMF/MeOH solution of **2.24**. The formula of the crystals was determined to be $[\text{Cu}_4(\text{L2})(\text{OH})(\text{NO}_3)(\text{OH})_2]$.

Anal. Calc.: C 36.89%, H 4.74%, N 9.41%, for $[\text{Cu}_4(\text{L2})(\text{OH})(\text{NO}_3)_2]\text{NO}_3$
2.EtOH (powder)

Found: C 37.12%, H 4.12%, N 10.05%

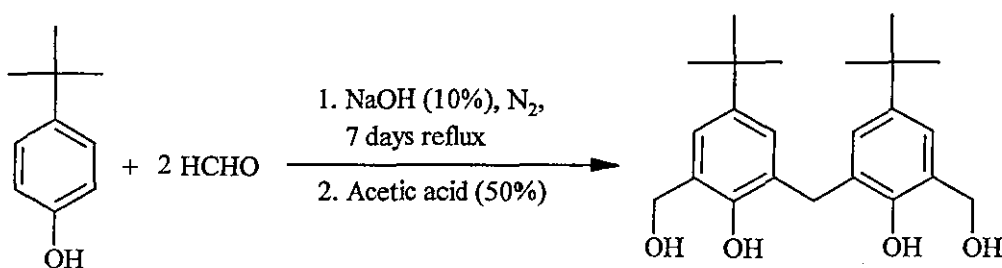
FAB-MS (% of relative abundance): 783(5); 1015(5); 1127(5)

IR (KBr, cm^{-1}): 3408(s,b); 2920(w); 1642(s, $\nu_{\text{C=N}}$); 1565(m, $\nu_{\text{C-O}}$); 1439(m, $\nu_3(\text{NO}_3)$); 1384(s, $\nu_3(\text{NO}_3)$); 1333(m, $\nu_3(\text{NO}_3)$)

E.3. Chapter 3

E.3.1. Organic preparations

E.3.1.1. Synthesis of 2,2'-dihydroxy-5,5'-di-*tert*-butyl-3,3'-methanediyl-dibenzyl alcohol (DHTMBA) (3.1)



This precursor was synthesised following a literature procedure¹²⁴ with some modifications. In this thesis, the work up of the reaction is discussed in more details (see section 3.2.1. in Chapter 3).

A mixture of 45 g of 4-*tert*-butylphenol, 60 mL of a 37% HCHO solution, and 140 mL of a 10 % NaOH solution was placed in a 500 mL round bottomed flask fitted with a reflux condenser. This mixture was heated at $50 \pm 5^\circ\text{C}$ for 7 days under an atmosphere of N_2 . It was then cooled and the resinous bright yellow precipitate was collected by filtration, re-dissolved in a minimum of acetone (50 to 100 mL). A

white insoluble product was filtered off if necessary. The resulting yellow filtrate was then acidified with 200 mL of cold 50% aqueous acetic acid. Most of the times an oil separated but it was not always the case. The aqueous layer was extracted several times with diethylether (100 mL) (3-4 times). The combined ether layers were washed (3-4 times) with water to remove the excess acetic acid and dried over MgSO_4 . The solvent was removed to give a coloured oil (the colour varying between pale yellow and red-purple). The oil was dissolved in 60-80 mL of benzene to which petroleum ether (bp 40-60°C) was added to turbidity. Within a day a white crystalline solid separated which was removed by filtration and washed with cold petroleum ether (13-16 g, 23-28%). The solid was analytically pure enough to carry out the next step of the synthesis.

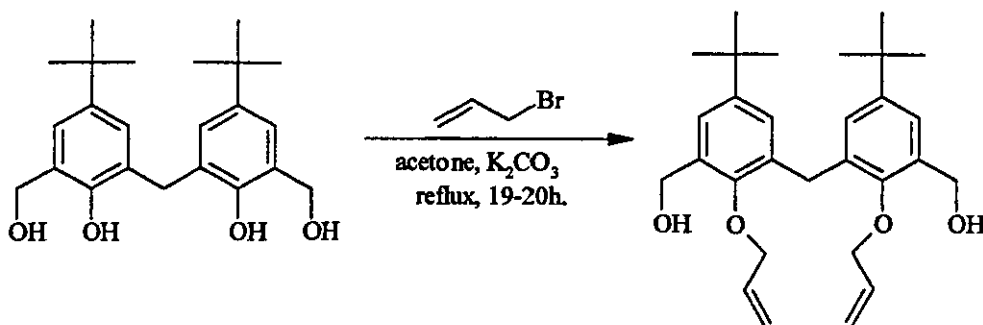
Anal. Calc.: C 74.16%, H 8.66%

Found: C 73.80%, H 9.13%.

NMR (CDCl_3 , ppm, ^1H): 7.26(d, 2, ArH), 6.94(d, 2 ArH), 4.77(s, 4, CH_2OH),
3.88(s, 2, ArCH_2Ar), 1.26(s, 18, $\text{C}(\text{CH}_3)_3$)

IR (KBr, cm^{-1}): 3420 and 3210(s, ν_{OH}); 1208 (s, $\nu(\text{ArOH})$); 875(m, 1,2,3,5 tetrasubstitution of Ar)

E.3.1.2. Synthesis of 2,2'-diallyloxy-5,5'-di-*tert*-butyl-3,3'-methanediyl-dibenzyl alcohol (AOTMBA) (3.2)



Compound 3.2 was prepared using a method frequently applied to phenols.¹²⁵

10 g (27 mmol) of DHTMBA, 7 g (58 mmol) of allylbromide, 7.42 g of anhydrous potassium carbonate and 100 mL of acetone were placed in a 250 mL three-necked round bottom flask fitted with a reflux condenser and sealed stirrer unit and refluxed for 20h. with stirring. The reaction mixture was then poured into 200 mL of water and the aqueous layer was extracted three times with diethyl ether. Then, the organic layer was washed with a 2M sodium hydroxide solution and dried over anhydrous potassium carbonate. The solvent was removed under vacuum leaving a white solid, which could be recrystallised from dichloromethane/n-hexane. The yield is 9 g (74 %). Colourless crystals suitable for X-ray studies were obtained by slow evaporation of a solution of petroleum ether/diethylether (50:50). TLC on silica gel (diethylether/pet-ether 40/60, 45:55) $R_f = 0.68$.

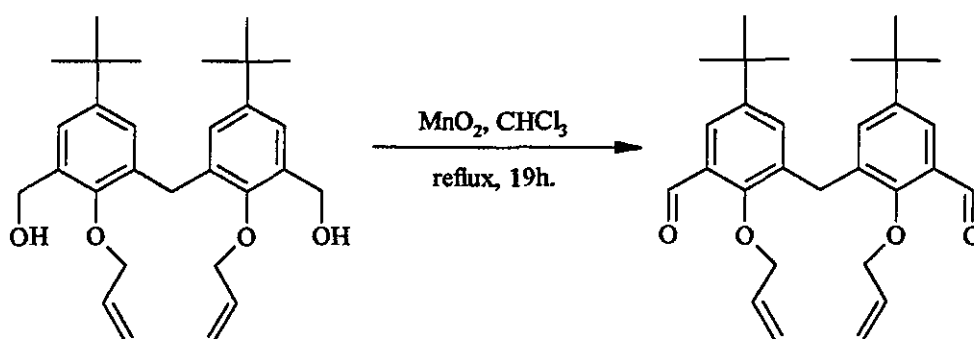
Anal.: Calc.: C 75.45%, H 8.95%, (3.2).1/2H₂O

Found: C 75.64%, H 9.06%.

NMR (CDCl₃, ppm, ¹H): 7.24(d, 2, ArH), 7.01(d, 2 ArH), 6.07(m, 2, allyl =CH), 5.34(dd, 2, allyl =CH₂), 5.30(dd, 2, allyl =CH₂), 4.73(d, 4, CH₂OH), 4.34(d, 4, allyl CH₂), 4.70(s, 4, CH₂OH), 4.07(s, 2, ArCH₂Ar), 1.26(s, 18, C(CH₃)₃)

IR (KBr, cm⁻¹): 3272(s, ν_{OH}), 3081(w, ν_{allyl=CH₂}), 883(m, 1,2,3,5 tetrasubstitution of Ar).

E.3.1.3. Synthesis of 2,2'-diallyloxy-5,5'-di-*tert*-butyl-3,3'-methanediyl-dibenzaldehyde (AOTMB) (3.3)



The method used is similar to the one reported by Taniguchi *et al.*¹²⁶

50 g of activated MnO₂ were added to 9 g (20 mmol) of AOTMBA in 200 mL of chloroform. The reaction mixture was refluxed for 19-20 h. after which time MnO₂ was filtered off and the organic layer dried over anhydrous magnesium sulphate. The solvent was removed under vacuum leaving a pale yellow oil that crystallised under vacuum over a week. The solid was then washed with cold methanol to remove the yellow impurities. Colourless crystals suitable for X-ray studies were obtained by slow evaporation of a diethylether solution of the product. The yield is 7 g (78%). The oil did not always crystallise but could be used without further purification, according to the NMR and elemental analysis data (no partially oxidised product present). TLC on silica gel (diethylether/pet-ether 40/60, 30:70) R_f = 0.50.

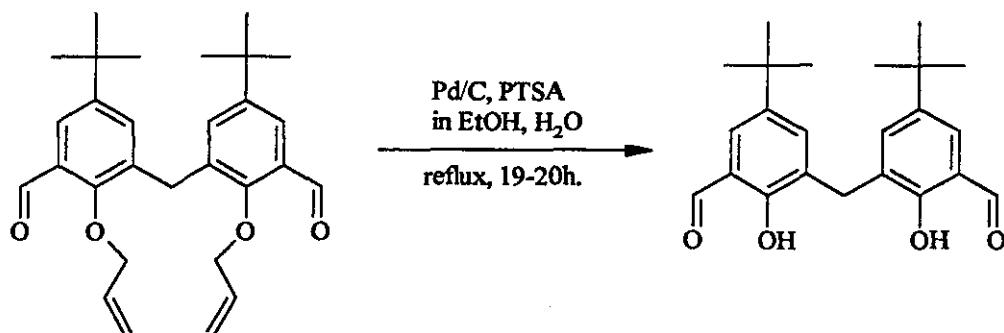
Anal: Calc.: C 76.11%, H 8.15%, (3.3).1/2H₂O

Found: C 76.08%, H 8.15%

NMR (CDCl₃, ppm. ¹H): 10.4(s, 2,CHO), 7.75(d, 2, ArH), 7.30(d, 2, ArH),
6.06(m, 2, allyl =CH), 4.40(dd, 2, allyl =CH₂), 4.44(dd,
2, allyl = CH₂), 4.13(s, 2, ArCH₂Ar), 1.26(s, 18,
C(CH₃)₃)

IR (KBr, cm⁻¹): 1660 (ν_{C=O}), 3081(w, ν_{allyl =CH₂}), 885(m, 1,2,3,5 tetrasubstitution of Ar)

E.3.1.4. Synthesis of 2,2'-dihydroxy-5,5'-di-*tert*-butyl-3,3'-methanediyl-dibenzaldehyde (DHTMB) (3.4)



The method used is similar to the one reported by Boss *et al.*¹²⁷

To a solution of AOTMB (7 g, 15.6 mmol) in 150 mL of ethanol, 1.5 g of Pd on activated charcoal and 0.7 g of p-toluenesulfonic acid in 5 mL of water were added. The stirred suspension was refluxed for 2 days after which time the reaction mixture was filtered hot. On cooling, the product precipitated out as a pale yellow powder, which was filtered off (1 g). An additional 3 g of DHTMB could be obtained on concentration of the resulting filtrate. Pale yellow crystals suitable for X-Ray studies were obtained by slow evaporation of a diethylether solution of the product. The yield is 4 g (70%), TLC on silica gel (diethylether/pet-ether 40/60, 30:70) $R_f = 0.64$.

Anal: Calc.: C 74.97%, H 7.66%

Found: C 74.51%, H 7.86%.

NMR (CDCl_3 , ppm, ^1H): 9.86(s, 2, CHO), 7.64(d, 2, ArH), 7.37 (d, 2, ArH),
4.03(s, 2, ArCH_2Ar), 1.26(s, 18, $\text{C}(\text{CH}_3)_3$)

IR (KBr, cm^{-1}): 1658($\nu_{\text{C=O}}$), 1270(s, $\nu(\text{ArOH})$), 1216(s)

E.3.2. Complex syntheses

E.3.2.1. $[\text{Mn}_2(\text{L8})](\text{ClO}_4)_2$ (3.5)

$\text{Mn}(\text{ClO}_4)_2 \cdot 6\text{H}_2\text{O}$ (0.13 g, 0.36 mmol) and DHTMB (0.20 g, 0.54 mmol) were dissolved in hot dry ethanol (80 mL). The solution was refluxed for 10-15 min. after which time a solution of *tris*(2-aminoethyl)amine (0.22 g, 1.52 mmol) in 10 mL of dry methanol was added drop-wise to the refluxing solution. The solution turned bright yellow. The reaction mixture was allowed to reflux for 1h. after which time it was left to cool. On standing, the solution turned dark green within 1 h. The solution was then concentrated to 15 mL and diethylether was allowed to diffuse slowly into the solution. After one or two days a green precipitate was visible, 0.20 g was collected and dissolved in dichloromethane. A small amount of impurities were filtered off and the solvent removed, 0.17 g of product was collected. Yield: 48%. Pale green needle-shaped crystals suitable for X-ray studies were isolated by

diethylether diffusion into an acetonitrile solution of **3.5**. As the crystals were small, data were collected using line 9.8 of the Synchrotron Radiation Source at Daresbury.

Anal. Calc.: C 54.32%, H 6.68%, N 8.44%, for $[\text{Mn}_2(\text{L8})](\text{ClO}_4)_2 \cdot 2\text{MeOH}$
(powder)

Found: C 54.24%, H 6.39%, N 8.23%

FAB-MS (% of relative abundance): 1063(100); 1163(10)

IR (KBr, cm^{-1}): 3416(b,s); 3135 (sh, bonding vibration of $-\text{NH}_2$); 3247 (sh, bonding vibration of $-\text{NH}_2$); 2955(s); 2864(s); 1631(s, $\nu_{\text{C}=\text{N}}$); 1616(s, $\nu_{\text{C}=\text{N}}$); 1599(s, $\nu_{\text{C}=\text{N}}$); 1545(s, $\nu_{\text{C}=\text{O}}$); 1438(s); 1327(m); 1268(s); 1089(s,b, $\nu_3(\text{ClO}_4^-)$); 624(m, $\nu_4(\text{ClO}_4^-)$)

E.3.2.2. $[\text{Co}_2(\text{L8})](\text{ClO}_4)_2$ (**3.6**)

$\text{Co}(\text{ClO}_4)_2 \cdot 6\text{H}_2\text{O}$ (0.13 g, 0.36 mmol) and DHTMB (0.20 g, 0.54 mmol) were dissolved in hot dry ethanol (80 mL). The solution was refluxed for 10-15 min. after which time a solution of *tris*(2-aminoethyl)amine (0.08 g, 0.55 mmol) in 10 mL of dry methanol was added drop-wise to the refluxing solution. The solution turned khaki green. The reaction mixture was allowed to reflux for 5 h. The resulting dark red-brown solution was left to cool, filtered, concentrated and diethylether was allowed to diffuse into the solution. A small amount of precipitate which appeared within one or two days was filtered off (0.02 g of a rusty powder) and identified as being $[\text{Co}_2(\text{L8a})(\text{OH})(\text{MeOH})](\text{ClO}_4)$ (**3.7**), according to the FAB results and elemental analysis.

Anal. Calc.: C 48.59%, H 7.13%, N 12.59%, for $[\text{Co}_2(\text{L8a})(\text{OH})(\text{MeOH})](\text{ClO}_4)$

Found: C 48.59%, H 7.13%, N 13.00%

FAB-MS (% of relative abundance): 839(100)

IR (KBr, cm^{-1}): 3422(b,s); 3269(sh,m); 1634(s, $\nu_{\text{C}=\text{N}}$); 1542(w, $\nu_{\text{C}=\text{C}}$); 1088(s, $\nu_3(\text{ClO}_4^-)$); 625(m, $\nu_4(\text{ClO}_4^-)$)

The remaining yellow filtrate was left to evaporate to dryness. The dark yellow powder was dissolved in acetonitrile and impurities were filtered off. The solvent was removed and 0.10 g of yellow powder was collected. Most likely due to poor solubility, only a small amount of $[\text{Co}_2(\text{L8a})(\text{OH})(\text{MeOH})](\text{ClO}_4)$ was detected. No traces of the compound $[\text{Co}_2(\text{L8})](\text{ClO}_4)_2$ were detected but this does not mean the compound did not form. No crystals suitable for X-ray studies have been obtained so far. Yield: 29%.

Anal. Calc.: C 55.20%, H 6.40%, N 11.1%, for $[\text{Co}_2(\text{L8})](\text{ClO}_4)_2 \cdot 3\text{CH}_3\text{CN}$ (powder)

Found: C 55.22%, H 6.67%, N 10.66%

FAB-MS (% of relative abundance): 840(20) (poor solubility)

IR (KBr, cm^{-1}): 3423(b,m); 3269(sh,m); 1956(s); 1632(s, $\nu_{\text{C}=\text{N}}$); 1542(w, $\nu_{\text{C}=\text{C}}$);
1475(m); 1096(s, $\nu_3(\text{ClO}_4^-)$); 624(m, $\nu_4(\text{ClO}_4^-)$)

E.3.2.3. $[\text{Ni}_2(\text{H}_4\text{L9})(\mu_2\text{-H}_2\text{O})(\text{EtOH})_2](\text{ClO}_4)_2$ (3.8)

$\text{Ni}(\text{ClO}_4)_2 \cdot 6\text{H}_2\text{O}$ (0.20 g, 0.54 mmol) and DHTMB (0.20 g, 0.54 mmol) were dissolved in hot dry ethanol (75 mL). The solution was refluxed for 10-15 min. after which time a solution of 1,3-diaminopropan-2-ol (0.053 g) in 10 mL of dry methanol was added drop-wise to the refluxing solution. The solution turned slightly darker green. The reaction mixture was left under reflux for 6-7 h. The solution was then left to cool, filtered, concentrated and left to evaporate slowly. Light green crystals for X-ray studies were isolated and data were collected using line 9.8 of the Synchrotron Radiation Source at Daresbury. 0.21 g of green crystals were collected (yield: 61%) and dried in vacuo. The green crystalline powder turned red over drying due to the loss of solvent molecules. The new mass is 0.195 g and the complex is assumed to be $[\text{Ni}_2(\text{H}_4\text{L2})](\text{ClO}_4)_2 \cdot 3\text{H}_2\text{O}$ (3.9) in the solid state. Yield: 58%.

Anal. Calc.: C 50.71%, H 5.89%, N 4.54%, for $[\text{Ni}_2(\text{H}_4\text{L2})](\text{ClO}_4)_2 \cdot 3\text{H}_2\text{O}$ (powder)

Found: C 51.09%, H 6.39%, N 4.26%

FAB-MS (% of relative abundance): 957(100); 995(5); 1094(5); 1108(5)

IR (KBr, cm^{-1}): 3433(b,s); 2962(s); 1636(s, $\nu_{\text{C=N}}$); 1560(w, $\nu_{\text{C-O}}$); 1394(m);
1364(m); 1475(m); 1438(m); 1120(b,s, $\nu_3(\text{ClO}_4^-)$); 626(m,
 $\nu_4(\text{ClO}_4^-)$)

E.3.2.4. [Co₂(H₄L9)(μ_2 -H₂O)(EtOH)₂](ClO₄)₂ (3.10)

Co(ClO₄)₂·6H₂O (0.40 g, 1.08 mmol) was dissolved in dry methanol (20 mL) and added to a hot solution of DHTMB (0.20 g, 0.54 mmol) in dry ethanol (60 mL). Nitrogen was bubbled through the mixture, which was refluxed for *ca.* 30 min. A solution containing 0.053 g (0.54 mmol) of 1,3-diaminopropan-2-ol in dry degassed methanol (10 mL) was added drop-wise to the reaction mixture. The solution turned slightly darker yellow/orange. The solution was left under reflux under nitrogen for 24 h. The resulting yellow/orange solution was concentrated in vacuo to *ca.* 5 mL and degassed diethylether (15 mL) added. A small amount of starting material was isolated by a quick filtration in air. The compound is not very air sensitive but the filtrate was degassed all the same, concentrated to 5 mL and degassed diethylether (15 mL) added. The pale yellow/orange solid was then quickly filtered in air and dried in vacuo (0.15 g, 45%). The isolated compound is assumed to be [Co₂(H₄L9)(H₂O)₃](ClO₄)₂ (3.11). Yellow crystals of [Co₂(H₄L9)(H₂O)(EtOH)₂](ClO₄)₂ (3.10) suitable for X-ray studies were isolated by slow evaporation of an ethanol solution of the compound. As the product is air sensitive in solution over a period of time the compound was partially oxidised and found to be a mixture of yellow crystals and brown powder. The attempts to separate the two compounds were unsuccessful. No crystals for X-ray studies were obtained for the brown compound.

Anal. Calc.: C 50.01%, H 5.97%, N 4.48%, for [Co₂(H₄L9)(H₂O)₃](ClO₄)₂.
2H₂O (powder)

Found: C 50.01%, H 5.63%, N 4.29%

FAB-MS (% of relative abundance): 959(25); 995(100); 1011(3); 1126(3)

IR (KBr, cm^{-1}): 3423(s,b); 2958(s); 1630(s, $\nu_{\text{C=N}}$); 1560(w, $\nu_{\text{C-O}}$); 1476(m);
1336(m); 1365(m); 1223(m); 1134(s, $\nu_3(\text{ClO}_4^-)$);
1117(s, $\nu_3(\text{ClO}_4^-)$); 1088(s, $\nu_3(\text{ClO}_4^-)$); 626(m, $\nu_4(\text{ClO}_4^-)$)

E.3.2.5. $[\text{Ni}_2(\text{H}_4\text{L9})(\text{H}_2\text{O})_3](\text{NO}_3)_2$ (3.12) / $[\text{Ni}_2(\text{H}_4\text{L9})(\text{NO}_3)(\text{DMF})_2](\text{NO}_3)$ (3.13)

$\text{Ni}(\text{NO}_3)_2 \cdot 6\text{H}_2\text{O}$ (0.16 g, 0.54 mmol) and DHTMB (0.20 g, 0.54 mmol) were dissolved in hot dry ethanol (75 mL). The solution was refluxed for 10-15 min. after which time a solution of 1,3-diaminopropan-2-ol (0.053 g) in 10 mL of dry methanol was added drop-wise to the refluxing solution. The solution turned slightly darker green. The reaction mixture was left under reflux for 6-7 h. The solution was then left to cool, filtered, and evaporated to dryness. The residue was washed with dichloromethane and 0.16 g (52%) of a pale yellow/green powder were filtered and washed with water.

Anal. Calc.: C 54.86%, H 6.37%, N 7.38%, for $[\text{Ni}_2(\text{H}_4\text{L9})(\text{H}_2\text{O})_3](\text{NO}_3)_2$ (powder)
Found: C 55.10%, H 6.20%, N 7.12%

FAB-MS (% of relative abundance): 958(100); 996(15)

IR (KBr, cm^{-1}): 3418(m,s); 2958(s); 1634(s, $\nu_{\text{C=N}}$); 1560(w, $\nu_{\text{C-O}}$); 1475(m);
1383(s, $\nu_3(\text{NO}_3^-)$)

This reaction was first tried with a metal/ligand ratio of 6:2 and left to reflux for 2 h. The powder isolated, then, was dissolved in dimethylformamide and left to evaporate slowly. Light green crystals for X-ray studies were isolated. The DMF molecules replaced the coordinated water molecules: $[\text{Ni}_2(\text{H}_4\text{L9})(\text{NO}_3)(\text{DMF})_2](\text{NO}_3)$ (3.13). No further characterisations were undertaken.

Another attempt was carried out with a metal/ratio of 2:2 and left to reflux for 4 h. The solution was left to cool, filtered and evaporated to dryness. The residue was washed with dichloromethane, dissolved in DMF and left to evaporate slowly. Within one or two weeks light green crystals ($[\text{Ni}_2(\text{H}_4\text{L9})(\text{NO}_3)(\text{DMF})_2](\text{NO}_3)$)

suitable for X-ray studies were isolated and washed with diethylether. 0.18 g (54%) of green crystals was isolated, ground and left under vacuo.

Anal. Calc.: C 55.79%, H 6.61%, N 8.97%, for $[\text{Ni}_2(\text{H}_4\text{L9})(\text{DMF})_2(\text{NO}_3)](\text{NO}_3)$
(powder)

Found: C 55.75%, H 6.81%, N 9.36%

FAB-MS (% of relative abundance): 903(5); 941(15); 973(100); 995(20);
1085(13); 1916(5); 1954(< 5); 2044(< 5)

IR (KBr, cm^{-1}): 3373(m); 2954(s); 2866(m); 1654(s, $\nu_{\text{C=O}}$); 1640(s, $\nu_{\text{C=N}}$);
1560(w, $\nu_{\text{C-O}}$); 1478(s); 1436(s, $\nu_3(\text{NO}_3^-)$); 1385(s, $\nu_3(\text{NO}_3^-)$);
1366(s, $\nu_3(\text{NO}_3^-)$)

E.3.2.6. $[\text{Ni}_2(\text{L10})]$ (3.14)

$\text{Ni}(\text{ClO}_4)_2 \cdot 6\text{H}_2\text{O}$ (0.20 g, 0.54 mmol) and DHTMB (0.20 g, 0.54 mmol) were dissolved in hot dry ethanol (75 mL). The solution was refluxed for 10-15 min. after which time a solution of 1,3-diaminopropane (0.041 g, 0.046 mL, 0.54 mmol) in 10 mL of dry methanol was added drop-wise to the refluxing solution. The solution turned darker yellow-brown. The reaction mixture was left under reflux for 4 h. after which time a precipitate had formed. 0.17 g (58%) of rusty brown powder was collected by filtration. The product is not very soluble in any of the solvents tried from low to high polarity, which is the reason why no crystals could be grown so far. The resulting yellow filtrate after evaporation to dryness did not give enough product to work with.

Anal. Calc.: C 64.35%, H 6.98%, N 5.17%, for $[\text{Ni}_2(\text{L10})] \cdot 3\text{EtOH} \cdot \text{H}_2\text{O}$

Found: C 64.11%, H 6.71%, N 5.67%

FAB-MS (% of relative abundance): 925(100); 947(50); 963(10); 1007(7)

IR (KBr, cm^{-1}): 3446(b,w); 2954(s); 1617(s, $\nu_{\text{C=N}}$); 1543(m, $\nu_{\text{C=C}}$); 1450(m)

E.3.2.7. $[\text{Mn}_2(\text{L10})(\text{EtOH})_2(\text{OAc})_2]$ (3.15)

$\text{Mn}(\text{OAc})_2 \cdot 4\text{H}_2\text{O}$ (0.40 g, 1.62 mmol) and DHTMB (0.20 g, 0.54 mmol) were dissolved in hot dry ethanol (80 mL). The solution was refluxed for 10-15 min. after which time a solution of 1,3-diaminopropane (0.041 g, 0.046 mL, 0.54 mmol) in 5-10 mL of methanol was added drop-wise to the refluxing solution. The solution turned darker yellow-brown. The reaction mixture was left under reflux for 1 h. On cooling the solution turned dark green/brown. It was then concentrated and diethylether was left to slowly diffuse into the solution. Dark green/brown crystals (0.06 g, 21%) were isolated. None of the recrystallisation techniques gave crystals suitable for X-ray studies. A second crop (0.10 g, 32%) was isolated as a dark green/brown powder.

1st crop: $\text{Mn}_2(\text{L10})(\text{OAc})_2(\text{MeOH})$ (3.16)

Anal. Calc.: C 64.00%, H 7.00%, N 5.20%, (powder)

Found: C 64.21%, H 6.99%, N 5.19%

FAB-MS (% of relative abundance): 918(100); 978(80); 1086(10); 1837(5);
1860(5)

IR(KBr, cm^{-1}): 3430(b,m); 2958(m); 1621(s, $\nu_{\text{C=N}}$); 1552(s, $\nu_{\text{C-O}}$); 1442(m,
acetate ν_{COO})

2nd crop: $\text{Mn}_2(\text{L10})(\text{OAc})_2(\text{EtOH})_2$ (3.15)

Anal. Calc.: C 62.82%, H 7.38%, N 4.88%, for (3.15). H_2O

Found: C 62.70%, H 6.77%, N 5.16%

FAB-MS (% of relative abundance): 919(80); 979(100); 1087(5)

IR(KBr, cm^{-1}): 3430(m); 2958(m); 1621(s, $\nu_{\text{C=N}}$); 1552(s, $\nu_{\text{C-O}}$); 1442(m, ν_{COO})

E.3.2.8. $[\text{Mn}_6(\text{H}_2\text{L9})_3(\text{H}_2\text{O})_6(\text{CO}_3)](\text{ClO}_4)_2$ (3.17)

This reaction was first carried out without dry-ice and brown crystals of $[\text{Mn}_6(\text{H}_2\text{L9})_3(\text{H}_2\text{O})_6(\text{CO}_3)](\text{ClO}_4)_2$ suitable for X-ray studies were obtained by slow diffusion of diethylether in a methanol solution of 3.17. Consequently, the reaction was tried as described below.

Mn(ClO₄)₂·4H₂O (0.39 g, 1.08 mmol) and DHTMB (0.20 g, 0.54 mmol) were dissolved in 70 mL of hot dry methanol. Dry ice was then added to the solution, which was refluxed for 10-15 min. A solution of 1,3-diaminopropan-2-ol (0.053 g, 0.54 mmol) in dry methanol (10 mL) was added drop-wise to the refluxing solution. The solution turned darker yellow. The reaction mixture was left under reflux for 1 h. On cooling the solution turned dark green. It was then filtered and the solvent evaporated to dryness. The dark green/brown residue was washed with dichloromethane followed by water. 0.15 g (47%) of dark green powder was collected.

Anal. Calc.: C 54.31%, H 6.00%, N 4.72%, for [Mn₆(H₂L9)₃(H₂O)₆(CO₃)](ClO₄)₂ · 4CH₂Cl₂ (powder)

Found: C 54.48%, H 6.18%, N 4.47%

FAB-MS (% of relative abundance): 899(50); 951(100); 987(25); 1089(35);

1266(7); 1319(7); 1795(3); 1848(3); 1900(3)

IR (KBr, cm⁻¹): 3425(s,b); 2958(m); 1616(s, ν_{C=N}); 1552(m, ν_{C=C}); 1441(m,

ν(CO₃⁻)); 1119(s, ν₃(ClO₄⁻)); 1010(s, ν₃(ClO₄⁻));

1088(s, ν₃(ClO₄⁻)); 874(w/m); 626(m, ν₄(ClO₄⁻))

E.3.2.9. [Mn₆(H₂L9)₃(H₂O)₃(OAc)₃(CO₃)] (3.18)

This reaction was first carried out without dry-ice and brown crystals of [Mn₆(H₂L9)₃(OAc)₃(H₂O)(EtOH)₂(CO₃)] suitable for X-ray studies were obtained by slow diffusion of diethylether in a methanol solution of 3.18. Consequently, the reaction was tried as described below.

Mn(OAc)₂·4H₂O (0.13 g, 0.54 mmol) and DHTMB (0.20 g, 0.54 mmol) were dissolved in 85 mL of hot dry ethanol. Dry ice was then added to the solution, which was refluxed for 10-15min. A solution of 1,3-diaminopropan-2-ol (0.053 g, 0.54 mmol) in dry methanol (10 mL) was added drop-wise to the refluxing solution. The solution turned darker yellow. The reaction mixture was left under reflux for 1 h. Within 10 min. of cooling the solution turned dark green. It was then filtered and the

solvent removed. The dark green brownish residue was washed with dichloromethane followed by water. 0.15 g (47%) of dark green powder was collected.

Anal. Calc.: C 56.53%, H 6.12%, N 4.70%, for $[\text{Mn}_6(\text{H}_2\text{L9})_3(\text{H}_2\text{O})_3(\text{OAc})_3(\text{CO}_3)] \cdot 5\text{CH}_2\text{Cl}_2$

Found: C 56.74%, H 6.51%, N 4.57%

FAB-MS (% of relative abundance): 949(30); 971(25); 1040(15);
1882(30); 1891(40); 1899(100); 1915(30)
1920(30); 1935(30); 2847(10); 2885(8);
2934(5); 2976(<3); 3062(<3)

IR (KBr, cm^{-1}): 3409(m,b); 2958(m); 1619(s, $\nu_{\text{C}=\text{N}}$); 1551(s, $\nu_{\text{C}=\text{O}}$); 1440(m,b, ν_{COO} and $\nu(\text{CO}_3^-)$); 1270(m); 875(w/m)

E.3.2.10. $[\text{Co}_6(\text{H}_2\text{L9})_3(\text{H}_2\text{O})_3(\text{OAc})_3\text{CO}_3]$ (3.19)

$\text{Co}(\text{OAc})_2 \cdot 4\text{H}_2\text{O}$ (0.40 g, 0.54 mmol) was dissolved in dry methanol (10 mL) and added to a solution of DHTMB (0.20 g, 0.54 mmol) in dry ethanol (60 mL). The mixture was refluxed for 30 min. A solution containing 0.053 g (0.54 mmol) of 1,3-diaminopropan-2-ol in 10 mL of dry methanol was added drop-wise to the refluxing solution. The solution turned orange-brown. The reaction mixture was allowed to reflux for 24 h. after which time the solution had turned darkish orange/red. On cooling the solution turned dark brown. The solution was then evaporated to dryness. The dark brown powder was dissolved in HPLC grade acetonitrile and a small amount of insoluble material was filtered off. The solution was left to evaporate slowly but no crystals suitable for X-ray studies were isolated. 0.26 g (90%) of a dark brown powder was collected. None of the crystallisation methods were successful in getting suitable crystals for X-ray studies.

Anal. Calc.: C 58.67%, H 6.31%, N 4.94%

Found: C 58.42%, H 6.60%, N 4.89%

FAB-MS (% of relative abundance): 952 (80); 981 (100); 1016(25); 1076 (10);
1937(50); 1993(20)

IR (KBr, cm^{-1}): 3430(s); 2957(m); 1629(s, $\nu_{\text{C=N}}$); 1561(s, $\nu_{\text{C=O}}$); 1442(s, ν_{COO} and $\nu(\text{CO}_3^-)$); 1392(m); 1269(m); 878(w/m)

E.3.2.11. [Fe₆(H₂L9)(OAc)₃(H₂O)₃(CO₃)] (3.20)

Fe(OAc)₂ (0.095 g, 0.54 mmol) was dissolved in dry methanol (10 mL) and added to a solution of DHTMB (0.20 g, 0.54 mmol) in dry ethanol (60 mL). The dark red-brown mixture was refluxed for 30 min. A solution containing 0.053 g (0.54 mmol) of 1,3-diaminopropan-2-ol in 10 mL of dry methanol was added drop-wise to the refluxing solution. The reaction mixture was allowed to reflux for 4.30 h. after which time the solution had turned deep purple-red. The solution was then left to cool, filtered and evaporated to dryness. The dark purple-red powder was washed with HPLC grade acetonitrile followed by water. 0.21 g (75%) of a dark purple-red powder was collected. None of the crystallisation methods were successful in getting suitable crystals for X-ray studies.

Anal. Calc.: C 62.16%, H 6.62%, N 5.33%

Found: C 62.70%, H 6.39%, N 5.08%

FAB-MS (% of relative abundance): 951(85); 975(100); 1007(60); 1078 (15);
1426(10); 1535(7); 1798(7)

IR (KBr, cm^{-1}): 3423(m); 2953(s); 2900(s); 1629(s, $\nu_{\text{C=N}}$); 1546(s, $\nu_{\text{C=C}}$); 1443(s, ν_{COO} and $\nu(\text{CO}_3^-)$); 1388(s); 1269(s); 873(w/m)

E.3.2.12. [Cu₄(H₂L9)(μ_2 -H₂O)₂(μ_2 -OH)₂](NO₃)₂ (3.21) / [Cu₃(L9)(MeOH)₂]_n (3.22)

Cu(NO₃)₂.6H₂O (0.24 g, 0.81 mmol) and DHTMB (0.20 g, 0.54 mmol) were dissolved in hot dry ethanol (80 mL). The solution was refluxed for 10 min. after which time a solution of 1,3-diaminopropan-2-ol (0.053 g, 0.54 mmol) in 10 mL of dry methanol was added drop-wise to the refluxing solution. The solution turned slightly darker green. Then, a solution of NaOH (0.023 g, 0.54 mmol) in 10 mL of dry methanol was added drop-wise to the refluxing solution. The reaction mixture

was refluxed for 3 h., left to cool, filtered and evaporated to dryness. 0.255 g of a dark green powder were collected and solubilised in dichloromethane. A small amount of insoluble material was filtered off and the solvent removed. Orange and green crystals formed by slow evaporation of an ethanol solution of the compound. The dark orange crystals were suitable for X-ray studies and proved to be $[\text{Cu}_3(\text{L9})(\text{MeOH})_2]_n$ (3.22). The data were collected using line 9.8 of the Synchrotron Radiation Source at Daresbury. As there was only a small amount of product isolated, no further characterisations were undertaken. It was only detected by FAB as part of the contaminated tetranuclear compound (3.21).

FAB-MS (% of relative abundance) for 3.21 and 3.22: 1015(35); 1031(100);
1093(35); 1459(5);
1653(10); 2137(45);
2202(15)

Anal. Calc.: C 45.70%, H 5.40%, N 6.00%, for 3.21. $\text{CH}_2\text{Cl}_2 \cdot \text{H}_2\text{O}$ (powder)

Found: C 45.65%, H 4.67%, N 6.35%

IR (KBr, cm^{-1}) for 3.21: 3430(m,s); 2958(s); 1644(s, $\nu_{\text{C}=\text{N}}$); 1562(w, $\nu_{\text{C}=\text{O}}$);
1460(m); 1384(s, $\nu_3(\text{NO}_3^-)$)

E.3.2.13. $[\text{Ni}_4(\text{H}_2\text{L9})(\mu_2\text{-OH})_2(\mu_2\text{-H}_2\text{O})_2(\text{EtOH})_4](\text{ClO}_4)_2$ (3.23)

$\text{Ni}(\text{ClO}_4)_2 \cdot 6\text{H}_2\text{O}$ (0.40 g, 1.08 mmol) and DHTMB (0.20 g, 0.54 mmol) were dissolved in hot dry ethanol (80 mL). The solution was refluxed for 10 min. after which time a solution of 1,3-diaminopropan-2-ol (0.053 g, 0.54 mmol) in 10 mL of dry methanol was added drop-wise to the refluxing solution. The solution turned slightly darker green. Then, a solution of NaOH (0.023 g, 0.54 mmol) in 10 mL of dry methanol was added drop-wise to the refluxing solution. The reaction mixture was left under reflux for 6-7 h. The solution was then left to cool, filtered, concentrated and left to evaporate slowly. Green crystals suitable for X-ray studies were isolated and data were collected using line 9.8 of the Synchrotron Radiation Source at Daresbury. 0.23 g of crystalline powder was collected and dried in vacuo. The powder kept its green colour. As the powder was contaminated (first elemental

analysis), it was dissolved in dichloromethane and a small amount of pink impurities were filtered off. The solvent was removed to give a green powder. Yield: 54%.

Anal. Calc.: C 46.13%, H 5.80%, N 3.53%, for $[\text{Ni}_4(\text{H}_2\text{L9})(\mu_2\text{-OH})_2(\mu_2\text{-H}_2\text{O})_2\text{-}(\text{EtOH})_4](\text{ClO}_4)_2 \cdot 2\text{H}_2\text{O}$ (powder)

Found: C 46.18%, H 5.60%, N 3.58%

IR (KBr, cm^{-1}): 3416(b,s); 2960(s); 2868(m); 1633(s, $\nu_{\text{C=N}}$); 1552(w, $\nu_{\text{C=O}}$); 1477(m); 1394(m); 1364(m); 1274(m); 1223(s); 1089(b,s, $\nu_3(\text{ClO}_4^-)$); 625(s, $\nu_4(\text{ClO}_4^-)$)

E.3.2.14. $[\text{Cu}_4(\text{H}_2\text{L9})(\mu_2\text{-H}_2\text{O})_2(\mu_2\text{-OH})_2](\text{NO}_3)_2$ (3.21)

$\text{Cu}(\text{NO}_3)_2 \cdot 6\text{H}_2\text{O}$ (0.32 g, 1.08 mmol) and DHTMB (0.20 g, 0.54 mmol) were dissolved in hot dry ethanol (80 mL). The solution was refluxed for 10 min. after which time a solution of 1,3-diaminopropan-2-ol (0.053 g, 0.54 mmol) in 10 mL of dry methanol was added drop-wise to the refluxing solution. The solution turned slightly darker green. Then, a solution of NaOH (0.046 g, 1.08 mmol) in 10 mL of dry methanol was added drop-wise to the refluxing solution. The reaction mixture was left under reflux for 3 h., left to cool, filtered and evaporated to dryness. The dark green residue was dissolved in dichloromethane and a light blue powder (copper salts) filtered off. The solvent was removed to give a dark green powder that was washed with water to completely remove the salts contaminating the compound. Yield: 0.19 g, 50%. Green crystals suitable for X-ray studies were isolated by slow-evaporation of an ethanol solution of 3.21. The formula of those crystals has been determined by X-ray as being $[\text{Cu}_4(\text{H}_2\text{L9})(\mu_2\text{-H}_2\text{O})_2(\mu_2\text{-OH})_2](\text{NO}_3)_2$ (3.21).

Anal. Calc.: C 47.10%, H 5.60%, N 6.30%, for $\text{Cu}_4(\text{H}_2\text{L9})(\mu_2\text{-H}_2\text{O})_2(\mu_2\text{-OH})_2\text{-}(\text{NO}_3)_2 \cdot 2\text{H}_2\text{O}$ (powder)

Found: C 47.25%, H 5.05%, N 6.16%

FAB-MS (% of relative abundance): 969(55); 1031(65); 1091(25); 1109(20); 1264(35); 1514(7); 1576(5)

IR (KBr, cm^{-1}): 3424(b,m); 2956(m); 1645(m, $\nu_{\text{C=N}}$); 1562(w, $\nu_{\text{C=O}}$); 1384(s, $\nu_3(\text{NO}_3^-)$)

E.3.2.15. [Cu₄(L9)(OAc)₂(HOAc)₃(DMF)] (3.24)

Cu(OAc)₂·H₂O (0.22 g, 1.08 mmol) and DHTMB (0.20 g, 0.54 mmol) were dissolved in hot dry methanol (100 mL). A bright green precipitate appeared. The solution was refluxed for 10 min. after which time a solution of 1,3-diaminopropan-2-ol (0.053 g, 0.54 mmol) in 10 mL of dry methanol was added drop-wise to the refluxing solution. The solution turned darker green. The reaction mixture was left under reflux for 16 h. after which time the solution was filtered hot and the dark green filtrate evaporated to dryness. The dark green residue was dissolved in dichloromethane. A small amount of copper salt was filtered off. 0.29 g of an emerald green powder was collected after the solvent was removed. The powder was dissolved in dimethylformamide and diethylether slowly diffused into the solution. After a week, 0.25 g of green powder was collected and washed with water. Yield: 0.23 g, 57%.

Anal. Calc.: C 53.33%, H 5.98%, N 4.78%, for [Cu₄(L9)(OAc)₂(AcOH)₃(DMF)]

Found: C 53.44%, H 6.00%, N 4.98%

FAB-MS (% of relative abundance): 989(45); 1448(<5); 1472(<5); 1579(<5)

IR (KBr, cm⁻¹): 3433(b,m); 2954(m); 1628(s, ν_{C=N}); 1567(s, ν_{C=O}); 1438(m,s,
ν_{COO})

E.3.2.16. [Co₄(L9)(μ₂-OH)₄(MeOH)₄](ClO₄)₂ (3.25)

Co(ClO₄)₂·6H₂O (0.40 g, 1.08 mmol) and DHTMB (0.20 g, 0.54 mmol) were dissolved in hot dry ethanol (80 mL). The solution was refluxed for 10 min. after which time a solution of 1,3-diaminopropan-2-ol (0.053 g, 0.54 mmol) in 10 mL of dry methanol was added drop-wise to the refluxing solution. The solution turned darker orange. Then, a solution of NaOH (0.023 g, 0.54 mmol) in 10 mL of dry methanol was added drop-wise to the refluxing solution. The orange-brown reaction mixture was left under reflux for 24 h. after which time the solution had turned dark brown. The solution was then left to cool, filtered, concentrated and left to evaporate slowly. The dark brown residue was dissolved in HPLC grade acetonitrile and a

small amount of pink powder (cobalt salts and unreacted ligand) was filtered off and the solvent removed to give a dark brown powder. Yield: 0.25 g, 60%.

Anal. Calc.: C 45.03%, H 5.79%, N 4.52%, for $[\text{Co}_4(\text{L9})(\mu_2\text{-OH})_4(\text{MeOH})_4](\text{ClO}_4)_2 \cdot \text{CH}_3\text{CN} \cdot 2\text{H}_2\text{O}$ (powder)

Found: C 45.02%, H 5.79%, N 4.47%

FAB-MS (% of relative abundance): 959(100); 1016(40); 1059(95); 1116(60);
1183(5); 1384(20); 1439(7); 1496(7)

IR (KBr, cm^{-1}): 3422(b,s); 2955(s); 1624(s, $\nu_{\text{C=N}}$); 1542(w, $\nu_{\text{C=C}}$); 1447(m);
1394(w); 1364(w); 1268(m); 1223(w); 1090(b,s, $\nu_3(\text{ClO}_4^-)$);
625(m, $\nu_4(\text{ClO}_4^-)$)

E.3.2.17. $[\text{Mn}_4(\text{L11})(\text{MeOH})_4(\text{MeO})_2(\text{OAc})_2]\text{Cl}_2$ (3.26)

$\text{Mn}(\text{OAc})_2 \cdot 4\text{H}_2\text{O}$ (0.27 g, 1.08 mmol) and DHTMB (0.20 g, 0.54 mmol) were dissolved in 60 mL of hot dry methanol and refluxed for 30 min. A solution containing 0.10 g (0.54 mmol) of 1,5-diaminopentan-3-ol (neutralised by KOH) in 10 mL of dry methanol was filtered directly into the refluxing solution and the reflux continued for 1 h. The resulting brown-green solution turned dark green on cooling. The solution was, then, filtered and reduced to approximately 30 mL and dark green crystals (0.10 g) suitable for X-ray studies were isolated after slow diffusion of diethyl ether into this solution over one week. A second crop (0.14 g) of a dark green powder was collected after a longer period. Yield (crystals): 24% (3.26) $\cdot 3\text{H}_2\text{O}$, Yield (powder): 33% (3.26) $\cdot 3\text{H}_2\text{O}$. Overall yield 57%.

Anal. Calc.: C 51.2%, H 6.77%, N 3.61%, for $[\text{Mn}_4(\text{L11})(\text{MeOH})_4(\text{MeO})_2(\text{OAc})_2] \cdot \text{Cl}_2 \cdot 3\text{H}_2\text{O}$ (powder)

Found: C 51.09%, H 6.14%, N 3.51%

FAB-MS (% of relative abundance): 901 (40); 954 (80); 990 (75); 1043 (100);
1096 (45); 1150(45); 1185 (30); 1489 (25);
1512 (10); 1584 (5)

IR (KBr, cm^{-1}): 3406(m); 2957(s); 2866(m); 1619(s, $\nu_{\text{C=N}}$); 1552(s, $\nu_{\text{C=O}}$); 1443(s,
 ν_{COO}); 1439(s, ν_{COO}); 1363(s); 1310(m)

E.3.2.18. [Mn₄(L11)(MeOH)₆(MeO)₂Cl₂](ClO₄)₂ (3.27)

Mn(ClO₄)₂·6H₂O (0.39 g, 1.08 mmol) and DHTMB (0.20 g, 0.54 mmol) were dissolved in 60 mL of hot dry methanol and refluxed for 30 min. Then, a solution containing 0.10 g (0.54 mmol) of 1,5-diaminopentan-3-ol (neutralised by KOH) in 10 mL of dry methanol was filtered directly into the refluxing solution and the reflux continued for 1 h. The resulting brown-green solution turned dark green on cooling. The solution was, then, filtered and reduced to approximately 30 mL and dark green crystals, suitable for X-ray studies, along with a dark green powder were isolated after slow diffusion of diethyl ether into this solution over a period of one week. The crystals were ground, mixed with the powder and washed with dichloromethane. Yield : 0.22 g, 50%.

Anal. Calc.: C 43.18%, H 5.43%, N 3.14%, for [Mn₄(L11)(MeOH)₆(MeO)₂Cl₂]-
(ClO₄)₂·2CH₂Cl₂ (powder)

Found: C 43.21%, H 5.55%, N 3.54%

FAB-MS (% of relative abundance): 955 (55); 991 (100); 1044(70); 1096 (25);
1108(20); 1223(15); 1287(10); 1337(10);
1490(10); 1518(10)

IR (KBr, cm⁻¹): 3421(b,m); 2957(m); 2867(w); 1618(s, ν_{C=N}); 1553(m, ν_{C-O});
1444(m); 1088(m, ν₃(ClO₄⁻)); 626(m, ν₄(ClO₄⁻))

E.3.2.19. [Co₄(L11)(MeOH)(HOAc)₃(MeO)₂(OAc)₂]Cl₂ (3.28)

Co(OAc)₂·4H₂O (0.27 g, 1.08 mmol) was dissolved in dry methanol (10 mL) and added to a solution of DHTMB (0.20 g, 0.54 mmol) in dry ethanol (60 mL). The mixture was refluxed for 30 min. A solution containing 0.10 g (0.54 mmol) of 1,5-diaminopentan-3-ol (neutralised by KOH) in 10 mL of dry methanol was filtered directly into the refluxing solution. The solution turned orange-brown. The reaction mixture was allowed to reflux for 24 h. after which time the solution had turned dark brown. The resulting solution was left to cool and evaporated to dryness. The dark brown powder was dissolved in HPLC grade acetonitrile and a small amount of

insoluble material was filtered off. The solution was left to evaporate slowly but no crystals suitable for X-ray studies were isolated. 0.23 g (57%) of a dark brown powder was collected. None of the crystallisation methods have been successful in getting suitable crystals for X-ray studies.

Anal. Calc.: C 51.98%, H 6.32%, N 3.51%

Found: C 52.27%, H 6.13%, N 2.96%

FAB-MS (% of relative abundance): 955 (40); 990 (100); 1038(100); 1065 (45);
1438(38); 1496(65)

IR (KBr, cm^{-1}): 3415(b,m); 2955(s); 2867(m); 1623(s, $\nu_{\text{C=N}}$); 1553(s, $\nu_{\text{C=O}}$);
1450(s, acetate ν_{COO}); 1362(m); 1270(m); 1218(m)

E.3.2.20. [Ni₄(L11)(MeOH)₅(HOAc)₃(OAc)₂] (3.29)

Ni(OAc)₂·4H₂O (0.27 g, 1.08 mmol) and DHTMB (0.20 g, 0.54 mmol) were dissolved in hot dry ethanol (60 mL). The solution was refluxed for 10-15 min. after which time, a solution containing (0.10 g, 0.54 mmol) of 1,5-diaminopentan-3-ol (neutralised with KOH) in 10 mL of dry methanol was filtered directly into the refluxing solution. The solution turned slightly darker green. The reaction mixture was allowed to reflux for 12 h. after which time the solution was left to cool, filtered and evaporated to dryness. The green residue was dissolved in dichloromethane, the impurities were filtered off and the solvent removed. 0.20 g of an olive green powder was collected. Yield: 48%.

Anal. Calc.: C 51.70%, H 6.60%, N 3.30%, for [Ni₄(L11)(MeOH)₅(HOAc)₃(OAc)₂].
2CH₂Cl₂

Found: C 51.38%, H 6.13%, N 2.87%

FAB-MS (% of relative abundance): 990(30); 1062(65); 1188(100); 1338(80);
1397(20); 1440(25); 1496(30); 1574(20)

IR (KBr, cm^{-1}): 3400(b,m); 2958(s); 1639(s, $\nu_{\text{C=N}}$); 1581(s, $\nu_{\text{C=O}}$); 1420(b,s, ν_{COO});
1363(m)

E.3.2.21. [Cu₄(L11)(OAc)₂(HOAc)₃(MeOH)](3.30) / [Cu₃(L11)]_n (3.31)

Cu(OAc)₂·4H₂O (0.28 g, 1.08 mmol) and DHTMB (0.20 g, 0.54 mmol) were dissolved in hot dry ethanol (60 mL). When DHTMB was added to the copper salt a green precipitate appeared. A solution containing (0.10 g, 0.54 mmol) of 1,5-diaminopentan-3-ol (neutralised with KOH) in 10 mL of dry methanol was filtered directly into the refluxing solution. The solution turned slightly darker green. Then, a solution of NaOH (0.046 g, 1.08 mmol) in 10 mL of dry methanol was added dropwise to the refluxing solution. The solution was refluxed for an additional 16 h. The resulting dark green solution was filtered and reduced to dryness. The residue was dissolved in dichloromethane and a small amount of copper salt filtered off. 0.15 g of a green powder was collected after the solvent was removed.

Anal. (3.30-3.31) Calc.(mixture1:1): C 57.54%, H 6.36%, N 4.36%

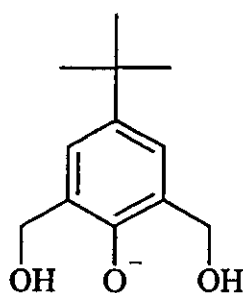
Found: C 57.73%, H 6.20%, N 3.11%

FAB-MS (% of relative abundance): 1515(15); 2091(7); 2269(10)

IR (KBr, cm⁻¹): 3432(b,m); 2954(m); 1620(s, ν_{C=N}); 1540(m, ν_{C=C}); 1449(m, ν_{COO})

E.4. / E.5. Chapter 4 and Chapter 5

Ligand used in chapters 4 and 5:



E.4.1. $[\text{Ni}_2(\text{C}_{12}\text{H}_{13}\text{O}_3)_2(\text{MeOH})_4](\text{ClO}_4)_2$ (4.1) / $[\text{Ni}_7(\text{C}_{12}\text{H}_{13}\text{O}_3)_6(\text{OH})_4(\text{MeO})_2](\text{ClO}_4)_2$ (5.1)

0.26 g (1.26 mmol) of 2,6-diformyl-4-*tert*-butylphenol (DFTP) and 0.58 g (1.57 mmol) of $\text{Ni}(\text{ClO}_4)_2 \cdot 6\text{H}_2\text{O}$ were dissolved in 250 mL of hot isopropanol. For complete dissolution, the suspension was heated under reflux. Then, 0.05 g (1.26 mmol) of sodium hydroxide was dissolved in 20 mL of methanol and added to the refluxing solution, which turned slightly darker green. The resulting mixture was refluxed for 2 h. The solution was then filtered, concentrated and left to evaporate slowly. 0.05 g (12%) of small green crystals of $[\text{Ni}_7(\text{C}_{12}\text{H}_{13}\text{O}_3)_6(\text{OH})_4(\text{MeO})_2](\text{ClO}_4)_2$ (5.1) was collected after 2-3 days and washed with isopropanol. Crystals suitable for X-ray studies were obtained from diethylether diffusion into a methanol solution of 5.1. The isopropanol solution was then concentrated to 10-20 mL and 0.30 g of $[\text{Ni}_2(\text{C}_{12}\text{H}_{13}\text{O}_3)_2(\text{MeOH})_4](\text{ClO}_4)_2$ (green powder) was collected. The powder was dissolved in methanol and diethylether allowed to diffuse into the solution. Green crystals suitable for X-ray studies were isolated after one day. After recrystallisation, 0.29 g (55%) of product was collected.

The reaction can also be performed at room temperature with similar yields for both products.

Anal. Calc.: C 34.20%, H 5.74%, N 0.00%, for $[\text{Ni}_2(\text{C}_{12}\text{H}_{13}\text{O}_3)_2(\text{MeOH})_4](\text{ClO}_4)_2 \cdot 7\text{H}_2\text{O}$ (powder)

Found: C 34.46%, H 5.52%, N 0.01%

IR (KBr, cm^{-1}): 3431(b,s); 2911(s); 1650(s, $\nu_{\text{C=O}}$); 1630(s, $\nu_{\text{C=O}}$); 1537(s, $\nu_{\text{C=C}}$); 1088(s, $\nu_3(\text{ClO}_4^-)$); 626(m, $\nu_4(\text{ClO}_4^-)$)

Anal. Calc.: C 44.28%, H 4.62%, N 0.00%, for $[\text{Ni}_7(\text{C}_{12}\text{H}_{13}\text{O}_3)_6(\text{OH})_4(\text{MeO})_2](\text{ClO}_4)_2 \cdot 2\text{H}_2\text{O}$ (powder)

Found: C 44.34%, H 4.62%, N 0.01%

FAB-MS (% of relative abundance): 526(100); 885(10); 1771(10); 1784(10);
1855(10); 1869(75); 1885(40)

IR (KBr, cm^{-1}): 3434(w,b); 2961(w); 1663(s, $\nu_{\text{C=O}}$); 1625(s, $\nu_{\text{C=O}}$); 1530(s, $\nu_{\text{C=C}}$);
1107(w,b, $\nu_3(\text{ClO}_4^-)$); 626(w, $\nu_4(\text{ClO}_4^-)$)

E.4.2. $[\text{Co}_2(\text{C}_{12}\text{H}_{13}\text{O}_3)_2(\text{MeOH})_4](\text{ClO}_4)_2$ (4.2) / $[\text{Co}_7(\text{C}_{12}\text{H}_{13}\text{O}_3)_6(\text{OH})_4(\text{MeO})_2](\text{ClO}_4)_2$ (5.2)

0.26 g (1.26 mmol) of 2,6-diformyl-4-*tert*-butylphenol (DFTP) and 0.58 g (1.57 mmol) of $\text{Co}(\text{ClO}_4)_2 \cdot 6\text{H}_2\text{O}$ were dissolved in 250 mL of hot isopropanol. For complete dissolution, the suspension is heated under reflux. Then, 0.05 g (1.26 mmol) of sodium hydroxide was dissolved in 20 mL of methanol and added to the refluxing solution which turns slightly darker orange. The resulting mixture was refluxed for 2 h. The solution was then filtered, concentrated and left to evaporate slowly. 0.08 g (22%) of small orange crystals of $[\text{Co}_7(\text{C}_{12}\text{H}_{13}\text{O}_3)_6(\text{OH})_4(\text{MeO})_2](\text{ClO}_4)_2$ (5.2) were collected after 2-3 days and washed with isopropanol. Orange crystals of $[\text{Co}_7(\text{C}_{12}\text{H}_{13}\text{O}_3)_6(\text{MeO})_6](\text{ClO}_4)_2$ suitable for X-ray studies were obtained by diethylether diffusion into a methanol solution of 5.2. The isopropanol solution was then concentrated to 10-20 mL and 0.25 g of $[\text{Co}_2(\text{C}_{12}\text{H}_{13}\text{O}_3)_2(\text{MeOH})_4](\text{ClO}_4)_2$ (orange powder) were collected. The powder was dissolved in methanol and diethylether allowed to diffuse into the solution. Crystals suitable for X-ray studies were isolated after one day. After recrystallisation, 0.24 g (45%) of product was collected.

The reaction can also be performed at room temperature with similar yields for both products.

Anal. Calc.: C 33.58%, H 5.83%, N 0.00%, for $[\text{Co}_2(\text{C}_{12}\text{H}_{13}\text{O}_3)_2(\text{MeOH})_4](\text{ClO}_4)_2 \cdot 8\text{H}_2\text{O}$ (powder)

Found: C 33.57%, H 5.41%, N 0.06%

IR (KBr, cm^{-1}): 3448(b,s); 2967(m); 1654(s, $\nu_{\text{C=O}}$); 1626(s, $\nu_{\text{C=O}}$); 1534(s, $\nu_{\text{C=C}}$);
1090(b,s, $\nu_3(\text{ClO}_4^-)$); 626(m, $\nu_4(\text{ClO}_4^-)$)

Anal. Calc.: C 43.42%, H 4.72%, N 0.00%, for $[\text{Co}_7(\text{C}_{12}\text{H}_{13}\text{O}_3)_6(\text{OH})_4(\text{MeO})_2]-(\text{ClO}_4)_2 \cdot 4\text{H}_2\text{O}$ (powder)

Found: C 43.40%, H 4.59%, N 0.39%

FAB-MS (% of relative abundance): 510(45); 608(35); 805(45); 950(35); 1150(30);
1165(35); 1179(45); 1221(75); 1414(20);
1605(20); 1623(45); 1638(58); 1654(40);
1674(25); 1690(25); 1704(20); 1719(35);
1734(37); 1750(15)

IR (KBr, cm^{-1}): 3448(b,w); 2956(w); 1664(s, $\nu_{\text{C=O}}$); 1631(s, $\nu_{\text{C=O}}$); 1530(s, $\nu_{\text{C=C}}$);
1097(b, s/m, $\nu_3(\text{ClO}_4^-)$); 623(m, $\nu_4(\text{ClO}_4^-)$)

E.4.3. $[\text{Mn}_2(\text{C}_{12}\text{H}_{13}\text{O}_3)_2(\text{MeOH})_4](\text{ClO}_4)_2$ (4.3)

0.26 g (1.26 mmol) of 2,6-diformyl-4-*tert*-butylphenol (DFTP) and 0.57 g (1.57 mmol) of $\text{Mn}(\text{ClO}_4)_2 \cdot 6\text{H}_2\text{O}$ were dissolved in 250 mL of hot refluxing isopropanol. Then, 0.05 g (1.26 mmol) of sodium hydroxide was dissolved in 20 mL of methanol and added to the refluxing solution, which turned slightly darker orange. The resulting mixture was refluxed for 2 h. The resulting mixture was refluxed for 2 h. after which time it was allowed to cool and some unreacted ligand was filtered off. The resulting filtrate was then concentrated to 50 mL, filtered again and left to evaporate slowly. After one day, needle-shaped yellow crystals appeared. Crystals were filtered off, ground and dried under vacuum. The resulting filtrate was concentrated and a yellow powder (4.3) precipitated. The powder was filtered off and dried in vacuo. Yield: 0.18 g, 34%. The powder was recrystallised by diethylether diffusion into a methanol solution of the complex. Yellow crystals suitable for X-ray studies were obtained using this method. The filtrate was darker orange and when evaporated to dryness, a small amount of dark brown powder believed to be a

multinuclear manganese cluster according to the FAB results (*cf.* tabulated data in chapter 4) was isolated.

Anal. Calc.: C 39.68%, H 4.99%, N 0.00%, (powder)

Found: C 39.01%, H 4.65%, N 0.15%

IR (KBr, cm^{-1}): 3435(b,w); 2960(w); 1654(s, $\nu_{\text{C=O}}$); 1532(s, $\nu_{\text{C=C}}$); 1096(m, $\nu_3(\text{ClO}_4^-)$); 624(m, $\nu_4(\text{ClO}_4^-)$)

E.4.4. $[\text{Cu}_2(\text{C}_{12}\text{H}_{13}\text{O}_3)_2(\text{MeOH})_2(\text{ClO}_4)_2]$ (4.4)

0.26 g (1.26 mmol) of 2,6-diformyl-4-*tert*-butylphenol (DFTP) and 0.58 g (1.57 mmol) of $\text{Cu}(\text{ClO}_4)_2 \cdot 6\text{H}_2\text{O}$ were dissolved in 250 mL of hot refluxing isopropanol. Then, 0.05 g (1.26 mmol) of sodium hydroxide was dissolved in 20 mL of methanol and added to the refluxing solution, which turned slightly darker green. The resulting mixture was refluxed for 2 h. after which time it was allowed to cool and some unreacted ligand was filtered off. The resulting filtrate was then concentrated to 50 mL, filtered again and left to evaporate slowly. 0.22 g (44%) of a green crystalline powder was isolated after 2-3 days and washed with isopropanol. Green crystals suitable for X-ray studies were obtained by diethylether diffusion into a methanol solution of 4.3.

Anal. Calc.: C 36.45%, H 4.70%, N 0.00, for $[\text{Cu}_2(\text{C}_{12}\text{H}_{13}\text{O}_3)_2(\text{MeOH})_2(\text{ClO}_4)_2] \cdot 3\text{H}_2\text{O}$ (powder)

Found: C 36.54%, H 3.81%, N 0.04%

IR (KBr, cm^{-1}): 3488(b,s); 2970(s); 1635(s, $\nu_{\text{C=O}}$); 1618(s, $\nu_{\text{C=O}}$); 1590(m); 1542(s, $\nu_{\text{C=C}}$); 1103 (b,m/s, $\nu_3(\text{ClO}_4^-)$); 626(m, $\nu_4(\text{ClO}_4^-)$)

E.4.5. $[\text{Ni}_2(\text{C}_{12}\text{H}_{13}\text{O}_3)_2(\text{MeOH})_2(\text{NO}_3)_2]$ (4.5)

This complex was isolated from a reaction in which we were aiming to form $[\text{Ni}_4(\text{L1})(\text{OH})](\text{NO}_3)_3$. 0.05 g of 4.5 was collected. No attempt to directly synthesise the complex, was made.

0.26 g (1.26 mmol) of 2,6-diformyl-4-*tert*-butylphenol (DFTP) and 0.92 g (2.60 mmol) of $\text{Ni}(\text{NO}_3)_2 \cdot 6\text{H}_2\text{O}$ were dissolved in 250 mL of hot ethanol. To the refluxed solution, a solution of the dinitrate salt of 1,5-diaminopentan-3-ol (achieved by adding AgNO_3 and filtering AgCl off) was added. The reaction mixture was refluxed for 2 h., left to cool, filtered and concentrated. The solution was left to evaporate slowly overnight. Green crystals of 4.5 appeared and were isolated. They were suitable for X-ray studies without any further recrystallisation.

Anal. Calc.: C 42.43%, H 4.65%, N 3.81%, for $[\text{Ni}_2(\text{C}_{12}\text{H}_{13}\text{O}_3)_2(\text{MeOH})_2(\text{NO}_3)_2]$.

H_2O (powder)

Found: C 42.37%, H 4.05%, N 4.05%

IR (KBr, cm^{-1}): 3422(b,m); 2964(m); 1648(s, $\nu_{\text{C=O}}$); 1626(s, $\nu_{\text{C=O}}$); 1534(s, $\nu_{\text{C=C}}$);
1450(w/m, $\nu(\text{NO}_3^-)$); 1384(s, $\nu_3(\text{NO}_3^-)$); 1322(w, $\nu(\text{NO}_3^-)$)

E.4.6. $[\text{Cu}(\text{C}_{12}\text{H}_{13}\text{O}_3)_2]$ (4.6)

0.26 g (1.26 mmol) of 2,6-diformyl-4-*tert*-butylphenol (DFTP) and 0.93 g (2.50 mmol) of $\text{Cu}(\text{ClO}_4)_2 \cdot 6\text{H}_2\text{O}$ were dissolved in 50 mL of acetonitrile at room temperature. Then, 0.05 g (1.26 mmol) of sodium hydroxide was dissolved in 25-30 mL of distilled water and added to the stirring solution. The resulting reaction mixture was left stirring for 2.1/2 h., turning cloudy after a while. The solution was filtered and concentrated. 0.16 g (54%) of 4.6 (khaki green powder) was isolated. Pale green crystals suitable for X-ray studies were obtained by slow diffusion of diethylether into a dichloromethane/acetonitrile solution of the complex.

Anal. Calc.: C 58.59%, H 5.73%, N 0.00%, for $[\text{Cu}(\text{C}_{12}\text{H}_{13}\text{O}_3)_2] \cdot \text{H}_2\text{O}$ (powder)

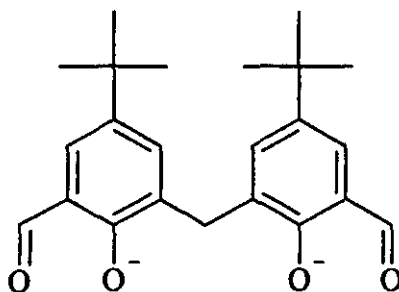
Found: C 58.52%, H 5.65%, N 0.06%

IR (KBr, cm^{-1}): 3447(m); 2959(m); 2867(w); 1671(s, $\nu_{\text{C=O}}$); 1625(s, $\nu_{\text{C=O}}$);
1601(m, $\nu_{\text{C=O}}$); 1527(s, $\nu_{\text{C=C}}$)

E.5 Chapter 5

For compounds $[\text{Ni}_7(\text{C}_{12}\text{H}_{13}\text{O}_3)_6(\text{OH})_4(\text{MeO})_2](\text{ClO}_4)_2$ (**5.1**) and of $[\text{Co}_7(\text{C}_{12}\text{H}_{13}\text{O}_3)_6(\text{OH})_4(\text{MeO})_2](\text{ClO}_4)_2$ (**5.2**): see section E.4/E.5

Ligand used for complex **5.3**:



$[\text{Mn}_3(\text{C}_{23}\text{H}_{26}\text{O}_4)_2(\text{MeOH})_4(\text{H}_2\text{O})](\text{ClO}_4)_2$ (**5.3**)

$\text{Mn}(\text{ClO}_4)_2 \cdot 6\text{H}_2\text{O}$ (0.30 g, 0.81 mmol) and DHTMB (0.20 g, 0.54 mmol) were dissolved in 80 mL of hot methanol and refluxed for 30 min. A solution containing (0.15 mL, 1.08 mmol) of triethylamine in 10 mL of methanol was added to the refluxing solution, which turned brighter yellow. The solution was left to reflux for 2.1/2 h. after which time it was allowed to cool. The orange-brown solution was then filtered, concentrated and left to evaporate. The residue was recrystallised in MeOH/ CH_3CN . Yield: 0.20 g, 57%. Yellow crystals suitable for X-ray studies were obtained by slow diffusion of diethylether into a MeOH/ CH_3CN solution of **5.3**.

Anal. Calc.: C 47.37%, H 5.92%, N 0.00%, for $[\text{Mn}_3(\text{C}_{23}\text{H}_{26}\text{O}_4)_2(\text{MeOH})_4(\text{H}_2\text{O})](\text{ClO}_4)_2 \cdot \text{MeOH}, \text{H}_2\text{O}$ (powder)

Found: C 47.76%, H 6.04%, N 0.21%

FAB-MS (% of relative abundance): 1074(15); 1265(50); 1288(15)

IR (KBr, cm^{-1}): 3427(b,m); 2961(s); 1647(s, $\nu_{\text{C=O}}$); 1591(m, $\nu_{\text{C=O}}$); 1540(m, $\nu_{\text{C=C}}$); 1459(m); 1268(m,s); 1215(m,s); 1121(b, m, $\nu_3(\text{ClO}_4^-)$); 626(w, $\nu_4(\text{ClO}_4^-)$)

REFERENCES

- (1) Lindoy, L. F. *The Chemistry of Macrocyclic Ligand Complexes*; Cambridge University Press: Cambridge, UK, 1989.
- (2) McKee, V. *Adv. Inorg. Chem.* **1993**, *40*, 323.
- (3) Guerriero, P.; Tamburini, S.; Vigato, P. A. *Coord. Chem. Rev.* **1995**, *139*, 17.
- (4) Constable, E. C. *Coordination Chemistry of Macrocyclic Compounds*; Oxford University Press: New York, 1999.
- (5) Vigato, P. A.; Tamburini, S.; Fenton, D. E. *Coord. Chem. Rev.* **1990**, *106*, 25.
- (6) Fenton, D. E. *Biocoordination Chemistry*; 1st ed.; Oxford University Press: Oxford, UK, 1995.
- (7) Lippard, S. J.; Berg, J. M. *Principles of Bioinorganic Chemistry*; University Science Book: Mill Valley (California), 1994.
- (8) Bertini, I.; Gray, H. B.; Lippard, S. J.; Valentine, J. S. *Bioinorganic Chemistry*; University Science Books: Mill Valley (California), 1994.
- (9) Gould, R. D. *Coord. Chem. Rev.* **1996**, *156*, 237.
- (10) Zagal, J. H. *Coord. Chem. Rev.* **1992**, *119*, 89.
- (11) Keizer, S. P.; Han, W.; Stillman, M. J. *Inorg. Chem.* **2002**, *41*, 353.
- (12) Guillaud, G.; Simon, J.; Germain, J. P. *Coord. Chem. Rev.* **1998**, *178-180*, 1433.
- (13) Gregory, P. J. *Porphyrins Phthalocyanines* **2000**, *4(4)*, 432.
- (14) Fenton, D. E. In *Structure and Bonding*: Berlin, 1987; Vol. 68; p 187.
- (15) Menif, R.; Martell, A. E.; Squattrito, P. J.; Clearfield, A. *Inorg. Chem.* **1990**, *29*, 4723.
- (16) Adams, H.; Bailey, N. A.; Debaecker, N.; Fenton, D. E.; Kanda, W.; Latour, J.-M.; Okawa, H.; Sakiyama, H. *Angew. Chem. Int. Ed.* **1995**, *34(22)*, 2535.
- (17) Okawa, H.; Furutachi, H.; Fenton, D. E. *Coord. Chem. Rev.* **1998**, *174*, 51.
- (18) Bailey, N. A.; Eddy, M. M.; Fenton, D. E.; Jones, G.; Moss, S.; Mukhopadhyay, A. *J. Chem. Soc., Chem. Commun.* **1981**, 628.
- (19) Bailey, N. A.; Eddy, M. M.; Fenton, D. E.; Moss, S.; Mukhopadhyay, A. *J. Chem. Soc., Dalton Trans.* **1984**, 2281.

- (20) Fenton, D. E.; Moody, R. *J. Chem. Soc., Dalton Trans.* **1987**, 219.
- (21) Tandon, S. S.; McKee, V. *J. Chem. Soc., Dalton Trans.* **1989**, 19.
- (22) Dutta, S. K.; Flörke, U.; Mohanta, S.; Nag, K. *Inorg. Chem.* **1998**, 5029.
- (23) Korupoju, S. R.; Zacharias, P. S. *Chem. Commun.* **1998**, 1267.
- (24) Jazwinski, J.; Lehn, J.-M.; Lilienbaum, D.; Ziessel, R.; Guilhem, J.; Pascard, C. *J. Chem. Soc., Chem. Commun.* **1987**, 1691.
- (25) McDowell, D.; Nelson, J. *Tetrahedron Lett.* **1988**, 29, 385.
- (26) Houjou, H.; Lee, S.-K.; Hishikawa, Y.; Nagawa, Y.; Hiratani, K. *Chem. Commun.* **2000**, 2197.
- (27) Schmidt, S.; Bauer, W.; Heinemann, F. W.; Lanig, H.; Grohmann, A. *Angew. Chem. Int. Ed.* **2000**, 39(5), 913.
- (28) Nelson, J.; McKee, V.; Morgan, G. *Prog. Inorg. Chem.* **1998**, 47, 167.
- (29) Brooker, S.; McKee, V. *J. Chem. Soc., Dalton Trans.* **1990**, 2397.
- (30) Nelson, S. M. *Pure & Appl. Chem.* **1980**, 52, 2461.
- (31) Adams, H.; Bailey, N. A.; Fenton, D. E.; Good, R. J.; Moody, R.; Barbarin, C. O. R. d. *J. Chem. Soc., Dalton Trans.* **1987**, 207.
- (32) Bailey, N. A.; Fenton, D. E.; Moody, R.; Barbarin, C. O. R. d.; Sciambarella, I. N.; Latour, J.-M.; Limosin, D.; McKee, V. *J. Chem. Soc., Dalton Trans.* **1987**, 2519.
- (33) Brooker, S.; McKee, V. *Chem. Commun.* **1989**, 619.
- (34) Brooker, S.; McKee, V.; Metcalfe, T. *Inorg. Chim. Acta* **1996**, 246, 171.
- (35) Brooker, S.; Kelly, R. J.; Moubaraki, B.; Murray, K. S. *Chem. Commun.* **1996**, 2579.
- (36) Robson, R. *Aust. J. Chem.* **1970**, 23, 2217.
- (37) Pilkington, N. H.; Robson, R. *Aust. J. Chem.* **1970**, 23, 2225.
- (38) Menif, R.; Martell, A. E. *J. Chem. Soc., Chem. Commun.* **1989**, 1521.
- (39) Atkins, A. J.; Black, D.; Blake, A. J.; Marin-Becerra, A.; Parsons, S.; Ruiz-Ramirez, L.; Schröder, M. *J. Chem. Soc., Chem. Commun.* **1996**, 457.
- (40) Black, D.; Blake, A. J.; Finn, R. L.; Lindoy, L. F.; Nezhadali, A.; Rougnaghi, G.; Tasker, P. A.; Schröder, M. *J. Chem. Soc., Chem. Commun.* **2002**, 340.
- (41) Huang, W.; Gou, S.; Hu, D.; Chantrapromma, S.; Fun, H.-K.; Meng, Q. *Inorg.*

- Chem.* **2001**, *40*, 1712.
- (42) Guerriero, P.; Vigato, P. A.; Bunzyl, J.-C. G.; Moret, E. *J. Chem. Soc., Dalton Trans.* **1990**, 647.
- (43) Lacroix, P.; Kahn, O.; Theobald, F.; Leroy, J.; Wakselman, C. *Inorg. Chim. Acta* **1988**, *142*, 129.
- (44) Thompson, L. K.; Mandal, S. K.; Tandon, S. S.; Bridson, J. N.; Park, M. K. *Inorg. Chem.* **1996**, *35*, 3117.
- (45) Bailey, N. A.; Fenton, D. E.; Moody, R.; Scrimshire, P. J.; Belorizky, E.; Fries, P. H.; Latour, J.-M. *J. Chem. Soc., Dalton Trans.* **1988**, 2817.
- (46) Crane, J. D.; Fenton, D. E.; Latour, J.-M.; Smith, A. J. *J. Chem. Soc., Dalton Trans.*, **1991**, 2979.
- (47) Yonemura, M.; Usuki, N.; Nakamura, Y.; Ohba, M.; Okawa, H. *J. Chem. Soc., Dalton Trans.* **2000**, 3624.
- (48) Gelling, O. J.; Meetsma, A.; Feringa, B. L. *Inorg. Chem.* **1990**, *29*, 2816.
- (49) Hoskins, B. F.; McLeod, N. J.; Schaap, H. A. *Aust. J. Chem.* **1976**, *29*, 515.
- (50) Mandal, S. K.; Thompson, L. K.; Newlands, M. J.; Gabe, E. J. *Inorg. Chem.* **1989**, *28*, 3707.
- (51) Gagné, R. R.; Henling, L. M.; Kistenmacher, T. J. *Inorg. Chem.* **1980**, *19*, 1226.
- (52) The United Kingdom Chemical Database Service, T. U. K. C. D.; Fletcher, D. A.; McMeeking, R. F.; Parkin, D. J. *J. Chem. Inf. Comput. Sci.* **1996**, *36*, 746.
- (53) Hoskins, B. F.; Williams, G. A. *Aust. J. Chem.* **1975**, *28*, 2697.
- (54) Chang, H.-R.; Larsen, S. K.; Boyd, P. D. W.; Pierpont, C. G.; Hendrickson, D. N. *J. Am. Chem. Soc.* **1988**, *110*, 4565.
- (55) Adams, H.; Bailey, N. A.; Bertrand, P.; Barbarin, C. O. R. D.; Fenton, D. E.; Gou, S. *J. Chem. Soc., Dalton Trans.* **1995**, 275.
- (56) Lambert, S. L.; Hendrickson, D. N. *Inorg. Chem.* **1979**, *18(10)*, 2683.
- (57) Spiro, C. L.; Lambert, S. L.; Smith, T. J.; Duesler, E. N.; Gagné, R. R.; Hendrickson, D. N. *Inorg. Chem.* **1981**, *20*, 1229.
- (58) Hoskins, B. F.; Robson, R.; Williams, G. A. *Inorg. Chim. Acta* **1076**, *16*, 121.

- (59) Wada, H.; Motoda, K.; Ohba, M.; Sakiyama, H.; Matsumoto, N.; Okawa, H. *Bull. Chem. Soc. Jpn.* **1995**, *68*, 1105.
- (60) Aono, T.; Wada, H.; Yonemura, M.; Ohba, M.; Okawa, H.; Fenton, D. E. *J. Chem. Soc., Dalton Trans.* **1997**, 1527.
- (61) Huang, W.; Gou, S.; Hu, D.; Chantrapromma, S.; Fun, H.-K.; Meng, Q. *Inorg. Chem.* **2002**, *41*, 864.
- (62) Gagné, R. R.; Spiro, C. L.; Smith, T. J.; Hamann, C. A.; Thies, W. R.; Shiemke, A. K. *J. Am. Chem. Soc.* **1981**, *103*, 4073.
- (63) Ohtsuka, S.; Kodera, M.; Motoda, K.; Ohba, M.; Okawa, H. *J. Chem. Soc., Dalton Trans.* **1995**, 2599.
- (64) Aono, T.; Wada, H.; Aratake, Y.; Matsumoto, N.; Okawa, H.; Matsuda, Y. *J. Chem. Soc., Dalton Trans.* **1996**, 25.
- (65) Mohanta, S.; Nanda, K. N.; Thompson, L. K.; Flörke, U.; Nag, K. *Inorg. Chem.* **1998**, *37*, 1465.
- (66) Kahn, O. In *Structure and Bonding*: Berlin, 1987; Vol. 68; p 89.
- (67) Yamami, M.; Usuki, N.; Nakamura, Y.; Ohba, M.; Okawa, H. *Inorg. Chem.* **1998**, *37*, 6832.
- (68) Furutachi, H.; Fujinami, S.; Suzuki, M.; Okawa, H. *J. Chem. Soc., Dalton Trans.* **2000**, 2761.
- (69) Tandon, S. S.; Thompson, L. K.; Bridson, J. N.; Benelli, C. *Inorg. Chem.* **1995**, *34*, 5507.
- (70) Tandon, S. S.; Thompson, L. K.; Bridson, J. N.; Mckee, V.; Downard, A. J. *Inorg. Chem.* **1992**, 4635.
- (71) Spodine, E.; Moreno, Y.; Garland, M. T.; Pena, O.; Baggio, R. *Inorg. Chim. Acta* **2000**, *309*, 57.
- (72) Downard, A. J.; McKee, V.; Tandon, S. S. *Inorg. Chim. Acta* **1990**, *173*, 181.
- (73) Drew, M. G. B.; Rodgers, A.; McCann, M.; Nelson, S. M. *J. Chem. Soc., Chem. Commun.* **1978**, 415.
- (74) Cook, D. H.; Fenton, D. E.; Drew, M. G. B.; Rodgers, A.; McCann, M.; Nelson, S. M. *J. Chem. Soc., Dalton Trans.* **1979**, 414.

- (75) Nelson, S. M.; Esho, F. S.; Drew, M. G. B. *J. Chem. Soc., Dalton Trans.* **1982**, 407.
- (76) Drew, M. G. B.; Cairns, C.; Lavery, A.; Nelson, S. M. *J. Chem. Soc., Chem. Commun.* **1980**, 1122.
- (77) Drew, M. G. B.; Nelson, J.; Nelson, S. M. *J. Chem. Soc., Dalton Trans.* **1981**, 1678.
- (78) Drew, M. G. B.; McCann, M.; Nelson, S. M. *J. Chem. Soc., Chem. Commun.* **1979**, 481.
- (79) Drew, M. G. B.; McCann, M.; Nelson, S. M. *J. Chem. Soc., Dalton Trans.* **1981**, 1868.
- (80) Nelson, S. M. *Pure Appl. Chem.* **1980**, *52*, 2461.
- (81) McKee, V.; Smith, J. *J. Chem. Soc., Chem. Commun.* **1983**, 1465.
- (82) Brooker, S.; McKee, V.; Shepard, W. B.; Pannell, L. K. *J. Chem. Soc., Dalton Trans.* **1987**, 2555.
- (83) McCann, V. H.; Jones, D. H.; McKee, V.; Faulalo, K. *Hyperfine Interactions* **1990**, *56*, 1465.
- (84) Dutton, J. C.; Fallon, G. D.; Murray, K. S. *J. Chem. Soc., Chem. Commun.* **1990**, 64.
- (85) Brooker, S.; Kelly, R. J.; Sheldrick, G. M. *J. Chem. Soc., Chem. Commun.* **1994**, 487.
- (86) Adams, H.; Elsegood, M. R. J.; Fenton, D. E.; Heath, S. L.; Ryan, S. J. *J. Chem. Soc., Dalton Trans.* **1999**, 2031.
- (87) Eppley, H. J.; Aubin, S. M. J.; Temple, M. W.; Adams, D. M.; Tsai, H.-L.; Grillo, V. A.; Castro, S. L.; Sun, Z.; Folting, K.; Huffman, J. C.; Hendrickson, D. N.; Christou, G. *Mol. Cryst. And Liq. Cryst.* **1997**, *305*, 167.
- (88) McKee, V.; Tandon, S. S. *Chem. Commun.* **1988**, 1334.
- (89) McCrea, J.; McKee, V.; Metcalfe, T.; Tandon, S. S.; Wikaira, J. *Inorg. Chim. Acta* **2000**, *297*, 220.
- (90) Kruger, P. E. *Unpublished work* **1996**.
- (91) Metcalfe, J. E. Ph.D, Queen's University of Belfast, Faculty of science and Agriculture, **1998**.

- (92) Nakatsugawa, H.; Iguchi, E. *Surf. Science* **1996**, 357-358, 96.
- (93) McKee, V.; Tandon, S. S. *J. Chem. Soc., Dalton Trans.* **1991**, 221.
- (94) McKee, V.; Tandon, S. S. *Inorg. Chem.* **1989**, 2901.
- (95) McKee, V.; Tandon, S. S. *Chem. Commun.* **1988**, 385.
- (96) Launay, F. M. Ph.D, The Queen's University Of Belfast, Faculty of Science and Agriculture, 2001.
- (97) Wikaira, J. Ph.D, University of Canterbury, 1996.
- (98) Lingga, N. Ph.D, University of Canterbury, 1996.
- (99) Kruger, P. E.; Launay, F.; McKee, V. *Chem. Commun.* **1999**, 639.
- (100) Xu, Z.; Lau, S.; Bohn, P. W. *Surf. Science* **1993**, 296, 57.
- (101) Bell, M.; Edwards, A. J.; Hoskins, B. F.; Kachab, E. H.; Robson, R. *Chem. Commun.* **1987**, 1852.
- (102) Edwards, A. J.; Hoskins, B. F.; Kachab, E. H.; Markiewicz, A.; Murray, K. S.; Robson, R. *Inorg. Chem.* **1992**, 31, 3585.
- (103) Bell, M.; Edwards, A. J.; Hoskins, B. F.; Kachab, E. H.; Robson, R. *J. Am. Chem. Soc.* **1989**, 111, 3603.
- (104) Grannas, M. J.; Hoskins, B. F.; Robson, R. *Inorg. Chem.* **1994**, 33, 1071.
- (105) Edwards, A. J.; Hoskins, B. F.; Robson, R.; Wilson, J. C.; Moubaraki, B.; Murray, K. S. *J. Chem. Soc., Dalton Trans.* **1994**, 1837.
- (106) Mohanta, S.; Nanda, K. K.; Werner, R.; Haase, W.; Mukherjee, A. K.; Dutta, S. K.; Nag, K. *Inorg. Chem.* **1997**, 36, 4656.
- (107) Nanda, K. K.; Venkatsubramanian, K.; Majumdar, D.; Nag, K. *Inorg. Chem.* **1994**, 33, 1581.
- (108) Yonemura, M.; Okawa, H.; Ohba, M.; Fenton, D. E.; Thompson, L. K. *Chem. Commun.* **2000**, 817.
- (109) Nakamura, Y.; Yonemura, M.; Arimura, K.; Usuki, N.; Ohba, M.; Okawa, H. *Inorg. Chem.* **2001**, 40, 3739.
- (110) Asato, E.; Furutachi, H.; Kawahashi, T.; Mikuriya, M. *J. Chem. Soc., Dalton Trans.* **1995**, 3897.
- (111) Tandon, S. S.; Thompson, L. K.; Bridson, J. N. *J. Chem. Soc., Chem. Commun.* **1992**, 911.

- (112) Hoskins, B. F.; Robson, R.; Smith, P. *Chem. Commun.* **1990**, 488.
- (113) Manura, J. J.; Manura, J. D., *Isotope Distribution Calculator, SIS*, 1996.
<http://www.sisweb.com/cgi-bin/mass10.pl>
- (114) Okawa, H.; Kida, S. *Bull. Chem. Soc. Jpn.* **1972**, *45*, 1759.
- (115) Mikes, O. In *Laboratory Handbook of Chromatographic Methods*; Mikes, O., Ed.; D. Van Nostrand Company Ltd: London, 1966; p 316.
- (116) Blake, A. J.; Danks, J. P.; Harrison, A.; Parsons, S.; Schooler, P.; Whittaker, G.; Schröder, M. *J. Chem. Soc., Dalton Trans.* **1998**, 2335.
- (117) Cromie, S.; Launay, F.; McKee, V. *Chem. Commun.* **2001**, 1918.
- (118) Asokan, A.; Varghese, B.; Caneschi, A.; Manoharan, P. T. *Inorg. Chem.* **1998**, *37*, 228.
- (119) Gou, S.; Fenton, D. E. *Inorg. Chim. Acta* **1994**, *223*, 169.
- (120) Atkins, A. J.; Blake, A. J.; Schröder, M. *J. Chem. Soc., Chem. Commun.* **1993**, 353.
- (121) McKee, V. *J. Chem. Soc., Dalton Trans.* **1989**, 19.
- (122) Deacon, G. B.; Phillips, R. J. *Coord. Chem. Rev.* **1980**, *33*, 227.
- (123) Blake, A. J.; Hyde, T. I.; Smith, R. S. E.; Schröder, M. *J. Chem. Soc., Chem. Commun.* **1986**, 334.
- (124) Dhawan, B.; C.D.; Gutsche J. *Org. Chem.* **1983**, *48(9)*, 1539.
- (125) Vogel, A. I. *Vogel's Textbook of Practical Organic Chemistry*; 5th. ed.; Prentice Hall, 1996.
- (126) Taniguchi, S. *Bull. Chem. Soc. Jpn.* **1984**, *57*, 2683.
- (127) Boss, R.; Scheffold, R. *Angew. Chem. Int. Ed. Engl.* **1976**, *15(9)*, 558.
- (128) Mandal, S. K.; Nag, K. J. *J. Chem. Soc., Dalton Trans.* **1984**, 2141.
- (129) Ginsberg, A. P.; Martin, R. L.; Brookes, R. W.; Sherwood, R. C. *Inorg. Chem.* **1972**, *11*, 2884.
- (130) Carlin, R. L. *Magnetochemistry*: Berlin Heidelberg, 1986.
- (131) Kennard, C. H. L.; O'Reilly, E. J.; Smith, G. *Polyhedron* **1984**, *3*, 689.
- (132) Barrios, A. M.; Lippard, S. J. *J. Am. Chem. Soc.* **1999**, *121*, 11751.
- (133) Volkmer, D.; Hommerich, B.; Griesar, K.; Haase, W.; Krebs, B. *Inorg. Chem.* **1996**, *35*, 3792.

- (134) Eremenko, I. L.; Nefedov, S. E.; Sidirov, A. A.; Golubnichaya, M. A.; Danilov, P. V.; Ikorskii, V. N.; Shvedenkov, Y. G.; Novotortsev, V. M.; Moiseev, I. I. *Inorg. Chem.* **1999**, *38*, 3764.
- (135) Meyer, F.; Kaifer, E.; Kircher, P.; Heinze, K.; Pritzow, H. *Chem. Eur. J.* **1999**, *5*(5), 1617.
- (136) Barrios, A. M.; Lippard, S. J. *Inorg. Chem.* **2001**, *40*, 1250.
- (137) Meyer, F.; Konrad, M.; Kaifer, E. *Eur. J. Inorg. Chem.* **1999**, 1851.
- (138) Scholz, F.; Meyer, B. *Electroanal. Chem.* **1998**, *20*, 1.
- (139) Bond, A. M.; Marken, F. J. *Electroanal. Chem.* **1994**, *372*, 125.
- (140) Bond, A. M.; Cooper, J. B.; Marken, F.; Way, D. M. *J. Electroanal. Chem.* **1995**, *396*, 407
- (141) Wilke, C. R.; Chang, P. *Am. Inst. Chem. Engrs.* **1955**, *1*(2), 264.
- (142) Black, D.; Blake, A. J.; Dancey, K. P.; Harrison, A.; McPartlin, M.; Parsons, S.; Tasker, P. A.; Whittaker, G.; Schröder, M. *J. Chem. Soc., Dalton Trans.* **1998**, 3953.
- (143) Okawa, H.; Tokii, T.; Muto, Y.; S.Kida *Bull. Chem. Soc. Jpn.* **1973**, *46*, 2464.
- (144) Nanda, K. K.; Addison, A. W.; Paterson, N.; Sinn, E.; Thompson, L. K.; Sakaguchi, U. *Inorg. Chem.* **1998**, *37*, 1028.
- (145) Ryback-Akimova, E. V.; Busch, D. H.; Kahol, P. K.; Pinto, N.; Alcock, N. W.; Clase, H. J. *Inorg. Chem.* **1998**, *36*, 510.
- (146) Luneau, D.; Oshio, H.; Okawa, H.; Kida, S. *J. Chem. Soc., Dalton Trans.* **1990**, 2283.
- (147) Luneau, D.; Oshio, H.; Okawa, H.; Koikawa, M.; Kida, S. *Bull. Chem. Soc. Jpn.* **1990**, *63*, 2212.
- (148) Zhong, Z. J.; Okawa, H.; Matsumoto, N.; Sakiyama, H.; Kida, S. *J. Chem. Soc., Dalton Trans.* **1991**, 497.
- (149) Ikeda, K.; Ohba, M.; Okawa, H. *J. Chem. Soc., Dalton Trans.* **2001**, 3119.
- (150) Krebs, C.; Winter, M.; Weyhermüller, T.; Eckhard, B.; Wiegardt, K.; Chaudhuri, P. *J. Chem. Soc., Chem. Commun.* **1995**, 1913.
- (151) Verani, C. N.; Weyhermüller, T.; Rentschler, E.; Bill, E.; Chaudhuri, P. *Chem. Commun.* **1998**, 2475.

- (152) Verani, C. N.; Rentschler, E.; Weyhermüller, T.; Bill, E.; Chaudhuri, P. J. *Chem. Soc., Dalton Trans.* **2000**, 251.
- (153) Fukita, N.; Ohba, M.; Shiga, T.; Okawa, H.; Ajiro, Y. *J. Chem. Soc., Dalton Trans.* **2001**, 64.
- (154) Abbati, G. L.; Cornia, A.; Frabretti, A. C.; Caneschi, A.; Gatteschi, D. *Inorg. Chem.* **1998**, *37*, 1430.
- (155) Steiner, T. *Angew. Chem. Int. Ed.* **2002**, *41*, 48.
- (156) Jeffrey, G. A. *An Introduction to hydrogen Bonding*; Oxford University Press: Oxford, 1997.
- (157) Goldberg, D. P.; Caneschi, A.; Delfs, C. D.; Sessoli, R.; Lippard, S. J. *J. Am. Chem. Soc.* **1995**, *117*, 5789.
- (158) McKee, V.; Shepard, W. *J. Chem. Soc., Chem. Commun.* **1985**, 158.
- (159) Lynch, M. W.; Hendrickson, D. N.; Fitzgerald, B. J.; Piermont, C. G. *J. Am. Chem. Soc.* **1984**, *106*, 2041.
- (160) Alzuet, G.; Casella, L.; Villa, M. L.; Carugo, O.; Gullotti, M. *J. Chem. Soc., Dalton Trans.* **1997**, 4789.
- (161) Pett, V. B.; Diaddario, L. L.; Dockal, E. R.; Corfield, P. W.; Ceccarelli, C.; Glick, M. D.; Ochrymowycz, L. A.; Rorabacher, D. B. *Inorg. Chem.* **1983**, *22*, 3661.
- (162) Drew, M. G. B.; McCann, M.; Nelson, S. M. *J. Chem. Soc., Dalton Trans.* **1981**, 1868.
- (163) Das, R.; Nag, K. *Inorg. Chem.* **1991**, *30*, 2833.
- (164) Alcock, N. W.; Balakrishnan, K. P.; Moore, P.; Omar, H. A. A. *J. Chem. Soc., Dalton Trans.* **1987**, 545.
- (165) Koike, T.; Kimura, E. *Inorg. Chem.* **1986**, *25*, 404.
- (166) Kimura, E.; Shionoya, M.; Mita, T.; Litaka, Y. *J. Chem. Soc., Chem. Commun.* **1987**, 1712.
- (167) Fortier, D. G.; McAuley, A. *Inorg. Chem.* **1989**, *28*, 655.
- (168) Kräutler, B.; Keller, W.; Hughes, M.; Caderas, C.; Kratky, C. *J. Chem. Soc., Chem. Commun.* **1987**, 1678.
- (169) Dong, Y.; Fujii, H.; Hendrich, M. P.; Leising, R. A.; Pan, G.; Randall, C. R.;

- Wilkinson, E. C.; Zang, Y.; Que, J. L.; Fox, B. G.; Kauffmann, K.; Münck, E. *J. Am. Chem. Soc.* **1995**, *117*, 2778.
- (170) Masuda, H.; Taga, T.; Osaki, K.; Sugimoto, H.; Yoshida, Z.-I.; Ogoshi, H. *Inorg. Chem.* **1980**, *19*, 950.
- (171) Alcock, N. W.; Liles, D. C.; McPartlin, M.; Tasker, P. A. *Chem. Commun.* **1974**, 727.
- (172) Hulsbergen, F. B.; Driessen, W. L.; Reedijk, J.; Verschoor, G. C. *Inorg. Chem.* **1984**, *23*, 3588.
- (173) O'Connor, C. *Prog. Inorg. Chem.* **1987**, *36*, 239.
- (174) Kahn, O. *Molecular Magnetism*; Wiley-VCH: New-York, 1993.
- (175) Sessoli, R.; Tsai, H.-L.; Schake, A. R.; Wang, S.; Vincent, J. B.; Folting, K.; Gatteschi, D.; Christou, G.; Hendrickson, D. N. *J. Am. Chem. Soc.* **1993**, *115*, 1804.
- (176) Eppley, H. J.; Tsai, H.-L.; Vries, N. D.; Folting, K.; Christou, G.; Hendrickson, D. N. *J. Am. Chem. Soc.* **1995**, *117*, 301.
- (177) Aubin, S. M. J.; Wemple, M. W.; Adams, D. M.; Tsai, H.-L.; Christou, G.; Hendrickson, D. N. *J. Am. Chem. Soc.* **1996**, *118*, 7746.
- (178) Aubin, S. M. J.; Dilley, N. R.; Wemple, M. W.; Maple, M. B.; Christou, G.; Hendrickson, D. N. *J. Am. Chem. Soc.* **1998**, *120*, 839.
- (179) Aubin, S. M. J.; Sun, Z.; Guzei, I. A.; Rheinhold, A. L.; Christou, G.; Hendrickson, D. N. *Chem. Commun.* **1997**, 2239.
- (180) Sun, Z.; Ruiz, D.; Rumberger, E.; Incarvito, C. D.; Folting, K.; Rheingold, A. L.; Christou, G.; Hendrickson, D. N. *Inorg. Chem.* **1998**, *37*, 4758.
- (181) Brechin, E. K.; Yoo, J.; Nakano, M.; Huffman, J. C.; Hendrickson, D. N.; Christou, G. *Chem. Commun.* **1999**, 783.
- (182) Yoo, J.; Yamaguchi, A.; Nakano, M.; Krzystek, J.; Streib, W. E.; Brunel, L.-C.; Ishimoto, H.; Christou, G.; Hendrickson, D. N. *Inorg. Chem.* **2001**, *40*, 4604.
- (183) Soler, M.; Artus, P.; Folting, K.; Huffman, J. C.; Hendrickson, D. N.; Christou, G. *Inorg. Chem.* **2001**, *40*, 4902.
- (184) Artus, P.; Boskovic, C.; Yoo, J.; Streib, W. E.; Brunel, L.-C.; Hendrickson, D.

- N.; Christou, G. *Inorg. Chem.* **2001**, *40*, 4199.
- (185) Castro, S. L.; Sun, Z.; Grant, C. M.; Bollinger, J. C.; Hendrickson, D. N. *J. Am. Chem. Soc.* **1998**, *120*, 2365.
- (186) Sangregorio, C.; Ohm, T.; Paulsen, C.; Sessoli, R.; Gatteschi, D. *Phys. Rev. Lett.* **1997**, *78*(24), 4645.
- (187) Barra, A.-L.; Caneschi, A.; Cornia, A.; Biani, F. F. d.; Gatteschi, D.; Sangregorio, C.; Sessoli, R.; Sorace, L. *J. Am. Chem. Soc.* **1999**, *121*, 5302.
- (188) Wernsdorfer, W.; Caneschi, A.; Sessoli, R.; Gatteschi, D.; Cornia, A.; Villar, V.; Paulsen, C. *Phys. Rev. Lett.* **2000**, *84*(13), 2965.
- (189) Oshio, H.; Oshino, N.; Ito, T. *J. Am. Chem. Soc.* **2000**, *122*, 12602.
- (190) Goodwin, J. C.; Sessoli, R.; Gatteschi, D.; Wernsdorfer, W.; Powell, A. K.; Heath, S. L. *J. Chem. Soc., Dalton Trans.* **2000**, 1835.
- (191) Gatteschi, D.; Sessoli, A.; Cornia, A. *Chem. Commun.* **2000**, 725.
- (192) Benelli, C.; Cano, J.; Journaux, Y.; Sessoli, R.; Solan, G. A.; Winpenny, R. E. *P. Inorg. Chem.* **2001**, *40*, 188.
- (193) Aubin, S. M. J.; Sun, Z.; Eppley, H. J.; Rumberger, E. M.; Guzei, I. A.; Folting, K.; Gantzel, P. K.; Rheingold, A. L.; Christou, G.; Hendrickson, D. N. *Inorg. Chem.* **2001**, *40*, 2127.
- (194) Ruiz, D.; Sun, Z.; Albela, B.; Folting, K.; Ribas, J.; Christou, G.; Hendrickson, D. N. *Angew. Chem. Int. Ed.* **1998**, *37*(3), 300.
- (195) Aubin, S. M. J.; Spagna, S.; Eppley, H. J.; Sager, R. E.; Christou, G.; Hendrickson, D. N. *Chem. Commun.* **1998**, 803.
- (196) Aubin, S. M. J.; Spagna, S.; Eppley, H. J.; Sager, R. E.; Folting, K.; Christou, G.; Hendrickson, D. N. *Mol. Cryst. and Liq. Cryst.* **1997**, *305*, 181.
- (197) Aubin, S. M. J.; Ruiz, D.; Rumberger, E.; Sun, Z.; Albela, B.; Wemple, M. W.; Dilley, N. R.; Ribas, J.; Maple, M. B.; Christou, G.; Hendrickson, D. N. *Mol. Cryst. and Liq. Cryst.* **1999**, *335*, 371.
- (198) Friedman, J. R.; Sarachik, M. P. *Phys. Rev. Lett.* **1996**, *76*, 3830.
- (199) Garanin, D. A.; Chudnovsky, E. M. *Phys. Rev. B.* **1997**, *56*, 11102.
- (200) Caneschi, A.; Gatteschi, D.; Sessoli, R. *J. Chem. Soc., Dalton Trans.* **1997**, 3963.

- (201) Ramirez, A. P. *J. Phys: Condens. Matter*. 1997, 9, 8171.
- (202) Taft, K. L.; Lippard, S. J. *J. Am. Chem. Soc.* 1990, 112, 9629.
- (203) Taft, K. L.; Delfs, C. D.; Papaefthymiou, G. C.; Foner, S.; Gatteschi, D.; Lippard, S. J. *J. Am. Chem. Soc.* 1994, 116, 823.
- (204) Benelli, C.; Parsons, S.; Solan, G. A.; Winpenny, R. E. P. *Angew. Chem. Int. Ed. Engl.* 1996, 35(16), 1825.
- (205) Frey, M.; Harris, S. G.; Holmes, J. M.; Nation, D. A.; Parsons, S.; Tasker, P. A.; Teat, S. J.; Winpenny, R. E. P. *Angew. Chem. Int. Ed.* 1998, 37(23), 3246.
- (206) Chiolero, A.; Loss, D. *Phys. Rev. Lett.* 1998, 80, 169.
- (207) Watton, S. P.; Fuhrman, P.; Pence, L. E.; Caneschi, A.; Cornia, A.; Abbati, G. L.; Lippard, S. J. *Angew. Chem. Int. Ed. Engl.* 1997, 36(24), 2774.
- (208) Caneschi, A.; Cornia, A.; Fabretti, A. C.; Gatteschi, D. *Angew. Chem. Int. Ed. Engl.* 1999, 38(9), 1295.
- (209) Ardizzoia, G. A.; Angaroni, M. A.; Monica, G. L.; Cariati, F.; Moret, M.; Masciocchi, N. *J. Chem. Soc., Chem. Commun.* 1990, 1021.
- (210) Lascialfari, A.; Jang, Z. H.; Borsa, F.; Gatteschi, D.; Cornia, A.; Rovai, D.; Caneschi, A.; P. Carreta *Phys. Rev. B* 2000, 61(10), 6839.
- (211) Blake, A. J.; Grant, C. M.; Parsons, S.; Rawson, J. M.; Winpenny, R. E. P. *J. Chem. Soc., Chem. Commun.* 1994, 2363.
- (212) Dearden, A. L.; Parsons, S.; Winpenny, R. E. P. *Angew. Chem. Int. Ed. Engl.* 2001, 40(1), 152.
- (213) Lah, M. S.; Pecoraro, V. L. *J. Am. Chem. Soc.* 1989, 111, 7258.
- (214) Lah, M. S.; Pecoraro, V. L. *Inorg. Chem.* 1991, 30, 878.
- (215) Lah, M. S.; Gibney, B. R.; Tierney, D. L.; Penner-Hahn, J. E.; Pecoraro, V. L. *J. Am. Chem. Soc.* 1993, 115, 5857.
- (216) Psomas, G.; Stemmler, A. J.; Dendrinou-Samara, C.; Bodwin, J. J.; Schneider, M.; Alexiou, M.; Kampf, J. W.; Kessissoglou, D. P.; Pecoraro, V. L. *Inorg. Chem.* 2001, 40, 1562.
- (217) Saalfrank, R. W.; Bernt, I.; Uller, E.; Hampel, F. *Angew. Chem. Int. Ed. Engl.* 1997, 36(22), 2482.
- (218) Waldmann, O.; Koch, R.; Schromm, S.; Bernt, I.; Schülein, J.; Müller, P.;

- Saalfrank, R. W.; Hampel, F.; Balthes, E. *Inorg. Chem.* **2001**, *40*, 2986.
- (219) Hasenknopf, B.; Lehn, J.-M.; Kneisel, B. O.; Braun, G.; Fenske, D. *Angew. Chem. Int. Ed. Engl.* **1996**, *108*, 1987.
- (220) Caneschi, A.; Cornia, A.; Lippard, S. J. *Angew. Chem. Int. Ed.* **1995**, *34(4)*, 467.
- (221) Abbati, G. L.; Cornia, A.; Fabretti, A. C.; Malvasi, W.; Schenetti, L.; Caneschi, A.; Gatteschi, D. *Inorg. Chem.* **1997**, *36*, 6443.
- (222) Cornia, A.; Affronte, M.; Jansen, A. G. M.; Abbati, G.-L.; Gatteschi, D. *Angew. Chem. Int. Ed.* **1999**, *38(15)*, 2264.
- (223) Ginsberg, A. *Inorg. Chim. Acta Rev.* **1971**, *5*, 45.
- (224) Blake, A. J.; Gould, R. O.; Milne, P. E. Y.; Winpenny, R. E. P. *Chem. Commun.* **1991**, 1453.
- (225) McConnell, S.; Motevalli, M.; Thornton, P. *Polyhedron* **1995**, *14(3)*, 459.
- (226) Blake, A. J.; Gould, R. O.; Grant, C. M.; Milne, P. E. Y.; Reed, D.; Winpenny, R. E. P. *Angew. Chem. Int. Ed.* **1994**, *33(2)*, 195.
- (227) Bolcar, M. A.; Aubin, S. M. J.; Folting, K.; Hendrickson, D. N.; Christou, G. *Chem. Commun.* **1997**, 1485.
- (228) Tesmer, M.; Müller, B.; Vahrenkamp, H. *Chem. Commun.* **1997**, 721.
- (229) Hendrickson, D. N. In *Research Frontier in Magnetochemistry*; O'Connor, C. J., Ed.; World Scientific: Singapore, 1993.
- (230) Abbati, G. L.; Cornia, A.; Fabretti, A. C.; Caneschi, A.; Gatteschi, D. *Inorg. Chem.* **1998**, *37*, 3759.
- (231) Heath, S. L.; Powell, A. K. *Angew. Chem. Int. Ed. Engl.* **1992**, *31*, 191.
- (232) Powell, A. K.; Heath, S. L.; Gatteschi, D.; Pardi, L.; Spina, G.; Giallo, F. D.; Pieralli, F. *J. Am. Chem. Soc.* **1995**, *117*, 2491.
- (233) Müller, U. *Inorganic Structural Chemistry*; J. Wiley & Sons: New-York, 1993.
- (234) Perrin *Purification of Laboratory Chemicals*; Armarego and Perrin, Pergammon Press, 1980.
- (235) Owen, G. R.; Reese, C. B. *Acta Crystallogr., Sect. C* **1970**, 2401.
- (236) Murase, I.; M.Hatano; M.Tanaka; S.Veno; Okawa, H.; S. Kida *Bull. Chem.*

- Soc. Jpn.* **1982**, *55*(8), 2404.
- (237) Drago, R. S.; Desmond, M. J.; Corden, B. B.; Miller, K. A. *J. Am. Chem. Soc.* **1983**, *105*, 2287.
- (238) Sheldrick, G. M. *SHELXTL version 5.03, Bruker-AXS, Madison WI* **1997**.
- (239) Sheldrick, G. M. *SHELXTL version 5.1, Bruker-AXS, Madison WI* **1998**.
- (240) Sluis, P. v. d.; Spek, A. L. *Acta Crystallogr., Sect. A* **1990**, *46*, 194.
- (241) Cernik, R. J.; Clegg, W.; Catlow, C. R. A.; Bushnell-Wye, G.; Flaherty, J. V.; Graves, G. N.; Hamichi, M.; Burrows, I.; Taylor, D. J.; Teat, S. J. *J. Synchrotron Radiat.* **1997**, *4*, 279.

SINGLE CRYSTAL X-RAY CRYSTALLOGRAPHY

The single crystals were mounted in oil on the tip of a quartz glass capillary and placed under a stream of nitrogen.

The data sets were corrected for Lorentz and polarisation effects. The data sets were solved by direct methods and refined by full-matrix least squares on F^2 . The structures were solved and refined using SHELXTL version 5.03 suites of program²³⁸ or SHELXTL version 5.1 suites of program.²³⁹ The crystal data and structure refinement table for all the structures is tabulated in annexes 1, 2, 3 and 4. Full details of the refinements in CIF format are available on CD.

ANNEX 1

**Tables for crystal data and refinement
for the
compounds described in chapter 2**

Table 1. Crystal data and structure refinement for [Ni₄(L2)(OH)(MeOH)₄(NO₃)₂](NO₃)

The X-ray reflection data were collected at 150K on a Bruker SMART1000 CCD diffractometer using graphite monochromated Mo-K α radiation ($\lambda = 0.71073 \text{ \AA}$) at Loughborough University.

Identification code	nina2lsq	
Empirical formula	C35.50 H63 N7 Ni4 O21.50	
Formula weight	1166.77	
Temperature	150(2) K	
Wavelength	0.71073 \AA	
Crystal system	Orthorhombic	
Space group	P2 ₁ 2 ₁ 2 ₁	
Unit cell dimensions	a = 7.5323(10) \AA	$\alpha = 90^\circ$
	b = 20.748(3) \AA	$\beta = 90^\circ$
	c = 28.603(4) \AA	$\gamma = 90^\circ$
Volume	4470.1(11) \AA^3	
Z	4	
Density (calculated)	1.734 Mg/m ³	
Absorption coefficient	1.751 mm ⁻¹	
F(000)	2436	
Crystal size	0.30 x 0.07 x 0.04 mm ³	
Theta range for data collection	1.21 to 25.00 $^\circ$.	
Index ranges	-8 \leq h \leq 8, -24 \leq k \leq 24, -34 \leq l \leq 34	
Reflections collected	41516	
Independent reflections	7779 [R(int) = 0.0336]	
Completeness to theta = 25.00 $^\circ$	99.0 %	
Absorption correction	Multiscan	
Max. and min. transmission	1.000 and 0.800	
Refinement method	Full-matrix least-squares on F ²	
Data / restraints / parameters	7779 / 0 / 520	
Goodness-of-fit on F ²	1.080	
Final R indices [I > 2 σ (I)]	R1 = 0.0628, wR2 = 0.1812	
R indices (all data)	R1 = 0.0638, wR2 = 0.1819	
Absolute structure parameter	0.53(3)	
Largest diff. peak and hole	0.855 and -1.087 e. \AA^{-3}	

Refinement and disorders details for [Ni₄(L2)(OH)(MeOH)₄(NO₃)₂](NO₃)

All the hydrogen atoms on the macrocycle were inserted at calculated positions. The hydrogen atoms H(51), H(61), H(71) and H(81) on the coordinated MeOH molecules were found and their positions and temperature factor fixed.

The model was refined as a racemic twin.

The uncoordinated nitrate anion and methanol solvates were severely disordered, occupying the spaces between the hydrogen-bonded columns of cations. These have been accounted for using the program Squeeze²⁴⁰ which located four equivalent voids of 223 \AA^3 (5% of the volume) each. The 'missing' electron count refined to 372 per unit cell or 94 per asymmetric unit. This was assigned to 1 NO₃⁻ anion and 3.5 methanol solvate molecules.

Table 2. Crystal data and structure refinement for [Mn₄(L2)(μ₄-O)(OAc)₄]

The X-ray reflection data were collected at 150K on a Bruker SMART1000 CCD diffractometer using graphite monochromated Mo-K α radiation ($\lambda = 0.71073 \text{ \AA}$) at Loughborough University.

Identification code	mn1207
Empirical formula	C41.80 H59 Mn4 N5.60 O14.25
Formula weight	1087.71
Temperature	150(2) K
Wavelength	0.71073 \AA
Crystal system	Monoclinic
Space group	C2/c
Unit cell dimensions	a = 34.157(2) \AA $\alpha = 90^\circ$ b = 12.3614(7) \AA $\beta = 103.3170(10)^\circ$ c = 23.7716(15) \AA $\gamma = 90^\circ$
Volume	9767.2(10) \AA^3
Z	8
Density (calculated)	1.479 Mg/m ³
Absorption coefficient	1.079 mm ⁻¹
F(000)	4504
Crystal size	0.77 x 0.20 x 0.11 mm ³
Theta range for data collection	1.76 to 25.00 $^\circ$.
Index ranges	-40 \leq h \leq 40, -14 \leq k \leq 14, -28 \leq l \leq 28
Reflections collected	34290
Independent reflections	8600 [R(int) = 0.0237]
Completeness to theta = 25.00 $^\circ$	99.9%
Absorption correction	Multiscan
Max. and min. transmission	1.000 and 0.861
Refinement method	Full-matrix least-squares on F ²
Data / restraints / parameters	8600 / 6 / 652
Goodness-of-fit on F ²	1.050
Final R indices [I > 2 σ (I)]	R1 = 0.0416, wR2 = 0.1149
R indices (all data)	R1 = 0.0526, wR2 = 0.1233
Largest diff. peak and hole	0.837 and -0.456 e. \AA^{-3}

Refinement and disorders details for [Mn₄(L2)(μ₄-O)(OAc)₄]

All the hydrogen atoms on the macrocycle and on the coordinated acetate molecules were inserted at calculated positions. The hydrogen atoms of the disordered CH₃CN and Et₂O solvate molecules were inserted at calculated positions and their temperature factor fixed.

One side chain of the macrocycle is disordered. Three carbon atoms are each sharing two sites with C10, C11 and C12 being 40% occupancy and C10', C11' and C12' being 60% occupancy.

Table 3. Crystal data and structure refinement for [Cu₄(L2)(μ₄-OH)(OH)₂(NO₃)]·6H₂O

The X-ray reflection data were collected at 150K on a Bruker SMART1000 CCD diffractometer using graphite monochromated Mo-Kα radiation (λ = 0.71073 Å) at Loughborough University.

Identification code	CuNaL	
Empirical formula	C ₂₈ H ₃₂ Cu ₄ N ₆ O ₁₇	
Formula weight	978.76	
Temperature	153(2) K	
Wavelength	0.71073 Å	
Crystal system	Monoclinic	
Space group	C2/m	
Unit cell dimensions	a = 7.8423(16) Å	α = 90°
	b = 20.163(4) Å	β = 93.577(4)°
	c = 11.456(2) Å	γ = 90°
Volume	1807.9(6) Å ³	
Z	2	
Density (calculated)	1.798 Mg/m ³	
Absorption coefficient	2.404 mm ⁻¹	
F(000)	988	
Crystal size	0.200 x 0.100 x 0.025 mm ³	
Theta range for data collection	1.78 to 24.99°.	
Index ranges	-9 ≤ h ≤ 9, -23 ≤ k ≤ 23, -13 ≤ l ≤ 13	
Reflections collected	6591	
Independent reflections	1648 [R(int) = 0.0312]	
Completeness to theta = 24.99°	99.9 %	
Absorption correction	Multiscan	
Max. and min. transmission	1.000 and 0.860	
Refinement method	Full-matrix least-squares on F ²	
Data / restraints / parameters	1648 / 0 / 145	
Goodness-of-fit on F ²	1.081	
Final R indices [I > 2σ(I)]	R1 = 0.0477, wR2 = 0.1404	
R indices (all data)	R1 = 0.0709, wR2 = 0.1585	
Largest diff. peak and hole	0.704 and -0.649 e.Å ⁻³	

Refinement and disorders details for [Cu₄(L2)(μ₄-OH)(OH)₂(NO₃)]·6H₂O

All the hydrogen atoms on the macrocycle were inserted at calculated positions. The hydrogen atoms on the water molecules and hydroxy groups were not found.

The atoms N(2) and O(4) belonging to the nitrate moiety are half occupancy whereas O(3) belonging to both nitrate and hydroxy groups is full occupancy. The explanation for the disorder model is given in chapter 2.

ANNEX 2

**Tables for crystal data and refinement
for the
compounds described in chapter 3**

Table 1. Crystal data and structure refinement for 2,2'-diallyloxy-5,5'-di-*tert*-butyl-3,3'-methanediyl dibenzyl alcohol (AOTMBA)

The X-ray reflection data were collected at 150K on a Bruker SMART CCD diffractometer using graphite monochromated Mo-K α radiation ($\lambda = 0.71073 \text{ \AA}$) at Queen's University, Belfast.

Identification code	111	
Empirical formula	C ₂₉ H ₄₀ O ₄	
Formula weight	452.61	
Temperature	150(2) K	
Wavelength	0.71073 \AA	
Crystal system	Triclinic	
Space group	$P\bar{1}$	
Unit cell dimensions	a = 10.5990(12) \AA	$\alpha = 64.537(2)^\circ$
	b = 11.9304(14) \AA	$\beta = 82.517(2)^\circ$
	c = 12.4287(14) \AA	$\gamma = 66.248(2)^\circ$
Volume	1297.0(3) \AA^3	
Z	2	
Density (calculated)	1.159 Mg/m ³	
Absorption coefficient	0.075 mm ⁻¹	
F(000)	492	
Crystal size	0.75 x 0.20 x 0.05 mm ³	
Theta range for data collection	1.82 to 24.00 $^\circ$.	
Index ranges	-12 \leq h \leq 12, -13 \leq k \leq 13, -14 \leq l \leq 14	
Reflections collected	11724	
Independent reflections	4073 [R(int) = 0.0273]	
Completeness to theta = 24.00 $^\circ$	99.9 %	
Absorption correction	Multiscan	
Max. and min. transmission	1.000 and 0.959	
Refinement method	Full-matrix least-squares on F ²	
Data / restraints / parameters	4073 / 0 / 304	
Goodness-of-fit on F ²	1.066	
Final R indices [I > 2 σ (I)]	R1 = 0.0678, wR2 = 0.1849	
R indices (all data)	R1 = 0.1022, wR2 = 0.2153	
Largest diff. peak and hole	0.492 and -0.250 e. \AA^{-3}	

Refinement and disorders details for 2,2'-diallyloxy-5,5'-di-*tert*-butyl-3,3'-methanediyl dibenzyl alcohol (AOTMBA)

All the hydrogen atoms were inserted at calculated positions except for the one on the hydroxy groups. The hydrogen atoms H(2A) and H(4A) on the hydroxy groups are disordered over two position with 50% occupancy each. They were found and their positions and temperature factors fixed.

Table 2. Crystal data and structure refinement for 2,2'-diallyloxy-5,5'-di-*tert*-butyl-3,3'-methanediylidibenzaldehyde (AOTMB)

The X-ray reflection data were collected at 150K on a Bruker SMART CCD diffractometer using graphite monochromated Mo-K α radiation ($\lambda = 0.71073 \text{ \AA}$) at Queen's University, Belfast.

Identification code	112
Empirical formula	C ₂₉ H ₃₆ O ₄
Formula weight	448.58
Temperature	150(2) K
Wavelength	0.71073 \AA
Crystal system	Monoclinic
Space group	P2 ₁ /c
Unit cell dimensions	a = 16.3126(13) \AA $\alpha = 90^\circ$ b = 10.2148(8) \AA $\beta = 108.4970(10)^\circ$ c = 16.4490(13) \AA $\gamma = 90^\circ$
Volume	2599.3(4) \AA^3
Z	4
Density (calculated)	1.146 Mg/m ³
Absorption coefficient	0.075 mm ⁻¹
F(000)	968
Crystal size	0.5 x 0.275 x 0.15 mm ³
Theta range for data collection	2.38 to 25.00 $^\circ$.
Index ranges	-19 \leq h \leq 19, -4 \leq k \leq 12, -19 \leq l \leq 16
Reflections collected	6185
Independent reflections	3855 [R(int) = 0.0205]
Completeness to theta = 25.00 $^\circ$	84.3 %
Absorption correction	Multiscan
Max. and min. transmission	1.000 and 0.949
Refinement method	Full-matrix least-squares on F ²
Data / restraints / parameters	3855 / 0 / 323
Goodness-of-fit on F ²	1.024
Final R indices [I > 2 σ (I)]	R1 = 0.0454, wR2 = 0.1136
R indices (all data)	R1 = 0.0739, wR2 = 0.1290
Largest diff. peak and hole	0.164 and -0.171 e. \AA^{-3}

Refinement and disorders details for 2,2'-diallyloxy-5,5'-di-*tert*-butyl-3,3'-methanediylidibenzaldehyde (AOTMB)

All the hydrogen atoms were inserted at calculated positions.

One of the oxoallyl group is disordered with C1 and C2 occupying two sites each. C1 and C2 are 67% occupancy while C1' and C2' are 33% occupancy.

Table 3. Crystal data and structure refinement for 2,2'-dihydroxy-5,5'-di-*tert*-butyl-3,3'-methanediyl dibenzaldehyde (DHTMB)

The X-ray reflection data were collected at 150K on a Bruker SMART CCD diffractometer using graphite monochromated Mo-K α radiation ($\lambda = 0.71073 \text{ \AA}$) at Queen's University, Belfast.

Identification code	12	
Empirical formula	C ₂₃ H ₂₈ O ₄	
Formula weight	368.45	
Temperature	150(2) K	
Wavelength	0.71073 \AA	
Crystal system	Tetragonal	
Space group	I ₄ /a	
Unit cell dimensions	a = 12.7930(7) \AA	$\alpha = 90^\circ$
	b = 12.7930(7) \AA	$\beta = 90^\circ$
	c = 24.158(2) \AA	$\gamma = 90^\circ$
Volume	3953.7(4) \AA^3	
Z	8	
Density (calculated)	1.238 Mg/m ³	
Absorption coefficient	0.083 mm ⁻¹	
F(000)	1584	
Crystal size	0.275 x 0.200 x 0.05 mm ³	
Theta range for data collection	1.80 to 24.97 $^\circ$.	
Index ranges	-15 \leq h \leq 15, -15 \leq k \leq 15, -28 \leq l \leq 28	
Reflections collected	19093	
Independent reflections	1736 [R(int) = 0.0557]	
Completeness to theta = 24.97 $^\circ$	100.0 %	
Absorption correction	Multiscan	
Max. and min. transmission	1.000 and 0.931	
Refinement method	Full-matrix least-squares on F ²	
Data / restraints / parameters	1736 / 0 / 127	
Goodness-of-fit on F ²	1.064	
Final R indices [I > 2 σ (I)]	R1 = 0.0427, wR2 = 0.0978	
R indices (all data)	R1 = 0.0711, wR2 = 0.1183	
Largest diff. peak and hole	0.148 and -0.206 e. \AA^{-3}	

Refinement and disorders details for 2,2'-dihydroxy-5,5'-di-*tert*-butyl-3,3'-methanediyl dibenzaldehyde (DHTMB)

All the hydrogen atoms were inserted at calculated positions.

Table 4. Crystal data and structure refinement for 2,2'-dihydroxy-5,5'-di-*tert*-butyl-3,3'-methanediyl dibenzaldehyde (DHTMB)

The X-ray reflection data were collected at 150K on a Bruker SMART CCD diffractometer using graphite monochromated Mo-K α radiation ($\lambda = 0.71073 \text{ \AA}$) at Queen's University, Belfast.

Identification code	sgnipelm	
Empirical formula	C ₂₃ H ₂₈ O ₄	
Formula weight	368.45	
Temperature	153(2) K	
Wavelength	0.71073 \AA	
Crystal system	Monoclinic	
Space group	C2/c	
Unit cell dimensions	a = 26.809(2) \AA	$\alpha = 90^\circ$
	b = 8.4543(7) \AA	$\beta = 120.6180(10)^\circ$
	c = 21.3720(18) \AA	$\gamma = 90^\circ$
Volume	4168.7(6) \AA^3	
Z	8	
Density (calculated)	1.174 Mg/m ³	
Absorption coefficient	0.079 mm ⁻¹	
F(000)	1584	
Crystal size	0.16 x 0.38 x 0.48 mm ³	
Theta range for data collection	1.77 to 25.00 $^\circ$.	
Index ranges	-31 $\leq h \leq$ 31, -10 $\leq k \leq$ 10, -25 $\leq l \leq$ 25	
Reflections collected	19806	
Independent reflections	3672 [R(int) = 0.0564]	
Completeness to theta = 25.00 $^\circ$	100.0 %	
Absorption correction	Multiscan	
Max. and min. transmission	1.000 and 0.896	
Refinement method	Full-matrix least-squares on F ²	
Data / restraints / parameters	3672 / 0 / 255	
Goodness-of-fit on F ²	1.036	
Final R indices [I > 2 σ (I)]	R1 = 0.0504, wR2 = 0.1263	
R indices (all data)	R1 = 0.0932, wR2 = 0.1491	
Largest diff. peak and hole	0.243 and -0.191 e. \AA^{-3}	

Refinement and disorders details for 2,2'-dihydroxy-5,5'-di-*tert*-butyl-3,3'-methanediyl dibenzaldehyde (DHTMB)

All the hydrogen atoms were inserted at calculated positions.

Table 5. Crystal data and structure refinement for [Mn₂(L8)](ClO₄)₂·4CH₃CN

The X-ray reflection data were collected at 150K on station 9.8 of the Synchrotron Radiation Source at Daresbury²⁴¹ on a Bruker SMART1000 CCD diffractometer using synchrotron radiation.

Identification code	MnO8O3	
Empirical formula	C66 H92 Cl2 Mn2 N12 O12	
Formula weight	1426.30	
Temperature	150(2) K	
Wavelength	0.68800 Å	
Crystal system	Orthorhombic	
Space group	Pbcn	
Unit cell dimensions	a = 25.578(2) Å	α = 90°
	b = 15.3262(13) Å	β = 90°
	c = 18.1531(16) Å	γ = 90°
Volume	7116.3(11) Å ³	
Z	4	
Density (calculated)	1.331 Mg/m ³	
Absorption coefficient	0.497 mm ⁻¹	
F(000)	3008	
Crystal size	0.18 x 0.04 x 0.02 mm ³	
Theta range for data collection	1.85 to 22.50°	
Index ranges	-28 ≤ h ≤ 22, -16 ≤ k ≤ 17, -20 ≤ l ≤ 20	
Reflections collected	25694	
Independent reflections	5124 [R(int) = 0.0843]	
Completeness to theta = 22.50°	99.9 %	
Absorption correction	none	
Refinement method	Full-matrix least-squares on F ²	
Data / restraints / parameters	5124 / 131 / 488	
Goodness-of-fit on F ²	1.026	
Final R indices [I > 2σ(I)]	R1 = 0.0613, wR2 = 0.1486	
R indices (all data)	R1 = 0.1075, wR2 = 0.1710	
Largest diff. peak and hole	0.933 and -0.491 e.Å ⁻³	

Refinement and disorders details for [Mn₂(L8)](ClO₄)₂·4CH₃CN

All the hydrogen atoms were inserted at calculated positions. In the asymmetric unit two solvate molecules (CH₃CN) are half occupancy and one perchlorate anion (Cl(1)O(15)O(16)O(17)O(18)) is disordered. The atoms Cl(1), O(16) and O(17) are disordered over two sites, with Cl(1), O(16) and O(17) having 70% occupancy and Cl(1'), O(16') and O(17') having 30% occupancy.

Table 6. Crystal data and structure refinement for $[\text{Ni}_2(\text{H}_4\text{L9})(\text{H}_2\text{O})(\text{EtOH})_2](\text{ClO}_4)_2$

The X-ray reflection data were collected at 150K on station 9.8 of the Synchrotron Radiation Source at Daresbury²⁴¹ on a Bruker SMART1000 CCD diffractometer using synchrotron radiation.

Identification code	ni1403	
Empirical formula	C ₆₅ H ₇₅ Cl ₂ N ₄ Ni ₂ O ₂₀	
Formula weight	1420.61	
Temperature	150(2) K	
Wavelength	0.6880 Å	
Crystal system	Orthorhombic	
Space group	Pnma	
Unit cell dimensions	a = 27.9469(13) Å	$\alpha = 90^\circ$
	b = 13.7059(7) Å	$\beta = 90^\circ$
	c = 18.8915(9) Å	$\gamma = 90^\circ$
Volume	7236.2(6) Å ³	
Z	4	
Density (calculated)	1.304 Mg/m ³	
Absorption coefficient	0.664 mm ⁻¹	
F(000)	2972	
Crystal size	0.14 x 0.14 x 0.14 mm ³	
Theta range for data collection	1.98 to 25.00°	
Index ranges	-33 ≤ h ≤ 16, -16 ≤ k ≤ 16, -21 ≤ l ≤ 22	
Reflections collected	36268	
Independent reflections	6657 [R(int) = 0.0363]	
Completeness to theta = 25.00°	99.9 %	
Absorption correction	None	
Refinement method	Full-matrix least-squares on F ²	
Data / restraints / parameters	6657 / 0 / 472	
Goodness-of-fit on F ²	1.167	
Final R indices [I > 2σ(I)]	R1 = 0.0858, wR2 = 0.2219	
R indices (all data)	R1 = 0.0978, wR2 = 0.2279	
Largest diff. peak and hole	1.225 and -0.558 e.Å ⁻³	

Refinement and disorders details for $[\text{Ni}_2(\text{H}_4\text{L9})(\text{H}_2\text{O})(\text{EtOH})_2](\text{ClO}_4)_2$

All the hydrogen atoms belonging to the macrocycle were inserted at calculated positions except those on O(14) (alkoxy oxygen), O(29) (coordinated ethanol molecule), O(1) (bridging water molecule), O(110) (phenoxy oxygen) and O(26) (phenoxy oxygen). The hydrogen atoms belonging to the solvate (ethanol) molecules were not included in the model.

The oxygen atom O(14) of the hydroxo group is disordered over two sites, one with 70% occupancy and the other with 30% occupancy.

The isotropic factor of the hydrogen atoms belonging to C(6), C(7), C(21), C(22), C(23), C(28), C(60) were fixed.

Table 7. Crystal data and structure refinement for [Co₂(H₄L9)(H₂O)(EtOH)₂](ClO₄)₂

The X-ray reflection data were collected at 150K on a Bruker SMART CCD diffractometer using graphite monochromated Mo-K α radiation ($\lambda = 0.71073 \text{ \AA}$) at Loughborough University.

Identification code	cop1210	
Empirical formula	C ₆₄ H _{112.50} Cl ₂ Co ₂ N ₄ O ₂₂	
Formula weight	1478.84	
Temperature	150(2) K	
Wavelength	0.71073 \AA	
Crystal system	Orthorhombic	
Space group	Pnma	
Unit cell dimensions	a = 27.9433(17) \AA	$\alpha = 90^\circ$
	b = 13.7494(8) \AA	$\beta = 90^\circ$
	c = 18.8620(11) \AA	$\gamma = 90^\circ$
Volume	7246.8(7) \AA^3	
Z	4	
Density (calculated)	1.355 Mg/m ³	
Absorption coefficient	0.606 mm ⁻¹	
F(000)	3154	
Crystal size	0.3 x 0.2 x 0.15 mm ³	
Theta range for data collection	1.81 to 25.00°	
Index ranges	-33 ≤ h ≤ 33, -16 ≤ k ≤ 16, -22 ≤ l ≤ 22	
Reflections collected	67564	
Independent reflections	6669 [R(int) = 0.0938]	
Completeness to theta = 25.00°	100.0 %	
Absorption correction	Multiscan	
Max. and min. transmission	1.000 and 0.767	
Refinement method	Full-matrix least-squares on F ²	
Data / restraints / parameters	6669 / 24 / 494	
Goodness-of-fit on F ²	1.029	
Final R indices [$I > 2\sigma(I)$]	R1 = 0.0848, wR2 = 0.2234	
R indices (all data)	R1 = 0.1233, wR2 = 0.2542	
Largest diff. peak and hole	1.234 and -0.631 e. \AA^{-3}	

Refinement and disorders details for [Co₂(H₄L9)(H₂O)(EtOH)₂](ClO₄)₂

All the hydrogen atoms were inserted at calculated positions except the hydrogen atoms on O(31) and O(41) belonging to the methanol solvate molecules, the hydrogen atom on O(29) belonging to the coordinated ethanol molecule, the hydrogen atoms on the bridging water O(1) and those on the phenoxo oxygen atoms O(11O) and O(26). The hydrogen atoms on O(31), O(41), O(29), O(1), O(11O) and O(26) were not found, thus not included in the model.

The oxygen atom O(14) of the hydroxo group is disordered over two sites, one with 70% occupancy and the other with 30% occupancy. One of the perchlorate anions is also disordered and was modelled with two oxygen atoms O(11) and O(13) sharing each two sites of 25% occupancy.

The anisotropic displacement factor of O(13), O(13'), O(11) and O(11') has been restrained to be approximately isotropic.

Table 8. Crystal data and structure refinement for $[\text{Ni}_2(\text{H}_4\text{L}9)(\text{NO}_3)(\text{DMF})_2](\text{NO}_3)$

The X-ray reflection data were collected at 150K on a Bruker SMART CCD diffractometer using graphite monochromated Mo-K α radiation ($\lambda = 0.71073 \text{ \AA}$) at Loughborough University.

Identification code	ni2111
Empirical formula	C61 H121.20 N9 Ni2 O16.90
Formula weight	1368.69
Temperature	150(2) K
Wavelength	0.71073 \AA
Crystal system	Monoclinic
Space group	$P2_1/c$
Unit cell dimensions	$a = 13.3462(5) \text{ \AA}$ $\alpha = 90^\circ$ $b = 31.9837(13) \text{ \AA}$ $\beta = 99.6140(10)^\circ$ $c = 16.4255(6) \text{ \AA}$ $\gamma = 90^\circ$
Volume	$6912.9(5) \text{ \AA}^3$
Z	4
Density (calculated)	1.315 Mg/m^3
Absorption coefficient	0.616 mm^{-1}
F(000)	2966
Crystal size	$0.22 \times 0.15 \times 0.04 \text{ mm}^3$
Theta range for data collection	1.27 to 25.00° .
Index ranges	$-15 \leq h \leq 15$, $-38 \leq k \leq 37$, $-19 \leq l \leq 19$
Reflections collected	50385
Independent reflections	12168 [R(int) = 0.0606]
Completeness to theta = 25.00°	100.0 %
Absorption correction	Multiscan
Max. and min. transmission	1.000 and 0.880
Refinement method	Full-matrix least-squares on F^2
Data / restraints / parameters	12168 / 0 / 819
Goodness-of-fit on F^2	1.049
Final R indices [I > 2 σ (I)]	R1 = 0.0771, wR2 = 0.2078
R indices (all data)	R1 = 0.1200, wR2 = 0.2450
Largest diff. peak and hole	1.286 and $-0.902 \text{ e. \AA}^{-3}$

Refinement and disorders details for $[\text{Ni}_2(\text{H}_4\text{L}9)(\text{NO}_3)(\text{DMF})_2](\text{NO}_3)$

All the hydrogen atoms were inserted at calculated positions except those belonging to O(11) and O(37) (phenoxo oxygen atoms) and that on O(14) (alkoxo oxygen).

The oxygen atom O(14) of the hydroxo group is disordered over two sites with 50% occupancy each. One of the methyl groups of the coordinated DMF molecule is disordered over two sites, one with 70% occupancy and the other with 30% occupancy. The free nitrate ion is disordered as well. The oxygen atoms O(91) and O(93) are disordered over two sites, one with 60% occupancy and the other with 40% occupancy.

The isotropic factor for the hydrogen atoms belonging to C(21), C(22), C(23), C(32), C(33), C(34), C(48), C(49), C(53), C(54), C(53'), C(54'), C(55'), C(59), C(60) and C(61) were fixed.

Table 9. Crystal data and structure refinement for $[(Mn_2(H_2L9))_3(OAc)_3(H_2O)(EtOH)_2CO_3]$

The X-ray reflection data were collected at 150K on station 9.8 of the Synchrotron Radiation Source at Daresbury²⁴¹ on a Bruker SMART1000 CCD diffractometer using synchrotron radiation.

Identification code	mn16051	
Empirical formula	C168.50 H200 Mn6 N12 O31.70	
Formula weight	3230.25	
Temperature	150(2) K	
Wavelength	0.6880 Å	
Crystal system	Triclinic	
Space group	P1	
Unit cell dimensions	a = 16.840(4) Å	$\alpha = 119.566(3)^\circ$
	b = 18.886(4) Å	$\beta = 102.642(3)^\circ$
	c = 18.986(4) Å	$\gamma = 95.862(3)^\circ$
Volume	4965.1(19) Å ³	
Z	1	
Density (calculated)	1.080 Mg/m ³	
Absorption coefficient	0.432 mm ⁻¹	
F(000)	1699	
Crystal size	0.33 x 0.30 x 0.09 mm ³	
Theta range for data collection	1.25 to 25.00°.	
Index ranges	-20 ≤ h ≤ 20, -22 ≤ k ≤ 22, -22 ≤ l ≤ 22	
Reflections collected	35180	
Independent reflections	31059 [R(int) = 0.0510]	
Completeness to theta = 25.00°	99.0 %	
Absorption correction	None	
Refinement method	Full-matrix least-squares on F ²	
Data / restraints / parameters	31059 / 57 / 2031	
Goodness-of-fit on F ²	0.933	
Final R indices [I > 2σ(I)]	R1 = 0.1062, wR2 = 0.2532	
R indices (all data)	R1 = 0.2288, wR2 = 0.3219	
Absolute structure parameter	0.35(3)	
Largest diff. peak and hole	1.094 and -0.655 e.Å ⁻³	

Refinement and disorders details for $[(Mn_2(H_2L9))_3(OAc)_3(H_2O)(EtOH)_2CO_3]$

All the hydrogen atoms belonging to the each macrocycle were inserted at calculated positions. The hydrogen atoms on the pendent alcohol groups, the coordinated water, the oxygen atoms belonging to the coordinated ethanol molecules and those belonging to the solvate molecules were not inserted. Due to poor data, the structure could not be refined to a reasonable factor.

Table 10. Crystal data and structure refinement for [Cu₃(L9)(CH₃OH)₂]_n

The X-ray reflection data were collected at 150K on station 9.8 of the Synchrotron Radiation Source at Daresbury²⁴¹ on a Bruker SMART1000 CCD diffractometer using synchrotron radiation.

Identification code	cu13032	
Empirical formula	C58 H84.53 Cu2.90 N4 O16	
Formula weight	1278.09	
Temperature	153(2) K	
Wavelength	0.6880 Å	
Crystal system	Orthorhombic	
Space group	Ibam	
Unit cell dimensions	a = 19.2316(13) Å	α = 90°
	b = 20.6093(14) Å	β = 90°
	c = 34.071(2) Å	γ = 90°
Volume	13503.9(16) Å ³	
Z	8	
Density (calculated)	1.257 Mg/m ³	
Absorption coefficient	0.968 mm ⁻¹	
F(000)	5381	
Crystal size	0.16 x 0.05 x 0.04 mm ³	
Theta range for data collection	1.88 to 25.00°	
Index ranges	-22<=h<=22, -24<=k<=24, -40<=l<=40	
Reflections collected	48862	
Independent reflections	6068 [R(int) = 0.0451]	
Completeness to theta = 25.00°	100.0 %	
Absorption correction	None	
Refinement method	Full-matrix least-squares on F ²	
Data / restraints / parameters	6068 / 12 / 399	
Goodness-of-fit on F ²	1.122	
Final R indices [I>2sigma(I)]	R1 = 0.0989, wR2 = 0.3059	
R indices (all data)	R1 = 0.1205, wR2 = 0.3354	
Largest diff. peak and hole	2.958 and -1.454 e.Å ⁻³	

Refinement and disorders details for [Cu₃(L9)(CH₃OH)₂]_n

All the hydrogen atoms belonging to the macrocycle were inserted at calculated positions. The hydrogen atoms on the solvate molecules (water and methanol) were not inserted.

The structure is disordered between a tricopper species and a dicopper species. The trinuclear copper structure is 45% occupancy while the dinuclear copper structure is 5% occupancy. One of the alkoxy side chains is disordered. The carbon atom C(24) is disordered over two positions with 50% occupancy each. The oxygen atom O(25) (O(25) is situated on the mirror plane, hence 50% occupancy) is disordered over two positions, one with 30% occupancy and the other 20% occupancy.

Table 11. Crystal data and structure refinement for $[\text{Ni}_4(\text{H}_2\text{L9})(\text{OH})_2(\text{H}_2\text{O})_2(\text{H}_2\text{O})_4](\text{ClO}_4)_2$

The X-ray reflection data were collected at 150K on station 9.8 of the Synchrotron Radiation Source at Daresbury²⁴¹ on a Bruker SMART1000 CCD diffractometer using synchrotron radiation.

Identification code	ni1601	
Empirical formula	C68.20 H82.50 Cl2 N4 Ni4 O30.10	
Formula weight	1745.62	
Temperature	150(2) K	
Wavelength	0.6880 Å	
Crystal system	Orthorhombic	
Space group	Pnma	
Unit cell dimensions	a = 21.9401(15) Å	$\alpha = 90^\circ$
	b = 14.9200(10) Å	$\beta = 90^\circ$
	c = 27.8332(18) Å	$\gamma = 90^\circ$
Volume	9111.1(11) Å ³	
Z	4	
Density (calculated)	1.273 Mg/m ³	
Absorption coefficient	0.945 mm ⁻¹	
F(000)	3626	
Crystal size	0.18 x 0.10 x 0.04 mm ³	
Theta range for data collection	1.81 to 25.00°	
Index ranges	-26 ≤ h ≤ 26, -17 ≤ k ≤ 17, -33 ≤ l ≤ 32	
Reflections collected	64152	
Independent reflections	8356 [R(int) = 0.0779]	
Completeness to theta = 25.00°	99.9 %	
Absorption correction	None	
Refinement method	Full-matrix least-squares on F ²	
Data / restraints / parameters	8356 / 0 / 425	
Goodness-of-fit on F ²	1.168	
Final R indices [I > 2σ(I)]	R1 = 0.1708, wR2 = 0.4103	
R indices (all data)	R1 = 0.1911, wR2 = 0.4214	
Largest diff. peak and hole	1.301 and -2.372 e.Å ⁻³	

Refinement and disorders details for $[\text{Ni}_4(\text{H}_2\text{L9})(\text{OH})_2(\text{H}_2\text{O})_2(\text{H}_2\text{O})_4](\text{ClO}_4)_2$

Due to poor data, the structure could not be refined to a reasonable factor.

Table 12. Crystal data and structure refinement for $[\text{Cu}_4(\text{H}_2\text{L9})(\text{H}_2\text{O})_2(\text{OH})_2](\text{NO}_3)_2$

The X-ray reflection data were collected at 150K on a Bruker SMART CCD diffractometer using graphite monochromated Mo-K α radiation ($\lambda = 0.71073 \text{ \AA}$) at Loughborough University.

Identification code	cu1109	
Empirical formula	C55.80 H65 Cu4 N6 O19.60	
Formula weight	1387.50	
Temperature	150(2) K	
Wavelength	0.6880 \AA	
Crystal system	Triclinic	
Space group	$P\bar{1}$	
Unit cell dimensions	$a = 11.849(7) \text{ \AA}$	$\alpha = 100.090(8)^\circ$
	$b = 14.272(8) \text{ \AA}$	$\beta = 94.985(8)^\circ$
	$c = 21.004(12) \text{ \AA}$	$\gamma = 90.021(9)^\circ$
Volume	$3483(4) \text{ \AA}^3$	
Z	2	
Density (calculated)	1.323 Mg/m^3	
Absorption coefficient	1.272 mm^{-1}	
F(000)	1429	
Crystal size	0.28 x 0.10 x 0.08 mm^3	
Theta range for data collection	0.99 to 25.00 $^\circ$.	
Index ranges	$-13 \leq h \leq 14$, $-16 \leq k \leq 16$, $-24 \leq l \leq 24$	
Reflections collected	24167	
Independent reflections	12066 [R(int) = 0.1412]	
Completeness to theta = 25.00 $^\circ$	98.7 %	
Absorption correction	Multiscan	
Max. and min. transmission	1.000 and 0.713	
Refinement method	Full-matrix least-squares on F^2	
Data / restraints / parameters	12066 / 0 / 605	
Goodness-of-fit on F^2	1.282	
Final R indices [$I > 2\sigma(I)$]	R1 = 0.1901, wR2 = 0.4194	
R indices (all data)	R1 = 0.2795, wR2 = 0.4592	
Largest diff. peak and hole	2.233 and -1.897 e.\AA^{-3}	

Refinement and disorders details for $[\text{Cu}_4(\text{H}_2\text{L9})(\text{H}_2\text{O})_2(\text{OH})_2](\text{NO}_3)_2$

Due to poor data, the structure could not be refined to a reasonable factor.

Table 13. Crystal data and structure refinement for $[\text{Mn}_4(\text{L11})(\text{MeOH})_6(\text{MeO})_2\text{Cl}_2](\text{ClO}_4)_2$

The X-ray reflection data were collected at 150K on a Bruker SMART CCD diffractometer using graphite monochromated Mo-K α radiation ($\lambda = 0.71073 \text{ \AA}$) at Queen's University, Belfast.

Identification code	mn2610
Empirical formula	C66 H108 Cl4 Mn4 N4 O24
Formula weight	1703.12
Temperature	150(2) K
Wavelength	0.71073 \AA
Crystal system	Monoclinic
Space group	C2/c
Unit cell dimensions	a = 30.526(2) \AA $\alpha = 90^\circ$ b = 11.5771(8) \AA $\beta = 105.5080(10)^\circ$ c = 23.4144(16) \AA $\gamma = 90^\circ$
Volume	7973.6(9) \AA^3
Z	4
Density (calculated)	1.419 Mg/m^3
Absorption coefficient	0.827 mm^{-1}
F(000)	3568
Crystal size	0.38 x 0.30 x 0.17 mm^3
Theta range for data collection	1.81 to 27.50 $^\circ$.
Index ranges	-39 \leq h \leq 39, -15 \leq k \leq 14, -30 \leq l \leq 30
Reflections collected	44477
Independent reflections	9095 [R(int) = 0.0235]
Completeness to theta = 27.50 $^\circ$	99.4 %
Absorption correction	Semi-empirical from equivalents
Max. and min. transmission	1.000 and 0.856
Refinement method	Full-matrix least-squares on F ²
Data / restraints / parameters	9095 / 0 / 466
Goodness-of-fit on F ²	1.075
Final R indices [I > 2 σ (I)]	R1 = 0.0426, wR2 = 0.1127
R indices (all data)	R1 = 0.0541, wR2 = 0.1204
Largest diff. peak and hole	0.712 and -0.562 e. \AA^{-3}

Refinement and disorders details for $[\text{Mn}_4(\text{L11})(\text{MeOH})_6(\text{MeO})_2\text{Cl}_2](\text{ClO}_4)_2$

All the hydrogen atoms belonging to the macrocycle were inserted at calculated positions. The hydrogen atoms on O(29), O(31) and O(32) belonging to the coordinated methanol molecules were found and their positions and temperature factors fixed.

Table 14. Crystal data and structure refinement for [Mn₄(L11)(MeOH)₄(MeO)₂(OAc)₂]Cl₂

The X-ray reflection data were collected at 150K on station 9.8 of the Synchrotron Radiation Source at Daresbury²⁴¹ on a Bruker SMART1000 CCD diffractometer using synchrotron radiation.

Identification code	mn0801sq	
Empirical formula	C66 H98.44 Cl2 Mn4 N4 O16.22	
Formula weight	1498.15	
Temperature	293(2) K	
Wavelength	0.68800 Å	
Crystal system	Rhombohedral	
Space group	R $\bar{3}$	
Unit cell dimensions	a = 37.1077(8) Å	$\alpha = 90^\circ$
	b = 37.1077(8) Å	$\beta = 90^\circ$
	c = 14.8540(5) Å	$\gamma = 120^\circ$
Volume	17713.4(8) Å ³	
Z	9	
Density (calculated)	1.264 Mg/m ³	
Absorption coefficient	0.755 mm ⁻¹	
F(000)	7076	
Crystal size	0.16 x 0.06 x 0.02 mm ³	
Theta range for data collection	1.81 to 27.50°.	
Index ranges	-42 ≤ h ≤ 49, -49 ≤ k ≤ 44, -17 ≤ l ≤ 19	
Reflections collected	40203	
Independent reflections	9961 [R(int) = 0.0407]	
Completeness to theta = 27.50°	99.9 %	
Absorption correction	None	
Refinement method	Full-matrix least-squares on F ²	
Data / restraints / parameters	9961 / 0 / 425	
Goodness-of-fit on F ²	1.115	
Final R indices [I > 2σ(I)]	R1 = 0.0486, wR2 = 0.1282	
R indices (all data)	R1 = 0.0561, wR2 = 0.1305	
Largest diff. peak and hole	1.167 and -0.648 e.Å ⁻³	

Refinement and disorders details for [Mn₄(L11)(MeOH)₄(MeO)₂(OAc)₂]Cl₂

All the hydrogen atoms belonging to the macrocycle were inserted at calculated positions. The hydrogen atoms on O(32) and O(33) belonging to the coordinated methanol molecules have been found and their positions and temperature factors fixed.

The methanol solvates that were severely disordered have been accounted for using the program Squeeze²⁴⁰ which located voids of 2293 Å³. The 'missing' electron count refined to 33 per unit cell. This was assigned to one methanol molecule per unit cell.

ANNEX 3

**Tables for crystal data and refinement
for the
compounds described in chapter 4**

Table 1: Crystal data and structure refinement for $[\text{Ni}_2(\text{C}_{12}\text{H}_{13}\text{O}_3)_2(\text{MeOH})_4](\text{ClO}_4)_2 \cdot 2\text{MeOH}$

The X-ray reflection data were collected at 150K on a Bruker SMART CCD diffractometer using graphite monochromated Mo-K α radiation ($\lambda = 0.71073 \text{ \AA}$) at Queen's University, Belfast.

Identification code	niper3
Empirical formula	C30 H44 Cl2 Ni2 O20
Formula weight	912.97
Temperature	150(2) K
Wavelength	0.71073 \AA
Crystal system	Monoclinic
Space group	$P2_1/n$
Unit cell dimensions	$a = 9.5039(8) \text{ \AA}$ $\alpha = 90^\circ$ $b = 21.3482(19) \text{ \AA}$ $\beta = 109.0030(10)^\circ$ $c = 10.5485(9) \text{ \AA}$ $\gamma = 90^\circ$
Volume	$2023.6(3) \text{ \AA}^3$
Z	2
Density (calculated)	1.498 Mg/m^3
Absorption coefficient	1.138 mm^{-1}
F(000)	948
Crystal size	$0.5 \times 0.3 \times 0.2 \text{ mm}^3$
Theta range for data collection	1.91 to 25.00° .
Index ranges	$-11 \leq h \leq 11$, $-25 \leq k \leq 25$, $-12 \leq l \leq 12$
Reflections collected	19414
Independent reflections	3557 [R(int) = 0.0249]
Completeness to theta = 25.00°	99.9 %
Absorption correction	Empirical
Max. and min. transmission	0.928 and 0.733
Refinement method	Full-matrix least-squares on F^2
Data / restraints / parameters	3557 / 1 / 254
Goodness-of-fit on F^2	1.072
Final R indices [$I > 2\sigma(I)$]	$R1 = 0.0571$, $wR2 = 0.1680$
R indices (all data)	$R1 = 0.0645$, $wR2 = 0.1756$
Largest diff. peak and hole	1.497 and $-0.677 \text{ e.\AA}^{-3}$

Refinement and disorders details for $[\text{Ni}_2(\text{C}_{12}\text{H}_{13}\text{O}_3)_2(\text{MeOH})_4](\text{ClO}_4)_2 \cdot 2\text{MeOH}$

All the hydrogen atoms on the coordinated ligands were inserted at calculated positions. The hydrogen atoms H(4) and H(5A) on the hydroxy group of the coordinated MeOH molecules were found and their positions and temperature factors fixed. The hydrogen atoms of the disordered MeOH solvate molecule were not included in the model.

In addition, the solvate methanol is disordered with O(10) being 70% occupancy and O(10') being 30% occupancy. One other feature to be mentioned about the structure is that the C-O distance for the disordered methanol molecule was restrained to be 1.5 \AA . The ClO_4^- counter-anion was also disordered. It was modelled with O(9) sharing two sites each with an occupancy of 50% above and below the triangular plane formed by the three other oxygen atoms O(6), O(7) and O(8).

Table 2. Crystal data and structure refinement for [Co₂(C₁₂H₁₃O₃)₂(MeOH)₄](ClO₄)₂·2MeOH

The X-ray reflection data were collected at 150K on a Bruker SMART CCD diffractometer using graphite monochromated Mo-K α radiation ($\lambda = 0.71073 \text{ \AA}$) at Queen's University, Belfast.

Identification code	coper2	
Empirical formula	C30 H50 Cl2 Co2 O20	
Formula weight	919.46	
Temperature	150(2) K	
Wavelength	0.71073 \AA	
Crystal system	Triclinic	
Space group	P $\bar{1}$	
Unit cell dimensions	$a = 10.9089(7) \text{ \AA}$	$\alpha = 80.6520(10)^\circ$
	$b = 12.6687(8) \text{ \AA}$	$\beta = 80.0630(10)^\circ$
	$c = 15.9332(10) \text{ \AA}$	$\gamma = 67.9810(10)^\circ$
Volume	1999.2(2) \AA^3	
Z	2	
Density (calculated)	1.527 Mg/m ³	
Absorption coefficient	1.041 mm ⁻¹	
F(000)	956	
Crystal size	0.52 x 0.45 x 0.40 mm ³	
Theta range for data collection	1.30 to 28.60 $^\circ$.	
Index ranges	-14 $\leq h \leq$ 14, -16 $\leq k \leq$ 16, -21 $\leq l \leq$ 20	
Reflections collected	23225	
Independent reflections	9014 [R(int) = 0.0310]	
Completeness to theta = 28.60 $^\circ$	88.1 %	
Absorption correction	Empirical	
Max. and min. transmission	1.000 and 0.719	
Refinement method	Full-matrix least-squares on F ²	
Data / restraints / parameters	9014 / 0 / 526	
Goodness-of-fit on F ²	0.963	
Final R indices [I > 2 σ (I)]	R1 = 0.0535, wR2 = 0.1523	
R indices (all data)	R1 = 0.0687, wR2 = 0.1614	
Largest diff. peak and hole	1.136 and -0.740 e. \AA^{-3}	

Refinement and disorders details for [Co₂(C₁₂H₁₃O₃)₂(MeOH)₄](ClO₄)₂·2MeOH

All the hydrogen atoms on the coordinated ligands were inserted at calculated positions. The hydrogen atoms H(7), H(8), H(9) and H(10) on the hydroxy group of the coordinated MeOH molecules were found and their positions and their temperature factors fixed. H(19A) and H(20A) on the hydroxy groups of the two non-coordinated MeOH molecule were treated the same way.

One of the ClO₄⁻ counter-anions is disordered with each oxygen atom around the chlorine atom sharing two sites with one set of oxygen atoms [O(11), O(12), O(13) and O(14)] being 38% occupancy and the other [O(11'), O(12'), O(13') and O(14')] being 62% occupancy. In addition, the solvate methanol is disordered with C being 72% occupancy and C' being 28% occupancy.

Table 3. Crystal data and structure refinement for $[\text{Mn}_2(\text{C}_{12}\text{H}_{13}\text{O}_3)_2(\text{MeOH})_4](\text{ClO}_4)_2 \cdot 2\text{MeOH}$

The X-ray reflection data were collected at 150K on a Bruker SMART CCD diffractometer using graphite monochromated Mo-K α radiation ($\lambda = 0.71073 \text{ \AA}$) at Queen's University, Belfast.

Identification code	mnper1
Empirical formula	C30 H50 Cl2 Mn2 O20
Formula weight	911.48
Temperature	153(2) K
Wavelength	0.71073 \AA
Crystal system	Triclinic
Space group	$P\bar{1}$
Unit cell dimensions	$a = 11.0145(15) \text{ \AA}$ $\alpha = 81.518(9)^\circ$ $b = 12.7239(13) \text{ \AA}$ $\beta = 79.904(10)^\circ$ $c = 15.9832(16) \text{ \AA}$ $\gamma = 67.441(10)^\circ$
Volume	2028.6(4) \AA^3
Z	2
Density (calculated)	1.492 Mg/m^3
Absorption coefficient	0.830 mm^{-1}
F(000)	948
Crystal size	0.46 x 0.42 x 0.20 mm^3
Theta range for data collection	2.02 to 25.00 $^\circ$
Index ranges	$-1 \leq h \leq 13$, $-14 \leq k \leq 15$, $-18 \leq l \leq 19$
Reflections collected	8335
Independent reflections	7116 [R(int) = 0.0255]
Completeness to theta = 25.00 $^\circ$	99.9 %
Absorption correction	Empirical
Max. and min. transmission	0.851 and 0.701
Refinement method	Full-matrix least-squares on F^2
Data / restraints / parameters	7116 / 0 / 536
Goodness-of-fit on F^2	1.039
Final R indices [$I > 2\sigma(I)$]	R1 = 0.0619, wR2 = 0.1429
R indices (all data)	R1 = 0.0929, wR2 = 0.1613
Largest diff. peak and hole	1.113 and -0.902 e.\AA^{-3}

Refinement and disorders details for $[\text{Mn}_2(\text{C}_{12}\text{H}_{13}\text{O}_3)_2(\text{MeOH})_4](\text{ClO}_4)_2 \cdot 2\text{MeOH}$

All the hydrogen atoms on the coordinated ligands were inserted at calculated positions. The hydrogen atoms H(7), H(8), H(9) and H(10) on the hydroxy group of the coordinated MeOH molecules were found and their positions and their temperature factors fixed. The hydrogen atoms on the disordered MeOH molecule were not included in the model.

One of the ClO_4^- counter-anion is disordered with each oxygen atom around the chlorine atom sharing two sites with one set of oxygen atoms [O(11), O(12), O(13) and O(14)] being 38% occupancy and the other [O(11'), O(12'), O(13') and O(14')] being 62% occupancy.

Table 4. Crystal data and structure refinement for [Cu₂(C₁₂H₁₃O₃)₂(MeOH)₂(ClO₄)₂]

The X-ray reflection data were collected at 150K on a Bruker SMART CCD diffractometer using graphite monochromated Mo-K α radiation ($\lambda = 0.71073 \text{ \AA}$) at Queen's University, Belfast.

Identification code	cuperr	
Empirical formula	C ₂₆ H ₃₄ Cl ₂ Cu ₂ O ₁₆	
Formula weight	800.51	
Temperature	150(2) K	
Wavelength	0.71073 \AA	
Crystal system	Monoclinic	
Space group	P2 ₁ /c	
Unit cell dimensions	a = 8.9898(18) \AA	$\alpha = 90^\circ$
	b = 10.864(2) \AA	$\beta = 103.912(4)^\circ$
	c = 17.542(3) \AA	$\gamma = 90^\circ$
Volume	1663.0(6) \AA^3	
Z	2	
Density (calculated)	1.599 Mg/m ³	
Absorption coefficient	1.510 mm ⁻¹	
F(000)	820	
Crystal size	.325 x .200 x .100 mm ³	
Theta range for data collection	2.22 to 25.00 $^\circ$.	
Index ranges	-10 \leq h \leq 8, -12 \leq k \leq 12, -20 \leq l \leq 20	
Reflections collected	10048	
Independent reflections	2905 [R(int) = 0.0745]	
Completeness to theta = 25.00 $^\circ$	99.4 %	
Absorption correction	Empirical	
Max. and min. transmission	1.000 and 0.598	
Refinement method	Full-matrix least-squares on F ²	
Data / restraints / parameters	2905 / 0 / 216	
Goodness-of-fit on F ²	0.920	
Final R indices [I > 2 σ (I)]	R1 = 0.0648, wR2 = 0.1550	
R indices (all data)	R1 = 0.0936, wR2 = 0.1682	
Largest diff. peak and hole	1.402 and -0.404 e. \AA^{-3}	

Refinement and disorders details for [Cu₂(C₁₂H₁₃O₃)₂(MeOH)₄(ClO₄)₂]

All the hydrogen atoms on the coordinated ligands were inserted at calculated positions. The hydrogen atom H(4) on the hydroxy group of the coordinated MeOH molecules was found and its position and temperature factor fixed.

Table 5. Crystal data and structure refinement for $[\text{Ni}_2(\text{C}_{12}\text{H}_{13}\text{O}_3)_2(\text{MeOH})_2(\text{NO}_3)_2]$

The X-ray reflection data were collected at 150K on a Bruker SMART CCD diffractometer using graphite monochromated Mo-K α radiation ($\lambda = 0.71073 \text{ \AA}$) at Queen's University, Belfast.

Identification code	ninit
Empirical formula	C ₂₆ H ₃₄ N ₂ Ni ₂ O ₁₄
Formula weight	715.97
Temperature	150(2) K
Wavelength	0.71073 \AA
Crystal system	Monoclinic
Space group	P2 ₁ /c
Unit cell dimensions	a = 8.8998(7) \AA $\alpha = 90^\circ$ b = 9.9928(8) \AA $\beta = 101.0610(10)^\circ$ c = 17.5245(14) \AA $\gamma = 90^\circ$
Volume	1529.6(2) \AA^3
Z	2
Density (calculated)	1.555 Mg/m^3
Absorption coefficient	1.302 mm^{-1}
F(000)	744
Crystal size	0.4 x 0.2 x 0.1 mm^3
Theta range for data collection	2.33 to 24.99 $^\circ$.
Index ranges	-10 \leq h \leq 10, -11 \leq k \leq 11, -20 \leq l \leq 20
Reflections collected	14460
Independent reflections	2693 [R(int) = 0.0353]
Completeness to theta = 24.99 $^\circ$	100.0 %
Absorption correction	Empirical
Max. and min. transmission	1.000 and 0.788
Refinement method	Full-matrix least-squares on F ²
Data / restraints / parameters	2693 / 0 / 203
Goodness-of-fit on F ²	1.067
Final R indices [I > 2 σ (I)]	R1 = 0.0457, wR2 = 0.1225
R indices (all data)	R1 = 0.0588, wR2 = 0.1325
Largest diff. peak and hole	0.615 and -0.319 e.\AA^{-3}

Refinement and disorders details for $[\text{Ni}_2(\text{C}_{12}\text{H}_{13}\text{O}_3)_2(\text{MeOH})_2(\text{NO}_3)_2]$

All the hydrogen atoms on the coordinated ligands were inserted at calculated positions. The hydrogen atom H(4) on the hydroxy group of the coordinated MeOH molecules was found and its position and its temperature factor fixed.

Table 6. Crystal data and structure refinement for [Cu(C₁₂H₁₃O₃)₂]

The X-ray reflection data were collected at 150K on a P4 diffractometer using graphite monochromated Mo-K α radiation ($\lambda = 0.71073 \text{ \AA}$) at Queen's University, Belfast.

Identification code	cuper2x	
Empirical formula	C ₂₄ H ₂₆ Cu O ₆	
Formula weight	473.99	
Temperature	293(2) K	
Wavelength	0.71073 \AA	
Crystal system	Monoclinic	
Space group	P2 ₁ /c	
Unit cell dimensions	a = 15.6358(15) \AA	$\alpha = 90^\circ$
	b = 6.0135(8) \AA	$\beta = 107.803(9)^\circ$
	c = 12.5470(16) \AA	$\gamma = 90^\circ$
Volume	1123.2(2) \AA^3	
Z	2	
Density (calculated)	1.401 Mg/m ³	
Absorption coefficient	1.009 mm ⁻¹	
F(000)	494	
Crystal size	0.78 x 0.24 x 0.22 mm ³	
Theta range for data collection	2.74 to 25.00 $^\circ$.	
Index ranges	-18 \leq h \leq 18, -1 \leq k \leq 7, -1 \leq l \leq 14	
Reflections collected	2722	
Independent reflections	1979 [R(int) = 0.0235]	
Completeness to theta = 25.00 $^\circ$	99.9 %	
Absorption correction	Semi-empirical	
Max. and min. transmission	0.933 and 0.814	
Refinement method	Full-matrix least-squares on F ²	
Data / restraints / parameters	1979 / 0 / 142	
Goodness-of-fit on F ²	1.032	
Final R indices [I > 2 σ (I)]	R1 = 0.0275, wR2 = 0.0739	
R indices (all data)	R1 = 0.0348, wR2 = 0.0777	
Largest diff. peak and hole	0.614 and -0.384 e. \AA^{-3}	

Refinement and disorders details for [Cu(C₁₂H₁₃O₃)₂]

All the hydrogen atoms on the coordinated ligands were inserted at calculated positions.

ANNEX 4

**Tables for crystal data and refinement
for the
compounds described in chapter 5**

Table 1: Crystal data and structure refinement for $[\text{Ni}_7(\text{C}_{12}\text{H}_{13}\text{O}_3)_6(\text{MeO})(\text{OH})_5](\text{ClO}_4)_2$

The X-ray reflection data were collected at 150K on station 9.8 of the Synchrotron Radiation Source at Daresbury²⁴¹ on a Bruker SMART1000 CCD diffractometer using synchrotron radiation.

Identification code	sandrb
Empirical formula	C74.40 H77 Cl2 Ni7 O33
Formula weight	1981.03
Temperature	150(2) K
Wavelength	0.68900 Å
Crystal system	Monoclinic
Space group	P2 ₁ /n
Unit cell dimensions	a = 12.6968(7) Å α = 90° b = 18.6255(10) Å β = 99.3320(10)° c = 24.2374(13) Å γ = 90°
Volume	5655.9(5) Å ³
Z	2
Density (calculated)	1.163 Mg/m ³
Absorption coefficient	1.249 mm ⁻¹
F(000)	2035
Crystal size	0.12 x 0.12 x 0.06 mm ³
Theta range for data collection	1.96 to 24.00°.
Index ranges	-14 ≤ h ≤ 14, -20 ≤ k ≤ 21, -28 ≤ l ≤ 28
Reflections collected	36291
Independent reflections	9590 [R(int) = 0.0909]
Completeness to theta = 24.00°	98.5 %
Absorption correction	None
Refinement method	Full-matrix least-squares on F ²
Data / restraints / parameters	9590 / 0 / 484
Goodness-of-fit on F ²	1.465
Final R indices [I > 2σ(I)]	R1 = 0.1314, wR2 = 0.3825
R indices (all data)	R1 = 0.1624, wR2 = 0.4078
Largest diff. peak and hole	1.450 and -1.735 e.Å ⁻³

Refinement and disorders details for $[\text{Ni}_7(\text{C}_{12}\text{H}_{13}\text{O}_3)_6(\text{MeO})(\text{OH})_5](\text{ClO}_4)_2$

All the hydrogen atoms on the coordinated ligands (DFTP) were inserted at calculated positions. The hydrogen atoms on the methoxy and hydroxy groups were not inserted. Due to weak data, the refinement factor of 13% could not be improved.

The carbon atoms on the two methoxy groups (C(40) and C(50)) are half occupancy.

The isotropic factor of the hydrogen belonging to C(10B), C(10C), C(11C) and C(12C) were fixed.

Table 2: Crystal data and structure refinement for [Co₇(C₁₂H₁₃O₃)₆(MeO)₆](ClO₄)₂

The X-ray reflection data were collected at 150K on a Bruker SMART CCD diffractometer using graphite monochromated Mo-K α radiation ($\lambda = 0.71073 \text{ \AA}$) at Queen's University, Belfast.

Identification code	coper1	
Empirical formula	C86 H100 Cl2 Co7 O36	
Formula weight	2193.07	
Temperature	150(2) K	
Wavelength	0.71073 \AA	
Crystal system	Monoclinic	
Space group	P2 ₁ /n	
Unit cell dimensions	a = 11.585(4) \AA	$\alpha = 90^\circ$
	b = 17.173(6) \AA	$\beta = 90.000(6)^\circ$
	c = 27.647(9) \AA	$\gamma = 90^\circ$
Volume	5501(3) \AA^3	
Z	2	
Density (calculated)	1.324 Mg/m ³	
Absorption coefficient	1.151 mm ⁻¹	
F(000)	2254	
Crystal size	0.25 x 0.17 x 0.13 mm ³	
Theta range for data collection	1.89 to 24.00 $^\circ$.	
Index ranges	-13 \leq h \leq 13, -19 \leq k \leq 19, -24 \leq l \leq 31	
Reflections collected	25076	
Independent reflections	8613 [R(int) = 0.0341]	
Completeness to theta = 24.00 $^\circ$	99.6 %	
Absorption correction	Multiscan	
Max. and min. transmission	1.000 and 0.713	
Refinement method	Full-matrix least-squares on F ²	
Data / restraints / parameters	8613 / 0 / 327	
Goodness-of-fit on F ²	2.417	
Final R indices [I > 2 σ (I)]	R1 = 0.1447, wR2 = 0.3743	
R indices (all data)	R1 = 0.1813, wR2 = 0.3924	
Largest diff. peak and hole	1.746 and -0.863 e. \AA^{-3}	

Refinement and disorders details for [Co₇(C₁₂H₁₃O₃)₆(MeO)₆](ClO₄)₂

All the hydrogen atoms on the coordinated ligands (DFTP) were inserted at calculated positions. The hydrogen atoms on the methoxy groups were not inserted. Due to weak data, the refinement factor of 14% could not be improved.

Table 3: Crystal data and structure refinement for $[\text{Mn}_3(\text{C}_{23}\text{H}_{26}\text{O}_4)_2(\text{CH}_3\text{OH})_4(\text{H}_2\text{O})](\text{ClO}_4)_2$

The X-ray reflection data were collected at 150K on a Bruker SMART1000 CCD diffractometer using graphite monochromated Mo-K α radiation ($\lambda = 0.71073 \text{ \AA}$) at Loughborough University.

Identification code	mn12	
Empirical formula	C52 H74 Cl6 Mn3 O21	
Formula weight	1412.63	
Temperature	150(2) K	
Wavelength	0.71073 \AA	
Crystal system	Monoclinic	
Space group	I2/a	
Unit cell dimensions	a = 15.3663(16) \AA	$\alpha = 90^\circ$
	b = 12.7963(14) \AA	$\beta = 98.732(2)^\circ$
	c = 32.615(3) \AA	$\gamma = 90^\circ$
Volume	6338.8(12) \AA^3	
Z	4	
Density (calculated)	1.480 Mg/m^3	
Absorption coefficient	0.912 mm^{-1}	
F(000)	2924	
Crystal size	0.42 x 0.06 x 0.03 mm^3	
Theta range for data collection	1.71 to 25.00 $^\circ$.	
Index ranges	-18 $\leq h \leq$ 18, -15 $\leq k \leq$ 15, -38 $\leq l \leq$ 38	
Reflections collected	22085	
Independent reflections	5582 [R(int) = 0.0787]	
Completeness to theta = 25.00 $^\circ$	99.8 %	
Absorption correction	Multiscan	
Max. and min. transmission	1.000 and 0.901	
Refinement method	Full-matrix least-squares on F ²	
Data / restraints / parameters	5582 / 0 / 373	
Goodness-of-fit on F ²	1.046	
Final R indices [I > 2 σ (I)]	R1 = 0.0600, wR2 = 0.1415	
R indices (all data)	R1 = 0.1048, wR2 = 0.1626	
Largest diff. peak and hole	0.456 and -0.918 e.\AA^{-3}	

Refinement and disorders details for $[\text{Mn}_3(\text{C}_{23}\text{H}_{26}\text{O}_4)_2(\text{CH}_3\text{OH})_4(\text{H}_2\text{O})](\text{ClO}_4)_2$

All the hydrogen atoms on the coordinated ligands (DHTMB) were inserted at calculated positions. The hydrogen atoms H(24), H(25) belonging to the two coordinated methanol molecules and H(1w) belonging to the coordinated water molecule were found and their positions fixed.

